



UNIL | Université de Lausanne

Unicentre
CH-1015 Lausanne
<http://serval.unil.ch>

Year : 2015

Evolution of the Helvetic shelf (Switzerland) during the Barremian–early Aptian: paleoenvironmental, paleogeographic and paleoceanographic controlling factors.

Bonvallet Lucie

Bonvallet Lucie, 2015, Evolution of the Helvetic shelf (Switzerland) during the Barremian–early Aptian: paleoenvironmental, paleogeographic and paleoceanographic controlling factors.

Originally published at : Thesis, University of Lausanne

Posted at the University of Lausanne Open Archive <http://serval.unil.ch>

Document URN : urn:nbn:ch:serval-BIB_8DF48AF8B7D54

Droits d'auteur

L'Université de Lausanne attire expressément l'attention des utilisateurs sur le fait que tous les documents publiés dans l'Archive SERVAL sont protégés par le droit d'auteur, conformément à la loi fédérale sur le droit d'auteur et les droits voisins (LDA). A ce titre, il est indispensable d'obtenir le consentement préalable de l'auteur et/ou de l'éditeur avant toute utilisation d'une oeuvre ou d'une partie d'une oeuvre ne relevant pas d'une utilisation à des fins personnelles au sens de la LDA (art. 19, al. 1 lettre a). A défaut, tout contrevenant s'expose aux sanctions prévues par cette loi. Nous déclinons toute responsabilité en la matière.

Copyright

The University of Lausanne expressly draws the attention of users to the fact that all documents published in the SERVAL Archive are protected by copyright in accordance with federal law on copyright and similar rights (LDA). Accordingly it is indispensable to obtain prior consent from the author and/or publisher before any use of a work or part of a work for purposes other than personal use within the meaning of LDA (art. 19, para. 1 letter a). Failure to do so will expose offenders to the sanctions laid down by this law. We accept no liability in this respect.

Evolution of the Helvetic shelf (Switzerland) during
the Barremian–early Aptian: paleoenvironmental,
paleogeographic and paleoceanographic controlling
factors.

Thèse de doctorat

présentée à la Faculté des géosciences et de l'environnement
de l'Université de Lausanne par

Lucie Bonvallet

diplômée de l'Université Joseph Fourier, Grenoble 1

Jury:

Prof. Karl B. Föllmi (Directeur, Univ. Lausanne, CH)

Dr. Thierry Adatte (Univ. Lausanne, CH)

Prof. Annie Arnaud-Vanneau (Association Dolomieu, Grenoble, F)

Prof. Alexis Godet (Univ. San Antonio, Texas, US)

Dr. PD. Jorge E. Spangenberg (Univ. Lausanne, CH)

sous la présidence du Prof. Eric Verrecchia (Univ. Lausanne, CH)



UNIL | Université de Lausanne

Institut des Sciences de la Terre

Evolution of the Helvetic shelf (Switzerland) during the Barremian–early Aptian: paleoenvironmental, paleogeographic and paleoceanographic controlling factors.

Thèse de doctorat

présentée à la Faculté des géosciences et de l'environnement
de l'Université de Lausanne par

Lucie Bonvallet

diplômée de l'Université Joseph Fourier, Grenoble 1

Jury:

Prof. Karl B. Föllmi (Directeur, Univ. Lausanne, CH)

Dr. Thierry Adatte (Univ. Lausanne, CH)

Prof. Annie Arnaud-Vanneau (Association Dolomieu, Grenoble, F)

Prof. Alexis Godet (Univ. San Antonio, Texas, US)

Dr. PD. Jorge E. Spangenberg (Univ. Lausanne, CH)

sous la présidence du Prof. Eric Verrecchia (Univ. Lausanne, CH)

Lausanne 2015



UNIL | Université de Lausanne
Décanat Géosciences et de l'Environnement
bâtiment Géopolis
CH-1015 Lausanne

IMPRIMATUR

Vu le rapport présenté par le jury d'examen, composé de

Président de la séance publique :	M. le Professeur Eric Verrecchia
Président du colloque :	M. le Professeur Eric Verrecchia
Directeur de thèse :	M. le Professeur Karl Föllmi
Experte externe :	Mme la Professeure Annie Arnaud
Expert externe :	M. le Docteur Alexis Godet
Expert interne :	M. le Docteur Jorge Spangenberg
Expert interne :	M. le Docteur Thierry Adatte

Le Doyen de la Faculté des géosciences et de l'environnement autorise l'impression
de la thèse de

Madame Lucie BONVALLET

Titulaire d'une
Master Professionnel « Géosciences, Exploration, Risques »
Université Joseph Fourier, Grenoble

intitulée

**EVOLUTION OF THE HELVETIC SHELF (SWITZERLAND)
DURING THE BARREMIAN-EARLY APTIAN :
PALEOENVIRONMENTAL, PALEOGEOGRAPHIC AND
PALEOCEANOGRAPHIC CONTROLLING FACTORS**

Lausanne, le 9 octobre 2015

Pour le Doyen de la Faculté des géosciences et
de l'environnement

Professeur Eric Verrecchia

Table of contents

<i>Abstract</i>	XI
<i>Résumé</i>	XIII
<i>Remerciements</i>	XV
Chapter 1 – General introduction	1
1.1 Foreword.....	3
1.2 The Cretaceous World	4
1.2.1 Paleogeographic context	4
1.2.2 Climatic conditions.....	5
1.2.3 Oceanic Anoxic Events (OAEs)	6
1.2.4 Sea level fluctuations.....	6
1.2.5 Cretaceous shallow-water carbonate platforms.....	6
1.3 The Helvetic Alps	8
1.3.1 Paleogeography of the Helvetic margin.....	8
1.3.2 Nappes and Palinspastic reconstruction.....	8
1.3.3 Intensity of the diagenesis of the Helvetic nappes.....	11
1.3.4 Stratigraphy of the late Hauterivian – early Aptian rocks in the Helvetic realm	11
1.3.4.1 <i>Lithostratigraphy and ages</i>	11
1.3.4.1.1 <i>Tierwis Formation</i>	11
The Altmann Member	13
The Drusberg Member	13
The Chopf Bed	13
1.3.4.1.2 <i>Schrattenkalk Fm.</i>	14
The Lower Schrattenkalk Mb.....	14
The Rawil Mb	14
Upper Schrattenkalk Mb.....	14

1.3.4.2 Sequence stratigraphy.....	15
1.4 Aims and organization of the thesis	15
1.5 References	16
 Chapter 2 – Installation of a shallow-water carbonate platform on top of hemipelagic sediments: example of the Drus- berg-Schrattenkalk platform in the Helvetic Alps (Barremian)..	25
2.1 Introduction	27
2.2 Geological setting	28
2.3 Methods	31
2.3.1 Microfacies analysis.....	31
2.3.2 Biostratigraphy.....	31
2.3.3 Sequence stratigraphy.....	33
2.3.4 Panorama of the Churfirsten range	35
2.4 Results.....	35
2.4.1 General description of the studied sections and the panorama.....	35
2.4.1.1 <i>Sequence B2: distribution of the facies along the Helvetic platform</i>	40
2.4.1.2 <i>Characterization of the SB B3</i>	47
2.4.1.3 <i>Depositional geometries associated with the SB B3</i>	48
2.4.1.4 <i>Description of the sequence B3 in the reference section of Valsloch and its sequence stratigraphic interpretation</i>	48
2.4.1.5 <i>Characterization of the LST B3</i>	50
2.4.1.6 <i>Description of the TST B3</i>	50
2.4.1.7 <i>Characterization of the mfs, HST B3 and SB B4</i>	50
2.4.2 Evolution of the depositional sequence B3 along the platform	53
2.5 Interpretations.....	54
2.5.1 Depositional model	54
2.5.2 The onset of the Urgonian platform	57
2.6 Conclusions	57
2.7 References	58

Chapter 3 – Development and demise of the Urgonian platform
along the NW Tethyan margin: the record of the Helvetic Alps

during the earliest Aptian.....	63
3.1 Introduction	66
3.2 Geological setting	68
3.3 Methods	68
3.3.1 Studied sections	68
3.3.2 Field work and samples preparation.....	71
3.3.3 Microfacies description	71
3.3.4 Component quantification in thin sections	71
3.3.5 Carbon and oxygen-isotope analysis.....	73
3.3.6 Phosphorus content.....	73
3.3.7 Bulk-rock mineralogy	73
3.4 Results.....	73
3.4.1 Facies, microfacies and biostratigraphy	73
3.4.1.1 <i>Lower Schrattenkalk Member</i>	74
3.4.1.2 <i>Rawil Member</i>	78
3.4.1.3 <i>Upper Schrattenkalk Member</i>	83
3.4.1.4 <i>Grünten Member</i>	87
3.4.2 Stable carbon isotope composition.....	87
3.4.3 Phosphorus content.....	88
3.5 Discussion and interpretations.....	88
3.5.1 Biostratigraphy	88
3.5.2 Sequence stratigraphy.....	92
3.5.3 Correlations along the northern margin of the Tethys.....	93
3.5.4 Preservation of the primary carbon stable isotope composition	95
3.5.5 Photozoan versus heterozoan carbonate production during the deposition of the Urgonian Formation	99
3.5.6 Interactions between tectonic processes and sea-level change.....	100
3.5.7 General paleoceanographic change and the evolution and termination of the Urgonian platform	102
3.6 Conclusions	103

3.7 References	104
Chapter 4 – Evolution of the Helvetic series (Switzerland) during the latest Hauterivian–early Aptian time: distribution and evolution of facies associated to sea-level, geochemistry and paleotopographic changes.....	115
4.1 Introduction	118
4.2 Geological setting	118
4.3 Studied sections	121
4.4 Methods	121
4.4.1 Field work and samples preparation.....	121
4.4.2 Microfacies description	121
4.4.3 Carbon and oxygen-isotope analysis.....	122
4.4.4 Phosphorus content.....	124
4.5 Results.....	124
4.5.1 Description of the studied sections	124
4.5.2 Temporal evolution: example of the Säntis nappe	142
4.5.3 Spatial and temporal evolution: paleogeographic distribution of facies and thickness variation of sediment on the Helvetic margin	144
4.5.3.1 Sequences H6 to B1 (<i>Altmann Mb</i>).....	144
Facies distribution	144
4.5.3.2 Sequence B2 (<i>Drusberg Mb</i>).....	146
Facies distribution	146
Micropaleontological markers.....	146
4.5.3.3 Sequence B3 (<i>Lower Schrattenkalk Mb – lower part</i>)	146
Facies distribution	146
Micropaleontological markers.....	147
4.5.3.4 Sequence B4 (<i>Lower Schrattenkalk Mb – middle part</i>)	147
Facies distribution	147
Micropaleontological markers.....	149
4.5.3.5 Sequence B5 (<i>Lower Schrattenkalk Mb – upper part</i>)	149
Facies distribution	149
Micropaleontological markers.....	150
4.5.3.6 TSTA1 (<i>Rawil Mb</i>)	150

Facies distribution	150
Micropaleontological markers.....	150
4.5.3.7 HSTA1 (<i>Upper Schrattenkalk Mb</i>)	150
Facies distribution	150
Micropaleontological markers.....	152
4.6 Geochemistry data.....	152
4.6.1 Total phosphorus content.....	152
4.6.2 Carbon isotope composition	152
4.6.2.1 <i>Individual hand-specimen subsamples</i>	152
4.6.2.2 <i>Whole-rock samples</i>	152
4.7 Discussion	155
4.7.1 The evolution of the Helvetic shelf: controlling factors.....	155
4.7.1.1 <i>Spatial and temporal evolution of the facies along the shelf</i>	155
4.7.1.2 <i>Subsidence and faulting</i>	157
4.7.1.3 <i>Architecture of the platform</i>	158
4.7.2 The carbon isotope record.....	159
4.7.3 Eustatic sea level change	162
4.7.4 Environmental and climatic changes	162
4.8 Conclusion	165
4.9 References	166
Chapter 5 – Main conclusions	181
Chapter 6 – Appendix	185
6.1 Affiliated paper	187
6.1.1 Introduction	190
6.1.2 Geological setting and location of the studied sections	191
6.1.2.1 <i>The Pilatus section</i>	191
6.1.2.2 <i>The Tierwis section</i>	192
6.1.2.3 <i>The Clos de Barral section</i>	193
6.1.3 Methods	195

6.1.4 Results.....	195
6.1.4.1 <i>Authigenetic and diagenetic phases composing the basal hard-ground of the Altmann Member at Pilatus</i>	195
6.1.4.2 <i>Late Hauterivian to Barremian isotope records</i>	197
The Pilatus section	197
The Tierwis section.....	201
The Clos de Barral section	201
6.1.5 Discussion	201
6.1.5.1 <i>Paragenetic sequence of the Altmann hardground at Pilatus</i>	201
6.1.5.2 <i>The imprint of sea-level fluctuations and palaeoenvironmental change on the diagenesis of the Altmann drowning unconformity</i>	204
6.1.5.3 <i>Sequence stratigraphic and biostratigraphic context of the Altmann Member drowning episode</i>	207
6.1.5.4 <i>Drowning surfaces as archives of palaeoceanographic changes</i>	210
6.1.6 Conclusions	211
6.1.7 Acknowledgements.....	212
6.1.8 References	212
6.2 Carbone and oxygen isotope data.....	219
Tierwis	221
L'Ecuelle	223
Valsloch	225
Harder.....	228
Justistal.....	230
Morschach	232
Rawil.....	234
Kistenpass	235
Interlaken.....	236
Lämmerenplatten.....	236
Cluses.....	237
6.3 Total Phosphorus data	239
Valsloch	241
Tierwis	244
Kistenpass	246

Harder.....	246
Harder.....	247
L'Ecuelle	248
Interlaken.....	250
6.4 XRD (bulk rock) data	251
Valsloch	253
Cluses.....	255
6.5 Valsloch component counting data	257
6.6 Microfacies and Dunham data	265
Justistal.....	266
Alvier.....	268
L'Ecuelle	270
Morschach	272
Tierwis	274
Valsloch	276
Rawil.....	279
Interlaken.....	280
Harder.....	280
6.7 Panorama	283
6.8 Additional boxplots for the chapter 3	323
6.9 Cluses section (Subalpine Chains).....	331

Abstract

The Early Cretaceous has experienced the development of large shallow-water carbonate platform in tropical and subtropical regions, favoured by exceptionally warm climatic conditions, optimal trophic conditions and a suitable tectonic and paleogeographic context. This period was also characterized by shorter intervals, in which the widespread deposition of marine sediments enriched in organic matter occurred (“oceanic anoxic episodes”). This study focuses on the Barremian-Aptian interval, during which the Urgonian platform developed throughout the northern Tethyan passive margin. Due to the Alpine orogeny, sediments belonging to this platform - named locally Schrattenkalk Formation, are presently outcropping in the Helvetic Alps.

This study aims to reconstruct the paleogeographic evolution of the Helvetic platform, and to define the environmental and oceanographic factors, which influenced its development. Several key episodes in the development of this platform have been identified:

- The installation of the platform, covering hemipelagic sediments of the Drusberg Member, near the limit between the early and late Barremian,
- The temporary change of carbonate production type during the basal Aptian, with the deposition of the Rawil Member,
- And finally the definitive interruption of photozoan carbonate platform sedimentation in the study area, during the early Aptian.

The sedimentological, biostratigraphical and chemostratigraphic ($\delta^{13}\text{C}$) data lead to the sequential subdivision of eleven sections and one core, located throughout the different Helvetic nappes of Switzerland. The sequence stratigraphic framework, initially defined for the Urgonian carbonate platform of the Vercors area (SE France), is confirmed in the Helvetic nappes, where the same number of sequences was observed. Many similarities between these two areas are put forward in this work. The sequence stratigraphic framework helped to highlight the installation of a bioclastic body, included in the Schrattenkalk Formation, since the middle Early Barremian (sequence B2). The age of the installation of the rudist-rich limestone, which corresponds to the Urgonian facies *sensu stricto*, is attributed to the late Barremian (maximum flooding surface of the sequence B3). This age coincides with the one determined in other northern Tethyan areas for the installation of the Urgonian platform.

The results of this study show a strong tectonic control of the platform architecture, with the presence of syn-sedimentary faults in a perpendicular position to the progradation direction of the platform. The presence of these faults was highlighted by the study of the evolution of the microfacies distribution and by thickness variations in different areas.

Sea level fluctuations also played an important role in the various life phases of the platform. Three major falls in sea level have been identified. A significant emersion of the proximal domain has been observed, involving an important drop of the relative sea level, leading to the exposure of the Drusberg Member hemipelagic series. A second major drop in sea level is identified near the Barremian-Aptian boundary, and a third is registered on the top of the Upper Schrattenkalk Member on the whole platform; it is associated with a karst affecting the underlying limestones to a depth of

over 20 meters. This observation sheds new light on the conditions linked to the demise of Urgonian platform, which was strongly influenced by this phase of emersion.

Résumé

Le Crétacé inférieur a vu le développement de grandes plateformes carbonatées dans les régions tropicales et subtropicales, favorisé par les conditions climatiques exceptionnellement chaudes, des conditions trophiques optimales et par un contexte paléogéographique et tectonique propice. Cette période est également caractérisée par le dépôt de nombreux niveaux enrichis en matière organique à l'échelle globale (OAE). Cette étude se concentre sur l'intervalle Barrémien–Aptien, au cours duquel la plateforme urgonienne s'est développée sur toute la marge passive nord téthysienne. Grace à l'orogenèse alpine, les nappes helvétiques mettent actuellement à l'affleurement des roches appartenant à cette plateforme urgonienne, localement nommées la formation du Schrattenkalk.

Cette étude vise à reconstituer l'évolution paléogéographique de la plateforme helvétique, ainsi qu'à définir les facteurs environnementaux et océanographiques qui ont influencé son développement. Plusieurs épisodes clefs dans le développement de cette plateforme ont été identifiés:

- l'installation de la plateforme, surmontant les sédiments hémiplégiques du membre du Drusberg,
- le changement momentané de type de production carbonatée durant l'Aptien basal, lors du dépôt du membre de Rawil,
- et finalement l'interruption définitive de la sédimentation carbonatée de plateforme photozoaires dans la région étudiée, durant l'Aptien inférieur.

Les observations sédimentologiques, biostratigraphiques et chimostratigraphiques ($\delta^{13}\text{C}$) ont permis le découpage séquentiel de onze coupes et d'un forage répartis sur l'ensemble des nappes helvétiques suisses. Le découpage séquentiel initialement défini pour la plateforme carbonatée urgonienne du Vercors est confirmé dans la plateforme helvétique, où le même nombre de séquences a été observé. De nombreuses similitudes entre ces deux plateformes ont été mises en avant dans ce travail. Le découpage séquentiel a permis de mettre en évidence l'installation de corps bioclastiques appartenant à la formation du Schrattenkalk dès le Barrémien inférieur moyen (séquence B2). L'âge de la mise en place des calcaires à rudistes, qui correspondent aux faciès urgoniens *sensu stricto*, reste cependant attribué au Barrémien supérieur (surface d'inondation maximale de la séquence B3). Cet âge est en accord avec celui déterminé dans les autres régions nord téthysiennes pour l'installation de la plateforme urgonienne.

Les résultats de cette étude montrent que l'organisation de la plateforme helvétique a été fortement influencée par la présence de failles syn-sédimentaires perpendiculaires à la direction de progradation de cette plateforme. La présence de ces failles a notamment été mise en évidence grâce à l'étude de l'évolution de la distribution des microfaciès, ainsi que par les variations d'épaisseurs des différents secteurs.

Les fluctuations du niveau marin ont également joué un rôle important dans les différentes

phases de vie de cette plateforme. Trois chutes majeures du niveau marin ont été identifiées. Une importante émersion du domaine interne a été mise en évidence, impliquant une chute relative du niveau marin mettant à nu des séries hémipélagiques appartenant au membre de Drusberg. Une seconde baisse majeure du niveau marin est présente à la limite Barrémien–Aptien, et une troisième est enregistrée au sommet du membre du Schrattenkalk supérieur sur l’ensemble de la plateforme ; elle est associée à un karst affectant sur plus de 20 mètres de profondeur les calcaires sous-jacents. Cette dernière observation apporte un éclairage nouveau sur les conditions liées à l’interruption finale de la plateforme urgonienne, qui serait fortement influencée par cette phase d’émersion.

Remerciements

Je tiens tout d'abord à remercier Karl Föllmi, l'instigateur de ce projet, grand connaisseur des sédiments crétacés et tertiaires des nappes helvétiques, sans qui je n'aurai jamais connu le Schrattenkalk. Je te remercie beaucoup de m'avoir aidé à mener à bien ce projet malgré les passages difficiles traversés pendant ces quatre ans. Merci de m'avoir permis d'apprendre autant, grâce aux nombreux congrès auquel tu m'as fait participer, aux camps de terrain de l'école doctorale ainsi qu'à l'excursion du Groupe Français du Crétacé en Oman.

Un très grand merci à Annie Arnaud-Vanneau pour ton enthousiasme et pour tout le temps et l'aide que tu as su m'apporter, tant devant le microscope tout au long de cette thèse que devant mon écran pour les derniers mois de rédaction.

Un très grand merci à Alexis Godet, pour ton aide si précieuse, tout au long de ce travail, d'abord en tant que post-doctorant, puis en tant que co-auteur et enfin en tant que membre du jury.

Merci aussi à Hubert Arnaud, pour toutes les discussions ainsi que pour votre aide dans l'interprétation du panorama des Churfirsten.

Je remercie également Thierry Adatte, pour l'intérêt que tu as porté à cette étude malgré ton anamour pour l'helvétique. Merci aussi pour les camps de terrain si enrichissants.

Merci à Jorge Spangenberg pour ton aide pour les isotopes stables.

Un très grand merci à Laurent Nicod, qui a accepté de m'enseigner les rudiments du métier de litho-lamelleur, merci encore pour tous ces bons moments. Pour leur aide au laboratoire, je remercie chaudement Tiffany Monnier et Cellia Trunz.

Mes remerciements vont également à Melody Stein, Stéphane Bodin et Quentin Ribaux pour m'avoir autorisé à utilisés leurs données et leurs échantillons pour les coupes de Tierwis/Säntis et de Brienz Rothorn, ainsi que pour les nombreuses et fructueuses conversations que nous avons partagé.

Merci également à Hans Peter Funk pour m'avoir fourni les photos aériennes du panorama des Churfirsten qui m'ont été d'une grande utilité.

Je remercie aussi Milena Pika de l'ETHZ pour m'avoir prêté les lames minces de Ueli Briegel et les échantillons de Lukas Wissler pour la coupe de Alvier.

Je remercie le Tiefbauamt du Canton de Schwyz ainsi que le bureau d'étude CSD ingénieurs SA de Kriens pour m'avoir fourni la carotte de Morschach, qui est stockée à l'Institut des Sciences de la Terre de l'Université de Lausanne.

Je remercie l'Université de Lausanne pour le support financier ainsi que la Société Académique Vaudoise pour m'avoir accordé un subside de recherche, afin de terminer plus sereinement.

Un immense merci à tous ceux qui sont venu braver les pentes herbeuses en portant des kilos de Schrattenkalk (Loïc, Alex, Chloé, Quentin, Miha, Brahim, Eric, Loraine, Laetitia, Arthur, Yoann, Antoine, Morgan, Caroline, Karl, mes parents, Audrey & Laurent, Nicolas).

Ces années lausannoises ont été synonyme pour moi de franches camaraderies et de profondes amitiés. Je remercie chaudement Anne-Marie, Krystel et Nadia, avec qui j'ai passé de merveilleux moments et qui ont été d'un très grand renfort, tant administratif que psychologique. Pour toutes ces sorties rocambolesques, je remercie Tonio, Remy, Bibi, Vivie, Clooney, Romain, Quentin et bien d'autres encore. Certaines soirées resteront inoubliables... Merci à mes collègues de bureau, si attentionnés malgré les (nombreuses) sautes d'humeur des derniers mois: Nicolas, Kathja et Cindy, ainsi que ceux du bureau d'à côté: Anne-Cécile, Evelyne et Eric. Je remercie aussi toute l'équipe des doctorants, post-doctorants, PAT et professeurs de l'institut, notamment Anders, Nathalie, Maria, Goran, Fabienne, Andres, Arthur, Mélina, Robert, Laurène, Pierre, David, Benita, Lukas, Jean-Luc (pour les discussions alpines et le Nutella), Melody, Fanny, Alicia et Iris. Un merci tout particulier à Anne-Marie et sa tribu qui m'ont souvent accueillis aux Rousses, et m'ont ainsi accordé des précieux moments de rigolade dans les derniers mois de rédaction.

Je tiens à remercier mes amis, Sarah, Yann, Armand, Clem, Myrtille, Suzy, Lyson, Jean, et toute l'équipe du Plan du loup, ainsi que les ex-claudebernardiens, Emilie, Etienne, Thomas, Charlotte, Elodie, Jocelyn, Sylvain, Myriam, Loïc et Ben, pour les moments de rires et de joie qui ont su me changer les idées tout au long de ces années.

Une pensée pour Mamie Paulette, Michel, Bruno, André et Mamie Raymonde qui n'ont pas eu le temps de voir l'achèvement de ce travail.

Enfin, un immense merci à ma famille, mes parents, ma sœur Audrey, mon beau-frère Laurent, leur petit Thomas, mon amour de Nicolas, pour m'avoir encouragé à commencer cette aventure, et soutenu pour que je puisse la finir.

Chapter 1 – General introduction

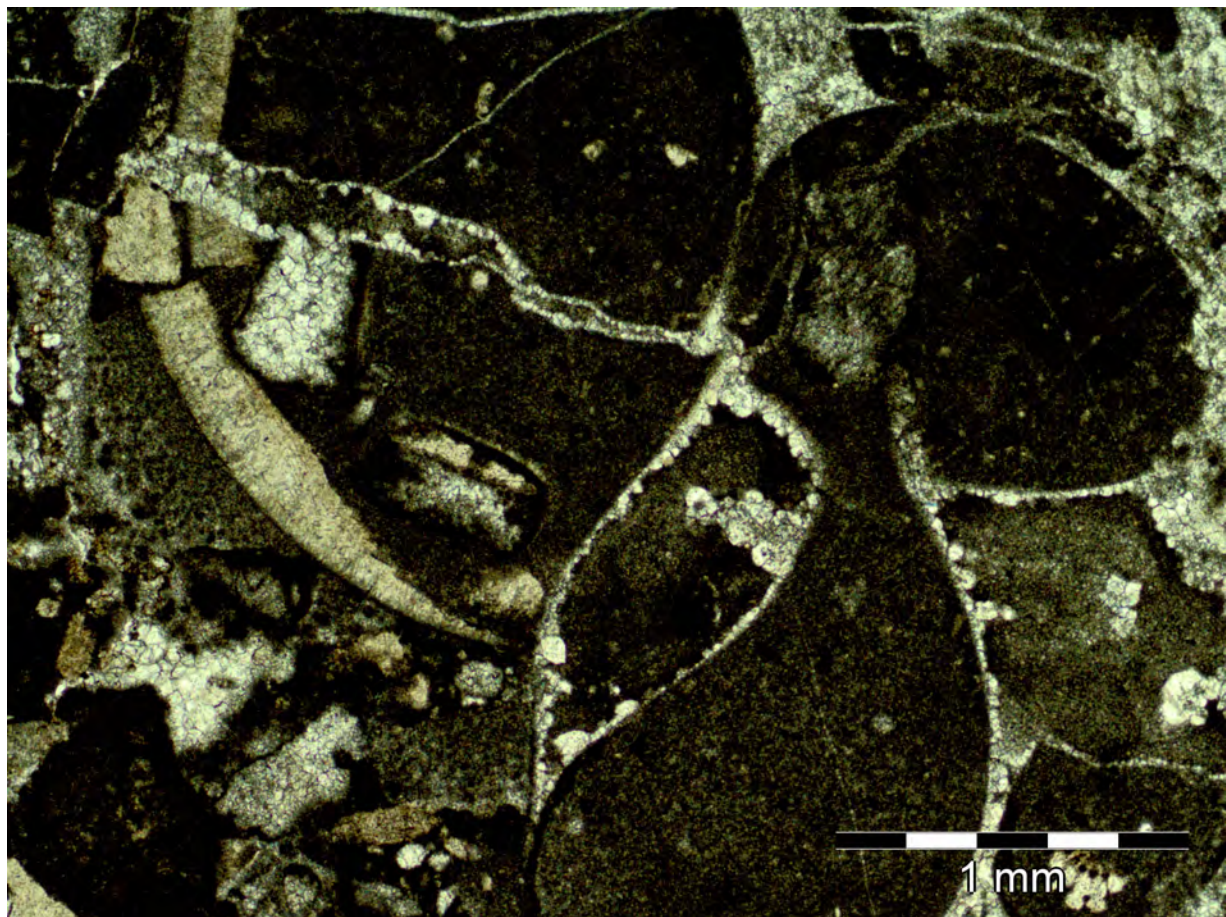


Fig. 1 Fractures filled by meteoritic cement (section of Harder, sample HA 401).

Chapter 1

General introduction

1.1 Foreword

Current tropical shallow-water carbonate factories are represented by coral reefs, such as those developed in the Bahamas, the Gulf of Mexico, the Great Barrier Reef of Australia and the Persian Gulf. These reefs are extremely important to the environment; although they occupy less than 1 % of the marine environment, they are home to more than one-quarter of marine wildlife species and represent one of the most biologically diversified ecosystems of the planet (McAllister, 1995 ; Doubilet, 1999). They also protect coastlines from storm and erosion. The health of a coral reef ecosystem depends on a complex, dynamic relationship between wildlife species and their environment. Specific conditions are needed for the development of this kind of ecosystem such as water temperature and water transparency or low trophic level (Hopley and Kinsey, 1988; Wilkinson and Buddemeier, 1994). These growth-limiting factors also controlled ancient carbonate platforms (Wilson, 1975). These specific environmental conditions render reefs and with them entire carbonate platforms extremely fragile and vulnerable to environmental change.

Since several decades, studies on present day carbonate platform highlight an important increase in their decline. According to Bryant et al. (1998), close to 60% of the world's coral reefs are already severely threatened by a number of human-induced stresses, including coastal de-

velopment, siltation triggered by deforestation, pollution by herbicide and fertilizer run-off, climate change and ocean acidification due to the anthropogenic increase in atmospheric CO₂ concentrations.

Emerging threats to coral reefs are bleaching and mortality associated with global warming. Elevated ocean temperatures are recognized as the primary cause of mass coral bleaching events (e.g. Hoegh-Guldberg, 1999; Hoegh-Guldberg et al., 2007). These events result from the loss of symbiotic algae - zooxanthellae, from coral tissues during times of stress (Glynn, 1993). Coral reefs are also threatened by the acidification of ocean (Orr et al., 2005), the intensification of tropical cyclones (Heron et al., 2008) and sea level rise (Field et al., 2011).

Because of their sensitivity to slight perturbations of their environment, the study of ancient carbonate platform ecosystems offers the possibility to understand the evolution of the paleoclimate and paleoenvironmental change during past time. The study of ancient ecosystems is also interesting to understand one of the most important parameters, which is time. The capacity of shallow-water carbonate systems to record environmental change is important, and their study allows to understand their capacity of recovery and adaptation through time.

This work deals with the study of a shallow-water carbonate platform, developed during the Early Cretaceous, which is today exposed in the Helvetic Alps.

1.2 The Cretaceous World

The Cretaceous Period is the last and the longest segment of the Mesozoic Era. It lasted approximately 79 million years, from the extinction event that closed the Jurassic period about 145 million years ago to the Cretaceous-Paleogene (K-T) extinction event dated at 66 million years ago (Cohen et al., 2013; updated).

1.2.1 Paleogeographic context

The evolution of Cretaceous paleogeography is linked to the break-up of the supercontinent Pangea, which started in the Early Jurassic by the formation of two distinct continents: Laurasia and Gondwana separated by an equatorial ocean (Tethys). The Central Atlantic Ocean, started to open during the Trias, extended eastwards to join the Tethys Ocean (Fig. 1.1). A hallmark of the Cretaceous period

is the presence of a narrow continuous equatorial seaway between Laurasia and Gondwana, which allowed ocean currents to flow between the two. However, several continental fragments and platforms constricted the western part of the Tethys (Stampfli and Borel, 2002; Stampfli et al., 2002), and offered a certain obstruction of this flow. Paleoceanographic currents were mostly oriented east-west (Pucéat et al., 2005). The Cretaceous is also characterized by the break-up of Gondwana leading to the opening of the South Atlantic Ocean, followed by its connection with the Central Atlantic. This break-up also gave rise to the Indian Ocean.

These phases of oceanisation are accompanied by strong magmatic activity (Hay, 2008), and by the development of large igneous provinces (LIPs) such as the Paraña–Etendeka in the Valanginian (cf. Martinez et al., 2015), Ontong–Java in the latest Barremian– early Aptian and Kerguelen in the late Albian (e.g. Neal et al., 1995).

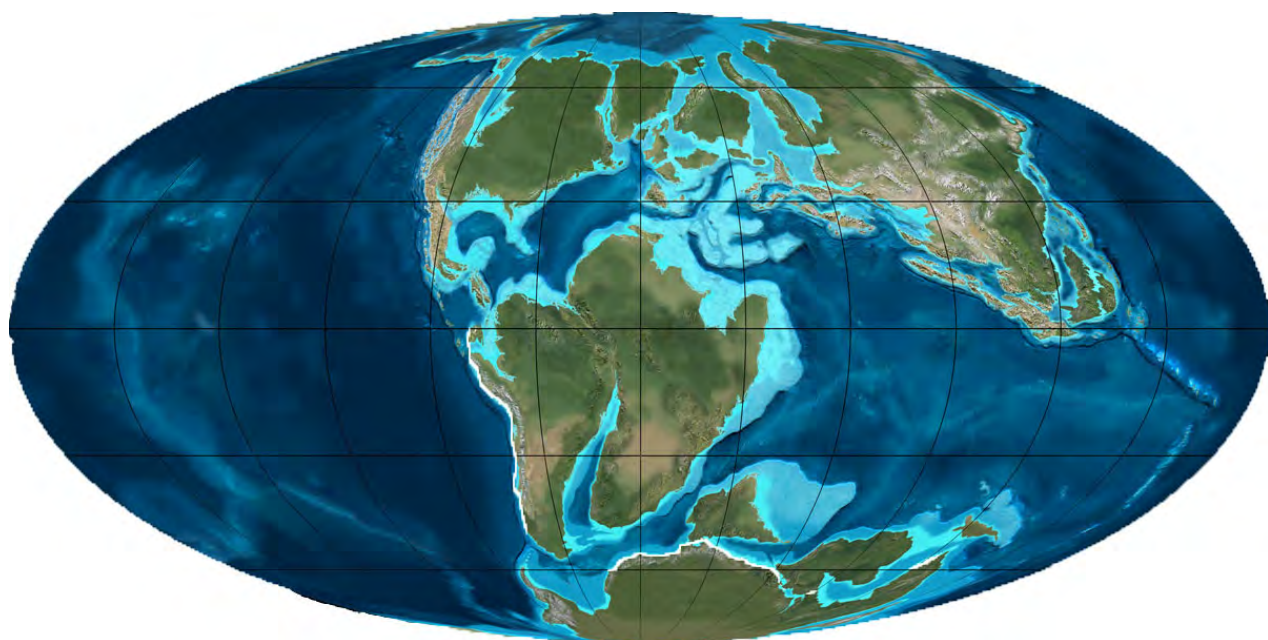


Fig. 1.1 Paleogeographic map for the Early Aptian (120 Ma). From Ron Blakey, Colorado Plateau Geosystems, Inc.; <http://cpgeosystems.com/paleomaps.html>

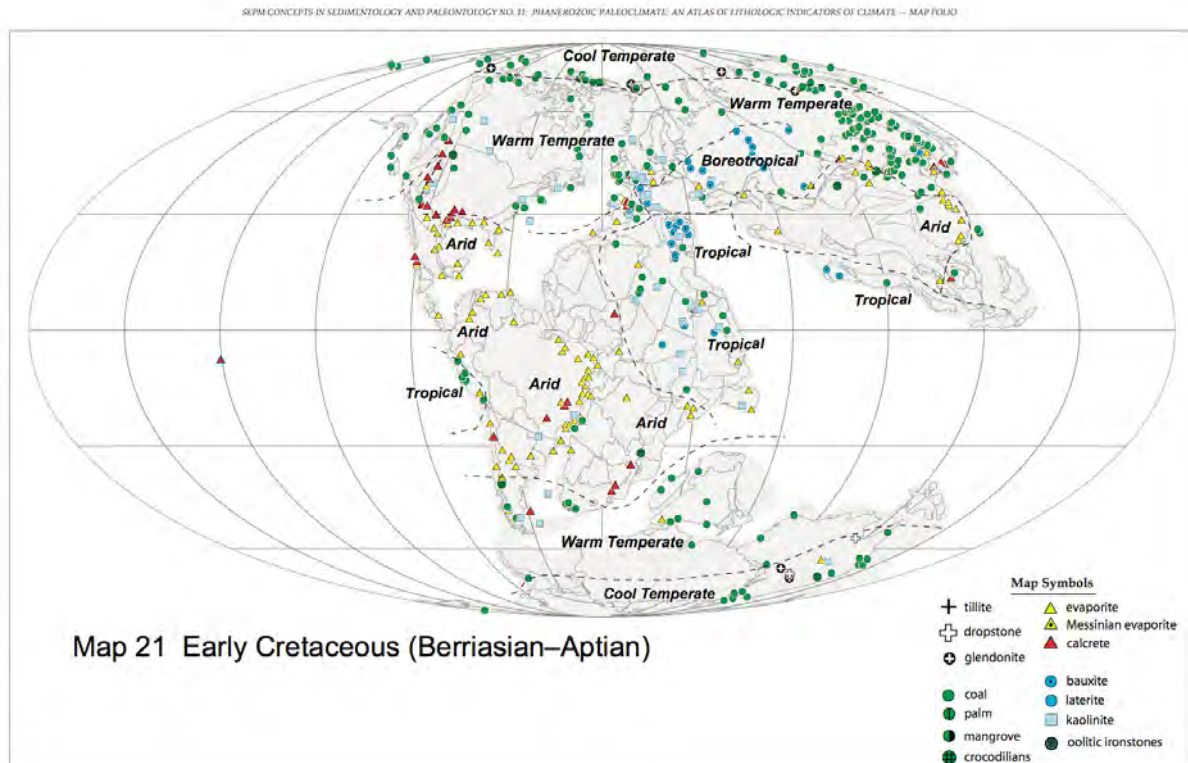


Fig. 1.2 Paleoclimate map for the Early Cretaceous (from Boucot et al., 2013).

1.2.2 Climatic conditions

It is generally admitted that the Cretaceous as a whole experienced extreme climatic warmth (e.g., Hallam, 1984; Francis and Frakes, 1993), with a low pole-to-equator temperature gradient (Chumakov et al., 1995). These conditions allowed tropical plants and animals to frequent the high paleolatitudes, as confirmed by the presence of crocodilian remains in Antarctica (Gasparini, 1980). The climatic belts of the Early Cretaceous are shown in Figure 1.2, with the main lithologic climate indicators (Boucot et al., 2013). It has been postulated since long time that ice caps were absent at the poles; nevertheless, this circumstance is presently widely debated (e.g., Kemper, 1987, Frakes and Francis, 1988; Frakes and Bolton, 1992; Price,

1999; Ahlberg et al., 2002; Jenkyns et al., 2004; Steuber et al., 2005). According to Hay (2008), if indeed polar ice would have occurred, it was only for short time intervals, and during most of the Cretaceous, the polar regions were ice free. However, sea-level fluctuations, deduced from the 3rd order sequences in Early Cretaceous, could imply glacio-eustacy (e.g., Immenhauser, 2005).

The warmer climate is explained by the high atmospheric pCO₂ rate, due to degassing linked to the installation of the LIPs (Berner et al., 2001; Royer, 2006). The pCO_{2atm} was between 2 and 6 times higher than the today's pre-industrial value (e.g., Barron and Washington, 1985; Berner, 1994; Veizer et al., 1999; Retallack, 2001; Heimhofer et al., 2004), and may have enhanced greenhouse conditions. Variations in the carbon

cycle and pCO_2 atm have triggered climatic perturbations during the Cretaceous time, which may ultimately have resulted in frequent oceanic anoxic events.

1.2.3 Oceanic Anoxic Events (OAEs)

The oceanic anoxic events (OAEs; Schlanger and Jenkyns, 1976; Jenkyns, 1980; Arthur et al., 1990) correspond to an interruption in normal pelagic sediment deposition by significant and widespread black-shale deposition under anoxic conditions. During the Cretaceous, these events were frequent, favoured by the specific paleoclimatic and paleoceanographic conditions (Wilson and Norris, 2001; Leckie et al., 2002). The most important Cretaceous events have been identified during the early Aptian (OAE 1a or Selli event, Erba et al., 1999), near the Aptian-Albian boundary (OAE 1b; e.g., Herrle et al., 2004), the late Albian (OAE 1c and OAE 1d; Arthur et al., 1990), the end Cenomanian (OAE 2) and the transition of the Coniacian to the Santonian (OAE 3; Arthur et al., 1990).

The mechanism responsible of these OAEs is assumed to be the release of volcanogenic CO_2 in the atmosphere (e.g., Weissert, 2000). Intensified greenhouse conditions inducing a more humid climate (Föllmi, 2012), intensifying continental rock weathering and erosion. This may have led to an increase in nutrient fluxes to the ocean, which enhanced primary productivity. The result is oceanic eutrophication, increasing the preservation of organic matter (Larson, 1991; Larson and Erba, 1999; Rullkötter, 2000; Mort, 2006) and the decrease or the disappearance of calcifying organisms associated with nutrient-enriched waters in both pelagic (nannoco-

nid crises, Erba, 2004) and neritic environments (Masse and Philip, 1981; Föllmi et al., 1994, 2007; Weissert et al., 1998).

1.2.4 Sea level fluctuations

According to Hardenbol et al. (1988), the Cretaceous period represents a first order transgressive phase, which resulted in the highest eustatic level of the entire Phanerozoic. During this time, sea level was in average more than 100 m higher than the currently one (Haq et al., 1987). The maximum in sea level occurred in the Late Cretaceous period (+250m during the Turonian; Haq, 2014). The rise of sea level is mainly due to the development of new oceans, inducing an increase in volume of mid-ocean ridges (Larson, 1991).

The relatively high sea level that prevailed during this period leads to the creation of many epicontinental seas and large shallow marginal marine areas (Haq et al., 1987; Ford and Golonka, 2003; Philip, 2003). The east-west orientation of the Tethys Ocean in the inter-tropical realm, and the multitude of shallow marine shelves during this time favoured the installation of carbonate platforms (Kiessling et al., 2003).

1.2.5 Cretaceous shallow-water carbonate platforms

The Cretaceous tropical belt hosted extensive shallow-water carbonate platforms, which have globally and episodically been interrupted in their growth (Skelton and Gili, 2012). These punctual crises are apparently linked to OAEs (e.g., Föllmi et al., 1994, 2006; Weissert et al., 1998). Despite these perturbations, the platforms

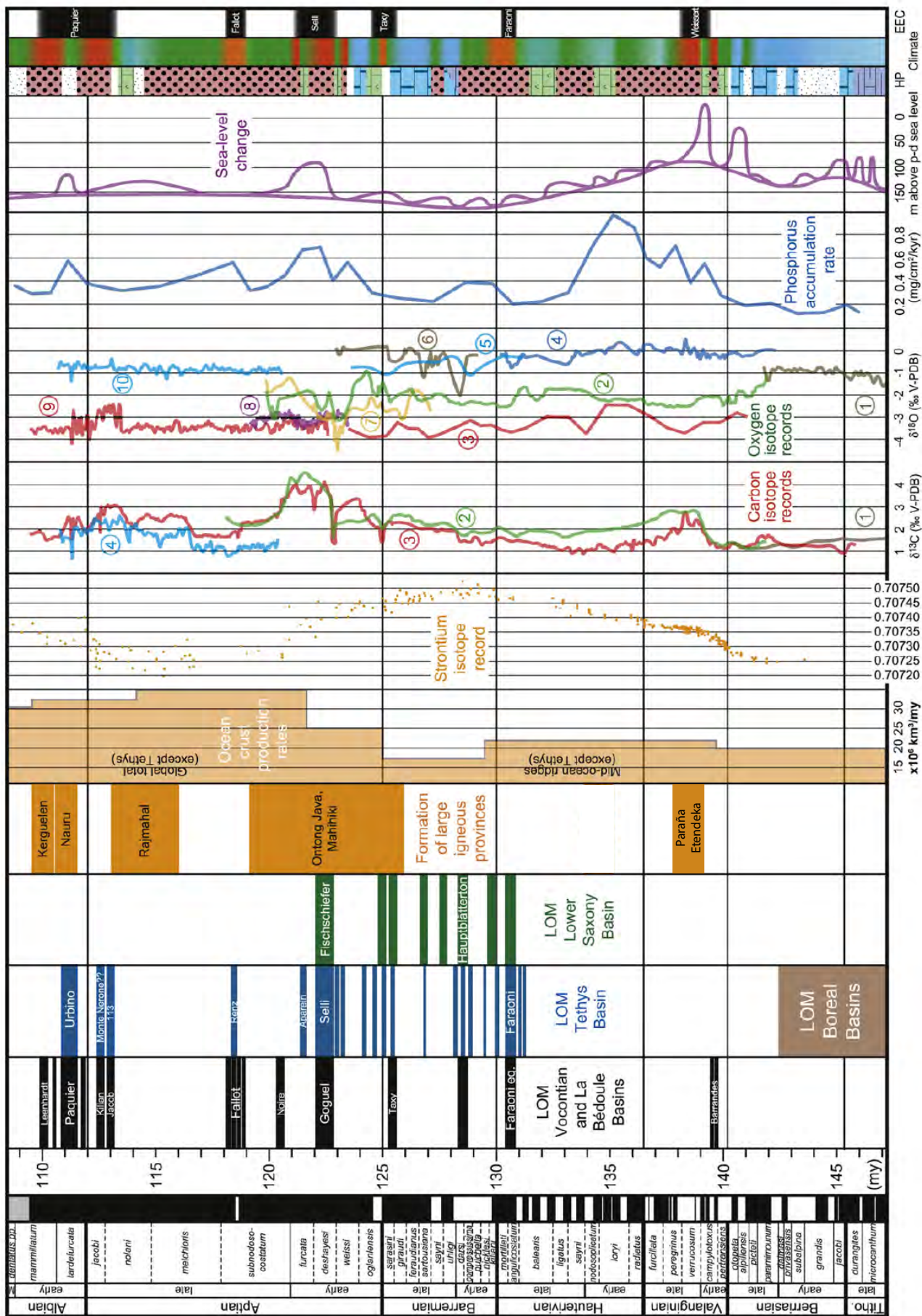


Fig. 1.3 Synthesis diagram showing the general evolution of paleoceanographic and paleoenvironmental conditions correlated with temporal trends in the Helvetic platform growth (From Föllmi 2012; modified after Martinez et al. 2015).

have had a prodigious capacity for rapid growth and expansion, thanks to the distinct benthic shelly biota that constituted their main carbonate factories. Contrary to modern tropical carbonate platforms, which carbonate factories are based on coral reefs and bioherms, the Cretaceous platforms were constituted by vast congregations of shelly organisms that spread across the whole platform. Various kinds of organisms were involved, such as bivalves, gastropods, green algae, calcareous sponges, benthic foraminifers, stromatoporoids and corals. The most abundant contributors were rudists, which are large-sized bivalves. These types of organisms are characteristic of photozoan assemblages, occurring in the photic zone, with oligotrophic conditions and normal oxygen and salinity levels. Slight variations of these environmental conditions can lead to a change in the biotic assemblage to a heterozoan one, characterized by abundance of suspension-filtering and feeding organisms such as crinoids, sponges and bryozoan (James, 1997; Föllmi et al., 1994; Mutti and Hallock, 2003).

1.3 The Helvetic Alps

1.3.1 Paleogeography of the Helvetic margin

The Helvetic Alps offer outcrops of the sedimentary record spanning the Late Paleozoic to Early Cenozoic, which represent the southern European margin. During most of the Mesozoic and the Early Cenozoic, these sediments were deposited along the northern Tethyan margin. Sediments of the latest Jurassic and Early Cretaceous represent the distal part of a shal-

low-water carbonate platform. The Helvetic platform experienced changes from photozoan to heterozoan assemblages several times during the Early Cretaceous (Fig. 1.3; Föllmi et al., 1994, 2007; Föllmi, 2012).

During the Early Cretaceous, the Helvetic realm was located approximately at subtropical paleolatitudes, at approximately 30°N (Fig. 1.4), on the northern margin of the Alpine Tethys. A shallow marine carbonate platform developed in a southward direction during the late Barremian and early Aptian. This platform was a part of a larger one, the Urgonian platform, including the Provencal, Gard, Ardèche, Vercors, Chartreuse, Bornes and Jura platforms (Arnaud-Vanneau et al., 1979; Arnaud-Vanneau and Arnaud, 1990; Arnaud and Arnaud-Vanneau, 1991; Arnaud et al., 1998), fringing the Hercynian basement of the Rhenish-Bohemian and Central Massifs. These massifs were covered by thick kaolinitic weathering mantles, and the reliefs of the paleolandscapes may had been significant, with probably high fault scarps which might have reached or exceeded 200m of elevation (Thiry et al., 2006). These massifs were separated by the Wealden gutter, in the Paris basin, a wide floodplain in which fluvio-deltaic sand and clays were deposited.

1.3.2 Nappes and Palinspastic reconstruction

The northern Alps in Switzerland are largely composed of late Paleozoic, Mesozoic and early Cenozoic sedimentary rocks, which belong to the former northern Tethyan margin. During the Alpine orogeny, the area was thrusted, over-thrusted and folded in a northward direction, forming the fold-and-thrust complex of the Hel-

thetic tectonic zone (Fig. 1.4A). It is divided in (1) the Helvetic nappes *sensu stricto* (Pfiffner, 1977; Trümpy, 1980) and (2) the underlying Infrahelvetic complex (Pfiffner, 1977). The first subunit comprises allochthonous sediments, consisting of large nappe systems and smaller slices, which were dislocated along a basal thrust fault over a distance of several tens of kilometres. The second subunit encompasses all units beneath the basal thrust of the Helvetic nappes. It consists of pre-Triassic crystalline basement rocks and their autochthonous and para-autochthonous sedimentary cover. It consists of intrinsically folded and partially thrusted sedimentary rocks.

Palinspastic reconstructions of the Helvetic area were proposed and discussed by Trümpy (1969), Ferrazzini & Schuler (1979), Funk (in Trümpy 1980), and Burkhard (1988). Recently, Kempf & Pfiffner (2004) proposed a palinspastic restoration of the Helvetic complex based on detailed cross sections, where infor-

mation on basement structures was provided by the interpretation of seismic lines of the Swiss NRP-20 project (Pfiffner et al., 1997, and papers therein). In the present contribution, the palinspastic reconstruction used is the one of Kempf & Pfiffner (2004; Fig. 1.4B), where only the relative position of the nappes is shown, in order to avoid the question of the relationship between the nappes and their roots in the crystalline massifs (especially for the Morcles nappe). The position between the nappes and their roots in the crystalline massifs (especially the Morcles nappe) is controversially treated by different authors. According to some authors (e.g. Ramsay, 1981, 1989; Dietrich & Casey, 1989; Pfiffner 1993), the nappe of Morcles is the cover of the entire Mont-Blanc massif, in contrast to other authors (e.g. Masson et al., 1980; Epard, 1990; Escher et al., 1993), who placed the core of this nappe only on the external part of the Mont-Blanc massif.

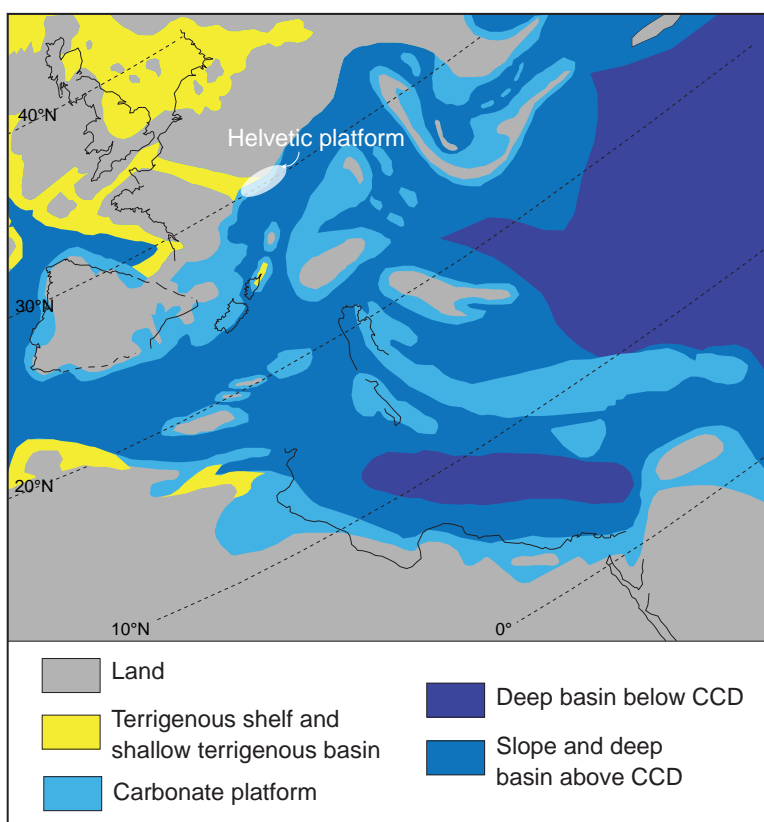
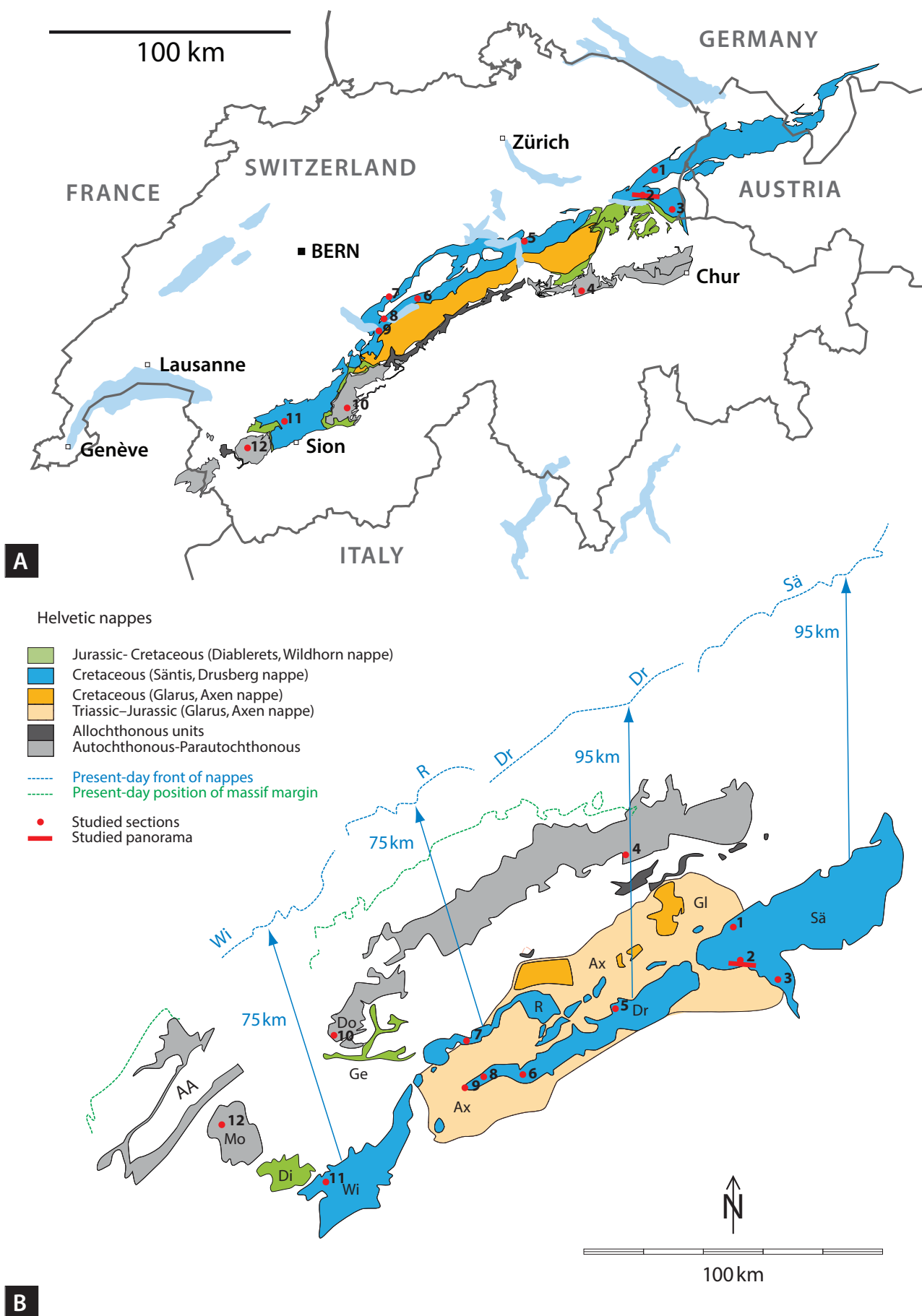


Fig. 1.4 Location of the Helvetic realm in a paleogeographic map of the western Tethys for the Aptian. (From Godet et al., 2013 ; redraw after Massé et al., 1993).



1.3.3 Intensity of the diagenesis of the Helvetic nappes

The folded and overthrusted Helvetic complex documents a low-grade metamorphism. The intensity of the metamorphism in the different nappes had been measured using the methods of illite crystallinity and vitrinite reflectivity by many authors (Frey et al. 1980; Breitschmid, 1982; Burkhard, 1988; Dietrich and Casey, 1989; Wang et al., 1996; Goy-Eggenberger, 1998; Burkhard and Goy-Eggenberger, 2001). These studies reveal an increase of the degree of metamorphism from tectonically higher to lower units, and from external to internal parts within the same tectonic unit.

The sections located in the nappes of Säntis (Tierwis, Valsloch and Alvier sections), Wildhorn (Rawil section) and Drusberg (Interlaken, Harder, Brienz Rothorn sections and Morschach core) and in the Border chain (Justistal section) record deep diagenetic conditions (temperatures $<200^{\circ}\text{C}$; Frey et al. 1980 and Burkhard and Goy-Eggenberger, 2001). Anchizone conditions (temperatures between 200 and 300°C ; Schmid, 1982; Groshong, 1988; Burkhard, 1990 and Burkhard and Goy-Eggenberger, 2001) are reached in the nappe of Morcles (L'Ecuelle section), while anchi- to epimetamorphism conditions (temperatures $>300^{\circ}\text{C}$; Frey et al. 1980 and Burkhard and Goy-Eggenberger, 2001) are found in the nappe of Doldenhorn (Lämmerenplatten section) and in the autoch-

thonous/para-autochthonous sedimentary cover of the Aar massif (Kistenpass section).

These different intensities of the diagenesis/low-grade metamorphism have modified the isotopic composition of the studied sections in function of the type of sediment (limestone vs. marls) by the circulation of fluids. This factor should be taken in consideration during the interpretation of the isotopic analyses.

1.3.4 Stratigraphy of the late Hauterivian – early Aptian rocks in the Helvetic realm

1.3.4.1 Lithostratigraphy and ages

The stratigraphy of the Helvetic Alps has been detailed by several authors (e.g. Funk et al., 1993; Föllmi et al., 2007). The main points are summarized here (Fig 1.6), based on the definitions provided in the Lithostratigraphic Lexicon of Switzerland (<http://www.strati.ch>).

1.3.4.1.1 Tierwis Formation

The Tierwis Fm has been defined by Föllmi et al. (2007), and was previously called “Drusberg Fm”. This formation includes the Alt-mann Mb, the Drusberg Mb and the Chopf Bed.

Fig. 1.5 A: Tectonic map of the Helvetic nappes, redrawn after the tectonical map of Switzerland 1: 500,000 (Swiss Federal Office of Topography – Swisstopo, Berne). B: Palinspastic reconstruction of the Helvetic nappes (redrawn after Kempf and Pfiffner, 2004). The same colours are used for the nappes on both figures. Studied sections: (1) Tierwis, (2) Valsloch, (3) Alvier, (4) Kistenpass, (5) Morschach, (6) Brienz Rothorn, (7) Justistal, (8) Harder, (9) Interlaken, (10) Lämmerenplatten, (11) Rawil and (12) L'Ecuelle.

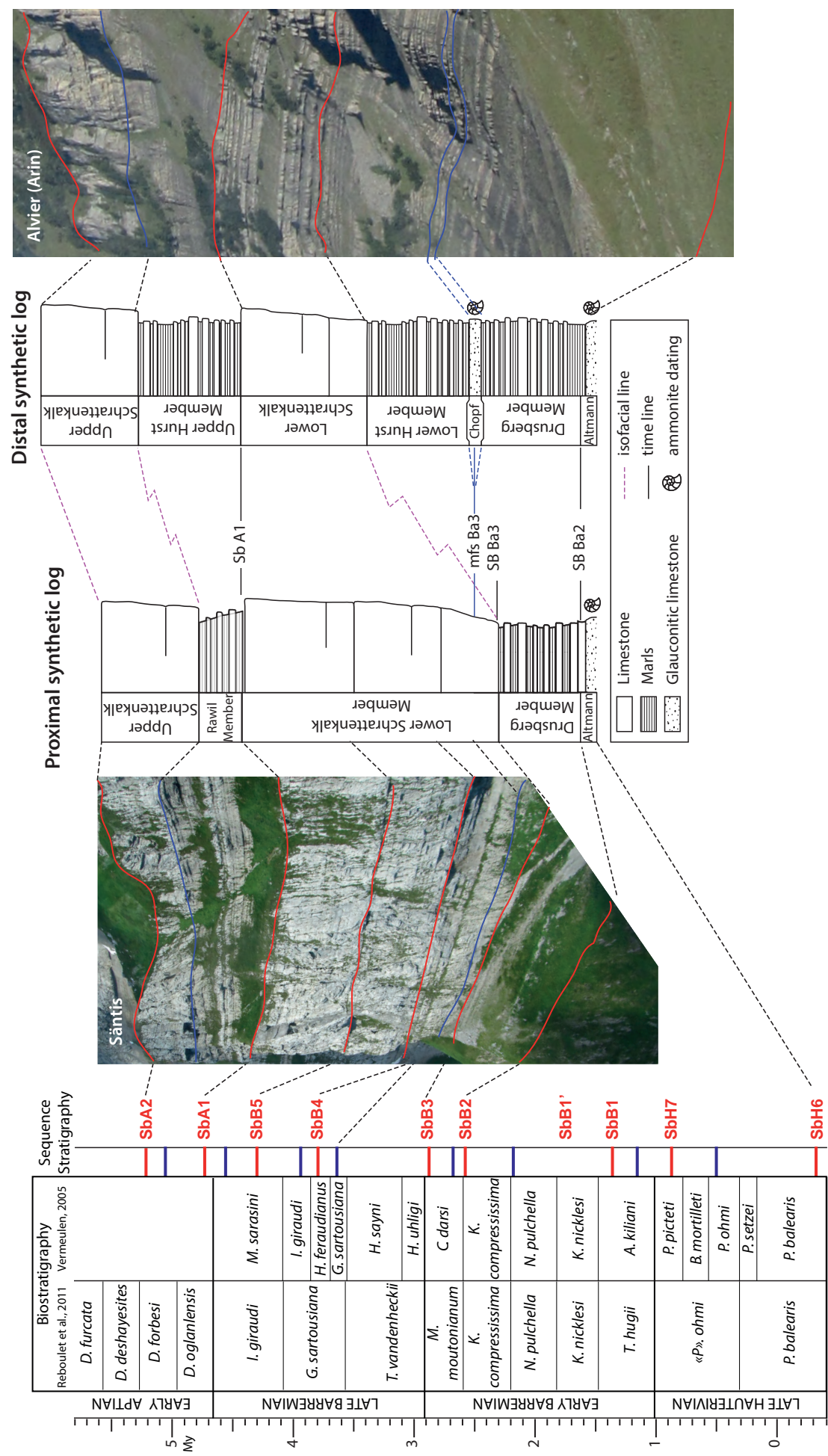


Fig. 1.6 Synthetic representation of the evolution of the lithostratigraphic units on a proximal to distal transect, and their relation with the sequence stratigraphic scheme (biostratigraphy from Reboulet et al., 2011 and Vermeulen, 2005; sequence stratigraphy adapted from Arnaud et al., 1998; synthetic logs modified after Bodin et al., 2006b).

The Altmann Member

The Altmann Member (Mb) has been described for the first time by Escher in Kaufmann (1867), in the locality type of Altmannsattel (canton of Saint Gallen). The paratype section is located in Tierwis (canton of Saint Gallen). This member consists of a thin and highly condensed (0 to 30m thick) unit rich in glauconite and phosphate nodules (Fichter 1934, Funk 1969, 1971; Wyssling 1986; Bodin 2006; Bodin et al., 2006a; Föllmi et al., 2007, Godet et al., 2013; Godet, 2013). In the most expanded sections (Säntis and Fluhbrig regions), it consists of a marly, crinoid-rich, limestone (Oberholzer, 1933; Rick, 1985; Bodin et al., 2006a). This unit covers the Hauterivian Kieselkalk Fm. Ammonites are common in this series and constrain the age of this member to the late Hauterivian *balnearis* zone and the late early Barremian *darsi* zone (Bodin et al., 2006a). In this study we consider that this member ends with the disappearance of limestone or sandstone beds, which is followed by the first occurrence of marls of the Drusberg Mb.

The Drusberg Member

The Drusberg Mb has been defined by Mayer-Eymar in 1867. Its distribution spans the Switzerland, and the Vorarlberg and Allgäu regions. This member starts with the first marl beds above the Altmann Mb, or directly above the Kieselkalk Fm, for example in the region of the Thun Lake (Ziegler, 1967). It consists of hemipelagic marly limestone–marl alternations. In proximal settings, oysters and irregular echinoids are frequent and form coquina levels (Oberholzer, 1933). The lower part of this

member is deposited on the whole Helvetic shelf but its end is diachronous. In the early Late Barremian, in the inner areas, this unit was overlain by shallow-water platform carbonate (Schrattenkalk Fm). In the outer-shelf realm, this member encompasses an up to 350m-thick succession and represents the distal equivalent of the Schrattenkalk Fm (Heim and Baumberger, 1933; Briegel, 1972; Bollinger, 1988). In the region of Alvier, Briegel (1972) splits this member into (1) “Drusberg beds” (Drusbergschichten), (2) “Chopf Beds”, (3) “Lower Hurst beds”, (Untere Hurstmergel) (4) Lower Schrattenkalk Mb, (5) “Upper Hurst Beds” (Obere Hurstmergel) which represents the distal equivalent of the Rawil Mb (see below) (6) Upper Schrattenkalk Mb. This complex nomenclature is now outdated. In distal areas, the Drusberg Mb is dated from the latest early Barremian *darsi* zone to the early Aptian *weissi* zone. This minimal age is obtained by ammonite stratigraphy of the overlying Grünten Mb (Garschella Fm; Linder et al., 2006).

The Chopf Bed

The Chopf Bed is a phosphate- and glauconite-rich condensed unit, formally described by Briegel (1972) in the region of Alvier (canton of St. Gallen). It has been also identified in Vorarlberg (Heim and Baumberger, 1933; Bollinger, 1988), in eastern Switzerland (Heim, 1910-1916; Oberholzer, 1933; Liennert, 1965, Briegel, 1972; Wissler et al., 2003, Bodin et al., 2006b) and in central Switzerland (Fichter, 1934; Staeger, 1944). In the section of Alvier it represents a 4m-thick bedded succession, dated by ammonite as the *sartousiana* zone, middle late Barremian (Briegel, 1972; Bodin et al., 2006b).

1.3.4.1.2 Schrattenkalk Fm

The Schrattenkalk Fm consists of massive light grey limestone rich in rudists. Studer first described this unit in 1834. The name is derived from the Swiss-German “Schratten” (a synonym of Karren) meaning clints or lapiés, a phenomena that frequently affects the Urgonian limestone. It is the spectacular lapiás of Schrattenfluh (canton of Lucerne) that gave its name to the Schrattenkalk Formation. In the French-speaking part of Switzerland, this unit was named Urgonian limestone (e.g., Lugeon, 1914). It is divided into 3 members: the Lower and the Upper Schrattenkalk Mbs and the Rawil Mb.

The Lower Schrattenkalk Mb

This member is characterized by light-coloured, thickly-bedded and massive limestone, overlying the hemipelagic marl-limestone alternations of the Drusberg Mb. This member reaches a maximal thickness of 100 m, and is mainly composed of oolites, bioclasts, rudist, stromatoporoid, chaetetidae, coral and gastropod remains. According to Bodin et al. (2006b), the age of the base of this member is diachronous, and is attributed to the middle Late Barremian *sartousiana* zone in proximal part of the platform. This diachrony is explained by the progradational character of this unit (Föllmi et al., 2006).

The Rawil Mb

This member was formerly named the “lower Orbitolina Beds”, and has been first

defined by Kaufmann (1867) as a sand-rich, dark-greyish to brownish limestone, which interrupts the Urgonian-type succession (i.e., Lower and Upper Schrattenkalk Mb). The name of Rawil for this unit (Schenk, 1992; Föllmi et al., 2007) comes from the region of the Rawil Pass (Canton of Bern). Stein et al. (2012) proposed a formal definition for this member. These authors constrain the Rawil Mb between the first and the last occurrence of marly or sandy, dark-colored well-bedded beds, which may contain one or several orbitolinid-rich beds. This member is not always well expressed, and can be calcareous in certain parts of the Helvetic Alps (i.e., in the western Austrian Helvetic nappes; Bollinger, 1988). It is dated as earliest Aptian, according to orbitolinid biostratigraphy (Bollinger, 1988; Schenk, 1992, Arnaud et al., 1998; Embry, 2005; Stein et al., 2012), and correlate with the Lower Orbitolina Beds in the Vercors platform (Arnaud-Vanneau, 1980).

Upper Schrattenkalk Mb

The Upper Schrattenkalk Mb is characterized by the reappearance of thickly-bedded massive limestone, of a maximal thickness of 100m. In terms of lithology and facies, this member is very similar to the Lower Schrattenkalk Mb, even though patch reefs have been more frequently described from this member in previous studies (e.g., Heim, 1910-1916; Oberholzer, 1933; Fichter, 1934; Lienert, 1965; Bollinger, 1988; Schenk, 1992). These patch reefs are composed by corals, rudists and stromatoporoids, separating the inner lagoonal environment from the distal platform margin (Bollinger, 1988; Linder et al., 2006). Ammonites coming from the overlying Garschella Fm give a minimum age for the Upper Schrattenkalk near the

boundary of the *weissi* and the *deshayesi* zones (Linder et al., 2006).

1.3.4.2 Sequence stratigraphy

In this study, the stratigraphy is based on the sequence stratigraphic concepts proposed in 1977 by Vail et al. of the EXXON Company, and subsequently described in numerous publications (e.g., Van Wagoner et al., 1988; Emery and Myers, 1996; Coe et al., 2003; Catuneanu et al., 2009). This model was originally based on the interpretation of seismic profiles. It is based on the recognition of the spatial organization of depositional sequences and their key surfaces, commonly generated by changing relative sea level. A depositional sequence starts by a remarkable erosive surface due to a drop in sea level, the sequence boundary (SB). The first deposits are found in distal parts and represent the lowstand systems tract (LST). The low rate of creation of accommodation space compared to the sedimentation rate generates a progradation of shallow-water facies toward the basin followed by a period of aggradation. The progressive rise of sea level is indicated by the transgressive surface (TS). The transgression is accompanied by backstepping of shallow-water facies, and the onlap of the sediments above the SB in a landward direction, forming the transgressive systems tract (TST). When the rate of sea level rise reaches its maximum, the sediments accumulated on the platform show the most external facies, on a surface or in a thin zone, which is known as the maximum flooding surface (mfs). The subsequent drop in sea level is accompanied by the progradation of shallow-water facies toward the basin, embodied by the highstand systems tract (HST), which is limited to its top by the SB of the overlying

depositional sequence.

The sequence stratigraphic framework used in this work is based on the one developed in the Vercors region of SE France by Arnaud and Arnaud Vanneau (1989, 1991), Arnaud-Vanneau and Arnaud (1990), Hunt and Tucker (1993) and Arnaud (2005). The sequence-stratigraphic model is chronostratigraphically calibrated in the Angles section of the Vocontian Trough, where the presence of ammonites allows for biostratigraphic time control. The same sequence-stratigraphic approach was applied in previous studies in the Helvetic Alps (Embry, 2005; Bodin et al., 2006a, 2006b; Stein et al., 2012). Figure 1.6 presents the sequential interpretation of the Barremian–Aptian series by these authors, and its relationships to the lithostratigraphic units. Bodin et al. (2006a) distinguished three sequences within the Almann Mb (Ha 6, Ha7 and Ba1). According to Bodin et al. (2006b), the onset of the Schrattenkalk Fm in proximal areas, and its distal equivalent Chopf Bed has been attributed to the mfs B3. The Lower Schrattenkalk Mb–Rawil Mb boundary represents the SB A1 (Embry, 2005, Stein et al., 2012), the upper part of the Rawil Mb is attributed to the mfs A1 by these authors, and the Upper Schrattenkalk Mb ends with the SB A2 (Linder et al., 2006; Stein et al., 2012).

1.4 Aims and organization of the thesis

The aim of this PhD thesis is to obtain a better understanding of the evolution of the Helvetic platform during the Barremian–early Aptian interval, by the reconstruction of its architecture and ecological distribution. We also intend to identify and prioritize the environ-

mental and oceanographic factors influencing the development of the Helvetic platform, by the study of the evolution of paleoecosystems, the paleotopography and paleogeography. Furthermore, this platform is placed into a larger context, by the comparison of its evolution with other well-studied platforms (e.g., Bas-Dauphiné platform, Jura platform).

Several key episodes in the life of this platform are examined to reach the aims of this thesis. The first point is the installation of the platform, covering hemipelagic sediments of the Drusberg Member, near the limit between the early and late Barremian. The second important episode is the temporary change in the type of carbonate production during the basal Aptian, with the deposition of the Rawil Member. And the final point is the definitive interruption of photozoan carbonate platform sedimentation in the study area, during the early Aptian. To understand the paleoenvironmental context associated with these episodes, the thesis is presented in five chapters:

Chapter 1 is this general introduction.

In chapter 2, the understanding of the timing and dynamics of the installation of the shallow-water platform in the Helvetic nappes is achieved, using an integrated sequence stratigraphic approach, by using microfacies, biostratigraphy data and the interpretation of a panorama.

Chapter 3 focuses on the Aptian period in the evolution of this platform, with the detailed study of six selected key sections, for which the microfacies succession, the isotopic record and the phosphorus content are examined. Similarities of the evolution of depositional environments with other sections of the NW Tethyan Platform (SE France) are discussed.

Chapter 4 aims at establishing the evolution of the Helvetic realm, from the latest Haute-

ravian to the early Aptian, in order to understand the architecture of the shelf. The distribution of microfacies is examined, and compared with carbon isotope and phosphorus records.

Chapter 5 presents the general conclusions of this PhD project, and the perspectives.

The annexes contain an affiliated paper, *Deciphering the message of Early Cretaceous drowning surfaces from the Helvetic Alps: What can be learnt from platform to basin correlations?* published in *Sedimentology* by Godet et al. (2013); the data of the analyses of stable isotopes, phosphorus contents, XRD bulk rock mineralogy, the interpretation of the Churfirsten panorama, and the microfacies interpretations.

1.5 References

- Ahlberg, A., Herman, A. B., Raikevich, M., Rees, A. and Spicer, R. A. (2002) Enigmatic Late Cretaceous high palaeo-latitude limestones in Chukotka, northeasternmost Asia. *GFF (Geologiska Föeningens i Stockholm Förhandlingar)*, **124**, 197-199.
- Arnaud, H. (2005) Sequence stratigraphy interpretation. In: *The Hauterivian-Lower Aptian sequence stratigraphy from Jura Platform to Vocontian Basin: A multidisciplinary approach* (Eds T. Adatte, A. Arnaud-Vanneau, H. Arnaud, M.-C. Blanc-Alétrou, S. Bodin, E. Carrio-Schaffhauser, K.B. Föllmi, A. Godet, M.C. Raddadi and J. Vermeulen), *Géologie Alpine, Série Spéciale «Colloques et Excursions» N°7*, pp. 174-179.
- Arnaud, H. and Arnaud Vanneau, A. (1989) Séquence de dépôt et variations du niveau de la mer au Barrémien et à l'Aptien inférieur dans les massifs subalpins septentrionaux et le Jura (Sud-Est de la France). *Bulletin de la*

- Société Géologique de France*, **V**, 651-660.
- Arnaud, H. and Arnaud-Vanneau, A.** (1991) Les calcaires urgoniens des Massifs subalpins septentrionaux et du Jura (France): âge et discussion des données stratigraphiques. *Géologie Alpine*, **67**, 63-79.
- Arnaud, H., Arnaud-Vanneau, A., Blanc-Alétrou, M.-C., Adatte, T., Argot, M., Delanoy, G., Thieuloy, J.-P., Vermeulen, J., Virgogne, A., Virlouvet, B. and Wermeille, S.** (1998) Répartition stratigraphique des orbitolinidés de la plate-forme urgonienne subalpine et jurassienne (SE de la France) *Géologie Alpine*, **74**, 87.
- Arnaud, H., Arnaud-Vanneau, A., Bulot, L.G., Beck, C., MacSotay, O., Stephan, J.-F. and Vivas, V.** (2000) Le Crétacé inférieur du Venezuela oriental : stratigraphie séquentielle des carbonates sur la transversale Casanay-Maturin (Etats de Anzoátegui, Monagas et Sucre). *Géologie Alpine*, **76**, 3-81.
- Arnaud-Vanneau, A.** (1980) Micropaléontologie, paléoécologie et sédimentologie d'une plate-forme carbonatée de la marge passive de la Téthys : l'Urgonien du Vercors septentrional et de la Chartreuse (Alpes occidentales). *Géologie Alpine, Grenoble Mém HS* **11**, 874 pp.
- Arnaud-Vanneau, A., Arnaud, H., Thieuloy, J.P.** (1976) Bases nouvelles pour la stratigraphie des calcaires urgoniens du Vercors. *Newsletter on Stratigraphy* **5**, 143-159.
- Arnaud-Vanneau, A., Arnaud, H., Charollais, J., Conrad, M.-A., Cotillon, P., Ferry, S., Masse, J.-P. and Peybernès, B.** (1979) Paléogéographie des calcaires urgoniens du sud de la France. *Geobios*, **12, Supplement 1**, 363-383.
- Arnaud-Vanneau, A. and Arnaud, H.** (1990) Hauterivian to Lower Aptian carbonate shelf sedimentation and sequence stratigraphy in the Jura and northern Subalpine chains (southeastern France and Swiss Jura). In: *Carbonate Platforms: Facies, Sequences and Evolution* (Eds M.E. Tucker, J.L. Wilson, P.D. Crevello, J.R. Sarg and J.F. Read), **9**, pp. 203-233. Blackwell Scientific Publications, Special Publication of the International Association of Sedimentologists.
- Arnaud-Vanneau, A. and Arnaud, H.** (2005) Carbonate facies and microfacies of the Lower Cretaceous carbonate platforms. In: *The Hauterivian-Lower Aptian sequence stratigraphy from Jura Platform to Vocontian Basin: A multidisciplinary approach* (Eds T. Adatte, A. Arnaud-Vanneau, H. Arnaud, M.-C. Blanc-Alétrou, S. Bodin, E. Carrio-Schafhauser, K.B. Föllmi, A. Godet, M.C. Raddadi and J. Vermeulen), *Géologie Alpine, Série Spéciale «Colloques et Excursions» N°7*, 39-68.
- Arthur, M.A., Jenkyns, H.C., Brumsack, H.-J. and Schlanger, S.O.** (1990) Stratigraphy, geochemistry, and paleoceanography of organic carbon-rich Cretaceous sequences. In: *Cretaceous resources, events, and rhythms* (Eds R.N. Ginsburg and B. Beaudoin), pp. 75-119. Kluwer, Dordrecht, Holland.
- Barron, E.J. and Washington, W.M.** (1985) Warm Cretaceous climates: High atmospheric CO₂ as a plausible mechanism. In: *The carbon cycle and atmospheric CO₂: Natural variations Archean to present* (Eds E.T. Sundquist and W.S. Broecker), **32**, pp. 546-553. Geophysical monograph, Washington, American Geophysical Union.
- Berner, R.A.** (1994) GEOCARB II: a revised model of atmospheric CO₂ over Phanerozoic time. *American Journal of Science*, **294**, 56-91.
- Bodin, S., Godet, A., Vermeulen, J., Linder, P. and Föllmi, K.B.** (2006a) Biostratigraphy,

- sedimentology and sequence stratigraphy of the latest Hauterivian – Early Barremian drowning episode of the Northern Tethyan margin (Altmann Member, Helvetic nappes, Switzerland) *Eclogae geologicae Helvetiae*, **99**, 157-174.
- Bodin, S., Vermeulen, J., Godet, A. and Föllmi, K.B.** (2006b) New data on the age of the installation of Urgonian-type carbonates along the northern Tethyan margin: biostratigraphy of the Chopf Member (Helvetic Alps, eastern Switzerland). *Comptes Rendus Geoscience*, **338**, 7.
- Bollinger, D.** (1988) *Die Entwicklung des distalen osthelvetischen schelfs im Barremian und Früh-Aptian. Drusberg-, Mittagspitz- und Schrattenkalk-Fm. im Vorarlberg und Allgäu.*, Universität Zürich, Zürich, 159 pp.
- Boucot, A.J., Xu, C., Scotese C.R.** (2013) Phanerozoic Paleoclimate: An Atlas of Lithologic Indicators of Climate. **11**.
- Burkhard, M.** (1988) L'Helvétique de la bordure occidentale du massif de l'Aar (évolution tectonique et métamorphique). *Eclogae Geologicae Helvetiae*, **81**, 63-114.
- Burkhard, M. and Goy-Eggenberger, D.** (2001) Near vertical iso-illite-crystallinity surfaces cross-cut the recumbent fold structure of the Morcles nappe, Swiss Alps. *Clay Minerals*, **36**, 159-170.
- Breitschmid, A.** (1982) Diagenese und schwache Metamorphose in den sedimentären Abfolgen der Zentralschweizer Alpen (Vierwaldstätter See, Uriotstock). *Eclogae geol. Helv.*, **75**, 331-380.
- Briegel, U.** (1972) Geologie der östlichen Alviergruppe (Helvetische Decken der Ostschweiz) unter besonderer Berücksichtigung der Drusberg- und Schrattenkalkformation (Unterkreide). *Eclogae geol. Helv.*, **65**, 425-483.
- Bryant, D., Burke, L., McManus, J.W. and Spalding, M.** (1998) *Reefs at Risk: A Map-Based Indicator of Potential Threats to the World's Coral Reefs*, Washington D.C., 60 pp.
- Catuneanu, O., Abreu, V., Bhattacharya, J.P., Blum, M.D., Dalrymple, R.W., Eriksson, P.G., Fielding, C.R., Fisher, W.L., Galloway, W.E., Gibling, M.R., Giles, K.A., Holbrook, J.M., Jordan, R., Kendall, C.G.S.C., Macurda, B., Martinsen, O.J., Miall, A.D., Neal, J.E., Nummedal, D., Pomar, L., Posamentier, H.W., Pratt, B.R., Sarg, J.F., Shanley, K.W., Steel, R.J., Strasser, A., Tucker, M.E. and Winker, C.** (2009) Towards the standardization of sequence stratigraphy. *Earth-Science Reviews*, **92**, 1-33.
- Chumakov, N.M., Zharkov, M.A., Herman, A.B., Doludenko, M.P., Kalandadze, N.N., Ponomarenko, A.G., Rautian, A.S.** (1995) Climatic zones in the middle of the Cretaceous Period. Stratigraphy and Geological Correlation, **3**, 3-14.
- Coe, A.L., Bosence, D.W.J., Church, K.D., Flint, S.S., Howell, J.A. and Wilson, R.C.L.** (2003) *The Sedimentary Record of Sea-Level Change*. Cambridge University Press.
- Cohen, K.M., Finney, S.C., Gibbard, P.L. & Fan, J.-X.** (2013; updated) The ICS International Chronostratigraphic Chart. *Episodes*, **36**, 199-204.
- Dietrich, D. and Casey, M.** (1989) A new tectonic model for the Helvetic nappes. *Geological Society, London, Special Publications*, **45**, 47-63.
- Doubilet, David.** (1999) Coral Eden. *National Geographic*, January 1999, 2-29.
- Escher, A., Masson, H. and Steck, A.** (1993) Nappe geometry in the Western Swiss Alps. *Journal of Structural Geology*, **15**.

- Emery, D. and Myers, K.** (1996) *Sequence Stratigraphy*. Blackwell Sciences.
- Embry, J.-C.** (2005) *Paléoécologie et architecture stratigraphique en haute résolution des plates-formes carbonatées du Barrémien–Aptian de la Néo-Téthys (Espagne, Suisse, Provence, Vercors) – impact respectif des différents facteurs de contrôle.*, MNHN-Paris/ IFP, 303 pp.
- Epard, J.L.** (1990) La nappe de Morcles au sud-ouest du Mont-Blanc. Université de Lausanne, *Mémoires de Géologie (Lausanne)*, **8**, 165 pp.
- Erba, E.** (2004) Calcareous nannofossils and Mesozoic oceanic anoxic events. *Marine Micropaleontology*, **52**, 85-106.
- Erba, E., Channell, J.E.T., Claps, M., Jones, C.E., Larson, R.L., Opdyke, B., Premoli-Silva, I., Riva, A., Salvini, G. and Torriceli, S.** (1999) Integrated stratigraphy of the Cismon APTICORE (Southern Alps, Italy): A «reference section» for the Barremian-Aptian interval at low latitudes. *Journal of Foraminiferal Research*, **29**, 371-391.
- Ferrazzini, B. and Schüler, P.** (1979) Versuch einer Abwicklung des Helvetikums zwischen Rhone und Reuss. *Eclogae geol. Helv.*, **72**, 439-454.
- Fichter, H.J.** (1934) Geologie der Bauen-Brisen-Kette am Vierwaldstättersee und die zyklische Gliederung der Kreide und des Malm der helvetischen Decken. Beiträge zur geologischen Karte der Schweiz NF 69, 129 pp.
- Field, M.E., Ogston, A.S. and Storlazzi, C.D.** (2011) Rising sea level may cause decline of fringing coral reefs. *Eos, Transactions American Geophysical Union*, **92**, 273-274.
- Föllmi, K.B., Weissert, H., Bisping, M. and Funk, H.** (1994) Phosphogenesis, carbon-isotope stratigraphy, and carbonate-plate evolution along the Lower Cretaceous northern Tethyan margin. *Geological Society of America Bulletin*, **106**, 729-746.
- Föllmi, K.B., Godet, A., Bodin, S. and Linder, P.** (2006) Interactions between environmental change and shallow water carbonate buildup along the northern Tethyan margin and their impact on the Early Cretaceous carbon isotope record. *Paleoceanography*, **21**, 16 pp.
- Föllmi, K.B., Bodin, S., Godet, A., Linder, P. and van de Shootbrugge, B.** (2007) Unlocking paleo-environmental information from Early Cretaceous shelf sediments in the Helvetic Alps: stratigraphy is the key! *Swiss Journal of Geosciences*, **100**, 349-369.
- Föllmi, K.B.** (2012) Early Cretaceous life, climate and anoxia. *Cretaceous Research*, **35**, 230-257.
- Ford, D. and Golonka, J.** (2003) Phanerozoic paleogeography, paleoenvironment and lithofacies maps of the circum-Atlantic margins. *Marine and Petroleum Geology*, **20**, 249-285.
- Funk, H.** (1969) Typusprofile der helvetischen Kieselkalk Formation und der Altmann Schichten. *Eclogae geol. Helv.*, **62**, 191–203.
- Funk, H.** (1971) Zur stratigraphie und lithologie des Helvetischen Kieselkalkes und der Altmannschichten im der Säntis-Churfirsten-Gruppe (Nordostschweiz). *Eclogae geol. Helv.*, **64**, 345–433.
- Funk, H., Föllmi, K.B. and Mohr, H.** (1993) Evolution of the Tithonian-Aptian Carbonate Platform Along the Northern Tethyan Margin, Eastern Helvetic Alps. In: *AAPG Special*
- Frakes, L. A. and Bolton, B.** (1992) Effects of ocean chemistry, sea level, and climate on the formation of primary manganese ore deposits. *Economic Geology*, **87**, 1207-1217.
- Frakes, L. A. and Francis, J. E.** (1988) A guide

- to Phanerozoic cold polar climates from high-latitudes ice-rafting in the Cretaceous. *Nature*, **333**, 547-549.
- Francis, J. E. and Frakes, L. A.** (1993) Cretaceous climates. *Sedimentology Review*, **1**, 17-30.
- Frey, M., Teichmüller, M., Teichmüller, R., Mullis, J., Künzi, B., Breitschmid, A., Gruner, U. and Schwizer, B.** (1980) Very low-grade metamorphism in external parts of the Central Alps : illite crystallinity, coal rank and fluid inclusion data. *Eclogae geol. Helv.*, **73**, 173-203.
- Gasparini, Z.de.** (1980) South American Mesozoic Crocodiles. *Mesozoic Vertebrate Life* **1**, 66-72.
- Glynn, P.W.** (1993) Coral reef bleaching: ecological perspectives. *Coral Reefs*, **12**, 1-7
- Godet, A.** (2013) Drowning unconformities: Palaeoenvironmental significance and involvement of global processes. *Sedimentary Geology*, **293**, 45-66.
- Godet, A., Föllmi, K.B., Spangenberg, J.E., Bodin, S., Vermeulen, J., Adatte, T., Bonvallet, L. and Arnaud, H.** (2013) Deciphering the message of Early Cretaceous drowning surfaces from the Helvetic Alps: What can be learnt from platform to basin correlations? *Sedimentology*, **60**, 152-173.
- Goy-Eggenberger, D.** (1998) *Faible métamorphisme de la nappe de Morcles. minéralogie et géochimie*, PhD thesis, Neuchâtel University, Switzerland.
- Groshong R.H.** (1988) Low temperature deformation mechanisms and their interpretation. *Geol. Soc. Am. Bull.* **100**, 1329-1360.
- Hallam, A.** (1984) Continental humid and arid zones during the Jurassic and Cretaceous. *Palaeogeography, Palaeoclimatology, Palaeoecology*, **47**, 195-223.
- Haq, B.U., Hardenbol, J. and Vail, P.R.** (1987) Chronology of fluctuating sea levels since the Triassic. *Science*, **235**, 1156-1167.
- Haq, B.U.** (2014) Cretaceous eustasy revisited. *Global and Planetary Change*, **113**, 44-58.
- Hardenbol, J., Thierry, J., Farley, M.B., Jacquin, T., Graciansky, P. and Vail, P.R.** (1998) Mesozoic and Cenozoic sequence chronostratigraphy framework of European basins. In: *Mesozoic and Cenozoic sequence stratigraphy of European basins* (Eds P. Graciansky, J. Hardenbol, T. Jacquin and P.R. Vail), **60**, pp. charts. SEPM Spec Publ.
- Hay, W.W.** (2008) Evolving ideas about the Cretaceous climate and ocean circulation. *Cretaceous Research*, **29**, 725-753.
- Heim, A.** (1910-1916) Monographie der Churfürsten-Mattstock-Gruppe: Beiträge zur Geologischen Karte der Schweiz 50: Bern. , 662 pp.
- Heim, A. and Baumberger, E.** (1933) Jura und Unterkreide in den helvetischen Alpen beiderseits des Rheines (Vorarlberg und Ostschweiz). *Denkschriften der Schweizerischen Naturforschenden Gesellschaft*, **68**, 155-220.
- Heimhofer, U., Hochuli, P.A., Herrle, J.O., Andersen, N. and Weissert, H.** (2004) Absence of major vegetation and palaeoatmospheric $p\text{CO}_2$ changes associated with oceanic anoxic event 1a (Early Aptian, SE France). *Earth and Planetary Science Letters*, **223**, 303-318.
- Herrle, J.O., Kößler, P., Friedrich, O., Erlenkeuser, H. and Hemleben, C.** (2004) High-resolution carbon isotope records of the Aptian to Lower Albian from SE France and the Mazagan Plateau (DSDP Site 545): a stratigraphic tool for paleoceanographic and paleobiologic reconstruction. *Earth and Planetary Science Letters*, **218**, 149-161.
- Heron, S. et al.** (2008) Hurricanes and their ef-

- fects on coral reefs. In: *Status of Caribbean Coral Reefs after Bleaching and Hurricanes in 2005*. (Eds C. Wilkinson and D. Souter). Townsville, Global Coral Reef Monitoring Network.
- Hoegh-Guldberg, O.** (1999) Climate change, coral bleaching and the future of the world's coral reefs. *Marine and Freshwater Research*, **50**, 839-866.
- Hoegh-Guldberg, O., Mumby, P.J., Hooten, A.J., Steneck, R.S., Greenfield, P., Gomez, E., Harvell, C.D., Sale, P.F., Edwards, A.J., Caldeira, K., Knowlton, N., Eakin, C.M., Iglesias-Prieto, R., Muthiga, N., Bradbury, R.H., Dubi, A. and Hatziolos, M.E.** (2007) Coral Reefs Under Rapid Climate Change and Ocean Acidification. *Science*, **318**, 1737-1742.
- Hopley, D. and Kinsey, D.W.** (1988) The effects of a rapid short-term sea level rise on the Great Barrier Reef. In: *Pearman, G.I. (ed.) Greenhouse: Planning for Climate Change*, E.J. Brill, New York, pp. 189-201.
- Hunt, D. and Tucker, M.E.** (1993) Sequence stratigraphy of carbonate shelves with an example from the mid-Cretaceous (Urgonian) of southeast France. *International Association of Sedimentologists, Special Publication* **18**, 307-341.
- Immenhauser, A., Hillgärtner, H. and Van Bentum, E.** (2005) Microbial-foraminiferal episodes in the Early Aptian of the southern Tethyan margin: ecological significance and possible relation to oceanic anoxic event 1a. *Sedimentology*, **52**, 77-99.
- James, N.P.** (1997) The cool-water carbonate depositional realm. In: *Cool-water carbonates* (Eds N.P. James and J.A.D. Clarke), **SEPM Special Publication N° 56**, pp. 1-20. Society for Sedimentary Geology, Tulsa, Oklahoma.
- Jenkyns, H.C.** (1980) Cretaceous anoxic events: from continents to oceans. *Journal of the Geological Society, London*, **137**, 171-188.
- Jenkyns, H.C., Forster, A., Schouten, S., and Sinninghe Damsté, J.S.** (2004) High temperatures in the Late Cretaceous Arctic Ocean. *Nature*, **432**, p. 888-892.
- Kaufmann, F.J.** (1867) Geologische Beschreibung des Pilatus. Beiträge zur geologischen Karte der Schweiz 5, 168 pp.
- Kemper, E.** (1987) Das Klima der Kreide-Zeit. *Geologisches Jahrbuch, Reihe A*, **96**, 5-185.
- Kempf, O. and Pfiffner, O.A.** (2004) Early Tertiary evolution of the North Alpine Foreland Basin of the Swiss Alps and adjoining areas. *Basin Research*, **16**, 549-567.
- Kiessling, W., Flügel, E. and Golonka, J.** (2003) Patterns of Phanerozoic carbonate platform sedimentation. *Lethaia*, **36**, 195-226.
- Larson, R.L.** (1991) Geological consequences of superplumes. *Geology*, **19**, 963-966.
- Larson, R.L. and Erba, E.** (1999) Onset of the mid-Cretaceous greenhouse in the Barremian-Aptian : Igneous events and the biological, sedimentary and geochemical responses. *Paleoceanography*, **14**, 663-678.
- Leckie, M.R., Bralower, T.J. and Cashman, R.** (2002) Oceanic anoxic events and plankton evolution: Biotic response to tectonic forcing during the mid-Cretaceous. *Paleoceanography*, **17**.
- Lienert, O.G.** (1965) *Stratigraphie der Drusbergschichten und des Schrattenkalks im Säntisgebirge unter besonderer Berücksichtigung der Orbitoliniden*. Diss. Naturwiss. ETH Zürich, Nr. 3707, ETH-HDB (Zürich)
- Linder, P., Gigandet, J., Hüsser, J.L., Gainon, F. and Föllmi, K.B.** (2006) The Early Aptian Grünten Member: Description of a new lithostratigraphic unit of the helvetic

- Garschella Formation. *Eclogae geologicae Helvetiae*, **99**, 327-341.
- McAllister, D. E.** (1995) Status of the World Ocean and its Biodiversity. Sea Wind, Bulletin of Ocean Voice International, Ottawa 9 (4): 1-72.
- Martinez, M., Deconinck, J.-F., Pellenard, P., Riquier, L., Company, M., Reboulet, S. and Moiroud, M.** (2015) Astrochronology of the Valanginian–Hauterivian stages (Early Cretaceous): Chronological relationships between the Paraná–Etendeka large igneous province and the Weissert and the Faraoni events. *Global and Planetary Change*, **131**, 158-173.
- Masse, J.-P. and Philip, J.** (1981) Cretaceous coral-rudist buildups of France. In: *European fossil reef models* (Ed. D.F. Toomey). *SEPM Spec. Publ.*, **30**, 399–426.
- Masse, J.-P., Bellion, Y., Benkhelil, J., Ricou, L.-E., Dercourt, J. and Guiraud, R.** (1993) Early Aptian (114 to 111 Ma). In: *Atlas Tethys paleoenvironmental maps*. (Ed R.L.-E. Dercourt J., Vrielynck B), pp. 135-152. Gauthier-Villars, Paris.
- Masson, H., Baud, A. and Escher, A.** (1980) Compte rendu de l'excursion de la Société Géologique Suisse du 1 au 3 octobre 1979 : coupe Préalpes-Hélicoïdale-Pennique en Suisse occidentale. *Eclogae geol. Helv.*, **73**, 331-349.
- Mort, H.P.** (2006) *Biogeochemical Changes during the Cenomanian-Turonian Oceanic Anoxic Event (OAE2)*. PhD thesis, University of Neuchâtel, Neuchâtel, 221 pp.
- Mutti, M. and Hallock, P.** (2003) Carbonate systems along nutrient and temperature gradients: some sedimentological and geochemical constraints. *Int. J. Earth Sci. (Geol. Rundsch.)*, **92**, 465-475.
- Neal, C. R., Mahoney, J. J., Kroenke, L. W., Duncan, R. A. and Petterson, M. G.** (1997) 'The Ontong Java Plateau', in *Large Igneous Provinces: Continental, Oceanic, and Planetary Flood Volcanism*, **100**, American Geophysical Union.
- Oberholzer, J.** (1933) *Geologie der Glarneralpen*. Beiträge zur geologischen Karte der Schweiz NF **28**, 626 pp.
- Ogg, J.G., Ogg, G. and Gradstein, F.M.** (2008) *The Concise Geologic Time Scale*. Cambridge University Press, New York, 177 pp.
- Orr, J.C., Fabry, V.J., Aumont, O., Bopp, L., Doney, S.C., Feely, R.A., Gnanadesikan, A., Gruber, N., Ishida, A., Joos, F., Key, R.M., Lindsay, K., Maier-Reimer, E., Matzear, R., Monfray, P., Mouchet, A., Najjar, R.G., Plattner, G.-K., Rodgers, K.B., Sabine, C.L., Sarmiento, J.L., Schlitzer, R., Slater, R.D., Totterdell, I.J., Weirig, M.-F., Yamanaka, Y. and Yool, A.** (2005) Anthropogenic ocean acidification over the twenty-first century and its impact on calcifying organisms. *Nature*, **437**, 681-686.
- Pfiffner, O. A.** (1977) Tektonische Untersuchungen im Infrahelvetikum der Ostschweiz. *Mitt. geol. Inst. ETH u. Univ. Zürich N.F.* **217**, 1-432.
- Pfiffner, O.A.** (1993) The structure of the Helvetic nappes and its relation to the mechanical stratigraphy. *Journal of Structural Geology*, **15**, pp. 511 to 521.
- Philip, J.** (2003) Peri-Tethyan neritic carbonate areas: distribution through time and driving factors. *Palaeogeography, Palaeoclimatology, Palaeoecology*, **196**, 19-37.
- Price, G.D.** (1999) The evidence and implications of polar ice during the Mesozoic. *Earth-Science Reviews*, **48**, 183-210.
- Pucéat, E., Lécuyer, C. and Reisberg, L.** (2005) Neodymium isotope evolution of

- NW Tethyan upper ocean waters throughout the Cretaceous. *Earth and Planetary Science Letters*, **236**, 705–720.
- Ramsay, J.G.** (1981) Tectonics of the Helvetic Nappes. *Geological Society, London, Special Publications*, **9**, 293–309.
- Ramsay, J.G.** (1989) Fold and fault geometry in the western Helvetic nappes of Switzerland and France and its implication for the evolution of the arc of the western Alps. *Geological Society, London, Special Publications*, **45**, 33–45.
- Retallack, G.J.** (2001) A 300-million-year record of atmospheric carbon dioxide from fossil plant cuticles. *Nature*, **411**, 287–290.
- Rick, B.** (1985) Geologie des Fluhbrig (Kt. Sz) unter besonderer Berücksichtigung der Alt-mannschichten und der “Gault”-Formation. Unpublished diploma thesis, ETH Zürich, 83 pp.
- Schenk, K.** (1992) *Die Drusberg- und Schratzenkalk-Formation (Unterkreide) im Helvetikum des Berner Oberlandes (2 vol)*. PhD thesis, University of Bern.
- Schlanger, S.O. and Jenkyns, H.C.** (1976) Cretaceous oceanic anoxic events: causes and consequences. *Geologie en Mijnbouw*, **55**, 179–184.
- Schmid S.M.** (1982) Microfabric studies as Indicators of Deformation Mechanisms and Flow Laws Operative in Mountain Building. Pp. 95–110 in: *Mountain Building Processes* (K.J. Hsü, editor). Academic Press, London.
- Skelton, P.W. and Gili, E.** (2012) Rudists and carbonate platforms in the Aptian: a case study on biotic interactions with ocean chemistry and climate. *Sedimentology*, **59**, 81–117.
- Staeger, D.** (1944) Geologie der Wilerhorngruppe zwischen Brienz und Lungern (Kantone Bern und Unterwalden). *Eclogae geologicae Helvetiae*, **37**, 99–188.
- Stampfli, G.M. and Borel, G.D.** (2002) A plate tectonic model for the Paleozoic and Mesozoic constrained by dynamic plate boundaries and restored synthetic oceanic isochrons. *Earth and Planetary Science Letters*, **196**, 17–33.
- Stampfli, G.M., Borel, G.D., Marchand, R. and Mosar, J.** (2002) Western Alps geological constraints on western Tethyan reconstructions. In: *Reconstruction of the evolution of the Alpine-Himalayan Orogen* (Eds G. Rosenbaum and G.S. Lister), **8**, pp. 77–106. Journal of the Virtual Explorer.
- Stein, M., Arnaud-Vanneau, A., Adatte, T., Fleitmann, D., Spangenberg, J.E. and Föllmi, K.B.** (2012) Palaeoenvironmental and palaeoecological change on the northern Tethyan carbonate platform during the Late Barremian to earliest Aptian. *Sedimentology*, **59**, 939–963.
- Studer, B.** (1834) Bemerkungen zu einem Durchschnitte durch die Luzerner Alpen. *N. Jb. Mineral. Geogn. Geol. Petrefaktenkd. Stuttgart*, **5**, p. 405.
- Thiry, M., Quesnel, F., Yans, J., Wyns, R., Vergari, A., Theveniaut, H., Simon-Coiçon, R., Ricordel, C., Moreau, M.-G., Giot, D., Dupuis, C., Bruxelles, L., Barbarand, J. and Baele, J.-M.** (2006) Continental France and Belgium during the early Cretaceous: paleoweatherings and paleolandforms. *Bull. Soc. géol. Fr.*, **177**, 155–175.
- Trümpy, R.** (1969) Die helvetischen Decken der Ostschweiz: Versuch einer palinspatischen Korrelation und Ansätze zu einer kinematischen Analyse. *Eclogae geol. Helv.*, **62**, 105–142.
- Trümpy, R.** (1980) *Geology of Switzerland: A guide-book. Part A: An Outline of the Geology of Switzerland*. Wepf & Co. Publishers,

- Basel - New York, 334 pp.
- Vail, P.R., Mitchum, R.M.J., Todd, R.G., Widmeri, J.W., Thompson, S., Sangree, J.B., Bubb, J.N. and Hatelid, W.G.** (1977) Seismic stratigraphy and global changes of sea level. In: *Seismic stratigraphy. Application to hydrocarbon exploration*, Am. Assoc. Pet. Geol. Mem., **26**, pp. 49-212, Tulsa.
- Van Wagoner, J.C., Posamentier, H.W., Mitchum, R.M., Vail, P.R., Sarg, J.F., Loutit, T.S. and Hardenbol, J.** (1988) An overview of the fundamentals of sequence stratigraphy and key definitions. In: *Sea Level Changes: An Integrated Approach* (Eds C.K. Wilgus, B.S. Hastings, C.G.S.C. Kendall, H.W. Posamentier, C.A. Ross and J.C. Van Wagoner), **42**, pp. 39-45. SEPM Special Publication, Tulsa, Oklahoma, U.S.A.
- Veizer, J., Ala, D., Azmy, K., Bruckschen, P., Buhl, D., Bruhn, F., Carden, G.A.F., Diener, A., Ebneth, S. and Godderis, Y.** (1999) $^{87}\text{Sr}/^{86}\text{Sr}$, $\delta^{13}\text{C}$ and $\delta^{18}\text{O}$ evolution of Phanerozoic seawater. *Chemical Geology*, **161**, 59-88.
- Vermeulen, J.** (2005) Boundaries, ammonite fauna and main subdivisions of the stratotype of the Barremian. In: *The Hauterivian-Lower Aptian Sequence Stratigraphy from Jura Platform to Vocontian Basin: A Multidisciplinary Approach* (Eds T. Adatte, A. Arnaud-Vanneau, H. Arnaud, M.-C. Blanc-Alétru, S. Bodin, E. Carrio-Schaffhäuser, K.B. Föllmi, A. Godet, M.C. Raddadi and J. Vermeulen), Géol. Alpine, Sér. Spéc. "Colloques et Excursions" No. 7, 147-173.
- Wang, H., Frey, M., Stern, W.B. and** (1996) Diagenesis and Metamorphism of Clay Minerals in the Helvetic Alps of Eastern Switzerland. *Clays and Clay Minerals*, **44**, 96-112.
- Weissert, H.** (2000) Deciphering methane's fingerprint. *Nature*, **406**, 356-357.
- Weissert, H., Lini, A., Föllmi, K.B. and Kuhn, O.** (1998) Correlation of Early Cretaceous carbon isotope stratigraphy and platform drowning events: a possible link? *Palaeogeography, Palaeoclimatology, Palaeoecology*, **137**, 189-203.
- Wilkinson, C. R. and Buddemeier R. W.** (1994) Global Climate Change and Coral Reefs: Implications for People and Reefs. *Report of the United Nations Environment Programme (UNEP), the Intergovernmental Oceanographic Commission (IOC), the Association of South Pacific Environmental Institutions (ASPEI) and The World Conservation Union (IUCN) Global Task Team on the Implications of Climate Change on Coral Reefs*.
- Wilson J. L.** (1975) Carbonate Facies in Geologic History, Springer-Verlag, 471 pp.
- Wilson, P.A. and Norris, R.D.** (2001) Warm tropical ocean surface and global anoxia during the mid-Cretaceous period. *Nature*, **412**, 425-429.
- Wissler, L., Funk, H. and Weissert, H.** (2003) Response of Early Cretaceous carbonate platforms to changes in atmospheric carbon dioxide levels. *Palaeogeography, Palaeoclimatology, Palaeoecology*, **Volume 200**, Pages 187-205.
- Wyssling, G.W.** (1986) Der frühkretazische helvetische Schelf im Vorarlberg und Allgäu. *Jahrbuch der Geologischen Bundesanstalt*, **129**, 161-265.
- Ziegler, M.A.** (1967) A study of the Lower Cretaceous facies developments in the Helvetic border chain, north of the Lake of Thun (Switzerland). *Eclogae Geologicae Helveticae*, **60**, 509-528.

Chapter 2 – Installation of a shallow-water carbonate platform on top of hemipelagic sediments: example of the Drusberg-Schrattenkalk platform in the Helvetic Alps (Barremian)

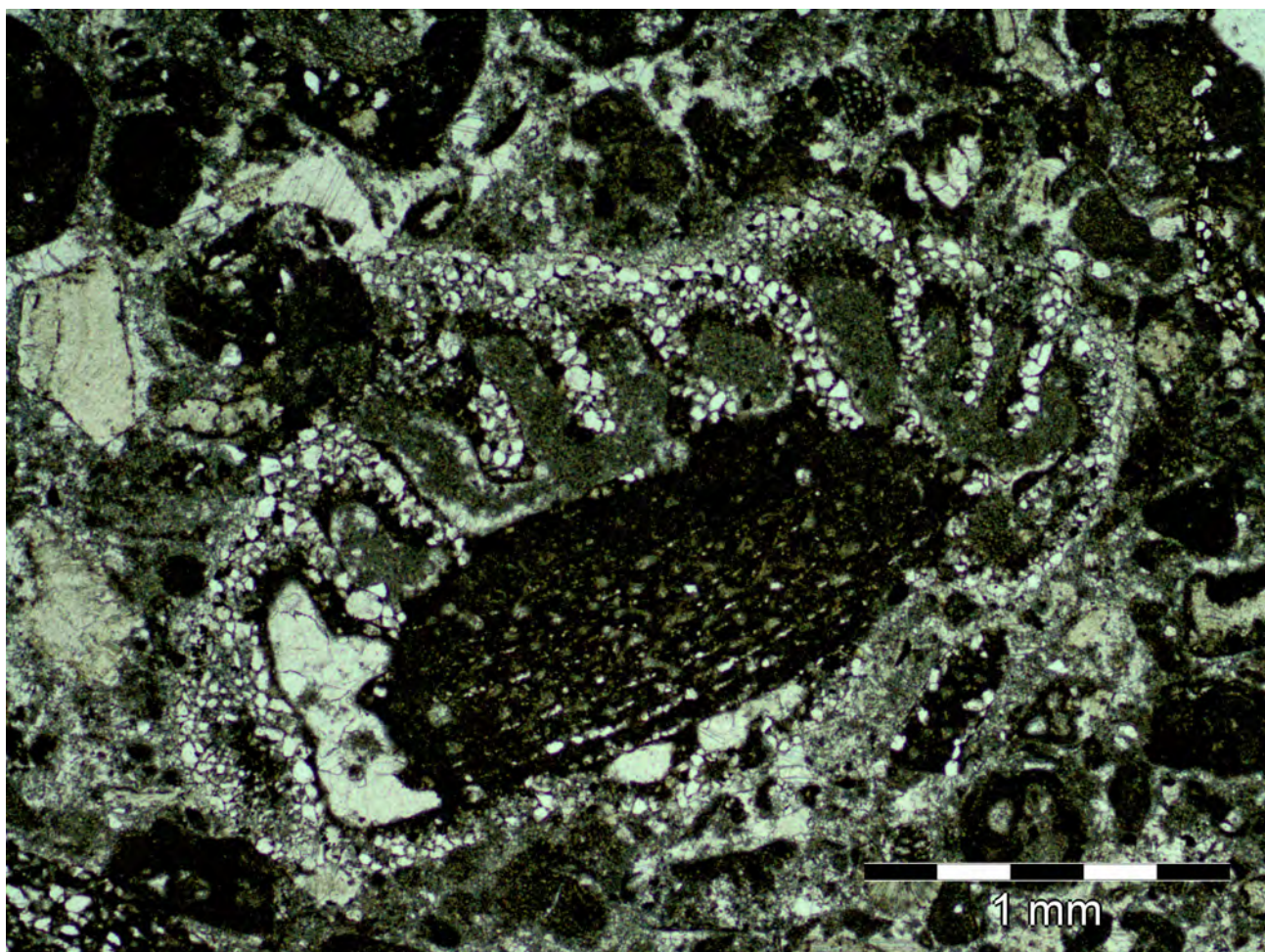


Fig. 2 *Acruliamina* uncrusting an orbitolind (section of Rawil, sample RW54)

The following chapter provides a contribution to a better understanding of the timing and dynamics of the installation of the shallow-water platform in the Helvetic nappes is achieved, using an integrated sequence stratigraphic approach, by using microfacies, biostratigraphy data and the interpretation of a panorama.

Chapter 2

Installation of a shallow-water carbonate platform on top of hemipelagic sediments: example of the Drusberg-Schrattenkalk platform in the Helvetic Alps (Barremian)

Abstract

In the Helvetic Alps, the Schrattenkalk Formation embodies the distal part of the Urgonian platform, which developed along the northern Tethyan margin. Mainly formed by photozoan organisms typical of a subtropical shallow-water carbonate platform, the sediments settled on top of the hemipelagic series of the Drusberg Member, which date from the early Barremian.

The timing and the dynamics of the installation of the Schrattenkalk carbonate platform are investigated here. To achieve it, nine sections and one panorama have been studied in the Helvetic thrust-and-fold belt. Based on the analyses of 800 thin sections and the determination of 12 microfacies, a sequence-stratigraphic framework has been established. The inherited paleotopography and the sea level changes associated with the deposit of the sequence B3 are the key of the understanding of the installation of the shallow-water photozoan facies. The sea-level record is characterized by an important regressive phase near the early-late Barremian boundary, which led to the emersion of hemipelagic sediments in the inner part of the platform, and to the deposition of a lowstand systems tract in the intermediate and distal domains. The deposition of platform carbonate occurred during the following important transgressive

phase, which flooded the entire platform. The associated faunal assemblages indicate an important increase in nutrient input linked to the transgression. The resulting sea-level highstand allowed for the deposition of shallow-water platform carbonates rich in corals and rudists. This depositional sequence terminated by important accommodation space infilling and a phase of sea level fall, which amplitude was at least 15 m below the base level, indicated by the presence and depth of karst features on the internal and intermediate platform.

Keywords

Helvetic Alps; Urgonian platform; Schrattenkalk Formation; Early Cretaceous; Barremian; Sea-level change; nutrients

2.1 Introduction

The Urgonian carbonate platforms developed in an important manner during the Barremian to build up one of the largest and most important shallow-water carbonate platforms of the entire Phanerozoic. Relicts of the Urgonian platform are outcropping in many places around the world, from Europe to Pakistan (Spain, Vilas et al., 1995; Italy, Amodio et al., 2013; Hungary,

Peybèrnes, 1979; Serbia, Sudar et al., 2008; central Iran, Wilmsen et al., 2013; Pakistan, Pudsey et al., 1985) on the northern Tethyan margin, and from Morocco to the Middle East (Morocco-Algeria-Tunisia, e.g. Canérot et al., 1986; Turkey, Masse et al., 2009; Oman, van Buchem et al., 2002) for the southern Tethyan margin, but also in the Pacific Ocean (Indonesia, Hashimoto and Matsumaru, 1971; Hokaido, Matsumaru, 2005; Resolution Guyot; Arnaud et al., 1995; Arnaud Vanneau et al., 1995), South America (Venezuela; Arnaud et al., 1994, 2000), and Central and North America (Mexico, Omana-Pulido and Pantoja-Alor, 1998; Barragan-Manzo and Diaz-Otero, 2004).

In spite of its importance, not much is known about the mechanisms and conditions leading to its development. The substratum on which the Urgonian Platform becomes installed is extremely variable in terms of age and lithology depending on the studied area. The best example is in the southeastern France: in the Gard region, this platform settled on top of uppermost lower Barremian hemipelagic sediments (Vermeulen et al., 2013). In the Vercors-Chartreuse area, the Urgonian Platform overlays an eroded surface due to the tilting of the substratum: in the Southern part of this platform, the sections are complete, while in northward directions the hiatus between older sediments and the Urgonian Platform becomes more and more important (e.g. Arnaud et al., 1998).

In this study, the installation of the Urgonian platform in the Helvetic platform, today outcropping in the Helvetic nappes (Switzerland – Austria), is examined. In this area, the Urgonian platform, embodied by the Schrattenkalk Formation, settled on top of the hemipelagic series of the Drusberg Member. The boundary between the hemipelagic Drusberg Member and

the shallow-water carbonate of the Schrattenkalk Fm has been previously described as a gradual transition. Nevertheless, a detailed analysis of the microfacies and the depositional geometries presented in this chapter, offers a new vision of the installation of the Urgonian platform in the Helvetic Alps.

2.2 Geological setting

The Helvetic nappes in the central European Alps consist of a thrust-and-fold complex, formed during the Alpine orogeny. They represent the northern passive margin of the Tethys, where Mesozoic and Cenozoic sediments were deposited. In the Helvetic nappes, intermediate to distal portions of the Urgonian platform are outcropping. The uppermost Hauterivian – lower Aptian succession is divided into two formations, the Tierwis Formation (Fm) and the Schrattenkalk Fm, which are themselves divided into Members (Mb; Fig. 2.1).

The succession of the Tierwis Fm starts with the condensed interval of the Altmann Mb, which has been studied in detail by Bodin et al. (2006a and b). This member is characterized by phosphate- and glauconite-rich sandstone, marl and coarse packstone rich in quartz, bryozoans and echinoderms. Ammonites and belemnites are common. In intermediate and distal parts of the Helvetic platform, condensation processes were very intense, and the entire Altmann Mb is less than a meter to a few meters thick, or is entirely lacking. In proximal parts, this unit can be more expanded and shows a more complete record (especially in the sections of Tierwis, Kistenpass and L'Ecuelle). However, there is a zone in between where the Altmann Mb is almost

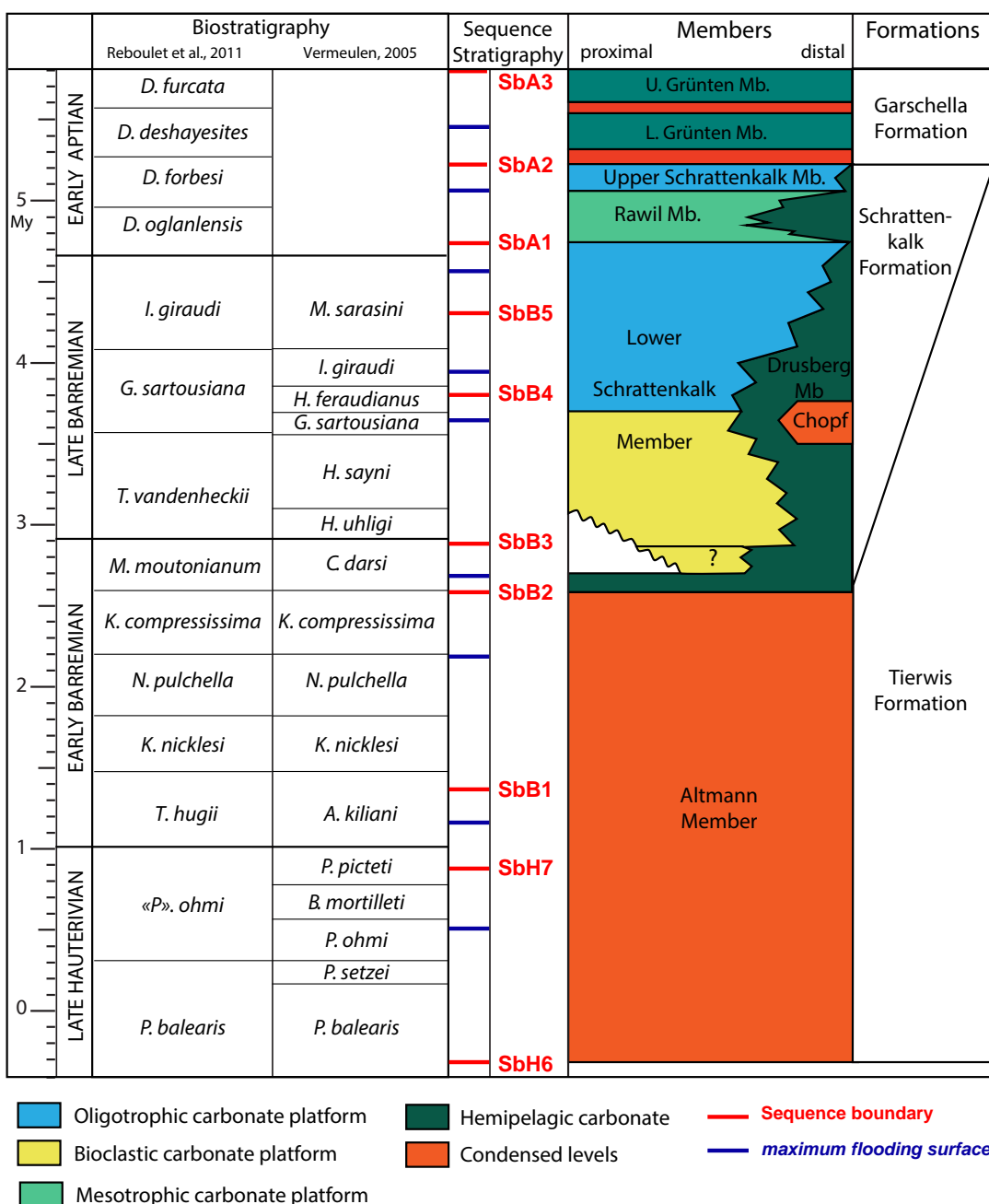


Fig. 2.1 Time-space diagram of the sedimentary successions of latest Hauterivian to early Aptian age through the Helvetic zone. Approximate position of the sequence stratigraphic framework (based on Arnaud et al. 2005; calibrated with the biostratigraphy from Vermeulen, 2005 and Reboulet et al., 2011). Mb = Member, Fm = Formation, Sb = Sequence Boundary.

completely missing, in the nappes of Glarus and Mürtschen for instance. Ammonites give a maximum age for this member from the latest Hauterivian to the late early Barremian (*Balearites balearis* to *Coronites darsi* ammonite zones). In this contribution, the boundary between the Altmann Mb and the Drusberg Mb is placed on top of a siliceous and phosphatic hardground in the reference section at Tierwis, which is lower

than the original boundary described by Bodin et al. (2006). This implies a readjustment of the sequence stratigraphic framework of Bodin et al. (2006), as will be discussed in the following.

The following lithostratigraphic unit is the Drusberg Mb, which sediments were deposited in a hemipelagic setting. The most abundant facies is rich in spicules, small-sized echinoderms, irregular echinoids, circalittoral

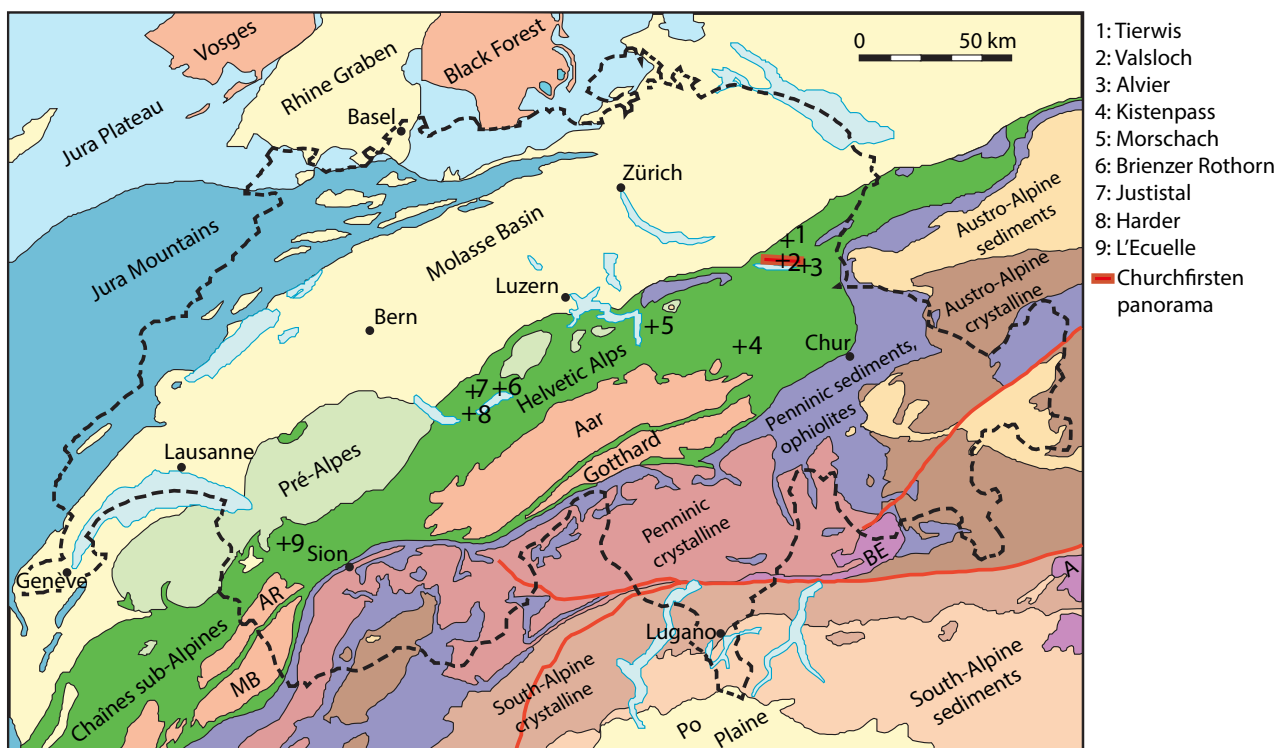


Fig. 2.2 Simplified tectonic map of Switzerland with the location of the analysed sections. (After Föllmi et al., 2013; Adapted from the Swiss Federal Office of Topography – Swisstopo, Bern. (<http://www.swisstopo.ch/internet/en/home/topics/geology/maps.html>)).

foraminifera, calcispheres, and radiolarians. This facies corresponds to fully marine sediments deposited in an outer-shelf environment. Sparse bioclastic beds occur, suggesting reworking of shallow-water carbonate particles and fossils, such as oolites, dasycladal algae, orbitolinids, and miliolids. Where it is overlain by the Schrattenkalk Fm, the age of the Drusberg Mb is restricted to the late early Barremian to middle late Barremian (Bodin et al., 2006b, c). In distal areas, the hemipelagic facies of the Drusberg Mb persisted during the late Barremian – earliest Aptian time period.

The Schrattenkalk Fm lies on top of the Drusberg Mb in the proximal and intermediate parts of the Helvetic realm. The lower and upper Schrattenkalk Mbs consist of shallow-water platform carbonate, showing lagoonal facies rich in rudists, in addition to reefal and oolitic shoal facies. In contrast, the Rawil Mb between the two Schrattenkalk Mbs is characterized by the deposition of marly limestone, which includes

layers rich in *Palorbitolina lenticularis* and contains a fauna and flora representative of seagrass environments. The Lower Schrattenkalk Mb is dated as late Barremian to the vicinity of the Barremian-Aptian boundary. The Rawil Mb is earliest Aptian in age, and the deposition of the Upper Schrattenkalk Mb is terminated by an episode of emersion. The demise of the Schrattenkalk platform is dated by ammonites as near the boundary between the *Deshayesites weissi* and *Deshayesites deshayesi* zones (middle early Aptian; Linder et al., 2006; Föllmi and Gainon, 2008).

The studied sections are at or near the localities of L'Ecuelle (Swiss coordinates: 579.336/124.832), part of the Morcles nappe; Justistal (628.427/176.557), Harder (631.250/170.991), Brienzer Rothorn (645.955/182.008), and Morschach (a drill core: 690.299/205.511), all in the Wildhorn-Drusberg nappe; Kistenpass (722.715/185.749) in the infrahelvetic complex; and Tierwis

(742.970/234.730), Valsloch (742.224/224.041), and Alvier (749.644/222.586) in the Säntis nappe. The section of Valsloch was chosen as the reference section for the Schrattenkalk Fm for the Helvetic platform in this study, because it includes one of the most complete sections through this formation. It is located in the Churfirsten range, and is part of the panorama of its south cliff, which was studied in detail. The location of the sections, the panorama and the nappes is presented in Fig. 2.2.

In this study we focus on the first depositional sequence of the Lower Schrattenkalk member to analyze the installation of the Urgonian platform in this particular part of the northern Tethyan margin.

2.3 Methods

2.3.1 Microfacies analysis

A total of 800 thin sections were studied, using the microfacies classification of Arnaud-Vanneau & Arnaud (2005; see Fig. 2.3). This classification is based on present-day environmental ecosystems. It consists on twelve microfacies types along a distal to proximal transect.

F0: marl and marly limestone with a significant amount of pelagic organisms (more than 50% of pelagic fragments). This facies is rarely present.

F1: marl and marly limestone with a hemipelagic association (less than 50% of pelagic fragments).

F2: marly limestone to wackestone rich in thin echinoid clasts.

F3: marly limestone to packstone and grainstone including small-size grains, rich in circalittoral foraminifera.

- F3a: abundance of annelids.

- F3b: important occurrence of the flat *Eopalorbitolina transiens*.

F4: packstone rich in crinoids and bryozoans.

F5: grainstone with large rounded clasts, showing good size sorting.

F6: oolitic grainstone.

F7: grainstone made of coral reef debris.

F8: packstone to wackestone, lagoonal facies rich in large rudists, miliolids and conical orbitolinids.

F9: wackestone, lagoonal facies rich in small rudists, miliolids and orbitolinids.

F10: wackestone, confined lagoonal facies. Abundant oncrolites indicate intense bacterial activity.

F11: supralittoral facies.

- F11a: beach environment: grainstone showing keystone vugs.

- F11b: muddy environment: mudstone showing algal mats, sheet cracks or bird's eyes.

These MF types were regrouped in five microfacies associations (AF1 to AF5), according to comparable bathymetries and grain-size sorting characteristics. An annex microfacies association is identified: AF6, which is used to characterize the main transgressive phases. It consists on wackestone/packstone showing lag and reworking grains.

2.3.2 Biostratigraphy

Benthic foraminifera and especially Orbitolinids are used to obtain a biostratigraphic framework and to correlate the sequences iden-

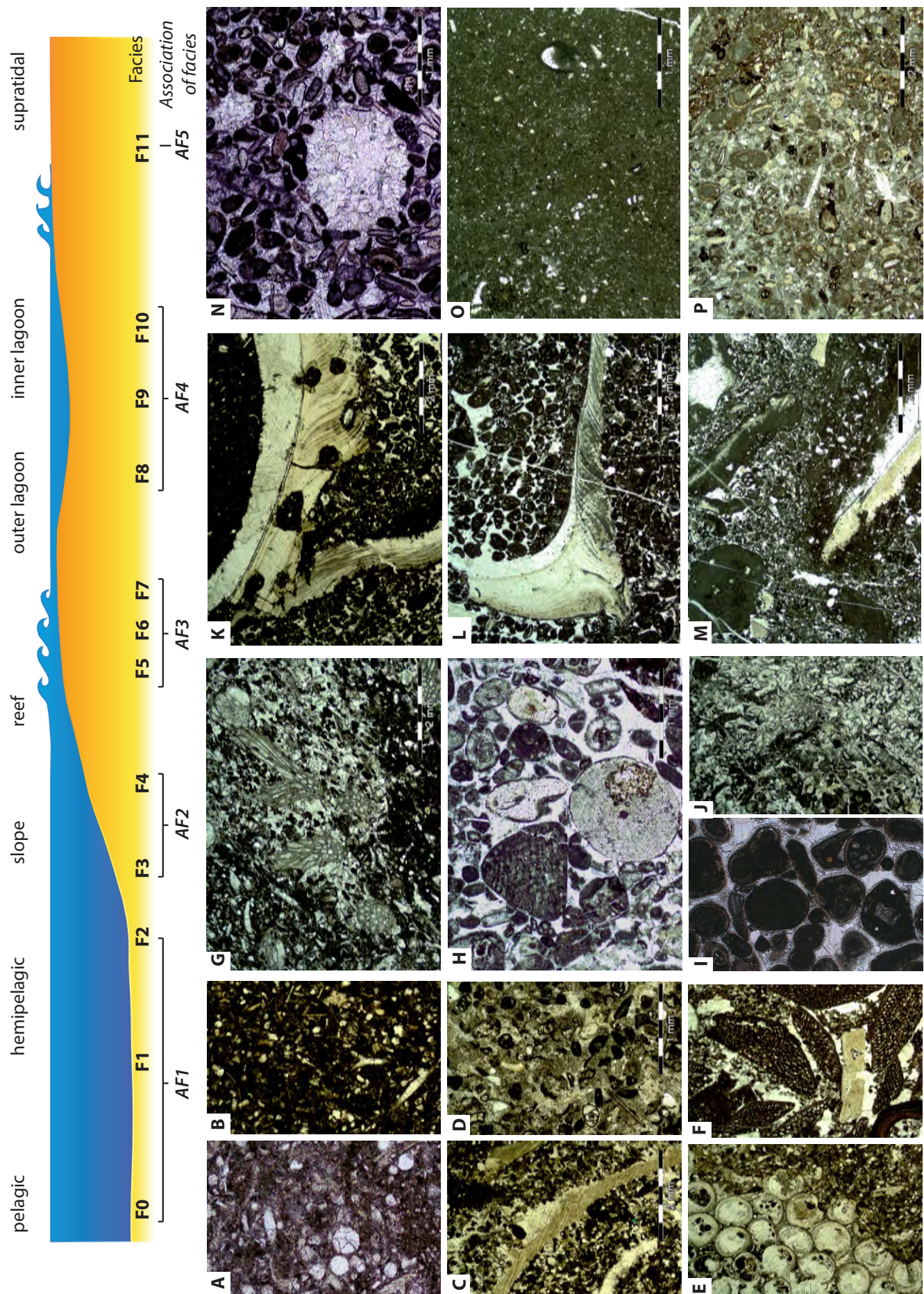


*Fig. 2.3 Microphotographs of microfacies types F0 to F11 and FT. A: F0, pelagic facies, rich in radiolaria (Valsloch, VA 317); B: F1, spicule-rich facies (Morschach, MC 259); C: F2, irregular sea urchin facies (Morschach, MC 238); D: F3, circalitoral foraminifera facies (Harder, HA46); E: F3a, colonial annelid facies (L'Ecuelle, EC 61); F: F3b, *Eopalorbitolina transiens* accumulation (Morschach, MC 206); G: F4, branched bryozoan facies (L'Ecuelle, EC 38); H: F5, rounded debris facies (Harder, HA 179); I: F6, oolite facies (Tierwis, TW 25); J: F7, coral facies (Morschach, MC 173); K: F8, canaliculate rudist facies (Morschach, MC 154); L: F9, rudist facies (Morschach, MC 163); M: F10, oncolite facies (Morschach, MC 165); N: F11a, keystone vugs facies (Valsloch, VA 26); O: F11b, confined supratidal facies (Tierwis, TW 32); P: FT, reworked facies (Valsloch, VA 255).*

tified in the Helvetic Alps with those from the Vercors, where the stratigraphic ranges of Orbitonilids were calibrated (e.g. Arnaud-Vanneau, 1980; Arnaud et al., 1998). Benthic foraminifera biostratigraphy works especially well in the Schrattenkalk Fm, because of its shallower facies and the presence and partly abundance of benthic foraminifera. *Praedictyorbitolina carthusiana*, *Palorbitolina /Eopalorbitolina transiens* - have a narrow stratigraphic distribution linked to sequence B3. *Paracoskinolina reicheli* and *Neotrocholina friburgensis* have a broader range and indicate the Late Barremian. Other species have a longer range that encompasses the whole Barremian stage, such as *Urgonina alpicensis*, and can even extend into the early Aptian such as *Paleodictyoconus* cf. *actinostoma*, *Falsurgonina* sp., *Cribellopsis neelongata* and the quartz-agglutinated *Pseudocyclammina ecougensis*. They are illustrated in Fig. 2.4.

2.3.3 Sequence stratigraphy

Sequence stratigraphy has been first defined by Vail et al. (1977) and subsequently described in numerous publications (e.g., Sarg, 1988; Van Wagoner et al., 1988; Emery and Myers, 1996; Coe et al., 2003; Catuneanu et al., 2009). It is based on the recognition of the spatial organization of depositional sequences and their

key surfaces, commonly generated by changing relative sea level. A depositional sequence starts with a remarkable erosive surface due to a drop in sea level, the sequence boundary (SB). The first deposits are found in distal parts and represent the lowstand systems tract (LST). The low rate of creation of accommodation space compared to the sedimentation rate generates a progradation of shallow-water facies toward the basin. The progressive rise of sea level triggers a retrogradational parasequence stacking patterns, for which the base is indicated by the transgressive surface (TS). The transgression is accompanied by backstepping of shallow-water facies, and the onlap of the sediments above the SB in a landward direction, forming the transgressive systems tract (TST). When the rate of sea level rise reaches its maximum, the sediments accumulated on the platform show the more external facies, on a surface or in a thin zone, which is known as the maximum flooding surface (mfs). The subsequent drop in sea level is accompanied by the progradation of shallow-water facies toward the basin, embodied by the highstand systems tract (HST), which is limited to its top by the SB of the overlying depositional sequence.

This study is based on the sequence stratigraphic framework described by Arnaud and Arnaud Vanneau (1989, 1991), Arnaud Vanneau and Arnaud (1990), and Hunt and Tucker (1993) in the Vercors and Chartreuse platform, which

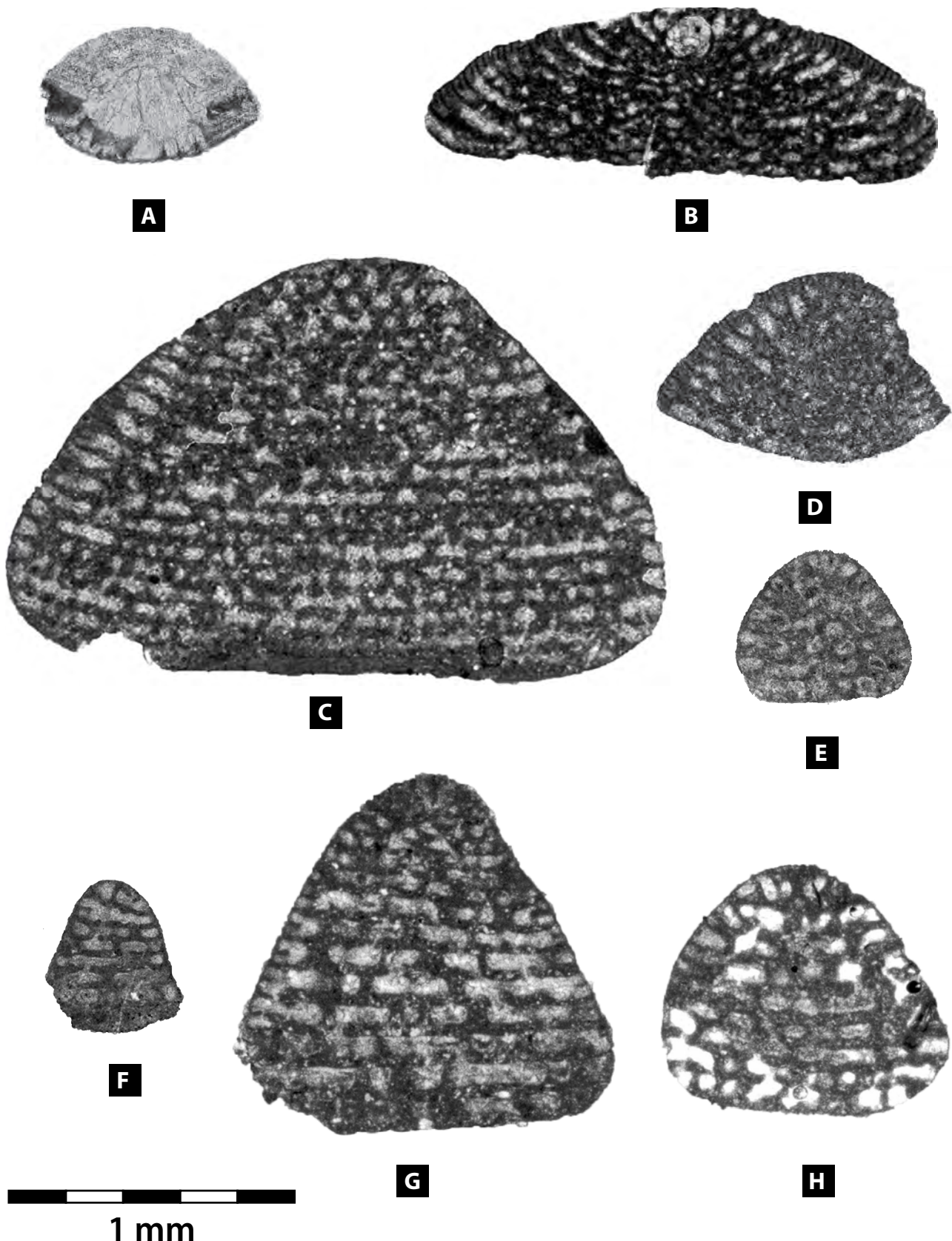


Fig. 2.4 Typical foraminifera of the depositional sequence B3. **A:** *Neotrocholina friburgensis*, oblique section (Tierwis, TW 4) **B:** *Palorbitolina-Eopalorbitolina transiens*, axial section through the embryonic apparatus (Valsloch, VA 186) **C:** *Praedictyorbitolina carthusiana*, oblique section (Valsloch, VA 170) **D:** *Paleodictyoconus cf. actinostoma*, axial section (Tierwis, TW 18) **E:** *Falsurgonina* sp., oblique section (Justistal, LB 218) **F:** *Urgonina alpicensis?*, oblique section (Justistal, LB 228) **G** and **H:** *Paracoskinolina reicheli*, oblique section (Justistal, LB 106 and LB 186).

was biostratigraphically calibrated by ammonite ages in the Vocontian basin. This sequence stratigraphic framework is also calibrated by the biostratigraphic scheme based on benthic foraminifera, which was successively developed by Arnaud Vanneau (1980), Arnaud Vanneau and Arnaud (1990), Arnaud et al. (1998), and Arnaud (2005), in the Vercors area. In the Helvetic nappes, the Barremian is divided in five sequences, from B1 to B5 (Fig. 2.1). The sequences B1 and B2 are dated as the early Barremian, and the sequences B3, B4 and B5 were deposited during the late Barremian. Bodin et al. (2006a) attributed the sequence B1 and the TST B2 to the Altmann Mb, whereas the HST B2 and the TST B3 belong to the Drusberg Mb, in proximal part. These authors identified the installation of the Schrattenkalk shallow-water platform during the HST B3. With the redefinition of the boundary between the Altmann and Drusberg Mbs at the reference locality of Tierwis, a readjustment of the sequence stratigraphic framework proposed Bodin et al. (2006a) is needed. The SB B3 is shifted upward and placed at the boundary between the Drusberg and the Schrattenkalk Mbs (for arguments, see below). We propose therefore that the whole depositional sequence B2 belongs to the Drusberg Mb at Tierwis.

2.3.4 Panorama of the Churfirsten range

The Churfirsten range exhibits a spectacular panorama, which provides information on the depositional geometries. A high-resolution panorama of the range has been performed from the south side of the Walensee Lake (Between Quartet and Oberterzen; 738.349/218.339) by the stacking of 460 pictures. The material

used for this panorama is composed by a camera *Canon EOS 7D*, a zoom lens *Canon EF image stabilizer 70-200 mm*, an automatic x2 tele-converter *Kenko Teleplus MC 7 DG* and a robotic camera mount *Gigapan Epic Pro*. The software used to combine the pictures is the Gigapan stitch software. The interpretation of this panorama is based on the visual observation of the evolution of beds through the picture. The sequence stratigraphy interpretation is calibrated on the section of Valsloch, which is located in the eastern part of the Churfirsten range.

2.4 Results

2.4.1 General description of the studied sections and the panorama

This study is based on the observations and analyses performed on 9 sections and one panorama. The complete logs and the facies association interpretations are shown in Figure 2.5.

(1) The section of Tierwis (Fig. 2.6-A) is located close to the Säntis summit, and represents a proximal part of the Helvetic platform. This section was logged and sampled in detail by Bodin et al. (2006a) for the Tierwis Fm. The Tierwis section presents a well-developed Altmann Mb (ca. 35 m), rich in ammonites and fish teeth (Bodin et al., 2006a.), overlain by a thin, 18m-thick Drusberg Mb. The latter consists of marly limestone alternating with marly intervals. The Schrattenkalk Fm is 150 m thick and is mainly composed of light grey colored massive limestone. The contact between the Drusberg

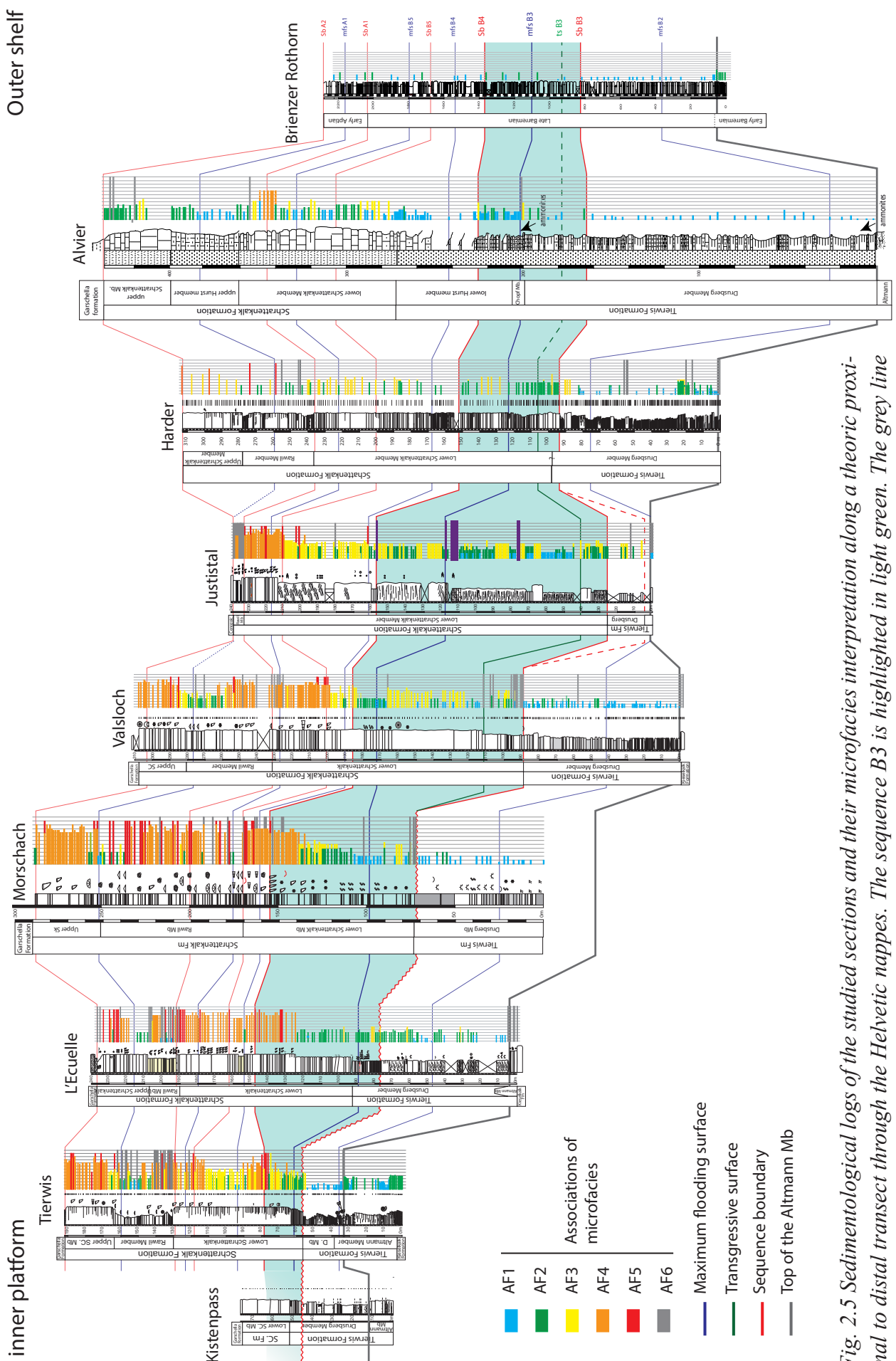


Fig. 2.5 Sedimentological logs of the studied sections and their microfacies interpretation along a theoric proximal to distal transect through the Helvetic nappes. The sequence B3 is highlighted in light green. The grey line corresponds to the top of the Altmann Mb.

Mb and the Schrattenkalk Fm is abrupt.

(2) The section of Valsloch (Fig. 2.6-B) is situated in the Churfirsten range and represents an intermediate position on the platform. The Valsloch section starts by 1m of dark sandy limestone rich in glauconite, forming the Altmann Mb, overlain by 100 m of poorly exposed marly and limestone alternations (Drusberg Mb). The Schrattenkalk Fm shows a bioclastic facies, with a horizon rich in annelids (Fig. 2.6-C), overlain by more lagoonal facies, rich in rudist remains.

(3) The section of Alvier (Fig. 2.6-D) is located on the eastern side of the Alvier Mount. It represents the distal part of the platform. This section is a composite section sampled and studied by Briegel (1972) for the upper part, in the locality of Glaennli, and by Wissler et al. (2003) at Riseten for the lower part of the section. The section starts with the Altmann Mb, where ammonites have been founded by Briegel (1972) and Bodin et al. (2006a). The Drusberg Mb consists of a 270m-thick alternation of marl and limestone, interrupted at 200m by a glauconitic horizon, rich in ammonites and belemnites, which is attributed to the Chopf Bed (Briegel, 1972; Bodin et al., 2006b). The Lower Schrattenkalk Mb is characterized by the decrease in marly beds, and the increase in bioclastic limestone.

(4) The Kistenpass section (Fig. 2.6-E) is located eastward of the Bifertenstock summit, in the Infrahelvetic complex. It represents a proximal part of the Helvetic platform. This section starts with 10m of Altmann Mb, rich in glauconitic sandstone and conglomeratic levels, overlain by 40 m of Drusberg Mb, which includes alternations of marly limestone and coquina levels rich in oysters (Fig. 2.6-G). The upper part of the section corresponds to 25 m of Urgonian-type limestone where only the basal part of the Lower Schrattenkalk Mb is preserved,

and ends by an erosional surface overlain by the Garschella Fm. Alpine deformation strongly affected the Urgonian part of the section.

(5) The borehole of Morschach is located on the golf course of Morschach, and represents an intermediate shelf position. The lower part is composed of a dark marly limestone, rich in oysters, irregular urchins and annelids. Some beds show bioturbation networks consisting of *Thalassinoides* (Fig. 2.6-F). This 75m-thick interval is attributed to the Drusberg Mb. The Schrattenkalk Fm is characterized by a 220 m-thick light grey limestone, bioclastic at the base and progressively richer in rudists and Orbitolinids.

(6) The Brienzer Rothorn section (Fig. 2.6-I) is located to the north of the Brienzer Lake, in the canton of Berne. This section is part of an overturned anticline, that represents a distal portion of the Helvetic platform. The section has been studied by Ribaux (2012) and starts with the Altmann Mb, which is 4 to 5m thick, and characterized by condensed levels and channelized, silt- and glauconite-rich limestone layers. It is overlain by more than 200 m of marly limestone–marl alternations of the Drusberg Mb. The following interval is attributed to the Rawil Mb.

(7) The section of Justistal (Fig. 2.6-J) is located on the northeastern side of the Lake of Thun. It represents an inner intermediate position on the platform. The section is precisely located in Loubenegg, in the southern part of the Valley of Justistal. Ziegler (1967) and Schenk (1992) previously studied this section. It consists of a 240m thick section, which starts with a 2m-thick glauconitic-rich dark sandy bed forming the Altmann Mb. The Drusberg Mb is missing and the following interval consists of a bioclastic limestone, attributed to the Lower Schrattenkalk Mb, interrupted by ledges of less massive limes-

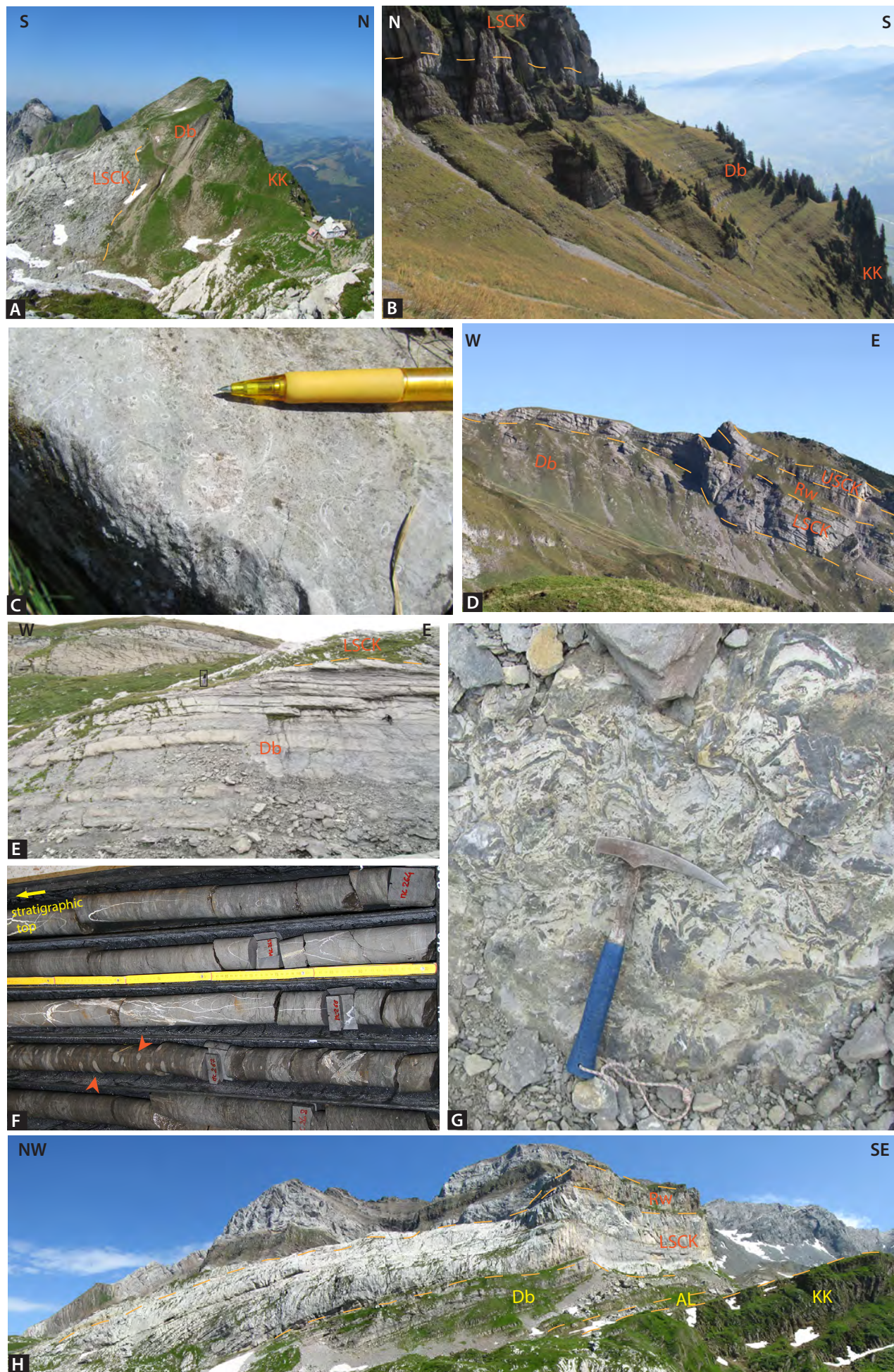




Fig. 2.6 Field photographs of the sections; KK = Kieselkalk Fm, AL = Alvier Mb, Db = Drusberg Mb, LSCK = Lower Schrattenkalk Mb, Rw = Rawil, USCK = Upper Schrattenkalk Mb. **A:** General overview of the lower part of the section of Tierwis, with the well-expressed change of competence between the Tierwis Fm and the Schrattenkalk Fm. **B:** Overview of the base of section of Valsloch. The Altman Mb is covered by vegetation. **C:** Detail of the annelid-rich interval in the section of Valsloch, in the Lower Schrattenkalk Mb. **D:** View of the section of Alvier. The right part is the upper part of the section sampled by Briegel, 1972 (Glännli). **E:** Drusberg Mb overview in the section of Kistenpass. Standing person is ca 1.9 m tall. **F:** View of a part of the core of Morschach, belonging to the Drusberg Mb (from the depth 308m to 313m). Alternation of dark marly-limestone, rich in bioturbations (arrows), and light grey limestone intervals are observable. **G:** Detail of a coquina level rich in oysters, in the marly interval of the Drusberg Mb in the Kistenpass section. **H:** General overview of the section of L'Ecuelle. **I:** Section of Brienzer Rothorn (Picture from Ribaux, 2012). **J:** Justistal section outcrop. **K:** Base of the section of Harder. **L:** Regular alternations of marls and limestones in the Drusberg Mb, in the section of Harder. **M:** Limestone banks intercalated in the hemipelagic series of the Drusberg Mb, with irregular top and base, interpreted as gravity flow deposits.

tones. The base of the Lower Schrattenkalk Mb shows channelized structures, which end by a truncation surface.

(8) The Harder section (Fig. 2.6-K) is situated on the eastern side of the cities of Interlaken and Unterseen. It represents the reversed sequence of the same overturned anticline as the section of Brienzer Rothorn. This section represents an intermediate position on the platform. The section starts with the Altmann Mb, a metric interval rich in glauconite, phosphate nodules and ammonites. This level has been studied by Ziegler (1967) and by Bodin et al. (2006a). It is covered by the Drusberg Mb, which consists of 90 m of marly limestone–marl alternations (Fig. 2.6-L) with several intercalated, calcareous banks. These beds are made of coarse grainstone and show erosive bases (Fig. 2.6-M). This interval is overlain by up to 140 m of thickly bedded carbonates assigned to the Lower Schrattenkalk Mb, which consists of bioclastic and peloidal limestone.

(9) The section of L'Ecuelle (Fig. 2.6-H) is located in the normal flank of the Morcles nappe, 2.5 km from Anzeindaz. The section represents an inner-platform position. The Altmann Mb is observed and represents 4m of coarse granular sandy limestone, overlain by 90 m of thinly-bedded marly limestone of the Drusberg Mb. The marly limestone is darkly colored and is rich in irregular urchin remains. This interval is overlain by the Lower Schrattenkalk Mb, which is characterized by a 100m-thick, rudist-rich photozoan limestone. The base of this member is affected by several faults.

(10) The panorama of the Churfisten (SG) encompasses the range between the Mount Schären (736.004/223.075) to the Mount Nideri (744.344/223.305). This panorama shows the superposition of two nappes (Säntis in upper position and Mürtschen in lower position). In

this study, only the Säntis nappe is examined. The panorama represents the transition from intermediate to distal, south eastward, parts of the platform, in a section oblique to the direction of platform progradation. The progradation of the Schrattenkalk Formation above the Drusberg Mb is observed at the base of the panorama.

2.4.1.1 Sequence B2: distribution of the facies along the Helvetic platform

The sequence B2 is latest early Barremian age, and spreads from the uppermost part of the *K. compressissima* zone to the uppermost part of the *M. moutonianum* zone. In the section of Tierwis, where the sequence stratigraphic scheme had been defined by Bodin et al. (2006a), the SB B2 is stacked with the sequence SB B1 on a hardground level above which the lithology is dominated by marls. This type of lithology and the microfacies are more coherent with the attribution of the Drusberg Mb for the interval above the hardground. In this study we propose to readjust the boundary between the Altmann Mb and the Drusberg Mb to this hardground level. This readjustment implies that the Altmann Mb ends at the SB B2.

Deposition of the Drusberg Mb occurred on the entire shelf exposed in the Helvetic nappes and maximal and minimal thicknesses in the sections analyzed here were recorded at Alvier (140 m) and Tierwis (30 m), respectively. The sequence B2 composes the entire Drusberg Mb in proximal parts and its base in distal parts. It is characterized by the presence of oyster lumachelles in the innermost part of the shelf (Kistenpass), and by hemipelagic facies (F0 to F3) in more distal areas. Figure 2.7 illustrates the qualitative/quantitative distribution of mi-

crofacies analysed in thin sections.

In the Churfirsten panorama, the sediments below SB B3, identified in the section of Valsloch, are more calcareous on the western side, and change laterally to marl towards the eastern side (Fig. 2.8). This carbonate body of the Lower Schrattenkalk Mb belonging to the HST of B2 shows eastward progradations, which reach up to the Schibenstoll. Above, the carbonate sequence B3 progrades further eastward to Tristencholben, along a distance of 2.5 km (Fig. 2.9).

In the section of Justistal, at the base of

the Schrattenkalk Fm, two clinoforms prograde south-westward, and their top is truncated. Two interpretations are possible. The first one is to consider this prograding carbonate body as belonging to the depositional sequence B2, probably the HST; the truncation surface would thus correspond to the SB B3. The second scenario is to consider that the base of the carbonate body is the base of the depositional sequence B3. At the base of the last clinoform, the beds are irregular and their morphology is similar to that of channels (Fig 2.10). In the section of Harder, the granular banks intercalated in the

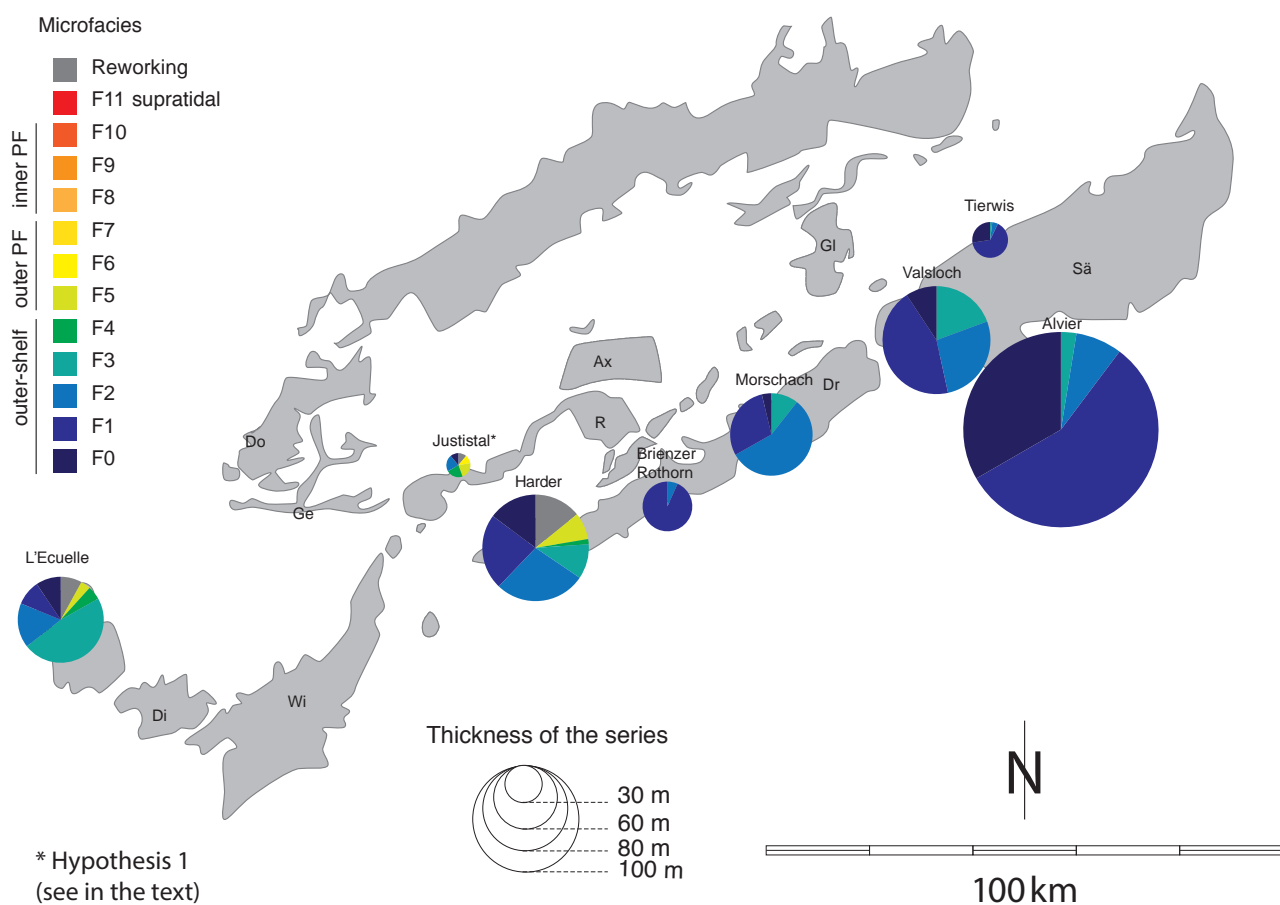


Fig. 2.7 Microfacies distribution in the sections of the sequence B2. The size of each pie chart is related to the thickness of the depositional sequence B2. Each analyzed site is plotted on the palin-spastic map of the nappes established by Trümpy (1969), Ferrazzini and Schuler (1979), and Kempf and Pfiffner (2004).

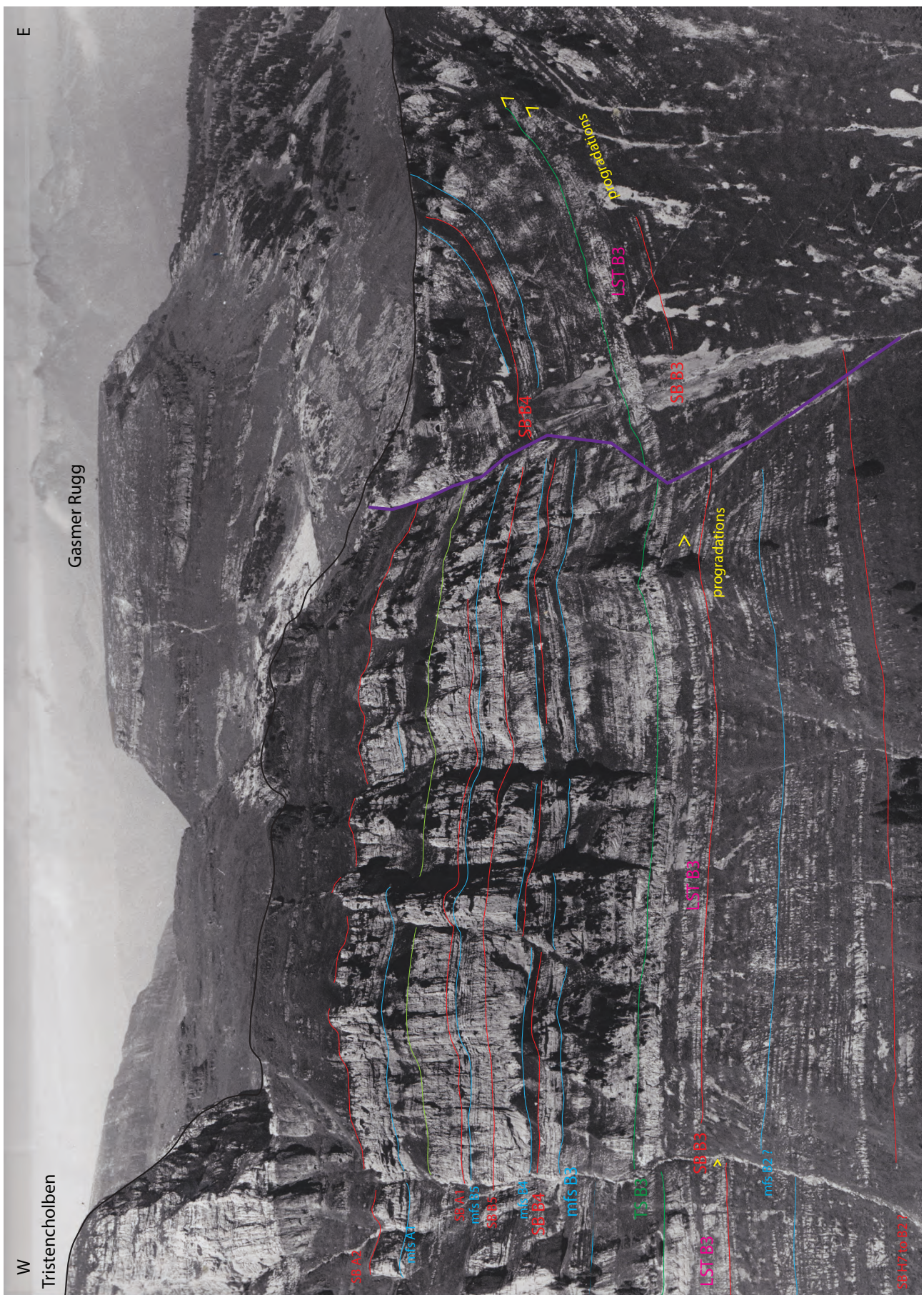


Fig. 2.8 Aerial photograph providing by Hanspeter Funk (Baden). East side of the Churfirsten panorama. Progradations of the LST B3 are pointed out.

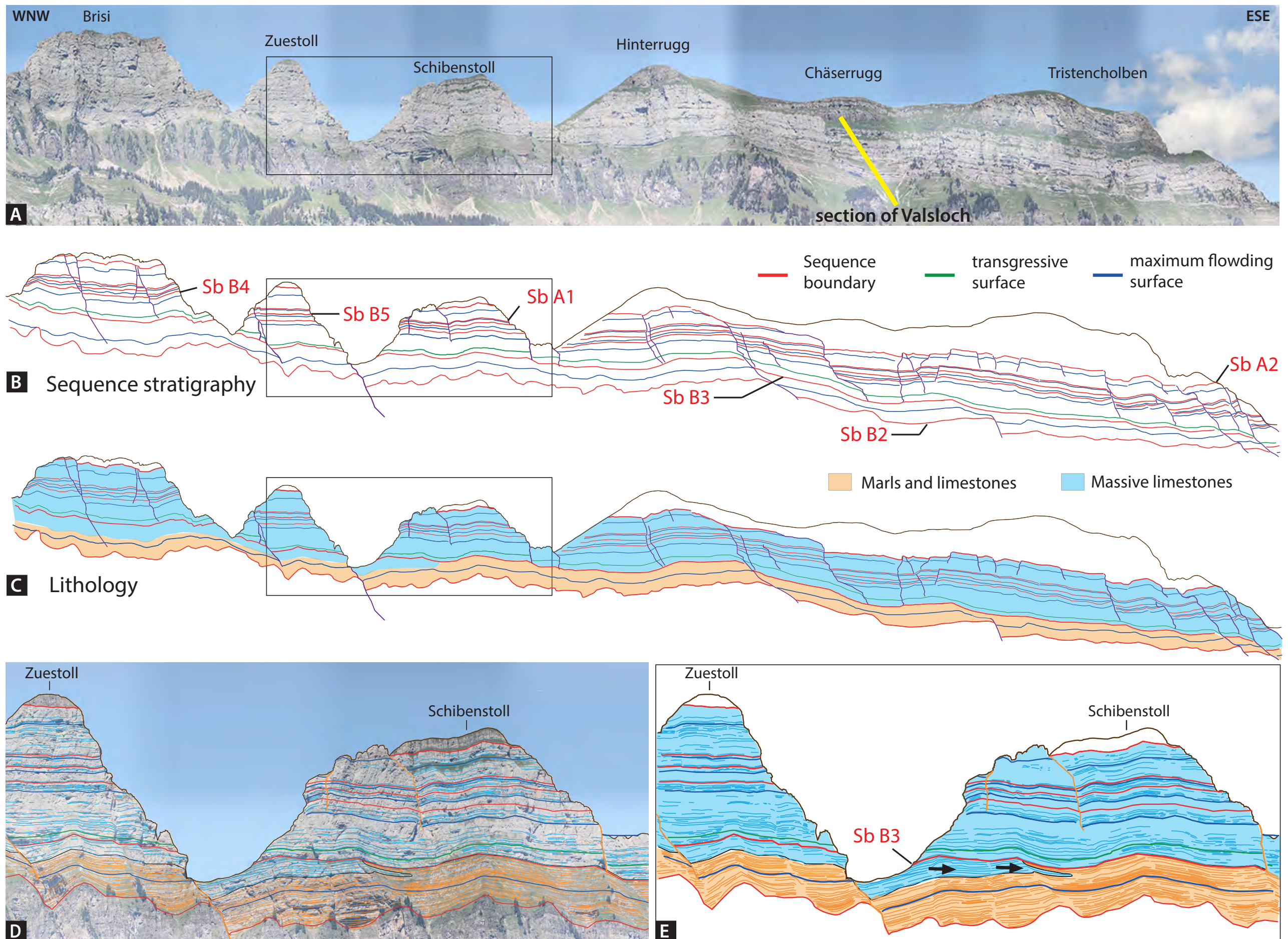


Fig. 2.9 **A**: Global overview of the Churfirsten panorama, the section of Valsloch is reported. **B**: and **C**: Interpretation of the panorama in terms of sequence stratigraphy (B) and in terms of lithology (C). **D** and **E**: Focus on the bioclastic body underneath the SB B3 (probably B2). A jump in the degree of progradation between this body and the LST B3 pointed out by a black arrow. The complete panorama is presented in Annex 6.7

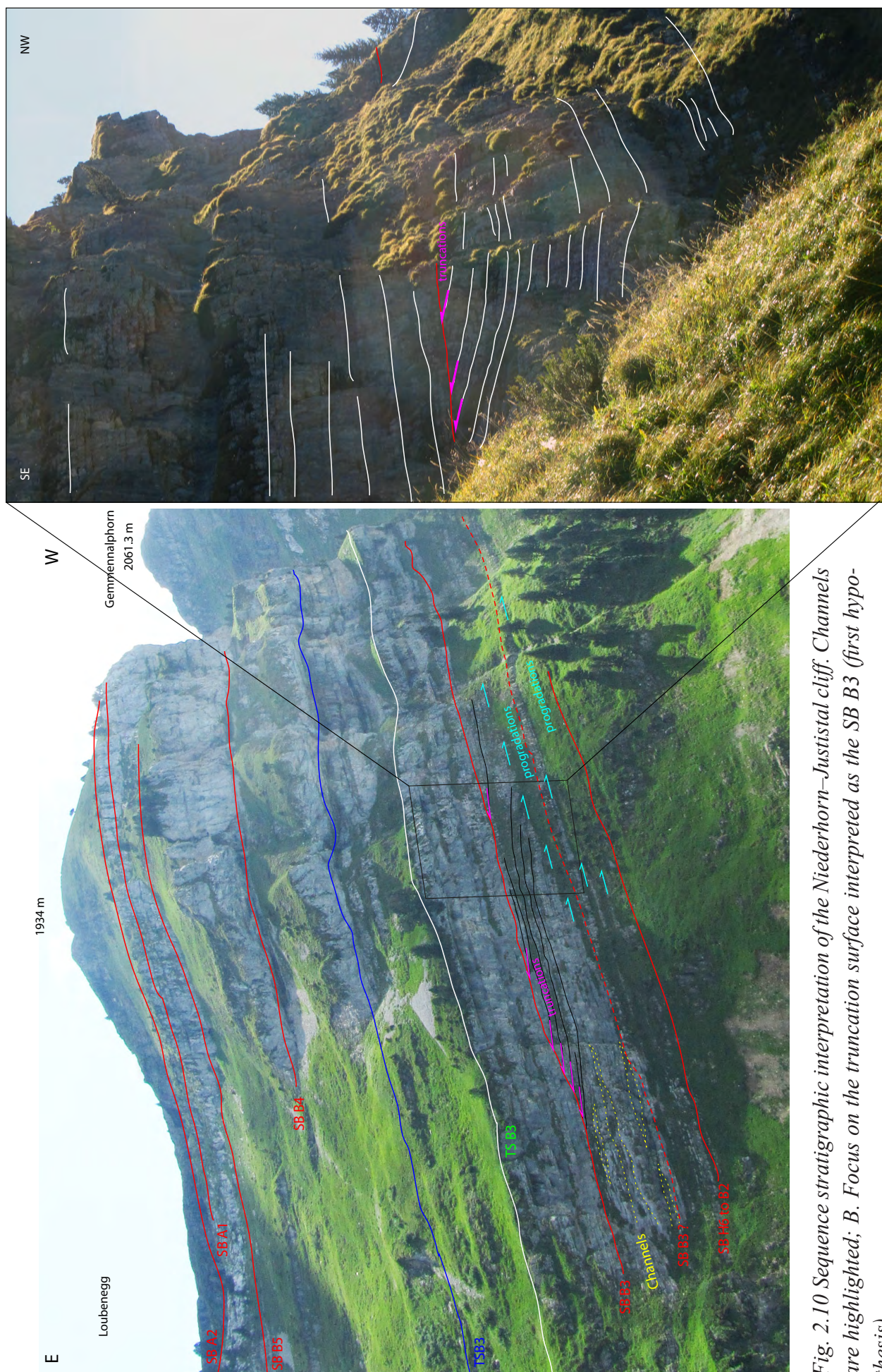
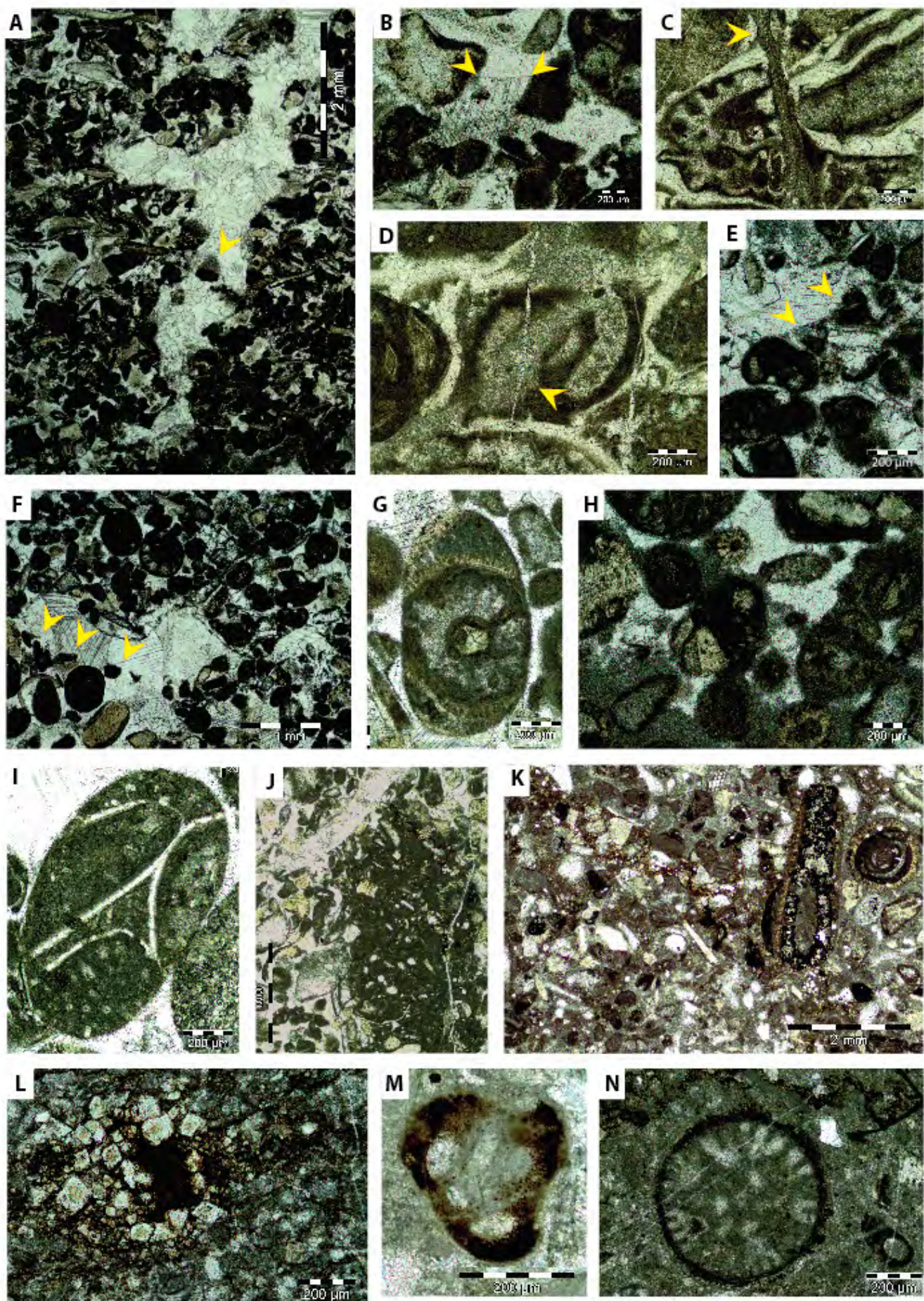


Fig. 2.10 Sequence stratigraphic interpretation of the Niederhorn-Justistal cliff. Channels are highlighted; B. Focus on the truncation surface interpreted as the SB B3 (first hypothesis).



hemipelagic successions of the Drusberg Mb are interpreted as storm-generated grainflows which were derived from a carbonate platform to the north, which developed during the deposition of B2.

2.4.1.2 Characterization of the SB B3

In proximal and intermediate parts of the inner shelf (sections of Tierwis and L'Ecuelle, and the core of Morschach) the contact between the hemipelagic sediments of the Drusberg Mb and the shallow-water carbonates of the Lower Schrattenkalk Mb represents an emersion surface. In the section of Tierwis, the top of the Drusberg Mb is represented by a 5m-thick bed of marls, covered by an early cemented, fractured grainstone. These fractures are filled by mud suggesting a synsedimentary origin for the fractures. The presence of micro-paleofractures and early infilling is an evidence of emersion and early cementation (Fig. 2.11-C and D). In the section of L'Ecuelle, facies types F3 and F4 facies are present in the upper part of the sequence B2 and in the base of the sequence B3. However, at 75m from the base of the Drusberg Mb, we observe a paleosol with rootcasts associated with partial early dissolution and a vadose silt present in the root molds. This paleosol had been interpreted

as the SB B3 (Fig. 2.11-A and B). In the section of Morschach, the Drusberg Mb is interrupted and covered by a bioclastic limestone showing various extraclasts from different origins: oolitic wackestone, orbitolinid-rich or calcisphere-rich packstone (Fig. 2.11-G, I and J). This level corresponds to a lag. The grainstone is early cemented and partially dissolved (Fig. 2.11-E and F). The shallow-water deposits are composed of a laminated tidal grainstone showing early cementation with meniscus cement (Fig. 2.11-H).

In more external parts of the Helvetic shelf, the evidence of the location of the SB B3 is given by lag deposits showing a mix of different types of grains. It is essentially marked by the presence of shallow-water grains in an outer-shelf matrix. This is the case in the section of Valsloch (Fig. 2.11-K). In the section of Harder, the deposition of granular facies above hemipelagic sediments (F1 and F2) supports the intense reworking of the grains. The presence of elements surrounded by a coating of iron oxide suggests that the reworked material was derived from soils (Fig. 2.11-L, M and N). In the sections of Alvier and Brienzer Rothorn the SB B3 is placed on top of the first occurrence of shallower facies. In Brienzer Rothorn, the position of the SB B3 is related to the decrease of the detrital index and the increase of the limestone to marl ratio (Ribaux, 2012).

Fig. 2.11 Microphotographs illustrating emersion associated with the SB B3; A: Root molds through a wackestone of microfacies F4, the arrow shows the vadose silt infilling (L'Ecuelle section; EC 47); B: Early dissolution of a cement (L'Ecuelle section; EC 47), C and D: Paleofractures (Tierwis section; TW 3); E and F: Truncation of grains by early dissolution (Morschach section; MC 227); G, I and J: pebbles of various origin (G: oolitic limestone; I: packstone with orbitolinidae; J: wackestone with spicules and calcispheres; Morschach section; MC 227); H: Meniscus cement (Morschach section; MC 225); K: Lag deposit containing large oolites in a deeper-water matrix (Valsloch section; VA 225); L: root traces (Harder section; HA 189); M and N: ferrous grains from a palaeosol (Harder section; HA 188).

2.4.1.3 Depositional geometries associated with the SB B3

In the proximal part of the platform, the SB B3 is marked by an abrupt change in lithology. This is the case for the Tierwis and Kistenpass sections. In the panorama of the Churfirsten, the SB B3 is associated with a jump in the progradation at the base of the calcareous cliff, between the HST B2, which ends in the western side of the Schibenstoll Mt, and the LST which ends eastward, on the eastern side of the Tristencholben Mt (Fig. 2.9).

In the case that the prograding cliniforms at the base of the section of Justistal belong to sequence B3, they can be interpreted as the lower part of the LST, which consists of slope fan and basin floor fan sediments (Fig. 2.10). The presence of this type of carbonate bodies attests that there is enough available space for the accumulation of granular sediments and their progradation. For these reasons, the section would be located on the platform margin or the upper slope. Nevertheless, the presence of granular facies reworked in the more external section of Harder (Fig. 2.6-M) in the sequence B2 argues for the interpretation of this body of Justistal as the HST of the sequence B2.

2.4.1.4 Description of the sequence B3 in the reference section of Valsloch and its sequence stratigraphic interpretation

The section of Valsloch is chosen as a reference section for the depositional sequence B3. The complete sedimentologic log is illustrated in Figure 2.12. Overlying almost 90 meters of hemipelagic deposits, a 10 m-thick, massive bed exhibits a succession of microfacies types from

F0 to F3 (Fig. 2.3-A, B, C and D), and evidence for lag deposits. This interval is composed of reworked grains such as oolites, orbitolinids, green algae, large-size miliolids, extraclasts and pebbles in a matrix rich in circalittoral foraminifera, spicules and echinoids (Fig. 2.3-P). Following this interval, a 50m-thick succession of bioclastic facies was deposited. The sediment is essentially composed of grainstone/packstone (microfacies F5 and F6; Fig. 2.3-H and I), with packstone intercalations, which contain more external fauna (microfacies F2 and F4; Fig. 2.3-C and G). The last meters of sediment are richer in oolites, but contain also many coral fragments and calcareous algae. The granular facies is sharply covered by a 20m-thick bed of wackestone, rich in colonial and isolated annelids, Choffatella and Eopalorbitolina transiens (microfacies F3a and F3b; Fig. 2.3-E and F). It is followed on top by the reoccurrence of granular facies (microfacies F5), overlain by outer lagunal facies (microfacies F7, F8; Fig. 2.3-J and K), which is rich in corals, chaetetidae, red algae and encrusting bryozoans at the base. Above, the sediments are dominated by rudists and miliolids. The top of the sequence B3 displays superficial karst with early dissolution features. The entire sequence has a thickness of 95 m.

The contact between the hemipelagic sediments and the lag deposits is interpreted as the SB B3. The basal part, which exhibits reworked facies, is attributed to the LST. The analysis of the panorama of the Churfirsten confirms this interpretation (Fig. 2.8 and 2.9).

The beds associated with LST B3 show indeed a maximum in basinward progradation in comparison to the over- and underlying beds. Following on top, the backstepping of the massive, bioclastic limestones is interpreted as the TST. The uppermost part of the TST, the mfs and the early HST are represented by wackestone.

Valsloch Churfirsten

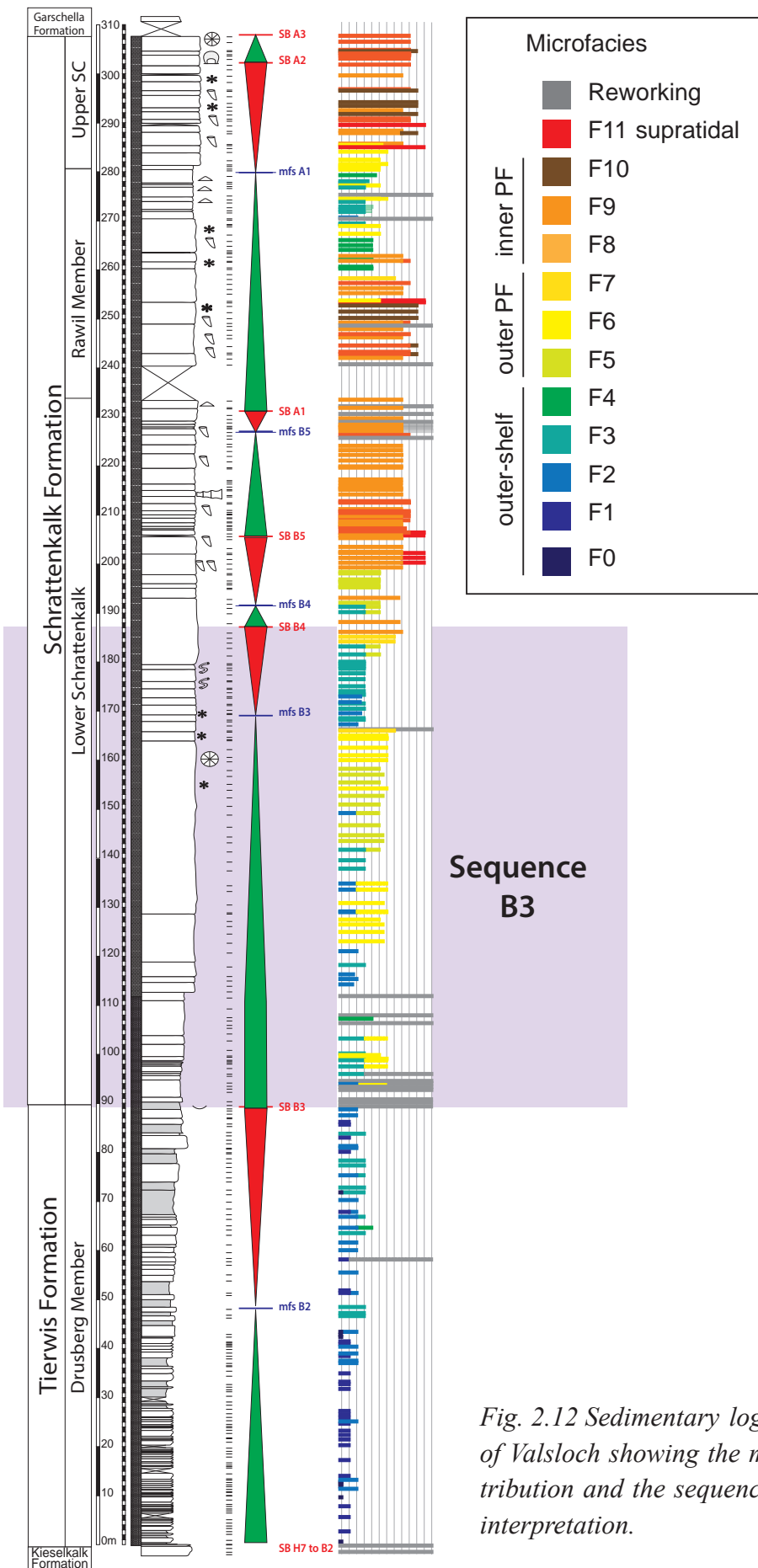


Fig. 2.12 Sedimentary log of the section of Valsloch showing the microfacies distribution and the sequence stratigraphic interpretation.

The HST is characterized by shallower facies and by the installation of lagoonal conditions. The SB B4 is identified based on the occurrence of emersion features.

2.4.1.5 Characterization of the LST B3

The LST is recorded in the sections located in intermediate and distal positions, especially those of Valsloch, Justistal and Harder. It consists of bioclastic accumulations (grainstone/packstone), showing various geometries and progradations. In the panorama of the Churfirsten (Fig. 2.8), the LST shows a maximum of progradation. Each bed grades basinward into marly-limestone and marl. In the section of Justistal, the beds above the truncation surface are composed of granular facies. In the Harder section, the first beds are forming a cliff, and are made of wackestone (allochthonous grains reworked into the mud). In the most distal sections, the characterization of the LST is not clear, due to the monotonous hemipelagic succession.

2.4.1.6 Description of the TST B3

In proximal part of the platform, the TST is extremely thin (only a few meters in Tierwis), and shows shallow-water facies at its base. The first beds include tidal laminations in granular facies. A rapid deepening-upward trend is then observed, with the deposition of F3 facies (wackestone).

In intermediate areas of the platform, the TST is characterized by recessive cliffs, made of decimetric beds of cross-bedded limestone. Its base is dominated by granular facies (F5, F6), mixed with more external facies (F2, F3). The deepening-upward trend is documented by the

increasing dominance of outer-shelf facies. In the section of Harder, the first granular beds are associated with downlap terminations, and we observe the presence of erosional scars on the slope (Fig. 2.13). In distal parts of the shelf, the LST and TST are characterized by hemipelagic facies composed of facies types F1, F2 and F3. In the section of Alvier, more and more marly beds are intercalated in the TST.

2.4.1.7 Characterization of the mfs, HST B3 and SB B4

The mfs of the depositional sequence B3 is indicated by the deepest facies recognized in the sections. The type of facies depends of the paleogeographic position of the section along a proximal to distal transect. In more distal settings, the deepening of the environment is marked by a reduced sedimentation rate, leading in certain places to the deposition of a condensed glauconitic and phosphatic interval, the Chopf Member. Ammonites are diagnostic of the *G. sartousiana* zone (Bodin et al. 2006b), which confirms the attribution of the mfs B3 for this member.

Above the mfs, facies constitutive of the HST also varies as a function of the paleogeographic position. In the inner and intermediate parts of the platform, a large accumulation of colonial and isolate annelids, associated with the occurrence of *Eopalorbitolina transiens* and *Choffatella*, is characteristic. This fauna association reflects dysoxic and mesotrophic conditions (Martínez-Taberner et al., 1993; Fornós et al., 1997). From the bottom to the top, facies usually evolve from oolitic and coral reef facies to lagoonal facies with rudists and confined environments. In the section of L'Ecuelle, oolitic facies is missing, so that confined lagoonal facies rich

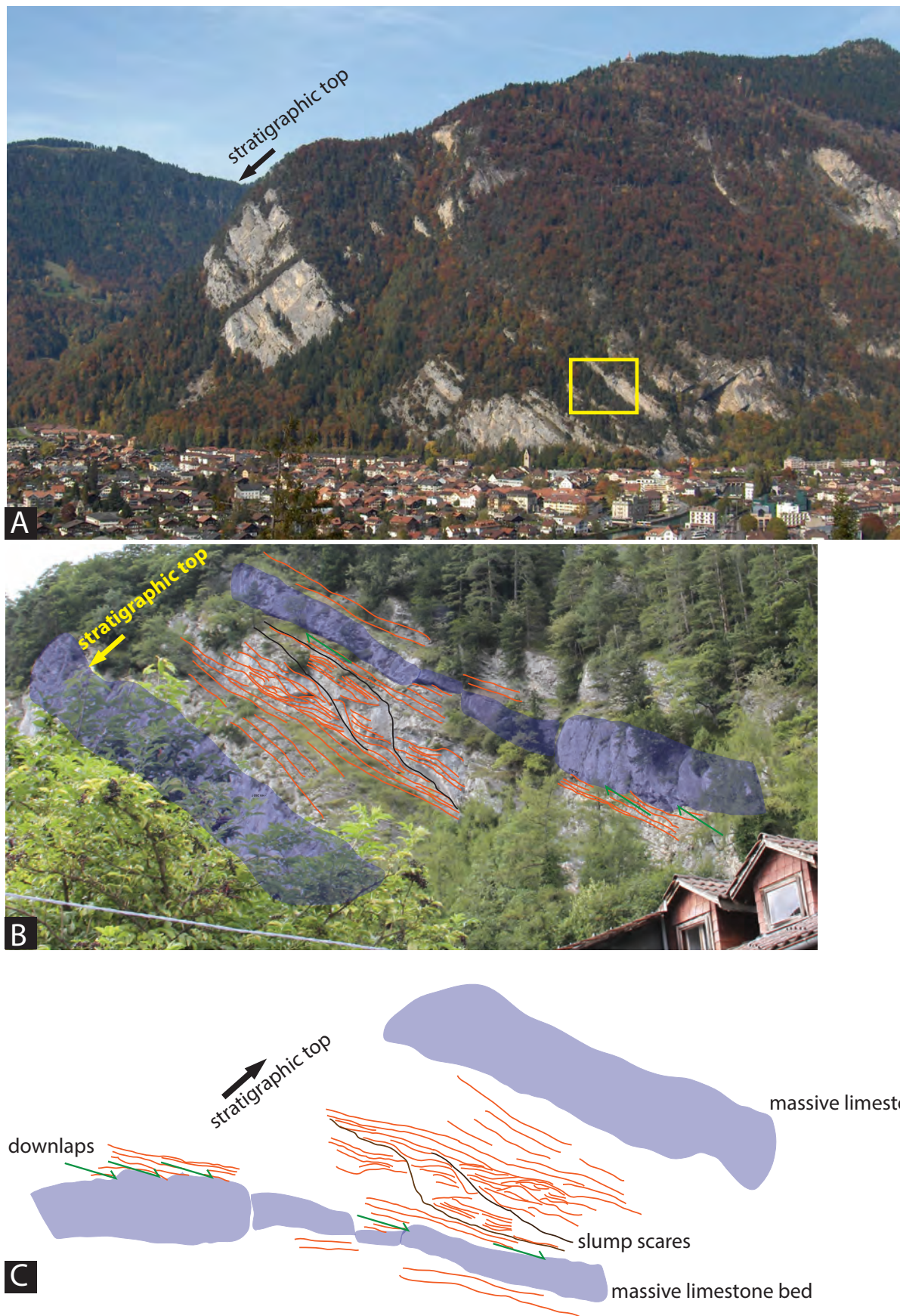


Fig. 2.13 Section of Harder. **A:** global view of the section of Harder, the section is overturned; the outlined area is detail in **B** and **C**. **B:** photo of the slump scars and progradations in the TST B3, overturned. **C:** scheme in the stratigraphic sense of the slump scars and downlaps of the marly limestones beds on the massive limestone bed.

in oncolids and beach deposits follow directly the mfs.

The depositional sequence B3 ends with shallower facies, exhibiting emersion and paleo-

sol features in the proximal part of the platform. The sections of L'Ecuelle and Valsloch show a superficial karst, which penetrates down to ca. 15 m below the SB B4 (Fig. 2.14-A, B). In the sections of Tierwis and Morschach, indications

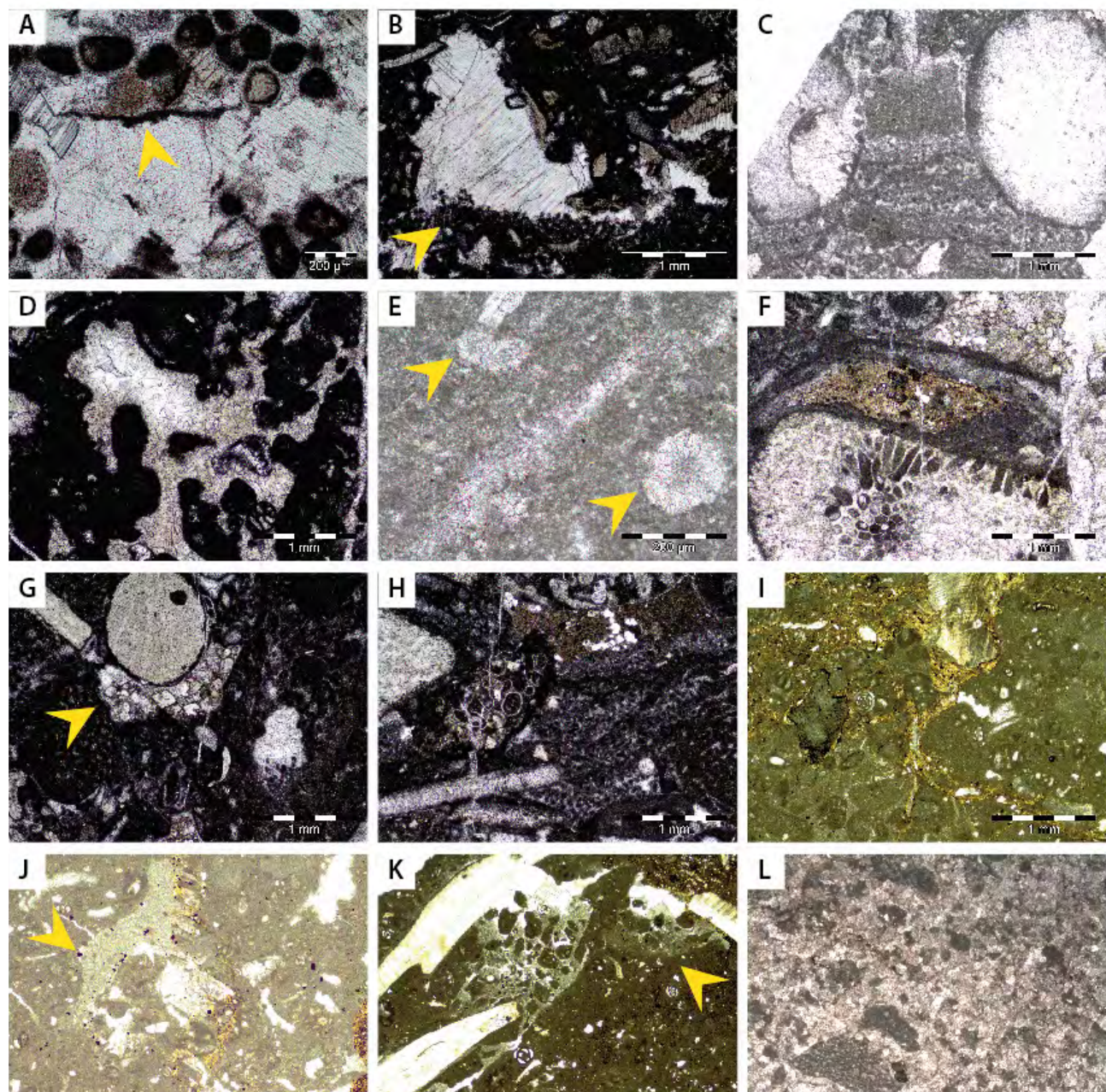


Fig. 2.14 Microphotographs illustrating the emersion associated with the SB B4; **A:** early dissolution, filled by endostromatolites (Valsloch section; VA 139); **B:** early dissolution, filled by microbial peloids (Valsloch section; VA 141); **C** and **H:** polyphase karstic infilling (Tierwis section; TW 34); **D:** amber meteoric cement (Tierwis section; TW 36); **E:** pedogenic cement in rosette (Tierwis section; TW 35); **F** and **I:** green marl associated with soil deposit (Tierwis and Morschach sections; TW 34 and MC 153); **G:** dolomitic infilling of early dissolution pocket (Tierwis section; TW 34); **J:** root trace (Morschach section; MC 152); **K:** epikarstic features (Morschach section; MC 152); **L:** dolomitic facies (Harder section; HA 251).

for dissolution are associated with paleosol features, such as root traces, deposition of green marls, and pedogenic cement (arranged in rosettes similar to *Microcodium*), illustrated in Figures 2.14-C, E, F, G, H, I and J. In the section of Tierwis, the last meters of the sequence B3 exhibit meteoric amber cement (Fig. 2.14-D). In the sections of Justistal and Harder, in the intermediate part of the platform, the top of this sequence is marked by intense dolomitization of the facies (Fig. 2.14-L). In Justistal, dissolution features are present and bioturbations are filled by dolomitic cement. In the distal part of the platform, the position of this boundary is hard to define. In Alvier, the SB B4 is placed above the bed showing a maximum of reworking of very shallow facies coming from the platform. In Brienzer Rothorn, the SB B4 is placed based on the variation of the microfacies, and in par-

ticular on the ratio of circalittoral foraminifera versus spicules (Ribaux, 2012), which decreases below the SB B4. It is also confirmed by the clay mineralogy, which shows a peak in the ratio of kaolinite versus smectite in this level (Ribaux, 2012). This key feature is well correlated with the Angles section from southwestern France (Godet et al., 2008).

2.4.2 Evolution of the depositional sequence B3 along the platform

The distribution of the facies constitutive of the sequence B3 is presented in Figure 2.15, and allows the distinction of three main areas. The first area represents the inner part of the platform, where the sections of Tierwis

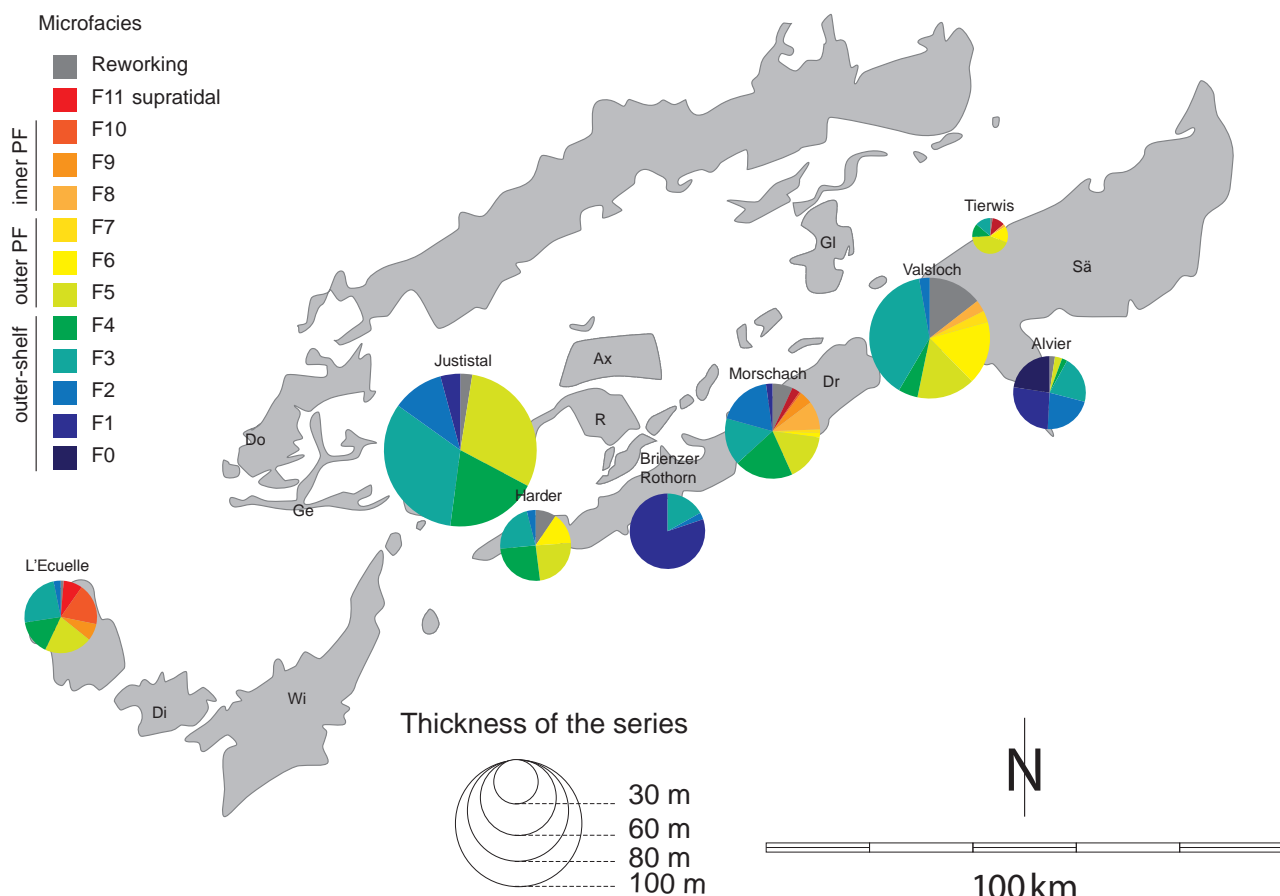


Fig. 2.15 Microfacies distribution of the depositional sequence B3 (see caption in Fig. 2.6).

(20m) and L'Ecuelle (60m) crop out. These successions are the thinnest and are characterized by the dominance of lagoonal and supratidal facies (more than 50%). The second area represents the intermediate part of the platform. Two groups of sections belong to this area: the first group ends with lagoonal deposits (sections of Morschach and Valsloch, where sequence B3 is 80m and 100m thick, respectively); the second group is composed of outer-shelf facies (F1 to F6) and grainstone/packstone with reworked platform grains (sections of Justistal and Harder, thicknesses of 130 m and 60 m for the B3 sequence, respectively). These latter sections show between 25 and 50% of shallow-water facies. The third area is the most distal one. It is part of the southern region of the nappes. It is characterized by the dominance of hemipelagic to circalittoral facies (F1 to F3). The sections of Alvier (60m) and Brienzer-Rothorn (60m) are representative of this area. The section of Brienzer-Rothorn represents the most external position of all sections studied and does not exhibit shallow-water carbonate platform deposits. The section of Alvier is mainly composed of hemipelagic to circalittoral facies (F0 to F3), and shows some granular facies F4 and F5, which are a mixture of in-situ and reworked grains coming from the inner platform.

To summarize, the thickness of the sequence B3 is minimal in landward and basinward directions, and maximal in the intermediate part of the shelf.

2.5 Interpretations

2.5.1 Depositional model

Following the condensation phase documented by the Altmann Mb, a phase of widespread hemipelagic sedimentation set in on the entire Helvetic realm. Landward, oyster lumachelles are interbedded within hemipelagic deposits. These deposits are early Barremian in age, and are part of the Drusberg Mb., which maximum thickness is observed seaward at Alvier for the sections investigated here (Fig. 2.11). The open-marine fauna of the Altmann Mb and the deposition of the hemipelagic Drusberg Mb indicates a relatively high sea level during the earlier Early Barremian. The presence of shallow-water carbonate in the HST of sequence B2 in proximal sections indicates the installation of a carbonate platform in proximal part of the Helvetic realm. The SB B3 documents a phase of important sea-level fall, leading to emersion on the inner part of the platform. In intermediate domains, the presence of bioclastic beds containing reworked shallow-water grains attests that carbonate shallow-water sedimentation occurred on the inner shelf.

The SB B3 is marked on the inner shelf by erosion and soil formation, on top of the hemipelagic facies of the Drusberg Mb, illustrating a time lag. On the outer platform, the hemipelagic facies record is continuous during this time. The transition between the inner and the external part of the shelf is extremely short (ca. 40 km between the sections of Tierwis and Alvier). This suggests a peculiar paleotopography of the shelf, with a steeper slope dividing the inner and outer shelf, which may have been triggered by syndimentary faulting, as was proposed by Trümpy (1980) for the eastern part of Switzerland. This author suggested the presence of a listric fault between the Säntis and Alvier sections, active until the Early Barremian. He demonstrated an important variation in subsidence rates in different places of the Helvetic shelf during the Early

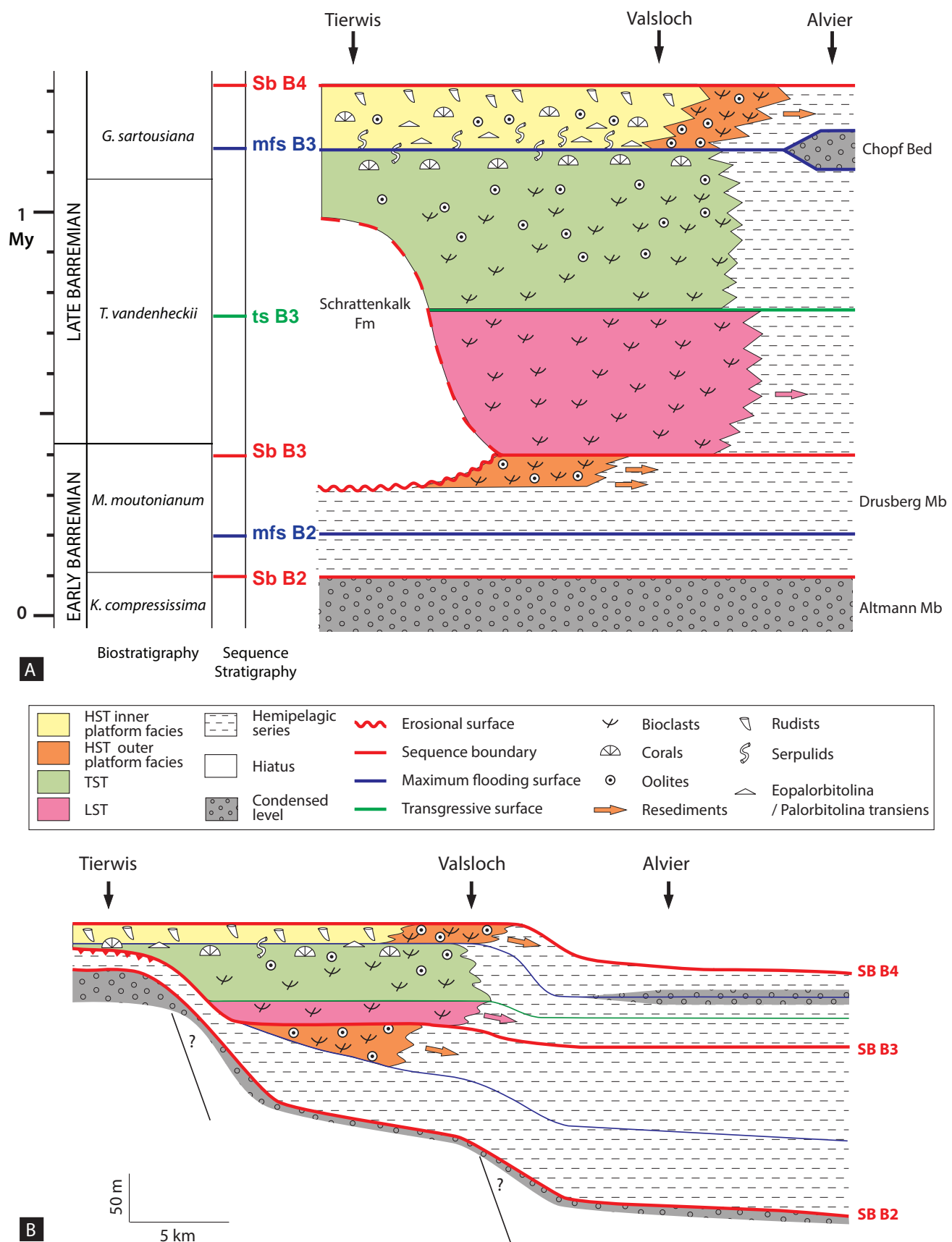


Fig. 2.16 A: Temporal and **B:** spatial representations of the depositional model of the uppermost lower Barremian – lower upper Barremian series in the Säntis nappe. (Biostratigraphy from Reboulet et al., 2011)

Cretaceous, and linked these observations with observed abrupt facies changes to assume the presence of tilted blocks.

The sequence B3 started with the deposition of the granular LST in intermediate parts of the shelf. The section of Justistal offers some specificities on the facies distribution within the LST. The section is dominated by granular facies. Ziegler (1967) explained that this type of facies was deposited on the top of tilted blocks. Nevertheless, the presence of granular facies at the base suggests that accommodation space was available to allow the deposition of the LST. However, the maximum thickness of the depositional sequence B3 is recorded in this section, suggesting that the accommodation rate was high, which is contradictory with the hypothesis of a paleotopographic high. The fact that the Drusberg Mb is not present in this section can be explained by the position of this section on the slope, explaining that a part of Drusberg Mb was exported basinward by gravity and storm-generated flows. The presence of several flow deposits in the section of Harder supports this hypothesis.

Shallower facies was deposited on top of LST B3. The accumulation of oolites preceded the development of corals and rudists in the inner and intermediate part of the platform. The maximum progradation of the sequence B3 occurred at this time, since reworked grains were found in the section of Alvier. Figure 2.16 summarizes the temporal (2.16-A) and spatial (2.16-B) evolution of this platform on a proximal to distal transect in the Säntis nappe.

The period of low sea-level documented in LST B3 is followed by an important transgressive phase, which is associated with the landward development of onlaps and the deposition of shallow-water granular facies above the emersion surface. The highest accumulation rate

occurs in the intermediate part of the platform. The deepening of the depositional environment through the whole shelf marks the maximum of marine transgression. In inner and intermediate locations, the organisms present in this interval are characteristic of mesotrophic environments, in particular indicated by the presence of isolated and colonial annelids and flat orbitolinids. This assemblage was already described in sequence B3 of the Vercors and Chartreuse area by Arnaud Vanneau (1980) and Arnaud (1981). Today, annelids prefer environments rich in organic matter, which may be dysoxic (Martínez-Taberner et al., 1993; Fornós et al., 1997, Hfaiedh et al., 2013). Total phosphorus contents show an enrichment in the corresponding sediments in L'Ecuelle and Valsloch, which indicate enhanced trophic conditions (see Chapter 3). The presence of the phosphatic and glauconitic Chopf Bed in the outer-shelf environment corresponding to the mfs of B3 embodies the macroscopic expression of the overall phosphorus enrichment during this transgressive time interval. We observe the same phenomenon in sediments characterized by important Orbitonilid accumulations in the Tethys, which are linked to the two major early Aptian transgressions. In our study area, we recognize those in the Rawil Mb (also called the Lower Orbitolina beds) and the Grünten Mb (Upper Orbitolina beds). In both cases, these transgressions are associated with increased detrital and nutrient input. The presence of the condensed phosphatic Chopf Bed and this comparison allow us to postulate that the transgression related to the sequence B3 was important and induced higher trophic levels and a possible diminution in oxygen conditions on the carbonate platform.

The sequence B3 is illustrated by the landward migration of the depocenter (Justistal, Valsloch, Morschach, L'Ecuelle). The thickness of the sequence B3 and its sediment and faunal

composition reflect the dynamic of deposition. In the proximal part of the platform, the sequence is extremely thin (30m in Tierwis). This is due to the late flooding of the area during the transgression of the TST, reflected by the only presence of the top TST, directly overlain by deep facies. In the intermediate realm, important accommodation space is present, which allows the deposition of granular limestone (F5, F6) forming the LST and a part of the TST with a thickness up to 140 m in Justistal and 95m in Valsloch. In the distal part of the platform, the entire sequence is characterized by hemipelagic facies (F0 to F3), showing a low sedimentation rate. In this domain, the thickness of this sequence does not exceed 60m.

2.5.2 The onset of the Urgonian platform

The installation of the Urgonian-type carbonate platform documented by the Schrattenkalk Fm in the Helvetic nappes was considered as gradual for a long time (Funk et al., 1993; Föllmi et al., 2007). In fact, the installation of this platform is not gradual and its history has two aspects: landward the installation of shallow water carbonate occurred without transition above an emersion surface. In the intermediate and distal part, there are resedimented bioclastic deposits forming a lowstand prograding wedge which prograde basinward (Justistal, Valsoch). This type of geometry indicates a paleotopography where the intermediate part corresponds to a slope sufficiently flooded to allow the deposition of a lowstand systems tract. This first depositional sequence is named B3. From a proximal to a distal direction, the maximum thickness is located in the intermediate part, and the mi-

nimum thicknesses are found in landward and basinward directions. The geometry is similar to the classical model defined by Vail et al. (1977) used in sequence stratigraphy.

Once installed, the platform was subjected to enhanced nutrient input during important transgression from which it was able to recover during the following sea-level highstand, where it developed oolite shoals, followed by the installation of coral patch reefs and a lagoon with rudists, which became more and more restricted.

The transgression documented by the TST B3 may have induced the deposition of organic-rich sediments in the Lower Saxony Basin (Mutterlose et al., 2010), and may be related to a minor positive excursion in the carbon-isotope record (Erba et al., 1999; Godet et al., 2006). An important transgression is also indicated for the early late Barremian in the most recent sea-level chart by Haq (2014).

The end of this sequence is associated to a phase of sea level fall. The associated regression is estimated at least at 15 m below the base level and attested by the development of karstification in internal and intermediate parts of the platform.

2.6 Conclusions

The installation of the Urgonian-type Schrattenkalk Formation in the Helvetic nappes was since long considered as gradual. This study reveals the presence of complex geometries for the basal part of this formation, which were triggered by the paleotopography and relative sea level variations. The depositional sequence B3 appears to be the key to understand the transition from the hemipelagic sedimentation documented by the Drusberg Mb to the shallow-water car-

bonate sedimentation of the Schrattenkalk Mb. This sequence records a phase of important sea level fall during the Barremian, which lead to the emersion of hemipelagic sediments in the inner part of the platform, and to the deposition of a lowstand systems tract in the intermediate and distal domains. This depositional sequence registers also the most important transgression of the Barremian, with a flooding of the entire platform. The specificity of the faunal assemblage deposited during the transgression B3 constitutes a major stratigraphic tool for sections of internal and intermediate locations and an indicator of the increase of nutrient input linked to the transgression. This transgression is followed by the deposition of shallow-water platform carbonates rich in corals and rudists. The end of this sequence is associated with an important phase of filling of the accommodation space and is followed by a phase of sea level fall. This fall is estimated at least at 15 m below the base level, as attested by the karstification features in internal and intermediate part of the platform.

2.7 References

- Amodio, S., Ferreri, V. and D'Argenio, B.** (2013) Cyclostratigraphic and chronostratigraphic correlations in the Barremian–Aptian shallow-marine carbonates of the central-southern Apennines (Italy). *Cretaceous Research*, **44**, 132–156.
- Arnaud, H.** (2005) Sequence stratigraphy interpretation. In: *The Hauterivian-Lower Aptian sequence stratigraphy from Jura Platform to Vocontian Basin: A multidisciplinary approach* (Eds T. Adatte, A. Arnaud-Vanneau, H. Arnaud, M.-C. Blanc-Alétrou, S. Bodin, E. Carrio-Schaffhauser, K.B. Föllmi, A. Godet,

- M.C. Raddadi and J. Vermeulen), *Géologie Alpine, Série Spéciale «Colloques et Excursions» N°7*, pp. 174–179.
- Arnaud, H. and Arnaud Vanneau, A.** (1989) Séquence de dépôt et variations du niveau de la mer au Barrémien et à l'Aptien inférieur dans les massifs subalpins septentrionaux et le Jura (Sud-Est de la France). *Bulletin de la Société Géologique de France*, **V**, 651–660.
- Arnaud, H. and Arnaud-Vanneau, A.** (1991) Les calcaires urgoniens des Massifs subalpins septentrionaux et du Jura (France): âge et discussion des données stratigraphiques. *Géologie Alpine*, **67**, 63–79.
- Arnaud, H., Bulot L. and Arnaud-Vanneau, A.** (1994) Stratigraphie séquentielle de l'Aptien et de l'Albien sur la transversal Pico Garcia–Casanay (Venezuela oriental), *rapport Aguasuelos*, 77p.
- Arnaud, H., Flood, P.G. and Strasser, A.** (1995) Resolution Guyot (Hole 866A, Mid-Pacific Mountains): Facies Evolution and Sequence Stratigraphy. In: *Proc. ODP, Sci. Results*, **143** (Ed S.W.W. Winterer E. L., Firth, J. V. and Sinton, J. M.), pp. 133–159, College Station, TX.
- Arnaud, H., Arnaud-Vanneau, A., Blanc-Alétrou, M.-C., Adatte, T., Argot, M., Delanoy, G., Thieuloy, J.-P., Vermeulen, J., Virgone, A., Virlouvet, B. and Wermeille, S.** (1998) Répartition stratigraphique des orbitolinidés de la plate-forme urgonienne subalpine et jurassienne (SE de la France) *Géologie Alpine*, **74**, 87 p.
- Arnaud, H., Arnaud-Vanneau, A., Bulot, L.G., Beck, C., MacSotay, O., Stephan, J.-F. and Vivas, V.** (2000) Le Crétacé inférieur du Venezuela oriental : stratigraphie séquentielle des carbonates sur la transversale Casanay-Maturín (Etats de Anzoátegui, Monagas et Sucre). *Géologie Alpine*, **76**, 3–81.

- Arnaud-Vanneau, A.** (1980) Micro-paléontologie, paléoécologie et sédimentologie d'une plate-forme carbonatée de la marge passive de la Téthys : l'Urgonien du Vercors septentrional et de la Chartreuse (Alpes occidentales). *Géologie Alpine, Grenoble Mém HS* **11**, 874 p.
- Arnaud-Vanneau, A. and Arnaud, H.** (1990) Hauterivian to Lower Aptian carbonate shelf sedimentation and sequence stratigraphy in the Jura and northern Subalpine chains (southeastern France and Swiss Jura). In: *Carbonate Platforms: Facies, Sequences and Evolution* (Eds M.E. Tucker, J.L. Wilson, P.D. Crevello, J.R. Sarg and J.F. Read), **9**, pp. 203-233. Blackwell Scientific Publications, Special Publication of the International Association of Sedimentologists.
- Arnaud Vanneau, A. and Sliter, W.V.** (1995) Early Cretaceous shallow-water benthic foraminifers and fecal pellets from Leg 143 compared with coeval faunas from the Pacific Basin, Central America, and the Tethys. In: *Proc. ODP, Sci. Results, 143* (Ed S.W.W. Winterer E. L., Firth, J. V. and Sinton, J. M.), pp. 537-564, College Station, TX.
- Barragan-Manzo, R. and Diaz-Otero, C.** (2004) Analisis de microfacies y datos micropaleontologicos de la transicion Barremiano-Aptiano en la Sierra de Rosario, Durango, Mexico. *Revista Mexicana de Ciencias Geologicas*, **21**, 247-259.
- Bodin, S., Godet, A., Vermeulen, J., Linder, P. and Föllmi, K.B.** (2006a) Biostratigraphy, sedimentology and sequence stratigraphy of the latest Hauterivian – Early Barremian drowning episode of the Northern Tethyan margin (Altmann Member, Helvetic nappes, Switzerland) *Eclogae geologicae Helvetiae*, **99**, 157-174.
- Bodin, S., Vermeulen, J., Godet, A. and Föllmi, K.B.** (2006b) New data on the age of the installation of Urgonian-type carbonates along the northern Tethyan margin: biostratigraphy of the Chopf Member (Helvetic Alps, eastern Switzerland). *Comptes Rendus Geoscience*, **338**, 7.
- Bodin, S., Godet, A., Föllmi, K.B., Vermeulen, J., Arnaud, H., Strasser, A., Fiet, N. and Adatte, T.** (2006c) The late Hauterivian Faraoni oceanic anoxic event in the western Tethys: Evidence from phosphorus burial rates. *Palaeogeography, Palaeoclimatology, Palaeoecology*, **235**, 245-264.
- Briegel, U.** (1972) Geologie der östlichen Alviergruppe (Helvetische Decken der Ostschweiz) unter besonderer Berücksichtigung der Drusberg- und Schrattenkalkformation (Unterkreide). *Eclogae geol. Helv.*, **65**, 425-483.
- Canérot, J., Cugny, P., Peybernès, B., Rahali, I., Rey, J. and Thieuloy, J.-P.** (1986) Comparative study on the lower and mid-Cretaceous sequences on different maghrebian shelves and basins - their place in the evolution of the north african atlantic and neotethysian margins. *Palaeogeography, Palaeoclimatology, Palaeoecology*, **55**, 213-232.
- Catuneanu, O., Abreu, V., Bhattacharya, J.P., Blum, M.D., Dalrymple, R.W., Eriksson, P.G., Fielding, C.R., Fisher, W.L., Galloway, W.E., Gibling, M.R., Giles, K.A., Holbrook, J.M., Jordan, R., Kendall, C.G.S.C., Macurda, B., Martinsen, O.J., Miall, A.D., Neal, J.E., Nummedal, D., Pomar, L., Posamentier, H.W., Pratt, B.R., Sarg, J.F., Shanley, K.W., Steel, R.J., Strasser, A., Tucker, M.E. and Winker, C.** (2009) Towards the standardization of sequence stratigraphy. *Earth-Science Reviews*, **92**, 1-33.
- Coe, A.L., Bosence, D.W.J., Church, K.D.,**

- Flint, S.S., Howell, J.A. and Wilson, R.C.L.** (2003) *The Sedimentary Record of Sea-Level Change*. Cambridge University Press.
- Emery, D. and Myers, K.** (1996) *Sequence Stratigraphy*. Blackwell Sciences.
- Erba, E., Channell, J.E.T., Claps, M., Jones, C., Larson, R., Opdyke, B., Premoli Silva, I., Riva, A., Salvini, G. and Torricelli, S.** (1999) Integrated stratigraphy of the Cismon Apticore (southern Alps, Italy); a «reference section» for the Barremian-Aptian interval at low latitudes. *Journal of Foraminiferal Research*, **29**, 371-391.
- Föllmi, K.B., Bodin, S., Godet, A., Linder, P. and van de Shootbrugge, B.** (2007) Unlocking paleo-environmental information from Early Cretaceous shelf sediments in the Helvetic Alps: stratigraphy is the key! *Swiss Journal of Geosciences*, **100**, 349-369.
- Föllmi, K.B. and Gainon, F.** (2008) Demise of the northern Tethyan Urgonian carbonate platform and subsequent transition towards pelagic conditions: The sedimentary record of the Col de la Plaine Morte area, central Switzerland. *Sedimentary Geology*, **205**, 142-159.
- Fornós, J., Forteza, V. and Martínez-Taber-ner, A.** (1997) Modern polychaete reefs in western Mediterranean lagoons: *Ficopomatus enigmaticus* (Fauvel) in the Albufera of Menorca, Balearic Islands. *Palaeogeography, Palaeoclimatology, Palaeoecology*, **128**, 175-186.
- Funk, H., Föllmi, K.B. and Mohr, H.** (1993) Evolution of the Tithonian-Aptian Carbonate Platform Along the Northern Tethyan Margin, Eastern Helvetic Alps. In: *AAPG Special Volumes, M 56: Cretaceous Carbonate Platforms*, pp. 387 - 407.
- Godet, A., S. Bodin, K. B. Föllmi, J. Vermeulen, S. Gardin, N. Fiet, T. Adatte, B. Zsolt, D. Stüben, and B. van de Schoot-brugge** (2006), Evolution of the marine stable carbon-isotope record during the Early Cretaceous: A focus on the late Hauterivian and Barremian in the Tethyan realm, *Earth Planet. Sci. Lett.*, **242**, 254– 271.
- Haq, B.U.** (2014) Cretaceous eustasy revisited. *Global and Planetary Change*, **113**, 44-58.
- Godet, A., Bodin, S., Adatte, T. and Föllmi, K.B.** (2008) Platform-induced clay-mineral fractionation along a northern Tethyan basin-platform transect: implications for the interpretation of Early Cretaceous climate change (Late Hauterivian-Early Aptian). *Cretaceous Research*, **29**, 830-847.
- Hashimoto, W. and Matsumaru, K.** (1971) Orbitolina from the Seberuang Cretaceous, Kalimantan Barat (West Kalimantan), Indonesia. *Geology and Palaeontology of Southeast Asia*, **CXLI**, 14, 89-99.
- Hfaiedh, R., Arnaud Vanneau, A., Godet, A., Arnaud, H., Zghal, I., Ouali, J., Latil, J.-L. and Jallali, H.** (2013) Biostratigraphy, palaeoenvironments and sequence stratigraphy of the Aptian sedimentary succession at Jebel Bir Oum Ali (Northern Chain of Chotts, South Tunisia): Comparison with contemporaneous Tethyan series. *Cretaceous Research*, **46**, 177-207.
- Hunt, D. and Tucker, M.E.** (1993) Sequence stratigraphy of carbonate shelves with an example from the mid-Cretaceous (Urgonian) of southeast France. *International Association of Sedimentologists, Special Publication* **18**, 307–341.
- Linder, P., Gigandet, J., Hüsser, J.L., Gainon, F. and Föllmi, K.B.** (2006) The Early Aptian Grünten Member: Description of a new lithostratigraphic unit of the helvetic Garschella Formation. *Eclogae geologicae Helvetiae*, **99**, 327-341.

- Martínez-Taberner, A., Forteza, V. and Fornós, J.** (1993) Colonization, structure and growth of *Ficopomatus enigmaticus* cf. TEN HOVE & WEERDENBURG (polychaeta, Serpulidae) in the Albufera of Menorca, Balearic Islands. *Internationale Vereinigung für Theoretische und Angewandte Limnologie Verhandlungen*, **25**, 1031-1034.
- Masse, J.-P., Tüysüz, O., Fenerci-Masse, M., Özer, S. and Sari, B.** (2009) Stratigraphic organisation, spatial distribution, palaeoenvironmental reconstruction, and demise of Lower Cretaceous (Barremian-lower Aptian) carbonate platforms of the Western Pontides (Black Sea region, Turkey). *Cretaceous Research*, **30**, 1170-1180.
- Matsumaru, K.** (2005) *Praeorbitolinoides*, a new Orbitolinid foraminiferal genus from the Lower Aptian (Cretaceous) of Hokkaido, Japan. *Micropaleontology*, **51**, 93-99.
- Mutterlose, J., Malkoč, M., Schouten, S., Singinghe Damsté, J.S. and Forster, A.** (2010) TEX₈₆ and stable δ¹⁸O paleothermometry of early Cretaceous sediments: Implications for belemnites ecology and paleotemperature proxy application. *Earth and Planetary Science Letters*, **298**, 286-298.
- Omana-Pulido, L. and Pantoja-Alor, J.** (1998) Early Aptian benthic foraminifera from the El Cajon formation, Huetamo, Michoacan, SW Mexico. *Revista Mexicana de Ciencias Geológicas*, **15**, 64-72.
- Peybernès, B.** (1979b) L'urgonien de Hongrie. *Geobios*, **12, Supplement 1**, 231-243.
- Pudsey, J.C., Schroeder, R. and Skelton, P.W.** (Eds) (1985) *Cretaceous (Aptian/Albian) Age for Island-Arc Volcanics, Kohistan, N. Pakistan*. V. J. Gupta et al., 150-168 pp.
- Ribaux** (2012) *Etude stratigraphique, sédimentologique et géochimique d'une succession helvétique de plateforme externe: l'intervalle Barrémien–Aptian du Brienz Rothorn (Ct Berne)*, Mc thesis, University of Lausanne, unpublished work.
- Sarg, J.F.** (1988) Carbonate Sequence Stratigraphy. In: *Sea-Level Changes - An Integrated Approach* (Ed SEPM), SEPM, **Special Publication n°42**, pp. 155-181.
- Sudar, M., Jovanovi, D., Maran, A. and Polavender, S.** (2008) Late Barremian-Early Aptian Urgonian Limestones from the south-eastern Kucaj Mountains (Carpatho-Balkanides, eastern Serbia). *Annales Géologiques De La Péninsule Balkanique*, **69**, 13-30.
- Trümpy, R.** (1980) *Geology of Switzerland: A guide-book. Part A: An Outline of the Geology of Switzerland*. Wepf & Co. Publishers, Basel - New York, 334 pp.
- Vail, P.R., Mitchum, R.M.J., Todd, R.G., Widmeri, J.W., Thompson, S., Sangree, J.B., Bubb, J.N. and Hatelid, W.G.** (1977) Seismic stratigraphy and global changes of sea level. In: *Seismic stratigraphy. Application to hydrocarbon exploration*, Am. Assoc. Pet. Geol. Mem., **26**, pp. 49-212, Tulsa.
- Van Buchem, F.S.P., Pittet, B., Hillgärtner, H.A., Al-Mansouri, A., Billing, I., Droste, H., Grötsch, J. and Oterdoom, H.** (2002) Regional sequence stratigraphic model for the Kharaib and Shuaiba Formations (Barremian, Aptian) in N. Oman and the UAE – depositional geometries and ecological change. *GeoArabia*, **7**, 461-500.
- Van Wagoner, J.C., Posamentier, H.W., Mitchum, R.M., Vail, P.R., Sarg, J.F., Loutit, T.S. and Hardenbol, J.** (1988) An overview of the fundamentals of sequence stratigraphy and key definitions. In: *Sea Level Changes: An Integrated Approach* (Eds C.K. Wilgus, B.S. Hastings, C.G.S.C. Kendall, H.W. Posamentier, C.A. Ross and J.C. Van Wagoner), **42**, pp. 39-45. SEPM Special Publication,

Tulsa, Oklahoma, U.S.A.

Vermeulen, J. (2005) Boundaries, ammonite fauna and main subdivisions of the stratotype of the Barremian. In: *The Hauterivian-Lower Aptian Sequence Stratigraphy from Jura Platform to Vocontian Basin: A Multidisciplinary Approach* (Eds T. Adatte, A. Arnaud-Vanneau, H. Arnaud, M.-C. Blanc-Alétru, S. Bodin, E. Carrio-Schaffhauer, K.B. Föllmi, A. Godet, M.C. Raddadi and J. Vermeulen), Géol. Alpine, Sér. Spéc. “Colloques et Excursions” No. 7, 147–173.

Vermeulen, J., Arnaud, H., Arnaud Vanneau, A., Lahondiere, J.-C., Lepinay, P. and Massonnat, G. (2013) L’Hauterivien supérieur et le Barrémien inférieur de la région de Seynes et Belvédère (Gard). *Annales du Muséum d’Histoire Naturelle de Nice*, **XXVIII**, 1-16.

Vilas, L., Masse, J.P. and Arias, C. (1995)

Orbitolina episodes in carbonate platform evolution: the early Aptian model from SE Spain. *Palaeogeography, Palaeoclimatology, Palaeoecology*, **119**, 35-45.

Wilmsen, M., Fürsich, F.T. and Majidifard, M.R. (2013) The Shah Kuh Formation, a latest Barremian – Early Aptian carbonate platform of Central Iran (Khur area, Yazd Block). *Cretaceous Research*, **39**, 183-194.

Wissler, L., Funk, H. and Weissert, H. (2003) Response of Early Cretaceous carbonate platforms to changes in atmospheric carbon dioxide levels. *Palaeogeography, Palaeoclimatology, Palaeoecology*, **Volume 200**, Pages 187-205.

Ziegler, M.A. (1967) A study of the Lower Cretaceous facies developments in the Helvetic border chain, north of the Lake of Thun (Switzerland). *Eclogae Geologicae Helveticae*, **60**, 509-528.

Chapter 3 – Development and demise of the Urgonian platform along the NW Tethyan margin: the record of the Helvetic Alps during the earliest Aptian

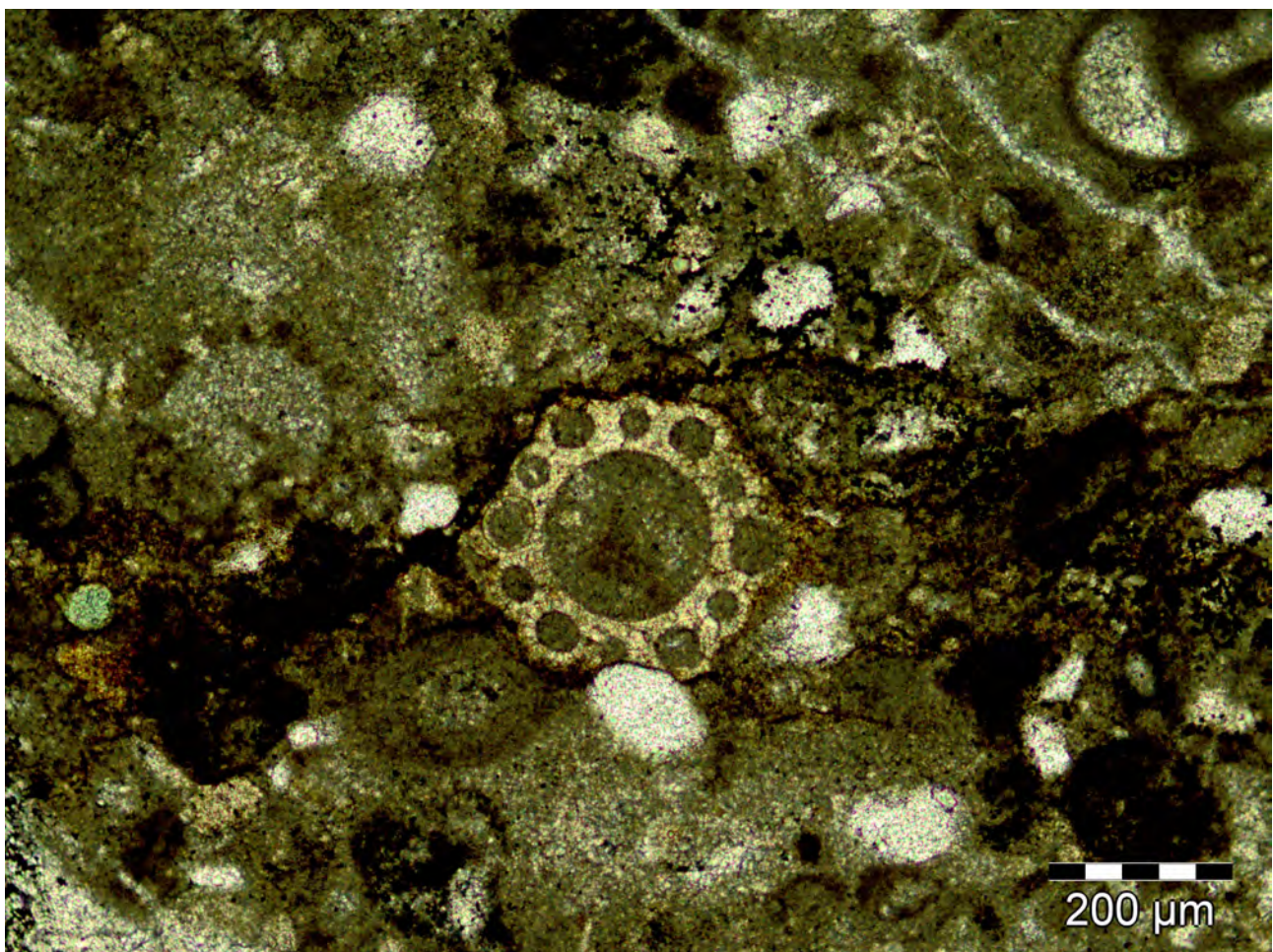


Fig. 3 Charophyta observed in the first mettrs of the Rawil Mb (Section of Justistal, sample LB 15)

Chapter 3 presents the development of the Urgonian limestone in the Helvetic nappes, and focuses on the Aptian period in the evolution of this platform, with the detailed study of six selected key sections, for which the microfacies succession, the isotopic record and the phosphorus content are examined. Similarities of the evolution of depositional environments with other sections of the NW Tethyan Platform (SE France) are discussed.

Chapter 3

Development and demise of the Urgonian platform along the NW Tethyan margin: the record of the Helvetic Alps during the earliest Aptian

Abstract

Urgonian-type carbonate platforms evolved rapidly and widely in subtropical and tropical shallow waters during the late Barremian and early Aptian to form one of the most widespread platforms of Earth history. The mechanisms leading to their proliferation are not well understood, especially since the Barremian and Aptian are periods of widespread regional to global oceanic anoxia. To this comes that the Barremian-Aptian boundary period and the earliest Aptian witnessed important environmental and climatic change, which partly anticipated the major changes associated with the unfolding of the Selli anoxic episode. These changes are recorded in the Urgonian platform, which developed on the Delphino-Helvetic shelf along the northern Tethys. Here we present an integrated high-resolution study of macro- and microfacies, benthic foraminiferal biostratigraphy, sequence stratigraphy, and carbon-isotope records on the Lower Schrattenkalk, Rawil and Upper Schrattenkalk Members (Mbs; equivalent of “Lower Urgonian Limestone”, “Lower Orbitolina Beds” and “Upper Urgonian Limestone” in the Dauphinois area) of the Swiss Helvetic Alps. The 6 sections analyzed include the L’Ecuelle section in the Morcles nappe, Rawil and Justistal sections and the Morschach core in

the Wildhorn/Drusberg nappe, and the Tierwis and Valsloch sections in the Säntis nappe. The data from the Lower Schrattenkalk Mb (late Barremian) records the installation of oligotrophic lagoonal facies, which was bordered by shoal-facies and back-reef facies. Two emersion phases were recorded during its deposition, and a further, major emersion phase marked its end (SB A1). This latter phase was triggered by important sea-level fall, estimated here at ca. 15m. The overlying Rawil Mb (earliest Aptian) shows the progressive deepening and eutrophication of the depositional environment. This resulted in mixed siliciclastic-carbonate platform buildup, characterized by a sea-grass facies and the massive occurrence of *Palorbitolina lenticularis*. The Upper Schrattenkalk Mb (early Aptian) witnessed the recovery of the typical rudist-rich photozoan platform, and terminated with a major emersive phase (SB A2), which triggered the demise of the Urgonian platform. The carbon-isotope records show an increase toward positive values during the Lower Schrattenkalk Mb and the base of the Rawil Mb, interrupted in most sections by a negative excursion near the Barremian–Aptian boundary. A negative shift occurred in the uppermost part of the Rawil Mb, followed by variable trends in the Upper Schrattenkalk Mb. The long-term trends are rather well correlated with the basinal record (Angles, La Bédoule). Deviations in the correlations are re-

lated to the influence of facies and microfacies, primary mineralogy and differential diagenesis on the carbon-isotope records. The succession of microfacies and the isotope trends are compared with those recorded in the Subalpine Chains (Bornes, Vercors, SE France). Its comparability confirms that the deposition of the Rawil Mb resulted from major environmental and climate change. It also confirms that the demise of the Urgonian platform occurred well before the Selli episode and was initiated by the emersion of the platform due to high-amplitude sea-level fall, followed by eutrophication during the following transgressive phase.

Keywords:

Barremian–Aptian; Northern Tethys; Helvetic nappes; Urgonian carbonate platform; Integrated stratigraphy; Carbon isotope records; Sea-level fluctuations

3.1 Introduction

Rudist-rich shallow-water platform carbonates are widespread in subtropical and tropical environments of the late Early Cretaceous. They include the so-called Urgonian platforms, which bordered the northern and southern Tethyan margins and which form one of the largest occurrences of carbonate platforms during Earth history (Arnaud-Vanneau et al., 1976; Ager, 1981; Michalik, 1994; Arnaud et al., 1998; Bernaus et al., 2003; Philip, 2003; Godet et al., 2014). The installation and evolution of these platforms mirror the general palaeoclimatic and environmental conditions, and especially the disappearance of the Urgonian platforms has been

linked to the unfolding of the early Aptian Selli episode or Oceanic Anoxic Event 1a (OAE1a, approximately 120 My ago; Schlanger and Jenkyns, 1976; Föllmi et al., 2006, 2007; Tejada et al., 2009; Jenkyns, 2010; Huck et al., 2011).

Several lines of evidence suggest that climate perturbations were already important during the late Barremian and earliest Aptian, well ahead of the Selli episode. The Ontong-Java LIP started to form during the latest Barremian (e.g., Kuroda et al., 2011), and a first period of regional anoxia is observed during the Barremian–Aptian boundary interval (“Taxy episode”; Föllmi, 2012; Föllmi et al., 2012; Stein et al., 2012). According to Haq (2014), the Barremian–Aptian boundary and the early Aptian *forbesi* ammonite zone are characterized by two major episodes of high-amplitude sea-level fall (> 75m), followed by phases of fast and important transgression. These two cycles of sea-level change are amongst the most important ones for the Early Cretaceous, in terms of their amplitude. In carbonate platforms of different regions, these cycles were associated with changes from a Urgonian-type facies rich in rudists and corals to a mixed siliciclastic–carbonate depositional system accompanied by the accumulation of orbitolinid-enriched deposits (“Lower and Upper Orbitolina Beds”; Wissler et al., 2003; Linder et al., 2006; Föllmi et al., 2007; Stein et al., 2012a,b; Carević et al., 2013). In general, these changes were also linked with climate perturbations associated with changes in terrigenous and nutrient input (Föllmi and Gainon, 2008; Stein et al., 2012a; Pictet et al., 2015). It is less well known in how far these important changes prepared the way for and interfered with OAE 1a, and, in general, the late Barremian and early Aptian time period is in need of more research integrating facies, sequence stratigraphy and chemostratigraphy in a high-resolution fashion,

in order to better understand palaeoenvironmental and palaeoclimatic changes and their effect on platform ecologies (e.g., Moreno-Bedmar et al., 2009; Keller et al., 2011; Huck et al., 2011, 2013; Di Lucia et al., 2012; Graziano, 2013; Godet et al., 2014).

On the northwestern Tethyan platform, the twofold change from photozoan carbonates

(Lower and Upper Schrattenkalk Members (Mbs), equivalent to the Urgonian Limestone) to mixed photozoan-heterozoan sediments (Rawil and Grünten Mbs, which are more traditionally named “Lower and Upper Orbitolina Beds”; e.g., Funk et al., 1993) during the early Aptian were studied by Wissler et al. (2003), Linder et al. (2006) and Stein et al. (2012a). Here we

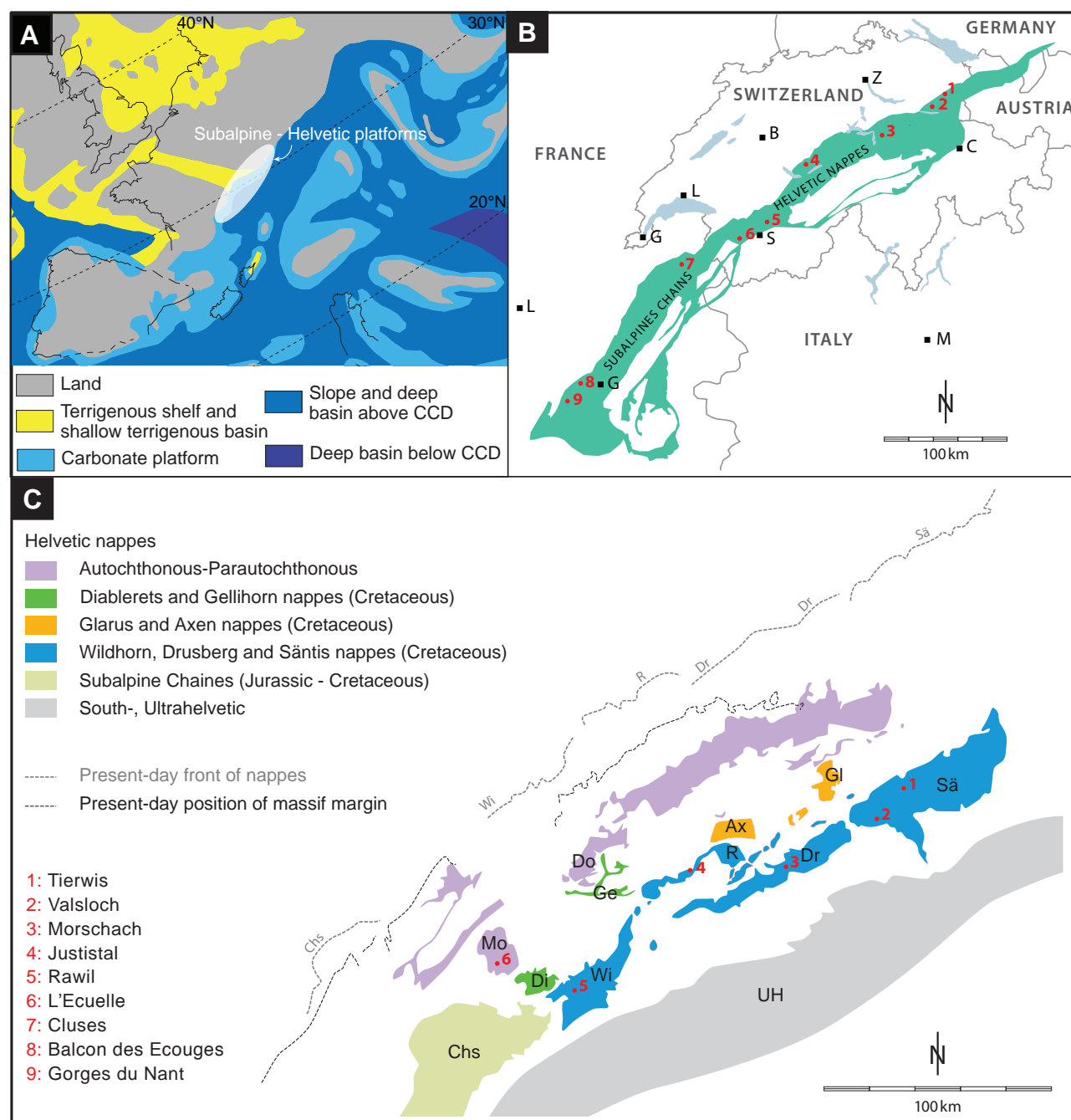


Fig. 3.1 **A:** Early Aptian paleomap of the western Tethyan realm showing the location of the Helvetic platform. (after Masse, 1993b). **B:** Location of the studied sections in the Helvetic nappes (green colored). **C:** Palinspastic reconstruction of the Helvetic nappes and restauration of the location of the sections (redrawn after Kempf and Pfiffner, 2004).

build up on these contributions and present a detailed study through the Lower Schrattenkalk, Rawil and Upper Schrattenkalk Mbs from the Helvetic thrust-and-fold belt in the Swiss Alps, where we logged and sampled six representative sections in high detail, established partly quantitative trends in facies and microfacies, proposed a sequence-stratigraphic framework and measured whole-rock carbon-isotopic composition. The sequence-stratigraphic trends and carbon-isotope records were used to correlate the sections and compare them with a detailed, synthetic reference section from the Vercors Massif (SE France), which is based on sedimentological, biostratigraphical, facies and microfacies observations (Arnaud-Vanneau, 1980; Raddadi, 2005). The aim of this study is to establish a detailed stratigraphic framework for the Helvetic platform using bio-, sequence, and $\delta^{13}\text{C}$ stratigraphies, in order to reconstruct the evolution of the Urgonian platform during the late Barremian and earliest Aptian and compare this with trends in other areas of the northern Tethyan platform. A further goal is to interpret the $\delta^{13}\text{C}$ records in terms of platform facies and changes therein, emersion events and global changes in the carbon cycle and as such to document the responses of the northern Tethyan carbonate platform to environmental conditions during the late Barremian and earliest Aptian.

3.2 Geological setting

The Helvetic tectonic unit represents the external part of the Alps, and extends across Switzerland and adjoining countries to the east (western Austria and southern Germany) and to the west (subalpine chains in eastern France). The Helvetic Alps are composed of a thrust-and-

fold complex formed during Cenozoic alpine orogenesis (e.g. Heim, 1916-1922; Ramsay, 1981; Pfiffner, 1993). It includes Mesozoic sediments representing the central part of the former northern Tethyan margin (Fig. 3.1-A). Trümpy (1969), Ferrazzini and Schüler (1979) and Kempf and Pfiffner (2004) proposed palinspastic reconstructions in order to place the Helvetic nappes in their original paleogeographic position on the northern Tethyan platform (Fig. 3.1-C). These reconstructions are used here to locate the sections in their original depositional context. The stratigraphic units corresponding to the Barremian–early Aptian Urgonian limestone are represented by the Schrattenkalk Formation (Fm), which is divided into a Lower and an Upper Schrattenkalk Member (Mb) by the Rawil Mb, an equivalent of the “Lower Orbitolina Beds” from the Vercors area (Fig. 3.2). The Upper Schrattenkalk Mb is overlain by the Grünten Mb, an equivalent of the “Upper Orbitolina Beds”.

3.3 Methods

3.3.1 Studied sections

Six sections were logged and sampled for this study. The section of Tierwies is part of the Säntis nappe and is located close to the Säntis summit (canton St. Gallen; Swiss coordinates: 742.970/234.730). This section was logged and sampled in detail by Stein et al. (2012a) for the Rawil Mb, and completed in this study for the Lower and Upper Schrattenkalk Mbs. The section of Valsloch is situated in the Churfirsten range (canton St. Gallen; Swiss

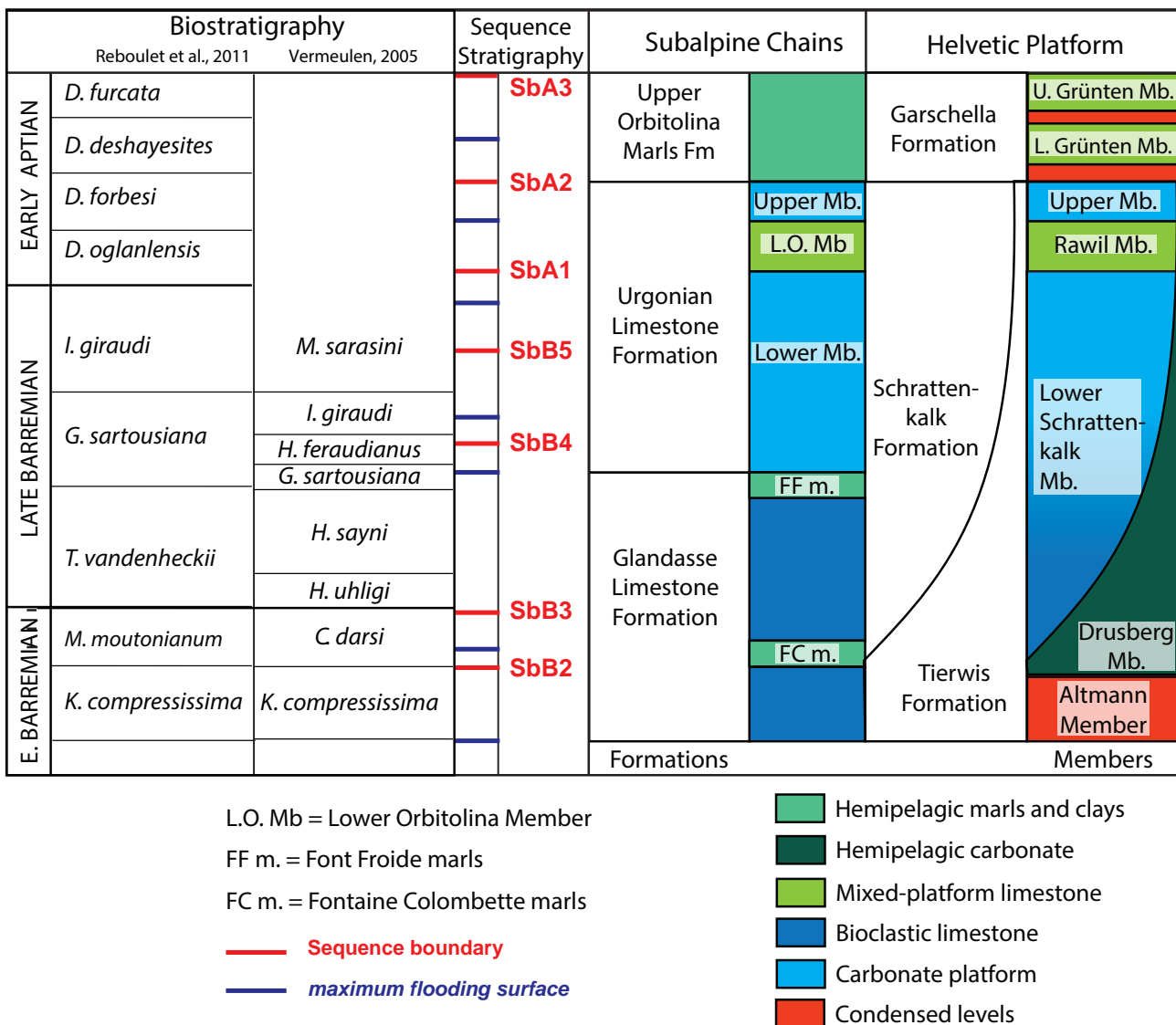


Fig. 3.2 Stratigraphic correlation diagram showing the temporal evolution of carbonate platform ecosystems along a SW-NE transect at the northern rim of the Tethyan Ocean. The calibration between the ammonite zones (Reboulet et al., 2011) and the sequence stratigraphy is based on the section of Angles (after Arnaud et al., 1998).

coordinates: 742.224/224.041) and also belongs to the Säntis Nappe. Near the base of the Rawil Mb, the outcrop becomes part of a cliff, which is inaccessible for about 7m. This interval outcrops also as a more recessive interval on the other side of the talweg – at a distance of ca. 140m, and there a second section was logged, narrowing the gap of observation to 2 meters. In the palinspastic reconstruction (Fig. 3.1-C), this section represents an outer-platform position. Nearby sections were previously studied by Wissler et al. (2003) and Stein et al. (2012a). The borehole of Morschach is located on the golf course of

Morschach (canton Schwyz; Swiss coordinates: 690.299/205.511); it represents an intermediate shelf position. The section of Justistal in the Wildhorn Nappe is located on the northeastern side of the Lake of Thun (canton Berne; Swiss coordinates: 628.427/176.557). Ziegler (1967) and Schenk (1992) previously studied this section. The section of Rawil is located underneath the midway station of the military cablecar of Rawil, to the south of Iffigenalp (canton Berne; Swiss coordinates: 601.187/137.250). This section, which is part of the Wildhorn Nappe, was previously studied by Schenk (1992) and Stein

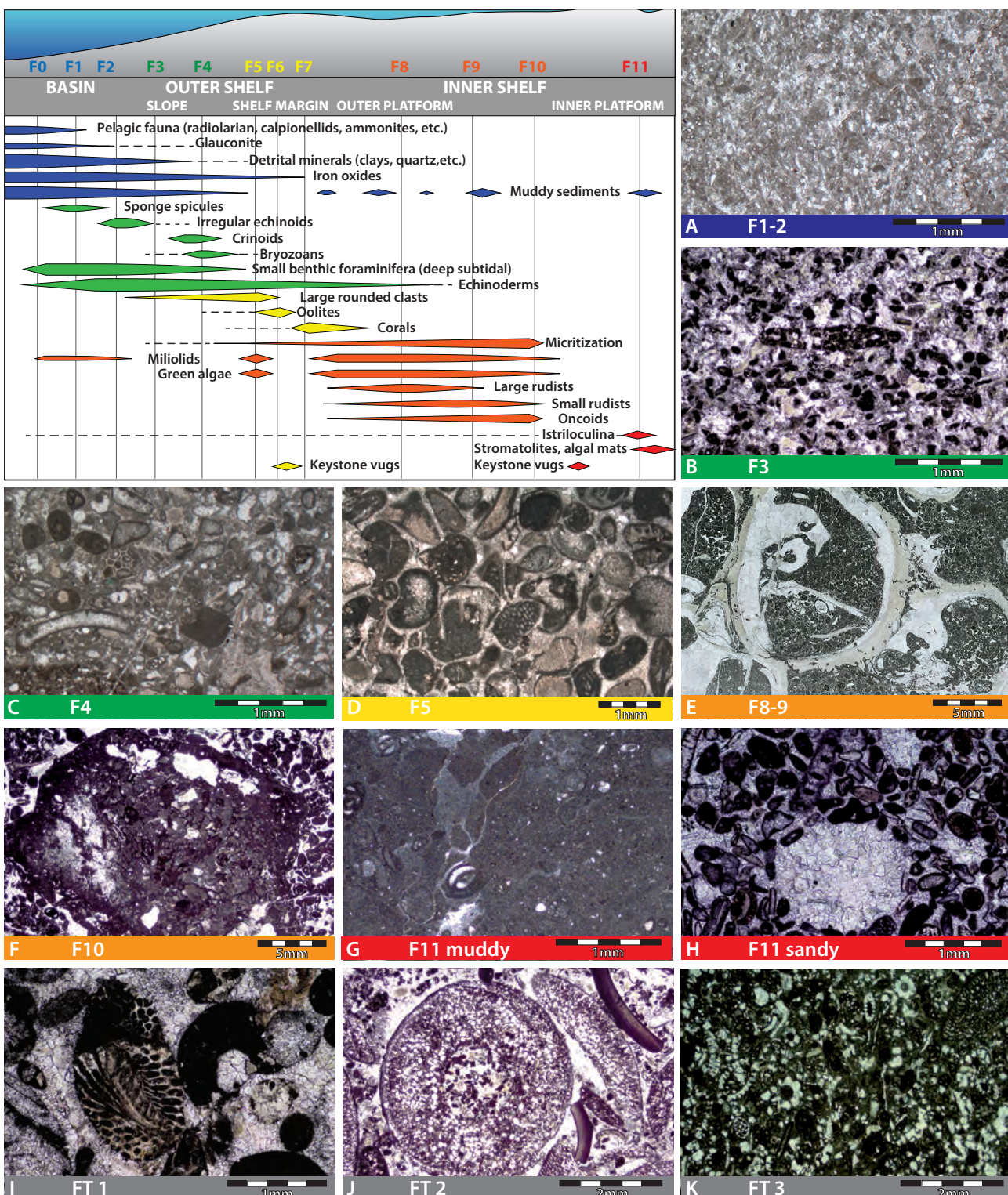


Fig. 3.3 Microfacies and microfacies–association chart (after Arnaud-Vanneau 2005). Distribution of principal microfacies types along a rimmed platform transect during the Barremian (redrawn after Arnaud-Vanneau, 2005). Microphotographs of the microfacies recognized in the studied sections. **A:** Facies F1, F2 with spicules of sponges. **B:** Facies F3 with small foraminifera and crinoidal remains. **C:** Facies F4 with bryozoans and crinoids. **D:** Facies F5 with rounded bioclasts. **E:** Facies F8-9 with rudist shells and miliolids. **F:** Facies F10 with *Bacinella* nodules and oncolites. **G:** Facies F11 in muddy environment, with bird's eyes. **H:** Facies F11 in sandy environment, with keystone vugs. **I:** Transgressive facies FT1 with reworked grains. **J:** Transgressive facies FT2 with accumulation of *Palorbitolina lenticularis*, associated with detrital quartz, annelids and *Choffatella decipiens*. **K:** Transgressive facies FT3 with accumulation of *Dasycladaceae* algae. The colours of the microphoto-

et al. (2012a). It represents the type locality of the Rawil Member. The section of L'Ecuelle is located close to Anzeindaz (canton Vaud; Swiss coordinates: 579.336/124.832). The section is part of the front of the Mörcoles nappe, and represents an inner-platform position.

3.3.2 Field work and samples preparation

The working approach used for sedimentological characterization involves an outcrop-based carbonate facies description supported by the analysis of 1094 samples. Samples for microfacies and geochemical investigations were taken at a spacing of 1 m or less. Higher sample densities were applied across facies boundaries and discontinuity surfaces. The samples were sawn in order to remove weathered surfaces and veins, and if present, the micritic part of the rock samples was privileged for the isotope analyses. Rock powders were obtained by using a mechanical agate crusher.

3.3.3 Microfacies description

The investigation of a total of 1035 thin sections was performed, using conventional optical microscopy. An Olympus BX51 microscope (Olympus, Tokyo, Japan) equipped with an Olympus Altra 20 camera and the Olympus Image Analysis © software was used for digital microphotography. The microfacies classification used in this study was the one established

by Arnaud-Vanneau and Arnaud (2005) in the Urgonian limestone of the Chartreuse and Vercors area (Fig. 3.3). Contrary to Stein et al. (2012a), who adapted this chart especially for the Rawil Mb, here we choose to follow the exact microfacies chart of Arnaud-Vanneau and Arnaud (2005), in order to use an identical approach throughout the different members and the different studied areas. This classification is based on actual analogues with regards to the environmental position of ecosystems, in addition to the effects of light, salinity, currents and trophic levels. It consists of twelve microfacies (MF) types, which are arranged on a distal-to-proximal transect, from the most external MF F0 characterized by a pelagic faunal association, to the shallowest MF F11, which represents an internal lagoonal facies close to emersion (Fig. 3.3). Three annex MF types are recognized: FT1, FT2 and FT3, which are used to characterize the main transgressive phases: FT1: reworking and lag; FT2: accumulation of *Palorbitolina lenticularis*, associated with detrital quartz, annelids and *Choffatella decipiens*; and FT3: accumulation of Dasycladaceae algae. These MF types were regrouped in six microfacies associations (AF1 to AF6), according to comparable bathymetries and grain-size sorting characteristics.

3.3.4 Component quantification in thin sections

For the section of Valsloch, the microfossil species of 77 thin sections were quantified us-

graphs indicate the facies association. AF1 in blue for the hemipelagic facies, F0, F1 and F2; AF2 in green for the outer-shelf facies F3 and F4; AF3 in yellow for the margin shelf facies F5, F6 and F7; AF4 in orange for the lagoonal facies F8, F9 and F10; AF5 in red for supratidal facies F11; and AF6 in grey for the transgressive facies FT1, FT2 and FT3.

Association	Microfossils and grains counted	Environment
A1	Circalittoral <i>Arenobulimina</i> sp., <i>Belorussiella</i> sp., Calcispheres, <i>Charentia nana</i> , <i>Conorboides</i> sp. (small size), <i>Earlandia brevis</i> , <i>Epistomina</i> sp., <i>Gavelinella</i> sp., <i>Gaudryina tuchaensis</i> , <i>Glaucony</i> , <i>Glomospirella</i> , <i>Circalittoral Istriloculina</i> , <i>Lenticulina</i> sp., <i>Marssonella</i> sp., Circalittoral Miliolidae, <i>Neotrocholina infragranulata</i> , Nodosariidae, Ophthalmolinidae, <i>Patelina</i> sp., <i>Patelina sub-cretacea</i> , Circalittoral Vercorsella, Radiolaria, <i>Sabaudia briacensis</i> , Sponges spicules, <i>Spirilina</i> sp., Textulariidae externe, Tristix, <i>Trochaminoidea coronus</i> , <i>Valvulinaria</i> sp1, <i>Verneuilina</i> sp.	Circalittoral
A2	Annelids, Arthropodes, Brachiopodes, Bryozoans, Circalittoral Choffatella, <i>Gaudryina cushmani</i> , <i>Nubecularia</i> sp., <i>Patellovalvulina</i> sp., <i>Spiroloculina</i> sp. (small size)	Circalittoral
Echinoderms		Circalittoral to Infralittoral
Ooids	Ooids (small and large)	Infralittoral
A3	Red algae, <i>Buccicrenata</i> sp., Corals, Calcareous sponges, <i>Ethelia alba</i> , Large agglutinated foraminifera, <i>Lithocodium aggregatum</i> , <i>Marinella lugeoni</i> , <i>Neomeris</i> sp., <i>Neotrocholina</i> sp.	Infralittoral
A4	Dasycladial algae, <i>Andersenolina rumania</i> , Infralittoral Arenobulimina, <i>Boueina</i> sp., <i>Choffatella</i> sp., <i>Clypeina nigra</i> , <i>Cribellopsis</i> sp., <i>Cribellopsis neoelongata</i> , <i>Derventina filipesculi</i> , <i>Dictyopsella</i> sp., <i>Dictyoconus cf vercorii</i> , <i>Falsurgonina</i> sp., <i>Falsurgonina pileola</i> , <i>Fisherina carinata</i> , Large size Miliolidae, <i>Orbitolinide</i> , <i>Orbitolinopsis buccifer</i> , <i>Orbitolinopsis kiliiani</i> , <i>Orbitolinopsis pygmaea</i> , <i>Orbitolinosis</i> sp., <i>Palorbitolina lenticularis</i> , <i>Palaeodictyoconus</i> sp., <i>Paracoskinolina</i> sp., <i>Paracoskinolina cf hispanica</i> , <i>Paracoskinolina maynci</i> , <i>Paracoskinolina reicheli</i> , Permocalculus sp., <i>Pfenderina aurelie</i> , <i>Pseudonumuloculina</i> sp., <i>Rumanoloculina</i> sp., <i>Sabaudia</i> sp., <i>Sabaudia minuta</i> , <i>Salpingoporella</i> sp., <i>Spiroloculina</i> sp., <i>Terquemella</i> sp., <i>Thaumathoporella parvovesiculifera</i> , <i>Valvulinaria</i> sp., <i>Valvulinaria?</i> sp.	External part of the inner platform, Infralittoral
A5	<i>Charentia</i> sp., <i>Charentia cretacea</i> , Condrodont, <i>Conorboides</i> sp., <i>Cuneolina</i> sp., <i>Debarina</i> sp., <i>Dobrogelina</i> sp., <i>Earlandia</i> sp., <i>Earlandia conradi</i> , <i>Gaudryina</i> sp., <i>Girariarella</i> sp., <i>Istiloculina</i> sp., <i>Istiloculina</i> sp., <i>Meandrospira</i> sp., <i>Melathrokerion</i> sp., <i>Miliolidae</i> , <i>Nautiloculina</i> sp., <i>Nezzazatinella</i> sp., <i>Novalesia</i> sp., <i>Novalesia distorta</i> , <i>Novalesia contorta</i> , <i>Pseudolituonella</i> sp., <i>Praereticulina</i> sp., <i>Praereticulina cuvillieri</i> , Rudists, Ruditapes with canals, <i>Sabaudia capitata</i> , Textulariidae ind., <i>Trocholina</i> sp., <i>Trocholina molesta</i> , <i>Valvulinaria</i> sp.2, <i>Vercorsella</i> sp.	Internal part of the inner platform, Infralittoral
A6	<i>Bacinella irregularis</i> , Oncolites, Oncolites with <i>Bacinella</i> , Oncolites with <i>Bacinella</i> and Lithocodium	Restricted environments
A7	<i>Arenobulimina</i> sp. (small size), <i>Girariarella</i> sp. (small size), <i>Glomospira</i> sp. (small size), <i>Istiloculina</i> sp. (small size), <i>Nubecularia</i> sp. (small size)	Restricted environments

Table 3.1 Microfossil description of the different assemblages of the component quantification and their depth attribution.

ing the counting technique discussed previously by Bernaus (1998), González-Lara (2001) and Hfaiedh et al. (2013); (see Raddadi et al., 2005 for a precise description). On a reference surface of 1.2x1.7 cm, all visible, entirely preserved or fragmented components (such as foraminifera, oncolites, algae, etc.) were counted for each selected thin section. The counted components are grouped in assemblages representing similar ecologic environments, which range from deeper, open marine environments to confined and even estuarine depositional settings. Nine assemblages were determined for the section of Valsloch and eight for the section of the Gorges du Nant, where the counting was performed by one of the co-authors (A. A.-V.). The details of the assemblages are shown in Table 3.1.

3.3.5 Carbon and oxygen-isotope analysis

A total of 1094 samples were analysed for their stable carbon and oxygen isotope composition at the Institute of Earth Surface dynamics of the University of Lausanne. Carbon and oxygen isotopes were analysed using procedures described by Revesz et al. (2001). Analyses of aliquots of all samples were performed using a Thermo Fisher Scientific (formerly Thermo-Quest/ Finnigan, Bremen, Germany) GasBench II preparation device interfaced with a Thermo Fisher Scientific Delta Plus XL continuous flow isotope ratio mass spectrometer (IRMS). The CO₂ extraction was executed at 90°C. The carbon and oxygen-isotope ratios were reported in the delta (δ) notation as the per mil (‰) deviation relative to the Vienna–Pee Dee belemnite standard (VPDB). Analytical uncertainty (2 σ), monitored by replicate analyses of the international calcite

standard NBS-19 and the laboratory standards Carrara Marble were not greater than $\pm 0.05\text{‰}$ for $\delta^{13}\text{C}$ and $\pm 0.1\text{‰}$ for $\delta^{18}\text{O}$.

3.3.6 Phosphorus content

The total phosphorus content was measured on 640 samples from the sections of L'Ecuelle, Tierwis and Valsloch, using the ascorbic acid molybdate blue method (Eaton et al., 1995) and following the procedure described in Bodin et al (2006). The phosphorus content was determined using a UV/Vis Perkin Elmer Lambda 25 spectrophotometer at the University of Lausanne, and calibrated with internal standard solutions providing a precision better than 5%.

3.3.7 Bulk-rock mineralogy

Bulk-rock mineralogy was analysed on 68 samples from the section of Valsloch on a Scintag XRD 2000 diffractometer at the University of Lausanne, based on procedures described by Kübler (1983) and Adatte et al. (1996). This method permits the semi-quantification of its mineralogy using external standards with an error of 5%.

3.4 Results

3.4.1 Facies, microfacies and biostratigraphy

The results of the analysis of the litholo-

gies, facies, microfacies and biostratigraphies of all sections are presented in Figures 3.4 to 3.9.

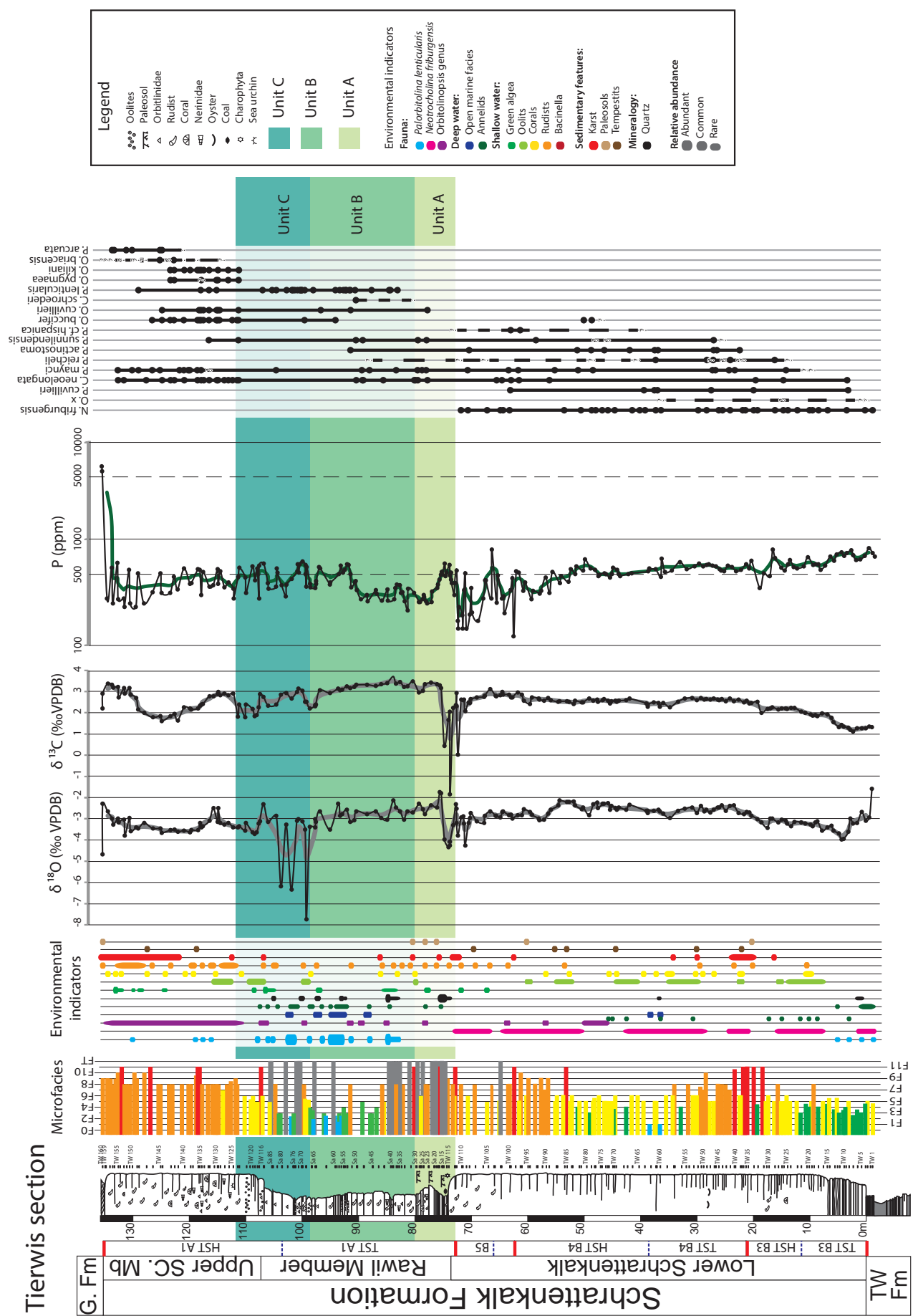
3.4.1.1 Lower Schrattenkalk Member

In all six sections, the Lower Schrattenkalk Mb consists of a massive limestone, which represents a shallow-water platform environment. Numerous Orbitolinids are present throughout this member, which are determined as *Paracoskinolina reicheli*, *Paracoskinolina hispanica*, *Paracoskinolina cf. hispanica*, *Paleodictyoconus cuvillieri* and *Paleodictyoconus actinostoma*, *Montseciella* sp., and *Praedictyorbitolina* sp. In the lower part of this member, bioclastic and oolitic facies (F4-F5-F6) were observed. In the sections of L'Ecuelle, Morschach and Tierwis, the dominant components are small echinoderm fragments, bryozoan clasts and conic Orbitolinids. The sections of Justistal, Valsloch and Rawil are dominated by oolitic shoals and bioclastic, partly reworked facies, rich in green algae, miliolids, *Neotrocholina*, *Sabaudia* and *Palorbitolina transiens*. In Rawil, numerous chaetetids are observed, which occur in outer-shelf facies rich in echinoderms, small foraminifera and spicules. The Lower Schrattenkalk Mb generally shows a shallowing upward trend in facies and its upper part is dominated by lagoonal microfacies types F8 to F10. Typical components of this interval are miliolids, rudists, oncolites, *Bacinella*, green algae and large benthic foraminifera (e.g. *Buccicrenata*, *Cuneolina*, *Derventina*). The sections of Tierwis and Valsloch include sediments of deeper-water

facies, which are intercalated in this lagoonal interval. Several emersive levels characterized by early dissolution, epikarst features, beachrock deposits, meteoric cements or vadose silts are observed through this interval in all investigated sections. In its uppermost metres, the Lower Schrattenkalk Member terminates with a supratidal facies (F11) with characteristic tempestite accumulations, beach facies including keystone vugs, or restricted environments (mudstone/wackestone rich in *Istriloculina* and bird's eyes). In the sections of Tierwis, Justistal and L'Ecuelle, *Neotrocholina friburgensis* is recorded throughout this interval and disappears suddenly at the top of the Lower Schrattenkalk Mb.

Different features indicate an important episode of emersion and karstification following the deposition of the Lower Schrattenkalk Mb, as is suggested by the presence of micro-caves, early dissolution, vadose silt and asymmetric cements, in particular in the sections of Valsloch, Rawil and Tierwis. In the section of Rawil, these dissolution features affected the substratum up to a depth of at least 15 meters below the base of the Rawil Mb, up to an interval characterized by deeper-water facies, rich in spicules, radiolarians and planktonic echinoderms (Fig. 3.10). The top surface of the Lower Schrattenkalk Mb is a spectacular emersion surface, in particular in L'Ecuelle. There, the surface is structured both by intense early dissolution of rudist shells, which are infilled by sandstone (Fig. 3.11-A), as well as by the presence of a dense network of *Thalassinoides*, which is also infilled by a yellowish sandstone (Fig. 3.11-B) and of dark

Fig. 3.4 Tierwis section: lithological-sedimentological log, sequence-stratigraphic interpretation, microfacies identification, environmental indicators, isotope stratigraphy, phosphorus content and biostratigraphy. The three green boxes correspond to the units A, B and C recognized by their microfacies and sedimentological observations (see text for details).



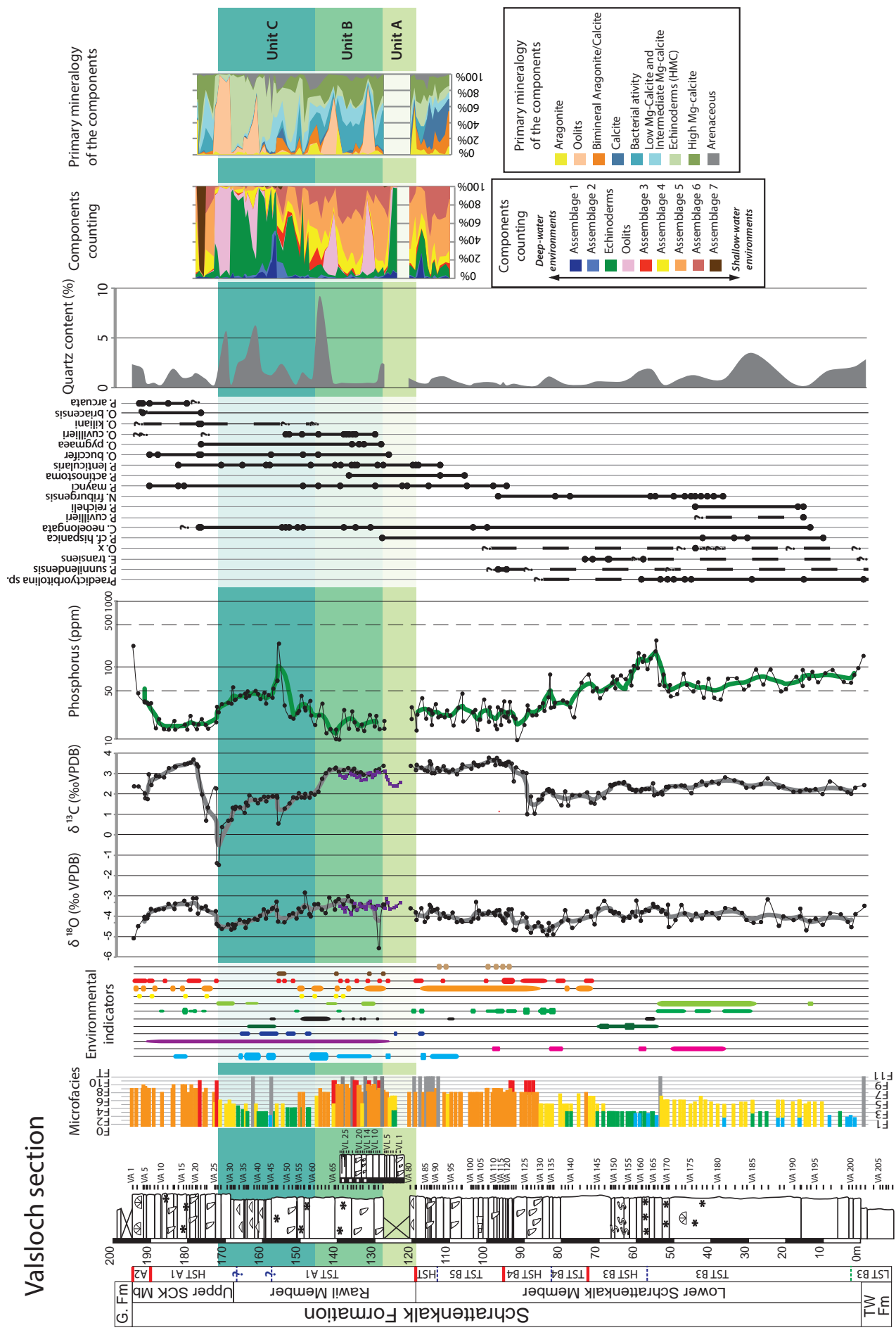


Fig. 3.5 Valsloch section: lithological-sedimentological log, sequence-stratigraphic interpretation, microfacies identification, environmental indicators, isotope stratigraphy, phosphorus content, biostratigraphy, Quartz content and component quantification in terms of assemblages and in terms of primary mineralogy of the components (legends in Fig. 3.4).

sandy infiltrations composing a vertical fracture network. In the Rawil section, this surface is marked by pockets of *terra rossa*. In the Justistal section, the complex history of this limit is recorded in a single thin section (Fig. 3.12), which shows that the initial depositional envi-

ronment is documented by a muddy supratidal facies (F11). The emersive phase is marked by early dissolution of aragonitic elements, such as Dasycladales, and void infills by vadose silt. This step is followed by the installation of palaeosols and karstification of the surface. The sea-level

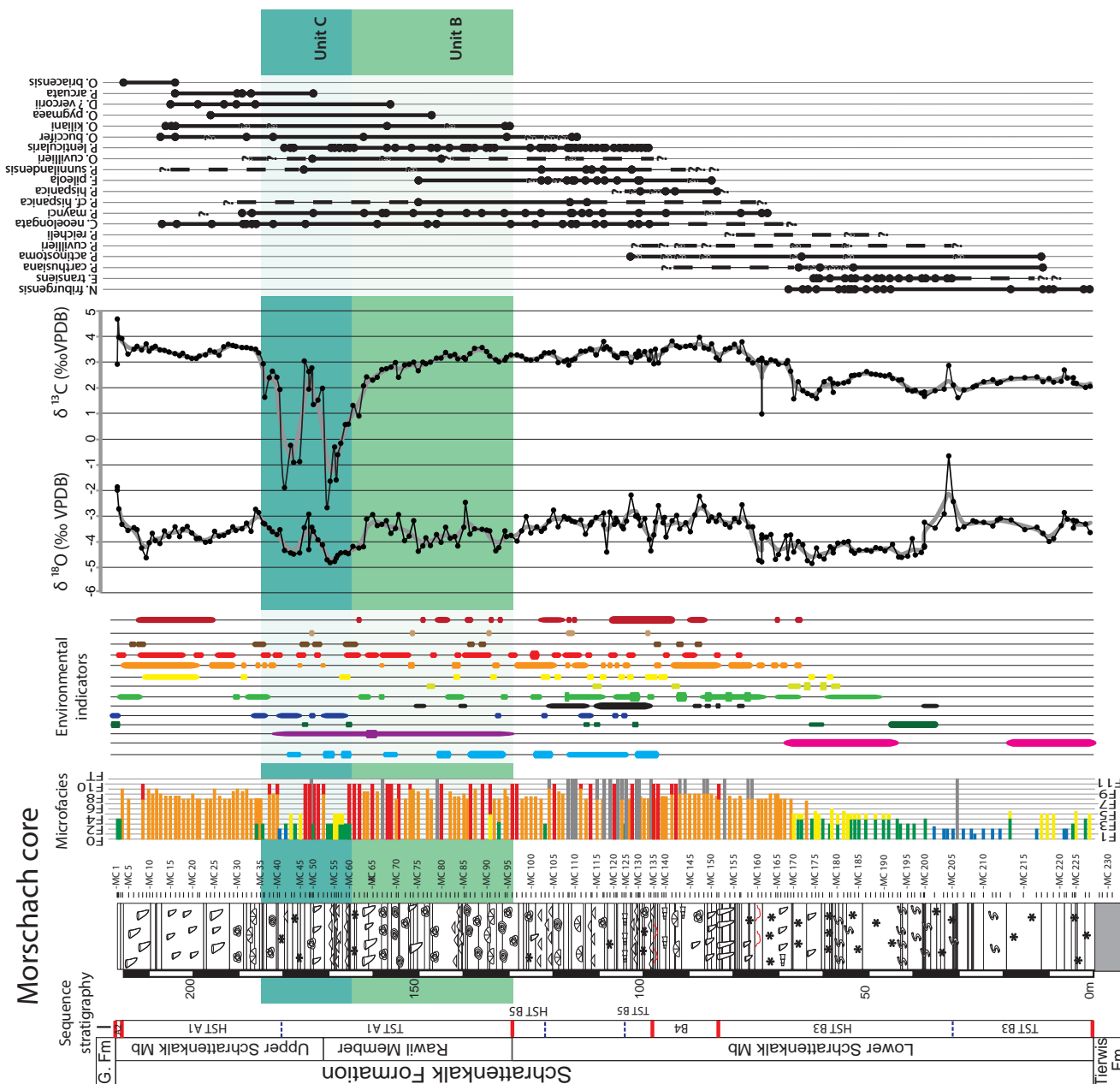


Fig. 3.6 Morschach section: lithological-sedimentological log, sequence-stratigraphic interpretation, microfacies identification, environmental indicators, isotope stratigraphy and biostratigraphy (legends in Fig. 3.4).

fall is consequent; the traces of karst associated with this SB are recorded up to 16 m below this sample.

3.4.1.2 Rawil Member

The Lower Schrattenkalk Mb is followed on top by the Rawil Mb, which distinguishes itself from the under- and overlying Schrattenkalk Mbs by an increase in detrital material and the

resulting presence of marls and sandy carbonates (Stein et al., 2012a). The regional distribution of detritus is quite variable, and in certain regions, such as in Vorarlberg (western Austria), detrital levels are very low and the Rawil Mb can not be distinguished as such (Heim and Baumberger, 1933; Bollinger, 1988; Stein et al., 2012a). Lateral variations in detrital input are also considerable in the sections investigated here. For example in the section of Tierwis, the base of the Rawil Mb consists of calcareous sandstones and sandy car-

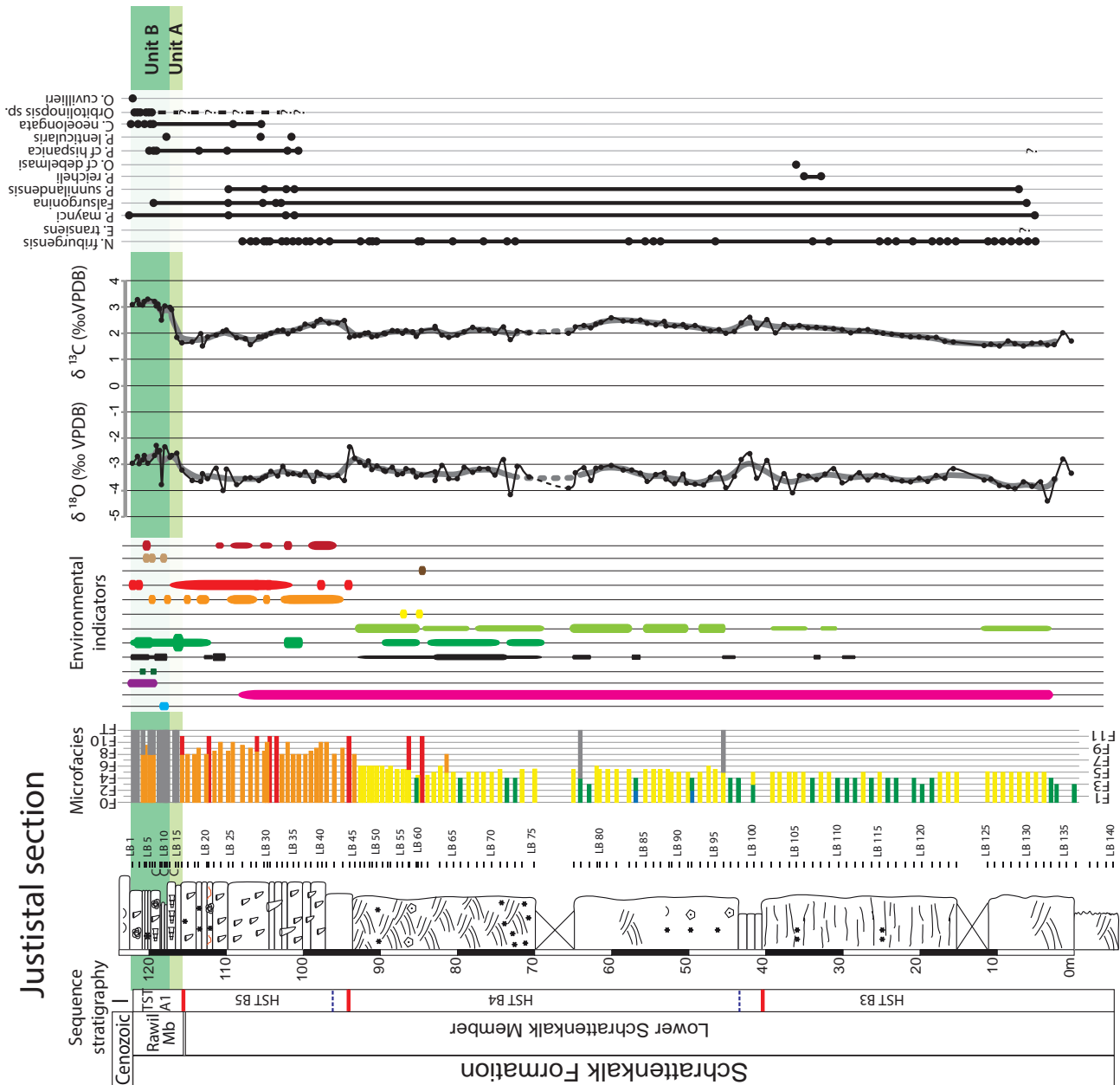


Fig. 3.7 Justistal section: lithological-sedimentological log, sequence-stratigraphic interpretation, microfacies identification, environmental indicators, isotope stratigraphy and biostratigraphy (legends in Fig. 3.4).

bonates, containing poorly sorted quartz grains, wood remains, and a marine fauna including miliolids (Embry, 2005, Stein et al., 2012a). In the section of L'Ecuelle, the first banks of the Rawil Mb show sandstone infiltrations at their top surfaces, which reach as deep down as 10 cm (Fig 3.11-D). They are covered by a carbonate breccia contained within a laminated sandstone (Fig 3.11-C). Based on the similar succession of the facies and on biostratigraphy, three units are distinguished within the Rawil Mb, which are labelled A, B and C. In general, the first meters

of the Rawil Mb are organized in several cm to dm thin parasequences, showing features of subaerial exposure at their top, such as palaeosols, beach deposits and beachrocks/washover deposits. Lag and transgressive microfacies type FT is common, and is associated with levels rich in quartz and clay, in particular in the sections of Rawil, Tierwis, L'Ecuelle and Justistal. Estimations of the quartz content are shown in Figures 3.4-3.9. Fragments of reworked charophytes are preserved in the sections of Tierwis, Rawil and Justistal. In this basal interval A, *Palorbitolina*

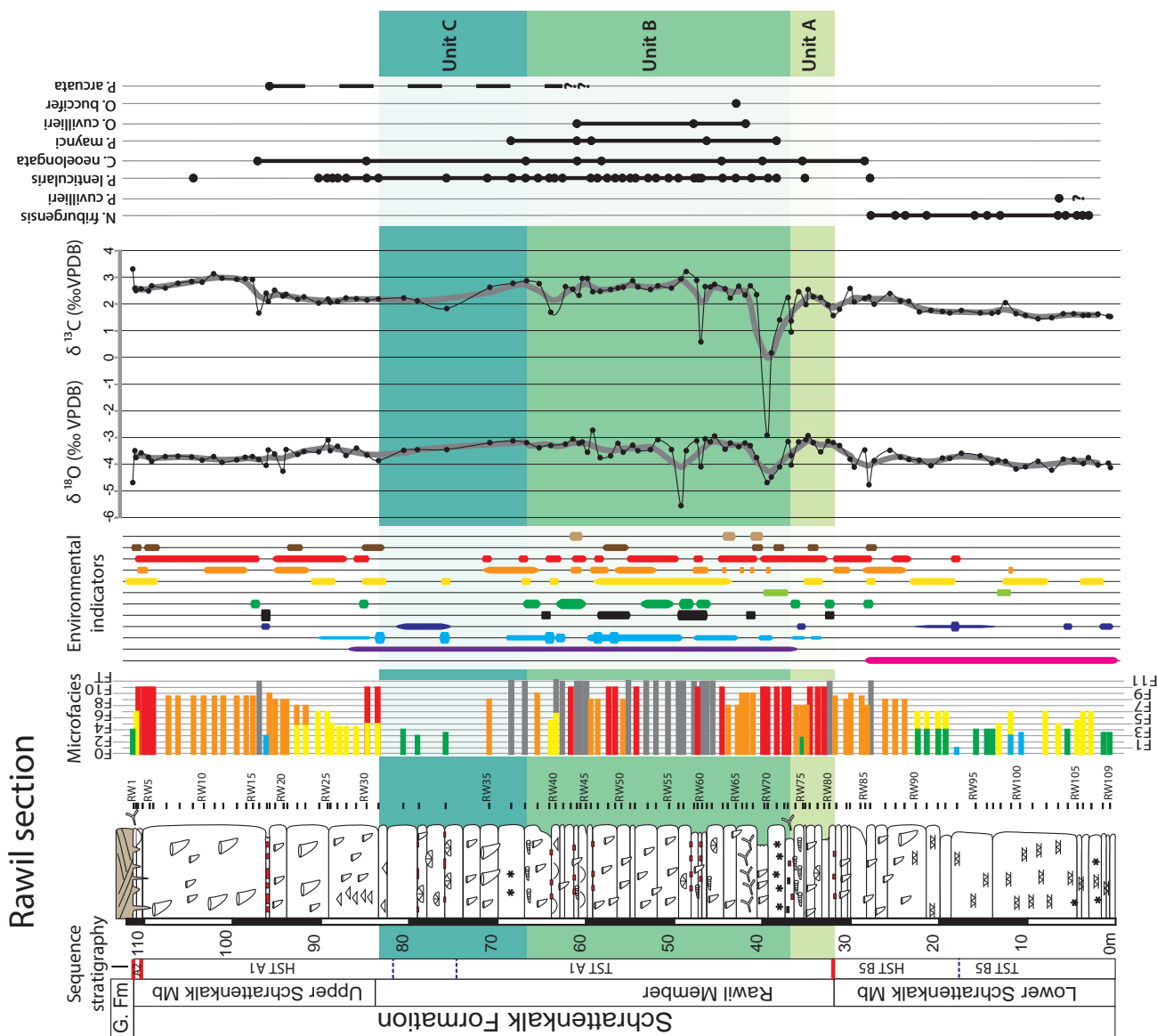


Fig. 3.8 Rawil section: lithological-sedimentological log, sequence-stratigraphic interpretation, microfacies identification, environmental indicators, isotope stratigraphy and biostratigraphy (legends in Fig. 3.4).

lenticularis or *Orbitolinopsis* were not observed, which is one of the criteria to distinguish this interval from the superjacent intervals B and C. These foraminifera are found in the Lower Schrattenkalk Mb, and their absence in the unit A supposed to be linked to peculiar environmental conditions associated with this unit. For the section of L'Ecuelle, *Palorbitolina* is found in

bioturbation infillings of the emersion surface on top of the Lower Schrattenkalk Mb, and it is likely that the unit A is missing in this section. In the section of Valsloch, following the two meters of the observational hiatus, the Rawil Mb is composed of a deeper-water facies (F3), which is followed by a more lagoonal facies including irregular urchins (*Nucleopygus roberti*), and by

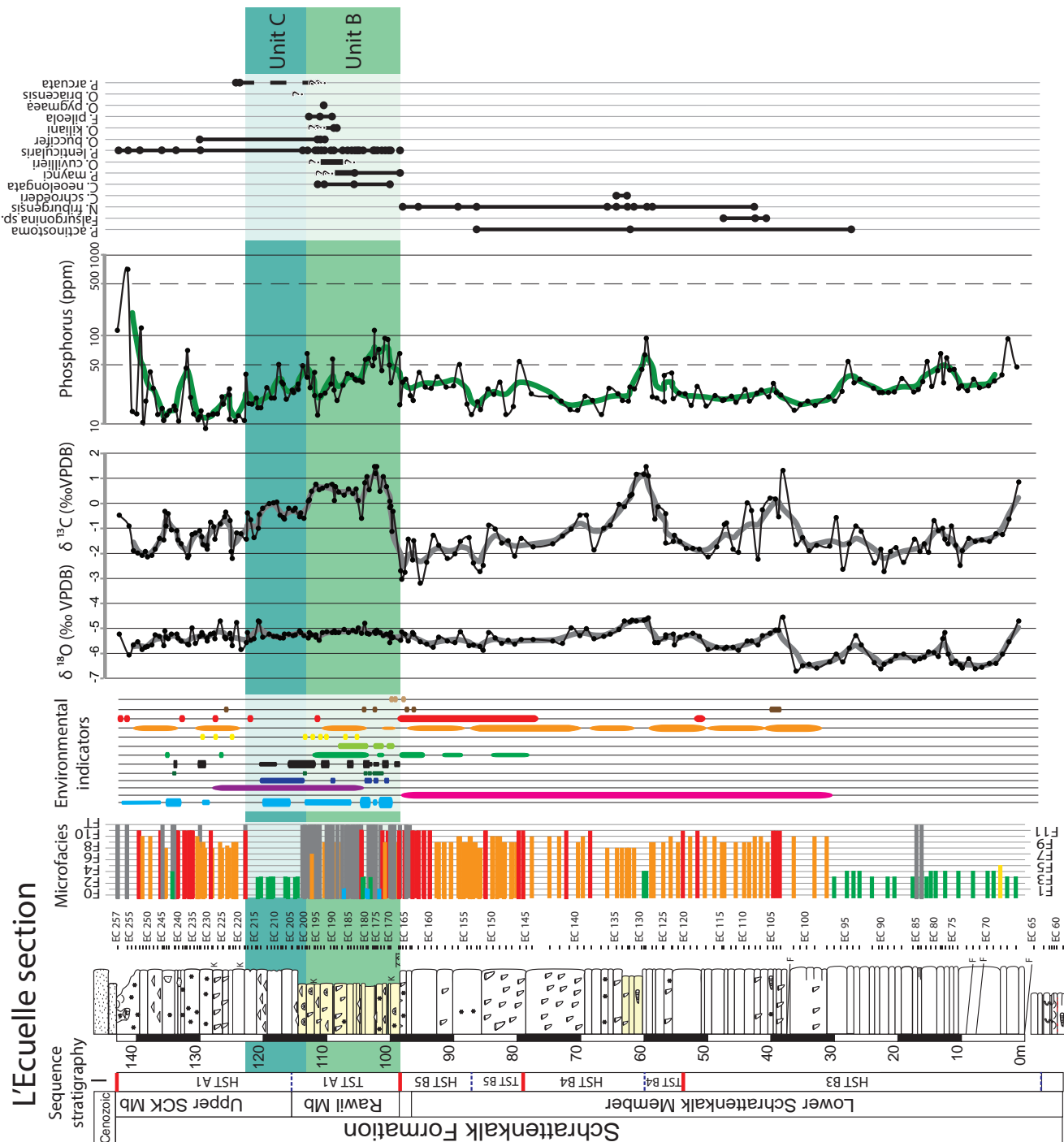


Fig. 3.9 L'Ecuelle section: lithological-sedimentological log, sequence-stratigraphic interpretation, microfacies identification, environmental indicators, isotope stratigraphy, phosphorus content and biostratigraphy (legends in Fig. 3.4).

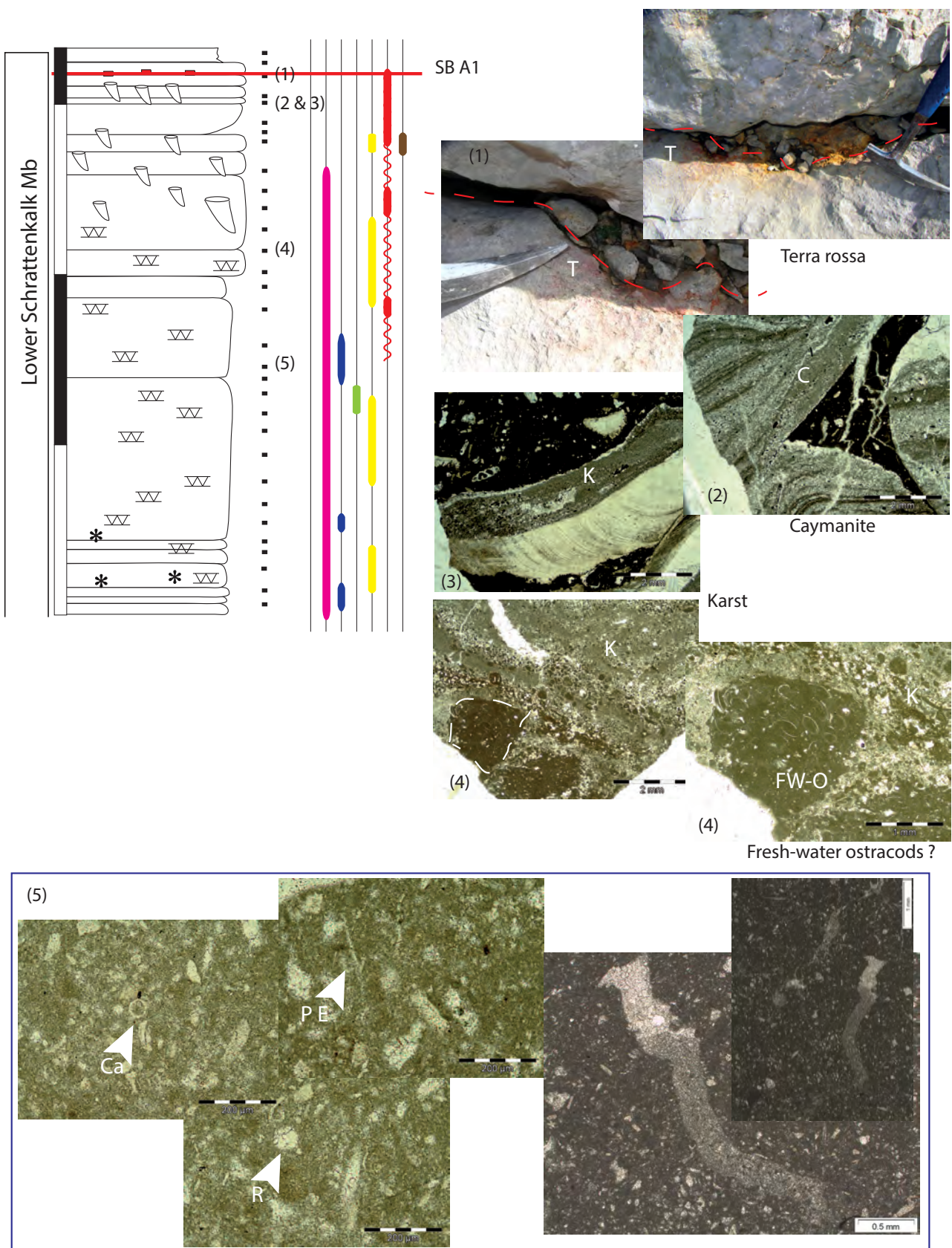


Fig. 3.10 Influence of the sea level fall associated with the SB A1 in the section of Rawil. Emersion evidence is given by terra rossa (T) deposits on the SB. Karst (K) evidence are given by caymanite (C) infilling, micro-breccia and vadose silt. The action of the karst is recorded up to the mfs B5 level (in hemipelagic facies showing calcispheres (Ca), radiolaria (R) and planktonic echinoderms (P E) remains). Microphotographs of sample RW 82 for (2) and (3); sample RW 89 for (4) and sample RW94 for (5).



a layer rich in small ooids (<100µm) and *Lithocodium-Bacinella* nodules. In the following, unit B consists of symmetrical parasequences (also described as “cyclic parasequences” in Bernaus, 1998 and Arnaud et al., 2000; or as “deep-water cycles” in Bernaus et al., 2003) showing progressively outer-shelf facies in most sections. These parasequences consist typically of a lag deposit at their base, containing reworked organisms from different habitats (FT1), followed by wackestones rich in green algae (FT3). The overlying sediments are associated with microfacies type FT2, and are rich in annelids, detrital quartz, and foraminifera attributed to sea-grass environments (e.g. *Choffatella decipiens*, *Palorbitolina* (*Palorbitolina*) *lenticularis lenticularis*; Arnaud-Vanneau, 1980). The parasequences continue with inner lagoonal sediments, which are rich in oncrites (F9-10), and end with supratidal facies, including tempestites or beach deposits (F11) (Fig. 3.11-G and H). In the section of L’Ecuelle, this interval composed of parasequences ends with a hardground on top of a bank rich in hermatypic corals, which is bioeroded and sealed by a reddish sandy matrix rich in orbitolinids and echinoids (Fig. 3.11-E and F). Unit C is characterized by the gradual appearance of an open-marine facies, within a thicker interval of approximately 20 m for the sections of Valsloch, Morschach and Tierwis, and 10 m for the section of Rawil and L’Ecuelle.

In these latter sections, the most external facies (F1, F2, and F3) are found within this interval, with sediments rich in sponge spicules, calcispheres, radiolarians and deeper-water benthic foraminifera (e.g., *Gaudryina*). Echinoderms are also abundant in this interval and lime mud corals are present in the section of Rawil. The core of Morschach offers some specificities, such as the enigmatic occurrence of a series of emergent horizons intercalated with sediments attributed to the external microfacies type F3, rich in circalittoral foraminifera and small echinoderm fragments. The Rawil Mb ends with one or several emersion levels, which define the boundary to the overlying Upper Schrattenkalk Mb.

3.4.1.3 Upper Schrattenkalk Member

The Upper Schrattenkalk Mb is composed of a massive limestone, which represents a succession of thinning- and shallowing-upward parasequences. In the sections of Valsloch, Rawil and Tierwis, its basal interval consists of oolitic microfacies (F6). In the sections of Morschach and L’Ecuelle, the Upper Schrattenkalk Mb directly starts with rudist-rich carbonates, which are attributed to a lagoonal environment (F8 to F9). In the section of Rawil, a reddish erosive surface overlain by a nodular level extremely

Fig. 3.11 A: Rudist shells, which are dissolved during an early phase and infilled by sandstone on the top surface of the Lower Schrattenkalk (L’Ecuelle; EC 166). **B:** network of Thalassinoides, infilled by yellowish sandstone on the top surface of the Lower Schrattenkalk (L’Ecuelle; EC 166). **C:** Carbonate breccia contained within laminated sandstone (L’Ecuelle; EC 172). **D:** Impregnations of dark sandstone of the top surface of the first beds of the Rawil Mb (L’Ecuelle; EC 170). **E:** Hardground on the top surface of the unit B, with bioeroded corals (orange lines) sealed by reddish orbitolinid-rich matrix (L’Ecuelle; EC 197). **F:** Zoom on a bioeroded coral and the orbitolinid-rich matrix (L’Ecuelle; EC 197). **G and H:** Accumulation of gasteropods in a tempestite level terminating a cyclic parasequence of the unit B (Rawil, RW 37).

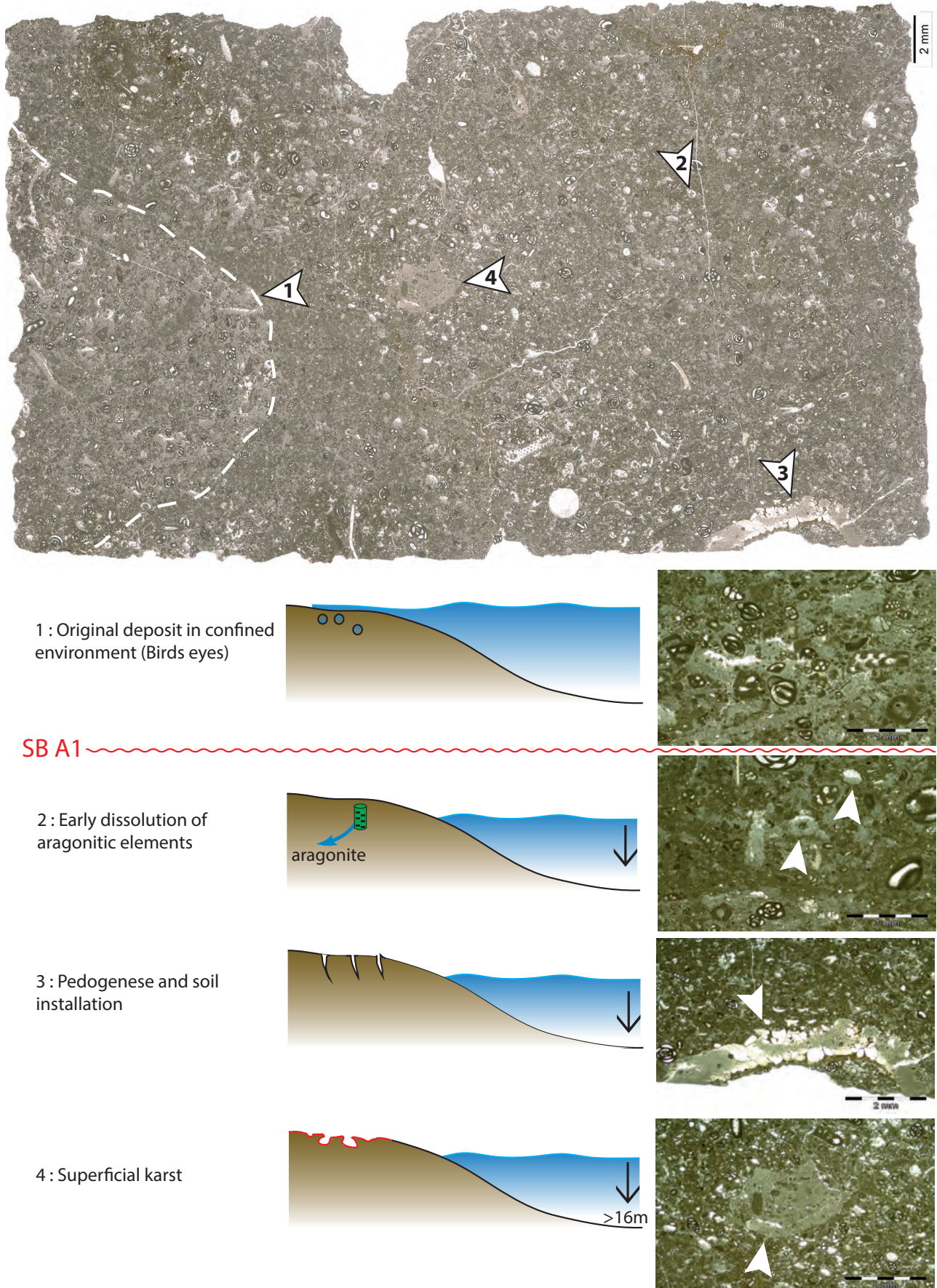


Fig. 3.12 Complete history of the sequence boundary A1 within one thin-section in the section of Jus-tistal (LB 16): (1) initial deposit: top of the HST B5; Sea level fall associated to the SB A1: evidences of emersion; (2) early dissolution of aragonitic organisms, (3) pedogenesis, (4) superficial karst (affecting sediments in a depth of more than 16m below this sample).

rich in quartz is observed; 15m below the top of the Rawil section, the Upper Schrattenkalk Mb includes a level of calcareous lithoclasts in a well-sorted sandy matrix. The matrix is composed of small angular quartz grains (around 50 µm), and includes small muscovite minerals and marine fossils and fossil debris (foraminifera, shells, green algae). Sigmoidal-shaped pebbles contain a lagoonal facies rich in miliolids (F8 type). In the section of Tierwis, a succession of parasequences is observed, which consist of rudist-rich carbonates followed by carbonates

containing corals and stromatoporoids, and ending by carbonates including *Nerineidae* accumulations. In the core of Morschach, an internal, confined microfacies containing oncolites (F10) and *Bacinella* nodules is dominant throughout the Upper Schrattenkalk Mb. Evidence of emersion is abundant in the upper part of Valsloch, Tierwis and Morschach, and affects a more than 20 meters thick interval underneath the upper boundary of the Upper Schrattenkalk Mb. The section of Rawil displays an important network of karstic caves within this member, occluded by

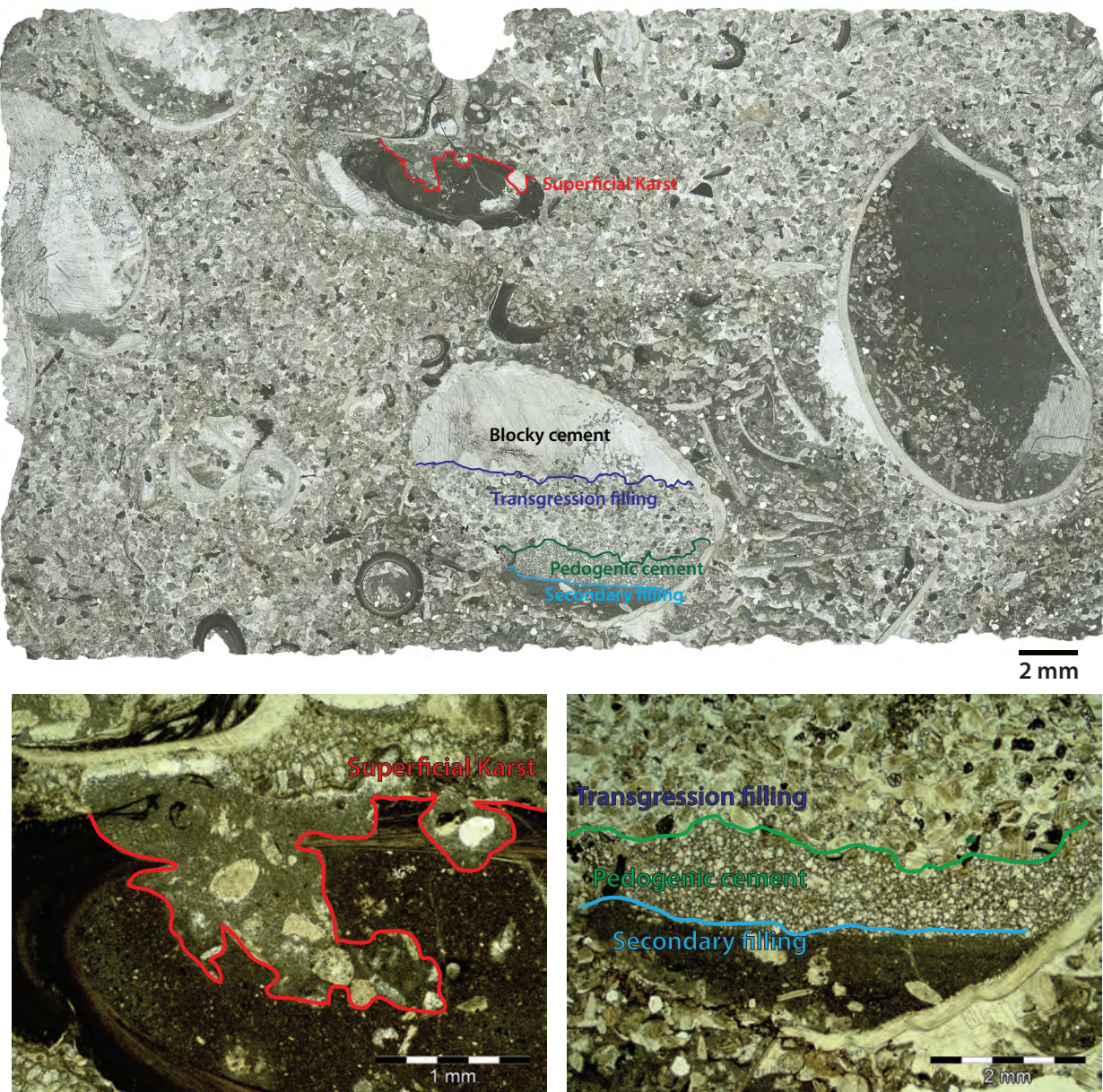


Fig. 3.13 Microphotographs of the Grünten Mb., in the borehole of Morschach. The facies is dominated by echinoderms, brachiopods and annelids. Numerous phases of dissolution and filling are highlighted.

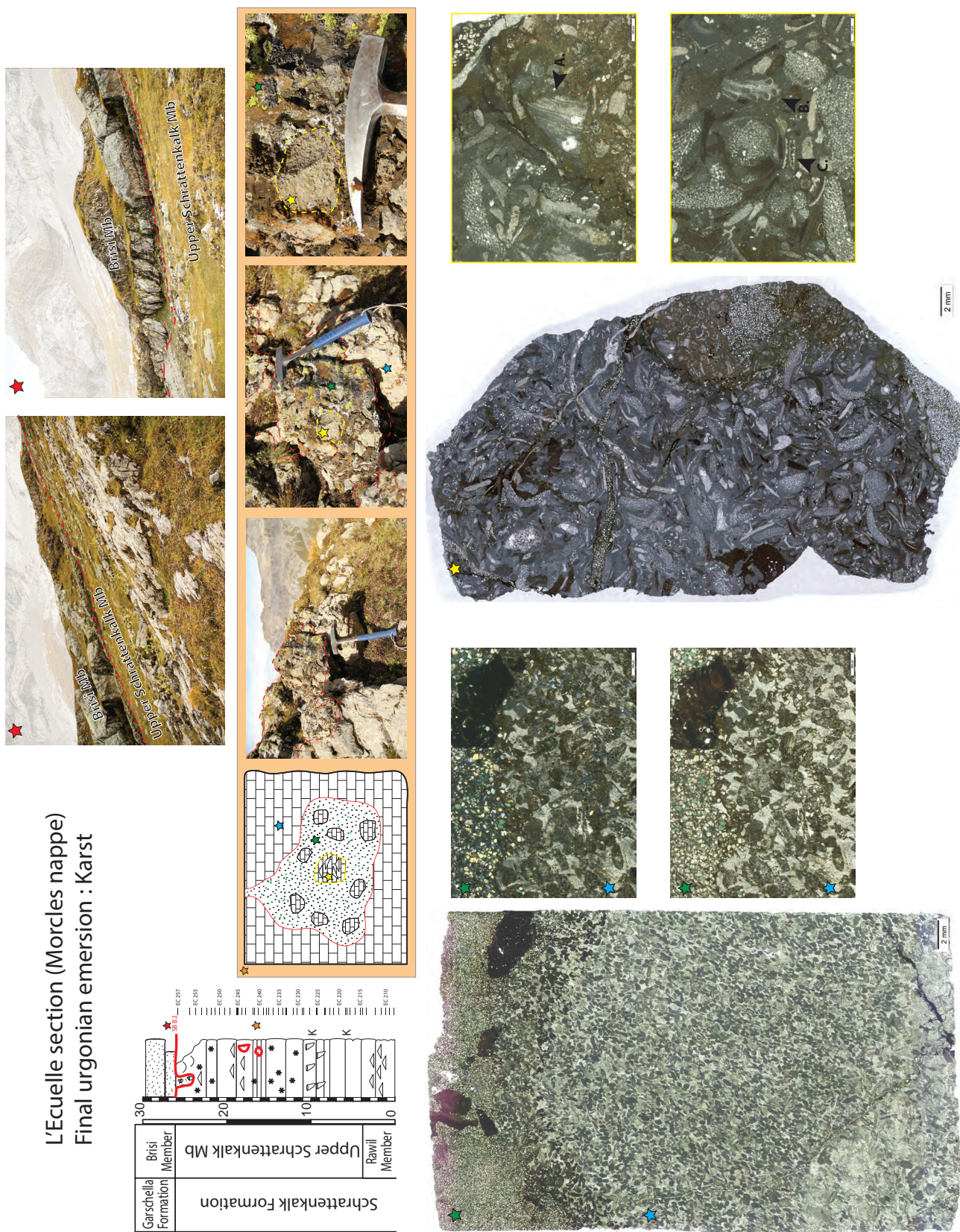


Fig. 3.14 Evidence of emersion on top of the Upper Schrattenkalk Mb. The photo with a red star illustrate the contact between the Upper Schrattenkalk Mb and the Brisi Mb, which is an irregular surface. The orange box shows the macroscopic aspect of the karstic pocket including blocks of the Grünten Mb. The blue stars indicate the shallow-water carbonate facies Upper Schrattenkalk Mb. The green stars indicate the sandy facies of the Brisi Mb. The yellow stars indicate the heterozoan facies of the Grünten Mb, rich in flat Orbitolina. A.: annelids; B.: bryozoan; C.: crinoids.

polyphased void filling.

3.4.1.4 Grünten Member

In the sections of Valsloch, Morschach and Rawil, the top of the Upper Schrattenkalk Mb is overlain by carbonates with a more external facies, rich in echinoderms and annelids. This unit is identified as representative of the overlying Grünten Mb. In Valsloch, their facies is rich in micrite, corals and stromatoporoids. Glauconitic infiltrations from the overlying Luitere Bed are observed in the top centimetres of this interval. In the Morschach core, these sediments consist of an echinodermal grainstone rich in brachiopods and annelids, and showing numerous karst phases (Fig. 3.13). Its top surface consists of the phosphatic condensed Luitere Bed. The preserved shells within this bed present different phases of infilling, one of which consists of a micrite rich in the planktonic foraminifer *Hedbergella*. In the section of L'Ecuelle, the top of the Schrattenkalk Fm is directly in contact with the Brisi Member, but large extraclasts composed of *Orbitolina*-rich carbonates of likely Grünten Mb origin are present in the infillings of the karst pockets on top of the Upper Schrattenkalk Mb (Fig. 3.14). In the sections of Valsloch and Morschach, the Luitere Bed overlays the studied sections. In Rawil and L'Ecuelle, coarse-grained sandstones of the Brisi Mb are directly covering the top of the Upper Schrattenkalk Mb. In Tierwis, the Schrattenkalk Fm is covered by glauconitic sediments of the Albian Selun Mb. In Justistal, the Upper Schrattenkalk Mb and the entire unit C and the upper part of unit B of the Rawil Mb are eroded. Eocene sediments directly overly the remainder of the Rawil Mb.

3.4.2 Stable carbon isotope composition

The results of the stable isotope analyses are shown aside the logs of each section in Figures 3.4-3.9. The lack of statically significant correlation between $\delta^{13}\text{C}$ and $\delta^{18}\text{O}$ values (covariance $R^2 = 0.11; 0.18; 0.31; 0.34, 0.13$ and 0.31 for the sections of Tierwis, Valsloch, Morschach, Justistal, Rawil and L'Ecuelle, respectively; Fig. 3.15) excludes diagenetic modification of the primary carbonate C isotope signature. The $\delta^{13}\text{C}$ values change progressively along a proximal-distal transect (Fig. 3.16). In the Lower Schrattenkalk Mb, a trend toward positive values is observed in all the sections, except for the section of L'Ecuelle, where the $\delta^{13}\text{C}$ record shows a negative trend at the base of the Lower Schrattenkalk Mb, followed by a plateau, which is interrupted by two positives excursions. In the sections of Tierwis and Rawil, the $\delta^{13}\text{C}$ values gradually increases. In contrast, the sections of Valsloch and Morschach show stable values at the base, which are followed by an abrupt positive shift to again stable values (+1.5‰ of amplitude). The section of Justistal shows stable values as well, which are interrupted by positive shifts. In the sections of Tierwis, Justistal, Rawil and L'Ecuelle, they show minimal values at or near the boundary between the Lower Schrattenkalk Mb and the overlying Rawil Mb, which are followed by a general positive shift, with an amplitude of up to +3‰ (L'Ecuelle). The $\delta^{13}\text{C}$ records evolve differently in the distal sections of Valsloch and Morschach, where they remain stable across the boundary between the Lower Schrattenkalk Mb and the Rawil Mb. The maximum in $\delta^{13}\text{C}$ values near the base of the Rawil Mb is followed by a trend towards more negative values in all sections (Fig. 3.16). This

trend is especially pronounced in the two distal sections of Morschach and Valsloch, where two distinctive minima occur in the upper part of the Rawil Mb, with a negative shift of up to -5‰. The boundary interval towards the Upper Schrattenkalk Mb is characterized by an evolution towards more positive values, which is especially pronounced in the distal sections, and which is not observed in the L'Ecuelle section. The maximum in the $\delta^{13}\text{C}$ record in the basal part of the Upper Schrattenkalk Mb is followed by an evolution towards more negative values (Fig. 3.16). In the sections of Tierwis and L'Ecuelle, this is followed by a positive trend in the top part of the Upper Schrattenkalk Mb.

3.4.3 Phosphorus content

The total phosphorus content was measured for the sections of L'Ecuelle (Fig 3.9), Tierwis (fig 3.4) and Valsloch (Fig 3.5). The Lower Schrattenkalk Mb shows a similar decrease in phosphorus values in all sections. This trend is interrupted by higher values in the marly levels. The uppermost part of the Lower Schrattenkalk Mb displays higher phosphorus values in the section of L'Ecuelle and pronounced fluctuations in the section of Tierwis. The base of the Rawil Mb is characterized by a peak in phosphorus values for the sections of Tierwis and l'Ecuelle. For the section of Tierwis and Valsloch, the upper part of the unit B shows a progressive increase in phosphorus values until a maximum content is reached in unit C. In these two sections this phase is followed by a decrease in phosphorus values until the Upper Schrattenkalk Mb. For the section of L'Ecuelle, a decrease occurs from the basal part of the unit B until the Upper Schrattenkalk Mb. In the Upper Schrattenkalk Mb,

phosphorus contents are extremely fluctuating for the sections of Tierwis and L'Ecuelle. The maximum content for all sections is recorded in the uppermost meters of the Upper Schrattenkalk Mb, where infiltrations from the overlying Garschella Fm are observed in the field.

3.5 Discussion and interpretations

3.5.1 Biostratigraphy

The biostratigraphic scheme used in this study is based on benthic foraminifera, which was developed by Arnaud-Vanneau (1980), Arnaud-Vanneau and Arnaud (1990), Arnaud et al. (1998), and Arnaud (2005). This group underwent a profound renewal at the Barremian–Aptian boundary, which is in particular characterized by the disappearance of *Neotrocholina friburgensis* GUILLAUME and REICHEL, 1957, *Paracoskinolina hispanica* (PEYBERNÈS, 1976), *P. reicheli* (GUILLAUME, 1956), *Paleodictyoconus cuvillieri* (FOURY, 1963), and *P. actinostoma* ARNAUD-VANNEAU and SCHROEDER, 1976 (temporary disappearance of this latter in the basal interval of the “Lower Orbitolina Beds”; unit A); the abundance of *Palorbitolina lenticularis* (BLUMENBACH, 1805), *Orbitolinopsis buccifer* ARNAUD-VANNEAU and THIEULOUY, 1972, *O. kiliani* SILVERSTRI, 1932, and *O. cuvillieri* MOULLADE, 1960; and the appearance of *Paracoskinolina arcuata* ARNAUD-VANNEAU, 1976, *Orbitolinopsis briacensis* ARNAUD-VANNEAU, 1980, and *O. pygmaea* ARNAUD-VANNEAU, 1980. The boundary of the units A and B within the Rawil Mb is marked by the occurrence of *Palorbitolina lenticularis*, *Orbitolinopsis buc-*

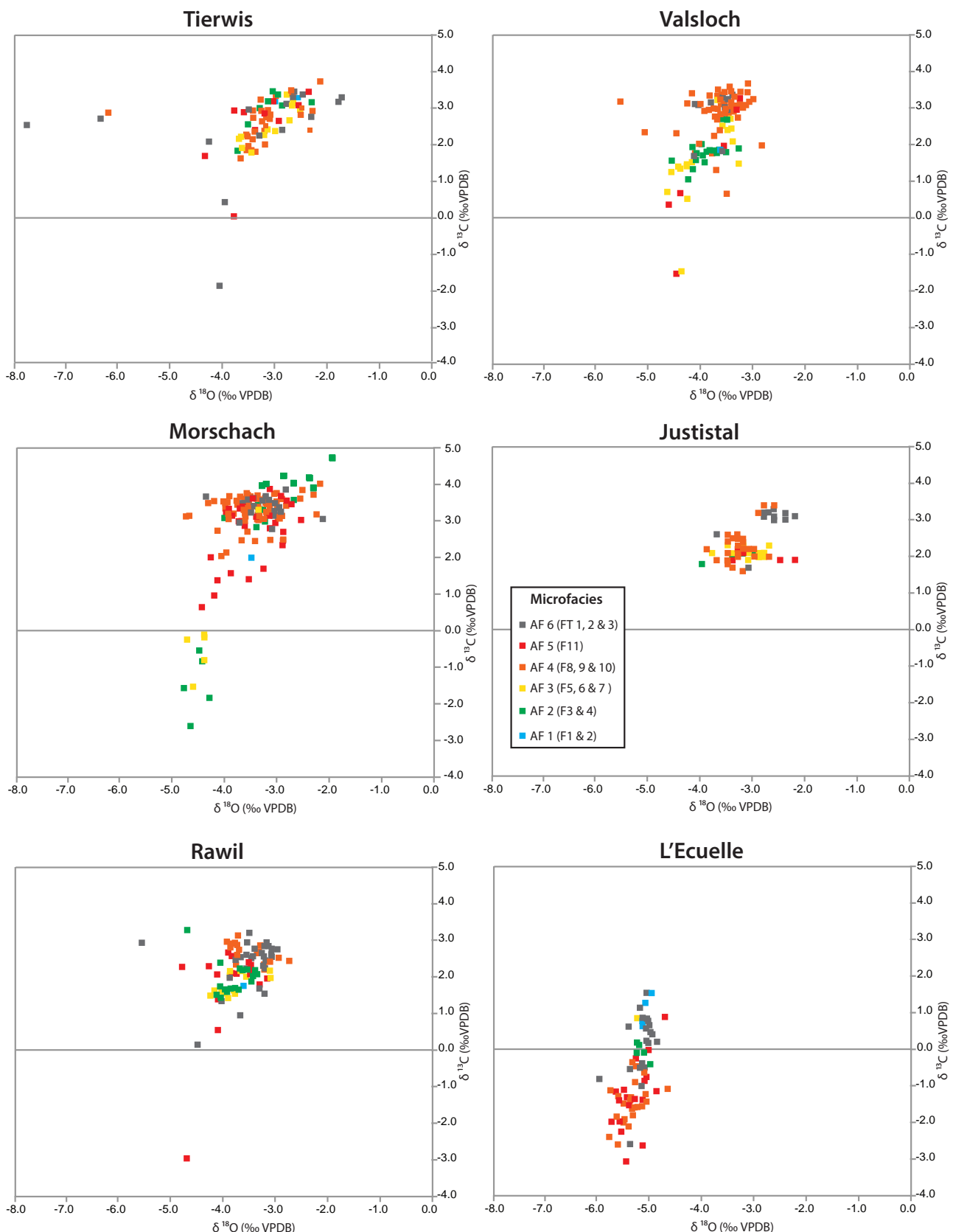


Fig. 3.15 Scatter plots of $\delta^{13}\text{C}$ vs. $\delta^{18}\text{O}$ values from the sections of Tierwis, Valsloch, Morschach, Justistal, Rawil and L'Ecuelle. The colours of squares represent the microfacies association.

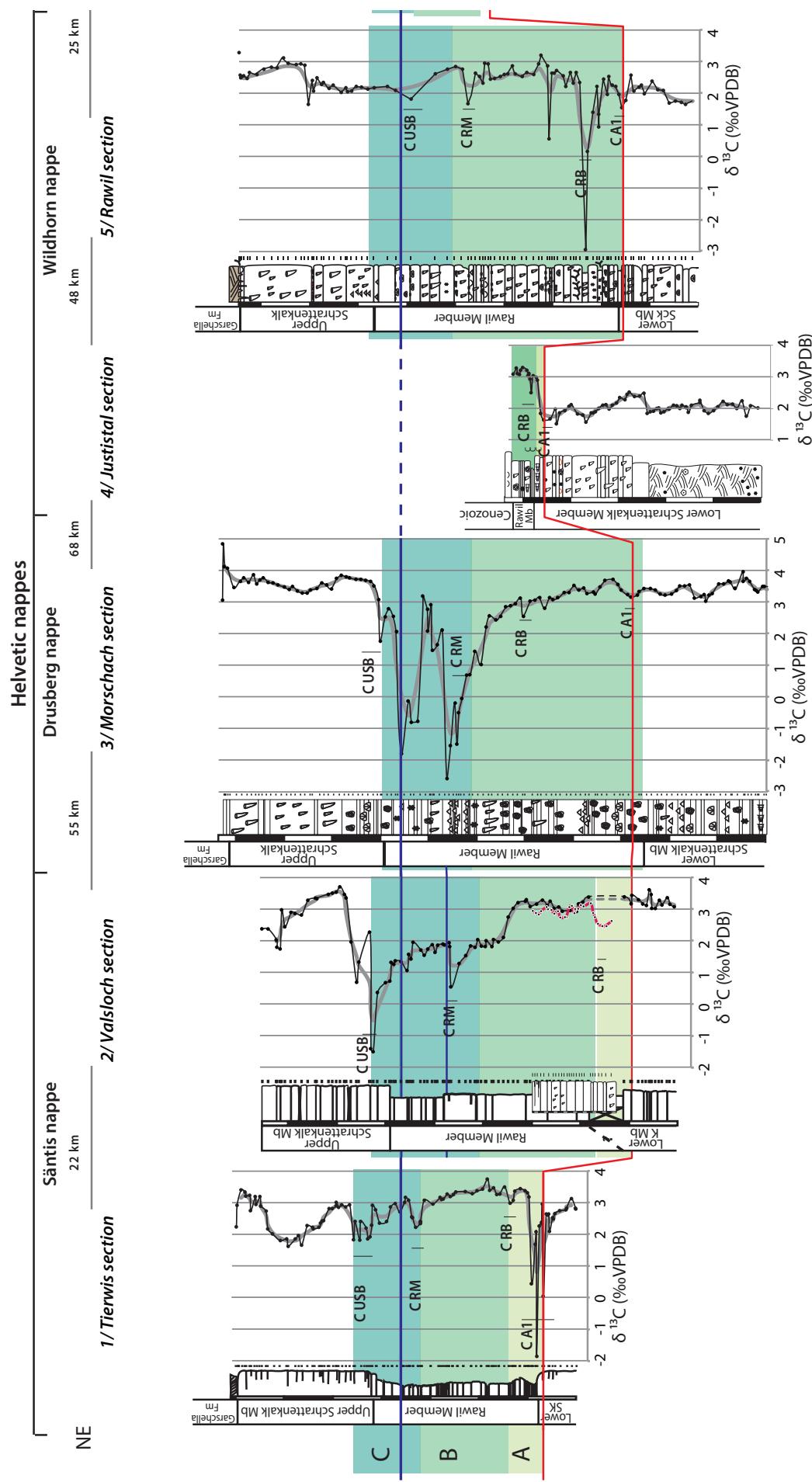


Fig. 3.16 Correlation of the sequence stratigraphy and the carbon-isotope record from the Schrattenkalk Fm in the Helvetic nappes with sections from the subalpine chains (Cluses (redraw after Wermeille 1996) and Huck et al. (2013)), Bornes Massif; Balcon des Ecouges (from Raddadi (2005) and Embry (2005)) and Gorges du Nant (from Raddadi (2005) and Bastide (2014)), Vercors massif) and the basinal record of the La Béoule section (from Stein et al., 2012b).

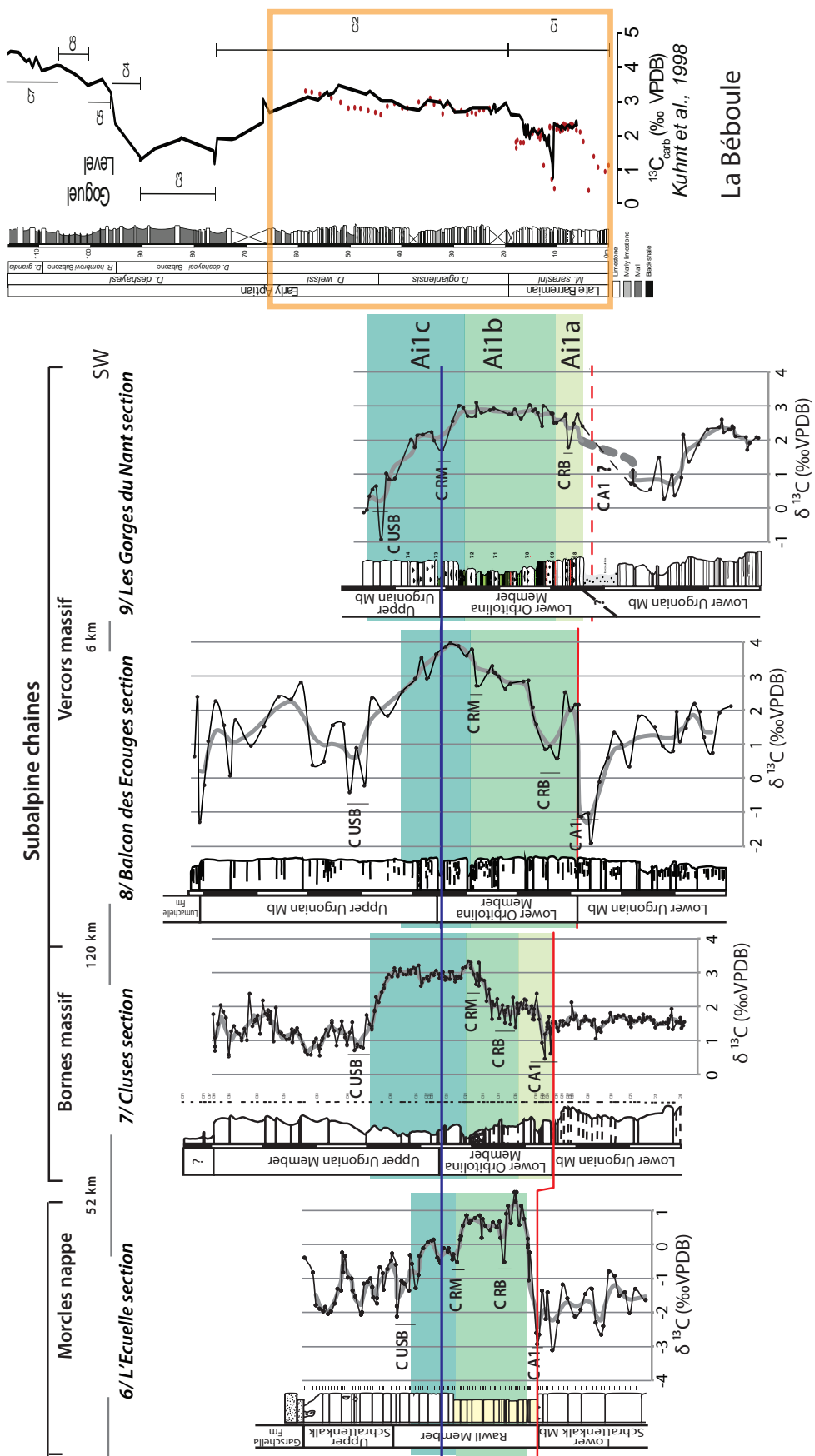


Fig. 3.14 Continued

cifer, *Orbitolinopsis kiliani* and *Orbitolinopsis cuvillieri*, according to Arnaud-Vanneau (1980) and Raddadi (2005)(see below). The transition to the Upper Schrattenkalk Mb is characterized by the first occurrence of *Orbitolinopsis briacensis*, *Orbitolinopsis pygmaea* and *Palorbitolina arcuata*. The benthic foraminiferal biostratigraphic events are well comparable between the Helvetic sections and also with the sections in the Subalpine Chains; this confirms their utility for dating purposes in this particular part of the Urgonian platform. The biostratigraphic observations indicate an age ranging from the *T. vandenheckii* to *G. sartousiana* zones for the onset of the Lower Schrattenkalk Mb, depending on the position on the platform. The Rawil Mb has an *D. oglanlensis* zone age, and the Upper Schrattenkalk as a whole is dated as the *D. forbesi* zone (Fig. 3.2).

3.5.2 Sequence stratigraphy

In this study, the key surfaces were identified using field observations and sedimentological and paleoecological analyses of thin sections. Once identified, the surfaces and trends in facies and microfacies allowed us to adopt a sequence-stratigraphic scheme, which is correlatable with the one developed in the Vercors region of SE France by Arnaud and Arnaud-Vanneau (1989, 1991), Arnaud-Vanneau and Arnaud (1990), and Hunt and Tucker (1993). Their model was derived from the one first defined by Vail et al. (1977) and subsequently described in numerous publications (e.g., Van Wagoner et al., 1988; Emery and Myers, 1996; Coe et al., 2003; Catuneanu et al., 2009). The sequence-stratigraphic model is chronostratigraphically calibrated in the Angles section of the Vocontian Trough,

where the presence of ammonites allows for biostratigraphic time control, as shown in Figure 3.2. The same sequence-stratigraphic approach was applied in previous studies for the Rawil Mb in the Helvetic Alps (Embry, 2005 and Stein et al., 2012a).

The Lower Schrattenkalk Mb corresponds to the sequences B3, B4 and B5. On the platform, the lowstand systems tracts (LST's) are not recorded and are embodied in the hiatus of the sequence boundaries (SB's). Exceptions are the sections of Valsloch and Justistal, where the Lower Schrattenkalk Mb starts with the LST B3, which consists of a bioclastic accumulation overlain by a lag deposit representing the transgressive surface (TS) B3. In the sections of Tierwis, L'Ecuelle and Morschach, the Lower Schrattenkalk Mb starts with the late transgressive systems tract (TST) B3. The maximum flooding surface (MFS) B3 is characterized by an important occurrence of annelids and the disappearance of *Eopalorbitolina transiens*. The lagoonal facies rich in rudists occurs in the HST B3, and are present in the sequences B4 and B5. These two sequences are characterized by shallow-water environment rich in rudists, mfs are placed in the intervals where microfacies are the most distal and the SBs are placed on the interval showing the maximum of emergent feature. The major emergent surface recorded in the sections near or at the top of the Lower Schrattenkalk Mb includes the Barremian-Aptian boundary and coincides with the SB A1. In the section of Tierwis, this SB is placed in the same position as previously proposed by Embry (2005) and Stein et al. (2012a), in the uppermost part of the massive limestone of the Lower Schrattenkalk Mb, where we observe a sudden stop in karstification and the presence of lag deposits and intense reworking above the SB. In the section of Rawil, the SB is marked by a thin

layer of *terra rossa* deposits; early dissolution and karstification affect the sediments at least 15 meters below this surface (Fig. 3.10). In the sections of Valsloch and Justistal, the SB A1 was not recognized in the field, but was identified based on microfacies analysis. In the Justistal section, emersion is shown by aragonite dissolution and the presence of paleosols and karstification. In the core of Morschach, two alternative positions are possible for the attribution of the SB A1. The first possible position is based on the $\delta^{13}\text{C}$ record and its correlation with the Valsloch section. The second possible position is based on microfacies analyses, and more precisely on the important occurrence of *Palorbitolina lenticularis*, green algae, and increased quartz content. In this core, evidence of subaerial exposures occurs in numerous intervals and none has been recognized as a major one.

The Rawil Mb as a whole corresponds to the TST of sequence A1. It is characterized by the progressive deepening of facies (Stein et al., 2012a). The unit A represents the early TST. It is characterized by the rapid filling of accommodation space, shown by the emergent tops of the parasequences and the thickness of these parasequences. In the most proximal section (L'Ecuelle), the absence of unit A indicates that the sediments associated with TST A1 did not yet arrive by retrogradational onlap. In the sections of Rawil and Morschach, the absence of unit A may reflect the effect of local palaeotopographic highs. Unit B corresponds to the middle TST, which shows cyclic parasequences. Unit C includes the late TST, the MSF and the early HST. In the section of Valsloch, two alternative intervals may represent the MFS; the first one occurs in the lower part of unit C, where the component quantification indicates maximum deepening and the presence of planktonic foraminifera. The second possible interval is the interval where the

last appearance of open marine facies (F3) was observed, in the upper part of unit C. A similar case was described for the Lower Orbitolina Beds in the Subalpine Massifs in southeastern France (Raddadi, 2005). According to Schlager (2005), in carbonate platforms where change is gradual, the MFS may be represented by an interval rather than a single surface. In this case, unit C would consist of the MF interval.

The Upper Schrattenkalk Mb embodies the HST of sequence A1. Overall, the member is characterized by shallowing-upward facies. SB A2 is placed on top of the Upper Schrattenkalk Mb. This emergent episode is associated with karstification, which affected the Upper Schrattenkalk Mb in an interval of up to more than 10 m below this surface.

In the core of Morschach, the base of the Grünten Member shows brachiopod accumulations and their shells are partially filled with sediment. The corresponding geopetal structures show various orientations, illustrating different phases of resedimentation. Several phases of karstification and erosion are recorded in this stratigraphic unit, which represents sequence A2.

3.5.3 Correlations along the northern margin of the Tethys

The sedimentary successions preserved in the Helvetic Alps are comparable to the Barremian–Aptian carbonate platform sediments present elsewhere along the northern margin of the Tethys. The Lower and Upper Schrattenkalk Mbs are the equivalent of the Lower and Upper Urgonian limestone in southeastern France, as discussed in Funk and Briegel (1979). The equivalent of the Rawil Mb, the “Lower

Orbitolina Beds”, includes a lithological and facies succession in the Subalpine Chains of the Vercors Massif (SE France), which is almost identical to that preserved in the Rawil Mb. The characteristics of the three units described in this study (namely A, B and C) are compared here with the ones identified by Arnaud Vanneau and Arnaud (1980), named Ai1a, Ai1b and Ai1c. The main lithological features, characteristic environmental markers and sequence stratigraphic stacking pattern according to Arnaud-Vanneau (1980) and Raddadi (2005) are shown in Figure 3.17. In our sections, unit A is overlying the

SB A1. It consists of cm- to dm-thick rhythmic calcareous parasequences showing the development of palaeosols and emersion features at their top. In proximal settings, *Charophytes* are preserved, and a coarse sandstone occurs, which is interpreted as lagoonal estuarine depositional environments (Embry, 2005). This interval is characterized by the absence of representatives of the genus *Orbitolinopsis* and the species *Palorbitolina lenticularis*. Unit A ends with an epikarstic surface, which is covered by unit B. Unit A shows the same characteristics as unit Ai1a in the Vercors Area. Unit Ai1a starts with

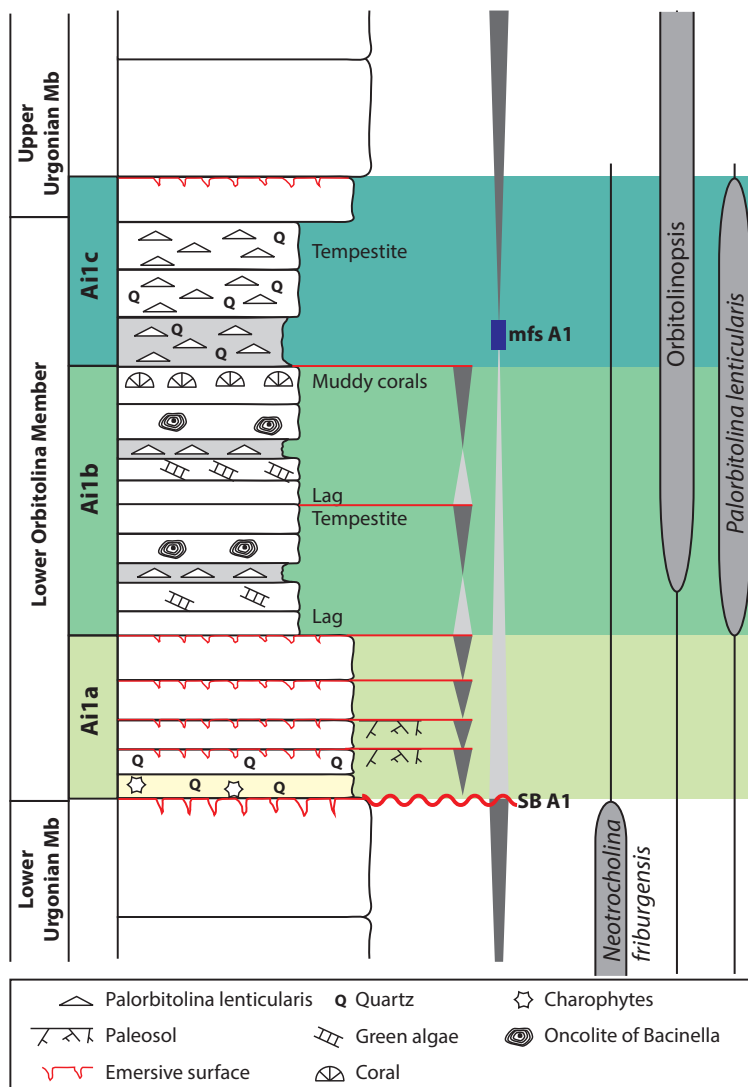


Fig. 3.17 Synthetic log the Lower Orbitolina Beds along the N-W Tethyan margin. The three units defined by Arnaud-Vanneau (1980): Ai1a, Ai1b and Ai1c are in light-, medium- and dark green, respectively; they are the equivalent of the units A, B and C in the Rawil Mb of the Helvetic nappes. Characteristics sedimentological and faunistic markers of each unit are shown (after observations of Arnaud-Vanneau, 1980 and Raddadi, 2005).

a brackish depositional environment, attested by the presence of *Charophytes*, followed by a gradual marine transgression, which is recorded by decimetric parasequences showing rubefaction, lag deposits and palaeosols. Ai1a is also characterized by the absence of marl and *Orbitolinopsis*. The presence of *Charophytes* above SB A1 was also documented in the Pyrenean section of Organya (Bernaus et al., 2003).

Unit B is arranged in cyclic parasequences. The gradual enrichment in sponge spicules and/or thin grainstone levels rich in small circalittoral foraminifera (e.g., *Gaudryina*) indicate a deepening phase, which goes along with the presence of *Palorbitolina lenticularis* and *Orbitolinopsis*. The top of this unit is generally characterized by the widespread occurrence of corals, stromatoporoids and chaetetids in muddy sediment, which may be associated with a hardground surface. In Vercors, the equivalent unit Ai1b consists of one or several marly beds, which are rich in *Palorbitolina lenticularis*, and includes wackestones rich in green algae, whereas evidence of emersion are absent. Cyclic parasequences are also characteristic of this interval, as is the appearance of *Orbitolinopsis cuvillieri* and the abundance of *Paracoskinolina maynci*. The upper part of this unit records a slow sedimentation rate as shown by a hardground, which terminates the bioherm development.

In the Helvetic Alps, the third unit C starts on top of this surface, with the mass accumulation of *Palorbitolina lenticularis* in wackestone to packstone marl and marly limestone. This unit represents a second deepening phase, interpreted as the maximum flooding interval. It becomes gradually more calcareous and ends with a surface showing evidence for subaerial exposure. The unit C is covered by the rudist-bearing Upper Schrattenkalk Mb. The first beds of the Upper Schrattenkalk Mb are included in the unit

C. In the Vercors Massive, the unit Ai1c starts with the last marly level of the Lower Orbitolina Beds and shows an increase in detrital sediments and an opening of the environment through deeper-marine facies. *Orbitolinopsis buccifer* and *Palorbitolina lenticularis* show a maximum in their occurrences and *Orbitolinopsis cuvillieri* evolved to *Orbitolinopsis kiliani*. This unit finishes with an emersive episode.

Using both benthic foraminiferal biostratigraphy, as well as trends in microfacies and the $\delta^{13}\text{C}$ records, we correlated the Helvetic sections with a selection of sections from the Subalpine chains (Fig. 3.18). The sections of Cluses in the Aravis-Bornes massif is based on Wermeille (1996) and Huck et al. (2011, 2013), the section of Les Gorges du Nant on Raddadi (2005) and Bastide (2014), and the section of Balcon des Ecouges on Embry (2005). The age of the Cluses section has been differently interpreted (Trabold, 1996; Wermeille, 1996; Huck et al., 2011, 2013). We concur with Wermeille (1996) and place the Barremian–Aptian boundary at the base of the positive C isotope excursion, based on lithological and microfacial trends.

3.5.4 Preservation of the primary carbon stable isotope composition

The assessment of the degree of possible diagenetic, hydrothermal or metamorphic overprints of the primary signature is discussed here.

We interpret the $\delta^{13}\text{C}$ records and trends therein as the result of different and partly interacting processes, which are related to local and regional differences in facies, microfacies, and mineralogical compositions, the local to regional diagenetic history, and overarching trends related to global changes in the carbon cycle.

As a first interpretation, the lack of statistically significant positive correlation between $\delta^{13}\text{C}$ and $\delta^{18}\text{O}$ values (R^2) and the generally positive values in the $\delta^{13}\text{C}$ records would suggest that diagenetic overprint of the primary isotopic signature can be excluded (Choquette and James, 1987). An exception is the section of L'Ecuelle, where the $\delta^{13}\text{C}$ records of both Schrattenkalk Mbs show low to negative values. This is explained by considerable diagenetic overprint due to the proximal depositional setting for this section, superimposed by low-grade metamorphism (from diagenetic conditions for the Säntis, Wildhorn and Drusberg nappes and up to anchizone conditions for the Morcles Nappes; Frey et al. 1980; Breitschmid, 1982; Burkhard, 1988; Dietrich and Casey, 1989; Wang et al., 1996; Goy-Eggenberger, 1998; Burkhard and Goy-Eggenberger, 2001). In addition, trends towards negative values occur also in relation to the presence of emersion surfaces (see below).

General trends are discernible in the sections, which consistently change going from proximal, shallower-water sections towards more distal, deeper-waters sections. In the Lower Schrattenkalk a similar trend is observed in most of the sections, which consists in an important positive shift of the $\delta^{13}\text{C}$ records, which coincide with the onset of the lagoonal facies F8 to F10. This trend is particularly well developed in the sections of Valsloch (+2‰) and Morschach (+1.5‰), but it is also visible in the sections of Justistal, Tierwis and Rawil. In the section of L'Ecuelle, the $\delta^{13}\text{C}$ record is less correlated with changes in facies, which is probably due to important diagenetic overprint. In proximal sections, the boundary between the Lower Schrattenkalk and the Rawil Mbs is characterized by minimal values (CA1 in Fig. 3.16), whereas the lower part of the Rawil Mb itself shows maximal values. In distal sections, the

transition between the Lower Schrattenkalk Mb and the Rawil Mb is not marked by large shifts in the $\delta^{13}\text{C}$ records, but the Rawil Mb shows an upwards trend towards more negative values. This upward trend towards more negative values is also observed for the upper part of the Rawil Mb in the proximal sections. Up to three shorter-term negative excursions occur superimposed on this long-term trend, which are designated here as CRB, CRM and CUSB. They mark the boundary of units A and B (CRB), occur near the boundary of units B and C (CRM, specifically in the sections of Tierwis and L'Ecuelle), and define or are close to the boundary between the Rawil and Upper Schrattenkalk Mbs (CUSB), respectively (Fig. 3.16). The CUSB negative excursion is especially well defined in the more distal sections, where the basal interval of the Upper Schrattenkalk Mb coincides with the upper limb of the excursion. In proximal sections, the long-term negative trend in the $\delta^{13}\text{C}$ continues well into the Upper Schrattenkalk Mb.

The overall trend in the proximal sections correlates quite well with the trend in the Angles and La Bédoule sections in southeastern France, which both provided a high-resolution $\delta^{13}\text{C}$ record for this time interval (Moullade et al., 1998; Renard et al., 2005; Godet et al., 2006; Kuhnt et al., 2011; Stein et al., 2012). Similar trends are also seen in the sections of Cluses (Huck et al., 2011, 2013), and the Balcon des Ecouges (Embry, 2005) and Gorges du Nant sections of the Vercors area (Bastide, 2014) (Fig. 3.16 and 3.18). These positive correlations confirm that changes in the global carbon cycle and its imprint in the $\delta^{13}\text{C}$ record are also recorded in the Urgonian platform, as was already shown by Wissler et al. (2003), Embry (2005), Huck et al. (2011, 2013) and Stein et al. (2012a).

Deviations from the general trends in the $\delta^{13}\text{C}$ record are related to the specificities of the

Urgonian platform and its diagenetic history. In the following, we explore potential relationships between the trends and deviations therein and the mineralogical composition (aragonite versus calcite), primary porosity (e.g., in echinoderms), and the presence of emersion surfaces. Positive $\delta^{13}\text{C}$ excursions on and near carbonate platforms, such as the one in the lower part of the Rawil Mb may be related to an increase in aragonitic components, as was proposed by Godet et al. (2006) and Föllmi et al. (2006, 2007), thereby following Swart and Eberli (2005). To estimate the initial content of aragonite in the sediments, a systematic quantification of components in thin sections was performed for the sections of Valsloch and Gorges du Nant (Fig. 3.5 and 3.16). Components which were originally aragonitic include green algae (Scholle and Ulmer-Scholle,

2003; Flügel, 2004), which are partly preserved as fossil debris (e.g., Dasycladals), and which may also have contributed to the production of lagoonal micrite (Udoteacean algae; Lowenstam and Epstein, 1957; Neumann and Land, 1975; Milliman et al, 1993; Seagrass, Enriquez and Schulbert, 2014). In our quantitative analysis, only the contribution of green algae in the form of preserved and recognizable fossils is considered. Aragonite is also important in rudists (Steuber, 2002; Skelton and Gili, 2012) and other mollusk groups such as gastropods (Bandel, 1990). As a first result, a surprisingly good correspondence is seen between reconstructed aragonite contents and the $\delta^{13}\text{C}$ record in the Gorges du Nant section, whereas the near-absence of aragonite in the Valsloch section concurs with the trend to more negative values in its $\delta^{13}\text{C}$ record (Fig.

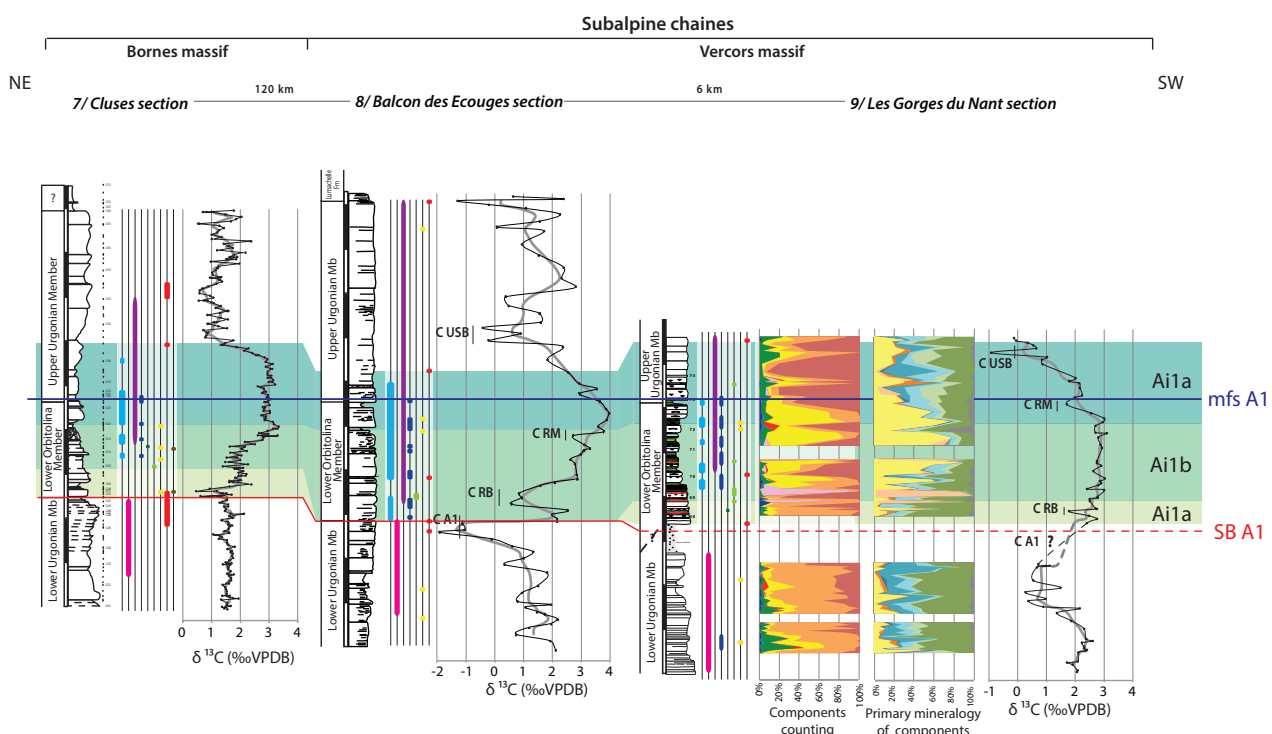


Fig. 3.18 Lithological-sedimentological log, sequence-stratigraphic interpretation environmental indicators and isotope stratigraphy for the sections of Cluses (redraw after Wermeille (1996) for the log and from Huck et al. (2013) for the isotope data), Le balcon des Ecouges (from Raddadi (2005) for the log and the data of environmental indicators; from Embry (2005) for the isotope data), Les gorges du Nant (from Raddadi (2005) for the log and the data of environmental indicators; from Arnaud-Vanneau (unpublished data) for the component counting; from Bastide (2014) for the isotope data).

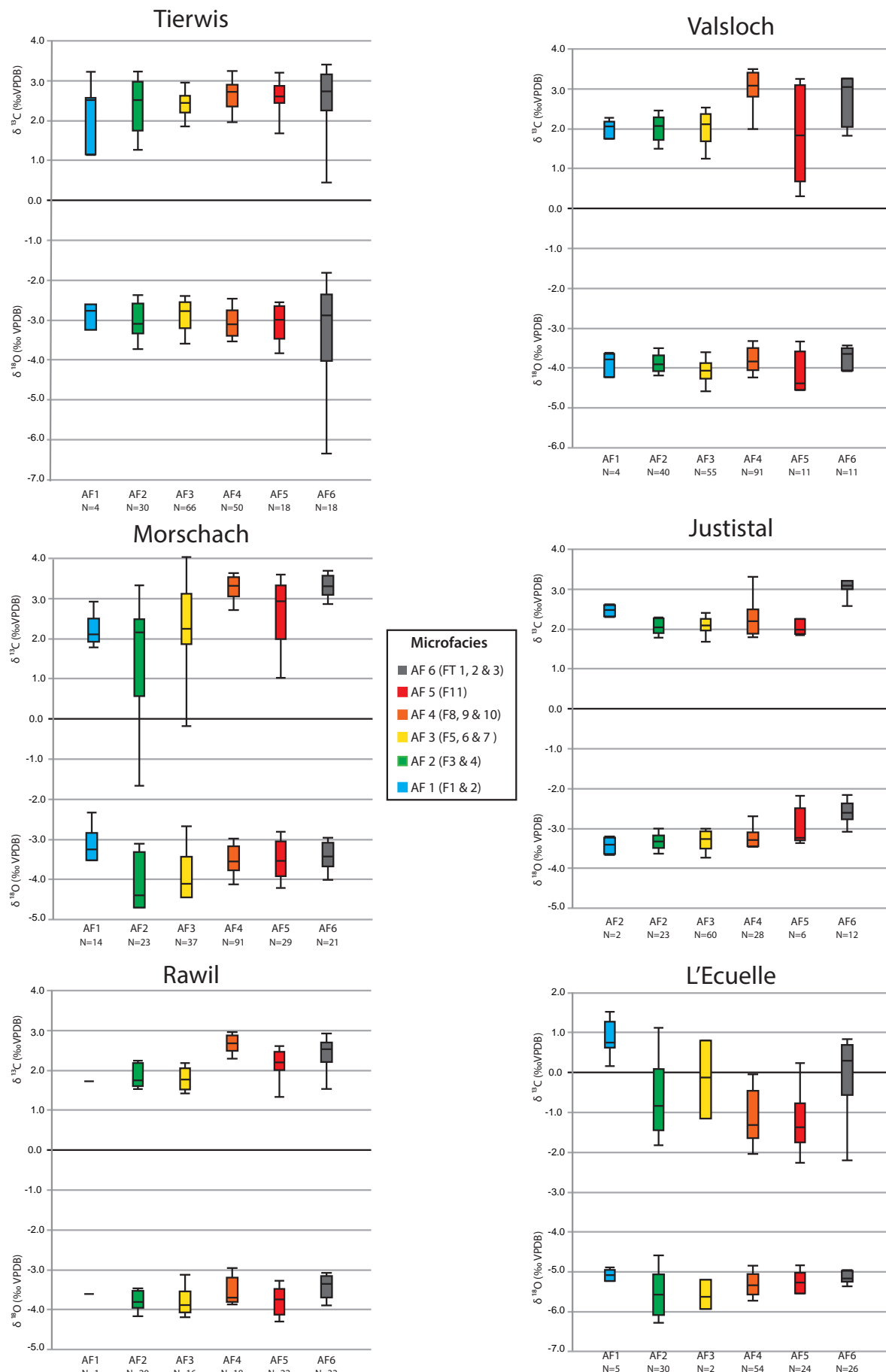


Fig. 3.19 Box plot of carbone and oxygen isotope values for facies associations for the sections of Tierwis, Valsloch, Morschach, Justistal, Rawil and L'Ecuelle.

3.5). Interestingly, the most negative values in the Valsloch section coincide with oolitic facies, in which cements are twinned and testify a phase of recrystallization. The plateau of negative values in the section of Valsloch corresponds to intervals highly enriched in echinoderms, which are composed of high-magnesium calcite, a carbonate mineral that is unstable under meteoric conditions (Kroh and Nebelsik, 2010). Mg-rich carbonates and dolomites are relatively more affected by diagenesis and associated isotopic resetting. Echinoderms are also characterized by important porosity, with a range of 10–70 % volume (Weber, 1969; Weber et al., 1969), which could also contribute to an easier circulation of post-depositional fluid in a certain way. These factors are likely implied in the generation of the observed trends towards more negative values in this section. The facies-dependent isotope variations are shown in boxplots for each section in Figure 3.19. The carbon-isotope values are lower for the association of outer-shelf microfacies types (AF1, AF2 and AF3) than of the AF4 (lagoonal facies), for the sections of Valsloch, Morschach and Rawil. This trend is less well expressed in the sections of Tierwis and Justital and is completely inverted in L'Ecuelle. Concerning the values of the AF5 (supratidal) and the AF6 (transgressive facies), no clear trends are discerned, except for lower medians than those of the AF4, and a larger dispersion, especially for the section of Tierwis.

A further factor to be considered is the coincidence of negative excursions with the presence of evidence for emersion. This relation is observed for CA1 of the boundary interval between the Lower Schrattenkalk and Rawil Mbs in proximal sections, as well as for the negative excursion within the Rawil Mb (CRB, CRM; e.g. in the sections of L'Ecuelle and Rawil) and near the base of the Upper Schrattenkalk Mb

(CUSB; e.g. in the sections of L'Ecuelle and Valsloch). It is clear, however, that not every emersion surface is associated with a negative $\delta^{13}\text{C}$ excursion and vice versa.

3.5.5 Photozoan versus heterozoan carbonate production during the deposition of the Urgonian Formation

The faunal and floral composition of the Urgonian Formation, the importance of detrital sediments and the phosphorus content are used here to infer trophic levels and their effect on the carbonate-producing ecosystems. For the Lower Schrattenkalk Mb, a progressive change towards detrital-poor carbonates is seen at its base, which goes along with the general decrease in phosphorus content. This decrease is correlated with the general shallowing-upward trend and the installation of a platform, which is characterized by a large lagoon, rimmed by oolitic shoals and small patch reefs. Its fauna is dominated by rudists, stromatoporoids, and corals, and represent a typical oligotrophic, photozoan association.

The importance of detrital material in the Rawil Mb relative to the underlying and overlying Schrattenkalk Mbs suggests that the Rawil Mb represents a mixed siliciclastic-carbonate platform. Based on clay mineralogy records and more particularly on the abundance of kaolinite in the Rawil Mb, Stein et al. (2012a) proposed that a change toward warmer and more humid climatic conditions triggered the increased input of nutrients and terrigenous materials, marking the deposition of the Rawil Mb. Phosphorus contents in the Rawil Mb are generally higher than those in the higher part of the Lower and the lower part of the Upper

Schrattenkalk Mbs (Stein et al., 2012a), which suggest that ambient trophic levels were indeed higher during deposition of the Rawil sediments. The persistence of dasycladacean green algae, patch-reef corals and rudists well into the lower part of the Rawil Mb suggests, however, that they were not higher than mesotrophic (Mutti and Hallock, 2003). It also shows that the carbonate-producing ecosystem was capable to adapt to the changing paleoenvironmental conditions. They were joined by organisms better adapted to mesotrophic conditions, such as the Orbitolinids (*Palorbitolina lenticularis*), annelids and the benthic foraminifera *Choffatella*, which became abundant and even dominant in certain time periods during the deposition of the Rawil Mb. During deposition of the upper part of the Rawil Mb, represented by the top of unit B and by unit C, light-independent fauna in the form of circalittoral foraminifera, echinoderms and bryozoans became the dominant groups in the carbonate-producing ecosystem, whereas corals, green algae and rudists were greatly reduced in numbers. This shift to a heterozoan association is explained by persistently elevated nutrient levels and the effect of relative sea-level rise (Lees and Buller, 1972; James and Clarke, 1997; Mutti and Hallock, 2003; Schlager, 2005). This is mirrored by the increase in phosphorus contents in the sections of Tierwis and Valsloch, whereas the section of L'Ecuelle shows a less well comprehensible inverse trend.

In the sediments of the Upper Schrattenkalk Member, we essentially find back the same facies types and same carbonate-producing ecosystems as in the Lower Schrattenkalk Mb. Also the detrital levels are very low, with the exception of a few discrete layers (e.g., in the section of Rawil). Carbonate production is essentially by photozoan organisms, well adapted to lower trophic levels, which is also shown by

a trend to lower values, relative to the upper part of the Rawil Mb.

3.5.6 Interactions between tectonic processes and sea-level change

In spite of its passive-margin configuration and the resulting tectonic stability (Trümpy, 1980), the northern Tethyan shelf underwent a certain tectonic readjustment during the Barremian-Aptian, which was related to the rotation of the Iberian subcontinent, the continuing opening of the Atlantic, and extension of the northern Tethyan Valais Basin (e.g., Arnaud, 1988; Olivet, 1996). As a consequence, subsidence rates were relatively high in the Helvetic domain, according to Funk et al. (1985). Furthermore, pre-existing faults became reactivated during this time period, leading to the tilting of block segments, as is observed on the platform preserved in the Vercors and Gard, and on the Provencal platform (Arnaud, 2005; Bastide, 2014). These tectonic rearrangements created a complex platform topography.

Changes in the thickness of stratigraphic sequences and their systems tracts may indicate the presence of a tectonically differentiated topography of the Helvetic platform. For instance, unit A is missing in the section of L'Ecuelle, as is shown by the first occurrence of *Palorbitolina lenticularis* in the infillings of the *Thalassinoides*, which occur directly on top of the SB A1. This suggests that the section of L'Ecuelle represents a proximal position, where sediment deposition by transgressive onlap started later (Stein et al., 2012a). The sections of Morschach and Rawil include a succession of emersive levels (tempestites, palaeosols) overlain by sediments of external facies. This constitutes

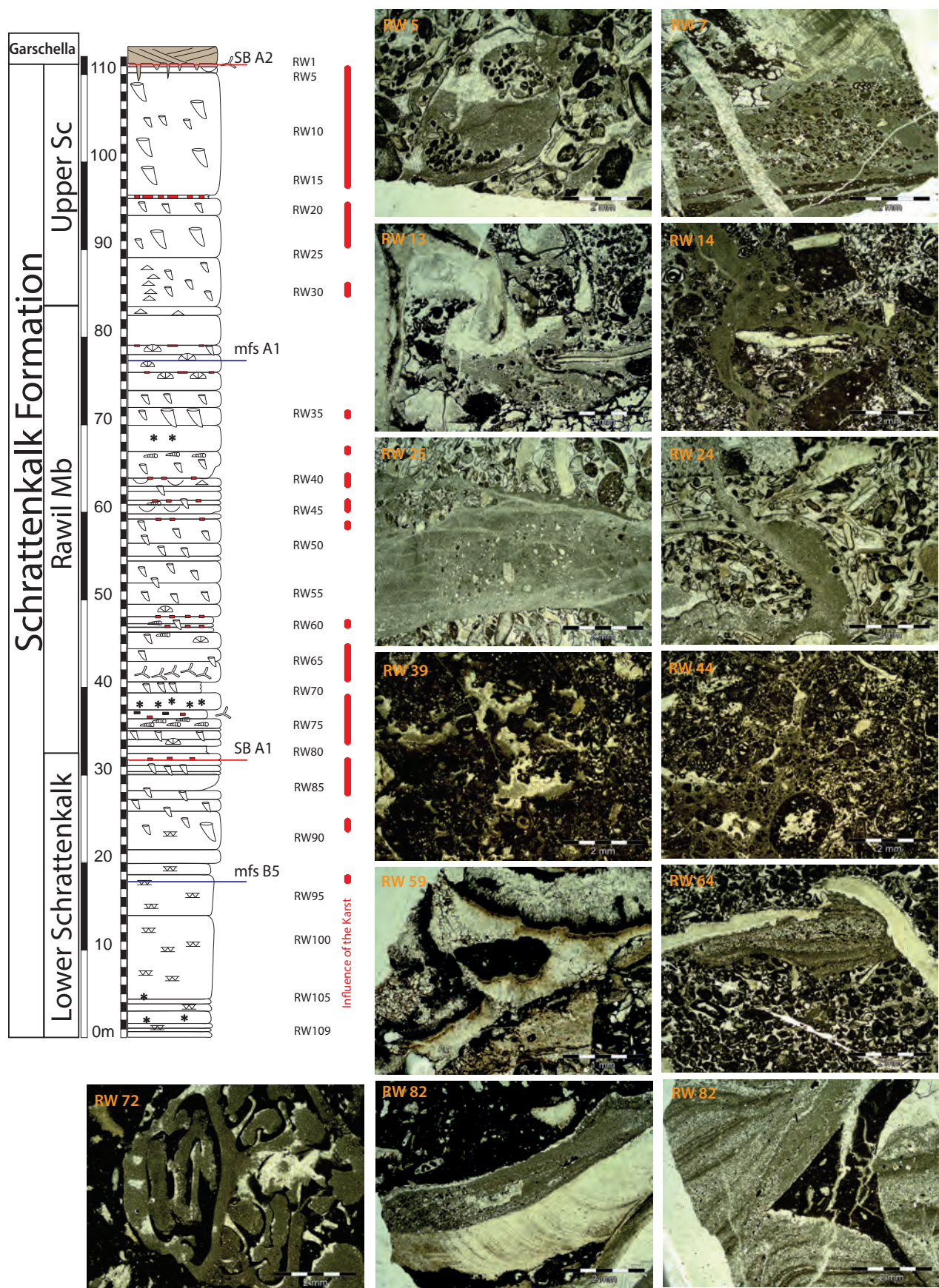


Fig. 3.20 Evidence of intense karstification affecting up to 90 m below the top surface of the Upper Schrattenkalk Mb in the section of Rawil.

an evidence for a paleotopographic high, where only the maximum transgression of each parasequence is recorded. Moreover, the presence of a complex karst system in the Rawil section, filled by caymanite-type deposits (Jones, 1992), which affects more than 90m of depth (Fig. 3.20), suggests recurrent subaerial exposure during and following the deposition of the Schrattenkalk Fm. The absence of quartz in the karst infilling indicates that this karstification phase and the following infilling phases occurred prior to the deposition of the Brisi Mb of the Garschella Fm, as opposed to the fracture infills observed in the section of L'Ecuelle.

Superimposed onto the tectonically induced changes in the topography, sea-level change was the major driver of facies change and the geometric configuration of the sediments investigated. This may also be related to the larger amplitudes of sea-level change, as proposed by Haq (2014). He suggested that the SB A1 and A2 were associated with major sea-level fall, with amplitudes of more than 75m. This range of amplitudes cannot be confirmed on the Helvetic platform, but nevertheless, in the section of Rawil, relative sea-level fall near the Barremian-Aptian boundary was at least 15m, as is indicated by karstification, which reached as deep down as this depth. Moreover, this marine regression may have induced an important hiatus, associated with the erosion of subjacent sediments, as is witnessed by the reduced thickness of the HST in sequence B5, especially in the sections of Valsloch and Tierwis. According to Haq (2014), the sea-level falls associated with SB A1 and A2 were followed by rapid transgressions. From our facies and microfacies analysis of Unit A at the base of the Rawil Mb, this cannot really be confirmed, as the change in facies was rather gradual. On the contrary, there are indications that sea-level rise following SB A2 was

important and was a likely factor implied in the drowning of the Urgonian platform (Föllmi and Gainon, 2008). They include the major emersive surface (SB A2), which terminates the Upper Schrattenkalk Mb, and which is associated with a karstic system of a depth of up to 20 m. The emersive surface is locally covered by a phosphatic hardground (Rohrbachstein Bed), which again is overlain by the mesotrophic sediments of the Lower Grunten Mb (Linder et al., 2006; Föllmi and Gainon, 2008).

3.5.7 General paleoceanographic change and the evolution and termination of the Urgonian platform

In the Helvetic Alps, the Urgonian Schrattenkalk platform shows a typically photozoan assemblage during the late Barremian and a change toward a photozoan-heterozoan mixed carbonate-siliciclastic platform during the earliest Aptian, followed by a return to photozoan conditions until the demise of this platform, which is dated as near the boundary between the *forbesi* and *deshayesi* zones (Föllmi and Gainon, 2008). These changes in the Urgonian carbonate factory are recorded also in other localities representing the Tethyan Ocean (Stein et al., 2012a), and were interpreted as the consequence of global paleoceanographic change. According to Stein et al (2012a), the Rawil Mb deposition was triggered by a transitional change towards more humid climatic conditions, which induced an increase in the detrital and nutrient fluxes, associated with general sea-level rise. The Rawil Mb occurring near the Barremian–Aptian boundary is coeval with the deposition of laminated organic-rich sediments recorded in many basinal sections of the western Tethys,

such as in the El Pui section in the south-central Pyrenees of northern Spain (Sanchez-Hernandez and Maurrasse, 2014), in the North-Atlantic-oriented sections of Spain (Igaratza section; Millà et al., 2009), in southeastern France (Cassis-La Bédoule; Stein et al., 2012 b), in Italy (Cismon; Menegatti et al., 1998; Gorgo a Cerbara; Stein et al., 2011; Capriolo; Föllmi et al., 2012) and also in the Lower Saxony Basin (Mutterlose et al., 2009). This interval was described as the Taxy episode (Föllmi, 2012), which may have coincided with the onset of the Ontong Java LIP in the Pacific, according to Tejada et al. (2009).

The return of the photozoan carbonate assemblage on the Helvetic platform took place during the relative sea-level fall following the earliest Aptian transgression. The renewal of the oligotrophic fauna as observed in the Upper Schrattenkalk Mb, is likely due to a renewed change in climate conditions toward dryer conditions, which triggered a reduction in continental run-off (Stein et al., 2012a, b). This is confirmed by the generally low values in phosphorus content. The Upper Schrattenkalk platform shows the maximum of progradation, which coincided with the general development of Urgonian platforms around the Tethys, as is observed, for instance, in Italy (Amodio et al., 2013), central Iran (Wilmsen et al., 2013), Spain (Vilas et al., 1995), Oman (van Buchem et al., 2002), Serbia (Sudar et al., 2008), Hungary (Peybernes, 1979), Turkey (Masse et al., 2009) and Mexico (Barragan and Melinte (2006) (see also Skelton and Gili, 2012).

The Lower and the Upper Schrattenkalk Mbs are well comparable in terms of lithologies, facies and microfacies, and fossil associations (rudists, miliolids, etc.). The twofold widespread appearance of oligotrophic facies during the late Barremian and early Aptian is remarkable, especially if one considers the rather high density

of anoxic episodes in the nearby basins during this time interval (Föllmi et al., 2012). This underlines both the exceptional position of the Urgonian platform in the late Early Cretaceous, in a time period, which was otherwise characterized by meso- to eutrophic conditions, as well as the potential of the late Early Cretaceous environment to rapidly shift between oligotrophic and eutrophic conditions as a consequence of volcanic activity, general climate change and associated rapid sea-level change.

The demise of the Urgonian Schrattenkalk platform near the boundary between the *forbesi* and *deshayesi* zones coincided with those of the Apulian carbonate platform (Graziano, 2013) and the subalpine chains (Huck et al., 2013). According to Huck et al. (2011), the time lag between the demise of the Urgonian platform and the onset of the Selli episode is estimated at 300 kyr. Platform demise was associated with a climate change toward warmer and more humid conditions, associated with an increase in nutrient fluxes (Stein et al., 2012b; Föllmi, 2012).

3.6 Conclusions

In this study we analysed the evolution of the Urgonian Schrattenkalk platform, which developed along the northern Tethyan margin and which is presently locked up in the Helvetic Alps of Switzerland. We studied six representative sections both for their facies, microfacies and biostratigraphy, as well as for their whole-rock $\delta^{13}\text{C}$ and phosphorus records.

In terms of the sequence-stratigraphic framework, sediments belonging to the Lower Schrattenkalk Mb include the upper part of sequence B3 and contain the entire sequences B4 and B5, which ends near the Barremian–Aptian

boundary. The following Rawil Mb includes the TSTA1 and the lowermost part of the early HST. The Upper Schrattenkalk Mb represents the HST A1. The here-deducted succession is well correlated to those established in southeastern France by Arnaud and Arnaud-Vanneau (1989, 1991), Arnaud-Vanneau and Arnaud (1990), and Hunt and Tucker (1993) and in the Vocontian basin (Angles section).

Three units were identified in the Rawil Mb, based on orbitolinid biostratigraphy, the succession of the facies and paleoenvironmental markers. These units A, B and C are correlatable with those described in the Vercors and Chartreuse area (SE France) and labelled as Ai1a, Ai1b and Ai1c by Arnaud-Vanneau (1980). This similarity of the succession of the environmental deposits along several hundred of kilometres of the NW Tethyan platform suggests the effects of paleoclimate and paleoceanographic changes, which outweighed the regional framework.

The overall long-term trends in the $\delta^{13}\text{C}$ records are comparable along the NW Tethyan Platform and correlate with those of the Vocontian Basin. Shorter-term deviations are related to the specifics of the mineralogy (aragonite versus calcite), diagenetic overprint (e.g., in porous echinodermal carbonates), and the presence of emersion surfaces. The presence of negative shifts in the $\delta^{13}\text{C}$ curves is used for correlation between the studied sections.

The changes from a pure carbonate platform dominated by an oligotrophic ecosystem (Lower Schrattenkalk Mb; late Barremian) to a mixed siliciclastic-carbonate platform with a mixed photozoan-heterozoan association (Rawil Mb; earliest Aptian), subsequently back to an almost pure carbonate platform built up by an essentially oligotrophic community (Upper Schrattenkalk Mb; early Aptian), and finally a platform drowning phase followed by the depo-

sition of mesotrophic carbonates (Grünten Mb; late early Aptian) are common to the northern Tethyan platforms in general. This is also seen by the detailed correlation of the three units within the Rawil Mb, which correlated very well with those on the Subalpine and Vercors platforms. Our reconstructions and the comparable changes across the northern Tethyan margin suggest that the overall evolution of the Urgonian platform was driven by paleoceanographic and paleoclimatic changes, which outweighed the regional frame. They were substantial and associated with rapid and larger amplitude sea-level change, which left their imprint on the evolution of the northern Tethyan Urgonian platform.

3.7 References

- Adatte, T., Stinnesbeck, W. and Keller, G.** (1996) Lithostratigraphic and mineralogic correlations of near K/T boundary sediments in northeastern Mexico: Implications for origin and nature of deposition. In: *The Cretaceous-Tertiary Event and Other Catastrophes in Earth History* (Eds G. Ryder, D. Fastovsky and S. Gartner), **Geological Society of America Special Paper 307**, pp. 211-226, Boulder, Colorado.
- Ager, D.V.** (1981) *The Nature of the Stratigraphical Record*. John Wiley and Sons, New York, 122 pp.
- Allmon, Warren D.** (2007) Cretaceous Marine Nutrients, Greenhouse Carbonates, and the Abundance of Turritelline Gastropods. *The Journal of Geology*, **115**, 509-523.
- Amodio, S., Ferreri, V. and D'Argenio, B.** (2013) Cyclostratigraphic and chronostratigraphic correlations in the Barremian–Aptian shallow-marine carbonates of the cen-

- tral-southern Apennines (Italy). *Cretaceous Research*, **44**, 132-156.
- Arnaud, H.** (1988) Subsidence in certain domains of southeastern France during the Ligurian Tethys opening and spreading stages. *Bull. Soc. Géol. Fr.*, **8**, 725-732.
- Arnaud, H.** (2005) Sequence stratigraphy interpretation. In: *The Hauterivian-Lower Aptian sequence stratigraphy from Jura Platform to Vocontian Basin: A multidisciplinary approach* (Eds T. Adatte, A. Arnaud-Vanneau, H. Arnaud, M.-C. Blanc-Alétrou, S. Bodin, E. Carrio-Schaffhauser, K.B. Föllmi, A. Godet, M.C. Raddadi and J. Vermeulen), *Géologie Alpine, Série Spéciale “Colloques et Excursions” N°7*, pp. 174-179.
- Arnaud, H. and Arnaud-Vanneau, A.** (1989) Séquence de dépôt et variations du niveau de la mer au Barrémien et à l'Aptien inférieur dans les massifs subalpins septentrionaux et le Jura (Sud-Est de la France). *Bulletin de la Société Géologique de France*, **V**, 651-660.
- Arnaud, H. and Arnaud-Vanneau, A.** (1991) Les calcaires urgoniens des Massifs subalpins septentrionaux et du Jura (France): âge et discussion des données stratigraphiques. *Géologie Alpine*, **67**, 63-79.
- Arnaud-Vanneau, A., Arnaud, H., Thieuloy, J.P.** (1976) Bases nouvelles pour la stratigraphie des calcaires urgoniens du Vercors. *Newsletter on Stratigraphy*, **5**, 143-159.
- Arnaud, H., Arnaud-Vanneau, A., Blanc-Alet-ru, M.-C., Adatte, T., Argot, M., Delanoy, G., Thieuloy, J.-P., Vermeulen, J., Virgone, A., Virlouvet, B. and Wermeille, S.** (1998) Répartition stratigraphique des orbitolinidés de la plate-forme urgonienne subalpine et jurassienne (SE de la France) *Géologie Alpine*, **74**, 87.
- Arnaud, H., Arnaud-Vanneau, A., Bulot, L.G., Beck, C., MacSotay, O., Stephan, J.-F. and Vivas, V.** (2000) Le Crétacé inférieur du Venezuela oriental : stratigraphie séquentielle des carbonates sur la transversale Casanay-Maturin (Etats de Anzoátegui, Monagas et Sucre). *Géologie Alpine*, **76**, 3-81.
- Arnaud-Vanneau, A.** (1980) Micropaléontologie, paléoécologie et sédimentologie d'une plate-forme carbonatée de la marge passive de la Téthys : l'Urgonien du Vercors septentrional et de la Chartreuse (Alpes occidentales). *Géologie Alpine, Grenoble Mém HS 11*, 874 p.
- Arnaud-Vanneau, A. and Arnaud, H.** (1990) Hauterivian to Lower Aptian carbonate shelf sedimentation and sequence stratigraphy in the Jura and northern Subalpine chains (southeastern France and Swiss Jura). In: *Carbonate Platforms: Facies, Sequences and Evolution* (Eds M.E. Tucker, J.L. Wilson, P.D. Crevello, J.R. Sarg and J.F. Read), **9**, pp. 203-233. Blackwell Scientific Publications, Special Publication of the International Association of Sedimentologists.
- Arnaud-Vanneau, A. and Arnaud, H.** (2005) Carbonate facies and microfacies of the Lower Cretaceous carbonate platforms. In: *The Hauterivian-Lower Aptian sequence stratigraphy from Jura Platform to Vocontian Basin: A multidisciplinary approach* (Eds T. Adatte, A. Arnaud-Vanneau, H. Arnaud, M.-C. Blanc-Alétrou, S. Bodin, E. Carrio-Schaffhauser, K.B. Föllmi, A. Godet, M.C. Raddadi and J. Vermeulen), *Géologie Alpine, Série Spéciale “Colloques et Excursions” N°7*, pp. 39-68.
- Barragan, R. and Melinte, M.C.** (2006) Palaeoenvironmental and palaeobiologic changes across the Barremian/Aptian boundary interval in the Tethys Realm, Mexico and Romania. *Cretaceous Research*, **27**, 529-541.

- Bastide, F.** (2014) *Synthèse de l'évolution de la plateforme urgonienne (Barrémien tardif à Aptien précoce) du Sud-Est de la France: Facies, micropaléontologie, géochimie, géométries, paléotectonique et géomodélisation.* PhD thesis, Université de Lausanne & Université Joseph Fourier, 452 p.
- Bandel, K.** (1990) Shell structure of the gastropoda excluding Archaeogastropoda, - in *Skeletal Biomineralization: Patterns Processes and Evolutionary Trends*, Vol I, J.G. Carter, (ed.) pp. 117-134, Van Nostrand, New York.
- Bernaus, J.M.** (1998) *L'Urgonien du Bassin d'Organya (NE Espagne): Micropaléontologie, Sédimentologie et Stratigraphie Séquentielle.* . PhD thesis, University Joseph Fourier, 208 p.
- Bernaus, J.M., Arnaud-Vanneau, A. and Caus, E.** (2003) Carbonate platform sequence stratigraphy in a rapidly subsiding area: the Late Barremian-Early Aptian of the Organya basin, Spanish Pyrenees. *Sedimentary Geology*, **159**, 177-201.
- Bodin, S., Godet, A., Föllmi, K.B., Vermeulen, J., Arnaud, H., Strasser, A., Fiet, N. and Adatte, T.** (2006) The late Hauterivian Faraoni oceanic anoxic event in the western Tethys: Evidence from phosphorus burial rates. *Palaeogeography, Palaeoclimatology, Palaeoecology*, **235**, 245-264.
- Bralower, T.J., Arthur, M.A., Leckie, M.R., Sliter, W.V., Allard, D.J. and Schlanger, S.O.** (1994) Timing and Paleoceanography of Oceanic Dysoxia / Anoxia in the Late Barremian to Early Aptian (Early Cretaceous). *Palaios*, **9**, 336-369.
- Breitschmid, A.** (1982) Diagenese und schwache Metamorphose in den sedimentären Abfolgen der Zentralschweizer Alpen (Vierwaldstätter See, Uriotstock). *Eclogae geol. Helv.*, **75**, 331-380.
- Bucur, I.I. and Săsăran, E.** (2005) Relationship between algae and environment: an Early Cretaceous case study, Trascău Mountains, Romania. *Facies*, **51**, 274-286.
- Burkhard, M.** (1988) L'Helvétique de la bordure occidentale du massif de l'Aar (évolution tectonique et métamorphique). *Eclogae geol. Helv.*, **81**, Pages 63-114.
- Burkhard, M. and Goy-Eggenberger, D.** (2001) Near vertical iso-illite-crystallinity surfaces cross-cut the recumbent fold structure of the Morcles nappe, Swiss Alps. *Clay Minerals*, **36**, 159-170.
- Carević, I., Taherpour Khalil Abad, M., Ljubović-Obradović, D., Vaziri, S.H., Mirković, M., Aryaei, A.A., Stejić P. and Ashouri, A.R.** (2013) Comparisons between the Urgonian platform carbonates from eastern Serbia (Carpatho-Balkanides) and northeast Iran (Kopet-Dagh Basin): Depositional facies, microfacies, biostratigraphy, palaeoenvironments and palaeoecology. *Cretaceous Research*, **40**, 110-130.
- Catuneanu, O., Abreu, V., Bhattacharya, J.P., Blum, M.D., Dalrymple, R.W., Eriksson, P.G., Fielding, C.R., Fisher, W.L., Gallaway, W.E., Gibling, M.R., Giles, K.A., Holbrook, J.M., Jordan, R., Kendall, C.G.S.C., Macurda, B., Martensen, O.J., Miall, A.D., Neal, J.E., Nummedal, D., Pomar, L., Posamentier, H.W., Pratt, B.R., Sarg, J.F., Shanley, K.W., Steel, R.J., Strasser, A., Tucker, M.E. and Winker, C.** (2009) Towards the standardization of sequence stratigraphy. *Earth-Science Reviews*, **92**, 1-33.
- Choquette, P.W. and James, N.P.** (1987) Diagenesis # 12. Diagenesis in Limestones - 3. The Deep Burial Environment. *Geoscience Canada*, **14**, 3-35.
- Coe, A.L., Bosence, D.W.J., Church, K.D.,**

- Flint, S.S., Howell, J.A. and Wilson, R.C.L.** (2003) *The Sedimentary Record of Sea-Level Change*. . Cambridge University Press.
- Di Lucia, M., Trecalli, A., Mutti, M. and Parente, M.** (2012) Bio-chemostratigraphy of the Barremian-Aptian shallow-water carbonates of the southern Apennines (Italy): Pinpointing the OAE1a in a Tethyan carbonate platform. *Solid Earth Discussions*, **3**, 28.
- Dietrich, D. and Casey, M.** (1989) A new tectonic model for the Helvetic nappes. *Geological Society, London, Special Publications*, **45**, 47-63.
- Eaton, A.D., Clesceri, L.S. and Greenberg, A.E.** (1995) *Standard Methods for examination of Water and Waste Water*. IXI, 4113-4114.
- Embry, J.-C.** (2005) *Paléoécologie et architecture stratigraphique en haute résolution des plates-formes carbonatées du Barrémien–Aptian de la Néo-Téthys (Espagne, Suisse, Provence, Vercors) – impact respectif des différents facteurs de contrôle.*, MNHN-Paris/ IFP, 303 pp.
- Emery, D. and Myers, K.** (1996) *Sequence Stratigraphy*. Blackwell Sciences.
- Enríquez, S. and Schubert, N.** (2014) Direct contribution of the seagrass Thalassia testudinum to lime mud production. *Nat Commun*, **5**.
- Ferrazzini, B. and Schüler, P.** (1979) Versuch einer Abwicklung des Helvetikums zwischen Rhone und Reuss. . *Eclogae geol. Helv.* , **72**, 439-454.
- Flügel, E.** (2004) *Microfacies of Carbonate Rocks - Analysis, Interpretation and Application*. Springer-Verlag, Berlin, Heidelberg, New York, 976 pp.
- Föllmi, K.B., Bodin, S., Godet, A., Linder, P. and van de Shootbrugge, B.** (2007) Unlocking paleo-environmental information from Early Cretaceous shelf sediments in the Helvetic Alps: stratigraphy is the key! *Swiss Journal of Geosciences*, **100**, 349-369.
- Föllmi, K.B. and Gainon, F.** (2008) Demise of the northern Tethyan Urgonian carbonate platform and subsequent transition towards pelagic conditions: The sedimentary record of the Col de la Plaine Morte area, central Switzerland. *Sedimentary Geology*, **205**, 142-159.
- Föllmi, K.B.** (2012) Early Cretaceous life, climate and anoxia. *Cretaceous Research*, **35**, 230-257.
- Föllmi, K.B., Bôle, M., Jammet, N., Froidevaux, P., Godet, A., Bodin, S., Adatte, T., Matera, V., Fleitmann, D. and Spangenberg, J.E.** (2012) Bridging the Faraoni and Selli oceanic anoxic events: late Hauterivian to early Aptian dysaerobic to anaerobic phases in the Tethys. *Clim. Past*, **8**, 171-189.
- Föllmi, K.B. and Gainon, F.** (2008) Demise of the northern Tethyan Urgonian carbonate platform and subsequent transition towards pelagic conditions: The sedimentary record of the Col de la Plaine Morte area, central Switzerland. *Sedimentary Geology*, **205**, 142-159.
- Frey, M., Teichmüller, M., Teichmüller, R., Mullis, J., Künzi, B., Breitschmid, A., Gruner, U. and Schwizer, B.** (1980) Very low-grade metamorphism in external parts of the Central Alps : illite crystallinity, coal rank and fluid inclusion data. *Eclogae geol. Helv.*, **73**, 173-203.
- Funk, H. and Briegel, U.** (1979) le facies Urgonien des nappes helvétiques en Suisse orientale. *Géobios, Mémoire spéciale n°3*, 9.
- Funk, H.** (1985) Mesozoische Subsidenzgeschichte im Helvetischen Schelf

- der Ostschweiz. *Eclogae geol. Helv.*, **78**, pp 249-272.
- Funk, H., Föllmi, K.B. and Mohr, H.** (1993) Evolution of the Tithonian-Aptian Carbonate Platform Along the Northern Tethyan Margin, Eastern Helvetic Alps. In: *AAPG Special Volumes, M 56: Cretaceous Carbonate Platforms*, pp. 387 - 407.
- Godet, A., S. Bodin, K. B. Föllmi, J. Vermeulen, S. Gardin, N. Fiet, T. Adatte, B. Zsolt, D. Stüben, and B. van de Schootbrugge** (2006a), Evolution of the marine stable carbon-isotope record during the Early Cretaceous: A focus on the late Hauterivian and Barremian in the Tethyan realm, *Earth Planet. Sci. Lett.*, **242**, 254– 271.
- Godet, A., Föllmi, K.B., Bodin, S., de Kaelnel, E., Matera, V. and Adatte, T.** (2010) Stratigraphic, sedimentological and palaeoenvironmental constraints on the rise of the Urgonian platform in the western Swiss Jura. *Sedimentology*, **57**, 1088-1125.
- Godet, A., Hfaiedh, R., Arnaud-Vanneau, A., Zghal, I., Arnaud, H. and Ouali, J.** (2014) Aptian palaeoclimates and identification of an OAE1a equivalent in shallow marine environments of the southern Tethyan margin: Evidence from Southern Tunisia (Bir Oum Ali section, Northern Chott Chain). *Cretaceous Research*, **48**, 110-129.
- González-Lara, J.C.** (2001) Le Paléocène du Chiapas (SE du Mexique): biostratigraphie, sédimentologie et stratigraphie séquentielle. *. Géologie Alpine H.S.*, **36**, 1-139.
- Goy-Eggenberger, D.** (1998) *Faible métamorphisme de la nappe de Morcles. minéralogie et géochimie*, Université de Neuchatel, Switzerland.
- Graziano, R.** (2013) Sedimentology, biostratigraphy and event stratigraphy of the Early Aptian Oceanic Anoxic Event (OAE1A) in the Apulia Carbonate Platform Margin – Ionian Basin System (Gargano Promontory, southern Italy). *Cretaceous Research*, **39**, 78-111.
- Gröcke, D.R., Hesselbo, S.P. and Jenkyns, H.C.** (1999) Carbon-isotope composition of Lower Cretaceous fossil wood : Ocean-atmosphere chemistry and relation to sea-level change. *Geology*, **27**, 155-158.
- Guillaume, H. and Reichel, M.** (1957) Neotricholina friburgensis, n. sp., foraminifère de l’Urgonien alpin. *Eclogae geol. Helv.*, **50**, 285-288.
- Haq, B.U.** (2014) Cretaceous eustasy revisited. *Global and Planetary Change*, **113**, 44-58.
- Heim, A.A.** (1916-1922) Geologie der Schweiz. Tauchnitz, Leipzig
- Heim, A. and Baumberger, E.** (1933) Jura und Unterkreide in den helvetischen Alpen beiderseits des Rheines (Vorarlberg und Ostschweiz). *Denkschriften der Schweizerischen Naturforschenden Gesellschaft*, **68**, 155–220.
- Hfaiedh, R., Arnaud Vanneau, A., Godet, A., Arnaud, H., Zghal, I., Ouali, J., Latil, J.-L. and Jallali, H.** (2013) Biostratigraphy, palaeoenvironments and sequence stratigraphy of the Aptian sedimentary succession at Jebel Bir Oum Ali (Northern Chain of Chotts, South Tunisia): Comparison with contemporaneous Tethyan series. *Cretaceous Research*, **46**, 177-207.
- Huck, S., Heimhofer, U., Immenhauser, A. and Weissert, H.** (2013) Carbon-isotope stratigraphy of Early Cretaceous (Urgonian) shoal-water deposits: Diachronous changes in carbonate-platform production in the north-western Tethys. *Sedimentary Geology*, **290**, 157-174.
- Huck, S., Heimhofer, U., Rameil, N., Bodin, S. and Immenhauser, A.** (2011) Strontium

- and carbon-isotope chronostratigraphy of Barremian-Aptian shoal-water carbonates: Northern Tethyan platform drowning predates OAE 1a. *Earth and Planetary Science Letters*, **304**, 547-558.
- Hunt, D. and Tucker, M.E.** (1993) Sequence stratigraphy of carbonate shelves with an example from the mid-Cretaceous (Urgonian) of southeast France. *International Association of Sedimentologists, Special Publication 18*, 307–341.
- Immenhauser, A., Della Porta, G., Kenter, J.A.M. and Bahamonde, J.R.** (2003) An alternative model for positive shifts in shallow-marine carbonates d13C and d18O. *Sedimentology*, **50**, 953-959.
- James, N.P. and Clarke, J.A.D.** (1997) *Cool Water carbonates*, Tulsa (Oklahoma), 440 pp.
- Jenkyns, H.C.** (1980) Cretaceous anoxic events: from continents to oceans. *Journal of the Geological Society, London*, **137**, 171-188.
- Jenkyns, H.C.** (2010) Geochemistry of oceanic anoxic events. *Geochemistry, Geophysics, Geosystems*, **11**, 30 pp.
- Keller, C.E., Hochuli, P.A., Weissert, H., Bernasconi, S.M., Giorgioni, M. and Garcia, T.I.** (2011) A volcanically induced climate warming and floral change preceded the onset of OAE1a (Early Cretaceous). *Palaeogeography, Palaeoclimatology, Palaeoecology*, **305**, 43-49.
- Kempf, O. and Pfiffner, O.A.** (2004) Early-Tertiary evolution of the North Alpine Foreland Basin of the Swiss Alps and adjoining areas. *Basin Research*, **16**, 549-567.
- Klicpera, A., Michel, J. and Westphal, H.** (2014) Facies patterns of a tropical heterozoan carbonate platform under eutrophic conditions: the Banc d'Arguin, Mauritania. *Facies*, **61**, 1-24.
- Kroh, A. and Nebelsick, J.H.** (2010) Echinoderms and Oligo-Miocene carbonate systems: potential applications in sedimentology and environmental reconstruction. *International Association of Sedimentologists Special Publication*, **42**, 201-228
- Kübler, B.** (1983) Dosage quantitatif des minéraux majeurs des roches sédimentaires par diffraction X. *Cahiers de l'Institut de Géologie, Université de Neuchâtel, Suisse, Série AX n°1.1 and 1.2*, 13 p.
- Kuhnt, W., Holbourn, A. and Moullade, M.** (2011) Transient global cooling at the onset of early Aptian oceanic anoxic event (OAE) 1a. *Geology*, **39**, 323-326.
- Kuroda, J., Tanimizu, M., Hori, R.S., Suzuki, K., Ogawa, N.O., Tejada, M.L.G., Coffin, M.F., Coccioni, R., Erba, E. and Ohkouchi, N.** (2011) Lead isotopic record of Barremian-Aptian marine sediments: Implications for large igneous provinces and the Aptian climatic crisis. *Earth and Planetary Science Letters*, **307**, 126-134.
- Larson, R.L.** (1991) Geological consequences of superplumes. *Geology*, **19**, 963-966.
- Larson, R.L. and Erba, E.** (1999) Onset of the mid-Cretaceous greenhouse in the Barremian-Aptian: Igneous events and the biological, sedimentary and geochemical responses. *Paleoceanography*, **14**, 663-678.
- Lees, A., and Buller, A.T.** (1972) Modern temperate water and warm water shelf carbonate sediments contrasted: *Marine Geology*, **13**, p. 1767-1773
- Linder, P., Gigandet, J., Hüsser, J.L., Gainon, F. and Föllmi, K.B.** (2006) The Early Aptian Grünen Member: Description of a new lithostratigraphic unit of the helvetic Garschella Formation. *Eclogae geologicae Helvetiae*, **99**, 327-341.
- Lowenstam, H.A. and Epstein, S.A.** (1957) On

- the origin of sedimentary aragonite needles of the Great Bahama Bank. *J. Geol.*, **65**, 364-375.
- Masse, J.P. and Philip, J.** (1986) L'évolution des rudistes au regard des principaux événements géologiques de Crétacé. *Bulletin des Centres de Recherches Elf-Aquitaine Exploration-Production*, **10**, 437-456.
- Masse, J.-P., Tüysüz, O., Fenerci-Masse, M., Özer, S. and Sari, B.** (2009) Stratigraphic organisation, spatial distribution, palaeoenvironmental reconstruction, and demise of Lower Cretaceous (Barremian-lower Aptian) carbonate platforms of the Western Pontides (Black Sea region, Turkey). *Cretaceous Research*, **30**, 1170-1180.
- Menegatti, A.P., Weissert, H., Brown, R.S., Tyson, R.V., Farrimond, P., Strasser, A. and Caron, M.** (1998) High-resolution ^{13}C stratigraphy through the early Aptian “Livello Selli” of the Alpine Tethys. *Paleoceanography*, **13**, 530-545.
- Michalik, J.** (1994) Lower Cretaceous carbonate platform facies, Western Carpathians. *Palaeogeography, Palaeoclimatology, Palaeoecology*, **111**, 263-277.
- Millan, M.I., Weissert, H.J., Fernandez-Mendiola, P.A. and García-Mondéjar, J.** (2009) Impact of Early Aptian carbon cycle perturbations on evolution of a marine shelf system in the Basque-Cantabrian Basin (Aralar, N Spain). *Earth and Planetary Science Letters*, **287**, 392-401.
- Milliman, J.D., Freile, D., Steinen, R.P. and Wilber, R.J.** (1993) Great Bahama aragonitic muds: mostly inorganically precipitated, mostly exported. *J. Sed. Petrol.*, **63**, 589-595.
- Moreno-Bedmar, J.A., Company, M., Bover-Arnal, T., Salas, R., Delanoy, G., Martínez, R. and Grauges, A.** (2009) Biostratigraphic characterization by means of ammonoids of the lower Aptian Oceanic Anoxic Event (OAE 1a) in the eastern Iberian Chain (Maestrat Basin, eastern Spain). *Cretaceous Research*, **30**, 864-872.
- Mutterlose, J., Pauly, S. and Steuber, T.** (2009) Temperature controlled deposition of early Cretaceous (Barremian-early Aptian) black shales in an epicontinental sea. *Palaeogeography, Palaeoclimatology, Palaeoecology*, **273**, 330-345.
- Mutti, M. and Hallock, P.** (2003) Carbonate systems along nutrient and temperature gradients: some sedimentological and geochemical constraints. *Int. J. Earth Sci. (Geol. Rundsch.)*, **92**, 465-475.
- Neumann, A.C. and Land, L.S.** (1975) Lime mud deposition and calcareous algae in the Bight of Abaco, Bahamas: a budget. *J. Sed. Petrol.*, **45**, 763-786.
- Olivet, J. L.** (1996). «La cinématique de la plaque ibérique.» *Bull. Cent. Rech. Explor. Prod. Elf Aquitaine*, **20**(1) : 131-195.
- Peybernès, B.** (1979a) Les algues du Jurassique et du Crétacé inférieur des Pyrénées franco-espagnoles. Interêt biostratigraphique et paléoécologique. *Bulletin des Centres de Recherches Expl.-Prod. Elf-Aquitaine*, **3**, 743-752.
- Peybernès, B.** (1979b) L'urgonien de Hongrie. *Geobios*, **12, Supplement 1**, 231-243.
- Pfiffner, O.A.** (1993) The structure of the Helvetic nappes and its relation to the mechanical stratigraphy. *Journal of Structural Geology*, **15**, pp. 511 to 521.
- Philip, J.** (2003) Peri-Tethyan neritic carbonate areas: distribution through time and driving factors: Palaeogeography, Palaeoclimatology, Palaeoecology, **196**, 1-2, p. 19-37.
- Pictet, A., Delanoy, G., Adatte, T., Spangenberg, J.E., Baudouin, C., Boselli, P., Bosel-**

- li, M., Kindler, P. and Föllmi, K.B.** (2015) Three successive phases of platform demise during the early Aptian and their association with the oceanic anoxic Selli episode (Ardèche, France). *Palaeogeography, Palaeoclimatology, Palaeoecology*, **418**, 101-125.
- Raddadi, M.C.** (2005) *Etude de la nature de la radioactivité gamma dans les roches carbonatées de plate-forme: analyses et interprétations environnementales, diagénétiques et géodynamiques*. Laboratoire de géodynamique des chaînes alpines, 221 pp.
- Raddadi, M.C., Arnaud Vanneau, A., Poupeau, G., Carrio-Schaffhauser, E., Arnaud, H. and Rivera, A.** (2005) Interpretation of gamma-ray logs: The distribution of uranium in carbonate platform. *Comptes Rendus Geoscience*, **337**, 1457-1461.
- Ramsay, J.G.** (1981) Tectonics of the Helvetic Nappes. *Geological Society, London, Special Publications*, **9**, 293-309.
- Revesz, K.M., Landwehr, J.M. and Keybl, J.** 2001. Measurement of delta¹³C and delta¹⁸O Isotopic Ratios of CaCO₃ Using a Thermoquest Finnigan GasBench II Delta Plus XL Continuous Flow Isotope Ratio Mass Spectrometer With Application to Devils Hole Core DH-11 Calcite, GEOLOGICAL SURVEY RESTON VA.
- Sanchez-Hernandez, Y. and Maurrasse, F.J.M.R.** (2014) Geochemical characterization and redox signals from the latest Barremian to the earliest Aptian in a restricted marine basin: El Pui section, Organya Basin, south-central Pyrenees. *Chemical Geology*, **372**, 12-31.
- Schenk, K.** (1992) *Die Drusberg- und Schratzenkalk Formation (Unterkreide) im Helvetikum des Berner Oberlandes (2 vol)*. PhD thesis, University of Bern.
- Schlager, W.** (2005) *Carbonate Sedimentology and Sequence Stratigraphy*. SEPM, Tulsa, Oklahoma, USA, 203 pp.
- Schlanger, S.O. and Jenkyns, H.C.** (1976) Cretaceous oceanic anoxic events: causes and consequences. *Geologie en Mijnbouw*, **55**, 179-184.
- Scholle, P.A. and Arthur, M.A.** (1980) Carbon Isotope Fluctuations in Cretaceous Pelagic Limestones: Potential Stratigraphic and Petroleum Exploration Tool. *American Association of Petroleum Geologists Bulletin*, **64**, 67-87.
- Skelton, P.W. and Gili, E.** (2012) Rudists and carbonate platforms in the Aptian: a case study on biotic interactions with ocean chemistry and climate. *Sedimentology*, **59**, 81-117.
- Stein, M., Arnaud-Vanneau, A., Adatte, T., Fleitmann, D., Spangenberg, J.E. and Föllmi, K.B.** (2012a) Palaeoenvironmental and palaeoecological change on the northern Tethyan carbonate platform during the Late Barremian to earliest Aptian. *Sedimentology*, **59**, 939–963.
- Stein, M., Westermann, S., Adatte, T., Matera, V., Fleitmann, D., Spangenberg, J.E. and Föllmi, K.B.** (2012b) Late Barremian - Early Aptian palaeoenvironmental change: The Cassis-La Bédoule section, southeast France. *Cretaceous Research*, **37**, 209-222.
- Steuber, T.** (2002) Plate tectonic control on the evolution of Cretaceous platform-carbonate production. *Geology*, **30**, 259-262.
- Sudar, M., Jovanovi, D., Maran, A. and Polavender, S.** (2008) Late Barremian-Early Aptian Urgonian Limestones from the south-eastern Kucaj Mountains (Carpatho-Balkanides, eastern Serbia). *Annales Géologiques De La Péninsule Balkanique*, **69**, 13-30.
- Swart, P.K. and Eberli, G.** (2005) The nature of the delta¹³C of periplatform sediments: Impli-

- cations for stratigraphy and the global carbon cycle. *Sedimentary Geology*, **175**, 115–129.
- Tejada, M.L.G., Suzuki, K., Kuroda, J., Coccioni, R., Mahoney, J.J., Ohkouchi, N., Sakamoto, T. and Tatsumi, Y.** (2009) Ontong Java Plateau eruption as a trigger for the early Aptian oceanic anoxic event. *Geology*, **37**, 855–858.
- Tomás, S., Löser, H. and Salas, R.** (2008) Low-light and nutrient-rich coral assemblages in an Upper Aptian carbonate platform of the southern Maestrat Basin (Iberian Chain, eastern Spain). *Cretaceous Research*, **29**, 509–534.
- Trabold, G.L.** (1996) Development of the Urgonian limestones in the Delphino Helvetic Realm (Northern Subalpine Chains, Haute-Savoie, France). *Sedimentology, Sequence Stratigraphy and Biostratigraphy. Université de Genève, Publications du Département de Géologie et Paléontologie*, **20**, 1–187.
- Trümpy, R.** (1969) Die helvetischen Decken der Ostschweiz: Versuch einer palinspatischen Korrelation und Ansätze zu einer kinematischen Analyse. *Eclogae geol. Helv.*, **62**, 105–142
- Vail, P.R., Mitchum, R.M.J., Todd, R.G., Widmeri, J.W., Thompson, S., Sangree, J.B., Bubb, J.N. and Hatelid, W.G.** (1977) Seismic stratigraphy and global changes of sea level. In: *Seismic stratigraphy. Application to hydrocarbon exploration, Am. Assoc. Pet. Geol. Mem.*, **26**, pp. 49–212, Tulsa.
- Valet, G.** (1979) Approche paléoécologique du monde des Dasycladales à partir d’écologie des formes actuelles. *Bulletin des Centres de Recherches Elf-Aquitaine Exploration-Production*, **3**, 859–866.
- Van Buchem, F.S.P., Pittet, B., Hillgärtner, H.A., Al-Mansouri, A., Billing, I., Droste, H., Grötsch, J. and Oterdoom, H.** (2002) Regional sequence stratigraphic model for the Kharaib and Shuaiba Formations (Barremian, Aptian) in N. Oman and the UAE – depositional geometries and ecological change. *GeoArabia*, **7**, 461–500.
- Van Wagoner, J.C., Posamentier, H.W., Mitchum, R.M., Vail, P.R., Sarg, J.F., Loutit, T.S. and Hardenbol, J.** (1988) An overview of the fundamentals of sequence stratigraphy and key definitions. In: *Sea Level Changes: An Integrated Approach* (Eds C.K. Wilgus, B.S. Hastings, C.G.S.C. Kendall, H.W. Posamentier, C.A. Ross and J.C. Van Wagoner), **42**, pp. 39–45. SEPM Special Publication, Tulsa, Oklahoma, U.S.A.
- Vermeulen, J.** (2005) Boundaries, ammonite fauna and main subdivisions of the stratiotype of the Barremian. In: *The Hauterivian-Lower Aptian Sequence Stratigraphy from Jura Platform to Vocontian Basin: A Multidisciplinary Approach* (Eds T. Adatte, A. Arnaud-Vanneau, H. Arnaud, M.-C. Blanc-Alétrou, S. Bodin, E. Carrio-Schaffhauser, K.B. Föllmi, A. Godet, M.C. Raddadi and J. Vermeulen), Géol. Alpine, Sér. Spéc. “Colloques et Excursions” No. **7**, 147–173.
- Vilas, L., Masse, J.P. and Arias, C.** (1995) Orbitolina episodes in carbonate platform evolution: the early Aptian model from SE Spain. *Palaeogeography, Palaeoclimatology, Palaeoecology*, **119**, 35–45.
- Wang, H., Frey, M., Stern, W.B. and** (1996) Diagenesis and Metamorphism of Clay Minerals in the Helvetic Alps of Eastern Switzerland. *Clays and Clay Minerals*, **44**, 96–112.
- Weber, J.N.** (1969) Origin of concentric banding in the spines of the tropical echinoid *Heterocentrotus*. *Pacific Sci.*, **23**, pp. 452–466.
- Weber, J., Greer, R., Voight, B., White, E. and**

- Roy, R.** (1969) Unusual strength properties of echinoderm calcite related to structure. *J. Ultrastruct. Res.*, **26**, pp. 355–366.
- Weissert, H.** (1989) C-Isotope stratigraphy, a monitor of paleoenvironmental change: a case study from the Early Cretaceous. *Surveys in Geophysics*, **10**, 1-61.
- Weissert, H., Lini, A., Föllmi, K.B. and Kuhn, O.** (1998) Correlation of Early Cretaceous carbon isotope stratigraphy and platform drowning events : a possible link ? *Palaeogeography, Palaeoclimatology, Palaeoecology*, **137**, 189-203.
- Wermeille, S.** (1996) *Etude sédimentologique, minéralogique et micropaléontologique des calcaires urgoniens de la région subalpine (Savoie, France). Coupes du Rocher de Cluses, du Borne et d'Andey.* Unpublished diploma thesis, University of Neuchâtel, Neuchâtel, 129 pp.
- Wilmsen, M., Fürsich, F.T. and Majidifard, M.R.** (2013) The Shah Kuh Formation, a latest Barremian – Early Aptian carbonate platform of Central Iran (Khur area, Yazd Block). *Cretaceous Research*, **39**, 183-194.
- Wissler, L., Funk, H. and Weissert, H.** (2003) Response of Early Cretaceous carbonate platforms to changes in atmospheric carbon dioxide levels. *Palaeogeography, Palaeoclimatology, Palaeoecology*, **Volume 200**, Pages 187-205.
- Ziegler, M.A.** (1967) A study of the Lower Cretaceous facies developments in the Helvetic border chain, north of the Lake of Thun (Switzerland). *Eclogae Geologicae Helveticae*, **60**, 509-528.

Chapter 4 – Evolution of the Helvetic series (Switzerland) during the latest Hauterivian–early Aptian time: distribution and evolution of facies associated to sea-level, geochemistry and paleotopographic changes.

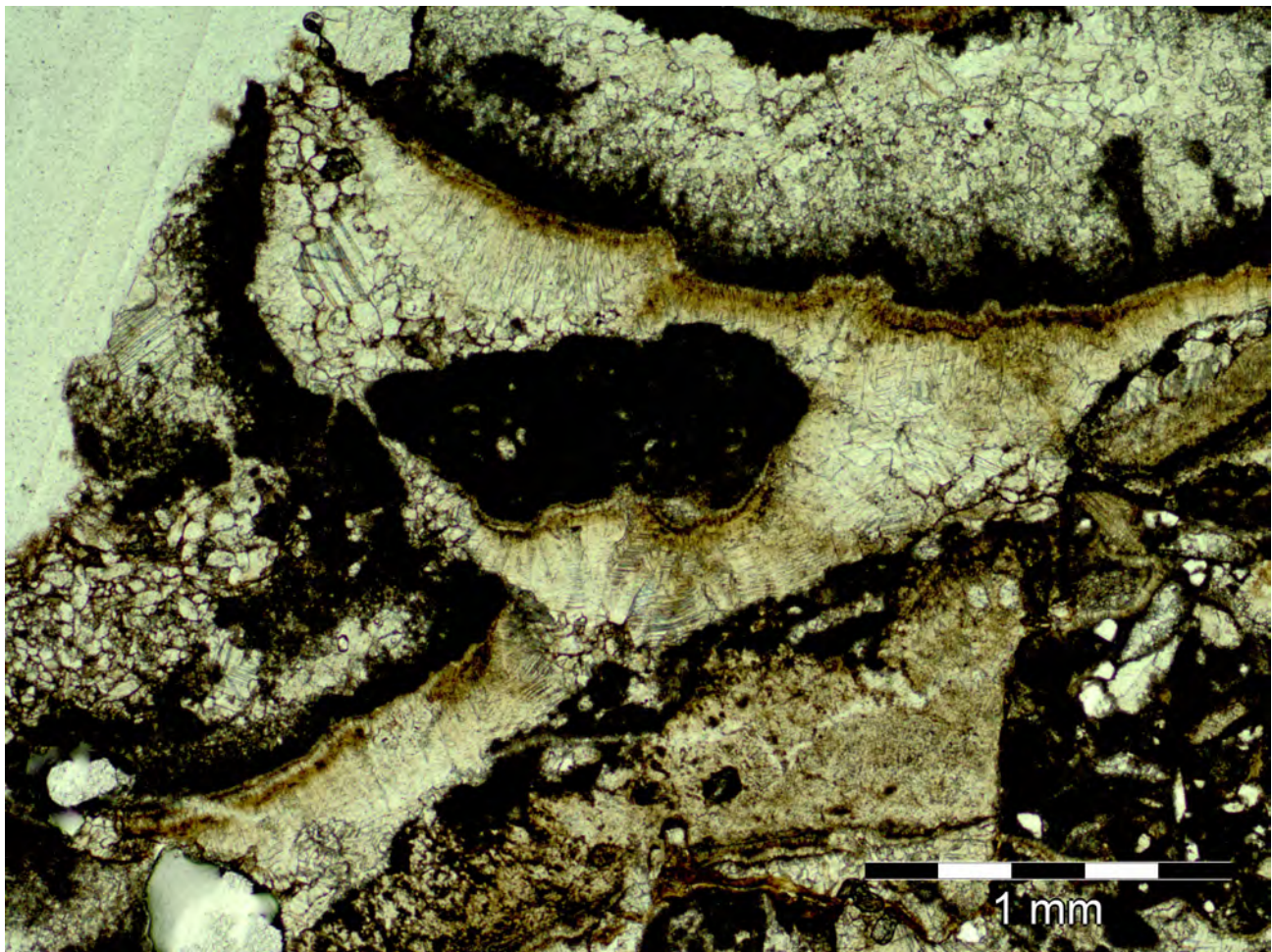


Fig. 4 Pending cement characteristic of beach rock deposits (section of Rawil; sample RW 59.)

The following chapter aims at establishing the evolution of the Helvetic realm, from the latest Hauterivian to the early Aptian, in order to understand the architecture of the shelf. The distribution of microfacies is examined, and compared with carbon isotope and phosphorus records. The principal controlling factors of the development of this platform are discussed in this chapter.

Chapter 4

Evolution of the Helvetic series (Switzerland) during the latest Hauterivian–early Aptian: distribution and evolution of facies associated to sea-level, geochemistry and paleotopographic changes.

Abstract

We report an integrated study of a platform to shelf succession of latest Hauterivian to early Aptian age, cropping out in the Helvetic Alps. The evolution of the Helvetic platform is examined using 12 sections across the Helvetic thrust-and-fold belt through the inner, intermediate and distal platform domains. The succession of microfacies, coupled with the biostratigraphy of the benthic foraminifera, permits to subdivide the series into 8 sequences. Geochemical analyses (stable isotopes and phosphorus content) have been performed in order to better constrain the paleoceanographic and paleoenvironmental conditions.

The distribution of microfacies for each sequence illustrates the development of the platform, starting with a phase of sedimentary condensation (Altmann Mb; late Hauterivian – early Barremian), followed by the deposition of hemipelagic sediments (Drusberg Mb; early Barremian), and the development of lagoonal shallow-water carbonate (Schrattenkalk Fm; early Barremian – early Aptian), which is characterized by important progradation and aggradation. The microfacies distribution and sequential geometry provide information on

the architecture of the platform, which changed from a ramp like toward a flat-topped platform. Changes of environmental conditions have been recognized, by the alternation of heterozoan/photozoan faunal assemblages and by the phosphorus content of the samples. During the development of the Schrattenkalk Fm, two intervals of more mesotrophic conditions have been recognized: one in the sequence B3 (early late Barremian) and the second one in the sequence A1 (earliest Aptian), which represents the Rawil Mb. The carbon-isotope trends are used to assess the importance of local environmental and diagenetic overprint relative to the global signal. The global signal is well preserved in the hemipelagic series, but is quite disturbed in the shallow-water carbonates by emersive phases, facies changes and late-stage diagenesis related to alpine orogenesis.

Keywords

Helvetic Alps; Urgonian platform; Altmann Mb; Drusberg Mb; Rawil Mb; Schrattenkalk Formation; Early Cretaceous; latest Hauterivian– early Aptian; Microfacies; Sequence stratigraphy; Carbon isotopes; Phosphorus

4.1 Introduction

The Helvetic carbonate platform belongs to one of the largest Mesozoic carbonate platforms, which developed over more than 2500 km along the northern Tethyan margin (Golonka, 2004). The structural fold-and-thrust system of the Helvetic realm exposes the distal part of the platform and the transition to the outer shelf, whereas the proximal part is located northward and preserved in the Jura Mountains (e.g., Godet et al., 2010).

The Early Cretaceous period is characterized by several changes in the type of carbonate production on the Helvetic shelf, which oscillated between photozoan and heterozoan assemblage phases, and phases of platform demise (e.g., Funk et al., 1993; Föllmi et al., 1994; Föllmi et al., 2007; Föllmi, 2012).

In this study, the succession of the uppermost Hauterivian – lower Aptian platform sediments in the Helvetic Alps is re-examined in detail. This interval of time records changes from a phase of condensation and suppressed platform carbonate production (Altmann Member (Mb)), followed by a phase of recovery in carbonate production (with the deposition of the hemipelagic Drusberg Mb), which led to the development of the photozoan Urgonian platform (Schrattenkalk Formation (Fm)). Amongst the first scientific descriptions and interpretations on the Urgonian in the Helvetic Alps, we list those by Kaufmann (1867), Heim (1916-1922), (Heim and Baumberger (1933), and Fichter (1934). More recent researches with a focus on facies and microfacies development were compiled by Bollinger (1988; Vorarlberg) and Schenk (1992; Bernese Alps). Funk et al. (1993) added the first sequence-stratigraphic interpretation. Combined sedimentological and geochemical approaches

constraining the evolution of the Urgonian carbonate depositional system are found in Bodin et al. (2006) for the Drusberg Fm and the transition to the Schrattenkalk Fm, and Stein (2011) for the Rawil Mb, which separates the Lower and Upper Schrattenkalk Mbs.

This analysis is based on the detailed study of 12 sections spread across the platform. The study links the analysis of microfacies, biostratigraphy, carbon-stable isotope records and phosphorus contents. A comparison and correlation of the sections are possible through the establishment of a sequence stratigraphic framework. The aims of this study are to illustrate the evolution of the platform by the variations in paleoenvironments, distribution of the facies, thickness of different sequences and characterization of the C-isotope record. The distribution of facies provides information on the relative water depth and is important in the interpretation of variations in the thickness of the sedimentary series, and their relationship with the inherent topography and local variations in subsidence due to synsedimentary tectonics, and finally to illustrate the dynamics of sediment deposition.

4.2 Geological setting

The Helvetic tectonic unit represents the external part of the Alps, and extends across the Switzerland and the adjoining countries to the east (western Austria and southern Germany) and to the west (subalpine chains in eastern France). The Helvetic Alps are composed of a thrust-and-fold complex formed during Cenozoic alpine orogenesis (e.g., Heim, 1916-1922; Ramsay, 1981; Pfiffner, 1993). It includes Mesozoic sediments representing the central part of the former northern Tethyan margin (Fig.

4.1). Trümpy (1969), Ferrazzini and Schüler (1979) and Kempf and Pfiffner (2004) proposed palinspastic reconstructions in order to place the Helvetic nappes in their original palaeogeographic position on the northern Tethyan platform (Fig. 4.1). These reconstructions are used here to locate the sections in their original depositional context.

The uppermost Hauterivian – lower

Aptian succession is divided into several lithostratigraphic units (Fig. 4.2). The uppermost Hauterivian to upper lower Barremian embodies the Altmann Mb, a condensed level forming the basal sub-unit of the Tierwis Fm. The superjacent member of this formation is the Drusberg Mb, which consists of hemipelagic marl and limestone alternations. This member is diachronically overlain by the Schrattenkalk Fm, which is the

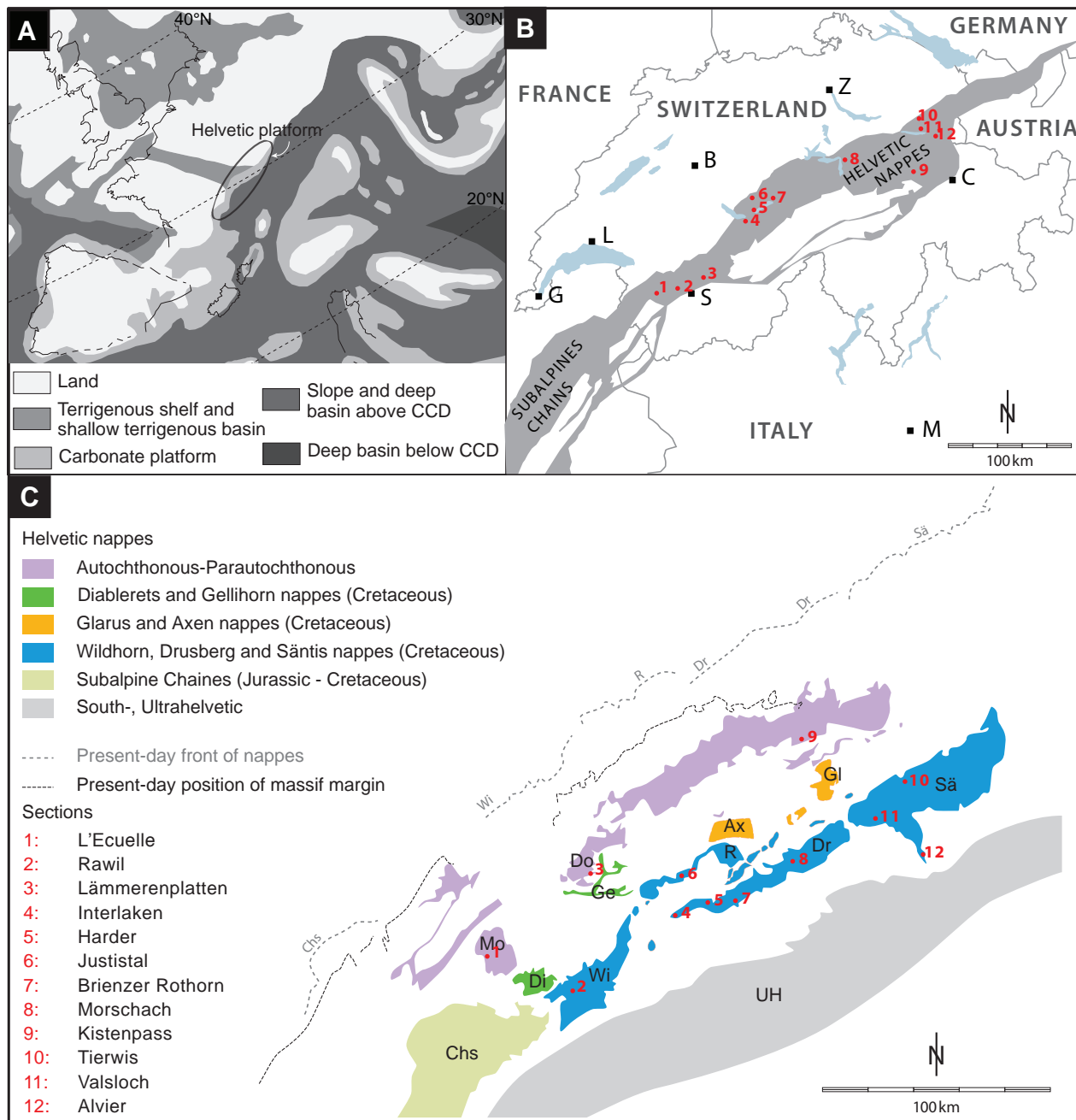


Fig. 4.1 A/ Early Aptian paleomap of the western Tethyan realm showing the location of the Helvetic platform. (after Masse, 1993b). B/ Location of the studied sections in the Helvetic nappes (grey colored). C/ Palinspastic reconstruction of the Helvetic nappes and restauration of the location of the sections (redraw after Kempf and Pfiffner, 2004).

equivalent of the Urgonian Fm in France (e.g., Arnaud-Vanneau, 1980). In proximal parts of the Helvetic shelf, the Schrattenkalk Fm starts in the latest early Barremian (see Chapter 2), whereas in the distal part of the shelf, the Drusberg Mb persists until the early Aptian. Like the Drusberg

Mb, the Schrattenkalk Fm ends in the early Aptian. The Schrattenkalk Fm is divided into a Lower and an Upper Schrattenkalk Member by the Rawil Mb, an equivalent of the “Lower Orbitolina Beds” (in the Vercors area of southeastern France). The Upper Schrattenkalk Mb

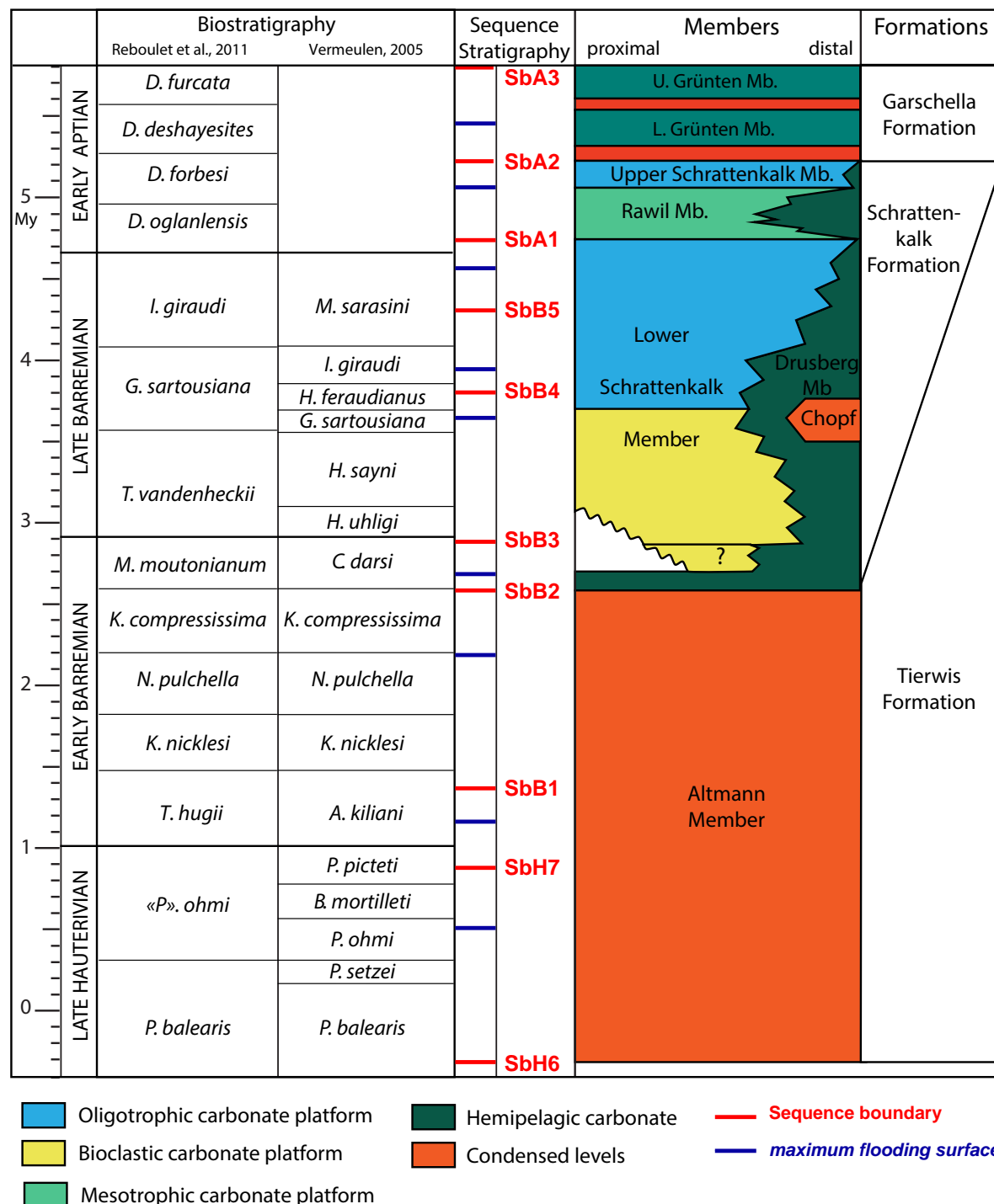


Fig. 4.2 Latest Hauterivian–earliest Aptian lithostratigraphy, biostratigraphy (Vermeulen, 2005 and Reboulet et al., 2011) and sequence stratigraphy of the Helvetic nappes. The sequence stratigraphic framework is based on the one defined by Arnaud et al., 1998 in the Vercors and Chartreuse massifs..

is overlain by the Grünten Mb, an equivalent of the “Upper Orbitolina Beds”.

4.3 Studied sections

This study is based on the observations and analyses performed on 12 sections and one panorama. The studied sections are: (1) L’Ecuelle (VD; Swiss coordinates: 579.336/124.832), (2) Rawil (BE; 601.157/137.186), (3) Lämmerenplatten (VS; 613.081/140.041), (4) Interlaken (BE; 631.347/169.493), (5) Harder (BE; 631.250/170.991), (6) Justistal (BE; 628.427/176.557), (7) Brienzer Rothorn (BE; 645.955/182.008), (8) Morschach (a drill core; SZ; 690.299/205.511), (9) Kistenpass (GR; 722.715/185.749), (10) Tierwis (SG; 742.970/234.730), (11) Valsloch (SG; 742.224/224.041) and (12) Alvier (SG; 749.644/222.586). The location of the sections and their position in the nappes are represented in the figure 4.1. The panorama of the Churfisten (SG) encompasses the range between the Mount Schären (736.004/223.075) to the Mount Nideri (744.344/223.305).

4.4 Methods

4.4.1 Field work and samples preparation

The working approach used for sedimentological characterization involves an outcrop-based carbonate facies description supported by the analysis of samples. Samples for microfacies and geochemical investigations were taken at a

spacing of 1 m or less. Higher sample densities were applied across facies boundaries and discontinuity surfaces. The samples were sawn in order to remove weathered surfaces and veins, and if present, the micritic part of the rock samples was privileged for the isotope analyses. Rock powders were obtained by using a mechanical agate crusher.

4.4.2 Microfacies description

A total of 1931 thin sections were studied, using conventional optical microscopy. An Olympus BX51 microscope (Olympus, Tokyo, Japan) equipped with an Olympus Altra 20 camera and the Olympus Image Analysis © software was used for digital microphotography. The microfacies classification used in this study was the one, established by Arnaud-Vanneau and Arnaud (2005) in the Urgonian limestone of the Chartreuse and Vercors area (Fig. 4.3). This classification is based on actual analogues with regards to the environmental position of ecosystems, in addition to the effects of light, salinity, currents and trophic levels. It consists of twelve microfacies (MF) types, which are arranged on a distal-to-proximal transect, from the most external MF F0 characterized by a pelagic faunal association, to the shallowest MF F11, which represents an internal lagoonal facies close to emersion (Fig. 4.3). Three annex MF types are recognized: FT1, FT2 and FT3, which are used to characterize the main transgressive phases: FT1: reworking and lag; FT2: accumulation of *Palorbitolina lenticularis*, associated with detrital quartz, annelids and *Choffatella decipiens*; and FT3: accumulation of Dasycladaceae algae. These MF types were regrouped in six microfacies associations (AF1 to AF6), according to

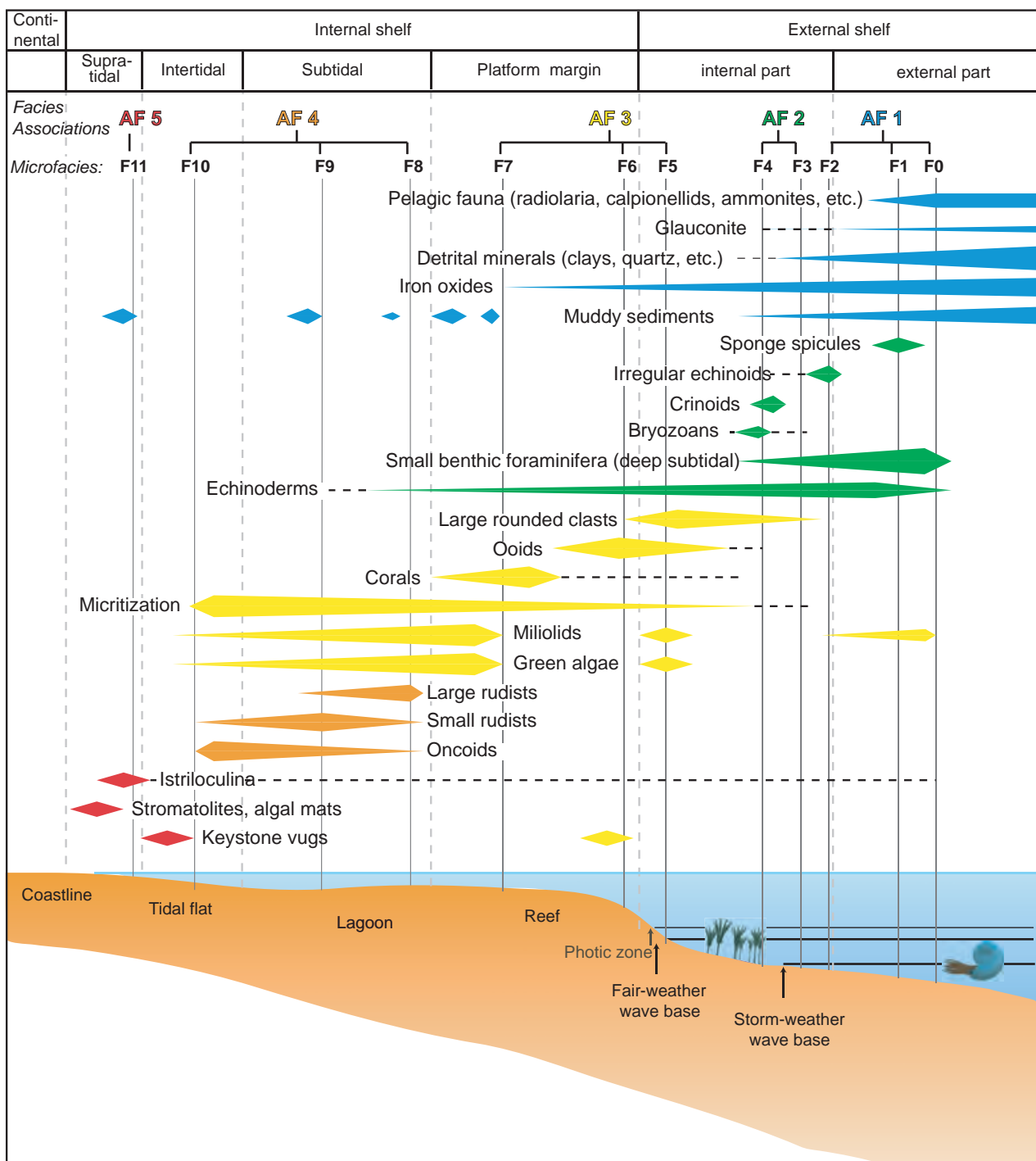


Fig. 4.3 Distribution of principal microfacies types along a rimmed platform transect during the Hauterivian–Barremian (redrawn after Godet et al., 2010, and Arnaud-Vanneau, 2005).

comparable bathymetries and grain-size sorting characteristics.

4.4.3 Carbon and oxygen-isotope analysis

A total of 1958 samples were analysed

for their stable carbon and oxygen isotope composition at the Institute of Earth Surface dynamics of the University of Lausanne. Carbon and oxygen isotopes were analysed using procedures described by Revesz et al. (2001). Analyses of aliquots of all samples were performed using a Thermo Fisher Scientific (formerly Thermo-Quest/Finnigan, Bremen, Germany) GasBench

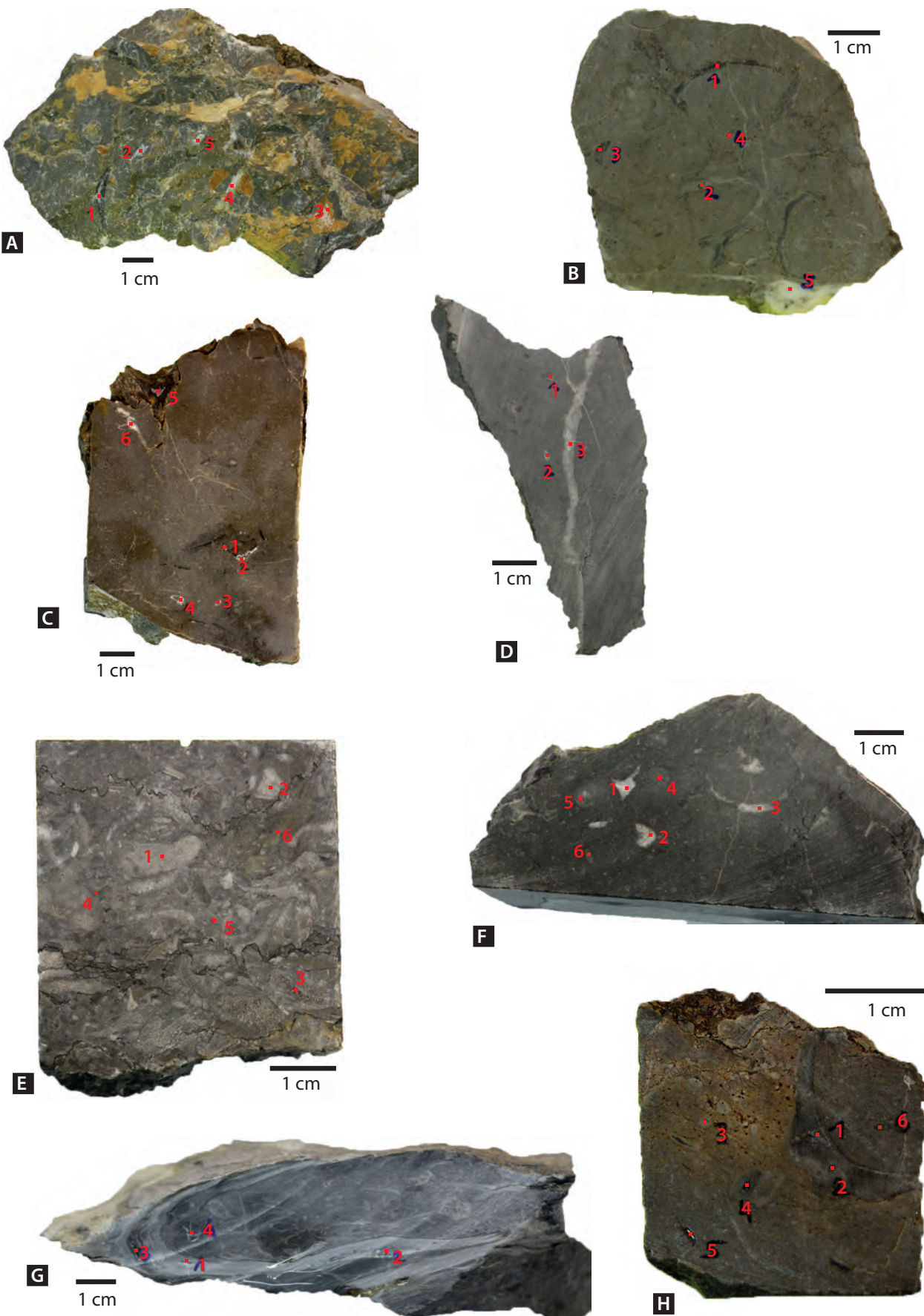


Fig. 4.4 Hand-specimens and position of the micro-drilling used to assess the heterogeneity of the isopotic compositions. **A:** sample EC 166 bis provides from the section of L'Ecuelle; **B:** sample LB 27 fro the section of Justistal; **C:** sample VA 122 from the section of Valsloch; **D:** sample TW 135

from the section of Tierwis; **E**: sample MC 137 from the core of Morschach **F**: sample VA 15 from the section of Valsloch; **G**: sample KP 61 from the section of Kistenpass; **H**: sample MC 10 from the core of Morschach.

II preparation device interfaced with a Thermo Fisher Scientific Delta Plus XL continuous flow isotope ratio mass spectrometer (IRMS). The CO₂ extraction was executed at 90°C. The carbon and oxygen-isotope ratios were reported in the delta (δ) notation as the per mil (‰) deviation relative to the Vienna–Pee Dee belemnite standard (VPDB). Analytical uncertainty (2σ), monitored by replicate analyses of the international calcite standard NBS-19 and the laboratory standards Carrara Marble was not greater than $\pm 0.05\text{‰}$ for $\delta^{13}\text{C}$ and $\pm 0.1\text{‰}$ for $\delta^{18}\text{O}$.

To assess the possible heterogeneity of the carbon and oxygen isotope composition within a hand-specimen, a detailed micro-drilling subsampling (100 to 300 µg) was performed on 8 selected samples. These samples contain facies-representative bioclasts, calcite veins and veinlets within the micritic matrix (Fig 3.4). A total of 54 subsamples were analysed for their C and O isotope composition as describer for the whole-rock powders.

4.4.4 Phosphorus content

The total phosphorus content was measured on 1182 samples from the sections of L'Ecuelle, Tierwis, Interlaken, Kistenpass, Harder, Brienzer-Rothorn and Valsloch, using the ascorbic acid molybdate blue method (Eaton et al., 1995) and following the procedure described in Bodin et al. (2006c). The phosphorus content was determined using an UV/Vis Perkin Elmer Lambda 25 spectrophotometer at the University of Lausanne, and calibrated with internal standard solutions providing a precision better than

5%.

4.5 Results

4.5.1 Description of the studied sections

(1) The section of L'Ecuelle (Fig. 4.5-A) is located in the normal flank of the Morcles nappe, 2.5 km from Anzeindaz (canton of Vaud). The section represents an inner-platform position. The complete log of this section is shown in Figure 4.6. The Altmann Mb is observed and represents 4m of coarse granular sandy limestone, overlain by 90 m of thinly-bedded marly limestone of the Drusberg Mb. The marly limestone is darkly colored and is rich in irregular urchin remains. This interval is overlain by the Lower Schrattenkalk Mb which is characterized by a 100m-thick, rudist-rich photozoan limestone. The base of this member is affected by several faults. A metric interval of yellowish marly limestone is observed in the middle part of this member. Above this interval, large oblique beds in a micritic lagoonal limestone are observed (Fig 4.5-B). At the top of the Lower Schrattenkalk Mb, a remarkable surface presents an important network of root traces, dissolved rudist shells and karst features (see Chapter 3). It marks the onset of the Rawil Mb, a 20m-thick interval of yellowish limestone rich in orbitolinids, corals and rudists. The 25 upper meters of the section correspond to the Upper Schrattenkalk shallow-water limestone,

with corals and rudists. Within the upper part of this member, fractures are infilled by glauconitic sandstones from the superjacent Garschella Fm including blocks from the Grünten Mb (see Chapter 3 for photo and more details).

(2) The section of Rawil (Fig. 4.5-C; Fig 4.7) is located underneath the midway station of the military cablecar of Rawil, south of Iffigenalp. This section, which is part of the Wildhorn Nappe, was previously studied by Schenk (1992) and Stein et al. (2012a). It represents the type locality of the Rawil Member. The section has only been logged from the upper part of the Lower Schrattenkalk Mb to the top surface of the Upper Schrattenkalk Mb. The logged Lower Schrattenkalk Mb consists of a 30m-thick interval of light grey limestone rich in corals and stromatoporoids. The last 5 meters are very rich in rudists. The Rawil Mb is characterized by a thinly-bedded limestone, rich in Orbitolinids, rudists and corals. The basal surface is marked by a thin reddish layer of terra rossa (see chapter 3), and the firsts meters show a succession of tempestites, which end with gastropod accumulations. The Upper Schrattenkalk Mb is rich in rudists and ends with an erosional surface, which is overlain by the Grünten Mb.

(3) The section of Lämmerenplatten (Fig. 4.5-D; Fig 4.8) is located close to the Gemipass, in the canton of Valais, in the nappe of Doldenhorn. There is a clear contact between the dark Kieselkalk Fm and the light grey overlying Tierwis and Schrattenkalk Fms. The first beds forming the Altmann Mb are rich in phosphate nodules (Fig 4.5-E). The rest of the section consists of a 35 m-thick limestone, which is metrically bedded, rich in silicified shells and *Microcodium*, and which is attributed to the Lower Schrattenkalk Mb. The series is covered by a white limestone of Eocene age, above an

erosional surface.

(4) The section of Interlaken (Fig. 4.5-F; Fig 4.9) is located west of the train station of Interlaken West. It is part of the Border Chains, in the frontal part of the Wildhorn nappe and represents an intermediate position on the Helvetic platform. It represents a reversed succession of an overturned anticline. The logged part of the section represents a 60m-thick carbonate interval belonging to the Upper Schrattenkalk Mb. Rudist remains are observed at the base of the section. This section allows the observation of the contact between the Upper Schrattenkalk Mb and the overlying Garschella Fm, which is erosive, perforated and shows traces of phosphate and pyrite (Fig 4.5-G). The section is affected by several faults and is extremely altered.

(5) The Harder section (Fig. 4.5-H; Fig 4.10) is situated on the eastern side of the cities of Interlaken and Unterseen, in the Wildhorn nappe. It also represents the reversed sequence of the same overturned anticline as the section of Interlaken, but a few kilometers more to the east. The section starts with the Altmann Mb, a metric interval rich in glauconite, phosphate nodules and ammonites. This level has been studied by Ziegler (1964) and by Bodin et al. (2006a). It is covered by the Drusberg Mb, which consists of 90 m of marly limestone–marl alternations with several intercalated, calcareous banks. This interval is overlain by up to 140 m of thickly bedded carbonates assigned to the Lower Schrattenkalk Mb, which consist of bioclastic and peloidal limestone. The following interval is composed of the Rawil Mb, which corresponds to a 40 m-thick succession of recessive beds of sandy marl and marly limestone very rich in large Orbitolinids (Fig 4.5-I). This member is overlain by a succession of thickly-bedded to massive carbonates, which consist of photozoan

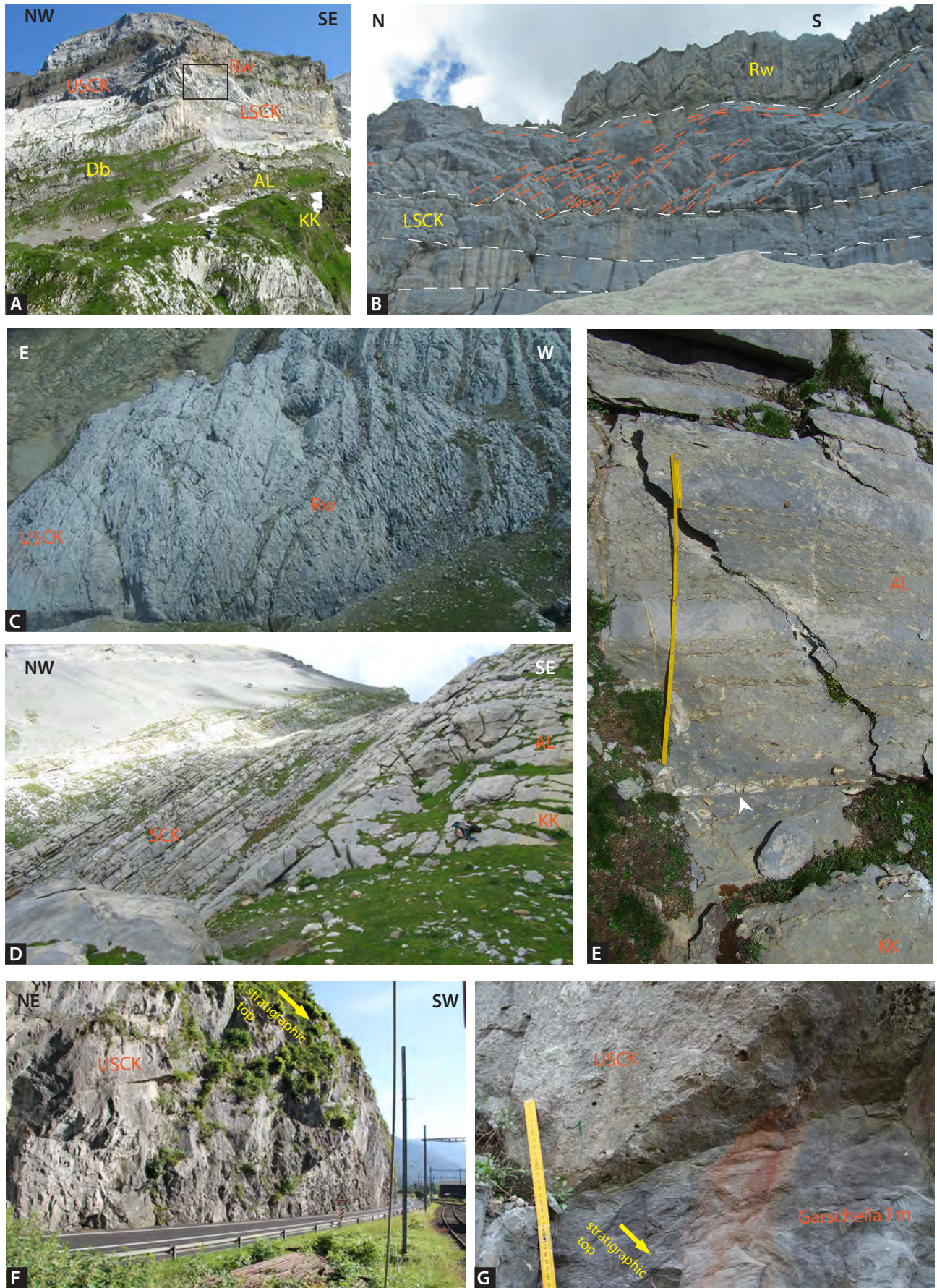
facies characterized by the occurrence of corals and rudists (Fig 4.5-J).

(6) The section of Justistal (Fig. 4.5-K:- Fig 4.11) in the Wildhorn Nappe is located on the northeastern side of the Lake of Thun. The section is precisely located in Loubenegg, in the southern part of the Valley of Justistal. Ziegler (1967) and Schenk (1992) previously studied this section. It consists of a 240m thick section, which starts with a 2m-thick glauconitic-rich dark sandy bed forming the Altmann Mb. The Drusberg Mb is missing and the following interval consists of a bioclastic limestone, attributed to the Lower Schrattenkalk Mb, interrupted by ledges of less massive limestones. The base of the Lower Schrattenkalk Mb shows channelized structures, which end by a truncation surface. Above this truncation, the bioclastic banks show cross-bedded stratifications (Fig 4.5-L). The upper 40 m of the sections are rich in ru-

dists and gastropods, and the uppermost meters correspond to the basal part of the Rawil Mb. An erosional surface ends the series, which is covered by a limestone of Eocene age.

(7) The Brienzer Rothorn (Fig. 4.5-M; Fig 4.12) section is located to the north of the Brienz Lake, in the canton of Berne. This section is part of the same overturned anticline as the Harder section, which represents a distal portion of the Helvetic platform. The section has been studied by Ribaux (2012) and starts with the Altmann Mb, which is 4 to 5m thick, and characterized by condensed levels and channelized, silt- and glauconite-rich limestone layers. It is overlain by more than 200 m of marly limestone–marl alternations of the Drusberg Mb. The following interval is attributed to the Rawil Mb. It starts with an intercalation of turbiditic calcareous banks in a marly interval. The presence of *Thalassinoides* burrows highlights these

Fig. 4.5 Field photographs of the sections; KK= Kieselkalk Fm, AL = Alvier Mb, Db=Drusberg Mb, LSCK=Lower Schrattenkalk Mb, Rw=Rawil, USCK=Upper Schrattenkalk Mb. A: Global view of L'Ecuelle section. Black box indicates the location of the picture B. B: Oblique stratifications in the section of L'Ecuelle. Different interpretations are discussed in the text. C: Overview of the Rawil section. D: Overview of the Lämmerenplatten section, with the contact between the Kieselkalk Fm and the Altmann Mb. The white arrow indicates the level of phosphate nodules. E: View of the upper part of the section of Interlaken. F: Detail of the top Schrattenkalk surface and the contact with the Garschella Fm. G: General overview of the section of Harder. I: Base of the Rawil Mb in the section of Harder, showing a recessive interval. J: Sample providing from the Upper Schrattenkalk Mb of the section of Harder, showing a shallow-water carbonate assemblage rich in corals (orange lines) and flats Orbitolina (orange arrow). K: Overview of the section of Justistal. L: cross-bedded stratifications, in the Lower Schrattenkalk Mb of the section of Justistal. M: Section of Brienzer Rothorn (Picture from Ribaux, 2012). N: Detail of the thalassinoides at the base of the beds, in the upper part of the section of Brienzer Rothorn (Picture from Ribaux, 2012). O: View of the section of Kistenpass. P: Detail of a coquina level rich in oyster, in the marly interval of the Drusberg Mb in Kistenpass section. Q: View of a part of the core of Morschach, belonging to the Drusberg Mb, rich in bioturbations. R: View of a part of the Rawil Mb of the core of Morschach, showing levels of lag associated to tempestite deposits. S: Part of the Upper Schrattenkalk Mb of the core of Morschach, showing light grey limestone rich in rudists. T: Tierwis section outcrop. U: General overview of the section of Valsloch. V: View of the section of Alvier. The right part is the upper part of the section sampled by Briegel, 1972 (Glännli).



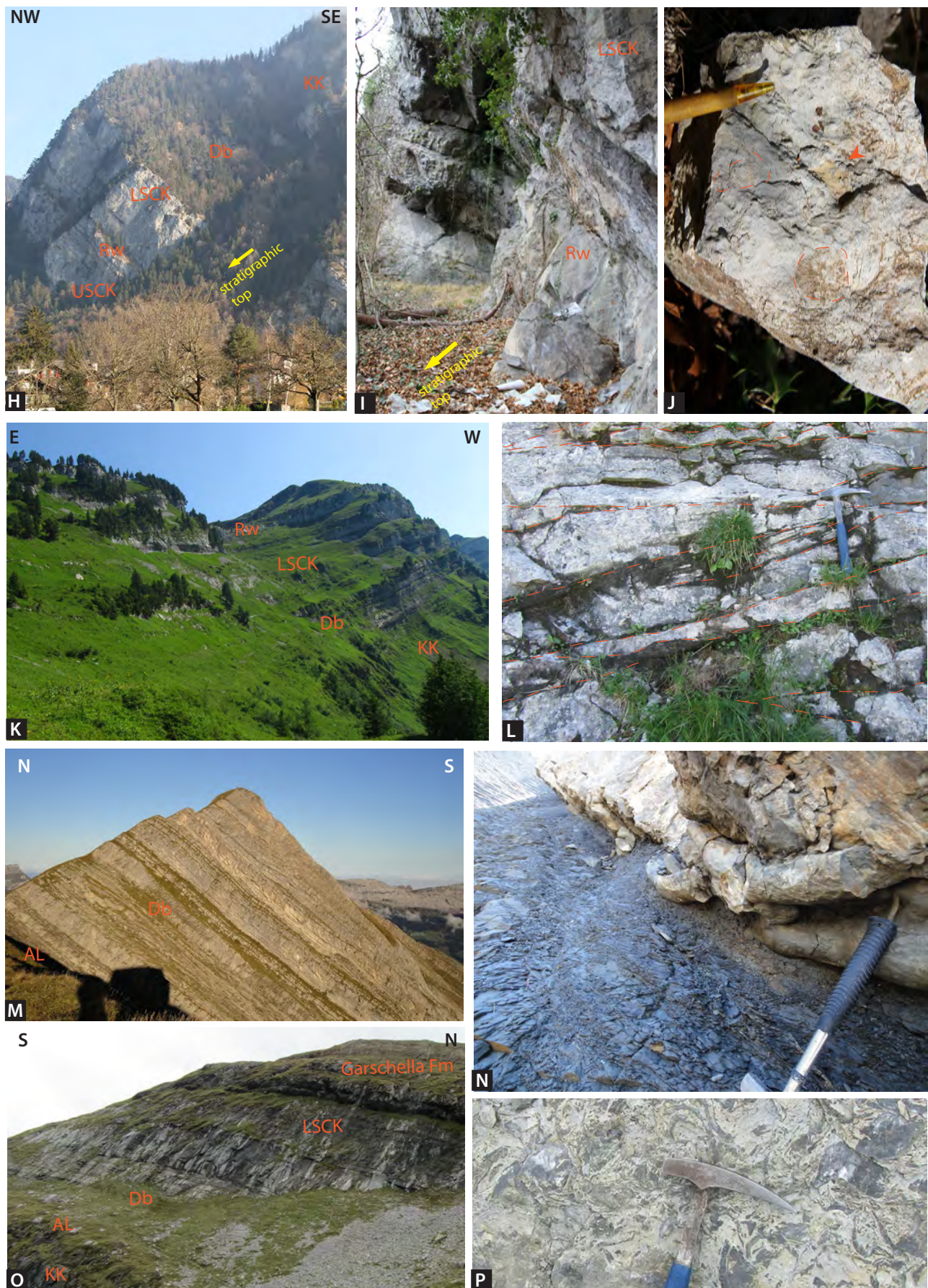


Fig. 4.5 (continued)



Fig. 4.5 (continued)

gravity-flow deposits (Föllmi and Grimm, 1990; Fig 4.5-N and -P).

(8) The borehole of Morschach (Fig. 4.14) is located on the golf course of Morschach, in the Drusberg nappe, and represents an intermediate shelf position. The lower part is composed of a dark marly limestone, rich in

oysters, irregular urchins and annelids. Some beds show bioturbation networks consisting of *Thalassinoides* (Fig 4.5-Q). This 75m-thick interval is attributed to the Drusberg Mb. The Lower Schrattenkalk Mb is characterized by a 125 m-thick light grey limestone, bioclastic at the base and progressively richer in rudists.

Corals, oncolites and Orbitolinids are abundant in the upper part of the Lower Schrattenkalk Mb. The Rawil Mb (50m) starts above a whitish interval characteristic of intense leaching associated to a succession of tempestite levels. The Rawil Mb shows several layers highly enriched in flat *Orbitolina* intercalated with level tempestites associated with intense reworking of bioclasts (Fig 4.5-R). The Upper Schrattenkalk Mb is characterized by the abundance of rudists, miliolids, *Bacinella* nodules and corals (Fig 4.5-S). The last meter shows the accumulation of echinoderms, brachiopods and annelids, and is attributed to the Grünten Mb.

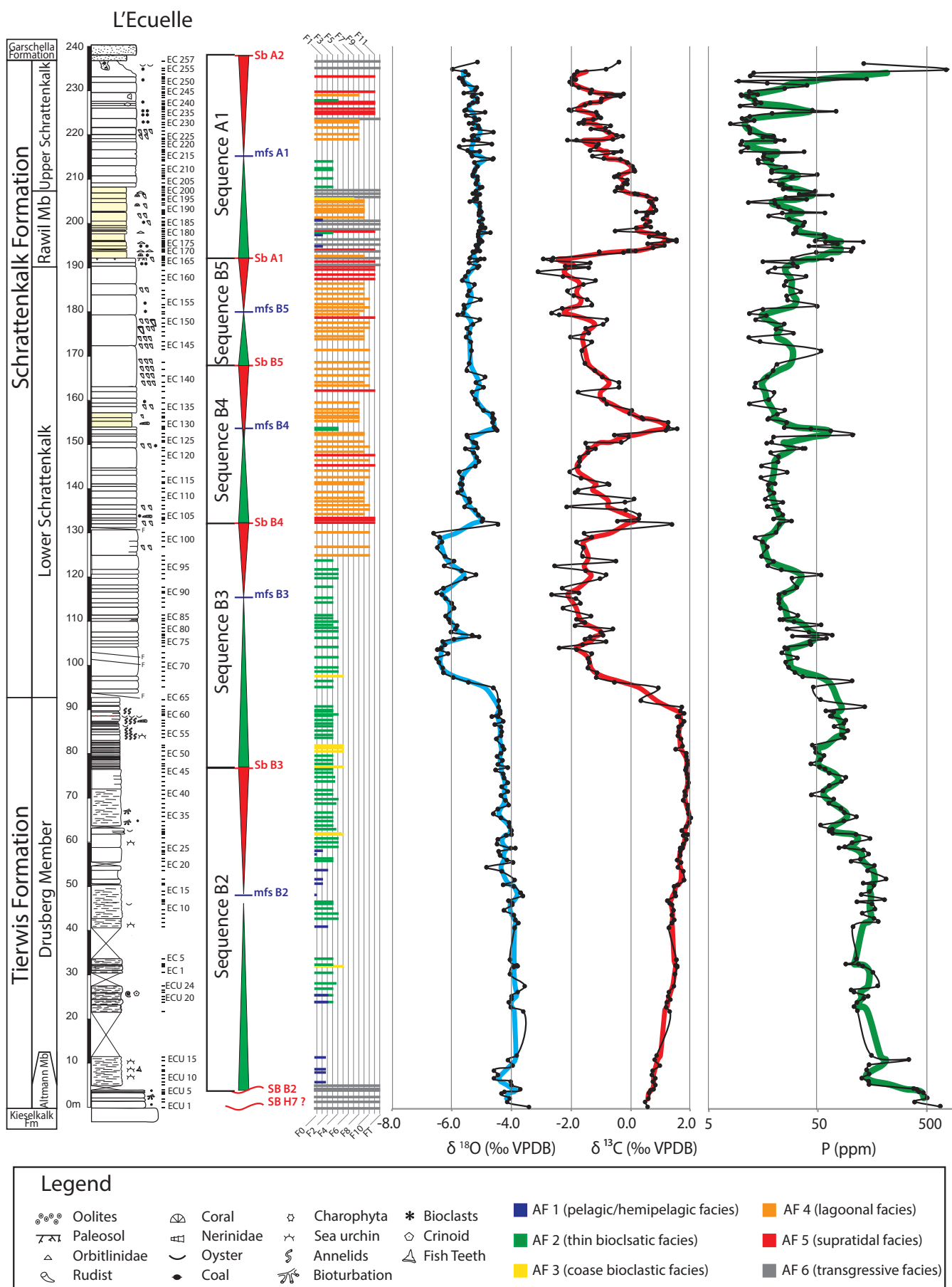
(9) The Kistenpass section (Fig. 4.5-O; Fig 4.14) is located eastward of the Biferstenstock, in the Infrahelvetic complex. This section starts with 10m of Altmann Mb, rich in glauconitic sandstone and conglomeratic levels, overlain by 40 m of Drusberg Mb, which includes alternations of marly limestone and coquina levels rich in oysters. The upper part of the section corresponds to 25 m of Urgonian-type limestone where only the basal part of the Lower Schrattenkalk Mb is preserved, and ends by an erosional surface overlain by the Garschella Fm. Alpine deformation strongly affected the Urgonian part of the section.

(10) The section of Tierwis (Fig. 4.5-T; Fig 4.15) is part of the Säntis nappe and is located close to the Säntis summit. This section was logged and sampled in detail by Bodin et al.

(2006a) for the Tierwis Fm and by Stein et al. (2012a) for the Rawil Mb, and completed in this study for the Lower and Upper Schrattenkalk Mbs. The Tierwis section presents a well-developed Altmann Mb (ca. 35 m), rich in ammonites and fish teeth (Bodin et al., 2006a.), overlain by a thin, 18m-thick Drusberg Mb. The latter consists of marly limestone alternating with marly intervals. The Lower Schrattenkalk Mb is 75 m thick and is mainly composed of a photozoan faunal assemblage (green algae, rudists, stromatoporoids). A recessive interval corresponds to the Rawil Mb, which includes a 30m-thick limestone intercalated with marly intervals, some of which show Orbitolinid accumulations (Stein, 2011). The Upper Schrattenkalk Mb is characterized by a succession of parasequences including corals at the bottom, rudists in the higher part and Nerineid gastropods near their top.

(11) The section of Valsloch (Fig. 4.5-U; Fig 4.16) is situated in the Churfirsten range and belongs to the Säntis Nappe. This section represents an outer-platform position. Nearby sections were previously studied by Wissler et al. (2003) and Stein et al. (2012a). The Valsloch section starts by 1m of dark sandy limestone rich in glauconite, forming the Altmann Mb, overlain by 100 m of poorly exposed marly and limestone alternations (Drusberg Mb). The Lower Schrattenkalk Mb shows a bioclastic facies, with a horizon rich in annelids, overlain by more lagoonal facies, rich in rudist remains.

Fig. 4.6 L'Ecuelle section: lithological-sedimentological log, microfacies identification, sequence-stratigraphic interpretation, isotope stratigraphy and phosphorus content. The microfacies are grouped in associations (see Figure 4.15). AF 1 is composed by microfacies F0, F1 and F2 and represents the external shelf. AF 2 is composed by microfacies F3 and F4, which are representative of the outer shelf close to the platform margin. AF 3 groups microfacies F5, F6 and F7, which indicate a platform margin position. AF 4 embodies microfacies F8, F9 and F10, typical for the inner platform. AF5 is in the supratidal part of the platform, and is the equivalent of microfacies F11 (muddy and sandy). AF 6 corresponds to the transgressive facies FT.



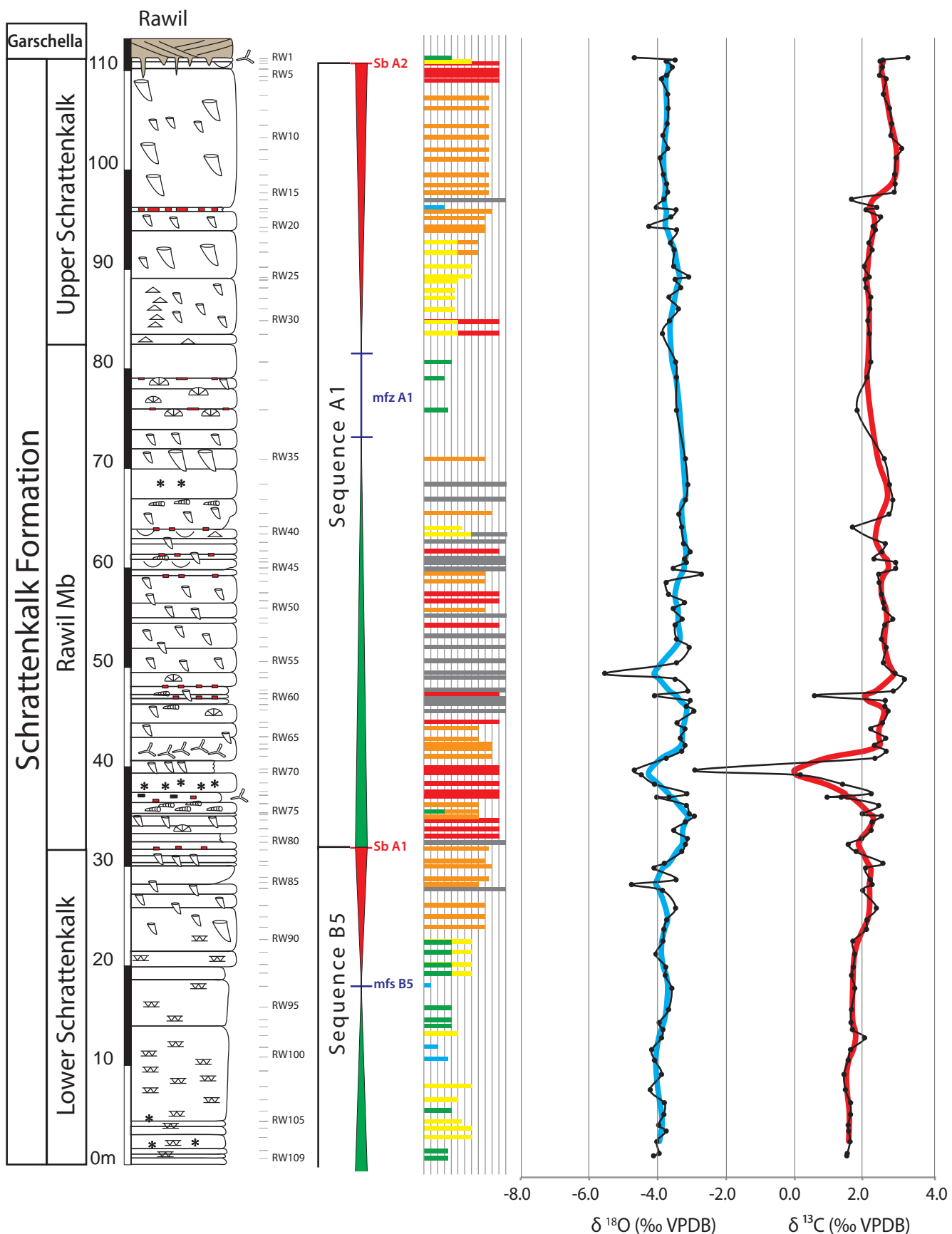


Fig. 4.7 Rawil section: lithological-sedimentological log, microfacies identification, sequence-stratigraphic interpretation, isotope stratigraphy. See Fig. 4.3 for the legend.

Lämmerenplatten

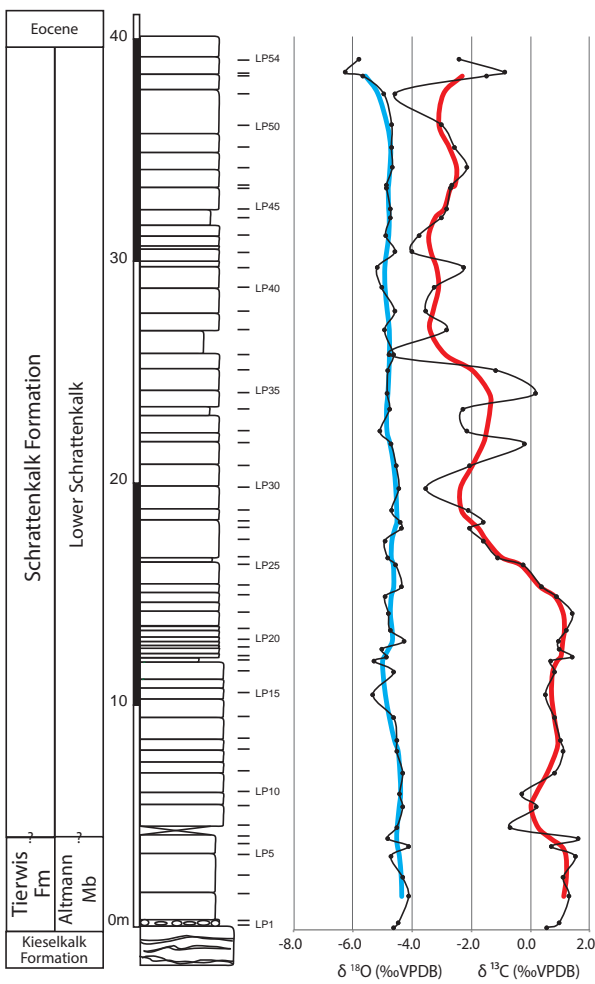


Fig. 4.8 Lämmerenplatten section: lithological-sedimentological log and isotope stratigraphy. See Fig. 4.3 for the legend.

Interlaken

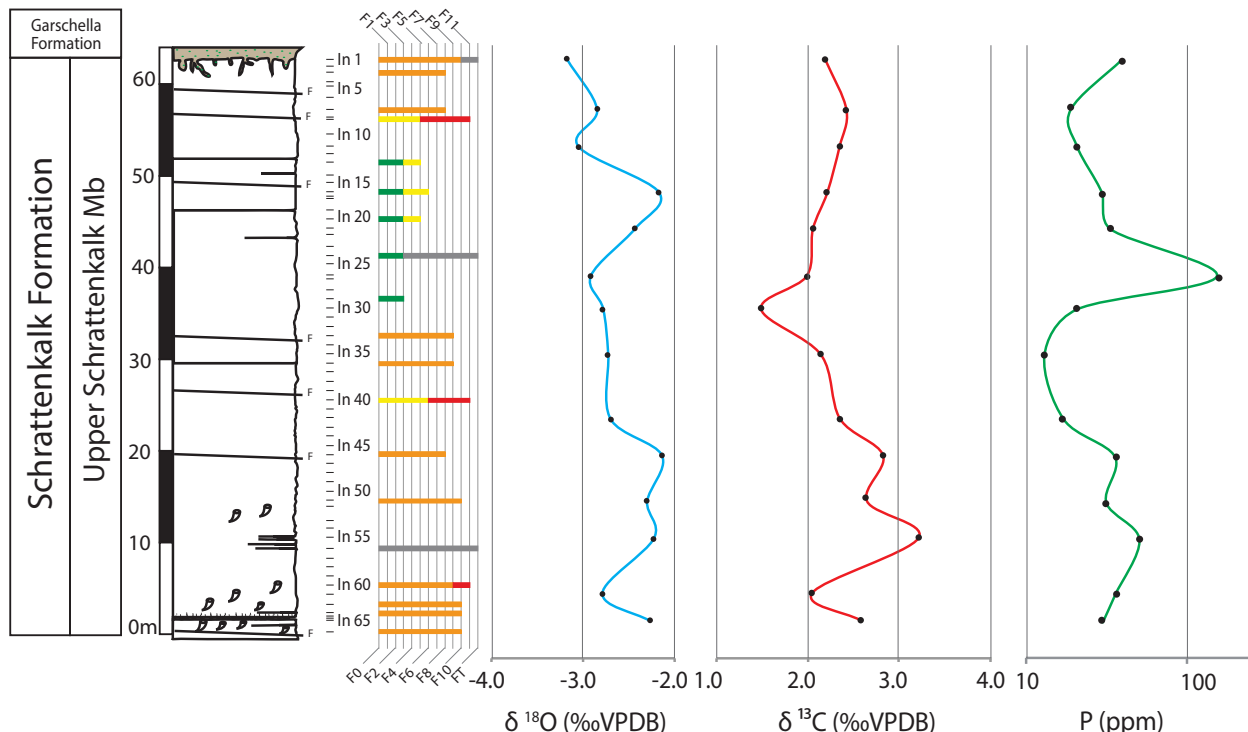


Fig. 4.9 Interlaken section: lithological-sedimentological log, microfacies identification, isotope stratigraphy and phosphorus content. See Fig. 4.3 for the legend.

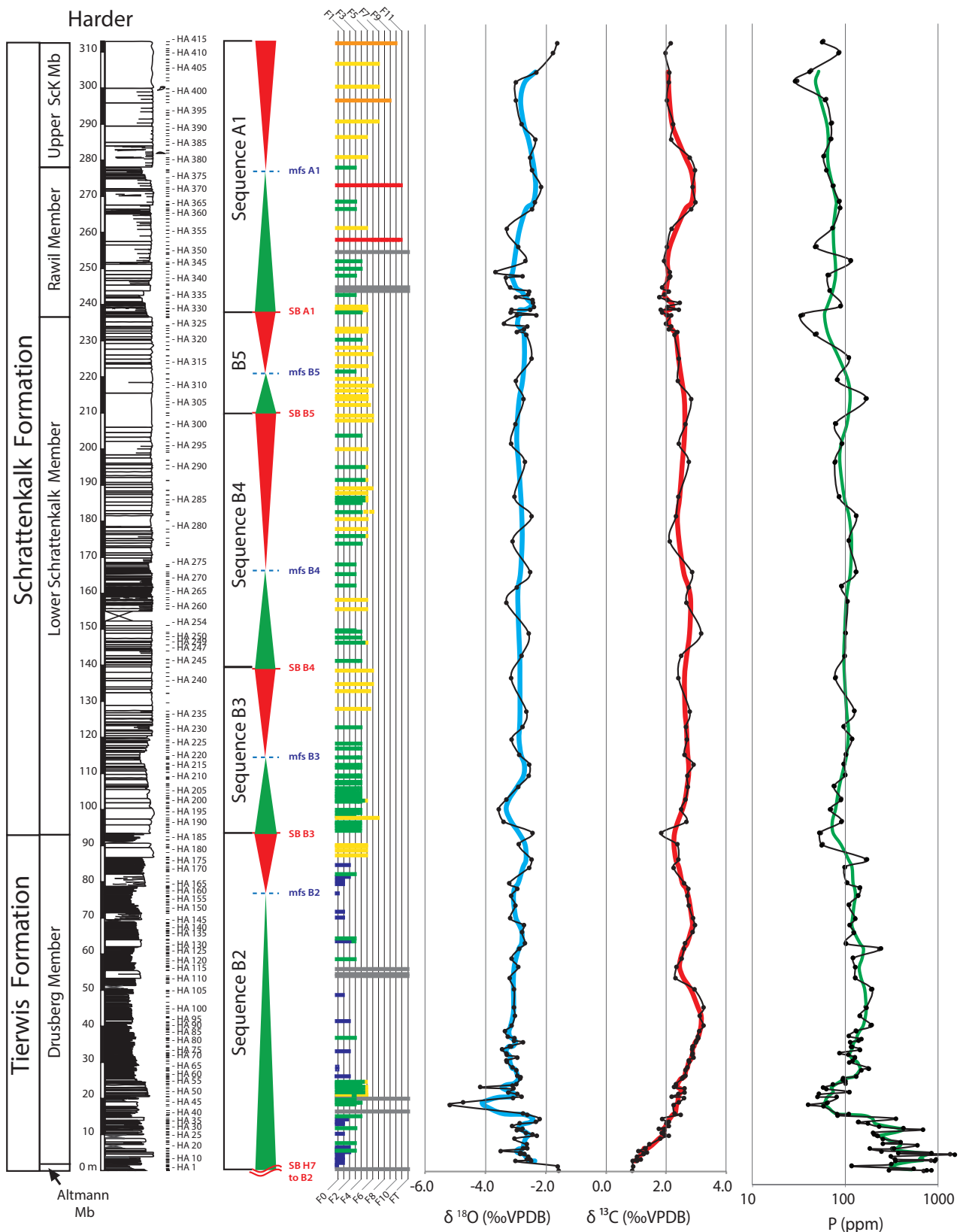


Fig. 4.10 Harder section: lithological-sedimentological log, microfacies identification, sequence-stratigraphic interpretation, isotope stratigraphy and phosphorus content. See Fig. 4.3 for the legend.

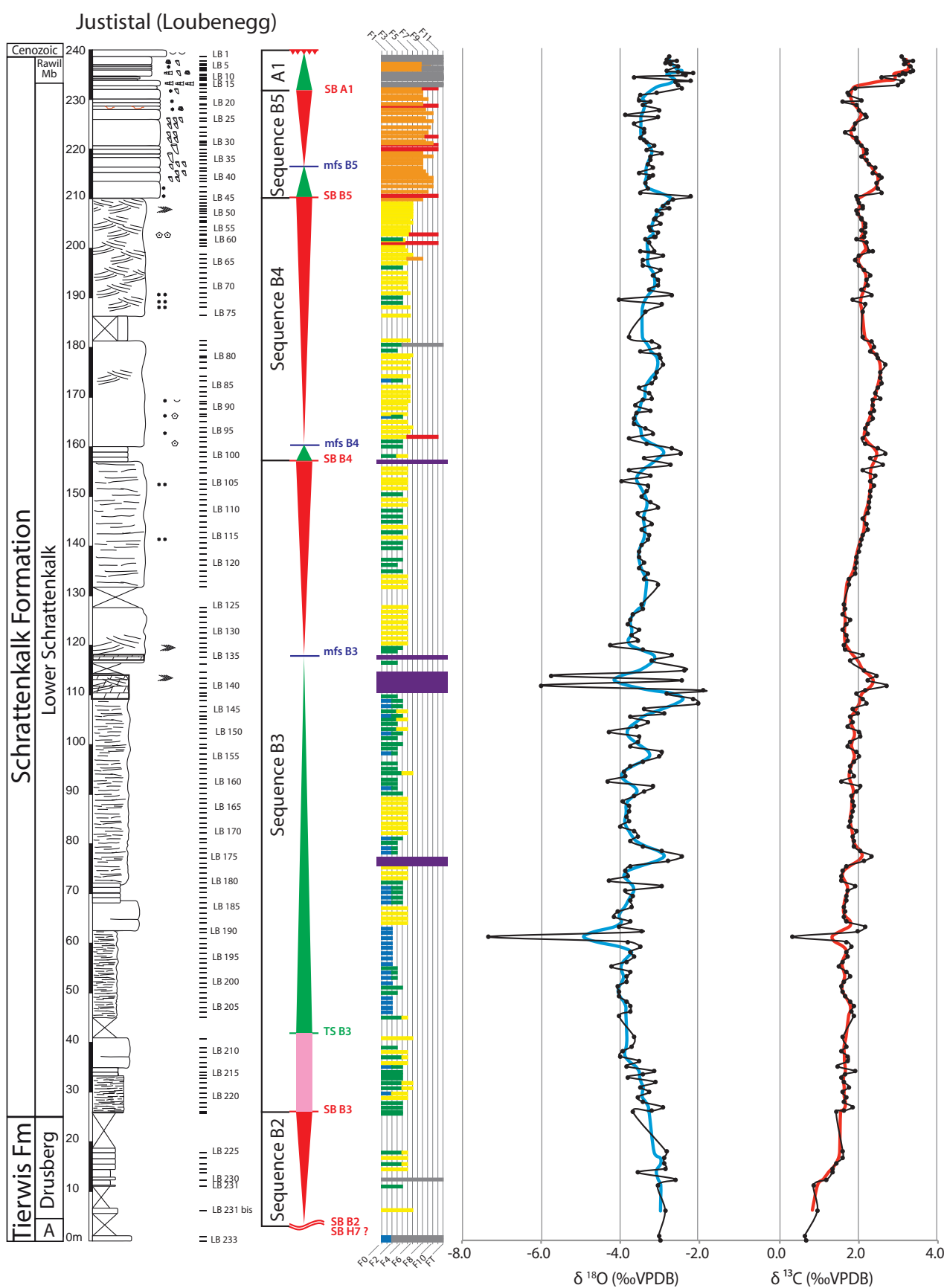


Fig. 4.11 Justistal section: lithological-sedimentological log, microfacies identification, sequence-stratigraphic interpretation and isotope stratigraphy. See Fig. 4.3 for the legend. Purple colour in the microfacies represent dolomitized sample.

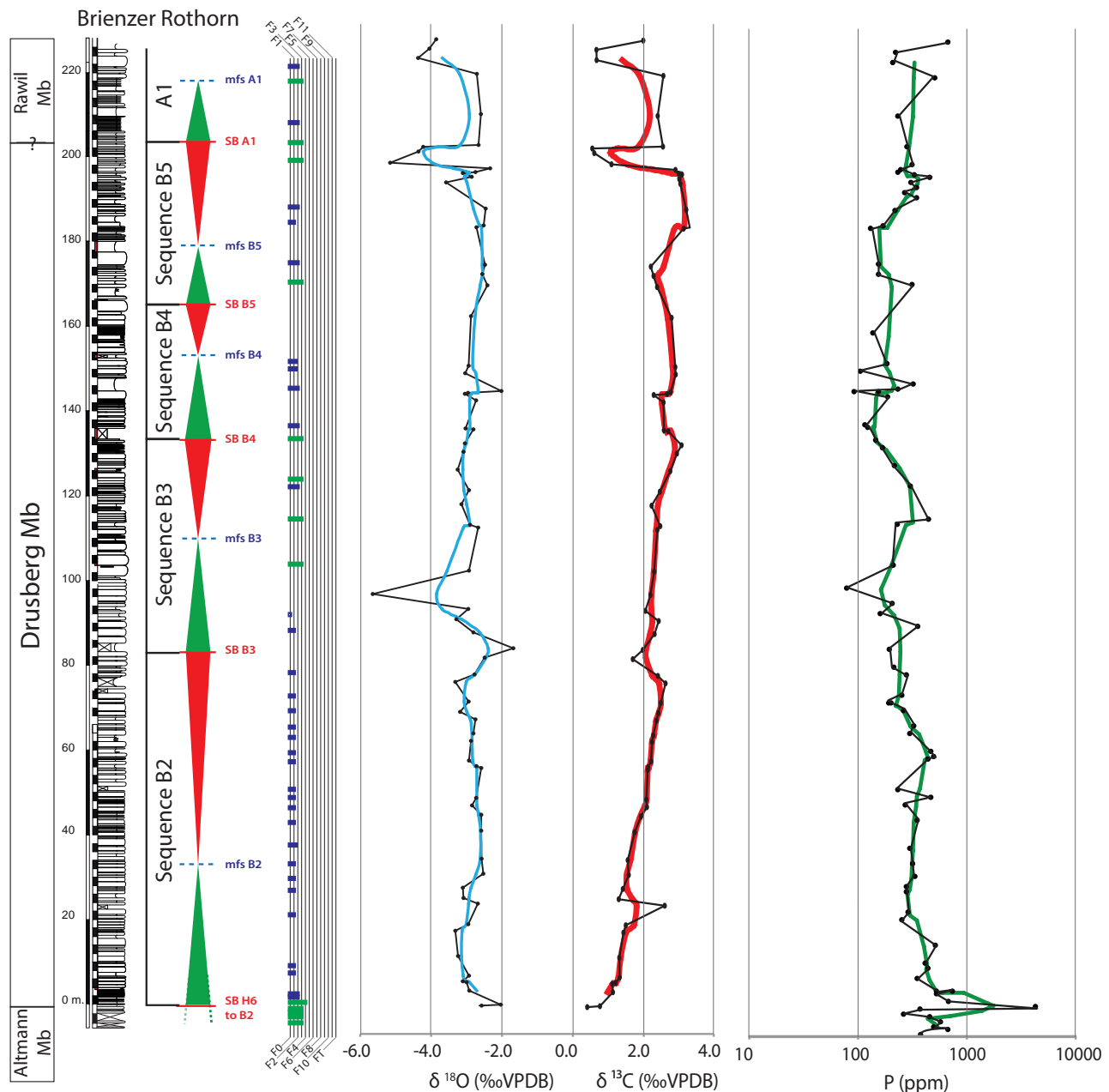


Fig. 4.12 Brienzer Rothorn section: lithological-sedimentological log, sequence-stratigraphic interpretation, microfacies identification, isotope stratigraphy and phosphorus content. The lithological log and the geochemical data are from Ribaux (2012). See Fig. 4.3 for the legend.

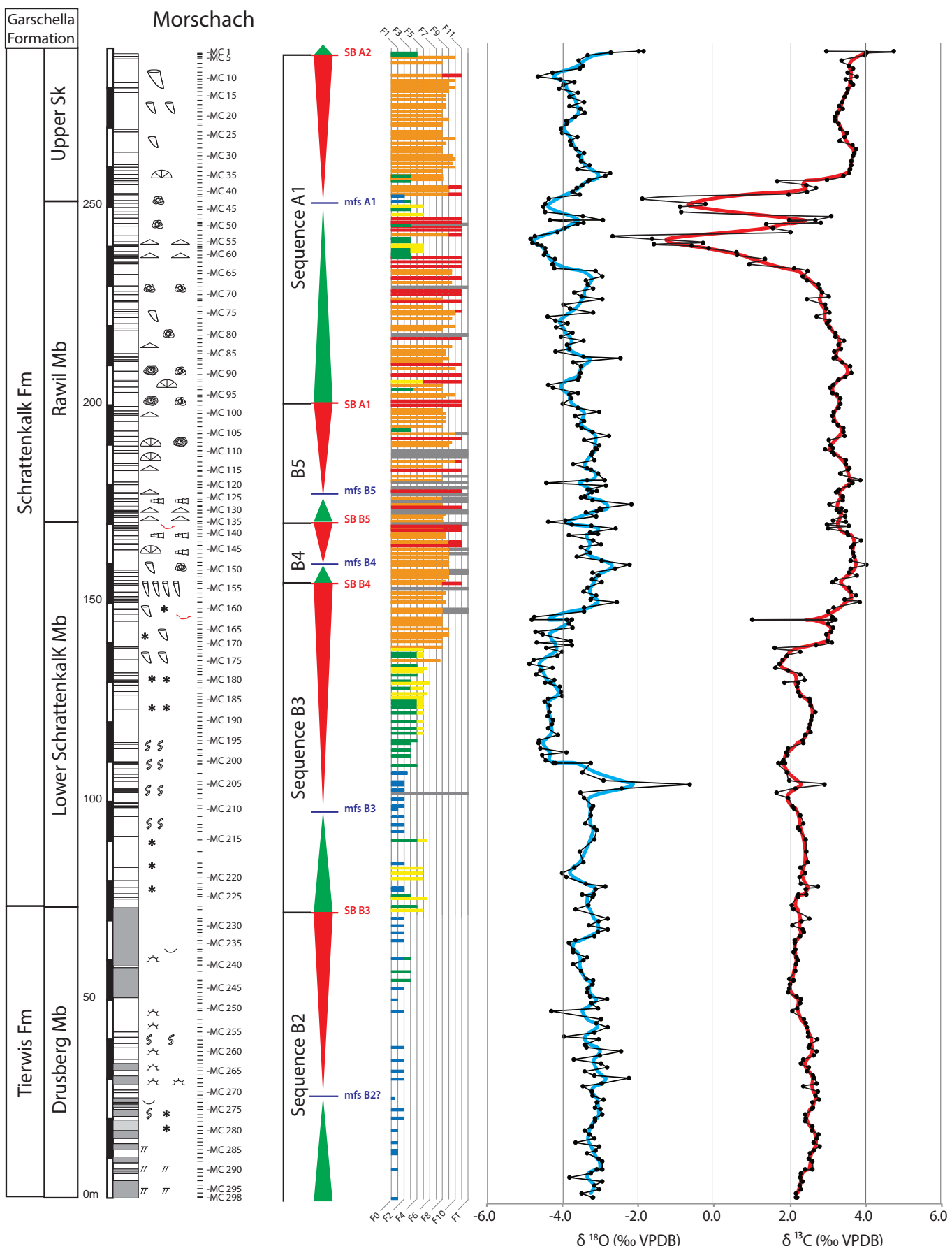


Fig. 4.13 Morschach section: lithological-sedimentological log, microfacies identification, sequence-stratigraphic interpretation and isotope stratigraphy. See Fig. 4.3 for the legend.

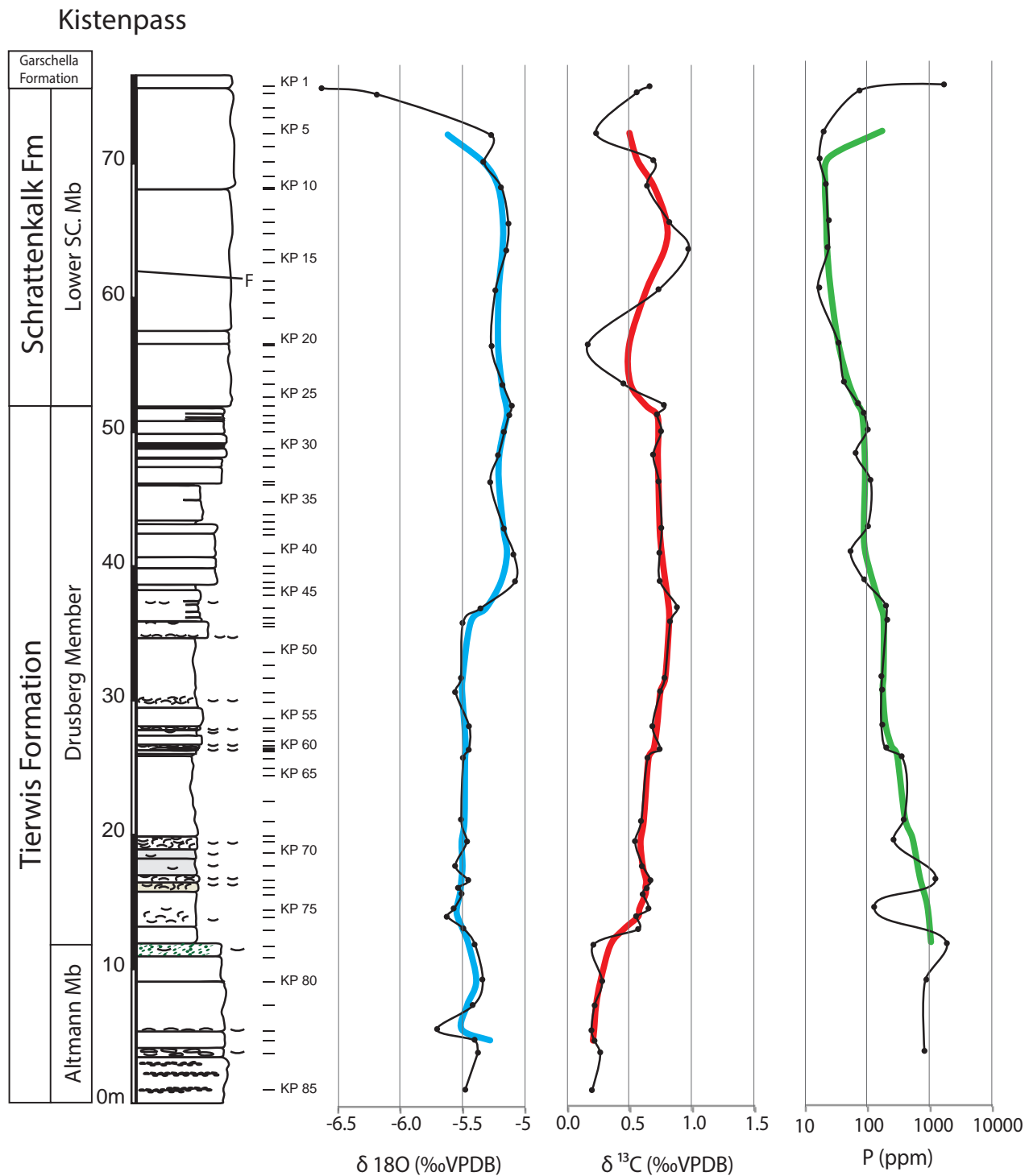


Fig. 4.14 Kistenpass section: lithological-sedimentological log, isotope stratigraphy and phosphorus content. See Fig. 4.3 for the legend.

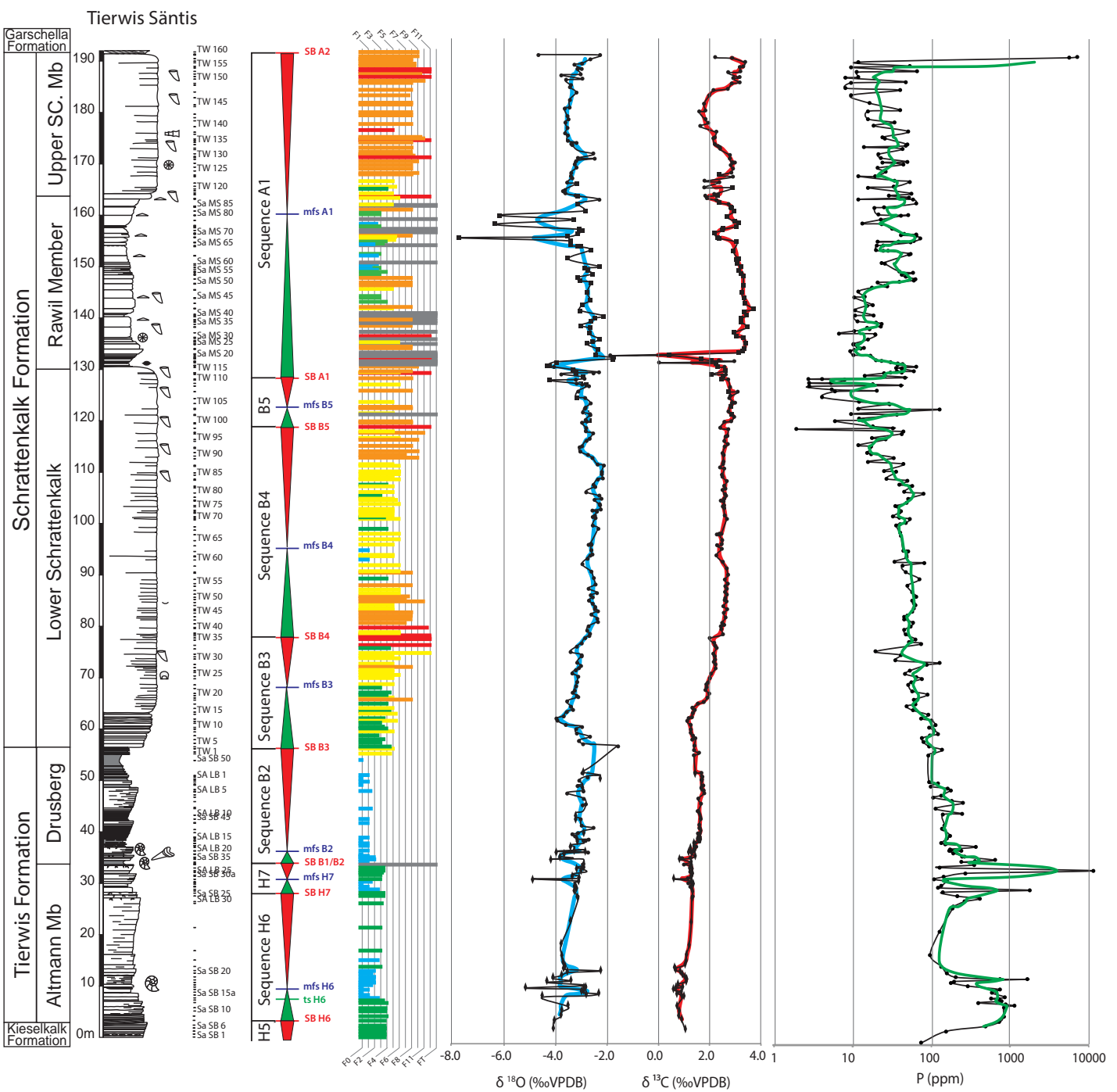


Fig. 4.15 Tierwis section: lithological-sedimentological log, microfacies identification, sequence-stratigraphic interpretation, isotope stratigraphy and phosphorus content. The carbon-isotope data (black diamonds) of the Tierwis Formation are from Godet et al. (2013); the lithological log of this interval is from Bodin et al. (2006a). The lithological log, the phosphorus data and the carbon-isotope data (black squares) of the Rawil Member are from Stein et al. (2012). See Fig. 4.3 for the legend.

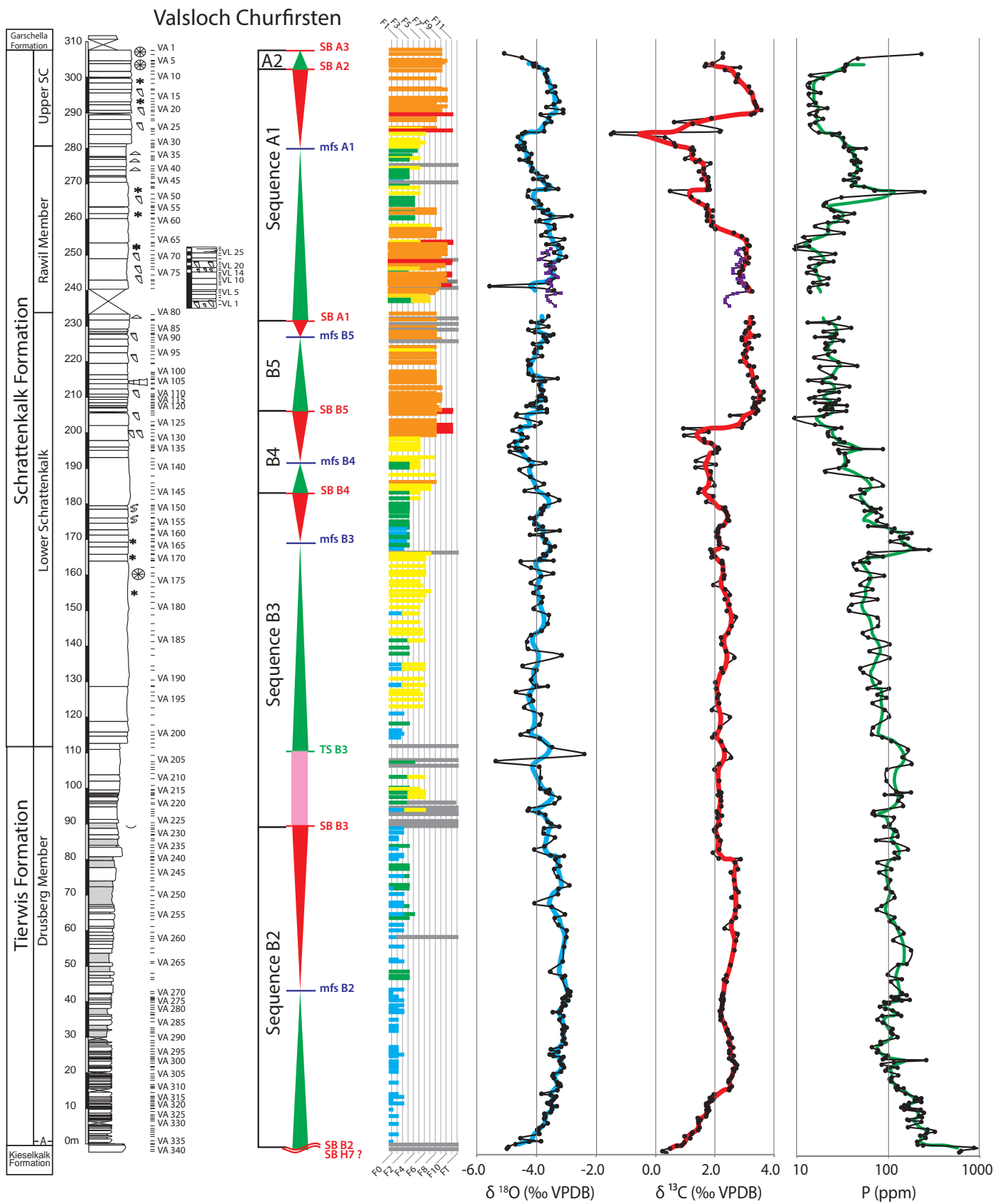


Fig. 4.16 Valsloch section: lithological-sedimentological log, microfacies identification, sequence-stratigraphic interpretation, isotope stratigraphy and phosphorus content. See Fig. 4.3 for the legend.

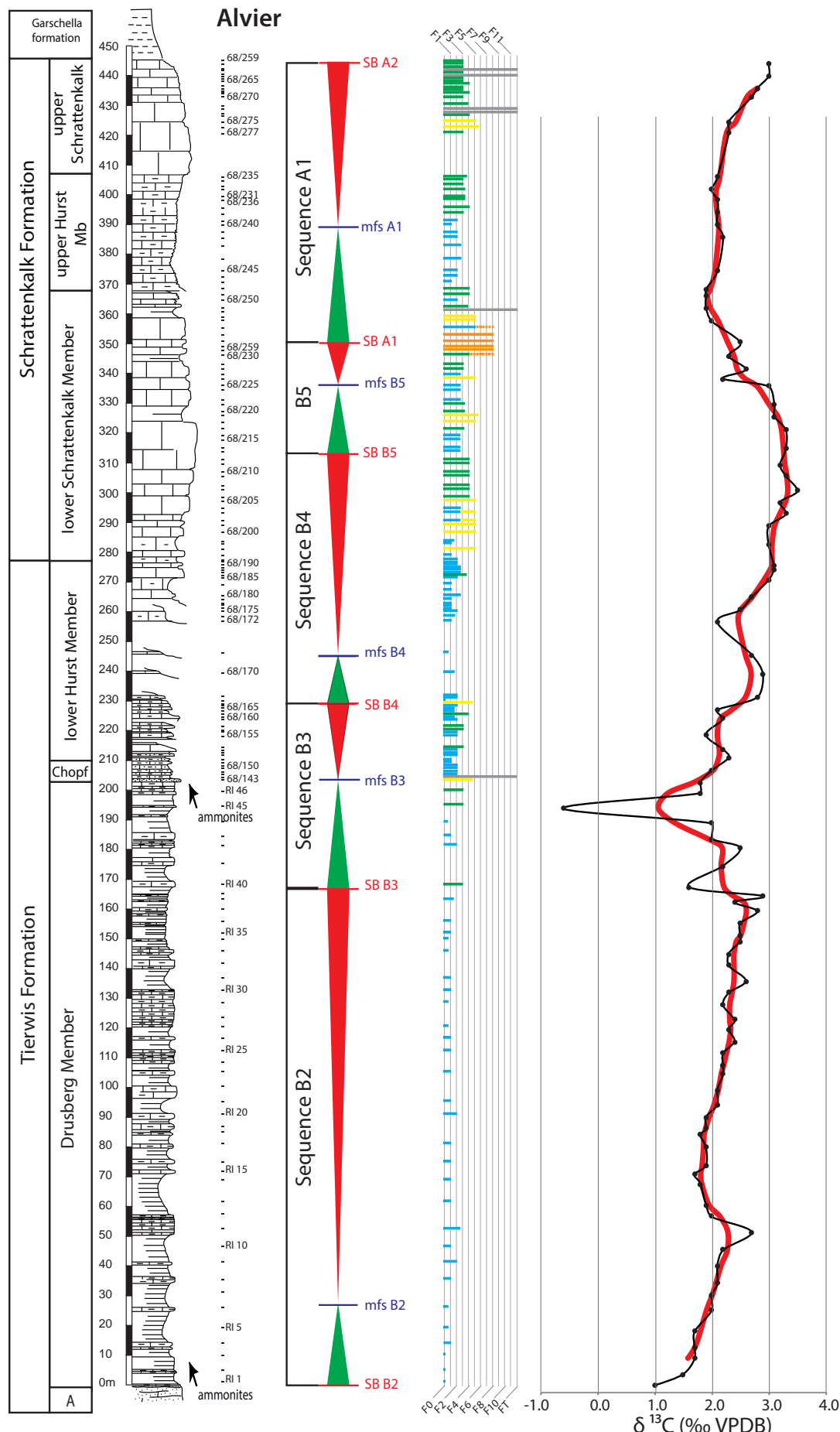


Fig. 4.17 Alvier section: lithological-sedimentological log, microfacies identification, sequence-stratigraphic interpretation and isotope stratigraphy. The sedimentological log is from Briegel (1972) and Wissler et al. (2003). The carbon-isotope data are from Wissler et al. (2003). See Fig. 4.3 for the legend.

The Rawil Mb is calcareous and is difficult to separate from the Schrattenkalk Mbs. The Upper Schrattenkalk Mb is characterized by a rudist- and coral-bearing boundstone. The contact between the Schrattenkalk and the Garschella Fms is covered.

(12) The section of Alvier (Fig. 4.5-V; Fig 4.17) is located on the eastern side of the Alvier, in the Säntis nappe. It represents the distal part of the platform. This section is a composite section sampled and studied by Briegel (1972) for the upper part, in the locality of Glaennli, and by Wissler et al. (2003) at Riseten for the lower part of the section. The section starts with the Altmann Mb, where ammonites were found by Briegel (1972) and Bodin et al. (2006a). The Drusberg Mb consists of a 270m-thick alternation of marl and limestone, interrupted at 200m by a glauconitic horizon, rich in ammonites and belemnites, which is attributed to the Chopf Bed (Briegel, 1972; Bodin et al., 2006b). The Lower Schrattenkalk Mb is characterized by the decrease in marly beds, and the increase in bioclastic limestone. The Upper Hurst Mb – a distal equivalent of the Rawil Mb - is characterized by the re-appearance of thinly-bedded alternations of marl and limestone, followed by the Upper Schrattenkalk Mb, which is more calcareous.

4.5.2 Temporal evolution: example of the Säntis nappe

For this study, we examined sections and a core in different nappes of the Helvetic thrust-and-fold belt. In this context, the Säntis nappe is of particular interest, because the sections in this nappe are stratigraphically much more complete than those in lower nappes. We used three sec-

tions in the Säntis nappe to establish a transect through the platform: (1) the proximal realm is represented by the section of Tierwis; (2) the intermediate area is embodied by the section of Valsloch and the panorama of the Churfirsten; and (3) the distal part in the direction of the outer shelf is illustrated by the Alvier section. This transect was already studied by several authors (in particular by Trümpy, 1969; Funk et al., 1979; Wissler et al., 2003; Embry, 2006; Huck et al., 2013).

The transect is shown in a chronostratigraphic representation in Figure 4.18, in order to illustrate the hiati and time gaps associated with emersions. The geological sections along this transect are interpreted in a sequence stratigraphic sense, thereby using the divisions defined by Arnaud and Arnaud-Vanneau (1989, 1991). The sections are presented including the microfacies data, which are grouped in facies assemblages (c.f. chart displaying the facies distribution in Figure 4.3). Biostratigraphy based on benthic foraminifera, sedimentological features and in particular identified sedimentary discontinuities are also shown in the figures of the sections.

During the transgressive systems tract (TST) B2, the platform is dominated by open-marine facies (F0 to F2). The variation in thickness between the inner and the most distal area is maximal during this interval. The Churfirsten panorama shows the development of a massive bioclastic body below the sequence boundary (SB) B3 (on the west side of Zuestoll; see chapter 2), which is interpreted as the highstand systems tract (HST) B2. A bioclastic microfacies type (F5, 6 or 7) is attributed to this interval, due to its massive structure and the nature of reworked grains identified in the section of Valsloch, below the SB B3. These grains consist of oolites, dasycladal algae, orbi-

tolinids, fragments of bivalves and bryozoans, and miliolids. It should be noted that in the section of Tierwis, the hemipelagic sediments are directly covered by the bioclastic sediments of the sequence B3. The area of Tierwis was likely emerged at that time. Sedimentological evidence of this emersion is described in chapter 2.

Sequence B3 starts on top of the SB B3 by the deposition of a lowstand systems tract (LST) B3 in intermediate and distal parts of the shelf. In Valsloch, the LST B3 is characterized by intense reworking and by the deposition of bioclastic facies (F5, F6 and F7). In the Churfirsten panorama, the SB B3 represents the base of the massive cliff on the eastern side, and the LST B3 shows a maximum in progradation (see chapter 2). In the section of Alvier, the LST B3 is characterized by the occurrence of outer-shelf facies F3 and F4. The following systems tract is the transgressive systems tract (TST) B3, which is extremely thick and bioclastic in Valsloch. The facies in TST B3 of this section is shallowing upward, with the development of patch reefs. Most sediment deposited in sequence B3 corresponds to the aggrading TST B3 in Valsloch. A similar sediment distribution was observed on the Upper Tortonian – Lower Messinian Llucmajor carbonate platform (Mallorca) studied by Pomar (1991; 1993); Pomar and Ward (1994; 1995; 1999) and Pomar and Kendall (2007).

A deepening phase occurred in the last meters of TST B3 in Valsloch with the accumulation of annelids, algae and flat orbitolinids (*Palorbitolina/Eopalorbitolina transiens*). In the inner part of the platform, the TST B3 onlaps onto the erosional surface of SB B3. The interval recording the highest sea level is characterized by facies F3 and F4 in a landward direction, and by a condensed level in a distal direction, on the platform margin (Chopf Mb). The mfs B3 is placed in this interval. The HST B3 starts

with bioclastic facies in Tierwis and Valsloch, followed by the installation of lagoonal facies, which arrives earlier on the inner platform at Tierwis than at Valsloch. The maximum of progradation of the HST B3 is shown by the presence of reworked bioclasts in the section of Alvier.

The SB B4 is associated with an erosional surface in the inner part of the platform, where dissolution and the formation of epikarst occurred below and at this surface. The sequence B4 is dominated by outer-shelf bioclastic facies. Development of lagoonal (Urgonian) facies is limited to the base and the top of the sequence. The TST B4 shows the backstepping of lagoonal and bioclastic facies. In the section of Alvier, outer platform facies (F3 and F4) is replaced by open-marine facies (F0, F1, F2). The depocenter was located in the inner part of the platform (Tierwis) and characterized by bioclastic accumulation. The HST B4 is shallowing upward on the inner and intermediate platform. The upper meters show the development of confined conditions and supratidal facies is widespread, both in Tierwis as well as in Valsloch, culminating in the widely developed exposure surface SB B5. The sequence B4 was less prograding than the previous one. In the distal part of the platform the shallowest facies, which reached the top of this sequence is outer-platform facies (F3 and F4).

Sequence B5 is characterized by the wide development of lagoonal facies. The TST is represented by aggradational parasequences covered by bioclastic and orbitolinid-rich facies, which represent the mfs B5. The HST is highly prograding, and some reworked lagoonal facies was recognized in the distal section of Alvier.

The TST of the sequence A1, which composes the Rawil Mb, is characterized by an increase in clay input. The base of the TST is still

rich in lagoonal facies, but important backstepping of shallow-water facies occurred. A thick atypical interval of outer-shelf facies (F3, F4) and transgressive facies (FT) mixed with dasycladal limestone and *Palorbitolina lenticularis*-rich facies is developed in Tierwis and Valsloch, and is laterally replaced by open-marine facies (F1, F2) at Alvier. The mfs A1 is placed in the upper part of this interval. The HST A1 marks a return to normal carbonate sedimentation on the shelf, with the development of lagoonal facies and rudist environments. Progradation is less important than in sequence B5 and the upper part of HST A1 in Alvier consists of outer-shelf facies (F3, F4). The terminal surface is an exposure surface, which shows intense karstification.

4.5.3 Spatial and temporal evolution: paleogeographic distribution of facies and thickness variation of sediment on the Helvetic margin

In chapter 2, three main spatial domains have been identified in the evolution of the Helvetic platform: the proximal area, which is the inner part of the platform, represented by the sections of Kistenpass, Tierwis and L'Ecuelle; the intermediate part, which is located close to the platform margin, with the sections of Justistal, Harder, Morschach and Valsloch; and the distal, outer part of the platform, with the sections of Brienz Rothorn and Alvier. This third domain gives us indications on the location of the platform margin. The geological map displays the position of the outer shelf with the disappearance of the Schrattenkalk Fm. In the southern part of the Wildhorn nappe (Prabé synclinal; Crête Besse–Chamosaire–Bella Lui area; Badoux et

al., 1959), the series is only represented by pelagic and hemipelagic sediments of the Drusberg Mb. This is also the case south of the Lake of Thun, in the southeastern part of Lungerersee and in the southern part of the Engelberg valley (Hankte, 1961). In the eastern part of the Säntis nappe, the outer shelf is defined as a “muddy shelf” (Bollinger, 1988), and is illustrated by the isopach maps of the Schrattenkalk Fm and the Drusberg Mb by Zerlauth et al. (2014).

The sequence stratigraphic divisions are grouped into seven units, which are each well defined at their bottom and top. To illustrate the distribution of the facies for each sequence, pie charts have been calculated for each section and placed on the palinspastic map.

4.5.3.1 Sequences H6 to B1 (Altmann Mb)

Facies distribution

The sediments of this unit were deposited from the late Hauterivian to the late early Barremian (Bodin et al., 2006a) and constitute the Altmann Mb. The age of these deposits is based on the recognition of ammonites, which indicate the time span between the *B. balearis* zone and the lower boundary of the *C. darsi* zone (Fichter, 1934; Rick, 1985; Wyssling, 1986; Bodin et al., 2006a). This unit is a condensed level rich in phosphatic particles and glauconite. It can be subdivided into three sequences – H6, H7 and B1 – in the more complete sections. This unit usually starts and ends with hardgrounds. The lower one is deposited above the Hauterivian Kieselkalk Fm, and the upper one is overlain by

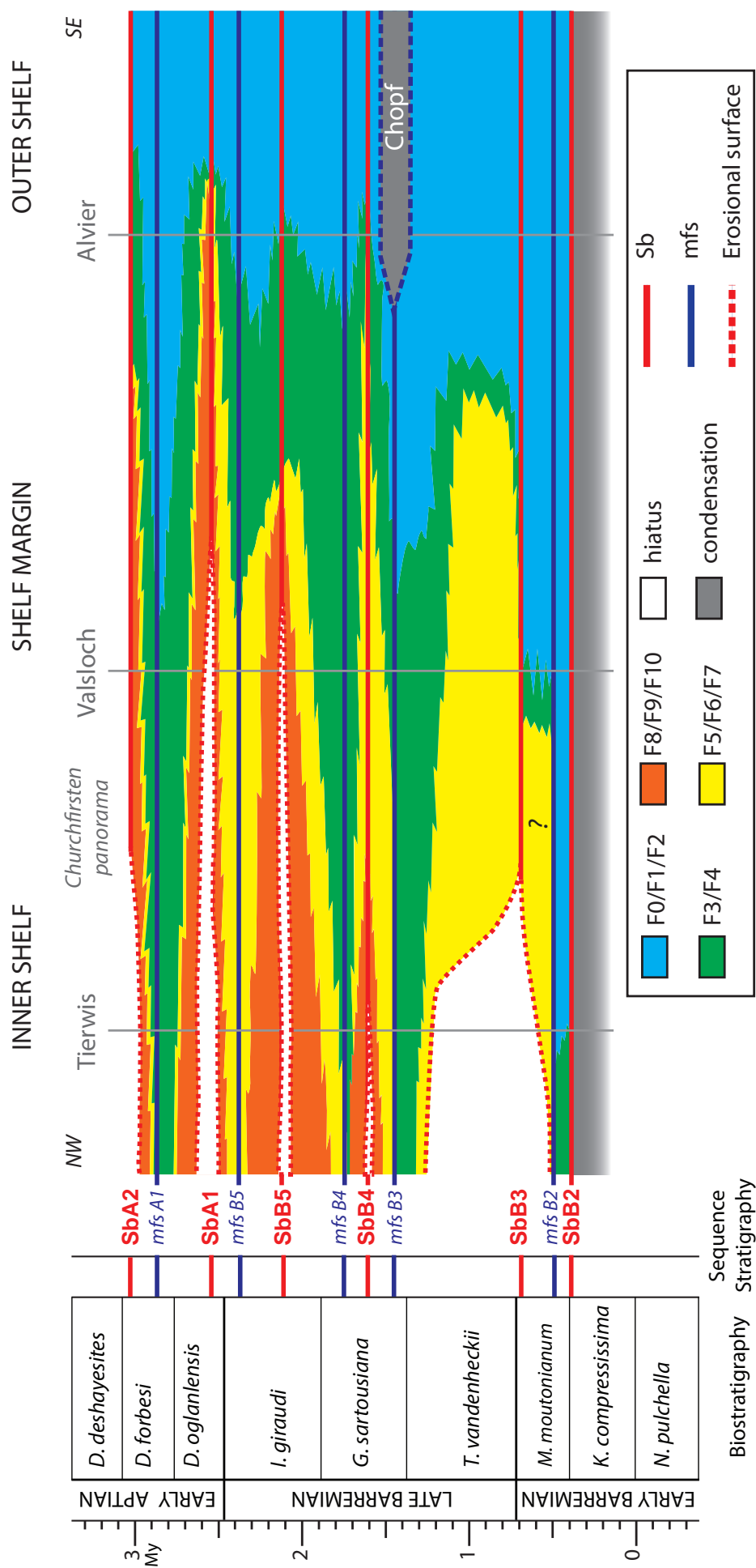


Fig. 4.18 Chronostratigraphic cross-section through the Säntis Nappe, calibrated by the biostratigraphic chart of Reboulet et al. (2011). This figure shows the temporal evolution of facies on the platform. The section of Tiervis represents the internal part of the platform, Valsloch is located on the edge of the platform margin and Alvier is in a distal position.

marl. Figure 4.19-A illustrates the thickness of this unit in the studied sections. The Altmann Mb is extremely thin in the sections of Justistal, Harder and Lämmerenplatten (less than 1m), in Valsloch, Brienzer Rothorn and Alvier it reaches approximately 4m and in the sections of L'Ecuelle and Kistenpass the Altmann Mb is more developed (8m and 10m, respectively). The section of Tierwis, studied in detail by Funk (1969, 1971) and Bodin et al. (2006), is more than 31m thick. In the field, this unit is characterized by a massive coarse granular limestone with a light grey colour, in comparison to the darkish underlying Kieselkalk Fm, and the overlying marly–limestone alternations of the Drusberg Mb. In the sections of L'Ecuelle and Kistenpass, the facies is a packstone rich in bryozoans, annelids and crinoids, with abundant glauconite and quartz (F4/FT).

4.5.3.2 Sequence B2 (Drusberg Mb)

Facies distribution

The second unit is the Drusberg Mb, which is attributed to sequence B2, described in chapter 2. This unit is characterized by the alternation of marl and marly limestone, and by oyster accumulations in proximal sections (Kistenpass). Sequence B2 is dominated by outer-shelf facies (F0, F1, F2 and F3) in the entire area (Fig. 4.19-B). The Drusberg Mb in the sections of Justistal and Harder include important intervals composed of bioclastic outer-platform facies (F4, F5 and F6) and reworked facies (FT). These intervals represent approximately 20% and 15% of the total Drusberg Mb for Harder and Justistal, respectively. The maximum thickness

of this member is observed in intermediate and external parts of the platform, and maximum accommodation occurred in the section of Alvier, where the thickness of the unit reaches 120m. The sediment-accumulation rate is minimal for sections located on the inner platform (Tierwis and Kistenpass). This unit ends in proximal area by an emersion surface, and in intermediate sections by the occurrence of reworked grains coming from more proximal environments.

Micropaleontological markers

In the hemipelagic sediments of sequence B2, the biostratigraphic markers are ammonites and circalittoral foraminifera (*Lenticulina*). In bioclastic beds, this unit is characterized by the presence of *Paleodictyoconus* sp., *Cribellopsis elongata*, *Falsurgonina* sp. and *Paracoskinolina sunnilandensis* (Fig. 4.20).

4.5.3.3 Sequence B3 (Lower Schrattenkalk Mb – lower part)

Facies distribution

Sequence B3 has been previously described in chapter 2. Here we treat variations in facies and thickness from proximal to distal regions. The special feature of this sequence is that it starts on top of the hemipelagic sediments of the Drusberg Mb with the influx of bioclastic grains derived from the shallow-water environment.

The thickness of the sequence varies, but the innermost sections are mostly thinner, with 20m at Kistenpass and in Tierwis. The maximum in thickness is observed in the intermediate

area (Fig. 4.19-C), in the sections of Justistal (130m), Valsloch (95m) and Morschach (80m). Sequence B3 reaches a maximum thickness where it is possible to recognize a LST showing characteristic progradation (Justistal, Valsloch) (see chapter 2).

All sections show outer-platform bioclastic facies (F3, F4) near the maximum water-depth (mfs). Bioclastic outer-platform facies (F5, F6) is, however, also well present in the LST of Justistal and Valsloch, but also at Harder (in the continuity of Justistal?). The same facies type is also observed in smaller proportions at Tierwis, Morschach and L'Ecuelle. The section of Kistenpass is dominated by lagoonal facies (F8, F10) and supratidal facies (F11), which are also observed at L'Ecuelle, Morschach and Valsloch. Sequence B3 is thinner in the distal domain, in the sections of Alvier and Brienzer Rothorn (around 60m thick) and characterized by outer-shelf facies (F0 to F3). The top of sequence B3 (SB B4) is marked in the inner and intermediate platform by an emersion surface and palaeosol, and in distal parts by the maximum abundance of grains reworked from the platform.

Micropaleontological markers

This unit is characterized by the presence of *Praedictyorbitolina carthusiana*, *Paleodictyoconus actinostoma*, *Paleodictyoconus cuvillieri*, *Eopalorbitolina/Palorbitolina transiens*, *Orbitolinopsis debelmasi*, *Falsurgonina* sp., *Montseciella* sp., and *Paracoskinolina sunnilandensis*, and the first occurrence of *Paracoskinolina reicheli*, and *Neotrocholina friburgensis* (Fig. 4.20).

4.5.3.4 Sequence B4 (Lower Schrat-tenkalk Mb – middle part)

Facies distribution

In the proximal area, TST B4 starts with lagoonal facies, which is rich in rudists (F8, F9), and becomes gradually more external, with the occurrence of oolitic and bioclastic facies up to the mfs. In the sections of L'Ecuelle and Morschach, the facies is extremely confined, with oncolites and *Bacinella* nodules (F10), intercalated in supratidal facies (F11), until the mfs. For the section of L'Ecuelle, this mfs is characterized in the field by a yellowish interval and in thin section by an increase in silt input. In the section of Morschach, the presence of more external lagoonal facies (F8) including some glauconite grains characterizes the mfs. In the section of Tierwis, the mfs is marked by the presence of radiolaria and sponge spicules.

In the intermediate area, in the sections of Valsloch, Justistal and Harder, TST B4 is characterized by a reduced thickness and consists mainly of bioclastic (F5) and outer-platform facies (F4). The sections of the distal realm are composed of open-marine facies (F2, F3) and the mfs is marked by the increase in marly beds.

HST B4 is characterized in the proximal part by an overall increase toward the top in confinement, which goes along with evidence for emersion, and which is associated with the deposition of supratidal facies and the development of early dissolution features. In the intermediate part of the platform, an evolution is observed in HST B4 from outer-platform facies (F3, F4) at the base to a lagoonal (F8, F9) and supratidal environment to the top. The sections

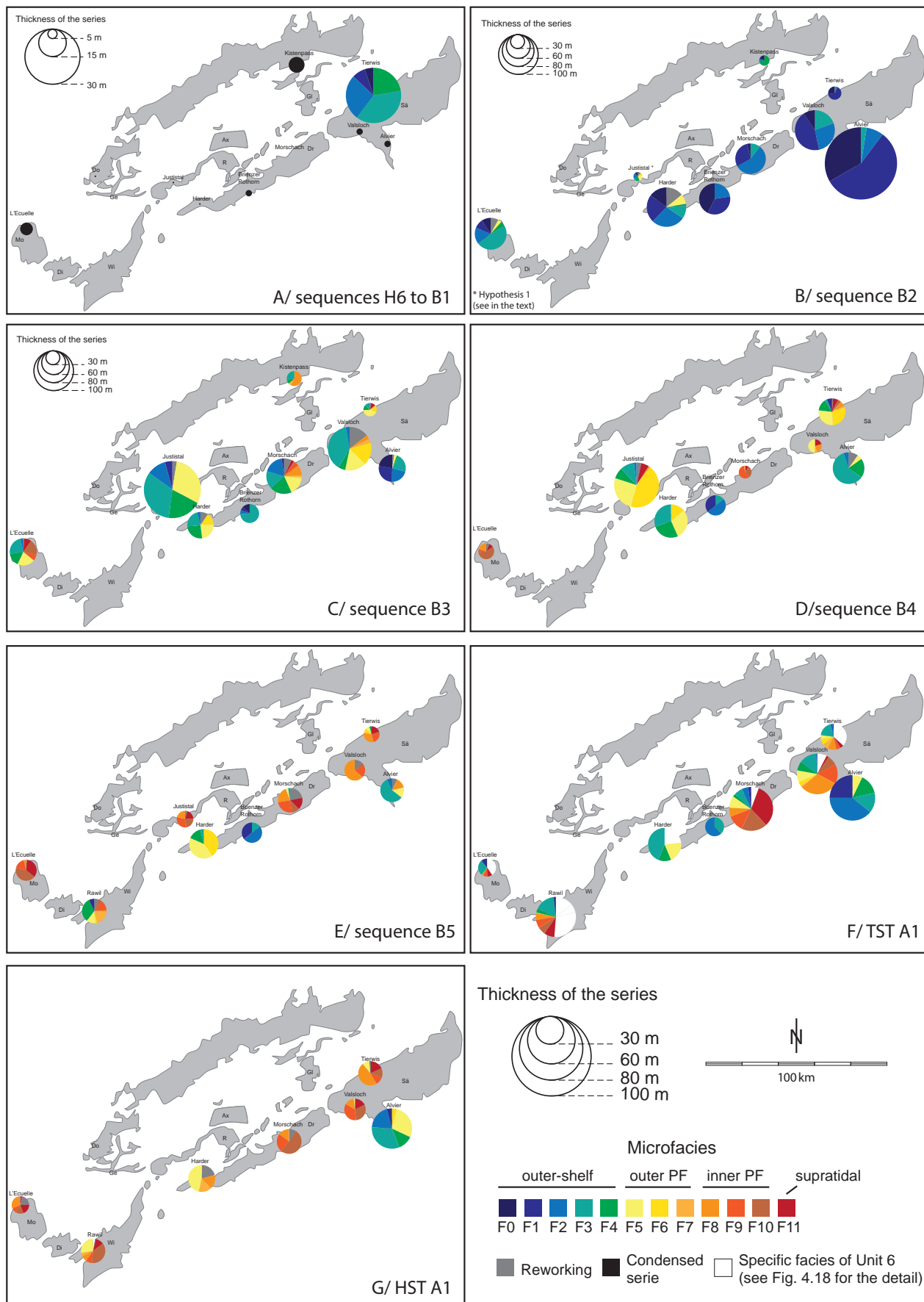


Fig. 4.19 Spatial distribution of the microfacies for the Altmann Mb to the Upper Schrattenkalk Mb. The size of each pie chart is related to the thickness of the unit. Each analyzed site is plotted on the palinspastic map of the nappes established by Trümpy (1969), Ferrazzini and Schuler (1979), and Kempf and Pfiffner (2004).

of Justistal and Harder are peculiar in this sense with the dominance of oolitic parasequences for Justistal, and intense grain reworking for Harder, where outer-platform facies occurs. In the distal part, sections exhibit pelagic and hemipelagic facies, which reaches facies F4 and F5 at the top of B4 at Alvier (Fig. 19-D).

Micropaleontological markers

Sequence B4 has not a proper faunal assemblage. It is characterized by the presence of *Neotrocholina friburgensis*, *Paleodictyoconus cuvillieri*, *Cribellopsis neelongata*, and *Parakoskinolina maynci*, like the sequences B3 and B5 (Fig. 4.20).

4.5.3.5 Sequence B5 (Lower Schrattenkalk Mb – upper part)

Facies distribution

In the proximal domain, SB B5 is marked by early dissolution, and TST B5 starts with supratidal facies, consisting of beach deposits with keystone vugs and palaeosols (root molds, green marl, pedogenic cements). The TST evolves from a restricted to outer lagoonal facies (F10, F8). The mfs is characterized by the occurrence of *Chondrodontes*, stromatoporoids and glauconite grains, which are the markers of an open-marine environment. In the intermediate part of the shelf, SB B5 is marked by superficial karstification. TST B5 begins with supratidal facies including beach deposits. In the section of Morschach, the TST starts with several levels of *Palorbitolina lenticularis* accumulations, which

are interpreted as beach deposits. TST B5 continues with outer lagoonal facies (F8), followed by outer platform facies (F5, F6 and F7). This is also the case for the section of Justistal, where lagoonal facies appears for the first time. The mfs is marked by deeper facies. In the section of Rawil, the mfs is characterized by outer-shelf facies, rich in planktonic echinoderms, calcispheres and radiolaria (F1). In the sections of Valsloch and Morschach, mfs B5 is marked by detrital input and the presence of flat *Palorbitolina*. In the section of Justistal, the mfs shows the presence of *Lithocodium* nodules without *Bacinella*. Presence of *Lithocodium* alone is an indication of more open-marine environments (Arnaud-Vanneau, 1980).

The section of Harder is particular. The SB B5 is marked by intense dolomitization. The following TST B5 is characterized by granular facies rich in reworked grains and oolites (F5, F6). The abundance of reworked grains in outer-shelf facies (F2, F3 and F4) indicates the mfs. In the distal area, facies forming TST B5 is characteristic of the outer shelf (F1, F2, F3). In the section of Alvier, some bioclasts are present in the matrix. Annelids are abundant. The mfs is indicated by a marly level.

HST B5 is characterized by restricted lagoonal to supratidal facies (F9, F10 and F11) in proximal and intermediate areas (Fig. 4.19-E). Oncolites and *Bacinella* nodules are abundant, and karst features overprint the facies in the upper part of the HST. In the section of Harder, a bioclastic facies (F5 and F6) forms the HST. In the section of Alvier, reworked rudist shells are recorded in the uppermost part of HST B5. The top of this unit is marked by a major emersion surface, associated with superficial karst, which is observed until 15 m below this surface (see chapter 3).

Micropaleontological markers

This unit is characterized by the last occurrence of *Neotrocholina friburgensis*, and by the presence of *Palorbitolina lenticularis*, *Orbitolinopsis buccifer*, *Paracoskinolina maynci*, and *Paracoskinolina cf. hispanica* (Fig. 4.20).

4.5.3.6 TST A1 (Rawil Mb)

Facies distribution

The following unit consists of the Rawil Mb, the equivalent of the Lower Orbitolina Beds. The microfacies succession is described in detail in chapter 3. This interval resulted from important transgression. The base of this unit is characterized by numerous decametric parasequences composed of inner lagoonal facies, which end with palaeosols. The first parasequences may contain *Charophyta* remains. The presence of *Charophyta* at the base of sequence A1 is observed from the Vercors Massif (French subalpine chains) to the Helvetic Alps. This shallow-water facies is progressively replaced by a microfacies characteristic of sea-grass environments, with a dominance of green algae (dasycladal algae), the massive accumulation of agglutinated *Palorbitolina lenticularis* and *Chofatella*, and the increase in quartz input, which led to the deposition of siltstone/sandstone beds. Figure 4.18 shows that this specific microfacies is mainly distributed on the proximal platform. The same facies is rare (less than 10%) in the intermediate sections of Morschach and Valsloch, and is missing on the outer platform (Alvier and Brienzer Rothorn). This unit ends with a marly

limestone rich in *Palorbitolina lenticularis*. This facies is close to facies F3 and is directly covered by massive limestones of the following unit, the Upper Schrattenkalk Mb.

The facies distribution and the thickness of the Rawil Mb are shown in figures 4.19-F and 4.21. The sediment thickness is minimal in the inner part of the platform (respectively 22 m and 32 m for the sections of L'Ecuelle and Tierwis) and in the section of Justistal, where only the first 6.5 m are recorded. In intermediate and distal parts, this unit has a comparable thickness, comprised between 40 m and 50 m.

Micropaleontological markers

This unit is characterized by the large abundance of *Palorbitolina lenticularis*, *Palorbitolina lenticularis lenticularis*, *Orbitolinopsis cuvillieri*, *Orbitolinopsis buccifer*, and *Paracoskinolina maynci*. The first occurrence of *Orbitolinopsis pygmaea* is observed in this unit (Fig. 4.20).

4.5.3.7 HST A1 (Upper Schrattenkalk Mb)

Facies distribution

The following unit corresponds to the Upper Schrattenkalk Mb, which is described in detail in chapter 3. This unit has more or less the same thickness: approximately 20 m at L'Ecuelle and 33 m at Rawil on the inner platform. The maximum thickness occurs in the outer shelf at Alvier (about 50 m). In this section, the maximum abundance of *Orbitolina* is observed in the last 5m and it is not excluded that this intervals

already belongs to the Grünten Mb. The facies distribution in the Upper Schrattenkalk Mb shows the development of inner lagoonal facies (F8 to F10) on the whole platform and supratidal facies represents at least 10% in the sections of Tierwis, Valsloch, Rawil and L'Ecuelle (Fig. 4.19-G). The two sections of Alvier and Harder display a different type of facies. At Alvier, more than 20% is occupied by granular facies (F5) showing evidence for maximal progradation of the carbonate platform. At Harder, the unit starts with bioclastic and oolitic facies, and finishes with lagoonal facies (20%), which again is indicative of the progradation of the carbonate

platform.

The top surface is eroded and deeply karstified. The terminal karst extends several meters below SB A2, with the maximum thickness in the intermediate part of the platform. It reaches up to 26 m in the section of Harder, around 20m in the sections of Valsloch, Morschach and L'Ecuelle, and 15 m in Tierwis. The section of Rawil is affected by intense karstification to a depth of 90 m, which shows polyphase fillings (see chapter 3). The oldest infills are sediments derived from the Grünten Mb.

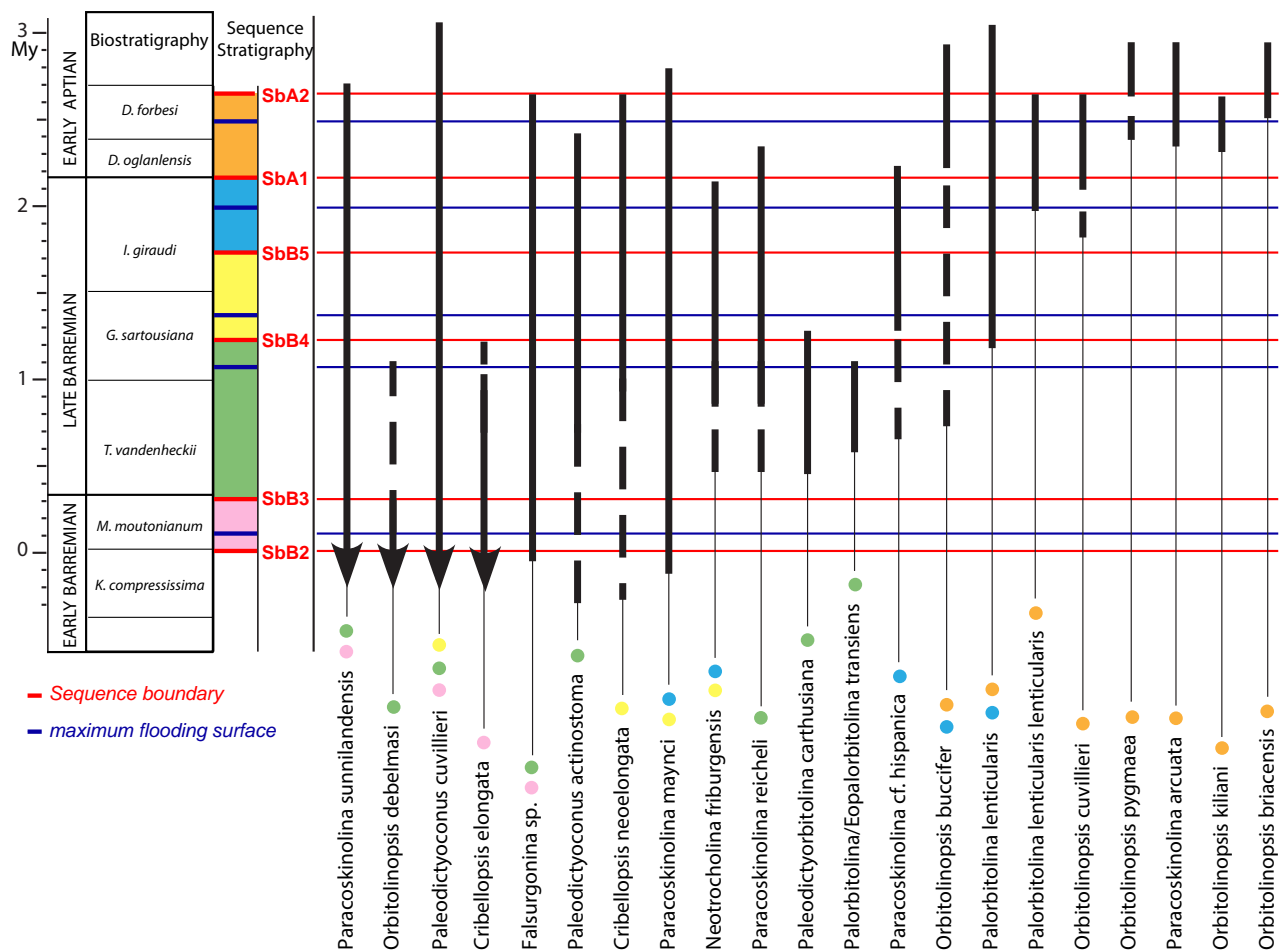


Fig. 4.20 Stratigraphic distribution of benthic foraminifera, especially Orbitolinids and Neotricholina friburgensis in the Helvetic nappes (modified after the one elaborated for the subalpine chaines by Arnaud et al., 1998). The colored markers correspond to the sequence in which these species are characteristic: pink marker for the B2 sequence; green marker for the B3 sequence; yellow marker for the B4 sequence; blue marker for the B5 sequence and orange marker for the A1 sequence. Biostratigraphy from Reboulet et al. (2011). Foraminifera are illustrated in the Plates 4.1 to 4.6.

Micropaleontological markers

The Upper Schrattenkalk Mb is characterized by the presence of *Orbitolinopsis briacensis* and *Paracoskinolina arcuata*, and by abundant *Orbitolinopsis pygmaea* (Fig. 4.20).

4.6 Geochemistry data

4.6.1 Total phosphorus content

The phosphorus (P) content has been measured in the sections of L'Ecuelle, Interlaken, Harder, Brienzer Rothorn, Tierwis, Valsloch and Harder (see Figures 4.6, 4.9; 4.10, 4.12, 4.15, 4.16 and 4.17, respectively). For all sections, the P content shows an upward decreasing trend. The highest values are recorded in the Altmann Mb and the first meters of the Drusberg Mb with values ranging between 500 ppm and 1000 ppm and maximum values of 11 700 ppm reached in the upper Altmann Mb hardground of Tierwis. Sequence B2 is characterized by a relatively high P content: above 100 ppm for the sections of Tierwis, Valsloch, Harder and Brienzer Rothorn, and above 50 ppm for L'Ecuelle (mean value 128 ppm). Sequence B3 is marked by a decrease in P content in all sections, with a mean value of 78, 44, 91, 87 and 121 ppm for the sections of Tierwis, L'Ecuelle, Valsloch, Harder and Brienzer Rothorn, respectively. An enrichment is observed in the interval showing the accumulation of *Eopalorbitolina transiens*, *Choffatella* and annelids at L'Ecuelle and Valsloch. Sequences B4 and B5 show a slight decrease in P values, with minimum values in the

upper part of HST B5 (4, 12, 10, 33 and 81 ppm for the sections of Tierwis, L'Ecuelle, Valsloch, Harder and Brienzer Rothorn, respectively. TST A1, forming the Rawil Mb, is characterized by an increase in P content (Stein et al., 2012a). In the sections of Tierwis, L'Ecuelle and Harder, this increase occurs directly above SB A1. In Valsloch, the P content exhibits higher values in the upper part of the TST and in the mfs interval. The values decrease in HST A1 until the last meters, where the P content reach higher values due to impregnations by the superjacent Garschella Fm.

4.6.2 Carbon isotope composition

4.6.2.1 Individual hand-specimen subsamples

The $\delta^{13}\text{C}$ and $\delta^{18}\text{O}$ values of the micro-drilled subsamples are presented in Table 4.1 and compared to the values obtained for the whole-rock powder of the same hand-specimens.

For most samples, the values obtained for the micro-drilled micrite and whole-rock powder differ less than 0.2‰ for $\delta^{13}\text{C}$ and 0.3‰ for $\delta^{18}\text{O}$. In some hand-specimens (samples EC 166, MC 137 and KP 61) the different subsamples (rudist, oncrite, oyster, recrystallized bioclasts, cement) differ up to 4‰ for $\delta^{13}\text{C}$ and 3.8‰ for $\delta^{18}\text{O}$ (both in EC 166).

4.6.2.2 Whole-rock samples

The whole-rock powders were obtained mostly from the micritic matrix of the hand-specimen, so minimizing the above-mentioned

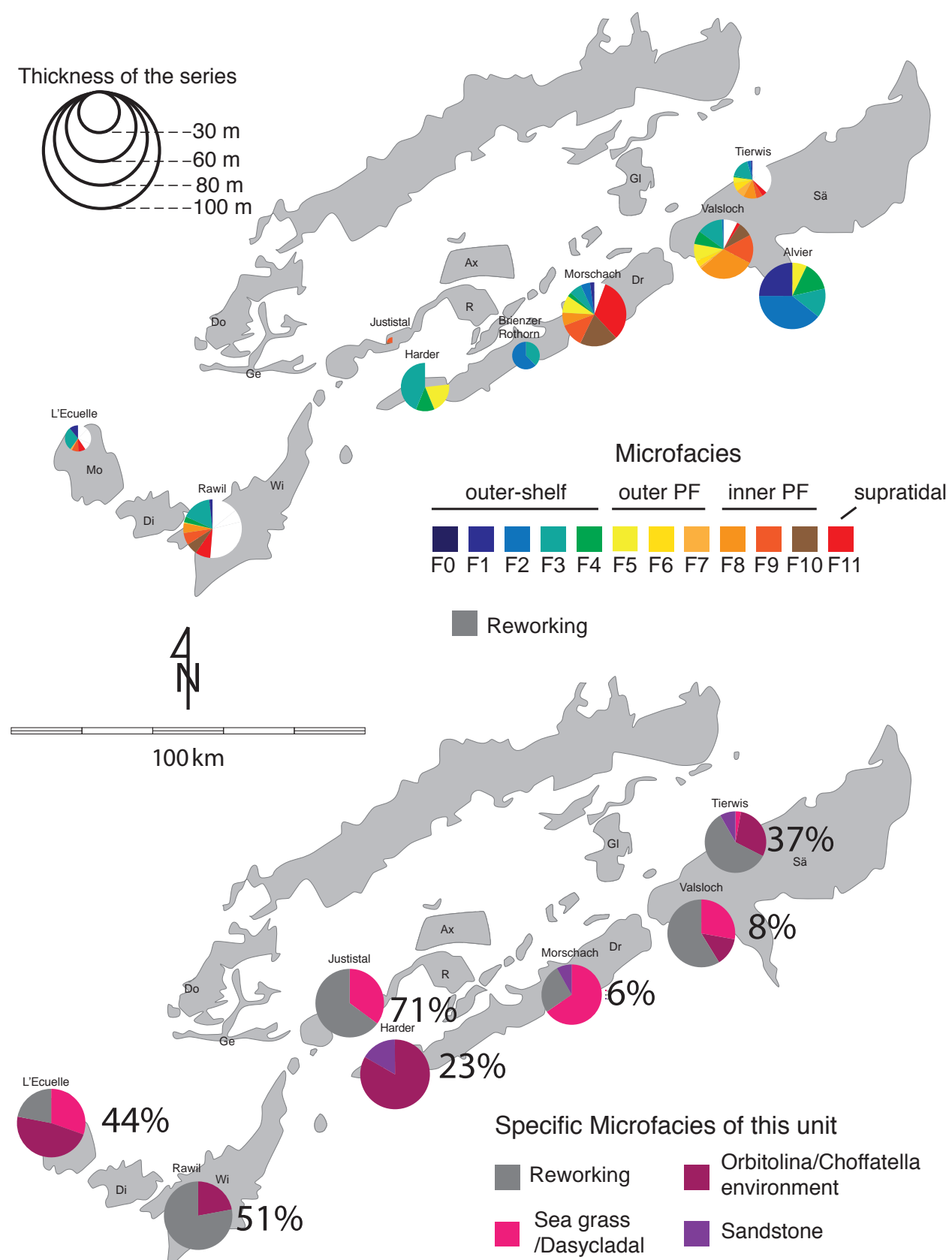


Fig. 4.21 Spatial distribution of the microfacies for TST A1 (Rawil Mb). The pie charts of the upper map represent microfacies F0 to F11 (facies FT is omitted), and their size is related to the thickness of the systems tracts in each section. The lower map represents the distribution of the specific facies of this unit (FT1: reworking and lag; FT2: accumulation of *Palorbitolina lenticularis*, associated with detrital quartz, annelids and *Choffatella decipiens*; FT3: accumulation of *Dasycladaceae* and sea-grass environment).

isotopic heterogeneity.

In the Altmann Mb, carbon isotope values are comprised between +0.5‰ and 1.5‰. For the Drusberg Mb, a distinction between three groups of sections can be made with regards to their $\delta^{13}\text{C}$ records. Those of Kistenpass, L'Ecuelle and Morschach, which are all part of the proximal platform domain, show a plateau with a mean value of 1.1‰; 1.5‰ and 2.4‰, respectively. The sections of Tierwis and Justistal show a positive excursion followed by a decrease in $\delta^{13}\text{C}$ values. The Valsloch, Harder, Alvier and Brienzer Rothorn, which are representative of the distal platform, show two well-developed trends toward positive values with a maximum amplitude recorded during the first positive shift of +2.5‰ for Harder and around +2‰ for the sections of Valsloch, Alvier and Brienzer Rothorn.

For sequence B3, the sections of Valsloch, Justistal, Harder and Brienzer Rothorn show a plateau in $\delta^{13}\text{C}$ values, with a mean value of 2.2‰, 1.8‰, 2.6‰ and 2.2‰, respectively. The $\delta^{13}\text{C}$ curves of Morschach and Tierwis show also a plateau (mean value = 2.2 ‰ and 1.5‰, respectively), followed in the last 10 m by a positive shift, which reaches maximum value of 3.8 ‰ and 2.5‰, respectively. The $\delta^{13}\text{C}$ record of L'Ecuelle shows an abrupt decrease to a negative plateau, with a minimum value of -2.6‰, interrupted by a positive excursion (maximum value 1.6‰) 10m below the top of this unit.

The Sequence 4 is characterized by a plateau for the sections of Tierwis (mean value 2.5‰), Morschach (mean value 3.5‰), Justistal (mean value 2.2‰) and Harder (mean value 2.7‰). For the section of L'Ecuelle, the $\delta^{13}\text{C}$ record shows a positive shift (maximum value -0.8‰) coinciding with the mfs. Valsloch shows saw-tooth variations in its $\delta^{13}\text{C}$ record, followed

by a negative excursion (minimum value 1‰), which is directly followed by a positive shift (maximum value 3‰). The sections of Alvier and Brienzer Rothorn are characterized by a slight increase in the $\delta^{13}\text{C}$ record (maximum values of 3.2‰ and 3‰, respectively).

The $\delta^{13}\text{C}$ record of sequence B5 represents a plateau in the sections of Morschach (mean value 3.3‰), Valsloch (mean value 3.3‰), Rawil (mean value 1.8‰) and Harder (mean value 2.5 ‰). A progressively negative shift is observed at L'Ecuelle (minimum value 1.5‰), Justistal (minimum value 1.6‰), and Alvier (minimum value 1‰). Tierwis and Brienzer Rothorn show a positive shift followed by a negative shift in the last meters (maximum values 3.1‰ and 3.3 ‰, and minimum values 0.1‰ and 0.6‰, respectively).

The Rawil Mb is characterized by a positive excursion, followed by a negative shift in the sections of Tierwis, L'Ecuelle, Justistal, Rawil and Brienzer Rothorn. In the sections of Valsloch and Morschach the plateau reached in the previous unit is maintained at the base, and is followed by a negative excursion (mean value of -1.5‰ and -2.6‰, respectively). In contrast, Harder shows a plateau followed by a positive excursion at the top of the Rawil Mb (maximum value 3‰).

The $\delta^{13}\text{C}$ record of the Upper Schrattenkalk Mb is highly fluctuating in the sections of Tierwis, L'Ecuelle and Valsloch. In the sections of Morschach and Rawil, a plateau is reached (mean value 3.5‰ and 2.4‰, respectively). In the section of Valsloch, the $\delta^{13}\text{C}$ record exhibits a positive trend toward the Grünten Mb (maximum value 3.7 ‰).

4.7 Discussion

4.7.1 The evolution of the Helvetic shelf: controlling factors

4.7.1.1 Spatial and temporal evolution of the facies along the shelf

Figure 4.19 shows the spatial and temporal evolution of the Helvetic realm in a step by step, sequence by sequence fashion, from the latest Hauterivian to the early Aptian. This evolution is based on the facies distribution and thickness variation figured in the pie charts. The evolution is summarized here:

The sequences H6 to B1 (Altmann Mb) are characterized by the presence of condensed beds, which are generally very thin (less than 10m). The thickest studied sections are located landward, close to the continent. At Tierwis, an expanded section of around 30m is present. This anomaly was explained by Bodin et al. (2006a) as the infill of a local depression, which was probably initiated by a normal fault. This trend is opposite to the one of Bodin et al. (2006 a) which observed a decrease in the thickness of the Altmann from basinward to landward positions. Nevertheless the deposition of the Altmann Mb was not homogenous along the platform. For instance in some areas, this member is completely missing, in particular in between the Säntis nappe and the Infrahelvetic complex, in the nappes of Glarus and Mürtschen (e.g., Funk, 1971; Funk et al., 1993).

The sequence B2 (Drusberg Mb) is composed of thick and usually hemipelagic

sediments, and the thickest sections are located basinward. The maximum thickness occurs at Alvier (160m), which is twice as thick as in the other sections. The Alvier section is located close to a listric paleofault, which was already described by Trümpy (1980) and which may have triggered an increasing subsidence rate during Jurassic time. The very thick Alvier section suggests that the tectonic mechanism may still have been active during early Barremian time.

The Sequence B3 is characterized by a complete change in sedimentation pattern and the important expansion of the shallow water carbonate factory, thereby covering the total investigated area except for two distal localities – Brienzer Rothorn and Alvier. The early late Barremian transgression flooded emerged landward areas, as is shown by the sections of L'Ecuelle, Tierwis and Morschach. In seaward directions, we note that the first bioclastic deposits belong to a LST, which is especially well developed in the thickest sections – Valsloch and Justistal – where progradations in parasequence are visible at and near the base (see chapter 2).

During the deposition of sequence B4, the existing topography is filled. The areas characterized by important sedimentation accumulation during sequence B3 are covered by thinner series composing sequence B4 (L'Ecuelle, Morschach and Valsloch). Tierwis is an exception, because the series above sequence B3 are thicker. In the section of L'Ecuelle, the mechanism leading to the deposition of large oblique stratifications in the HST could be interpreted in different ways. A first explanation of these structures is a fore-set origin; nevertheless the lagoonal facies F9-F10 is contradictory to such type of dynamic deposition. A second hypothesis could be the presence of syn-sedimentary folds, associated to a tectonic phase during the sequence B3, which increase the local topography and could lead to

a slumping along a slope. Similar structures are observed in the Chartreuse area (Boloyan, 1991, unpublished memoir). Finally a third explanation is an artefact linked to fracturation associated to the Alpine orogenesis (this section is located in the nappe of Morcles, in an anticline). Justistal and Harder were probably located in a depre-

sion because the depositional sequence B4 is very thick and rich in oolitic accumulations (possible shoals). On the outer shelf, sequence B4 in the Alvier and Brienz Rothorn sections still consists of hemipelagic sediments, which include bioclastic grains in Alvier.

Sequences B5 and A1 are characterized

Identifier	Carb-gen.	d13C VPDB	d18O VPDB
EC 166 BIS (1)	Rudist	-1.5	-4.2
EC 166 BIS (2)	Micrite	-2.3	-4.9
EC 166 BIS (3)	Vein (yellow cement)	-1.8	-8.1
EC 166 BIS (4)	Vein (white cement)	-5.5	-5.3
EC 166 BIS (5)	Bioturbation	-3.8	-5.2
EC 166 carb (W-R)	Bulk-rock (micrite)	-2.9	-5.0
EC 166 biot (W-R)	Bulk-rock (bioturbation)	-3.9	-8.2

Identifier	Carb-gen.	d13C VPDB	d18O VPDB
LB 27 (1)	Rudist 1	1.8	-3.2
LB 27 (2)	Rudist 2	1.5	-3.0
LB 27 (3)	Bioclaste	1.6	-3.1
LB 27 (4)	Micrite	2.0	-3.0
LB 27 (5)	Calcareous vein	1.6	-4.8
LB 27 (W-R)	Bulk-rock	1.7	-3.4

Identifier	Carb-gen.	d13C VPDB	d18O VPDB
VA 122 (1)	Rudist (calcite)	1.9	-3.3
VA 122 (2)	Rudist (recrystallized aragonite)	2.4	-3.7
VA 122 (3)	Oncolite	2.7	-3.8
VA 122 (4)	Micrite	2.6	-4.1
VA 122 (5)	Dark micrite	2.7	-3.6
VA 122 (6)	Calcareous vein	2.9	-6.3
VA 122 (W-R)	Bulk-rock	2.6	-4.6

Identifier	Carb-gen.	d13C VPDB	d18O VPDB
VA 15 (1)	Recrystallized bioclast 1	2.4	-6.5
VA 15 (2)	Recrystallized bioclast 2	2.3	-6.1
VA 15 (3)	Bivalve	2.6	-7.0
VA 15 (4)	Coral 1	3.5	-3.6
VA 15 (5)	Coral 2	3.4	-4.2
VA 15 (6)	Micrite	3.6	-3.7
VA 15 (W-R)	Bulk-rock	3.4	-3.2

Identifier	Carb-gen.	d13C VPDB	d18O VPDB
MC 10 (1)	Rudist 1	3.1	-2.4
MC 10 (2)	Rudist 2	3.9	-3.4
MC 10 (3)	Echinoderm	3.9	-3.4
MC 10 (4)	Bioclast	3.3	-3.7
MC 10 (5)	Micrite 1	3.8	-3.7
MC 10 (6)	Micrite 2	3.7	-3.4
MC 10 (W-R)	Bulk-rock	3.5	-4.0

Identifier	Carb-gen.	d13C VPDB	d18O VPDB
MC 137 (1)	Recrystallized bioclast 1	2.3	-2.6
MC 137 (2)	Recrystallized bioclast 2	3.6	-5.2
MC 137 (3)	Recrystallized bioclast 3	1.9	-2.5
MC 137 (4)	Orbitolinidae	3.3	-2.4
MC 137 (5)	Micrite 1	3.2	-2.1
MC 137 (6)	Micrite 2 (dark)	4.4	-3.8
MC 137 (W-R)	Bulk-rock	3.0	-2.5

Identifier	Carb-gen.	d13C VPDB	d18O VPDB
KP 61 (1)	Oyster layer 1	2.9	-3.9
KP 61 (2)	Oyster layer 2	1.4	-4.6
KP 61 (3)	Oyster layer 3	1.5	-4.7
KP 61 (4)	Micrite	1.4	-4.8
KP 61 (W-R)	Bulk-rock	1.5	-4.9

Identifier	Carb-gen.	d13C VPDB	d18O VPDB
TW-145 (1)	Orbitolinidae	2.0	-3.2
TW-145 (2)	Micrite	2.0	-3.6
TW-145 (3)	Calcareous vein	2.1	-5.1
TW-145 (W-R)	Bulk-rock	1.9	-3.5

Table 4.1 Stable isotope composition ($\delta^{13}\text{C}$ and $\delta^{18}\text{O}$) of the micro-drilled samples and of the whole-rock samples (W-R) from the selected samples presented in the Fig. 4.4.

by the absence of topography on the platform, as shown by the comparable thicknesses in all sections. Nevertheless, TST A1 forming the Rawil Mb is characterized by a global trend toward open-marine facies, illustrating the deepening of the environment.

The Helvetic realm evolved in two distinct phases: the first phase is the recovery in sediment accumulation after a phase of drowning (Altmann Mb). This phase witnessed the creation of topography during the deposition of the sequences B2 and B3. The second phase comprises the development of the “Urgonian” platform s.s., during which the topography is levelled out (sequences B4, B5, and A1).

A peculiarity in the evolution of the platform is observed in the region of the Lake of Thun (sections of Justistal and Harder), where a specific evolution of thickness and facies is observed. The Altmann Mb is extremely thin (less than 1m) and highly condensed. Ziegler (1967) reported that the Altmann Mb is even missing in some places in this area. During the deposition of the following Drusberg Mb, bioclastic facies is present in the western part of the Helvetic realm (L’Ecuelle, Justistal and Harder). Scheeberger (1927) and Ziegler (1967) postulated the presence of a shoal around the Niedernhorn. This hypothesis serves to explain the early development of the Schrattenkalk Fm in this area. Ziegler (1967) postulated the presence of a fault, which explains the absence of the Altmann Mb and the presence of granular facies directly above the Kieselkalk formation, which change landward (Rothorn) into the hemipelagic succession of the Drusberg Mb.

The extremely thin Drusberg Mb at Justistal is interpreted as the consequence of sediment removal by gravity flow (see chapter 2). The shoal bathymetry of this area would explain

the dominance of bioclastic and oolitic facies. The filling of the accommodation space and the progradation of this shoal in a seaward direction are illustrated by the decrease in thickness at Justistal between sequences B3 and B5, which are inversely related to the evolution of thickness at Harder during deposition of the same units. The infilling is also revealed by the installation of lagoonal facies in Justistal during deposition of sequence B5. Nevertheless, the observations of Ziegler (1967) of the presence of a hemipelagic succession in the northern, landward part of Justistal and Niederhorn suggest that channels have incised the oolitic shoal.

The presence of shallow-water platform particles in grain-flow deposits in the B2 sequence (Harder, Justistal, Valsloch) suggests the development of a shallow-water carbonate factory on the inner platform, possibly located on that part of the platform, which is presently exposed in the Jura Mountains.

4.7.1.2 Subsidence and faulting

The platform edge is defined by the lateral transition between the Schrattenkalk Fm and the Drusberg Mb, which is located in the higher Helvetic nappes. The transition occurs in a zone, which can be traced from the Wildhorn in the west to the Alvier in the eastern part of Switzerland, and which runs almost parallel to the Alps (i.e., W30°S) according to Heim (1916–1922). In this zone the lateral change between shallow-water platform and hemipelagic facies, is accomplished in less than 10 km across strike (Heim, 1916–1922; Ziegler, 1967).

It is likely that the platform margin coincide with a listric paleofault zone (Trümpy, 1960, 1980, for the east; Badoux et al., 1959 and Badoux and Lombard, 1962, for the west). These

authors postulated a Jurassic age for these paleofaults, for which their presence has been essentially deducted from the important thickness of the Helvetic Jurassic and Cretaceous succession in the distal part of the platform, to explain the associated high subsidence rate. Unfortunately, not much evidence exists in the field for the presence and location of these paleofaults. Wildi et al. (1989) established that the subsidence rate was high during the Jurassic, and increased a second time during the Early Cretaceous (120 my +/- 3 my) in the Helvetic realm.

Extensional tectonism linked to the rifting and opening of the Alpine Tethys (Stampfli, 1993) in the Middle–Late Jurassic was accommodated by continental drift and widespread oceanic crust production in the most internal sectors of the basin. The geodynamic context during the Early Cretaceous is characterized by the opening of the southern Atlantic Ocean and consequently by the convergence between Africa and Europe (Philips and Forsyth, 1972; Ziegler, 1987; Rosenbaum and Lister 2004). Several studies show that continuing extension following the break-up phase has significantly affected both margins of the Alpine Tethys from the Middle and late Jurassic until the Eocene (e.g. Güntzler-Seiffert 1942, 1952; Montanari, 1988; Manatschal and Bernouilli, 1999; Graziano, 2000; Santantonio et al. 2013; Cardello and Mancktelow, 2014).

The section of Rawil, where karst developed through more than 90m from the top of the Upper Schrattenkalk Mb (see details in chapter 2), may have been deposited on a paleo-high. The presence of paleofaults has been reported for this area by Föllmi and Gainon (2008) and Cardello and Mancktelow (2014) (Eaux froides and Chamossaire paleofaults). According to these latter authors, these listric paleofaults were active in the Turonian–Santonian for the first

one and in the Early Maastrichtian for the second one.

Tilted blocks affecting the Urgonian platform have been described in southeastern France, more precisely in the Jura and the northern Subalpine chains (Mojon, 2002), in the Vercors–Chartreuse area (e.g. Arnaud Vanneau 1980; Arnaud et al. 2005), and in the Gard and Ardèche areas (Bastide, 2014).

4.7.1.3 Architecture of the platform

The spatial facies distribution and their evolution during time provide us information on the morphology of the Helvetic platform. During the latest Hauterivian–early Barremian (Altmann and Drusberg Mb deposits), the morphology of the platform was a ramp *sensu* Burchette and Wright (1992), according to Bodin et al. (2006a). The morphology of the platform changed toward a flat-topped platform, with the installation of the Urgonian limestone (“open platform” according to Pomar et al., 2012). This is supported by the equivalent thickness of the sequences and the similarity of the facies distribution in the inner and intermediate parts of the platform. The rapid facies change in the area of the platform slope suggests the presence of a distally steepened platform. The change of morphology occurs during the sequence B3, with the deposition of an aggradational bioclastic TST B3 (Pomar and Kendall, 2008) in the section of Valsloch, which indicates a flat-topped platform morphology for the sequence B3. The presence of a distally-steepened platform break is constrained by the maximum in progradation, which never reached the most distal sections, except for grain-by-grain reworking of some platform material (such as the presence of turbidites in the upper part of the section of Brienzer Rothorn; Ribaux, 2012), and

may have been related to the presence of paleo-faults and associated differential subsidence as stated before.

4.7.2 The carbon isotope record

The carbon-isotope composition of carbonate is widely used to interpret geological and biological phenomena and to obtain information on the sedimentary environment (e.g., Anderson and Arthur, 1983). The $\delta^{18}\text{O}$ vs. $\delta^{13}\text{C}$ plot serves to assess the degree of alteration of, and the possible diagenetic or metamorphic overprint on the isotope record of the studied samples. The covariance values are 0.16, 0.11, 0.62, 0.14, 0.06, 0.29, 0.18, 0.13, 0.03, 0.02 and 0.1 for the sections of Morschach, Valsloch, L'Ecuelle, Tierwis, Harder, Interlaken, Justistal, Rawil, Lämmerenplatten, Kistenpass and Brienz Rothorn, respectively (Fig. 4.22). As a first interpretation, the lack of statically significant correlation between $\delta^{13}\text{C}$ and $\delta^{18}\text{O}$ values excludes diagenetic modification of the primary carbonate C isotope signature, according to Choquette and James (1987). As from the observed different carbonate textures, the lack of a strict chemostratigraphic correlation (discrepancies in the position of the isotopic excursion compared to the position of the SBs) and some very negative excursions in most sections and simple geological considerations (overprint through alpine orogenesis) would suggest that significant diagenetic alteration overprinted the primary isotope signature for several sections. The most affected are the sections of Kistenpass, Lämmerenplatten and L'Ecuelle that show low to negative values, probably due low-grade metamorphic overprint (See Chapter 3; and Fig. 4.22).

The $\delta^{18}\text{O}$ vs. $\delta^{13}\text{C}$ scatter plot of the selected samples on which a micro-drilling sub-sampling were performed, are presented in the Fig. 4.23. We observed variations between the different micro-drilled phases or organisms and the values obtained on the powder of the whole-rock sample. Nevertheless, the values between the micro-drilled micrite and the powder of the whole-rock show that even if a heterogeneity exists within hand-specimen, the bulk-rock powder reflects the stable isotopic composition of the matrix.

In the lower part of the sections (sequences B6 to B2), the $\delta^{13}\text{C}$ values show two prominent positive excursions without any associated facies change (hemipelagic facies F0 to F3). These two excursions can be correlated with the positive excursions observed in the section of Angles (SE France; Godet et al., 2006), which occurred in the uppermost lower Barremian (first one in the *K. compressissima* zone, and the second one in the *C. darsi* zone).

A phase of subaerial erosion and the formation of superficial karst and palaeosols associated with SB 3 in the proximal part of the platform (sections of Tierwis, L'Ecuelle and Morschach) is not reflected in the carbon-isotope record. This may be best explained by the fact that the emerged “substratum” is composed of hemipelagic micritic facies (mudstone and wackestone), with low porosity and which is therefore less affected by diagenesis.

In the Lower Schrattenkalk Mb, the $\delta^{13}\text{C}$ record is highly influenced by the type of facies present. The installation of lagoonal and associated facies (F8, F9 and F10) is directly linked with positive excursions. This is especially the case in the sections of Morschach and Valsloch with amplitudes of +1.5‰ and +2‰, respectively. The same is also visible in sections

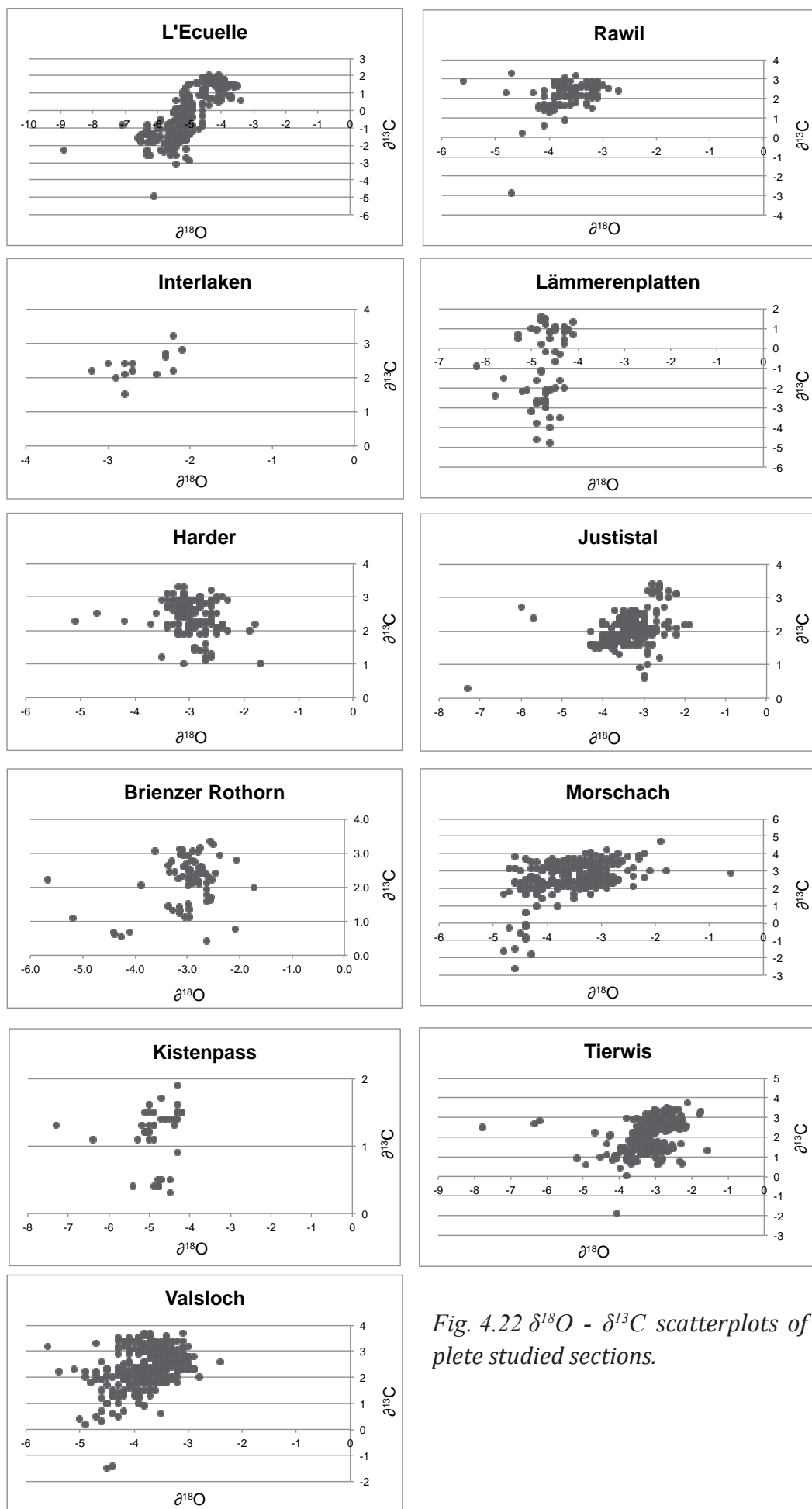
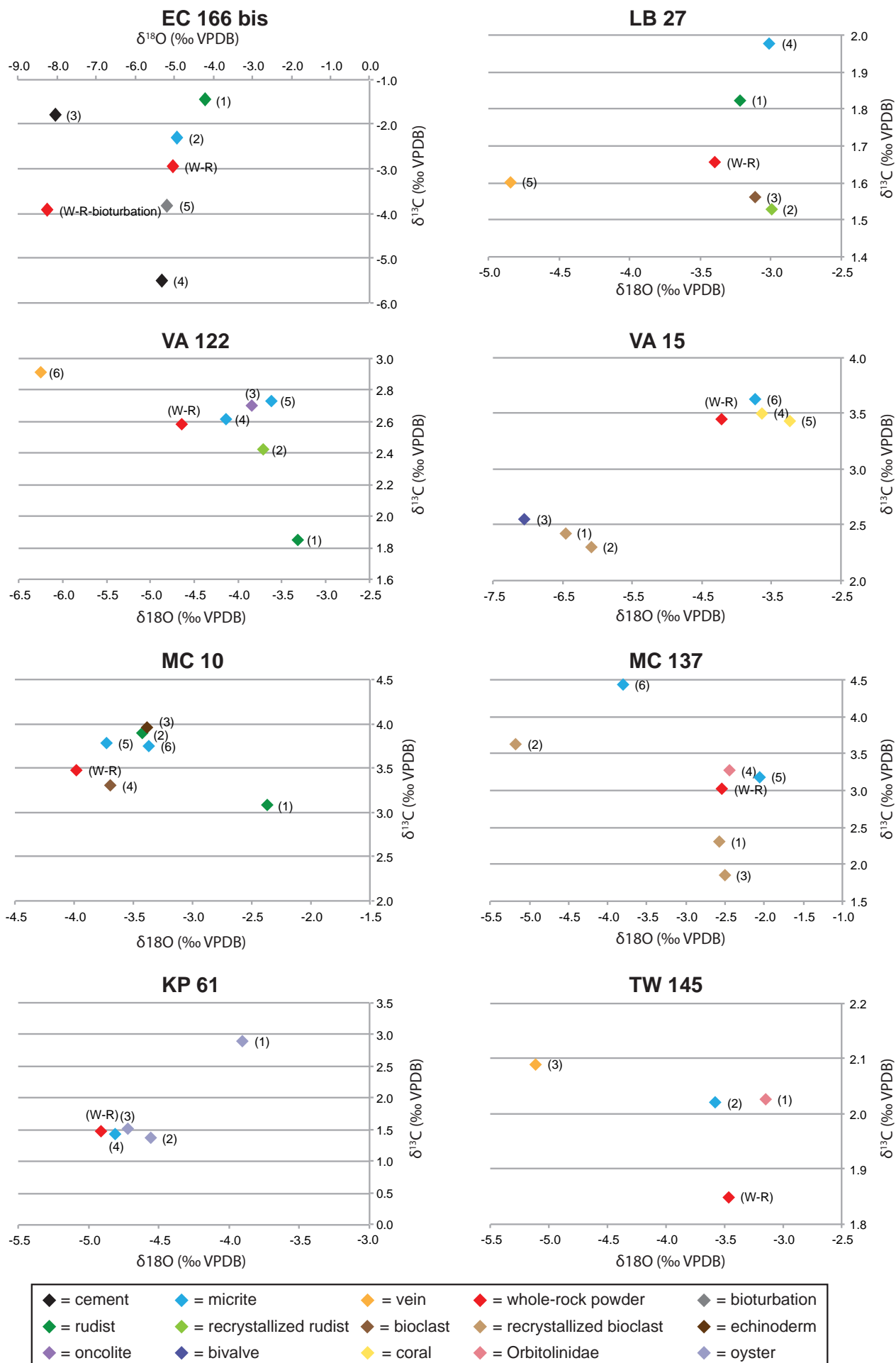


Fig. 4.22 $\delta^{18}\text{O}$ - $\delta^{13}\text{C}$ scatterplots of the complete studied sections.


 Fig. 4.23 $\delta^{18}\text{O}$ - $\delta^{13}\text{C}$ scatterplots of the micro-sampled isotopic data of the 8 selected samples.

of Rawil, Justistal and Tierwis and to a lesser extent in L'Ecuelle. This trend is diachronous, depending of the position of the section on the platform. In proximal to inner intermediate sections it occurs in sequence B3 (HST B3; at Morschach, Tierwis and L'Ecuelle), and higher up in intermediate sections (sequence B4 – HST B4 – at Valsloch; sequence B5 at Justistal). The high values in the often confined lagoons may be the result of recycling of carbon and the loss of lighter carbon, and the presence of aragonite (Swart and Eberli, 2005; Godet et al., 2006; Föllmi et al., 2006).

The presence of oolitic and bioclastic facies (F5, F6) tends also to lower $\delta^{13}\text{C}$ values (e.g., TST B3 at Valsloch; sequences B2 to B4 at Justistal; sequences B3 to B5 at Harder). This may be explained by the fact that these facies are grainstones with corresponding amounts of diagenetic cements (e.g. meteoric), and that the grains may be porous as well (e.g., crinoid particles).

In distal sections (Alvier and Brienzer Rothorn), the $\delta^{13}\text{C}$ record is less influenced by biological and diagenetic overprint, the exportation of material from the shelf may, however, explain the higher values (maximum value +3.0‰) compared to the Vocontian record (Angles; Fig. 4.24). The $\delta^{13}\text{C}$ record of the Rawil Mb and variations therein are discussed in chapter 3.

4.7.3 Eustatic sea level change

The use of a sequence stratigraphic approach allows to better constrain the timing and amplitude of relative sea level change. To this comes that the variations in the subsidence rate are known through the contributions of Funk

(1985), Lemoine and Trümpy (1987) and Wildi (1989), which helps to disentangle regional from global components in sea-level change.

The TST B2 is represented by an open-marine to hemipelagic facies sediments (Drusberg Mb) for most of the platform and outer shelf, which resulted from high sea level. HST B2 documents the onset of shallow-water carbonate deposition in the intermediate platform realm (sections of Justistal, Valsloch and panorama of the Churfirsten range).

The terminal surface of sequence A1 consists of a major emersion surface, associated with karst on the whole platform (SB A2). The comparable depth of karst influence (between 15 and 26 m) through the inner and intermediate platform confirms the absence of topography, and indicates a sea-level fall of at least 30 m. Moreover, it suggests that erosion of the limestone was accommodated by karstification.

4.7.4 Environmental and climatic changes

Prior to the deposition of the “Urgonian” facies during the late Barremian, the Helvetic platform was dominated by heterozoan assemblages and condensation phases from the Valanginian onward (Föllmi et al., 2006, 2007; Föllmi, 2012). The heterozoan assemblage is dominated by crinoids and bryozoans, and reflects an adaptation of the ecosystem to mesotrophic palaeoenvironmental conditions, which was likely due to a general increase in the phosphorus concentrations in the ocean (van de Schootbrugge et al., 2003; Godet, 2013). According to Kuhn (1996), van de Schootbrugge et al. (2003) and Godet (2013), the condensation phases observed in the Helvetic realm during the Early Cretaceous have

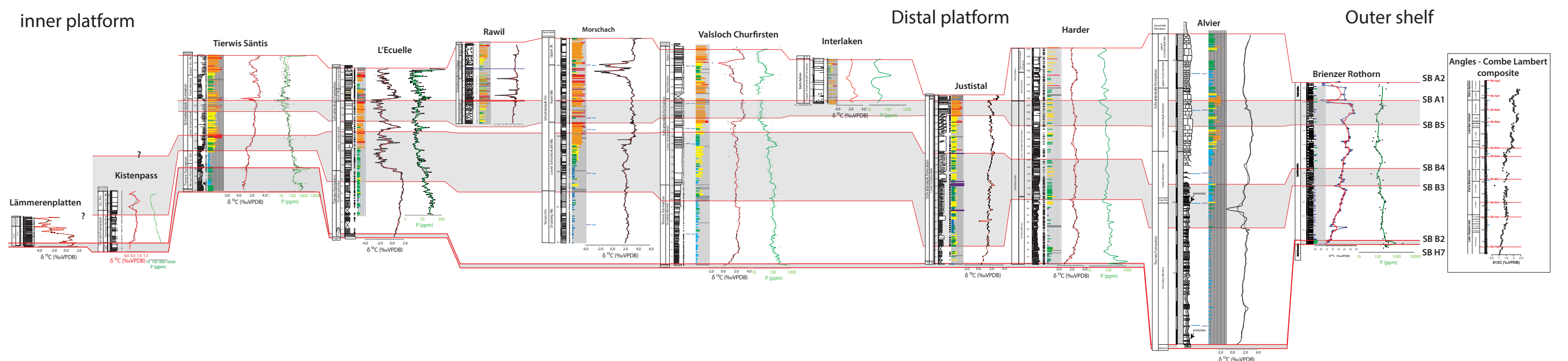


Fig. 4.24 Palinspastic transect along the Helvetic nappes with correlation of the studied sections based on their sequence stratigraphy, the carbon-isotope records, the phosphorus content and microfacies.

been related to upwelling currents, which led to the demise of the heterozoan ecosystems. The onset of the condensed Altmann Mb is coarsely correlated to the Faraoni anoxic event recorded in the basin (Föllmi et al., 2007; Föllmi, 2012). This member is deposited during a nutrient-rich phase (mesotrophic to eutrophic conditions) during which strong currents occurred. The nutrient content is still high during the deposition of the hemipelagic sediments of the Drusberg Mb (sequence B2), but decreased from the installation of the shallow-water oligotrophic carbonate to the demise of the platform, as is indicated by the progressive decrease in P contents. The long-term trend is superimposed by two positive shifts, which occurred during the deposition of sequences B3 and A1, which correspond both to main transgressive sequences, and which are associated with mixed photozoan – heterozoan assemblages.

Climatic conditions during the late Hauterivian–early Barremian were warm and humid according to Godet et al. (2008). According to Ruffel (2002), the climatic conditions during the Barremian time became gradually more arid. The temperature increased near the end of the Barremian, decreased during the earliest Aptian, and increased during the phase prior the oceanic anoxic episode 1a, according to Stein et al. (2012a). The climatic fluctuations suggest that the installation of the Urgonian shallow-water carbonate platform, characterized by oligotrophic conditions, has been triggered by climatic and paleoenvironmental conditions. The development of the Urgonian-type platforms, widespread in the tropical and inter-tropical area, occurred during a phase of arid climate, between the phases of intense warming, associated to oceanic anoxic events (Faraoni event in the Hauterivian and Selly event (OA1a) in the early Aptian). The late Barremian–earliest Aptian re-

presents a period of optimal climate conditions and of relative stability of the paleoenvironmental conditions, which allow the development of large Urgonian-types platforms. The change of carbonate production-style recorded during the earliest Aptian, forming the Rawil Mb, testifies to the response of the ecosystems to environmental fluctuations.

4.8 Conclusion

The evolution of the Helvetic shelf is studied for the time period between the latest Hauterivian and the early Aptian. The stratigraphic development in microfacies, biostratigraphy based on benthic foraminifera, $\delta^{13}\text{C}$ records and phosphorus data are used to propose a sequence-stratigraphic subdivision of the sediments. The sequence stratigraphic framework established in the Subalpine Chains is adapted here.

The sedimentary record started with the deposition of condensed, phosphate and glauconite-rich beds of the Altmann Mb, which was followed by a phase of widespread hemipelagic sedimentation (Drusberg Mb). Both units were accumulated during high relative sea level. The therein contained $\delta^{13}\text{C}$ records show two positive excursions, which are correlated with the basinal record of the Vocontian basin, and which as such date from the early–late Barremian boundary interval. The difference in thickness of the series between the inner and intermediate platform and the distal shelf, suggests the presence of a distally steepened edge created by listric paleofaults, especially in the eastern region.

The presence of an emersion surface above these hemipelagic sediments (cf. chapter 2) in the proximal part of the platform suggests a

major sea-level fall resulting in the formation of SB B3. The following sequence forming the base of the Lower Schrattenkalk Mb on the platform is characterized by the development of a LST on the border of the platform, which is followed by a major transgression documented by a particular facies rich in flat orbitolinids and annelids. An increase in phosphorus content is observed in this interval in the inner and intermediate sections, and condensation occurred in the distal sections (Chopf Bed). HST B3 exhibits the installation of the shallow-water carbonate factory of typical Urgonian facies in most places of the platform. In this sequence, the $\delta^{13}\text{C}$ record is affected by facies change. Sequence B4 is characterized by the filling of the paleotopography inherited from the Hauterivian Kieselkalk platform, which was accentuated since then. In the central part of the platform (Justistal and Harder), anomalous thick successions and their facies distribution suggest the presence of a locally accentuated topography, which may have resulted from the action of a conjugate fault. During the deposition of sequence B5, the associated depression has been filled in. At that time, lagoon facies is developed in most places of the inner and intermediate platform. Sequence A1 is characterized by a major transgression associated with increased clay input, which led to the deposition of a thick TST (Rawil Mb) showing the replacement of lagoonal facies by outer-platform facies and by the development of particular facies, close to the one developed during sequence B3. The overlying HST A1 shows the recovery of the partly restricted lagoonal environment on the entire platform, and ends by an important emersion horizon accompanied by major karstification of the upper 20m sediments of HST A1. Sea-level fall linked to this emersion is estimated at least at 26m.

4.9 References

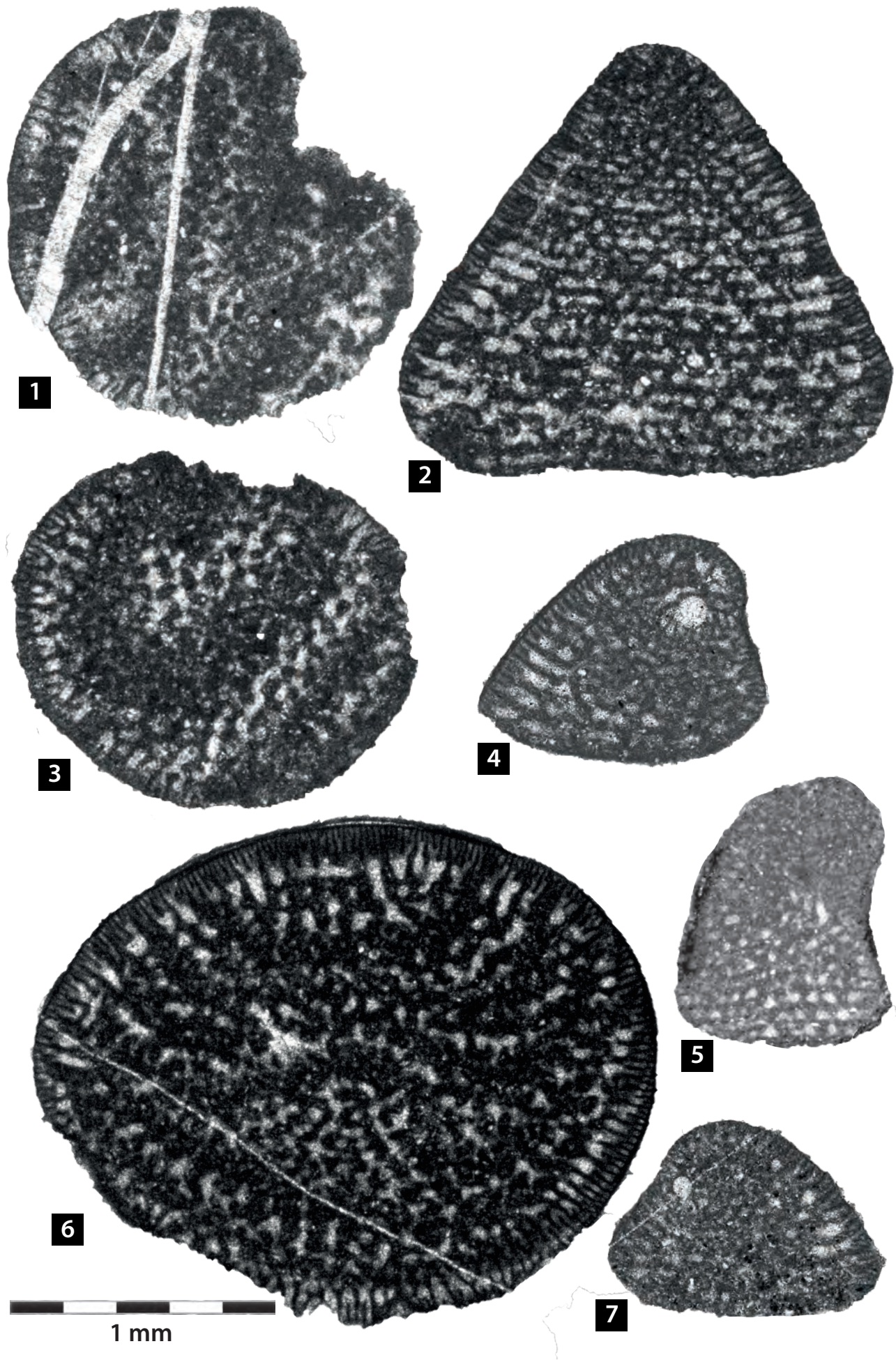
- Andreson, T.F. and Arthur, M.A.** (1983) Stable isotope of oxygen and carbon and their application to sedimentologic and paleo-environmental problems. *Society of economic palaeontologists and mineralogists, Short Course*, **10**, 1–151
- Arnaud, H. and Arnaud Vanneau, A.** (1989) Séquence de dépôt et variations du niveau de la mer au Barrémien et à l’Aptien inférieur dans les massifs subalpins septentrionaux et le Jura (Sud-Est de la France). *Bulletin de la Société Géologique de France*, **V**, 651–660.
- Arnaud, H. and Arnaud-Vanneau, A.** (1991) Les calcaires urgoniens des Massifs subalpins septentrionaux et du Jura (France): âge et discussion des données stratigraphiques. *Géologie Alpine*, **67**, 63–79.
- Arnaud, H., Arnaud-Vanneau, A., Blanc-Aletru, M.-C., Adatte, T., Argot, M., Delanoy, G., Thieuloy, J.-P., Vermeulen, J., Virgogne, A., Virlouvet, B. and Wermeille, S.** (1998) Répartition stratigraphique des orbitolinidés de la plate-forme urgonienne subalpine et jurassienne (SE de la France) *Géologie Alpine*, **74**, 87.
- Arnaud-Vanneau, A.** (1980) Micropaléontologie, paléoécologie et sédimentologie d'une plate-forme carbonatée de la marge passive de la Téthys : l’Urgonien du Vercors septentrional et de la Chartreuse (Alpes occidentales). *Géologie Alpine, Grenoble Mém HS* **11**, 874 p.
- Arnaud-Vanneau, A. and Arnaud, H.** (1990) Hauterivian to Lower Aptian carbonate shelf sedimentation and sequence stratigraphy in the Jura and northern Subalpine chains (southeastern France and Swiss Jura). In: *Carbonate Platforms: Facies, Sequences*

- and Evolution* (Eds M.E. Tucker, J.L. Wilson, P.D. Crevello, J.R. Sarg and J.F. Read), **9**, pp. 203-233. Blackwell Scientific Publications, Special Publication of the International Association of Sedimentologists.
- Arnaud-Vanneau, A. and Arnaud, H.** (2005) Carbonate facies and microfacies of the Lower Cretaceous carbonate platforms. In: *The Hauterivian-Lower Aptian sequence stratigraphy from Jura Platform to Vocontian Basin: A multidisciplinary approach* (Eds T. Adatte, A. Arnaud-Vanneau, H. Arnaud, M.-C. Blanc-Alétru, S. Bodin, E. Carrio-Schafhauser, K.B. Föllmi, A. Godet, M.C. Raddadi and J. Vermeulen), *Géologie Alpine, Série Spéciale “Colloques et Excursions” N°7*, pp. 39-68.
- Badoux, H., Bonnard, E.G., Burri, M., Vischer, A.** (1959). Feuille 35 St-Leonard et notice explicative. Atlas geol. Suisse 1:25'000. Comm. Geol. Suisse. Basel.
- Badoux, H., Lombard, A.** (1962). Feuille 41 Lenk et notice explicative. Atlas geol. Suisse 1:25'000. Comm. Geol. Suisse. Bern
- Bastide, F.** (2014) *Synthèse de l'évolution de la plateforme urgonienne (Barrémien tardif à Aptien précoce) du Sud-Est de la France : Facies, micropaléontologie, géochimie, géométries, paléotectonique et géomodélisation*. PhD thesis, Université de Lausanne & Université Joseph Fourier, 452 p.
- Bodin, S., Godet, A., Vermeulen, J., Linder, P. and Föllmi, K.B.** (2006a) Biostratigraphy, sedimentology and sequence stratigraphy of the latest Hauterivian – Early Barremian drowning episode of the Northern Tethyan margin (Altmann Member, Helvetic nappes, Switzerland) *Eclogae geologicae Helvetiae*, **99**, 157-174.
- Bodin, S., Vermeulen, J., Godet, A. and Föllmi, K.B.** (2006b) New data on the age of the installation of Urgonian-type carbonates along the northern Tethyan margin: biostratigraphy of the Chopf Member (Helvetic Alps, eastern Switzerland). *Comptes Rendus Geoscience*, **338**, 7.
- Bodin, S., Godet, A., Föllmi, K.B., Vermeulen, J., Arnaud, H., Strasser, A., Fiet, N. and Adatte, T.** (2006c) The late Hauterivian Faraoni oceanic anoxic event in the western Tethys: Evidence from phosphorus burial rates. *Palaeogeography, Palaeoclimatology, Palaeoecology*, **235**, 245-264.
- Bollinger, D.** (1988) *Die Entwicklung des distalen osthelvetischen schelfs im Barremian und Früh-Aptian. Drusberg-, Mittagspitz- und Schrattenkalk-Fm. im Vorarlberg und Allgäu.*, Universität Zürich, Zürich, 159 pp.
- Boloyan, C.** (1993) *Etude d'une série réduite dans les calcaires urgoniens du massif de la Chartreuse – implications tectoniques possibles.*, Université Joseph Fourier Grenoble 1, 51 pp.
- Briegel, U.** (1972) Geologie der östlichen Alviergruppe (Helvetische Decken der Ostschweiz) unter besonderer Berücksichtigung der Drusberg- und Schrattenkalkformation (Unterkreide). *Eclogae geol. Helv.*, **65**, 425-483.
- Cardello, G.L. and Mancktelow, N.** (2014) Cretaceous syn-sedimentary faulting in the Wildhorn Nappe (SW Switzerland). *Swiss Journal of Geosciences*, **107**, 223-250.
- Cecca, F., Marini, A., Pallini, G., Baudin, F. and Begouen, V.** (1994) A guide-level of the uppermost Hauterivian (lower Cretaceous) in the pelagic succession of Umbria-Marche Apennines (central Italy): the Faraoni level. *Riv. It. Paleont. Strat.*, **99**, 551-568.
- Choquette, P.W. and James, N.P.** (1987) Diagenesis # 12. Diagenesis in Limestones - 3. The Deep Burial Environment. *Geoscience Canada*, **14**, 3-35.

- Eaton, A.D., Clesceri, L.S. and Greenberg, A.E.** (1995) *Standard Methods for examination of Water and Waste Water*. IXI, 4113-4114.
- Embry, J.-C.** (2005) *Paléoécologie et architecture stratigraphique en haute résolution des plates-formes carbonatées du Barrémien–Aptian de la Néo-Téthys (Espagne, Suisse, Provence, Vercors) – impact respectif des différents facteurs de contrôle.*, MNHN-Paris/ IFP, 303 pp.
- Ferrazzini, B. and Schüler, P.** (1979) Versuch einer Abwicklung des Helvetikums zwischen Rhone und Reuss. . *Eclogae geol. Helv.* , **72**, 439-454.
- Fichter, H.J.** (1934) Geologie der Bauen-Brisen-Kette am Vierwaldstättersee und die zyklische Gliederung der Kreide und des Malm der helvetischen Decken. Beiträge zur geologischen Karte der Schweiz NF 69, 129 pp.
- Föllmi, K.B. and Grimm, K.A.** (1990) Doomed pioneers : Gravity-flow deposition and bioturbation in marine oxygen-deficient environments. *Geology*, **18**, 1069-1072.
- Föllmi, K.B., Weissert, H., Bisping, M. and Funk, H.** (1994) Phosphogenesis, carbon-isotope stratigraphy, and carbonate-platform evolution along the Lower Cretaceous northern Tethyan margin. *Geological Society of America Bulletin*, **106**, 729-746.
- Föllmi, K.B., Godet, A., Bodin, S. and Linder, P.** (2006) Interactions between environmental change and shallow-water carbonate build-up along the northern Tethyan margin and their impact on the early Cretaceous carbon-isotope record. *Paleoceanography*, **21**, 16 pp.
- Föllmi, K.B., Bodin, S., Godet, A., Linder, P. and van de Shootbrugge, B.** (2007) Unlocking paleo-environmental information from Early Cretaceous shelf sediments in the Helvetic Alps: stratigraphy is the key! *Swiss Journal of Geosciences*, **100**, 349-369.
- Föllmi, K.B. and Gainon, F.** (2008) Demise of the northern Tethyan Urgonian carbonate platform and subsequent transition towards pelagic conditions: The sedimentary record of the Col de la Plaine Morte area, central Switzerland. *Sedimentary Geology*, **205**, 142-159.
- Föllmi, K.B.** (2012) Early Cretaceous life, climate and anoxia. *Cretaceous Research*, **35**, 230-257.
- Funk, H.** (1969) Typusprofile der helvetischen Kieselkalk Formation und der Altmann Schichten. . *Eclogae geol. Helv.* , **62**, 191–203.
- Funk, H.** (1971) Zur stratigraphie und lithologie des Helvetischen Kieselkalkes und der Altmannschichten im der Säntis-Churfirsten-Gruppe (Nordostschweiz). *Eclogae geol. Helv.* , **64**, 345–433.

Plate 4.1

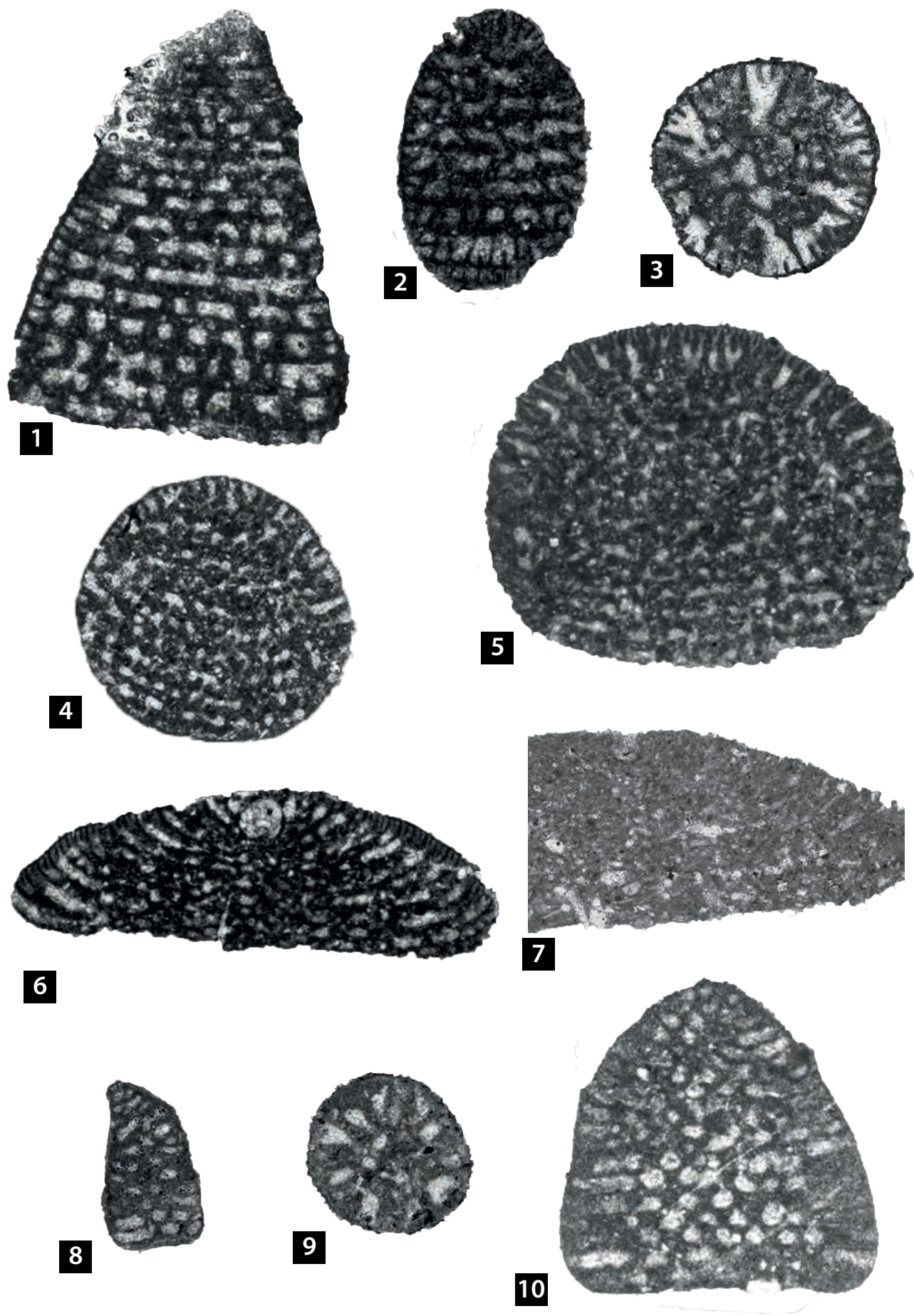
- 1/ *Paleodictyoconus*, transverse section (Tierwis section, sample TW23, HST B3)
- 2/ *Paleodictyoconus cuvillieri*, sub-axial section (Tierwis section, sample TW 47, TST B4)
- 3/ *Paleodictyoconus cuvillieri*, transverse section (Tierwis section, sample TW 99, HST B4)
- 4/ *Paleodictyoconus actinostoma*, axial section through the embryonic apparatus (Tierwis section, sample TW 62, TST B4)
- 5/ *Paleodictyoconus*, sub-axial section (Valsloch section, sample VA 255, HST B2)
- 6/ *Paleodictyoconus actinostoma*, transverse section (Tierwis section, sample TW 62, TST B4)
- 7/ *Paleodictyoconus actinostoma*, axial section (Tierwis section, sample TW 82)



- Funk, H. and Briegel, U.** (1979) Le facies Urgonien des nappes helvétiques en Suisse orientale. *Géobios, Mémoire spéciale n°3*, 9.
- Funk, H.** (1985) Mesozoische Subsidenzgeschichte im Helvetischen Schelf der Ostschweiz. *Eclogae geol. Helv.*, **78**, pp 249-272.
- Funk, H., Föllmi, K.B. and Mohr, H.** (1993) Evolution of the Tithonian-Aptian Carbonate Platform Along the Northern Tethyan Margin, Eastern Helvetic Alps. In: *AAPG Special Volumes, M 56: Cretaceous Carbonate Platforms*, pp. 387 - 407.
- Godet, A.** (2013) Drowning unconformities: Palaeoenvironmental significance and involvement of global processes. *Sedimentary Geology*, **293**, 45-66.
- Godet, A., Bodin, S., Adatte, T. and Föllmi, K.B.** (2008) Platform-induced clay-mineral fractionation along a northern Tethyan basin-platform transect: implications for the interpretation of Early Cretaceous climate change (Late Hauterivian-Early Aptian). *Cretaceous Research*, **29**, 830-847.
- Godet, A., S. Bodin, K. B. Föllmi, J. Vermeulen, S. Gardin, N. Fiet, T. Adatte, B. Zsolt, D. Stüben, and B. van de Schootbrugge** (2006), Evolution of the marine stable carbon-isotope record during the Early Cretaceous: A focus on the late Hauterivian and Barremian in the Tethyan realm, *Earth Planet. Sci. Lett.*, **242**, 254– 271.
- Godet, A., Föllmi, K.B., Bodin, S., de Kaelnel, E., Matera, V. and Adatte, T.** (2010) Stratigraphic, sedimentological and palaeoenvironmental constraints on the rise of the Urgonian platform in the western Swiss Jura. *Sedimentology*, **57**, 1088-1125.
- Golonka, J.** (2004) Plate tectonic evolution of the southern margin of Eurasia in the Mesozoic and Cenozoic. *Tectonophysics*, **381**, 235-273.
- Graziano, R.** (2000) The Aptian-Albian of the Apulia Carbonate Platform (Gargano Promontory, southern Italy): evidence of paleogeographic and tectonic controls on the stratigraphic architecture of the platform margin *Cretaceous Research*, **21**, 107-126.
- Günzler-Seiffert, H.** (1942) Persistente Brücke im Jura der Wildhorn Decke des Berner Oberlandes. *Eclogae Geologicae Helvetiae*, **34**, 2. 164 – 172.
- Günzler-Seiffert, H.** (1952) Alte Brücke im Kreide/Tertiär-anteil der Wildhorndecke zwischen Rhone und Rhein. *Geologisches Rundshau*. **40**, 2, 211
- Hantke, R.** (1961) Tektonik der helvetischen

Plate 4.2

- 1/ *Paracoskinolina reicheli*, sub-axial section (Tierwis section, sample TW40, TST B4)
- 2/ *Montseciella*, oblique section (Tierwis section, sample TW 46, TST B4)
- 3/ *Montseciella* ?, transverse section (Justistal section, sample LB 34, HST B5)
- 4/ *Praedictyorbitolina* ?, oblique section (Morschach section, sample MC 217, TST B3)
- 5/ *Praedyctiorbitolina*, oblique section (Justistal section, sample LB 217, LST B3)
- 6/ *Palorbitolina/Eopalorbitolina transiens*, axial section through the embryonic apparatus (Tierwis section, sample TW 62, TST B4)
- 7/ *Palorbitolina/Eopalorbitolina transiens*, axial section through the embryonic apparatus (Tierwis section, sample TW 82, HST B4)
- 8/ *Cribellopsis elongata*, sub-axial section (Justistal section, sample LB 226, HST B2)
- 9/ *Cribellopsis elongata*, transverse section (Justistal section, sample LB 230, HST B2)
- 10/ *Orbitolinopsis debelmasi*, sub-axial section (Tierwis section, sample TW 23, HST B3)

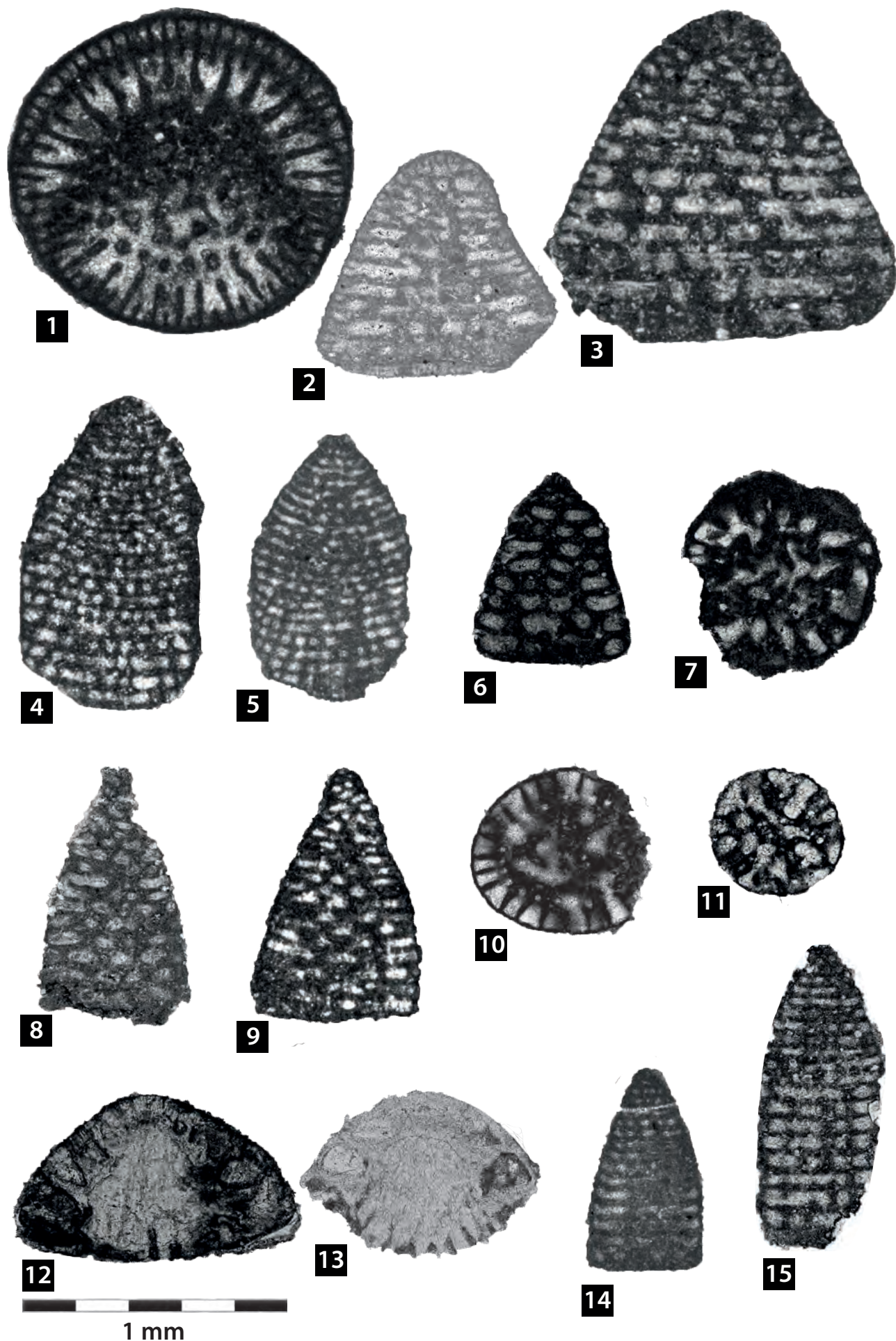


1 mm

- Kalkalpen zwischen Obwalden und dem St. Galler Rheintal. *Mitteilungen des Geologischen Institutes der ETH und der Universität Zürich, Serie B* **16**, 210 pp.
- Haq, B.U.** (2014) Cretaceous eustasy revisited. *Global and Planetary Change*, **113**, 44–58.
- Heim, A.A.** (1916–1922) Geologie der Schweiz. Tauchnitz, Leipzig
- Heim, A. and Baumberger, E.** (1933) Jura und Unterkreide in den helvetischen Alpen beiderseits des Rheines (Vorarlberg und Ostschweiz). *Denkschriften der Schweizerischen Naturforschenden Gesellschaft*, **68**, 155–220.
- Huck, S., Heimhofer, U., Immenhauser, A. and Weissert, H.** (2013) Carbon-isotope stratigraphy of Early Cretaceous (Urgonian) shoal-water deposits: Diachronous changes in carbonate-platform production in the north-western Tethys. *Sedimentary Geology*, **290**, 157–174.
- Kaufmann, F.J.** (1867) Geologische Beschreibung des Pilatus. Beiträge zur geologischen Karte der Schweiz 5, 168 pp.
- Kuhn, O.** (1996) Der Einfluss von Verwitterung auf die Paläoceanographie zu Beginn des Kreide-Treibhausklimas (Valanginian und Hauterivian) in der West-Tethys, Universität Zürich, Zürich, 380 pp.
- Pfiffner, O.A.** (1993) The structure of the Helvetic nappes and its relation to the mechanical stratigraphy. *Journal of Structural Geology*, **15**, pp. 511–521.
- Kempf, O. and Pfiffner, O.A.** (2004) Early Tertiary evolution of the North Alpine Foreland Basin of the Swiss Alps and adjoining areas. *Basin Research*, **16**, 549–567.
- Lemoine, M. and Trümpy, R.** (1987) Pre-oceanic rifting in the alps. *Tectonophysics*, **133**, 305–320.
- Manatschal, G. and Bernoulli, D.** (1999). Rifting and early evolution of ancient ocean basins: the record of the Mesozoic Tethys and of the Galicia-Newfoundland margins. *Marine Geophysical Research*, **20**, 371–381.
- Masse, J.-P., Bellion, Y., Benkhelil, J., Ricaou, L.-E., Dercourt, J. and Guiraud, R.** (1993) Early Aptian (114 to 111 Ma). In:

Plate 4.3

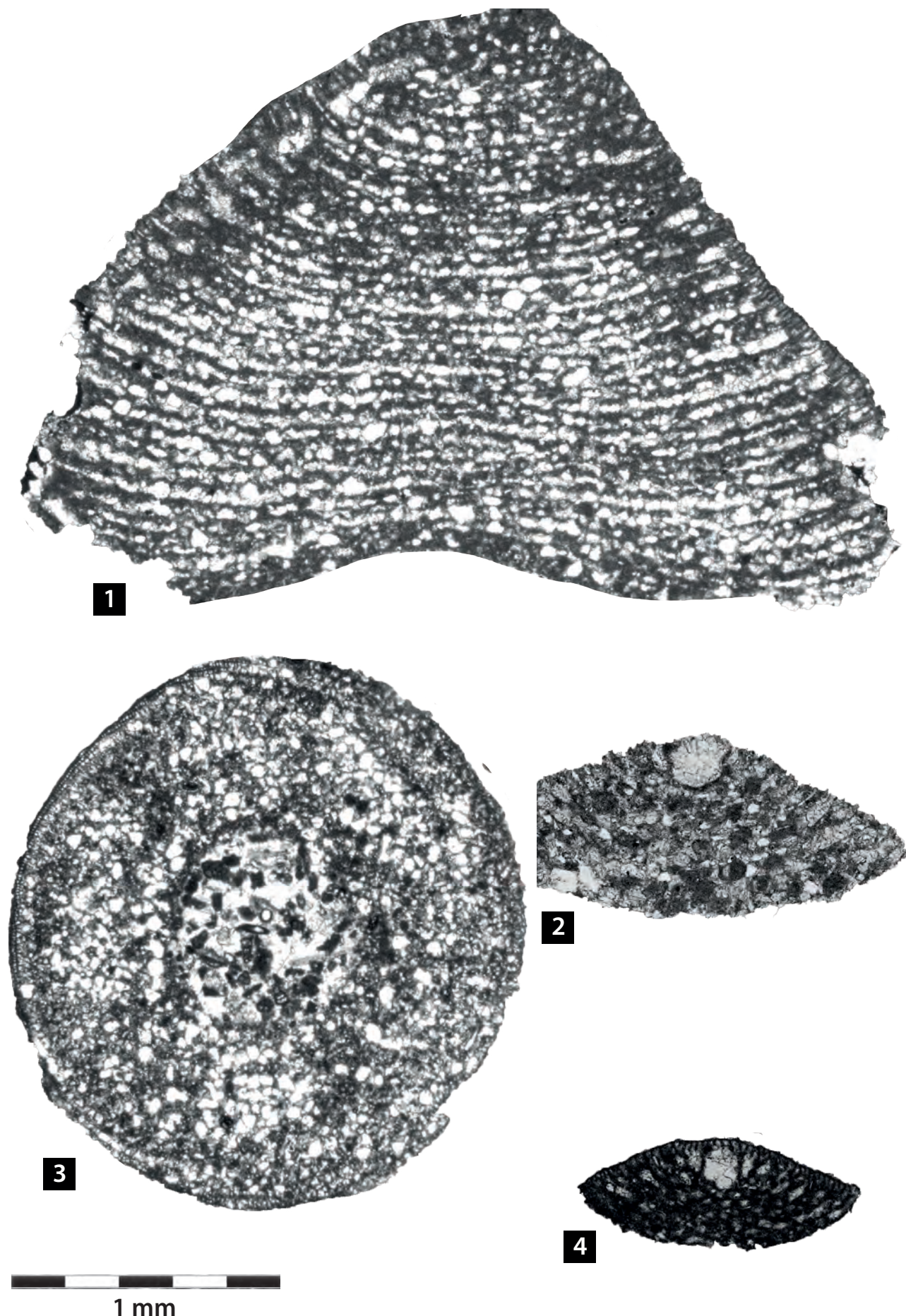
- 1/ *Paracoskinolina reicheli*, transverse section (Tierwis section, sample TW 46, TST B4)
- 2/ *Paracoskinolina reicheli*, sub-axial section (Valsloch section, sample VA 178, TST B3)
- 3/ *Paracoskinolina reicheli*, sub-axial section (Justistal section, sample LB 106, HST B3)
- 4/ *Paracoskinolina sunnilandensis*, sub-axial section (Tierwis section, sample TW 46, TST B4)
- 5/ *Paracoskinolina sunnilandensis* of large size, sub-axial section (Morschach section, sample MC 112, HST B5)
- 6/ *Falsurgonina*, sub-axial section (Tierwis section, sample TW 57, TST B4)
- 7/ *Falsurgonina*, transverse section (Morschach section, sample MC 150, TST B4)
- 8/ *Cribellopsis neelongata*, sub-axial section (Harder section, sample HA 247, TST B4)
- 9/ *Cribellopsis neelongata*, axial section (Tierwis section, sample TW 89, HST B4)
- 10/ *Cribellopsis neelongata*, transverse section showing a row of pores (Valsloch section, sample VA 70, TST A1)
- 11/ *Falsurgonina*, transverse section (Morschach section, sample MC 110, HST B5)
- 12/ *Neotrocholina friburgensis*, axial section (Tierwis section, sample TW 82, HST B4)
- 13/ *Neotrocholina friburgensis*, sub-axial section (Tierwis section, sample TW 100, TST B5)
- 14/ *Paracoskinolina cf hispanica*, sub-axial section (Morschach section, sample MC 112, HST B5)
- 15/ *Paracoskinolina cf hispanica*, sub-axial section (Harder section, sample HA 244, TST B4)



- Atlas Tethys paleoenvironmental maps.* (Ed R.L.-E. Dercourt J., Vrielynck B), pp. 135–152. Gauthier-Villars, Paris.
- Montanari, A.** (1988). Tectonic implications of hydrothermal mineralization in the Late Cretaceous – Early Tertiary pelagic basin of the Northern Apennines. *Bollettino della Società Geologica Italiana*, **107**, 399–411.
- Mojon, P.-O.** (2002) Les formations mésozoïques à Charophytes (Jurassique moyen–Crétacé inférieur) de la marge téthysienne nord-occidentale (Sud-est de la France, Suisse occidentale, nord-est de l’Espagne). Sédimentologie, micropaléontologie, biostratigraphie. *Géologie alpine, Mémoire HS* **41**, 1–386.
- Phillips, J.D. and Forsyth D.** (1972). Plate Tectonics, Paleomagnetism, and the Opening of the Atlantic. *Geological Society of America Bulletin*, **83**, 1579–1600.
- Pomar, L.** (1991) Reef geometries, erosion surfaces and high-frequency sea-level changes, upper Miocene Reef Complex, Mallorca, Spain. *Sedimentology*, **38**, 243–269.
- Pomar, L.** (1993) High-resolution Sequence Stratigraphy in Prograding Carbonates: Application to Seismic Interpretation. In: Louks, B., Sarg, R.J. (Eds.), Carbonate Sequence Stratigraphy: Recent Advances and Applications, *AAPG Memoir*, **57**, pp. 389–407. Tulsa.
- Pomar, L.** (2001) Ecological control of sedimentary accommodation: evolution from carbonate ramp to rimmed shelf, Upper Miocene, Balearic Islands. *Palaeogeography, Palaeoclimatology, Palaeoecology*, **175**, 249–272.
- Pomar, L., Kendall, C.G.S.C.** (2008) Architecture of carbonate platforms: A response to hydrodynamics and evolving ecology. In: Lukasik, J., Simo, A. (Eds.), *Controls on Carbonate Platform and Reef Development: SEPM Special Publication*, **89**, pp. 187–216. Tulsa.
- Pomar, L., Bassant, P., Brandano, M., Ruchonnet, C. and Janson, X.** (2012) Impact of carbonate producing biota on platform architecture: Insights from Miocene examples of the Mediterranean region. *Earth-Science Reviews*, **113**, 186–211.
- Pomar, L., Ward, W.C.** (1994) Response of a Miocene carbonate platform to highfrequency eustasy. *Geology*, **22**, 131–134.
- Pomar, L., Ward, W.C.** (1995) Sea level change, carbonate production and platform architecture. In: Haq, B. (Ed.), *Sequence stratigraphy and depositional response to eustatic, tectonic and climatic forcing*. Kluwer Academic Press, pp. 87–112.
- Pomar, L., Ward, W.C.** (1999) Reservoir-scale heterogeneity in depositional packages and diagenetic patterns on a reef-rimmed platform, Upper Miocene, Mallorca, Spain.
- Ramsay, J.G.** (1981) Tectonics of the Helvetic

Plate 4.4

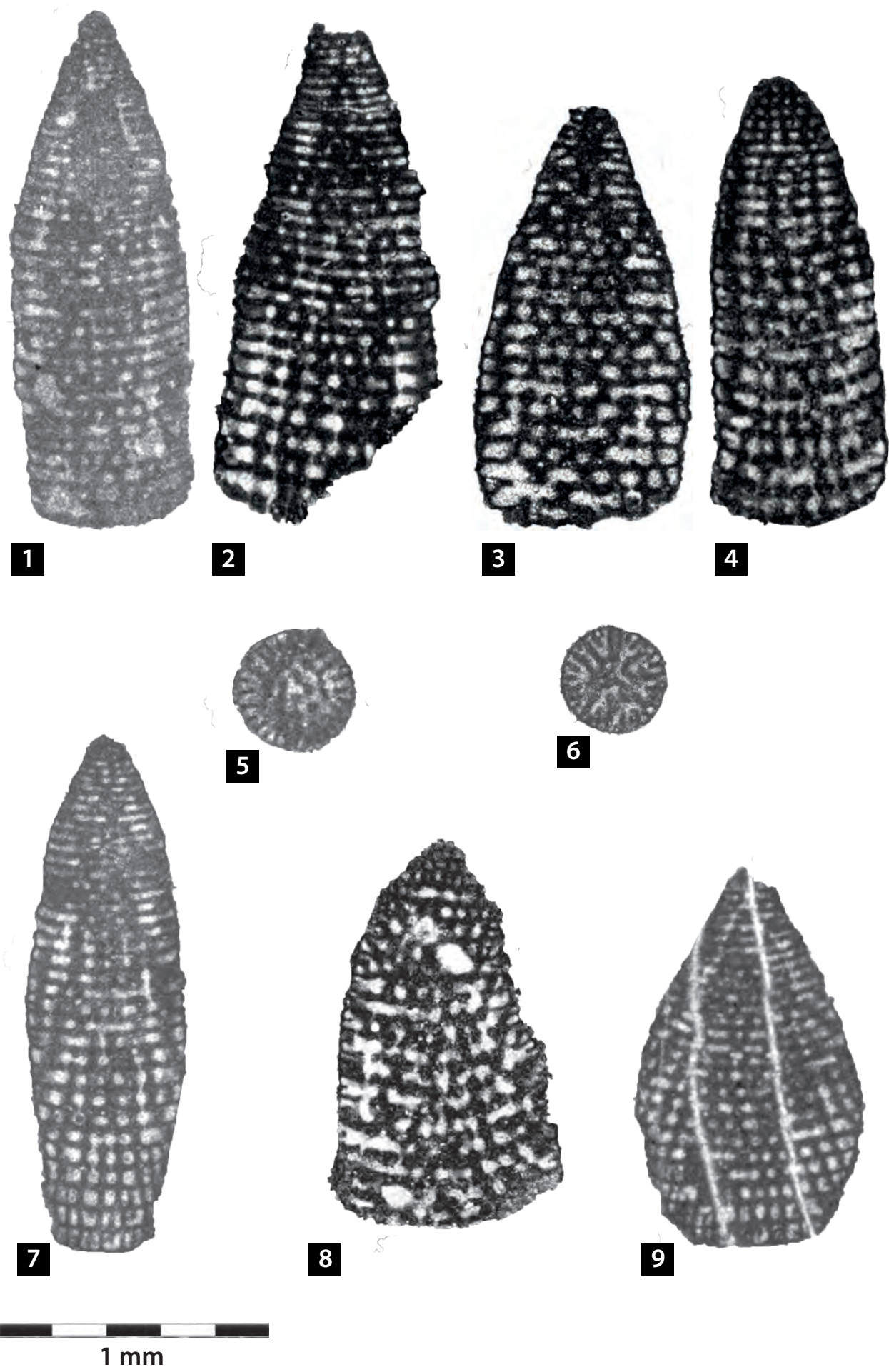
- 1/ *Palorbitolina arenaceus*, sub-axial section (Valsloch section, sample VA 63, TST A1)
- 2/ *Palorbitolina lenticularis lenticularis*, axial section through the embryonic apparatus (Morschach section, sample MC 43, mfs A1)
- 3/ *Palorbitolina lenticularis* with annular chambers, transverse section (Valsloch section, sample VA 45, TST A1)
- 4/ *Palorbitolina lenticularis*, axial section through the embryonic apparatus (Harder section, sample HA 378, HST A1)



- Nappes. *Geological Society, London, Special Publications*, **9**, 293-309.
- Revesz, K.M., Landwehr, J.M. and Keybl, J.** (2001) Measurement of delta13C and delta18O Isotopic Ratios of CaCO₃ Using a Thermoquest Finnigan GasBench II Delta Plus XL Continuous Flow Isotope Ratio Mass Spectrometer With Application to Devils Hole Core DH-11 Calcite, Geological Survey Reston VA.
- Ribaux** (2012) *Etude stratigraphique, sédimentologique et géochimique d'une succession helvétique de plateforme externe: l'intervalle Barrémien–Aptian du Brienzer Rothorn (Ct Berne)*, Msc thesis, University of Lausanne, unpublished work.
- Rick, B.** (1985) Geologie des Fluhbrig (Kt. Sz) unter besonderer Berücksichtigung der Alt-mannschichten und der “Gault”-Formation. Unpublished diploma thesis, ETH Zürich, 83 pp.
- Rosenbaum, G. and Lister G.** (2004). Formation of arcuate orogenic belts in the western Mediterranean region. *Spec. Pap. Geol. Soc. Am.*, **8**, 107– 130.
- Ruffell, A., Mc Kinley, J. and Worden, R.** (2002) Comparison of clay mineral stratigraphy to other proxy palaeoclimate indicators in the Mesozoic of NW Europe. *Phil. Trans. R. Soc. Lond.*, **360**, 675-693.
- Santantonio, M., Scrocca, D. and Lipparini,**
- L.** (2013) The Ombrina-Rospo Plateau (Apulian Platform): Evolution of a Carbonate Platform and its Margins during the Jurassic and Cretaceous. *Marine and Petroleum Geology*, **42**, 4-29.
- Schneeberger W.** (1927): Die stratigraphischen Verhältnisse von Kreide und Tertiär der Randkette nördlich des Thunersees. *Mitt. naturf. Ges. Bern* 1926.
- Schenk, K.** (1992) *Die Drusberg– und Schratzenkalk Formation (Unterkreide) im Helvetikum des Berner Oberlandes (2 vol)*. PhD thesis, University of Bern.
- Stampfli, G.M.** (1993) Le Briançonnais, terrain exotique dans les Alpes? *Eclogae Geologicae Helvetiae* , **86** ,1, 1– 45.
- Stein, M.** (2011) *Paleoenvironmental evolution of the Helvetic shallow-water carbonate platform near the Barremian-Aptian boundary, and its relationship with paleoceanographic and paleoclimatic change in the Tethys*. PhD thesis, University of Lausanne, Lausanne, 209 pp.
- Stein, M., Arnaud-Vanneau, A., Adatte, T., Fleitmann, D., Spangenberg, J.E. and Föllmi, K.B.** (2012a) Palaeoenvironmental and palaeoecological change on the northern Tethyan carbonate platform during the Late Barremian to earliest Aptian. . *Sedimentology*, **59**, 939–963.
- Stein, M., Westermann, S., Adatte, T., Mat-**

Plate 4.5

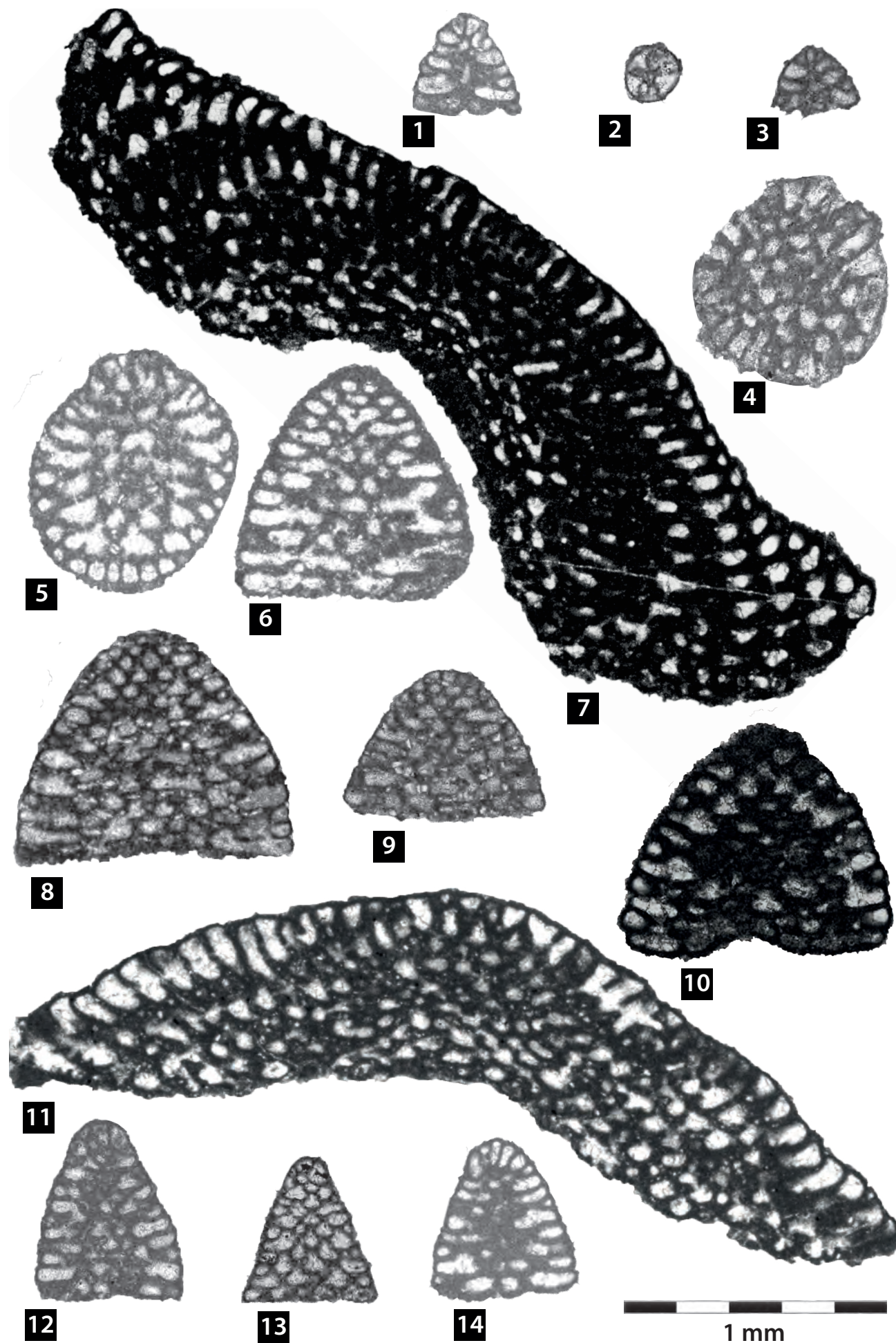
- 1/ *Paracoskinolina maynci*, sub-axial section (Valsloch section, sample VA 14, HST A1)
- 2/ *Paracoskinolina maynci*, sub-axial section (Morschach section, sample MC 99, HST B5)
- 3/ *Paracoskinolina maynci*, sub-axial section (Tierwis section, sample TW 100, TST B5)
- 4/ *Paracoskinolina maynci*, sub-axial section (Justistal section, sample LB 36, HST B5)
- 5/ *Paracoskinolina maynci*, transverse section (Valsloch section, sample VA 102, TST B5)
- 6/ *Paracoskinolina arcuata*, transverse section (Tierwis section, sample TW 145, HST A1)
- 7/ *Paracoskinolina arcuata*, sub-axial section (Tierwis section, sample TW 144, HST A1)
- 8/ *Paracoskinolina arcuata*, sub-axial section (Tierwis section, sample TW 156, HST A1)
- 9/ *Paracoskinolina arcuata*, sub-axial section (Valsloch section, sample VL 26, TST A1)



- era, V., Fleitmann, D., Spangenberg, J.E. and Föllmi, K.B.** (2012b) Late Barremian - Early Aptian palaeoenvironmental change: The Cassis-La Bédoule section, southeast France. *Cretaceous Research*, **37**, 209-222.
- Swart, P.K. and Eberli, G.** (2005) The nature of the $\delta^{13}\text{C}$ of periplatform sediments: implications for stratigraphy and the global carbon cycle. *Sedimentary Geology*, **175**, 115-129.
- Trümpy, R.** (1960) Paleotectonic evolution of the central and western Alps. *Bull. Soc. Geol. Am.*, **71**, 843– 908.
- Trümpy, R.** (1969) Die helvetischen Decken der Ostschweiz: Versuch einer palinspastischen Korrelation und Ansätze zu einer kinematischen Analyse. *Eclogae geol. Helv.*, **62**, 105–142
- Trümpy, R.** (1980) *Geology of Switzerland: A guide-book. Part A: An Outline of the Geology of Switzerland*. Wepf & Co. Publishers, Basel - New York, 334 pp.
- Vail, P.R., Mitchum, R.M.J., Todd, R.G., Widmeri, J.W., Thompson, S., Sangree, J.B., Bubb, J.N. and Hatelid, W.G.** (1977) Seismic stratigraphy and global changes of sea level. In: *Seismic stratigraphy. Application to hydrocarbon exploration*, Am. Assoc.
- Pet. Geol. Mem.*, **26**, pp. 49-212, Tulsa.
- van de Schootbrugge, B., Kuhn, O., Adatte, T., Steinmann, P. and Föllmi, K.B.** (2003) Decoupling of P- and Corg-burial following Early Cretaceous (Valanginian-Hauterivian) platform drowning along the NW Tethyan margin. *Palaeogeography, Palaeoclimatology, Palaeoecology*, **199**, 315-331.
- Vermeulen, J.** (2005) Boundaries, ammonite fauna and main subdivisions of the stratotype of the Barremian. In: *The Hauterivian-Lower Aptian Sequence Stratigraphy from Jura Platform to Vocontian Basin: A Multidisciplinary Approach* (Eds T. Adatte, A. Arnaud-Vanneau, H. Arnaud, M.-C. Blanc-Alétru, S. Bodin, E. Carrio-Schaffhauser, K.B. Föllmi, A. Godet, M.C. Raddadi and J. Vermeulen), Géol. Alpine, Sér. Spéc. “Colloques et Excursions” No. **7**, 147–173.
- Wildi, W., Funk, H. and Loup, B.** (1989) Mesozoic subsidence history of the European marginal shelves of the alpine Tethys (Helvetic realm, Swiss Plateau and Jura). *Eclogae geol. Helv.*, **82**, 870-840.
- Wissler, L.** (2001) *Response of early cretaceous sedimentary systems to perturbation in global carbon cycling: insights from stra-*

Plate 4.6

- 1/ *Orbitolinopsis pygmaea*, sub-axial section (Valsloch section, sample VL 23, TST A1)
- 2/ *Orbitolinopsis pygmaea*, transverse section (Tierwis section, sample TW 129, HST A1)
- 3/ *Orbitolinopsis pygmaea*, sub-axial section (Tierwis section, sample TW 129, HST A1)
- 4/ *Orbitolinopsis kiliani*, transverse section (Valsloch section, sample VA 45, TST A1)
- 5/ *Orbitolinopsis briacensis*, sub-axial section (Valsloch section, sample VA 6, HST A1)
- 6/ *Orbitolinopsis briacensis* ?, sub-axial section (Valsloch section, sample VA 23, TST A1)
- 7/ *Orbitolinopsis buccifer*, sub-axial section (Morschach section, sample MC 15, HST A1)
- 8/ *Orbitolinopsis briacensis*, sub-axial section (Tierwis section, sample TW 137, HST A1)
- 9/ *Orbitolinopsis kiliani*, sub-axial section (Tierwis section, sample TW 123, HST A1)
- 10/ *Orbitolinopsis kiliani*, sub-axial section (Morschach section, sample MC 15, HST A1)
- 11/ *Orbitolinopsis buccifer*, sub-axial section (Morschach section, sample MC 95, HST B5)
- 12/ *Orbitolinopsis cuvillieri*, sub-axial section (Valsloch section, sample VL 19, TST A1)
- 13/ *Orbitolinopsis cuvillieri*, sub-axial section (Tierwis section, sample TW 130, HST A1)
- 14/ *Orbitolinopsis cuvillieri*, sub-axial section (Valsloch section, sample VA 70, TST A1)



- tigraphy, sedimentology and geological modeling, ETH Zürich.
- Wissler, L., Funk, H. and Weissert, H.** (2003) Response of Early Cretaceous carbonate platforms to changes in atmospheric carbon dioxide levels. *Palaeogeography, Palaeoclimatology, Palaeoecology, Volume 200*, Pages 187-205.
- Wyssling, G.W.** (1986) Der frühkretazische helvetische Schelf im Vorarlberg und Allgäu. *Jahrbuch der Geologischen Bundesanstalt, 129*, 161–265.
- Zerlauth, M., Ortner, H., Pomella, H., Adrian Pfiffner, O. and Fügenschuh, B.** (2014) Inherited tectonic structures controlling the deformation style: an example from the Helvetic nappes of the Eastern Alps. *Swiss Journal of Geosciences, 107*, 157-175.
- Ziegler, M.A.** (1967) A study of the Lower Cretaceous facies developments in the Helvetic border chain, north of the Lake of Thun (Switzerland). *Eclogae Geologicae Helveticae, 60*, 509-528.

Chapter 5 – Main conclusions



Fig. 5 Dissolved nerinid infilled by vadose silt (Rawil section, sample RW 76).

Chapter 5

Main conclusions

The influence of paleoclimatic and paleoenvironmental conditions on the development of the platform was put forward in this thesis through the study of the evolution of palaeoecosystems and paleobathymetric indicators.

The Helvetic platform recorded three main phases of falling sea level, (1) at the base of the Lower Schrattenkalk Mb in its inner part (SB B3), (2) at the top of this member (SB A1), (3) and finally at the top of the Upper Schrattenkalk Mb (SB A1). These episodes were highlighted both by sedimentological observations (karstification, paleofractures, paleosols, lag), as well as by the carbon-isotope record (negative shifts, especially for the last two episodes). The response of ecosystems to these eustatic fluctuations shows similarities, despite the different contexts in all three cases. The transgressive phases following these sequence boundaries are accompanied by a change in the type of dominant organisms.

The first emersion occurred on top of hemipelagic series, over which the sedimentation of the shallow-water carbonate platform started. The first phase of transgression following SB B3 allows the development of large bioclastic lowstand systems tracts in external parts, while in inner parts we observe the development of organisms characteristic of mesotrophic conditions (annelids, orbitolinids, flat *Choffatella*). Such environments spread over the entire platform, with a deepening of depositional environments, which peaked at mfs B3. This range corresponds in the distal part of the platform to the condensation phase of the Chopf bed. According to Föllmi (2012), a brief climate change towards warmer and more humid conditions might be related to this condensation. HST B3 shows a shallowing-upward, until the installation of rudist facies (Urgonian-platform *sensu stricto*) in the inner and intermediate parts of the platform.

The second transgression (TST A1) also includes the installation of mesotrophic fauna within the member of Rawil. A detailed study of microfacies and environmental markers revealed an evolution on the Helvetic platform similar to that found in other subalpine platforms, inspite of their separation by several hundred kilometers. These observations show how this phenomenon is beyond the regional framework in terms of its importance. Stein et al. (2012) has highlighted climate change to warmer and more humid conditions, which may have accelerated continental weathering, increasing the nutrient transfer rate to the oceans. This phase of eutrophication is followed by a recovery of the photozoan-type carbonate production as documented in the Upper Schrattenkalk Mb.

The last emergence recorded by this platform, on the top surface of the Upper Schrattenkalk Mb, appears to have been related to a major drop in sea level, as we found traces of karstification on the entire platform, in depths of maximally 20m underneath the emersion surface. The demise of the photozoan Urgonian-type Helvetic platform occurred with this emersion. This termination is synchronous for a majority of carbonate platforms of the same age (Föllmi and Gainon, 2008). The climatic conditions intensified to lead to the global oceanic anoxic event A1. In the Helvetic nappes,

the top of the Schrattenkalk formation is drowned and covered by a condensed level followed by the deposition of heterozoan-type sediments (Grünten Mb).

These observations highlight a strong link between eustatic variations and climatic perturbations. Indeed, transgression phases seem to have been accompanied by short phases of intensified greenhouse climate.

Geochemical studies showed a strong influence of facies and lithology on the carbon isotope record, which interfered with the overall record. The isotope records show a strong enrichment in heavy carbon isotopes during the installation of lagoonal facies, probably related to the increasing aragonite content. The presence of karst modified negatively the isotopic record, and the levels showing abundant echinoderms in the Member Rawil seem also to record a similar trend, probably due to the high porosity of these organisms promoting diagenesis. These observations show that the use of chemostratigraphy on shallow-water carbonate platform should be taken with caution and should be done as part of a multidisciplinary study to differentiate the overall record from local effects.

Finally the study of the distribution of facies in space and time shows a strong progradation of the platform during the latest Barremian, despite the important paleotopographic heritage. Maximum progradation is reached in the sequence B5. The fact that the sequence A1 does not exceed the level of progradation of the sequence B5 raises the issue of the platform edge type. The variations in subsidence suggest the presence of a platform edge structured by listric fault systems perpendicular to the direction of progradation. However no evidence of fault breccias have been found which could confirm the presence of a bypass border in this region.

References

- Föllmi, K.B. (2012) Early Cretaceous life, climate and anoxia. *Cretaceous Research*, **35**, 230-257.
- Föllmi, K.B. and Gainon, F. (2008) Demise of the northern Tethyan Urgonian carbonate platform and subsequent transition towards pelagic conditions: The sedimentary record of the Col de la Plaine Morte area, central Switzerland. *Sedimentary Geology*, **205**, 142-159.
- Stein, M., Arnaud-Vanneau, A., Adatte, T., Fleitmann, D., Spangenberg, J.E. and Föllmi, K.B. (2012) Palaeoenvironmental and palaeoecological change on the northern Tethyan carbonate platform during the Late Barremian to earliest Aptian. . *Sedimentology*, **59**, 939–963.

Chapter 6 – Appendix

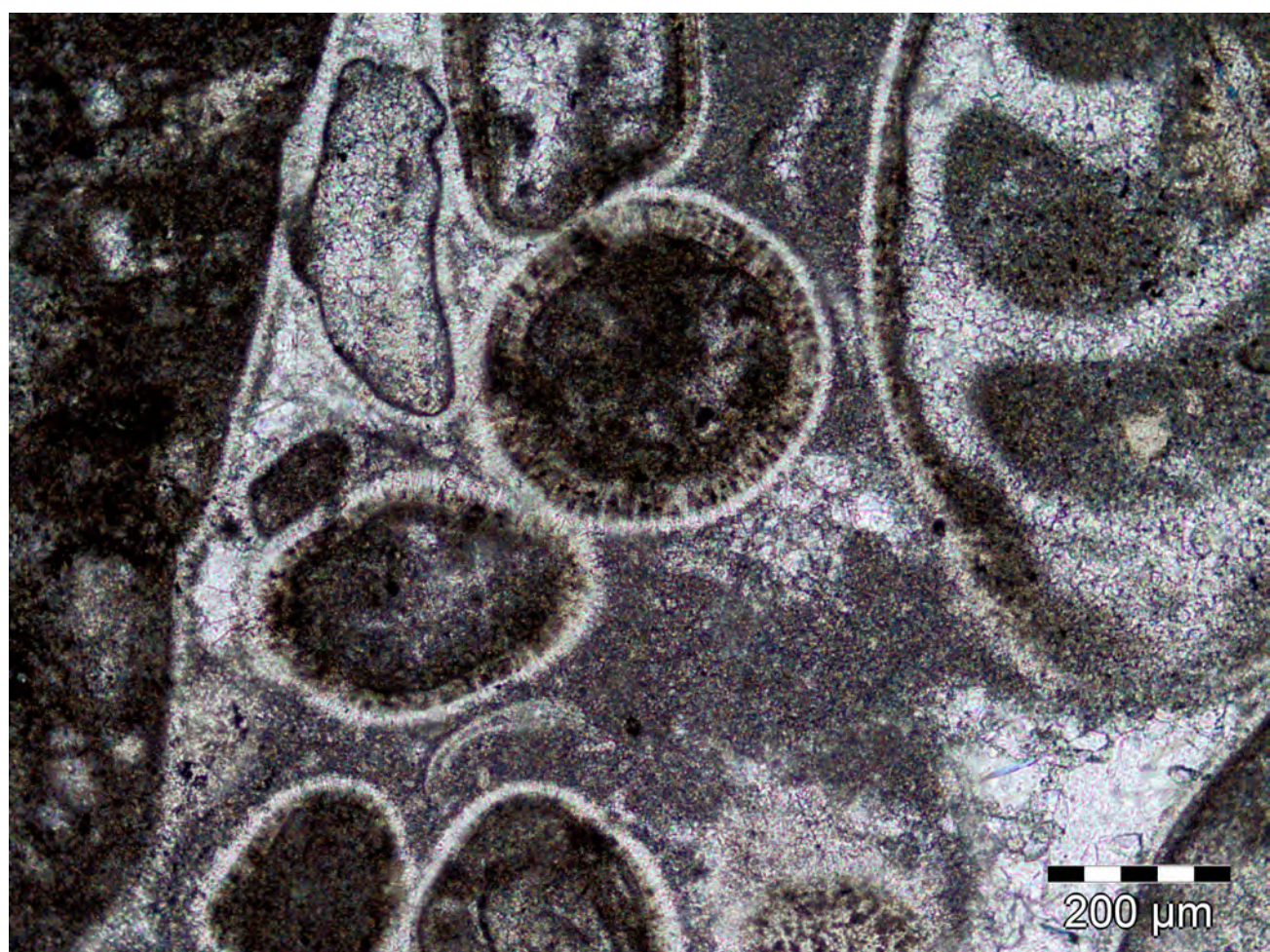


Fig. 6 Early aragonitic rimmed cement (Tierwis section, sample TW 69).

6.1 Affiliated paper

Deciphering the message of Early Cretaceous drowning surfaces from the Helvetic Alps: What can be learnt from platform to basin correlations?

ALEXIS GODET^{a*}, KARL B. FÖLLMI^a, JORGE E. SPANGENBERG^a, STÉPHANE BODIN^b, JEAN VERMEULEN^c, THIERRY ADATTE^a, LUCIE BONVALLET^a and HUBERT ARNAUD^d

^aUniversity of Lausanne, Institute of Earth Sciences, UNIL Mouline, Geopolis building, CH-1015 Lausanne, Switzerland

^bRuhr-Universität, Bochum, Institute for Geology, Mineralogy and Geophysics, Universitätsstrasse 150, D-44801 Bochum, Germany

^cGrand Rue, F-04330 Barrême, France

^dAssociation Dolomieu, F-38000 Grenoble, France

*Corresponding author. Email address: alexis.godet@unil.ch

Published in *Sedimentology*, Vol. 60, 2013, pp. 152-173

Abstract

Drowning unconformities are a frequent feature of carbonate platforms and generally express the incapacity of shallow-marine ecosystems to adapt to abrupt sea-level rise and/or palaeoenvironmental change. During the late Hauterivian and early Barremian, the Helvetic carbonate platform experienced a major drowning phase documented by the phosphate and glauconite-rich Altmann Member. It has been shown that a drowning unconformity in the form of a hardground at the base of the Altmann Member on the Pilatus summit (central Switzerland) results from a complex, polyphased diagenetic history which includes two main phases of phosphogenesis. Using carbon-isotope stratigraphy, biostratigraphy and sequence stratigraphy, the correlation of this drowning unconformity from the Helvetic domain with more distal and more complete sedimentary archives allows reconstruction of the sequence-stratigraphic

context of the drowning surface, and also an estimation of the amount of time represented by the episodes of condensation. Unconformities associated with the Altmann Member drowning phase developed during transgressive episodes, when strong currents arrived onto the previously subaerially exposed platform, and periods of phosphogenesis may have lasted up to 2.8 Ma. Variations in trophic levels and hitherto less well-known intervening emersion phases played an essential triggering role for the Altmann drowning phase. High-resolution studies of drowning unconformities unravel the diversity of palaeoenvironmental parameters involved in the unfolding of such crises during the evolution of carbonate platforms.

Keywords

Helvetic carbonate platform; phosphogenesis; drowning; diagenesis; subaerial exposure, Hauterivian, Barremian

6.1.1 Introduction

Drowning surfaces constitute some of the most intriguing unconformities within carbonate successions. In geological archives, these unconformities are expressed by the superposition of (hemi-)pelagic or authigenic sediments on top of carbonates deposited in shallow-marine platform settings (Schlager 1981 and references therein; see also Föllmi et al., 1994; 2006; Mutti et al., 1997; Schlager, 1998; Bodin et al., 2006b; Gawlick & Schlagintweit, 2006; Sattler et al., 2009; Marino & Santantonio, 2010); this reflects a rapid increase in accommodation space by enhanced subsidence rates or eustatic sea-level, which outpaces the capacity of shallow-marine ecosystems to produce carbonate within the photic zone (e.g. Schlager, 1981; Catuneanu, 2006). From a sequence stratigraphic point of view, drowning unconformities can be interpreted either as sequence boundaries (SB) or maximum flooding surfaces (mfs), depending on the depiction of an intervening emergent phase (e.g. Catuneanu, 2006). Drowning unconformities have been associated with platform emersion prior to the drowning phase, as indicated by karstification features, and in such cases the drowning surfaces were identified as sequence boundaries (Camoin et al., 1998; Schlager, 1998; Marino & Santantonio, 2001). Emersion may also be evidenced by the presence of rhizoliths, early dissolution of aragonite particles or early dolomitisation (e.g. Camoin et al., 1998; Immenhauser et al., 2000). On the other hand, emersion may not necessarily constitute a prerequisite for drowning. The drowning unconformity may represent a maximum flooding surface or a type-3 sequence boundary, which is formed during transgression following a sea-level highstand, without intervening eustatic sea-level fall (Schlager, 1999). For

example, based on petrographic and geochemical data, Wilson et al. (1998) concluded that the drowning of five different Pacific Guyots during the Cretaceous was not preceded by emersion, because the cements held only slightly negative oxygen isotope ratios ($\delta^{18}\text{O}$ values versus Vienna Pee Dee belemnite standard, VPDB) and positive carbon isotope ratios ($\delta^{13}\text{C}$). This geochemical evidence was, however, challenged by textural and facies-related indications for emersion and karstification (for example, calcrete horizons, dissolution cavities with speleothems and geopetal infills; Sager et al., 1993), thus highlighting the complexity of drowning surfaces in general. The understanding of the drowning of a platform (emersion and/or rapid flooding, eutrophication) is fundamental for understanding the recovery processes of shallow-marine ecosystems responding to major environmental crises. The estimation of the time included within such key surfaces is also problematic and gains a special interest, because they often represent several sequence boundaries and thus major time gaps in shallow-marine deposits.

In the well-preserved Lower Cretaceous succession of the northern Tethyan margin in France and Switzerland, several key horizons have been interpreted as drowning surfaces (e.g. Funk et al., 1993; Föllmi et al., 1994, 2006, 2007; Weissert et al., 1998; Huck et al., 2011; Masse & Fenerci-Masse, 2011; Stein et al., 2012, among others). Spanning a period ranging from the late Hauterivian up to the early to late Barremian transition (*Pseudothurmannia seitzi* to *Coronites darsi* ammonite zones; Bodin et al., 2006b), the Altmann Member (Mb) in the Helvetic Alps is of special interest since it corresponds to a major turning point in the evolution of the Helvetic carbonate platform. This lithostratigraphic unit documents a phase of major condensation and associated authigenesis

of phosphate and glauconite in the Helvetic platform, which is interpreted as expression of a major and long-lasting platform-drowning phase (e.g. Funk et al., 1993; Föllmi et al., 1994, 2006, 2007). The platform-drowning phase separated a period of platform growth in a heterozoan mode, dominated by crinoid–bryozoan–sponge ecosystems, during most of the Hauterivian from a subsequent period of platform growth in a combined heterozoan–photozoan mode, including green algal–coral–rudist–stromatoporoid ecosystems, during the late Barremian. In most sections, the base of the Altmann Member is materialised by a phosphatic hardground, which is condensed and represents several stacked sequence boundaries (Bodin et al., 2006b). The strong degree of condensation renders difficult the differentiation of the superimposed sequence boundaries, the determination of their exact age, and also their attribution to specific eustatic cycles.

The goal of this article is to precisely document the sedimentary and diagenetic processes which led to the formation of the phosphatic hardground in the Helvetic Altmann Member. For this purpose, the highly condensed Pilatus section was investigated, which was located in an intermediate platform position. A correlation is proposed with two more expanded sections from the Helvetic Alps (Tierwis) and the Provence region (Clos de Barral), by combining and comparing biostratigraphic, sequence stratigraphic and chemostratigraphic anchor points. This correlation may unravel potential time gaps associated with drowning episodes examined in this study, and may also help in estimating their duration. Such an approach aims to: (i) shed more light on the sequential framework in which the drowning surfaces developed; and (ii) provide more information on the character and timing of palaeoceanographic phenomena that were invol-

ved in the development of the drowning surfaces considered here. Splitting the Altmann Member drowning unconformity into several sequence stratigraphic key-surfaces may also bring new insights into the general understanding of such episodes, in particular their relation with more widespread palaeoceanographic change.

6.1.2 Geological setting and location of the studied sections

The shallow-water Pilatus and Tierwis sections in the vicinity of the cities of Luzern and Appenzell, respectively, are located within the Helvetic Alps of Switzerland (Fig. 6.1). Sediments of these sections were deposited on a vast, shallow-water carbonate platform that developed from the latest Jurassic to the late Early Cretaceous over a lateral distance of more than 2500 km (Golonka, 2004). These sediments have subsequently been involved in the Alpine orogenesis, creating the Helvetic thrust and fold belt. Palinspastic reconstruction of proximal to distal transects highlighted the importance of condensation in the history of this platform (Funk et al., 1993). The hemipelagic Clos de Barral section crops out in the south of France near the Clavel pass (region of Var), and its sediments were deposited on the southern slope of the Vocontian Basin, where condensation was highest during the Barremian (e.g. Goguel, 1944).

6.1.2.1 The Pilatus section

The Pilatus section is relatively condensed, because the Altmann Member

does not exceed 8 m. The lower part of the section comprises upper Hauterivian bioclastic grainstone belonging to the upper Kieselkalk Member ('Echinodermenbreccie bed'; Bodin et al., 2006b). This 1.5 m thick bed is topped by a phosphatic and glauconitic hardground. The hardground is covered by two beds (4 m and 3 m thick) composed of glauconite-rich, bioclastic wackestone to packstone, which have been interpreted as gravity-flow deposits (Bodin et al., 2006b). Finally, a thick marly interval marks the end of the Altmann Member and the following Drusberg Member is characterized by alternations of limestone and marl.

Bodin et al. (2006b) provided a sequence-stratigraphic interpretation (Fig. 6.2) for the Pilatus section and proposed the superposition of five sequence boundaries (SB Ha6 to SB Ba2) within the phosphatic and iron-bearing hardground. The mfs Ba2 is interpreted to be present in the marly interval of the Altmann Member.

6.1.2.2 The Tierwis section

The 56 m thick Tierwis section (Fig. 6.3) has been logged and described in detail by Bodin et al. (2006b). The top of the Kieselkalk Formation (bioclastic grainstone) is marked by an erosive surface, which is covered by sediments rich in bryozoans and crinoids (8 m). An ammonite-bearing bed (indicating the *Pseudothurmannia ohmi* to *Balearites mortilleti* ammonite zones interval) follows at 10 m depth; it has been interpreted as the climax of a deepening-upward trend (Bodin et al., 2006b). This bed is succeeded by a 17 m thick interval of packstone with peloids, bioclasts and, to a lesser extent, crinoids. Several bioturbated horizons precede the main condensed interval, which corresponds to a phosphatic and glauconitic hardground. Ammonites were found in this stratigraphic level, dating it to the (late) *Nicklesia pulchella* to *Kotetishvilia compressissima* ammonite zones. On the other hand, ammonites found in a marly interval 3 m above this hardground are indicative

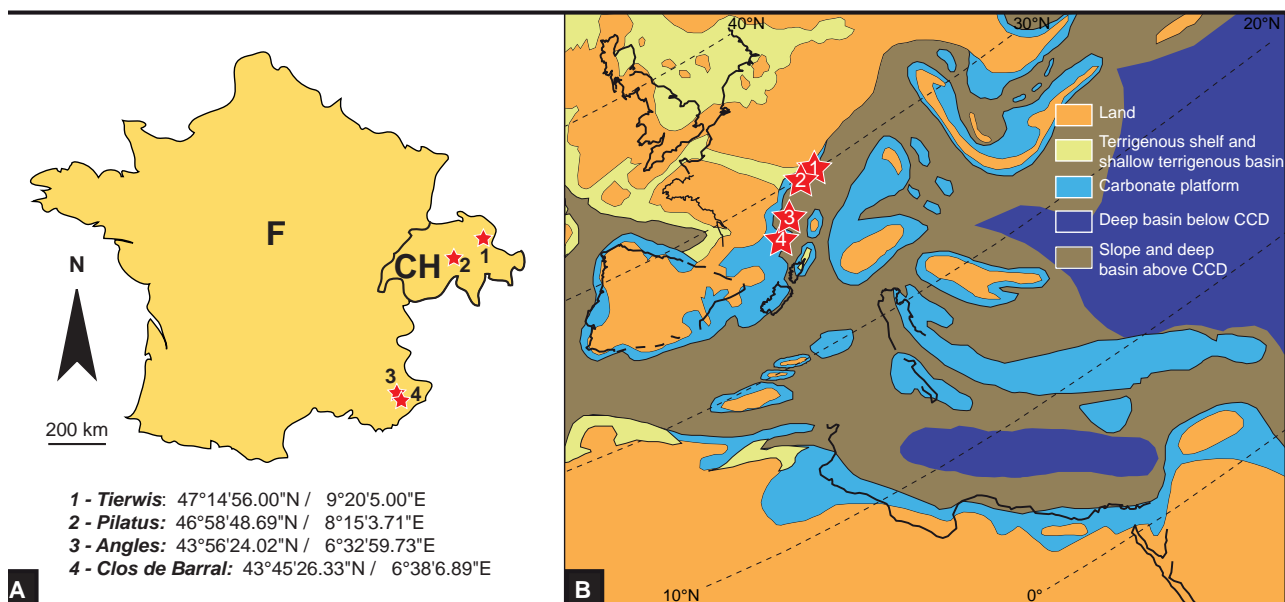


Fig. 6.1 Location of the Pilatus, Tierwis, Clos de Barral and Angles sections on present-day geography (A) and Early Cretaceous (early Aptian) palaeogeographic reconstruction (modified after Masse et al., 1993).

Pilatus section

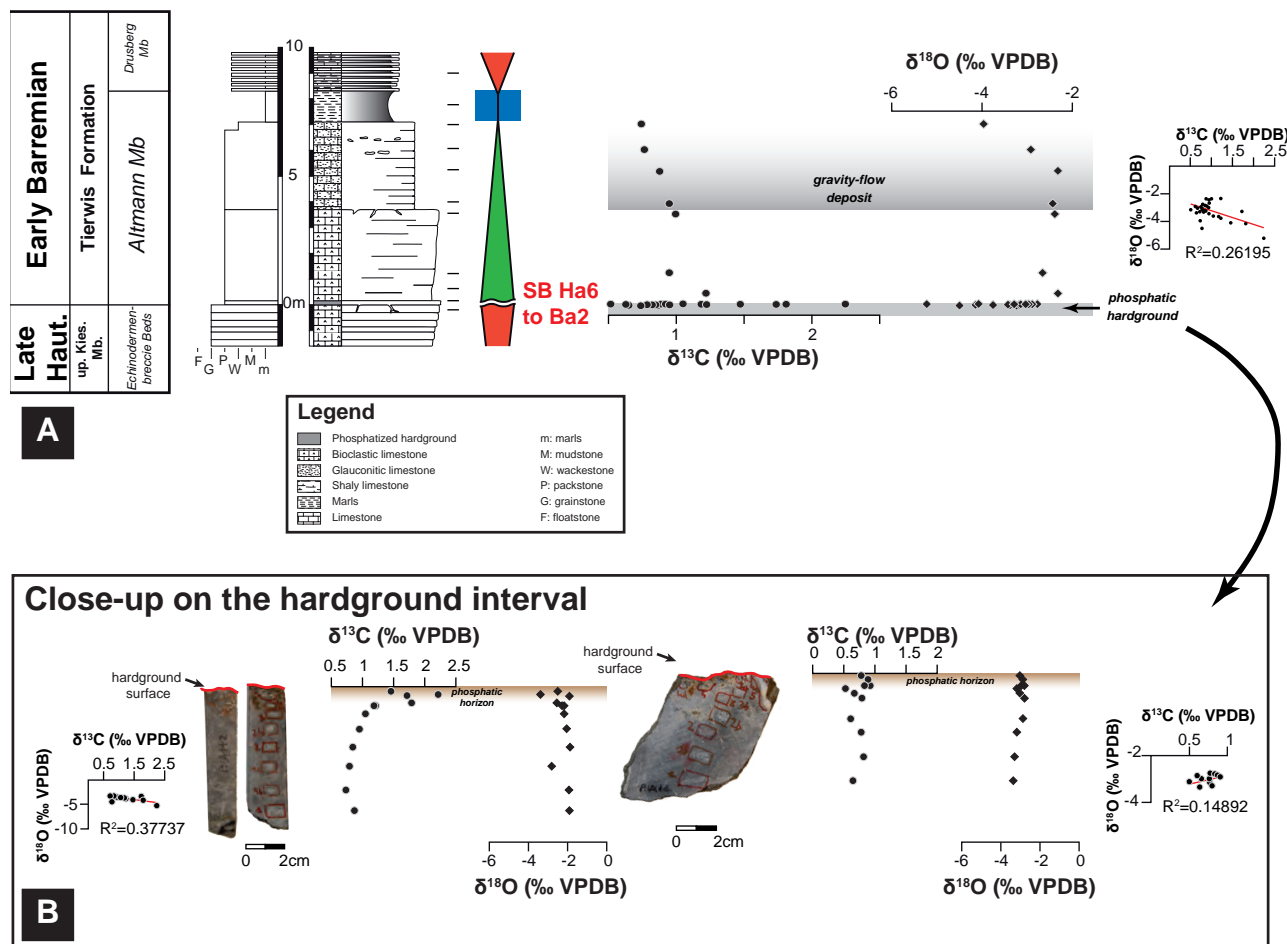


Fig. 6.2 Sedimentary succession of the Pilatus section showing the boundary between the Upper Kieselkalk Member and the Tierwis Formation, exhibiting the phosphatic hardground at the base of the Altmann Member (A). Carbon and oxygen stable isotopes have been measured for bulk-rock samples, especially in the 5 cm below the hardground surface where a high-resolution signal has been achieved using a microsampling device (B). Lithological, sequence stratigraphy and dating after Bodin et al. (2006b).

of the *K. compressissima* ammonite zone (Bodin et al., 2006b). After a last interval of bioturbated and spicule-rich biomicrite, the onset of marl and alternations of limestone and marl mark the base of the Drusberg Member.

Following the sequence stratigraphic framework for the Tierwis section (Fig. 6.3) of Bodin et al. (2006b), the siliceous and phosphatic hardground in the upper part of the Altmann Member includes three stacked sequence boundaries (SB Ba1, SB Ba1' and SB Ba2). Maximum flooding surface Ba2 coincides with a marly interval near the top of the Altmann Member, whereas the SB Ba3 caps a several

metre thick limestone bed which is overlain by a marl-limestone alternation.

6.1.2.3 The Clos de Barral section

The 82 m thick Clos de Barral section is mainly composed of white to grey limestone beds with subordinate marly intervals, which correspond to hemipelagic facies deposited on the drowned Provencal platform (Arnaud, 2005a). The faunal content includes numerous ammonites and belemnites, and to a lesser extent bivalves and echinoids. Glauconite represents up

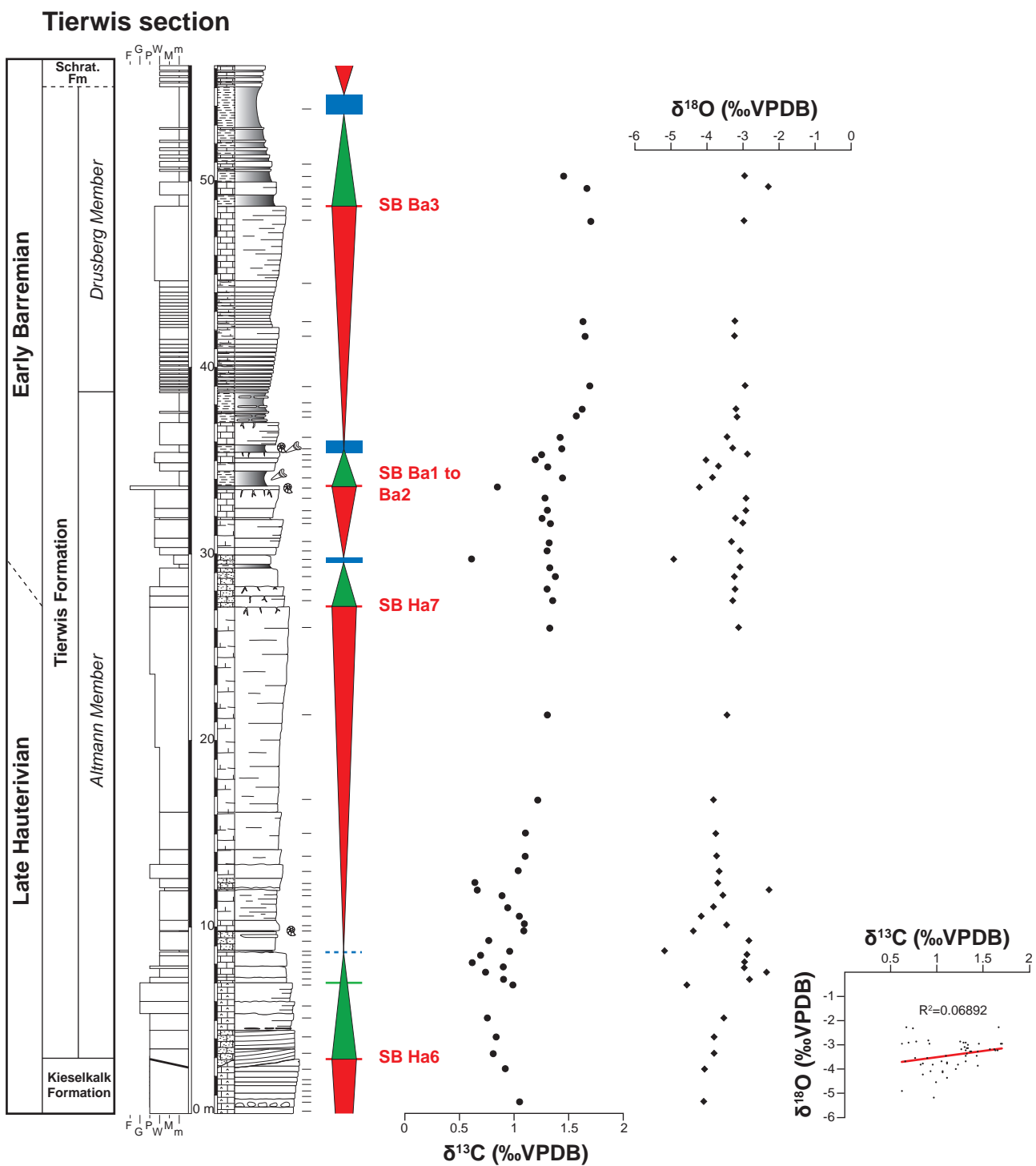


Fig. 6.3 Sedimentary succession and sequence stratigraphic interpretation of the Tierwis section (modified after Bodin et al., 2006b). Several ammonite-bearing levels ensure the precise dating of the upper part of the Altmann Member (see Bodin et al., 2006b for the corresponding fossil list). The evolution of the carbon and oxygen stable isotope composition is reported alongside the section, whereas a $\delta^{13}\text{C}$ versus $\delta^{18}\text{O}$ (right-hand side of the figure) reveals no correlation.

to 30 to 35% in discrete horizons at 52.5 m and 61 m depth, as shown in Fig. 6.4. The layers have been dated as *Psilotissotia colombiana* subzone to lowermost *Kotetishvilia nicklesi*, *N. pulchella* to *C. darsi* and *Heinzia sayni* ammonite zones. A first age model by means of ammonite bios-

trigraphy was provided for the entire section by Vermeulen (1980) which was subsequently revised (e.g. Vermeulen, 2002, 2005; Arnaud, 2005a).

Arnaud (2005a) developed a sequence-stratigraphic framework for the hemipe-

lagic Clos de Barral section (Fig. 4). Following this author, the transitions between thinly-bedded intervals and thick limestone beds represent sequence boundaries. Thick marly intervals were interpreted as maximum flooding surfaces, characterized by the highest abundance and diversity of ammonites. According to Arnaud (2005a), transgressive surfaces (TS) would occur at the base of thickening-upward successions in limestone beds (see the explanatory cartoon in Fig. 6.4), but these surfaces were difficult to identify in the Clos de Barral section. Moreover, Arnaud (2005a) did not observe the presence of lowstand systems tracts (LST) in this section.

6.1.3 Methods

The investigation of eight representative thin sections of the hardground at Pilatus has been performed at the Institute of Earth Sciences of the University of Lausanne using conventional optical microscopy. An Olympus BX51 microscope (Tokyo, Japan) equipped with an Olympus Altra 20 camera and Olympus Image Analysis[©] software was used for digital microphotography. The geometrical relation of grains, matrix and cements was examined under high magnification on an Olympus BX61 microscope coupled to a motorized, computer-controlled stage, and an Olympus UC30 camera. Images were captured and processed with Stream Motion[©] software. Cathodoluminescence microscopy of all thin sections was performed on an Opea Cathodyne cold-cathode luminescence device (Vincennes, France) with an acceleration voltage and a current ranging from 15 to 18 kV and from 200 to 300 μ A, respectively. Selected thin sections were subsequently leached and stained by an acid solution of alizarin red-S and potassium

ferricyanide, following the procedure of Dickson (1965). This process allows differentiation between calcite and dolomite, and between iron-rich and non-ferroan phases.

Stable-isotope analyses were completed on samples from the Pilatus ($n = 29$), Tierwis ($n = 52$) and Clos de Barral ($n = 128$) sections, at the Institute of Earth Sciences of the University of Lausanne using a Thermo Fisher Scientific carbonate-preparation device and Gas Bench II connected to a Thermo Fisher Delta Plus XL isotope ratio mass spectrometer (IRMS; Thermo Fisher Scientific, Bremen, Germany), which was operated in the continuous He flow mode. The stable carbon and oxygen-isotope ratios are reported in the delta (δ) notation as the per mil (‰) deviation relative to the VPDB. A set of aliquots of laboratory standard Carrara Marble standard, ranging from 10 to 110 μ g, was used to evaluate the linearity and correct for eventual size effects. For analysis with less than 20 μ g the error was between 0.1‰ and 0.4‰. Consequently, only samples of a weight at least 20 μ g were analysed, for which the error was better than $\pm 0.05\text{‰}$ for $\delta^{13}\text{C}$ and $\pm 0.1\text{‰}$ for $\delta^{18}\text{O}$, based on analytical reproducibility estimated from replicate analyses of Carrara Marble.

6.1.4 Results

6.1.4.1 Authigenetic and diagenetic phases composing the basal hardground of the Altmann Member at Pilatus

Based on conventional optical microscopy completed by cathodoluminescence and stable-isotope ($\delta^{13}\text{C}$, $\delta^{18}\text{O}$) data, six phases of

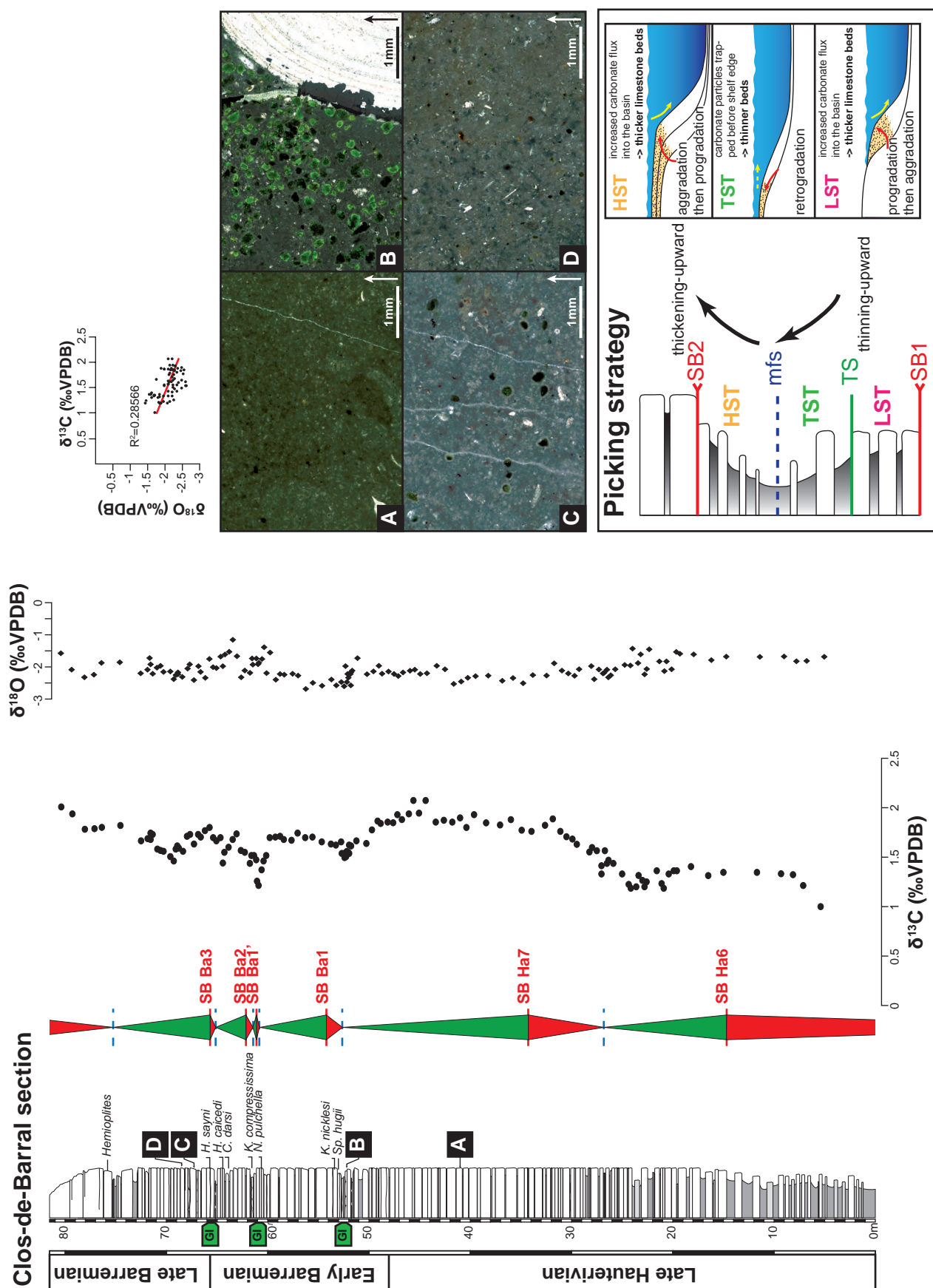


Fig. 6.4 Stable isotopes and sequence stratigraphy of the Clos de Barral section. A cartoon illustrating the strategy used to interpret sequence boundaries, transgressive and maximum flooding surfaces is provided on the right-hand side of the figure; the sequence stratigraphic interpretation is here based on the stacking pattern (variation in bed thickness), which relies on variation in carbonate production in neritic environments. On the right-hand side of the figure, microphotograph (B) illustrates facies

enriched in dark-green glauconite (Gl, up to 20%), whereas the panels (A), (C) and (D) correspond to classical mudstones of the Clos de Barral section with a glauconite content ranging from 0 to 5%.

cementation and two main phases of phosphogenesis are differentiated within the basal hardground of the Altmann Member at Pilatus. In the following, IFC, SC and BC designate ‘Isopach Fibrous Cement’, ‘Scalenohedral Cement’ and ‘Blocky Calcite’, respectively.

Microfacies associated with the Altmann hardground is composed of oolitic and bioclastic grainstone. In intergranular porosity, micrite is preferentially deposited at the bottom of pores, and is intercalated between a first phase of cementation (IFC1) and a phosphatic, dark brown infill (Fig. 6.5E and F). The presence of IFC1 between the micrite and the walls of the pore confirms this chronology; IFC1 is characterized by dull brown, 30 µm long ferroan calcite fibres, as indicated by pale pink staining. Cathodoluminescence imaging reveals the development of a second phase of cementation with dogtooth cements (SC1), which are characterized by 50 µm long crystals with non-luminescent cores and bright orange rims (Fig. 6.5A and B). The remaining porosity is filled in either by a brown phosphatic sediment which exhibits a dark blue luminescence (Ph1, reaching from the hardground surface down to *ca* 1 cm below it; Figs. 6.5C, 6.5D, 6.6C and 6.6D), or by a sparitic cement. The latter consists of blocky calcite (BC1) with well-defined twins and a dull brown luminescence with dark cores (Fig. 6.5A and B). Truncation of Ph1 by a second brown and phosphate-rich material is observed on the hardground surface itself (Ph2; Fig. 6.5C and D). Unlike Ph1, the abundance of glauconite and quartz is high in Ph2. The contact between Ph1 and Ph2 may be underlined by a thin (*ca* 10 µm) crust of isopach fibrous cement, the identification of which is made difficult by its

tiny crystals size and the dark colour of both phosphatic sediments. Ph2 seems to be found only in bioturbations that belong to the *Glossifungites* ichnofacies. Dolomite rhombs are found within Ph2, whereas they are absent in Ph1 (Fig. 6.6A and B). Cathodoluminescence reveals the presence of two types of dolomitic minerals. The first one (Dol1) is characterized by large (mean values for diagonals of 153 µm and 117 µm), idiopathic and equigranular rhombs with a cloudy centre, exhibiting twins and dull, brown to orange luminescence similar to that of BC1. The second dolomite type (Dol2) is composed of smaller (mean values for diagonals of 117 µm and 108 µm), equigranular and idiopathic rhombs with dark cores and bright orange to reddish luminescent, thick rims. Rhombs belonging to the latter type are also apparent in the former type of dolomite. Finally, calcitic veins are filled by dark brown, dull luminescence cement, BC2. The veins are cross-cutting grains, IFC1, SC1 and Ph1 (Fig. 6.6C and D).

The carbon and oxygen-isotope composition of BC1, BC2, Ph1 and Ph2 phases are reported in Fig. 7. All analysed sparitic or phosphatic areas hold negative $\delta^{18}\text{O}$ values ranging between -3‰ and -6.2‰. BC1, BC2 and Ph1 have $\delta^{13}\text{C}$ values from 0.1 to 1.2‰, with a progressive enrichment in heavy isotopes from BC1 and BC2 to Ph1. A trend toward lighter values (up to 2.0‰) is observed for Ph2 microsamples.

6.1.4.2 Late Hauterivian to Barremian isotope records

The Pilatus section

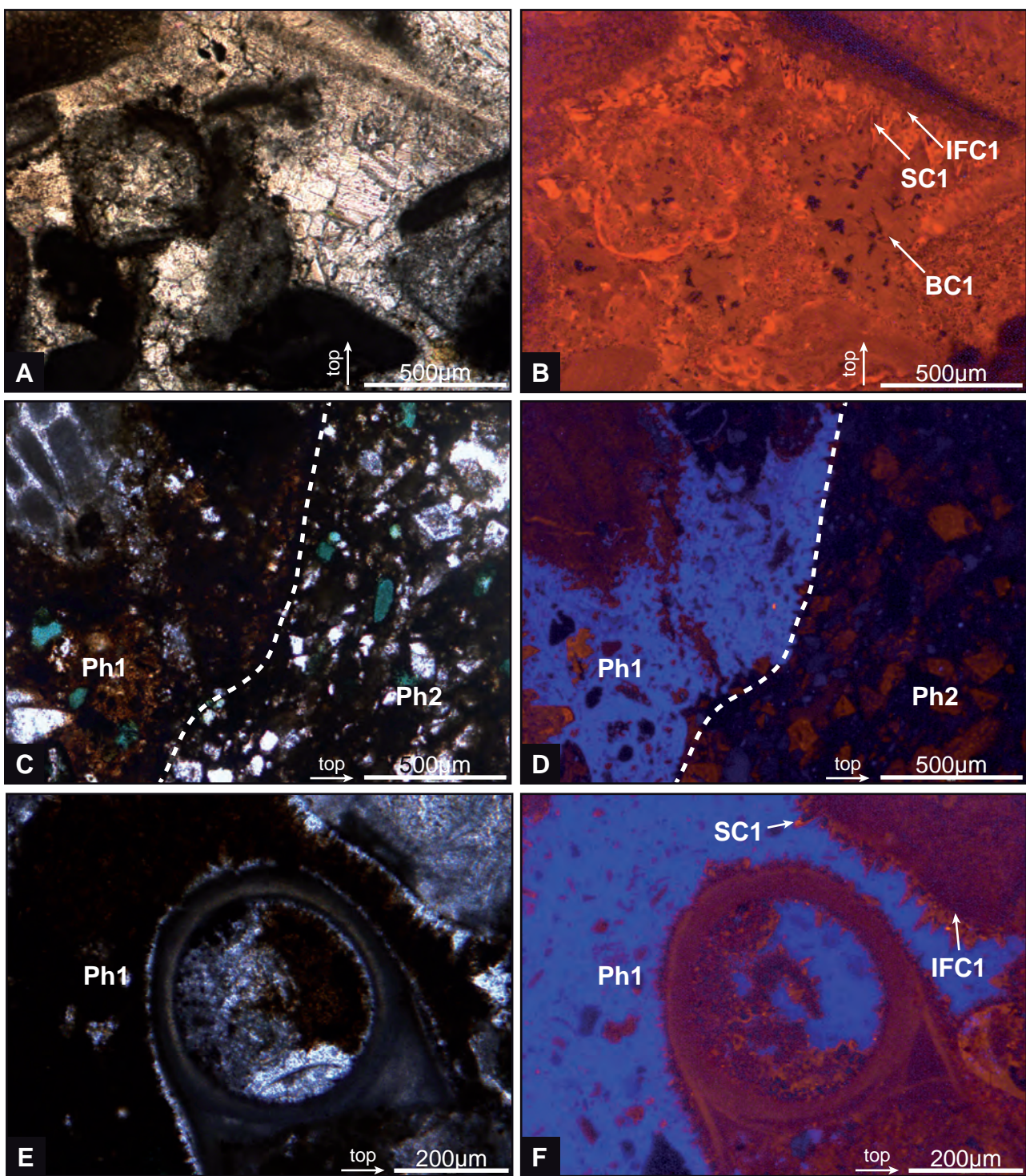
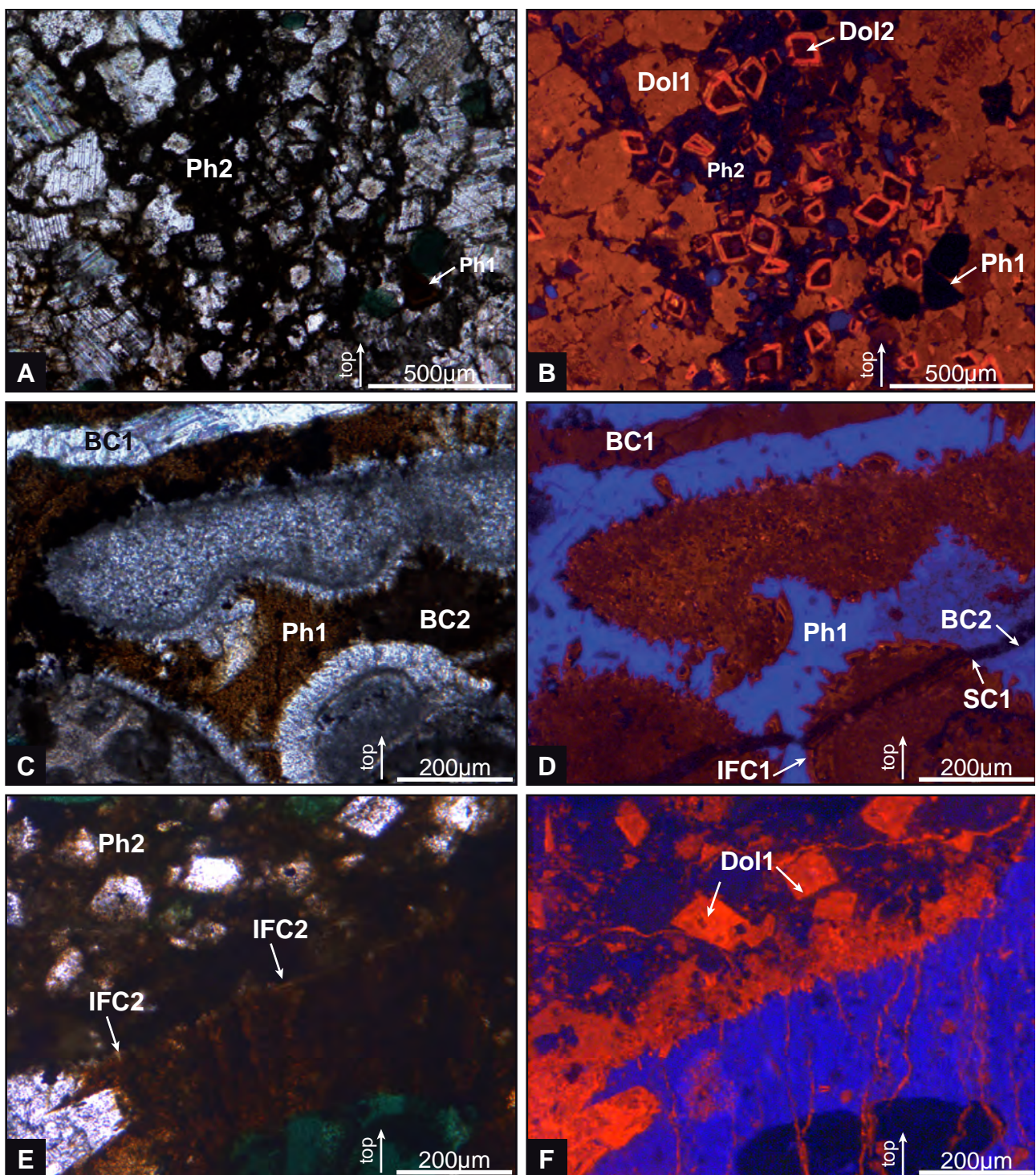
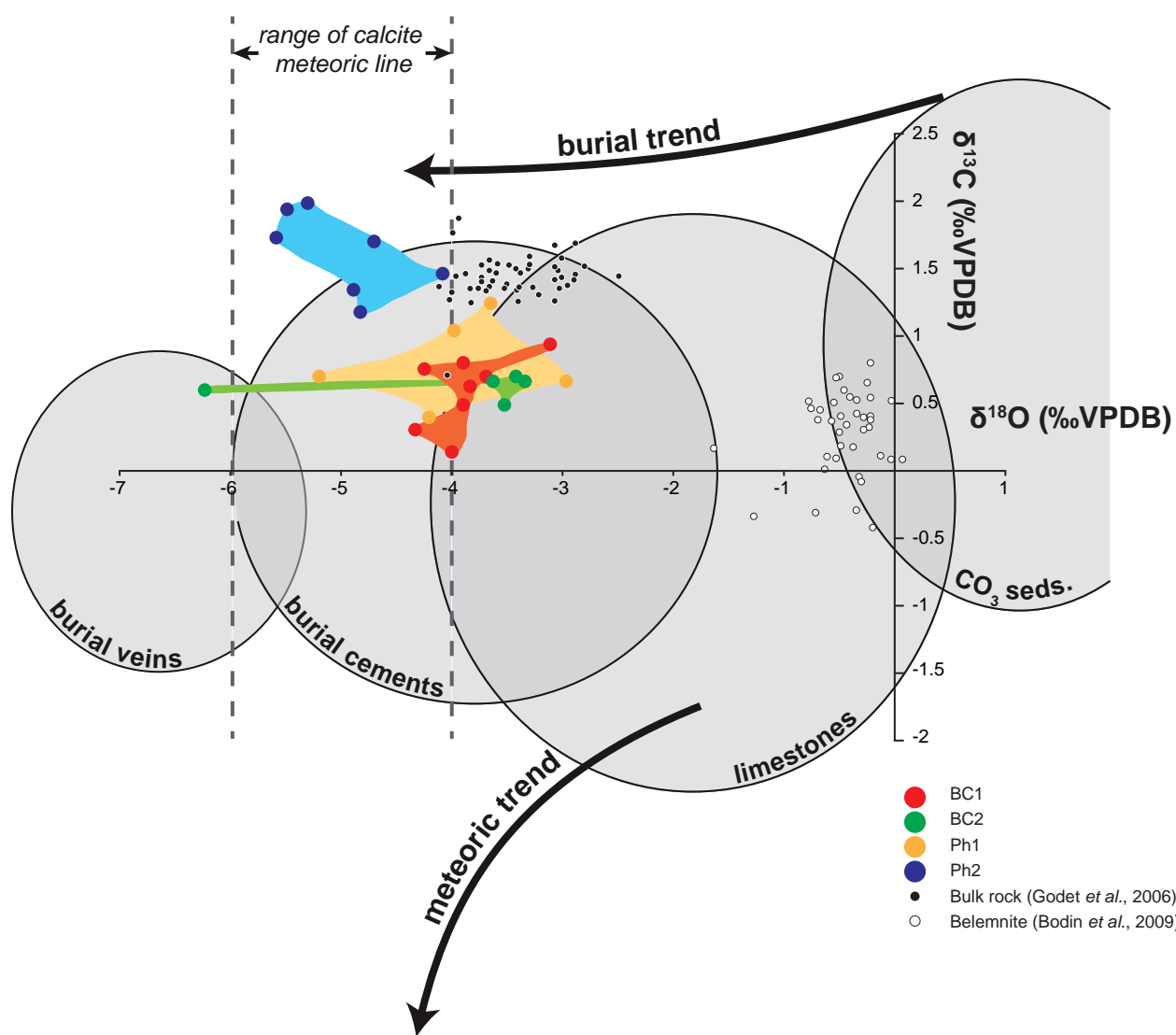


Fig. 6.5 Optical (A), (C) and (E) and cathodoluminescence (B), (D) and (F) microscopy of the main cementation phases constituting the Altmann hardground at Pilatus. (A) Cementation began with Isopachous Fibrous Calcite ('IFC1') whereas the habitus of the subsequent Scalanoedral Calcite ('SC1') rather suggests a vadose meteoric environment before burial cements ('BC1') occluded the remaining porosity. (B) Note the dark core of SC1 reflecting its precipitation from an oxidizing fluid. (C) Sharp and irregular contact between the two generations of phosphate-rich infills ('Ph'). Note that rhombs and quartz grains are mainly present in Ph2 whereas glauconite is equally distributed between Ph1 and Ph2. (D) Bright dark blue luminescence of Ph1 and nearly absence of luminescence in Ph2. (E) and (F) Geopetal infill developed in a serpulid, suggesting that SC1 developed after the formation of an internal sediment;



*Fig. 6.6 Optical (A), (C) and (E) and cathodoluminescence (B), (D) and (F) microscopy of the main cementation phases constituting the Altmann hardground at Pilatus. (A) and (B) Dolomite rhombs preserved in the infill of a bivalve burrow (*Glossifungites* ichnofacies). The luminescence of Dolomite ('Dol') 1 crystals is typical of the one of BC1 (compare with Fig. 5B), whereas Dol2 retained primary characteristics. (C) and (D) The bioclast in the centre has been dissolved relatively early during diagenesis, potentially after an early phase of cementation ('IFC1'), which helped to preserve this new porosity. The latter has been filled in by BC1, whereas BC2 cement developed in association with fractures which cross-cut IFC1, SC1, Ph1 and BC1, and thus were formed during burial diagenesis. (E) and (F) Close-up of the boundary between Ph1 and Ph2, underlain by a thin transparent, fibrous crust interpreted as a second phase of early marine cementation IFC2.*



	n	$\delta^{13}\text{C}$ (‰ VPDB)			$\delta^{18}\text{O}$ (‰ VPDB)		
		mean	max	min	mean	max	min
BC1	8	0.6	0.9	0.1	-3.9	-3.1	-4.3
BC2	5	0.6	0.7	0.5	-4.0	-3.4	-6.2
Ph1	5	0.8	1.2	0.4	-4.0	-3.0	-5.2
Ph2	7	1.6	2.0	1.2	-5.0	-4.1	-5.6

Fig. 6.7 $\delta^{13}\text{C}$ and $\delta^{18}\text{O}$ values for BC1 and BC2 cements, and Ph1 and Ph2 phosphate-rich infills. Cross-plot of $\delta^{13}\text{C}$ (‰) versus $\delta^{18}\text{O}$ (‰) of BC1 and BC2 cements, and Ph1 and Ph2 phosphate rich infills. Bulk-rock (Godet et al., 2006) and belemnite (Bodin et al., 2009) values from the same time interval (i.e. from the *Spathicrioceras angulicostatum* to the *Coronites darsi* ammonite zone) are reported to provide insights on stable isotope compositions of shallow and deep water masses of the western Tethys. Values for the calcite meteoric line is after Lohmann (1988), and fields of values for carbonate components are after Knoerich & Mutti (2006).

The $\delta^{13}\text{C}$ record ($n = 29$) directly below the phosphatic hardground of the Altmann Member exhibits a positive trend from 0.5 to 2.2‰ (Fig. 6.2B). Above the hardground, a

trend toward slightly lower values is observed, from 0.9 to 0.5‰, whereas $\delta^{18}\text{O}$ values remain relatively constant (Fig. 6.2A). Both the $\delta^{13}\text{C}$ and $\delta^{18}\text{O}$ isotope records show a slightly nega-

tive trend in the upper part (5 to 8 m depth) of the Altmann Member.

The Tierwis section

The $\delta^{13}\text{C}$ record ($n = 52$) exhibits a long-term evolution toward heavier values (from $0.8\text{\textperthousand}$ up to $1.7\text{\textperthousand}$) from the upper Kieselkalk Member up to the Drusberg Member. Within the Kieselkalk Member, the $\delta^{13}\text{C}$ is decreasing from 1 to $0.8\text{\textperthousand}$ (Fig. 3). The lowermost and upper part of the Altmann Member [TST (Transgressive Systems Tract) – HST (Highstand Systems Tract) Ha6 and TST Ha7 up to TST Ba2] show short-term decreasing-increasing trends with amplitudes of $0.4\text{\textperthousand}$ and $0.8\text{\textperthousand}$ at 8.5 m and 12 m depth, respectively. These parts are separated by an increasing trend between 12 m and 17 m (amplitude *ca* $0.5\text{\textperthousand}$). Near the top of the Altmann Member (35 to 40 m depth), the $\delta^{13}\text{C}$ values increase rapidly from 1.2 to $1.7\text{\textperthousand}$, before a stabilisation at $1.6\text{\textperthousand}$ in the remainder of the section. Oxygen isotopes exhibit an increasing trend, with $\delta^{18}\text{O}$ values changing from -4.5 to $-2.9\text{\textperthousand}$ from the base to the top of the section. The correlation coefficient (R^2) between $\delta^{13}\text{C}$ and $\delta^{18}\text{O}$ is 0.069.

The Clos de Barral section

In total, 128 samples from the Clos de Barral section have been analysed. In the basal part of the section (between 5 m and 8 m), an increasing trend in $\delta^{13}\text{C}$ values has been measured with an amplitude of $0.3\text{\textperthousand}$. Then, values oscillate around $1.35\text{\textperthousand}$. This plateau is followed by a large positive excursion of more than $0.65\text{\textperthousand}$ (between 23.7 m and 32 m; Fig. 6.4), reaching a second plateau characterized by the

highest $\delta^{13}\text{C}$ values of the section (1.9 to $2.1\text{\textperthousand}$), from 32 to 45.6 m (latest Hauterivian). A trend toward lighter values is subsequently observed, and minimal values ($1.5\text{\textperthousand}$) are recorded at 52.3 m. Up section, the $\delta^{13}\text{C}$ curve describes a second plateau between 52.3 m and 60 m (mean value of $1.6\text{\textperthousand}$), which corresponds to the first occurrence (FO) of *K. nicklesi* and *N. pulchella*, respectively. Upward, the $\delta^{13}\text{C}$ record increases in three main steps: from 61 to 63.2 m (FO of *Heinzia caicedi*; maximal value of $1.7\text{\textperthousand}$), from 64.6 to 65.8 m (FO of *Heinzia sayni*, maximal value of $1.8\text{\textperthousand}$), and from 69.4 m to the end of the section where the $\delta^{13}\text{C}$ record reaches the maximal value of 2\textperthousand . Each of these positive excursions is interrupted by negative shifts in the order of 0.4 to $0.6\text{\textperthousand}$ (at 61 m, 64.6 m and 69.5 m, respectively).

The $\delta^{18}\text{O}$ record describes an antagonistic evolution compared with that of the $\delta^{13}\text{C}$ record. An overall decreasing trend is observed from the base of the section up to 41.9 m (minimal value of $-2.5\text{\textperthousand}$), then a plateau develops between 43.5 m and 51.3 m (mean value of $-2.1\text{\textperthousand}$). After an interval where the most negative values of the section are recorded (average of $-2.4\text{\textperthousand}$ between 52 m and 56.4 m, with a minimum of $-2.7\text{\textperthousand}$ at 56.4 m), the record returns toward heavier values and describes two peaks at 60.5 m and 63.6 m ($-1.4\text{\textperthousand}$ and $-1.2\text{\textperthousand}$, respectively). Finally, the last part of the section is characterized by a return toward more negative values oscillating around $-2.1\text{\textperthousand}$ (from 66.7 m to the top).

6.1.5 Discussion

6.1.5.1 Paragenetic sequence of the Altmann hardground at Pilatus

Biogenic carbonates are precipitated in geochemical equilibrium with sea water, and their subsequent contact with diagenetic fluids, such as fresh water or brines, induces their leaching and dissolution, mostly during early diagenesis (e.g. James & Choquette, 1984). The correct identification of diagenetic phases and their relative timing assists in identifying the triggering mechanisms responsible for the build-up of submarine hardgrounds. The Altmann hardground from Pilatus represents an appropriate candidate for such an approach, since both its complex nature and the estimated long duration (e.g. Föllmi et al., 1994, 2006) reflect the superposition of several sea-level cycles.

A first step consists of identifying all periods during which authigenesis occurred, and this can only be achieved by understanding how the different diagenetic phases are arranged in time. Based on macroscopic and microscopic observations, a synthetic diagram illustrating the

paragenetic sequence of the Altmann Member hardground is proposed in Fig. 8. Following the deposition of the oolitic and bioclastic grainstone (upper Kieselkalk Member), a micritic, internal sediment blankets the bottom of some pores, which have subsequently been occluded by a late phase of sparitic cementation. Moreover, this material is covered by one of the earliest phases of cementation (SC1; see below). Because of its geometry, its micritic nature and its timing of deposition in shallow marine facies, this internal sediment is interpreted as a vadose silt, thus reflecting the influence of gravitational sedimentation within the meteoric vadose domain (James & Choquette, 1984; Tucker & Wright, 1990). First cements consist of IFC1, rapidly followed by SC1. For SC1, a progressive transition from oxidizing to reducing environments may have taken place during crystallisation, reflecting an early phase during which the influence of vadose, meteoric fluids prevailed, followed by a progres-

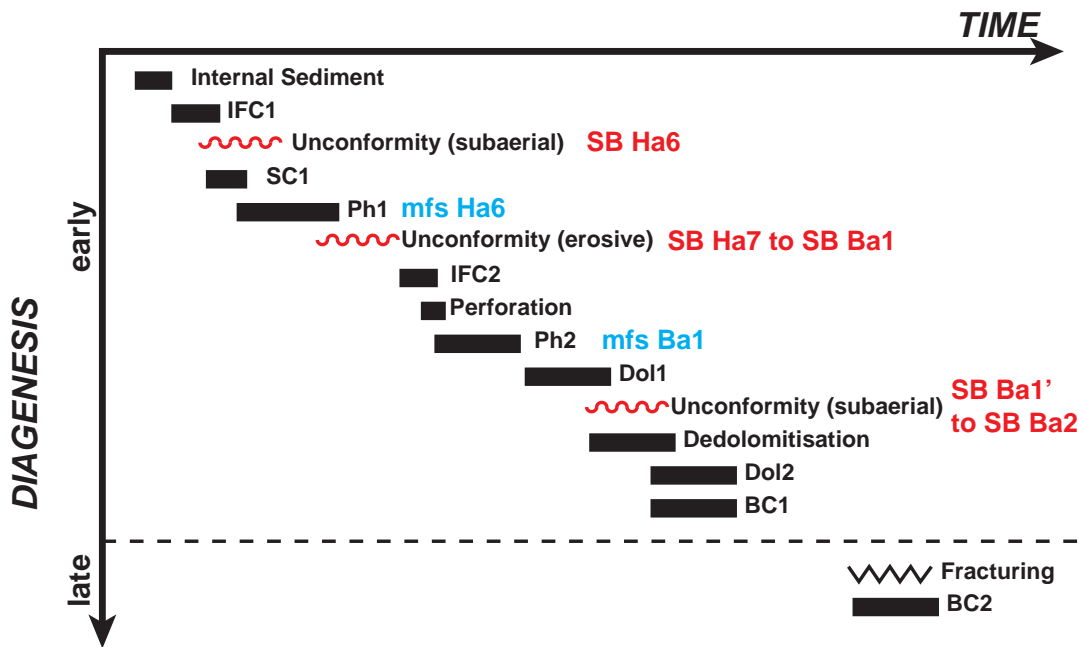


Fig. 6.8 Paragenetic sequence interpreted for the genesis of the Altmann hardground at Pilatus and based on cross-cut relations observed in thin sections, as well as on the stable isotope compositions obtained for the different cement phases ('IFC' Isopachous Fibrous Calcite; 'SC' Scalanoedral Calcite; 'Ph' Phosphatic infill; 'Dol' Dolomite). Sequence boundary (SB) and maximum flooding surface (mfs) nomenclature is after Arnaud (2005b); their dating is based on biostratigraphic provided for the Altmann Member by Bodin et al. (2006b).

sive decrease of the $\text{Fe}^{2+}/\text{Mn}^{2+}$ ratio, because the latter mainly drives luminescence activation or quenching (Barbin & Schvoerer, 1997). The preferential development of SC1 on the lower side of grains (dripstone-like structure; Fig. 6.5A and B) supports an early diagenetic phase in the meteoric vadose environment. This observation suggests that the deposition of sediments of the upper Kieselkalk Member was followed rapidly by a phase of subaerial exposure after their early cementation by IFC1 in a phreatic, marine environment. This suggestion is also coherent with the thickness of IFC1, which becomes irregular toward the base of the Altmann hardground. The alteration of this cement and partly also the included bioclasts, argues in favour of a meteoric influence, and would constitute the source material of the vadose silt that pre-dates the development of SC1, because the latter developed on top of it (Fig. 6.5E and F). This emersion phase is interpreted to have produced a first sequence boundary, which is probably dated as late Hauterivian and potentially as a *P. seitzi* ammonite zone or slightly older, following the oldest age postulated for the Altmann Member by Bodin et al. (2006b). A coeval sea-level drop is defined in global sequence stratigraphic schemes. Both Haq et al. (1987) and Hardenbol et al. (1998) placed their medium-scale SB Ha6 in the uppermost *Balearites balearis* ammonite zone.

Geometrical and superposition features constrain the occurrence of Ph1. The latter is dark brown in natural light, whereas it is characterized by dark blue luminescence (Figs 6.5D, 6.5F and 6.6D), which may be related to a relatively high iron content compared to carbonate particles, as suggested by the occurrence of rusty patches. Of special interest is the infill of an annelid illustrated in Fig. 6.5E and F. The present geopetal structure indicates that Ph1 occurred both after deposition of the first internal sediments, as well

as after the formation of IFC1 and SC1 since the latter are blanketing the serpulid shell both on its internal and external side, except for where the vadose silt is in direct contact with the serpulid. Some doubts remain on the chronology of IFC1 and the vadose silt, since clear observations are difficult on the geometrical relation between these two phases. Finally, directly at the surface of the Altmann hardground, Ph1 is cut by an erosive unconformity that is blanketed by a second early phase of marine cementation (IFC2; Fig. 6.6E and F). The first phase of phosphogenesis is either accompanied by a phase of enhanced current activity triggering the development of a truncation surface, or followed by a second subaerial exposure and associated erosion. Since both erosive pockets and burrows are filled in by the same phosphatic material rich in glauconite and dolomite (Ph2; Figs 6.5C, 6.5D, 6.6A and 6.6B), marine conditions may have been preserved throughout the development of this erosive surface, which is subsequently interpreted as a second SB lacking subaerial exposure.

Two different types of dolomite are described within Ph2. Optical characteristics of Dol1 minerals suggest a dedolomitization phase, and the calcitic mineral found within the newly-created moulds mimics that of the cement that occludes the remaining porosity in phosphate-free areas, implying that BC1 developed after Ph1, Ph2 and Dol1. Its relation with the second phase of dolomitization (Dol2) is, however, less clear. On the one hand, BC1 may have crystallised prior to or synchronously with Dol2, because these rhombs are in direct contact or even included within dedolomitized Dol1 rhombs. On the other hand, Dol2 crystals may have developed well before BC1, thus occupying part of the porosity created by dedolomitization of Dol1. In the latter case, BC1 sparite may have developed during burial diagenesis,

which is confirmed by its $\delta^{18}\text{O}$ values ranging from -4.3 to $-3.1\text{\textperthousand}$ (Fig. 6.7). Moreover, isotopic data for this cement phase fall outside fields defined for shallow-water and deep-water masses, as deduced from isotopic analysis performed on bulk-rock samples and belemnites of the same age. These cements, however, exhibit relatively heavy carbon-isotope compositions (0.1 to $0.9\text{\textperthousand}$), revealing a minor contribution from organic-rich sources. Finally, since dedolomitization processes may occur as a response to subaerial exposure (e.g. Flügel, 2004), a third unconformity may be placed between Dol1 and Dol2, prior to the early lithification of Ph2, because both dolomite generations crystallised within it. Microscopic characteristics of the BC1 cementation phase suggest that the porosity created by dedolomitization of Dol1 may have remained open for a substantial amount of time. In the Tierwis section, ammonites found on top of the uppermost hardground of the Altmann Member are indicative of the late *N. pulchella* to *K. compressissima* ammonite zones (Bodin et al., 2006b), suggesting another unconformity after the second phase of phosphogenesis. It may correspond to SBBa1' and SBBa2.

All of the above-mentioned stages can be attributed to epidemiogenesis (Fig. 6.8). Effects of anadiagenesis (late diagenesis or burial diagenesis; e.g. Fairbridge, 1967; Choquette & Pray, 1970) consist of compaction features associated with cementation phases. A first one (BC1) occluded all the remaining porosity. Its luminescence (dull brown and black core) reflects the influence of oxidizing fluids, during the early stages of burial diagenesis (Tucker & Wright, 1990; see also Sattler et al., 2004 for a case study). It pre-dates the main fracturing phase, which may be related to alpine orogenesis, whereas the cement BC2 post-dates it since it fills in open fractures. It also precipitated from

oxidizing fluids, because it displays an even darker, brown luminescence; its linkage to burial diagenesis is confirmed by its isotope composition (mean values of -4.0 and 0.6 for $\delta^{18}\text{O}$ and $\delta^{13}\text{C}$, respectively; Fig. 6.7).

6.1.5.2 The imprint of sea-level fluctuations and palaeoenvironmental change on the diagenesis of the Altmann drowning unconformity

The several centimetre-thick hardground of the Altmann Member may include three sequence boundaries, and the two intervening main phases of phosphogenesis may be related either to a TST or mfs. In the case of the Helvetic platform, the onset of phosphogenesis is classically explained by the installation of northward upwelling currents subordinated to a general westward current (e.g. Kuhn, 1996); the upward motion of nutrient-rich bottom sea waters may have fertilized the shallow marine water and, at the same time, decreased the sea water temperature. Sea water fertilization by upwelling currents and subsequent drowning has also been postulated for the demise of the shallow marine carbonate megabank on the northern Nicaragua Rise and the Maiella carbonate during the Miocene (Mutti & Bernouilli, 2003; Mutti et al., 2005). The coexistence of phosphate-rich sediments with evolved glauconitic grains within the Altmann Member basal hardground at Pilatus supports the identification of upwelling currents as triggering mechanisms. For instance, enhanced upwelling currents along the shelf edge may have induced the phosphate-rich and glauconite-rich, Albian deposits of the Sierra de Espuña (Spain; Debrabant & Paquet, 1975). In this case, compensation currents, the path of

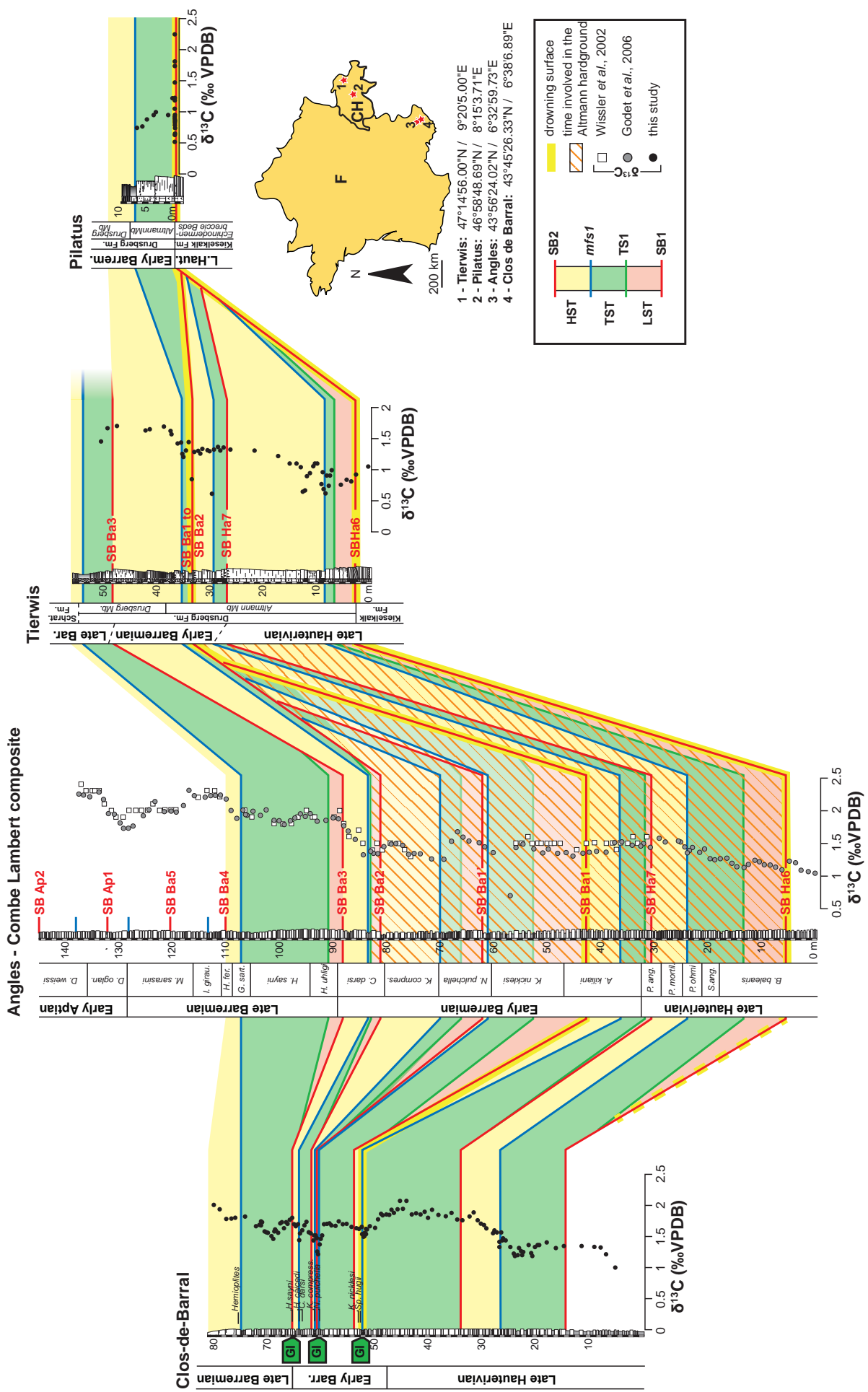


Fig. 6.9 Correlation of the Clos de Barral, Angles, Tierwis and Pilatus sections, by means of chemostratigraphy, biostratigraphy and sequence stratigraphy. A yellow line indicates the position of the drowning surfaces.

which may have followed the shelf-break edge, may have contributed to the phosphogenesis and glauconitisation. On the other hand, during the Altmann hardground formation, an enhanced input of fresh water into the marine realm is deduced from the switch from smectite to kaolinite-dominated clay assemblages between the late Hauterivian and the Barremian along the northern Tethyan margin (Godet et al., 2008). Moreover, during the latest Hauterivian, an enhanced stratification of the water column is also seen through the comparison of $\delta^{18}\text{O}$ measured on bulk-rock samples and belemnites, thus suggesting more input of fresh water from the continents (Bodin et al., 2009). An increase in phosphorus contents in coeval hemipelagic sediments (*P. mortilleti* to *C. darsi* ammonite zones; Bodin et al., 2006a) mirrors an enhanced input of nutrients by increased continental runoff, especially during TSTs. During such periods of a sea-level cycle, reworking is indeed favoured and may lead to the regeneration of nutrients previously preserved in flooded soils (Jarvis et al., 2002; see also Bodin et al., 2006a for an in-depth review of this process). This process may have sustained phosphogenesis by providing more phosphorus into the oceanic reservoir.

The development of SC1 in association with the sequence boundary Ha6 and the lack of an apparent sedimentary gap between SC1 and Ph1 in the Altmann hardground suggest a parallel with the first phase of phosphogenesis in the TST of Ha6. This is coeval with the development of the Faraoni event, a short-lived anoxic event well-documented in the Tethyan domain (e.g. Cecca et al., 1994; Föllmi et al., 2012, amongst numerous others). Although low phosphorus mass accumulation rates are described from this period, an increased trophic level has been postulated as responsible for this event and associated anoxia which favoured the recy-

cling of phosphorus and its return to the water column, explains the lack of high phosphorus mass accumulation rates (PMAR) in sediments (Bodin et al., 2006a).

Concerning the second phase of phosphogenesis recorded within the Altmann hardground, the contact between Ph1 and Ph2 can be dated as after the maximum flooding surface Ha6 and before the maximum flooding surface B2, because the latter has been identified in marly intervals above the Altmann Member hardground at Pilatus and Tierwis (Bodin et al., 2006b). The rise in PMAR values up to the maximum flooding surface Ba1 (Bodin et al., 2006a), associated with an intertropical, humid climate as identified from clay mineral assemblages (Godet et al., 2008), may have triggered the second phase of phosphogenesis on the Helvetic platform. Associated enhanced continental runoff may have also favoured the development of short-lived suboxic to anoxic conditions in deeper waters (e.g. Bordenave & Burwood, 1995), potentially leading to a better preservation of organic matter in intermediate to deep settings of the Tethys ocean. In pelagic sections that are exposed in southern Switzerland and Italy, organic-rich levels are documented in the early Barremian, with total organic carbon (TOC) values of up to 6 wt.% (Breggia section; Bitterli, 1965; Weissert et al., 1979; Föllmi et al., 2012). Although a robust correlation of these phenomena is hampered by a lack of precise dating, the enhanced burial of organic carbon would have depleted the oceanic pool in light carbon isotope ^{12}C . Carbonate particles precipitating in equilibrium with sea water would thus get a heavier $\delta^{13}\text{C}$ signature; this is the case for Ph2, for which $\delta^{13}\text{C}$ values were shifted by a mean value of +0.9‰ toward heavier values compared with Ph1. By taking these palaeoceanographic and palaeoclimatic

events into consideration, the timing of the Ph2 phosphogenesis can be narrowed down to the *K. nicklesi* ammonite zone of the early Barremian.

6.1.5.3 Sequence stratigraphic and biostratigraphic context of the Altmann Member drowning episode

Numerous publications have been dedicated to drowning events and surfaces, either from a conceptual point of view or by describing field case studies (e.g. Schlager, 1981; Hallock & Schlager, 1986; Simone & Carannante, 1988; Graziano, 1999; Mallarino et al., 2002; Gawlick & Schlagintweit, 2006). The resulting geometry constitutes a true paradox since it resembles the one produced by a sea-level fall, whereas a drowning unconformity is by definition generated during a relative sea-level rise (Schlager, 1981). On the other hand, a complementary model for the demise of shallow-marine carbonate platforms invokes a relatively long-lasting exposure of marine ecosystems to abnormal trophic levels and/or temperatures, in the absence of emersion, which may have previously weakened them (e.g. Hallock & Schlager, 1986; Wilson et al., 1998). Other palaeoenvironmental factors may have contributed to the demise of shallow-marine communities; in particular sea water acidification associated with the onset of the Oceanic Anoxic Event 1a may have weakened rudist-dominated ecosystems during the early Aptian (Wissler et al., 2003; Millán et al., 2011; Skelton & Gili, 2012). In southern France, tectonic movements may have triggered the drowning of the Provencal platform during the *Globigerinelloides blowi* foraminiferal zone of the early Aptian (Renard et al., 2005).

As stated by Catuneanu (2006), confu-

sion may arise when interpreting a drowning unconformity as a sequence boundary, especially if the duration of the drowning episode responsible for it encompasses several sea-level cycles, as postulated for the Gemsmättli and the Lidernen Members (*Saynoceras verrucosum* to *Criosarasinella furcillata* and *Lyticoceras nodosoplicatum* to *Plesiospitidiscus ligatus* ammonite zones, respectively; Funk et al., 1993; Föllmi et al., 2006). A drowning episode corresponds to the entire time period during which shallow-marine ecosystems are weakened and are not able to recover from the initial palaeoenvironmental perturbation. This is the case for the Altmann Member: it mirrors a major phase of slow-down of activity on the Helvetic carbonate platform with a major drowning unconformity at or near its base, and the associated drowning phase lasted for more than four 3rd-order depositional sequences (Bodin et al., 2006b; see also Föllmi et al., 2006). In proximal areas of the northern Tethyan margin, ascertaining the exact timing of the onset of the drowning unconformity is difficult and requires both an in-depth sedimentological approach and an integrated biostratigraphic and chemostratigraphic dating framework (e.g. Huck et al., 2011), because the differentiation between sequence boundary, transgressive and drowning surfaces is made difficult, if not impossible, by the superimposition of the aforementioned key surfaces. This is relevant to the sedimentary record preserved at Pilatus, but also to other locations of the Helvetic realm. In the Tierwis section (Fig. 6.3), which represents one of the most expanded sections in which a hardground and phosphates associated with the Altmann Member drowning episode are preserved (Bodin et al., 2006b), the most condensed interval consists of three stacked sequence boundaries instead of five in the Pilatus section. The difference in time gaps represented

by hardgrounds in different sections implies that the temporal correlation of a drowning unconformity between several sections is biased, if only based on sedimentology, because this specific drowning unconformity does not necessarily represent the same amount of time involved in their genesis.

In distal settings of the northern Tethyan margin, more expanded and complete sections encompass the time span of the Altmann Member drowning phase. In Provence, the Clos de Barral section includes three levels that are strongly enriched in glauconite (up to 20%; Fig. 4B); in the rest of the section, glauconite content varies between 0% and 5% (Fig. 6.4A, C and D). The dark-green colour and the rather angular shape of glauconitic grains suggest a para-autochthonous to autochthonous origin. These levels are interpreted as maximum flooding surfaces (Arnaud, 2005a), and their dating by ammonite biostratigraphy (Vermeulen, 1980; see also the detailed biostratigraphic scheme provided by Vermeulen in Arnaud, 2005a, and this article) suggests that they may correspond to part of the drowning phase documented in the Altmann Member. Similar and potentially coeval glauconite-rich intervals occur within the upper Hauterivian and Barremian sedimentary succession of the Nice area (Delanoy, 1992). In this area, the Barremian succession results in a 5 m thick, condensed interval rich in glauconite (Vermeulen, 1980; Arnaud, 2005a). Also in Ardèche (southern France), glauconite-rich levels are described below Urgonian-type limestones and are dated as the *K. compressissima* ammonite zone (Lafarge, 1978). Finally in the neighbouring region of Gard, recent fieldwork highlighted the occurrence of at least one hardground and of several condensed levels, as deduced from the high amount of glauconite. These condensed intervals from southern France

have been attributed to the *N. pulchella* to *K. compressissima* ammonite zones, indicating that this region witnessed a widespread period of condensation during the early Barremian. In contrast to the Helvetic realm where phosphogenesis prevailed, it is expressed by enhanced glauconite formation.

The combination of sequence stratigraphy and available biostratigraphy is complemented by chemostratigraphic correlations based on the $\delta^{13}\text{C}$ records, in order to assess the synchronicity of these Provencal glauconitic levels with the Helvetic phosphatic ones (Fig. 6.9). Although it has been included on the correlation panel, it is impossible to correlate the $\delta^{13}\text{C}$ curve of the Pilatus section with the others based on the evolution of the $\delta^{13}\text{C}$ signal, because this section exhibits the most intense condensation. However, because the Tierwis section is more expanded and well-correlated with the sedimentary succession at Pilatus both by biostratigraphy and sequence stratigraphy (Bodin et al., 2006b), the trends in $\delta^{13}\text{C}$ values observed at Tierwis were used as a reference pattern for the Helvetic carbonate platform. When comparing the $\delta^{13}\text{C}$ evolution at Tierwis and Clos de Barral with that previously published for the Angles section (stratotype for the Barremian stage; Wissler et al., 2002; Godet et al., 2006), the following trends can be used as correlatable anchor points:

In the TST Ha6 (late Hauterivian), a slight decrease of between 0.2‰ and 0.4‰ pre-dates a positive trend of 0.8‰ and 0.7‰ in the Clos de Barral and Tierwis sections, respectively. This evolution toward heavier values lasts up to the latest Hauterivian and thus runs through an entire depositional sequence since it ends within the TST Ha7. By taking into account the sequence stratigraphic and biostratigraphic framework of the Angles section, the climax of this positive trend probably falls within the

Pseudothurmannia angulicostata (Spath 1923, previously *P. picteti*; Vermeulen et al., 2008) ammonite zone.

Then, in the early Barremian of the Clos de Barral section, the transition between the HST Ba1 and TST Ba1' is marked by a sharp decrease (0.4‰) in $\delta^{13}\text{C}$ values followed by an increase of comparable amplitude; although this negative peak is not firmly documented at Angles, a similar bell-shaped trend characterizes the TST Ba1'. The smoother evolution at Angles is certainly due to the presence of a LST in this section (Arnaud, 2005a).

From the *C. darsi* ammonite zone upward, a complex although characteristic behaviour of the $\delta^{13}\text{C}$ is documented at Angles, Clos de Barral and, partially, also at Tierwis. An increase (HST Ba2) of nearly 0.5‰ in all sections marks the end of the phosphatic and glauconitic sediments at Tierwis and Clos de Barral, respectively; it is also well marked at Angles, where it has been thought to represent an increased shedding of material from the Urgonian carbonate platform, which started again at that time in peri-tethyan areas and included aragonite-producing organisms (Godet et al., 2006; Föllmi et al., 2007).

During the subsequent and final depositional sequences studied both at Tierwis and Clos de Barral, a decrease initiated within the LST Ba3 (Angles section) is accentuated during the TST Ba3 where minimal values are encountered (1.5‰ at Clos de Barral). Finally, an increase toward heavier values characterizes the HST of Ba3 (*Gerardthia sartousiana* ammonite zone).

These chemostratigraphic correlations are in line with the sequential stratigraphic interpretations, and permit confirmation of the stratigraphic location of some key surfaces. For instance at Tierwis, the maximum flooding surface Ba3 has been previously identified within a 2 m thick marly sediment deposited in

an outer-shelf environment (microfacies HF0 of Bodin et al., 2006b). However, a thinner, ammonite-bearing and fish-teeth-bearing marly interval located 1.5 m below the aforementioned bed also corresponds to microfacies HF0, and constitutes another candidate for a maximum flooding surface. The positive trend in $\delta^{13}\text{C}$ values initiated within the latter interval of marls perfectly mimics the one recovered within the HST Ba3 at Angles and, to a lesser extent, in the Clos de Barral section, suggesting a lower stratigraphic position for the maximum flooding surface Ba3 at Tierwis than previously stated.

In sections where biostratigraphic anchor points are scarce or where their resolution is lower than time gaps involved within a drowning phase, chemostratigraphic correlations may help in estimating the amount of time leading to a condensed interval, especially if coupled with a sequence stratigraphic framework. At Pilatus, the Altmann Member hardground represents at least the time interval between the sequence boundary Ha6 and the sequence boundary Ba2 (Bodin et al., 2006b), which corresponds to the time interval between the base of the *P. seitzi* to the base of the *C. darsi* ammonite zones (Arnaud, 2005a, b). In proximal settings such as represented by the Pilatus section, however, a certain diachroneity can be postulated for the age of a sequence boundary compared with its basinal correlative conformity (Catuneanu, 2006), because emersion occurred on the platform whereas the basin remained inundated, allowing continuous sedimentation. Correlation of the $\delta^{13}\text{C}$ patterns highlights the time intervals, which are not preserved in the Helvetic sections; they are shown by the orange hatched polygon on the Angles $\delta^{13}\text{C}$ curve in Fig. 9. The main phase of condensation occurred during the time interval from the late *A. kiliani* to the mid *C. darsi* ammonite zones, whereas the remainder of

the *C. darsi* zone is attributed to the Drusberg Member. Using official calibration of ammonite zonation against time scales (Ogg et al., 2008), as well as available cyclostratigraphic data (Bodin et al., 2006a), the duration of the Altmann Mb drowning phase can be estimated to have lasted between 1.27 Ma and 1.42 Ma (Tierwis section), and 1.79 Ma and 2.82 Ma (Pilatus section), respectively.

6.1.5.4 Drowning surfaces as archives of palaeoceanographic changes

The link between episodes of carbonate platform drowning and more widespread, profound environmental crises has long been postulated in the Helvetic realm (Föllmi et al., 1994; Weissert et al., 1998; Föllmi and Godet, this volume). In other parts of the world the precise study of drowning surfaces, or of discontinuities reflecting the cessation of carbonate platform activity, revealed that the interaction of subaerial exposures with submarine hardgrounds is rare (e.g. Camoin et al., 1998; Immenhauser et al., 2000), and that these are often linked to major biotic or palaeoenvironmental crises (e.g. van de Schootbrugge et al., 2003; Mutti et al., 2005). Several polygenic discontinuity surfaces are described from the early and middle Cretaceous of Oman and, in most cases, they consist of two submarine hardgrounds including a subaerial exposure surface in between (Immenhauser et al., 2000; Rameil et al., 2012). Although these authors did not equate such surfaces with drowning episodes *sensu stricto*, they underlined their complexity and their importance in terms of palaeoenvironmental reconstructions. In fact, integration of the processes involved in the genesis of such surfaces helps in understanding how large-scale palaeoceanographic changes

have impacted shallow-marine ecosystems, the latter being of relatively small geographic extent in comparison. For example Léonide et al. (2012) remarkably exemplified such interactions by linking a drowning episode to the Pliensbachian–Toarcian boundary and the early Toarcian Oceanic Anoxic Event (T-OAE). Around the Pliensbachian–Toarcian boundary in Provence (south of France), a polyphased hardground, initiated by the Pliensbachian–Toarcian boundary environmental perturbation, directly precedes in time the sharp, negative $\delta^{13}\text{C}$ excursion characteristic of the T-OAE. Léonide et al. (2012) grouped the different cementation phases into diagenetic sequences, which have subsequently been related to these major environmental perturbations by means of $\delta^{13}\text{C}$ chemostratigraphy. This approach, as well as the one applied to the Altmann drowning event, requires not only a deep understanding of feedback mechanisms between neritic and open-marine domains, but also demands an estimation of the time represented by these surfaces, which can be variable. For instance a period of non-deposition and erosion of up to 10 Ma is postulated for the duration of the top Shu'aiba surface (late Aptian to early Albian, Oman; Rameil et al., 2012), whereas the aforementioned Early Jurassic drowning episode of the Provence Platform may have lasted from 0.5 to 2 Ma, depending on the cyclostratigraphic interpretation chosen for the determination of the duration of the implied ammonite zones. It is also important to bear in mind that the time gap represented by drowning unconformities may vary, depending on palaeotopography. This is the case for the duration of the Altmann Member drowning episode, where the time span ranges from 1.42 to 2.82 Ma between Tierwis and Pilatus, respectively. These different estimations confirm the importance of recognizing drowning surfaces as such, and also of segregating them

into single sequence stratigraphic key-surfaces, since they may include subaerially-exposed sequence boundary (-ies) and thus important hiatus, during which major palaeoceanographic changes took place.

As far as the Altmann Member hardground is concerned, the in-depth understanding of its genesis not only confirms its link to palaeoenvironmental and palaeoceanographic changes at the scale of the Tethys, but also suggests a long period of climate-induced environmental disturbance. The development of phosphate-rich sediments may also be a sign of eutrophication on the platform in relation to the drowning episode. This is especially true for the first phase of phosphogenesis documented in the Altmann Member, which has been correlated with the Faraoni anoxic event. Not all drowning episodes, however, are characterized by phosphate-rich sediments. For instance, the drowning of a small platform belonging to the Fennosarmatia shelf is dated to the late Devonian to Early Carboniferous (Szulcewski et al., 1996); its stepwise development is punctuated by emersions without any phosphatic sedimentation. Another example is given by Sattler et al. (2009), who studied a Miocene carbonate platform from the South China Sea. In this peculiar setting, a complex interaction between tectonic, sea-level and trophic level variations may have triggered platform drowning, with evidence neither for emersion nor for the development of phosphogenesis. It thus seems that a general model for carbonate platform drowning episodes cannot be proposed, because the effect of local palaeoenvironmental parameters may be superimposed onto global palaeoceanographic changes.

6.1.6 Conclusions

Based on cross-cutting relations established from optical and cathodoluminescence microscopy as well as on stable-isotope analysis of sparitic cements, a complete diagenetic history is proposed for the hardground developed at the base of the Altmann Member at Pilatus in the Helvetic Alps. Prior to the main phase of phosphogenesis, a relatively brief period of subaerial exposure may have exposed the shallow marine ecosystem to meteoric waters and thus induced its early dissolution/cementation. Two distinct phases of phosphogenesis are preserved and their development is linked to periods of high sea-level associated with the onset of palaeoceanographic perturbations, which are documented in the Tethyan realm or at least at the scale of the northern Tethyan margin. The drowning phase itself lasted for up to 2.8 Ma and encompasses several depositional sequences. This observation is based on a chemostratigraphic, biostratigraphic and sequence stratigraphic correlation of sections from the Helvetic realm with the Angles and the Clos de Barral sections from south-eastern France. In the latter depositional environment, the drowning phase may have led to the formation of glauconitic-rich intervals.

Direct access to the sedimentary expression of drowning unconformities is often hampered by the associated condensation. However, successful characterisation by means of geochemistry, sequence stratigraphy and optical and cathodoluminescence microscopy brings new arguments in favour of a link between major environmental perturbations recorded in the open-marine realm and neritic crises, whereas erroneous interpretation may induce a bias in, for example, past sea-level reconstructions. Drowning episodes may display a large range of sedimentological expressions, reflecting the complex interaction of environmental pa-

rameters, such as nutrient supply, sea-surface temperature and sea-level variations, which may have led to the development of such crises in the evolution of shallow-marine ecosystems. The identification of the dominant biolimiting factor, which induced a specific drowning episode, will ultimately increase current understanding of environmentally-driven sedimentary pattern.

6.1.7 Acknowledgements

We thank Laurent Nicod and Claudia Baumgartner (both from the University of Lausanne) for the confection of thin sections (Pilatus and Clos de Barral) and for the help with the cathodoluminescence microscope, respectively. We are grateful to Guillaume Suan (Lyon) for sharing his knowledge of Jurassic ammonite biostratigraphy and cyclostratigraphy. The comments and suggestions of Stefan Huck (Hannover) and an anonymous reviewer, as well as of guest editor Helmut Weissert (Zürich) and Sedimentology editors Stephen Rice and Elaine Richardson, greatly improved the quality of this manuscript. Financial support of the Swiss National Foundation (project 20021_127013) is gratefully acknowledged.

6.1.8 References

- Arnaud, H.** (2005a) Sequence stratigraphy interpretation. In: *The Hauterivian-Lower Aptian sequence stratigraphy from Jura Platform to Vocontian Basin: A multidisciplinary approach* (Eds T. Adatte, A. Arnaud-Vanneau, H. Arnaud, M.-C. Blanc-Alétrou, S. Bodin, E. Carrio-Schaffhauser, K.B. Föllmi, A. Godet, M.C. Raddadi and J. Vermeulen), *Géologie Alpine, Série Spéciale «Colloques et Excursions» N°7*, 174-179.
- Arnaud, H.** (2005b) The South-East France Basin (SFB) and Its Mesozoic Evolution. In: *The Hauterivian-Lower Aptian sequence stratigraphy from Jura Platform to Vocontian Basin: A multidisciplinary approach* (Eds T. Adatte, A. Arnaud-Vanneau, H. Arnaud, M.-C. Blanc-Alétrou, S. Bodin, E. Carrio-Schaffhauser, K.B. Föllmi, A. Godet, M.C. Raddadi and J. Vermeulen), *Géologie Alpine, Série Spéciale «Colloques et Excursions» N°7*, 5-28.
- Barbin, V. and Schvoerer, M.** (1997) Cathodoluminescence et géosciences. *C.R. Acad. Sc. Paris, Sciences de la terre et des planètes / Earth & Planetary Sciences*, **325**, 157-169.
- Bitterli, P.** (1965) Bituminous Intercalations in the Cretaceous of the Breggia River, S. Switzerland. *Vereinigung Schweizerischer Petroleum-Geologen und -Ingenieure Bulletin*, **31**, 179-185.
- Bodin, S., Fiet, N., Godet, A., Matera, V., Westermann, S., Clément, A., Janssen, N.M.M., Stille, P. and Föllmi, K.B.** (2009) Early Cretaceous (late Berriasian to early Aptian) palaeoceanographic change along the northwestern Tethyan margin (Vocontian Trough, southeastern France): $\delta^{13}\text{C}$, $\delta^{18}\text{O}$ and Sr-isotope belemnite and whole-rock records. *Cretaceous Research*, **30**, 1247-1262.
- Bodin, S., Godet, A., Vermeulen, J., Arnaud, H., Strasser, A., Fiet, N., Adatte, T. and Föllmi, K.B.** (2006a) The late Hauterivian Faraoni oceanic anoxic event in the western Tethys: Evidence from phosphorus burial rates. *Palaeogeography, Palaeoclimatology, Palaeoecology*, **235**, 245-264.
- Bodin, S., Godet, A., Vermeulen, J., Linder, P. and Föllmi, K.B.** (2006b) Biostratigraphy, sedimentology and sequence stratigraphy

- of the latest Hauterivian - early Barremian drowning episode of the Northern Tethyan margin (Altmann Member, Helvetic Nappes, Switzerland). *Eclogae Geologicae Helveticae*, **99**, 157-174.
- Bordenave, M.L. and Burwood, R.** (1995) The Albian Kazhdumi Formation of the dezful Embayment, Iran: One of the Most Efficient Petroleum Generating Systems. In: *Petroleum Source Rocks* (Ed B. Katz), 183-207. Springer-Verlag, Berlin-Heidelberg-New York-London-Paris-Tokyo-Hong Kong-Barcelona-Budapest.
- Camoin, G.F., Arnaud-Vanneau, A., Bergersen, D.D., Enos, P. and Ebren, P.** (1998) Development and demise of mid-oceanic carbonate platforms, Wodejebato Guyot (NW Pacific). In: *Reefs and Carbonate Platforms in the Pacific and Indian Oceans* (Eds G.F. Camoin and P.J. Davies), *Spec. Publs. int. Ass. Sediment.*, **25**, 39-67.
- Catuneanu, O.** (2006) *Principles of Sequence Stratigraphy*. Elsevier, Amsterdam. 375 pp.
- Cecca, F., Marini, A., Pallini, G., Baudin, F. and Begouen, V.** (1994) A guide-level of the uppermost Hauterivian (lower Cretaceous) in the pelagic succession of Umbria-Marche Apennines (central Italy): the Faraoni level. *Riv. It. Paleont. Strat.*, **99**, 551-568.
- Choquette, P.W. and Pray, L.C.** (1970) Geologic Nomenclature and Classification of Porosity in Sedimentary Carbonates. *AAPG Bulletin*, **54**, 207-250.
- Debrabant, P. and Jaquet, J.** (1975) L'association glauconites-phosphates-carbonates (Albien de la Sierra de Espuña, Espagne méridionale). *Chemical Geology*, **15**, 61-75.
- Delanoy, G.** (1992) Les Ammonites du Barrémien supérieur de Saint-Laurent de l'Escarène (Alpes-Maritimes, sud-est de la France). *Annales du Muséum d'Histoire Naturelle de Nice*, **IX**, 148 pp.
- Dickson, J.A.D.** (1965) A Modified Staining Technique for Carbonates in Thin Section. *Nature*, **205**, 587.
- Fairbridge, R.W.** (1967) Phases of diagenesis and authigenesis. In: *Diagenesis in Sediments: Developments in Sedimentology* (Eds G. Larsen and G.V. Chilingar), **8**, 179-322. Elsevier Pub. Co., Amsterdam.
- Flügel, E.** (2004) *Microfacies of Carbonate Rocks - Analysis, Interpretation and Application*. Springer-Verlag, Berlin, Heidelberg, New York. 976 pp.
- Föllmi, K.B., Bodin, S., Godet, A., Linder, P. and van de Shootbrugge, B.** (2007) Unlocking paleo-environmental interaction from Early Cretaceous shelf sediments in the Helvetic Alps: stratigraphy is the key! *Swiss Journal of Geosciences*, **100**, 349-369.
- Föllmi, K.B., Bôle, M., Jammet, N., Froidevaux, P., Godet, A., Bodin, S., Adatte, T., Matera, V., Fleitmann, D. and Spangenberg, J.E.** (2012) Bridging the Faraoni and Selli oceanic anoxic events: short and repetitive dys- and anaerobic episodes during the late Hauterivian to early Aptian in the central Tethys. *Climate of the Past*, **8**, 171-189.
- Föllmi, K.B., Godet, A., Bodin, S. and Linder, P.** (2006) Interactions between environmental change and shallow-water carbonate build-up along the northern Tethyan margin and their impact on the early Cretaceous carbon-isotope record. *Paleoceanography*, **21**, 16 pp.
- Föllmi, K.B., Weissert, H., Bisping, M. and Funk, H.** (1994) Phosphogenesis, carbon-isotope stratigraphy, and carbonate-platform evolution along the Lower Cretaceous northern Tethyan margin. *Geological Society of America Bulletin*, **106**, 729-746.
- Funk, H., Föllmi, K.B. and Mohr, H.** (1993)

- Evolution of the Tithonian-Aptian carbonate platform along the northern Tethyan margin, eastern Helvetic Alps. In: *Cretaceous carbonates platforms* (Eds J.A.T. Simo, R.W. Scott and J.P. Masse), AAPG (American Association of Petroleum Geologists) Memoir 56, 387-407. Tulsa, OK, United States.
- Gawlick, H.-J. and Schlagintweit, F.** (2006) Berriasian drowning of the Plassen carbonate platform at the type-locality and its bearing on the early Eoalpine orogenic dynamics in the northern Calcareous Alps (Austria). *International Journal of Earth Sciences (Geologisches Rundschau)*, **95**, 451-462.
- Godet, A., Bodin, S., Adatte, T. and Föllmi, K.B.** (2008) Platform-induced clay-mineral fractionation along a northern Tethyan basin-platform transect: implications for the interpretation of Early Cretaceous climate change (Late Hauterivian-Early Aptian). *Cretaceous Research*, **29**, 830-847.
- Godet, A., Bodin, S., Föllmi, K.B., Vermeulen, J., Gardin, S., Fiet, N., Adatte, T., Berner, Z., Stüben, D. and van de Schootbrugge, B.** (2006) Evolution of the marine stable carbon-isotope record during the early Cretaceous: A focus on the late Hauterivian and Barremian in the Tethyan realm. *Earth and Planetary Science Letters*, **242**, 254-271.
- Goguel, J.** (1944) Contribution à l'étude paléogéographique du Crétacé inférieur dans le Sud-Est de la France. *Bulletin du Service de la Carte Géologique de France*, **44**, 1-38.
- Golonka, J.** (2004) Plate tectonic evolution of the southern margin of Eurasia in the Mesozoic and Cenozoic. *Tectonophysics*, **381**, 235-273.
- Graziano, R.** (1999) The Early Cretaceous drowning unconformities of the Apulia carbonate platform (Gargano Promontory, southern Italy): local fingerprints of global palaeoceanographic events. *Terra Nova*, **11**, 245-250.
- Hallock, P. and Schlager, W.** (1986) Nutrient Excess and the Demise of Coral Reefs and Carbonate Platforms. *Palaios*, **1**, 389-398.
- Haq, B.U., Hardenbol, J. and Vail, P.R.** (1987) The chronology of fluctuating sea level since the Triassic. *Science*, **235**, 1156-1167.
- Hardenbol, J., Thierry, J., Farley, M.B., Jacquin, T., Graciansky, P. and Vail, P.R.** (1998) Mesozoic and Cenozoic sequence chronostratigraphy framework of European basins. In: *Mesozoic and Cenozoic sequence stratigraphy of European basins* (Eds P. Graciansky, J. Hardenbol, T. Jacquin and P.R. Vail), **60**, charts. SEPM Spec Publ.
- Huck, S., Heimhofer, U., Rameil, N., Bodin, S. and Immenhauser, A.** (2011) Strontium and carbon-isotope chronostratigraphy of Barremian-Aptian shoal-water carbonates: Northern Tethyan platform drowning predates OAE 1a. *Earth and Planetary Science Letters*, **304**, 547-558.
- Immenhauser, A., Creusen, A., Esteban, M. and Vonhof, H.B.** (2000) Recognition and Interpretation of Polygenic Discontinuity Surfaces in the Middle Cretaceous Shu'aiba, Nahr Umr, and Natih Formations of Northern Oman. *GeoArabia*, **5**, 299-322.
- James, N.P. and Choquette, P.W.** (1984) Diagenesis 9 - Limestones - The Meteoric Diagenetic Environment. *Geoscience Canada*, **11**, 161-194.
- Jarvis, I., Mabrouk, A., Moody, R.T.J. and de Cabrera, S.** (2002) Late Cretaceous (Campanian) carbon isotope events, sea-level change and correlation of the Tethyan and Boreal realms. *Palaeogeography Palaeoclimatology Palaeoecology*, **188**, 215-248.
- Knoerich, A.C. and Mutti, M.** (2006) Epitaxial calcite cements in Earth history: a cooler-wa-

- ter phenomenon during aragonite-sea times? In: *Cool-Water Carbonates: Depositional Systems and Palaeoenvironmental Controls* (Eds H.M. Pedley and G. Carannante), **255**, 323-335. Geological Society of London, London.
- Kuhn, O.** (1996) *Der Einfluss von Verwitterung auf die Paläoceanographie zu Beginn des Kreide-Treibhausklimas (Valanginian und Hauterivian) in der West-Tethys*. PhD thesis, ETH Zürich, Zürich, 380 pp.
- Lafarge, D.** (1978) *Etude géologique du plateau de St. Remèze, Ardèche. Stratigraphie, cartographie, sédimentologie, tectonique*. Thèse 3ème cycle, Université Claude Bernard, Lyon, 119 pp.
- Leonide, P., Floquet, M., Durlet, C., Baudin, F., Pittet, B. and Lécuyer, C.** (2012) Drowning of a carbonate platform as a precursor stage of the Early Toarcian global anoxic event (Southern Provence sub-Basin, South-east France). *Sedimentology*, **59**, 156-184.
- Lohmann, K.C.** (1988) Geochemical Patterns of Meteoric Diagenetic Systems and Their Application to Studies of Paleokarst. In: *Paleokarst* (Eds N.P. James and P.W. Chouquette), 58-80. Springer-Verlag, New-York Berlin Heidelberg London Paris Tokyo.
- Mallarino, G., Goldstein, R.H. and Di Stefano, P.** (2002) New approach for quantifying water depth applied to the enigma of drowning of carbonate platforms. *Geology*, **30**, 783-786.
- Marino, M. and Santantonio, M.** (2010) Understanding the geological record of carbonate platform drowning across rifted Tethyan margins: Examples from the Lower Jurassic of the Apennines and Sicily (Italy). *Journal of Sedimentary Research*, **225**, 116-137.
- Masse, J.-P., Bellion, Y., Benkhelil, J., Dercourt, J., Guiraud, R. and Ricou, L.E.** (1993) Lower Aptian Palaeoenvironments (114 to 112 Ma). In: *Atlas Tethys Palaeoenvironmental Maps* (Eds J. Dercourt, L.E. Ricou and B. Vrielynck), Maps. BEICIP-FRAN-LAB, Rueil-Malmaison. Gauthier-Villars, Paris.
- Masse, J.-P. and Fenerci-Masse, M.** (2011) Drowning discontinuities and stratigraphic correlation in platform carbonates. The late Barremian-Early Aptian record of southeast France. *Cretaceous Research*, **in press**.
- Millan, M.I., Weissert, H.J., Owen, H., Fernández-Mendiola, P.A. and Garcia-Mondejar, J.** (2011) The Madotz Urgonian plarform (Aralar, northern Spain): Paleocological changes in response to Early Aptian global environmental events. *Palaeogeography, Palaeoclimatology, Palaeoecology*, **in press**.
- Mutti, M. and Bernouilli, D.** (2003) Early marine lithification and hardground development on a Miocene ramp (Maiella, Italy): Key surfaces to track changes in trophic resources in nontropical carbonate settings. *Journal of Sedimentary Research*, **73**, 296-308.
- Mutti, M., Bernouilli, D. and Stille, P.** (1997) Temperate carbonate platform drowning linked to Miocene oceanographic events: Maiella platform margin, Italy. *Terra Nova*, **9**, 122-125.
- Mutti, M., Droxler, A.W. and Cunningham, A.D.** (2005) Evolution of the Northern Nicaragua Rise during the Oligocene-Miocene: Drowning by environmental factors. *Sedimentary Geology*, **175**, 237-258.
- Ogg, J.G., Ogg, G. and Gradstein, F.M.** (2008) *The Concise Geologic Time Scale*. Cambridge University Press, New York. 177 pp.
- Rameil, N., Immenhauser, A., Csoma, A.É. and Warrlich, G.** (2012) Surfaces with a

- long history: the Aptian top Shu'aiba Formation unconformity, Sultanate of Oman. *Sedimentology*, **59**, 212-248.
- Renard, M., de Rafélis, M., Emmanuel, L., Moullade, M., Masse, J.-P., Kuhnt, W., Bergen, J.A. and Tronchetti, G.** (2005) Early Aptian $\delta^{13}\text{C}$ and manganese anomalies from the historical Cassis-La Bédoule stratotype sections (S.E. France): relationship with a methane hydrate dissociation event and stratigraphic implications. *Carnets de Géologie / Notebooks on Geology, Article 2005/04 (CG2005_A04)*, 18 p.
- Sager, W.W., Winterer, E.L., Firth, J.V., Arnaud, H., Baker, P.A., Baudin, F., Brälower, T.J., Castillo, P., Cooper, P., Flood, P.G., Golovchenko, X., Iryu, Y., Ivanov, M., Jenkyns, H.C., Kenter, J.A.M., Murdmaa, I., Mutterlose, J., Nogi, Y., Paull, C.K., Polgreen, E., Röhl, U., Sliter, W.V., Strasser, A., Swinburne, N.H.M., Tarduno, J.A. and van Waasbergen, R.** (1993) Site 867/868. *Proceedings of the Oceanic Drilling Program, Initial Reports*, **143**, 273-296.
- Sattler, U., Immenhauser, A., Schlager, W. and Zampetti, V.** (2009) Drowning history of a Miocene carbonate platform (Zhujiang Formation, South China Sea). *Sedimentary Geology*, **219**, 318-331.
- Sattler, U., Zampetti, V., Schlager, W. and Immenhauser, A.** (2004) Late leaching deep burial conditions: a case study from the Miocene Zhujiang Carbonate Reservoir, South China Sea. *Marine and Petroleum Geology*, **21**, 977-992.
- Schlager, W.** (1981) The paradox of drowned reefs and carbonate platforms. *Geological Society of America Bulletin*, **92**, 197-211.
- Schlager, W.** (1998) Exposure, drowning and sequence boundaries on carbonate platforms. In: *Reefs and Carbonate Platforms in the Pacific and Indian Oceans* (Eds G.F. Camoin and P.J. Davies), *Spec. Publs. int. Ass. Sediment.*, **25**, 3-21.
- Schlager, W.** (1999) Type 3 Sequence Boundaries. In: *Advances in Carbonate Sequence Stratigraphy: Application to Reservoirs, Outcrops and Models* (Ed SEPM), *SEPM Special Publication*, n°**63**, 35-45.
- Simone, L. and Carannante, G.** (1988) The fate of foramol («temperate-type») carbonate platforms. In: *Non-Tropical Shelf Carbonates - Modern and Ancient* (Ed C.S. Nelson), *Sedimentary Geology*, **60**, 347-354.
- Skelton, P. and Gili, E.** (2012) Rudists and carbonate platforms in the Aptian: a case study on biotic interactions with ocean chemistry and climate. *Sedimentology*, **59**, 81-117.
- Stein, M., Westermann, S., Adatte, T., Materia, V., Fleitmann, D., Spangenberg, J.E. and Föllmi, K.B.** (2012) Late Barremian - Early Aptian palaeoenvironmental change: The Cassis-La Bédoule section, southeast France. *Cretaceous Research*, **in press**.
- Szulczewski, M., Belka, Z. and Slompski, S.** (1996) The drowning of a carbonate platform: an example from the Devonian-Carboniferous of the southwestern Holy Cross Mountains, Poland. *Sedimentary Geology*, **106**, 21-49.
- Tucker, M.E. and Wright, V.P.** (1990) *Carbonate Sedimentology*. Blackwell Science, Victoria, Australia. 482 pp.
- van de Schootbrugge, B., Kuhn, O., Adatte, T., Steinmann, P. and Föllmi, K.** (2003) Decoupling of P- and Corg-burial following Early Cretaceous (Valanginian-Hauterivian) platform drowning along the NW Tethyan margin. *Palaeogeography, Palaeoclimatology, Palaeoecology*, **199**, 315-331.
- Vermeulen, J.** (1980) Biozonation homophylé-

- tique du Barrémien du Clos de Barral (Var). In: *Ammonites* (Ed G. Thomel), 181-184. Editions Serre, Nice.
- Vermeulen, J.** (2002) Etude stratigraphique et paléontologique de la famille des Pulchellidae (Ammonoidea, Ammonitina, Endomocerataceae). *Géologie Alpine, Mémoire H.S.* N°42, 333 pp.
- Vermeulen, J.** (2005) Boundaries, ammonite fauna and main subdivisions of the stratotype of the Barremian. In: *The Hauterivian-Lower Aptian sequence stratigraphy from Jura Platform to Vocontian Basin: A multidisciplinary approach* (Eds T. Adatte, A. Arnaud-Vanneau, H. Arnaud, M.-C. Blanc-Alétrou, S. Bodin, E. Carrio-Schaffhauser, K.B. Föllmi, A. Godet, M.C. Raddadi and J. Vermeulen), *Géologie Alpine, Série Spéciale «Colloques et Excursions» N°7*, 147-173.
- Vermeulen, J., Duyé, J.-P., Lazarin, P., Leroy, L. and Mascarelli, E.** (2008) Nouvelles données taxinomiques sur la famille des Crioceratitidae Gill, 1871 (Ancyloceratina, Ancyloceratoidea). *Riviéra Scientifique*, 92, 65-76.
- Weissert, H., Lini, A., Föllmi, K.B. and Kuhn, O.** (1998) Correlation of Early Cretaceous carbon isotope stratigraphy and platform drowning events : a possible link ? *Palaeogeography, Palaeoclimatology, Palaeoecology*, 137, 189-203.
- Weissert, H., McKenzie, J. and Hochuli, P.** (1979) Cyclic anoxic events in the Early Cretaceous Tethys Ocean. *Geology*, 7, 147-151.
- Wilson, P.A., Jenkyns, H.C., Elderfield, H. and Larson, R.L.** (1998) The paradox of drowned carbonate platforms and the origin of Cretaceous Pacific guyots. *Nature*, 392.
- Wissler, L., Funk, H. and Weissert, H.** (2003) Response of Early Cretaceous carbonate platforms to changes in atmospheric carbon dioxide levels. *Palaeogeography, Palaeoclimatology, Palaeoecology*, 200, 187-205.
- Wissler, L., Weissert, H., Masse, J.-P. and Bulot, L.G.** (2002) Chemostratigraphic correlation of Barremian and lower Aptian ammonite zones and magnetic reversals. *Int. J. Earth Sci. (Geol. Rundsch.)*, 91, 272-279.

6.2 Carbone and oxygen isotope data

Tierwis

Sample	Depth (cm)	$\delta^{13}\text{C}$	$\delta^{18}\text{O}$
TW160	19260	2.22	-4.68
TW159	19250	2.91	-2.28
TW 158	19165	3.40	-2.66
TW157	19085	3.33	-2.98
TW 156	19065	3.20	-3.28
TW155	18985	3.23	-3.00
TW 154	18970	2.74	-3.16
TW 153	18875	3.19	-3.03
TW 152	18860	2.93	-3.79
TW151	18780	3.18	-2.98
TW 150	18760	2.88	-3.60
TW 149	18660	2.72	-3.42
TW148	18620	2.16	-3.45
TW 147	18520	2.00	-3.20
TW 146	18370	1.79	-3.46
TW145	18230	1.85	-3.46
TW 144	18210	1.62	-3.66
TW 143	18060	1.84	-3.55
TW142	17990	1.95	-3.52
TW 141	17930	1.65	-3.63
TW140	17815	2.26	-3.55
TW 139	17710	2.21	-3.64
TW138	17685	2.16	-3.53
TW137	17570	2.22	-3.54
TW136	17537	2.35	-3.19
TW135	17512	2.40	-3.40
TW134	17482	2.43	-3.36
TW132	17372	2.80	-3.10
TW131	17302	2.80	-2.50
TW130	17227	2.89	-3.14
TW129	17217	3.00	-2.50
TW128	17177	2.85	-3.21
TW 127	17107	2.92	-3.27
TW 126	17037	2.86	-3.19
TW125	16947	2.92	-3.40
TW 124	16867	1.82	-3.41
TW123	16842	2.40	-3.36
TW122	16742	1.80	-3.56
TW 120	16612	2.19	-3.65
TW119	16572	1.85	-3.73
TW 118	16532	1.92	-3.64
TW117	16497	2.27	-3.23
TW116	16417	2.76	-2.31
TW115	13128	-1.85	-4.08
TW 114	13028	2.37	-2.32
TW113	13013	2.95	-2.53
TW 112	12988	0.04	-3.79
TW111	12898	2.60	-2.89
TW 110	12878	2.64	-3.23
TW108	12758	2.65	-2.72
TW 107	12653	2.74	-3.13
TW 106	12518	2.81	-2.87
TW105	12418	3.12	-2.64
TW 104	12328	2.81	-2.85
TW 103	12308	2.79	-2.87
TW102	12208	3.00	-2.67
TW 101	12188	2.88	-2.66
TW 100	12048	2.75	-2.80
TW99	12028	2.75	-2.99
TW 98	11938	2.97	-2.83
TW97	11858	2.86	-2.84
TW 96	11828	2.59	-2.55

Sample	Depth (cm)	$\delta^{13}\text{C}$	$\delta^{18}\text{O}$
TW95	11718	2.43	-2.69
TW 94	11688	2.74	-2.82
TW93	11568	2.70	-2.98
TW 92	11548	2.64	-3.07
TW 91	11468	2.59	-3.06
TW90	11398	2.72	-2.76
TW 89	11348	2.61	-2.57
TW88	11218	2.52	-2.38
TW 87	11198	2.55	-2.14
TW 86	11068	2.56	-2.21
TW 85	11028	2.54	-2.21
TW84	10948	2.43	-2.18
TW 83	10928	2.58	-2.36
TW 82	10808	2.51	-2.54
TW 81	10778	2.51	-2.48
TW80	10678	2.68	-2.82
TW 79	10598	2.58	-2.31
TW78	10538	2.64	-2.22
TW 77	10523	2.52	-2.50
TW 76	10433	2.62	-2.30
TW 75	10408	2.66	-2.29
TW74	10338	2.58	-2.25
TW 73	10308	2.45	-2.58
TW 72	10283	2.56	-2.40
TW 71	10213	2.58	-2.49
TW70	10188	2.53	-2.57
TW 69	10158	2.58	-2.46
TW 68	10018	2.61	-2.57
TW67	9958	2.68	-2.35
TW 66	9668	2.46	-2.64
TW 65	9648	2.30	-2.73
TW 64	9648	2.40	-2.63
TW63	9538	2.51	-2.63
TW 62	9448	2.48	-2.59
TW 61	9433	2.31	-2.66
TW60	9373	2.49	-2.77
TW 59	9253	2.28	-2.97
TW 57	9113	2.53	-2.62
TW56	8993	2.68	-2.53
TW54	8858	2.72	-2.46
TW 53	8778	2.61	-2.73
TW 52	8703	2.72	-2.40
TW51	8643	2.64	-2.64
TW 50	8608	2.67	-2.56
TW49	8543	2.64	-2.72
TW 48	8483	2.67	-2.57
TW 47	8413	2.63	-2.47
TW 46	8388	2.61	-2.48
TW 45	8338	2.67	-2.36
TW 44	8268	2.56	-2.62
TW43	8198	2.69	-2.39
TW 42	8128	2.57	-2.37
TW40	8038	2.64	-2.72
TW 39	7948	2.51	-2.79
TW 37	7895	2.57	-2.67
TW36	7855	2.46	-2.70
TW35	7810	2.47	-2.86
TW 34	7710	2.53	-3.00
TW 33	7640	2.02	-3.18
TW32	7535	2.20	-3.43
TW 31	7485	2.23	-3.00
TW 30	7445	2.28	-3.00

Tierwis

Sample	Depth (cm)	$\delta^{13}\text{C}$	$\delta^{18}\text{O}$
TW 29	7335	2.16	-3.17
TW28	7275	2.22	-3.03
TW 27	7215	2.23	-3.10
TW 26	7180	2.19	-3.23
TW25	7115	2.24	-3.36
TW 24	7055	2.25	-3.14
TW 23	6940	2.07	-3.17
TW22	6870	2.02	-3.22
TW 21	6773	1.94	-3.27
TW 20	6731	1.89	-3.35
TW19	6686	1.90	-3.18
TW 18	6646	1.85	-3.13
TW 17	6566	1.99	-3.56
TW 16	6476	1.92	-3.42
TW15	6406	1.78	-3.33
TW 14	6364	1.56	-3.57
TW 13	6275	1.34	-3.70
TW12	6230	1.43	-3.98
TW 11	6185	1.35	-3.94
TW 9	6107	1.32	-3.62
TW8	6075	1.20	-2.99
TW 7	6023	1.14	-3.22
TW 6	5948	1.28	-3.19
TW 5	5868	1.28	-2.68
TW4	5798	1.27	-3.10
TW3	5733	1.37	-2.94
TW1	5690	1.34	-1.58
TW 0.1	5683.78	1.46	-3.25
TW 0.2	5548.78	1.42	-3.00
TW 0.3	5468.78	1.41	-3.59
TW 0.4	5398.78	1.60	-3.50
TW 0.5	5348.78	1.42	-2.50
TW 0.6	5038.78	1.45	-3.95
SALB1	5018.78	1.69	-2.97
SALB2	4953.78	1.71	-2.77
SALB3	4878.78	1.69	-3.10
SALB4	4778.78	1.75	-3.15
SALB5	4728.78	1.69	-2.98
SALB6	4673.78	1.78	-2.93
SALB7	4628.78	1.80	-3.57
SALB8	4523.78	1.57	-2.92
SALB9	4423.78	1.68	-2.83
SALB10	4273.78	1.56	-2.96
SALB11	4128.78	1.65	-3.04
SALB12	3998.78	1.61	-3.00
SALB13	3948.78	1.61	-2.53
SALB14	3848.78	1.62	-3.14
SALB15	3833.78	1.56	-3.36
SALB16	3778.78	1.63	-3.26
SALB17	3733.78	1.56	-2.73
SALB18	3698.78	1.60	-2.93
SALB19	3658.78	1.44	-2.91
SALB20	3588.78	1.49	-3.27
SALB21	3533.78	1.40	-3.31
SALB22	3483.78	1.34	-2.80
SALB23	3373.78	1.26	-3.33
SALB24c	3353.78	0.93	-3.72
SALB24s	3353.78	0.86	-2.95
SALB25	3253.78	1.01	-3.01
SALB26	3108.78	1.26	-2.82
SALB27	2978.78	1.17	-3.22
SALB28	2898.78	1.18	-3.31

Sample	Depth (cm)	$\delta^{13}\text{C}$	$\delta^{18}\text{O}$
SALB29	2818.78	1.25	-3.19
SALB30	2618.78	1.34	-3.16
SA MS 90	16727	2.40	-3.20
SA MS 88	16483	2.91	-3.13
SA MS 86	16332	2.35	-3.16
SA MS 84	16191	2.39	-2.87
SA MS 82	16106	2.86	-6.19
SA MS 80	16018	2.96	-3.29
SA MS 79	15925	2.70	-6.35
SA MS 78	15830	3.00	-3.08
SA MS 76	15803	3.15	-3.01
SA MS 74	15736	3.06	-3.11
SA MS 72	15681	2.54	-3.52
SA MS 70	15662	2.52	-7.77
SA MS 68	15600	2.21	-3.39
SA MS 67	15510	2.34	-3.40
SA MS 66	15499	2.38	-3.01
SA MS 65	15498	2.39	-3.15
SA MS 63	15425	3.07	-2.64
SA MS 61	15247	2.95	-3.51
SA MS 60	15098	3.15	-2.30
SA MS 59	15068	3.09	-2.87
SA MS 58	15030	3.10	-2.78
SA MS 56	14952	3.26	-2.58
SA MS 53	14883	3.18	-3.15
SA MS 52	14819	3.24	-3.06
SA MS 50	14782	3.33	-2.64
SA MS 47	14593	3.34	-2.77
SA MS 45	14436	3.28	-2.65
SA MS 44	14342	3.36	-2.97
SA MS 42	14237	3.42	-3.04
SA MS 41	14130	3.73	-2.13
SA MS 39	14082	3.38	-2.47
SA MS 37	14007	3.46	-2.65
SA MS 35	13942	3.24	-3.04
SA MS 33	13883	3.27	-2.66
SA MS 32	13778	3.49	-2.70
SA MS 30	13674	2.97	-2.30
SA MS 28	13609	3.06	-2.56
SA MS 26	13571	3.36	-2.78
SA MS 23	13465	3.43	-2.36
SA MS 21	13360	3.37	-2.46
SA MS 19	13308	3.30	-1.74
SA MS 17	13283	3.17	-1.79
SA MS 15	13228	0.44	-3.97
SA MS 13	13159	1.68	-4.35
SA MS 11	13133	2.07	-4.27
SA MS 9	13074	2.25	-3.30
SA MS 6	13013	2.32	-3.21
SA MS 4	12934	2.63	-2.93
SA MS 2	12864	2.09	-4.26
SA MS 1	12803	2.51	-3.19
SA MS 200	12778	2.48	-2.97
SA MS 202	12531	2.76	-3.20
SA MS 204	12239	2.85	-2.95
SA MS 206	12087	2.87	-2.84

L'Ecuelle

Sample	Depth (cm)	$\delta^{13}\text{C}$	$\delta^{18}\text{O}$
EC257	23365	-0.38	-5.14
EC256	23215	-0.82	-5.96
EC255	23145	-1.80	-5.55
EC254	23075	-1.90	-5.43
EC253	23005	-1.98	-5.73
EC252	22965	-1.84	-5.64
EC251	22915	-2.05	-5.61
EC250	22860	-1.98	-5.55
EC249	22800	-1.74	-5.15
EC248	22730	-1.32	-5.21
EC247	22665	-1.36	-5.58
EC246	22650	-0.24	-5.00
EC245	22635	-0.82	-5.26
EC244	22595	-0.34	-5.31
EC243	22545	-0.97	-5.14
EC242	22465	-1.00	-5.13
EC241b	22445	-2.33	-8.91
EC241a	22395	-1.36	-5.29
EC240	22330	-1.53	-5.40
EC238	22295	-2.07	-5.51
EC237	22270	-1.98	-5.56
EC236	22225	-1.15	-4.88
EC235	22165	-1.11	-5.50
EC234	22105	-1.00	-5.23
EC233	22070	-1.25	-5.07
EC232	22055	-1.57	-5.14
EC231vert	21985	-1.74	-5.40
EC231	21935	-1.58	-5.27
EC230	21875	-0.68	-5.11
EC229	21860	-0.85	-5.09
EC228	21785	-1.34	-5.31
EC227	21715	-0.72	-4.60
EC226	21700	-0.46	-5.25
EC225	21615	-0.27	-5.30
EC224	21605	-0.61	-5.10
EC223	21595	-1.82	-5.31
EC222	21520	-2.12	-5.60
EC221	21455	-1.09	-4.65
EC220	21365	-1.14	-5.74
EC219	21350	-1.35	-5.45
EC218	21305	-0.31	-5.07
EC217	21245	-0.57	-5.37
EC216	21180	-1.27	-5.31
EC215	21165	-0.90	-4.60
EC214	21105	-0.35	-4.62
EC213	21015	-0.12	-5.24
EC212	20940	0.07	-5.14
EC211	20890	0.11	-5.21
EC210	20835	0.13	-5.23
EC209	20785	-0.40	-5.29
EC208	20765	-0.48	-5.28
EC207	20705	-0.54	-5.13
EC206	20625	-0.12	-5.12
EC205	20605	-0.22	-5.17
EC204	20535	-0.12	-5.17
EC203	20515	-0.45	-4.99
EC202	20455	-0.29	-5.06
EC201	20395	-0.53	-5.17
EC200	20375	0.15	-5.27
EC199	20335	0.23	-5.05
EC198	20274	0.55	-5.15
EC197	20265	0.84	-5.15

Sample	Depth (cm)	$\delta^{13}\text{C}$	$\delta^{18}\text{O}$
EC196	20215	0.85	-5.24
EC195	20175	0.63	-5.38
EC194	20105	0.69	-5.06
EC193	20015	0.78	-5.05
EC192	19975	0.85	-5.06
EC191	19960	0.19	-5.01
EC190	19905	0.74	-5.08
EC189	19825	0.54	-5.07
EC188	19760	0.42	-4.94
EC187	19755	0.66	-5.07
EC186	19685	-0.80	-7.10
EC185	19640	0.48	-4.98
EC184	19613	0.67	-5.02
EC183	19550	0.20	-4.87
EC182	19505	-0.52	-5.09
EC181	19470	0.89	-4.70
EC180	19425	1.13	-5.10
EC179	19345	0.63	-5.11
EC178	19323	1.53	-5.04
EC177	19320	1.26	-5.08
EC176	19265	1.54	-4.98
EC175	19213	0.56	-5.08
EC174	19160	1.14	-5.17
EC173	19104	0.75	-5.13
EC172carb	19090	0.17	-5.18
EC172karst	19070	-0.09	-5.45
EC171	19055	-0.02	-5.05
EC170	18935	-1.04	-5.28
EC169	18922	-0.24	-5.25
EC168	18917	-2.59	-5.37
EC167	18915	-4.91	-6.05
EC166	18875	-2.93	-5.03
EC165	18820	-2.66	-5.13
EC164	18750	-1.35	-5.41
EC163	18725	-2.18	-5.08
EC162	18625	-1.40	-5.13
EC161	18525	-3.11	-5.44
EC160	18425	-2.27	-5.54
EC159	18335	-1.18	-5.64
EC158	18195	-1.59	-5.24
EC157	18085	-2.12	-5.40
EC156	17995	-1.92	-5.47
EC155	17865	-1.45	-5.04
EC154	17795	-1.29	-5.60
EC153	17695	-2.30	-5.56
EC152	17645	-2.64	-5.61
EC151	17545	-2.40	-5.78
EC150	17445	-0.79	-5.06
EC149	17345	-0.93	-5.29
EC148	17245	-1.50	-5.49
EC147	17145	-1.40	-5.38
EC146	17045	-2.02	-5.51
EC145	16845	-1.32	-5.35
EC144	16545	-1.64	-5.33
EC143	16395	-1.53	-5.40
EC142	16245	-1.21	-5.49
EC141	16115	-0.95	-4.87
EC140	16010	-0.40	-5.18
EC139	15900	-0.40	-4.92
EC138	15745	-1.76	-5.32
EC137	15635	-0.90	-5.21
EC136	15495	-0.79	-5.13

L'Ecuelle

Sample	Depth (cm)	$\delta^{13}\text{C}$	$\delta^{18}\text{O}$
EC135	15415	0.03	-4.94
EC134	15320	-0.05	-4.62
EC133	15295	0.37	-4.63
EC132	15225	0.43	-4.57
EC131	15110	1.24	-4.62
EC130	15075	1.25	-4.57
EC129	15035	1.56	-4.53
EC128	14940	1.19	-4.48
EC127	14890	-0.55	-5.48
EC126	14770	-0.06	-5.47
EC125	14760	-0.32	-5.26
EC124	14640	-1.50	-5.17
EC123	14630	-1.43	-5.14
EC122	14535	-1.19	-5.54
EC121	14435	-1.44	-5.25
EC120	14335	-1.71	-5.14
EC119	14235	-1.72	-5.08
EC118	14095	-1.73	-5.21
EC117	13965	-2.05	-5.75
EC116	13835	-1.65	-5.65
EC115	13813	-0.77	-5.71
EC113	13695	-0.71	-5.65
EC112	13625	-1.75	-5.65
EC111	13485	-1.86	-5.79
EC110	13415	0.11	-5.40
EC109	13315	-0.20	-5.39
EC108	13235	-2.13	-5.56
EC107	13120	-0.16	-5.20
EC106	13040	0.29	-5.11
EC105	12990	0.26	-4.96
EC104	12920	-0.45	-4.98
EC103	12715	1.39	-4.46
EC102	12615	-1.57	-6.59
EC101	12510	-1.30	-6.39
EC100	12390	-1.81	-6.33
EC99	12185	-1.58	-6.49
EC98	12075	-1.61	-6.22
EC97	11975	-0.50	-5.92
EC96	11870	-2.55	-6.24
EC95	11770	-1.52	-5.67
EC94	11680	-0.83	-5.19
EC93	11475	-1.03	-5.54
EC92	11370	-2.29	-6.28
EC91	11325	-1.75	-6.50
EC90	11230	-2.64	-6.32
EC89	11130	-1.84	-6.19
EC88	11015	-1.69	-6.00
EC87	10840	-2.28	-5.93
EC86	10760	-1.33	-6.20
EC85	10750	-1.82	-6.10
EC84	10700	-1.54	-6.04
EC83	10625	-1.87	-5.82
EC82	10545	-0.60	-5.87
EC81	10470	-1.00	-6.01
EC80	10405	-0.92	-5.31
EC79	10375	-1.34	-5.07
EC78	10320	-1.52	-5.91
EC77	10260	-0.82	-6.29
EC76	10195	-1.60	-6.21
EC75	10125	-2.40	-6.35
EC74	9990	-1.80	-6.47
EC73	9890	-1.31	-6.12

Sample	Depth (cm)	$\delta^{13}\text{C}$	$\delta^{18}\text{O}$
EC72	9790	-1.42	-6.50
EC71	9660	-1.38	-6.43
EC70	9560	-1.44	-6.30
EC69	9455	-1.12	-6.28
EC68	9350	-1.15	-5.93
EC67	9210	-0.53	-5.44
EC66	8930	0.92	-4.60
EC65	8775	0.34	-4.43
EC64	8685	1.71	-4.43
EC63	8646	1.65	-4.38
EC62	8567	1.78	-4.38
EC61	8560	1.55	-4.65
EC60	8460	1.61	-4.44
EC59	8394	1.78	-4.26
EC58	8329	1.71	-4.55
EC57	8224	1.61	-4.34
EC56	8139	1.61	-4.31
EC55	8069	1.57	-4.35
EC54	7894	1.68	-4.51
EC53	7834	1.74	-4.30
EC52	7747	1.50	-4.25
EC51	7659	1.87	-4.34
EC50	7570	1.85	-4.47
EC49	7480	1.88	-4.30
EC48	7420	1.91	-4.45
EC47	7355	1.87	-4.11
EC46	7275	1.83	-4.53
EC45	7175	1.89	-4.26
EC44	7075	1.91	-4.25
EC43	6975	1.93	-4.11
EC42	6875	1.91	-4.32
EC41	6775	1.82	-4.12
EC40	6675	1.83	-4.34
EC39	6575	1.75	-4.19
EC38	6475	1.91	-4.09
EC37	6375	1.91	-4.44
EC36	6275	1.94	-4.61
EC35	6175	2.01	-4.36
EC34	6080	1.97	-4.06
EC33	5990	1.87	-4.06
EC32	5940	1.70	-3.99
EC31	5905	-4.54	-20.20
EC29	5880	1.77	-4.17
EC28	5785	1.87	-4.45
EC27	5685	1.77	-4.47
EC26	5590	1.73	-4.00
EC25	5585	1.67	-3.86
EC24	5515	1.66	-4.42
EC23	5425	1.66	-4.38
EC22	5325	1.57	-4.15
EC21	5275	1.68	-3.94
EC20	5165	1.59	-4.82
EC19	5065	1.75	-4.33
EC18	4865	1.79	-3.89
EC17	4765	1.58	-4.26
EC16	4735	1.45	-3.91
EC15	4585	1.47	-3.69
EC14	4515	1.51	-3.61
EC13	4405	1.22	-4.10
EC12	4355	1.30	-3.97
EC11	4305	1.38	-3.96
EC10	4185	1.43	-4.23

L'Ecuelle

Sample	Depth (cm)	$\delta^{13}\text{C}$	$\delta^{18}\text{O}$
EC9	4085	1.37	-3.91
EC8	3975	1.45	-3.87
EC7	3895	1.39	-3.77
EC6	3795	1.27	-3.88
EC5	3060	1.54	-4.05
EC4	2940	1.51	-3.81
EC3	2930	1.55	-3.80
EC2	2900	1.55	-3.92
EC1	2750	1.49	-4.05
ECU24	2745	1.40	-3.50
ECU22	2600	1.30	-3.80
ECU21	2505	1.30	-4.00
ECU20	2455	1.30	-4.00
ECU19	2375	1.20	-4.10
ECU18	2270	1.20	-4.00
ECU17	2175	1.30	-3.60
ECU16	1170	0.90	-3.80
ECU15	1070	0.80	-4.10
ECU14	950	1.00	-3.90
ECU12	830	0.80	-4.50
ECU11	740	0.70	-4.40
ECU10	660	0.80	-4.50
ECU9	580	0.80	-4.00
ECU8	510	0.80	-4.00
ECU7	407	0.80	-3.70
ECU6	385	0.70	-3.70
ECU5	355	0.60	-4.20
ECU4	320	0.70	-4.30
ECU3	200	0.60	-4.00
ECU2	120	0.50	-4.10
ECU1	5	0.60	-3.40

Valsloch

Sample	Depth (cm)	$\delta^{13}\text{C}$	$\delta^{18}\text{O}$
VA1	30983	2.34	-5.07
VA2	30863	2.33	-4.48
VA3	30693	1.98	-4.03
VA4	30683	1.75	-4.11
VA5	30618	1.71	-4.09
VA6	30588	2.93	-3.94
VA7	30518	2.41	-3.64
VA8	30393	2.86	-3.71
VA9	30308	2.83	-3.66
VA10	30178	2.78	-3.64
VA11	30048	3.24	-3.39
VA12	29888	3.31	-3.64
VA13	29868	3.30	-3.37
VA15	29623	3.44	-3.24
VA16	29543	3.46	-3.43
VA17	29463	3.50	-3.67
VA18	29388	3.67	-3.12
VA19	29298	3.43	-3.11
VA20	29258	3.32	-3.86
VA21	29158	1.94	-3.58
VA22	29048	0.65	-3.51
VA23	28998	1.29	-3.72
VA24	28778	2.23	-3.75
VA25	28758	-1.45	-4.37
VA26	28708	-1.54	-4.48
VA27	28618	0.33	-4.61
VA28	28453	0.65	-4.39
VA29	28363	0.69	-4.65
VA30	28333	1.28	-4.39
VA31	28278	1.22	-4.57
VA32	28253	1.33	-4.42
VA33	28138	1.31	-4.17
VA34	28013	1.03	-4.26
VA35	27978	1.53	-4.56
VA36	27928	1.39	-4.27
VA37	27888	1.90	-4.18
VA38	27733	1.67	-4.13
VA39	27658	1.51	-4.17
VA40	27588	1.70	-3.97
VA41	27493	1.83	-3.66
VA42	27433	1.60	-4.11
VA43	27383	1.83	-3.77
VA44	27268	1.85	-3.63
VA45	27248	1.84	-3.60
VA46	27148	1.88	-3.28
VA47	27138	1.79	-3.70
VA48	27108	0.51	-4.25
VA49	26938	1.24	-4.29
VA50	26808	1.50	-3.94
VA51	26708	1.80	-3.85
VA52	26613	1.75	-4.10
VA54	26558	2.00	-3.62
VA55	26488	1.80	-3.79
VA56	26403	1.78	-3.54
VA57	26388	1.97	-2.84
VA58	26268	1.79	-3.89
VA59	26233	2.00	-4.00
VA60	26133	1.93	-3.41
VA61	26033	2.08	-3.40
VA62	25933	2.71	-3.67
VA63	25833	2.99	-3.84
VA64	25733	3.17	-3.08

Valsloch

Sample	Depth (cm)	$\delta^{13}\text{C}$	$\delta^{18}\text{O}$
VA65	25583	3.22	-3.67
VA66	25563	3.26	-3.27
VA67	25483	3.05	-3.15
VA68	25353	3.13	-3.41
VL28	25278	2.90	-3.44
VA69	25233	3.24	-3.02
VL27	25213	2.84	-3.55
VL26	25158	2.79	-3.71
VA70	25133	3.09	-3.26
VL25	25108	2.90	-3.51
VA71	25073	3.21	-3.52
VL24	24993	3.03	-3.76
VA72	24993	2.99	-3.69
VL23	24978	2.96	-3.84
VL22	24893	2.93	-3.31
VA73	24893	3.03	-3.39
VL21	24838	2.82	-3.61
VA74	24823	2.91	-3.54
VL20	24758	2.90	-3.35
VL19	24713	2.69	-3.45
VA75	24663	2.92	-3.34
VL18	24618	2.71	-3.49
VL17	24583	2.71	-3.60
VL15	24583	2.96	-3.52
VA76	24533	2.89	-3.54
VL14	24523	2.71	-3.49
VA77	24493	3.13	-3.61
VL13	24473	3.04	-3.31
VL12	24423	3.05	-3.19
VL16	24403	2.83	-3.47
VL11	24403	2.91	-3.51
VA78	24403	3.19	-5.55
VL10	24348	2.98	-3.56
VL9	24288	3.09	-3.42
VA79	24283	3.35	-3.42
VL8	24233	3.04	-3.41
VL7	24083	3.15	-3.53
VL6	24033	2.84	-3.08
VL5	23998	2.73	-3.29
VL4	23943	2.50	-3.58
VL3	23833	2.43	-3.52
VL2	23773	2.45	-3.43
VL1	23653	2.58	-3.27
VA80	23553	3.35	-3.61
VA81	23413	3.14	-3.81
VA82	23393	3.40	-4.18
VA83	23263	3.26	-3.60
VA84	23173	3.13	-4.27
VA85	23100	3.09	-4.06
VA86	23040	3.58	-3.44
VA87	23005	3.43	-3.54
VA88	22985	2.99	-3.77
VA89	22915	2.99	-3.69
VA90	22835	3.24	-3.64
VA91	22775	3.10	-4.11
VA92	22670	3.33	-3.84
VA93	22615	3.12	-4.02
VA94	22525	3.03	-4.08
VA95	22425	3.16	-3.82
VA96	22310	2.94	-4.28
VA97	22190	3.24	-4.19
VA98	22165	3.41	-4.27

Sample	Depth (cm)	$\delta^{13}\text{C}$	$\delta^{18}\text{O}$
VA99	21925	3.21	-4.26
VA101	21860	3.51	-4.10
VA102	21795	3.38	-3.30
VA103	21735	3.33	-4.10
VA104	21720	3.38	-3.72
VA105	21620	3.40	-3.91
VA107	21480	3.52	-3.86
VA108	21455	3.75	-3.77
VA109	21325	3.63	-3.82
VA110	21280	3.39	-3.94
VA111	21240	3.74	-3.71
VA113	21170	3.60	-3.70
VA114	21155	3.44	-3.97
VA115	21085	3.44	-4.10
VA116	21070	3.42	-4.20
VA117	21010	3.48	-4.33
VA118	21000	3.36	-3.85
VA119	20945	3.54	-3.95
VA120	20920	3.55	-3.66
VA121	20840	3.46	-3.66
VA122	20785	2.59	-4.64
VA123	20725	3.27	-4.67
VA124	20545	3.04	-3.86
VA125	20445	2.99	-4.06
VA126	20425	0.97	-4.54
VA127	20325	1.84	-4.79
VA128	20225	1.00	-4.49
VA129	20125	1.68	-4.30
VA130	20035	1.70	-4.50
VA131	20005	1.93	-4.72
VA132	19885	2.17	-4.91
VA133	19845	2.20	-4.33
VA134	19830	2.09	-4.69
VA135	19745	2.12	-4.49
VA136	19725	2.01	-4.88
VA137	19505	1.40	-4.25
VA138	19405	2.09	-3.70
VA139	19325	1.39	-4.19
VA140	19215	1.91	-4.56
VA141	19015	1.91	-4.21
VA142	18815	2.04	-3.75
VA143	18715	1.54	-4.01
VA144	18615	1.48	-4.39
VA145	18515	2.01	-3.62
VA146	18355	1.76	-3.24
VA147	18195	2.41	-3.74
VA148	18165	2.35	-3.74
VA149	18105	2.42	-3.85
VA150	18065	2.45	-3.79
VA151	17965	2.51	-3.84
VA152	17845	2.49	-4.21
VA153	17825	2.55	-4.07
VA154	17695	2.35	-4.02
VA155	17675	2.23	-4.07
VA156	17605	2.17	-3.79
VA157	17515	2.10	-4.00
VA158	17495	2.17	-3.23
VA159	17375	2.11	-4.21
VA160	17345	2.21	-3.80
VA161	17245	2.20	-3.68
VA163	17155	2.20	-3.73
VA164	17045	2.49	-3.39

Valsloch

Sample	Depth (cm)	$\delta^{13}\text{C}$	$\delta^{18}\text{O}$
VA165	17015	1.90	-3.53
VA166	16925	1.96	-3.54
VA167	16825	2.06	-3.78
VA168	16795	1.94	-3.69
VA169	16695	2.31	-3.89
VA170	16645	2.29	-3.44
VA171	16625	2.33	-4.52
VA172	16445	2.33	-4.18
VA173	16285	2.39	-3.45
VA174	16195	2.37	-3.84
VA175	16015	2.01	-4.19
VA176	15895	2.41	-3.87
VA177	15735	2.58	-4.10
VA178	15615	2.40	-3.80
VA179	15465	2.56	-3.83
VA180	15285	2.47	-4.09
VA181	15110	2.78	-3.59
VA182	14860	2.64	-3.63
VA183	14660	2.52	-3.83
VA184	14540	2.27	-4.17
VA185	14350	2.29	-4.31
VA186	14150	2.44	-4.27
VA187	13970	2.73	-3.16
VA188	13670	2.28	-4.46
VA189	13550	2.34	-4.00
VA190	13275	2.07	-4.18
VA191	13105	2.10	-4.00
VA192	13095	2.10	-3.62
VA193	12935	2.19	-4.68
VA194	12835	2.14	-4.21
VA195	12685	2.21	-4.11
VA196	12495	1.96	-4.41
VA197	12295	2.58	-3.85
VA198	12010	2.24	-3.90
VA199	11820	2.05	-4.27
VA200	11725	1.97	-4.52
VA201	11615	2.27	-3.89
VA203	11375	2.40	-3.48
VA204	11155	2.62	-2.44
VA205	10980	2.21	-5.35
VA207	10820	2.04	-3.91
VA210	10505	2.20	-3.86
VA212	10200	2.21	-3.87
VA213	10170	2.28	-3.57
VA215	10100	2.16	-3.68
VA216	10065	2.26	-3.58
VA218	9940	2.28	-3.24
VA220	9785	2.28	-3.40
VA221	9640	2.12	-4.24
VA222	9580	2.16	-4.29
VA223	9520	2.30	-3.92
VA224	9460	2.14	-3.71
VA225	9265	2.23	-3.63
VA226	9200	2.10	-3.51
VA227	9125	2.03	-3.24
VA228	9080	2.05	-3.75
VA230	8935	2.14	-3.76
VA232	8820	2.26	-3.39
VA235	8570	2.21	-3.74
VA236	8480	1.99	-4.07
VA238	8315	2.19	-3.53
VA239	8297	2.95	-3.09

Sample	Depth (cm)	$\delta^{13}\text{C}$	$\delta^{18}\text{O}$
VA241	8202	2.75	-3.37
VA243	8012	2.86	-3.22
VA244	7927	2.61	-3.41
VA246	7707	2.72	-3.29
VA248	7467	2.78	-2.91
VA249	7367	2.88	-3.27
VA250	7217	2.63	-3.29
VA252	6962	2.90	-4.06
VA253	6862	2.76	-3.50
VA255	6647	2.79	-3.06
VA256	6542	2.63	-3.39
VA257	6347	2.39	-3.27
VA258	6192	2.84	-3.00
VA260	6002	2.79	-3.01
VA262	5732	2.74	-3.08
VA265	5317	2.60	-3.13
VA266	5027	2.45	-3.54
VA267	4907	2.37	-3.05
VA268	4847	2.47	-3.14
VA269	4517	2.33	-2.97
VA270	4462	2.31	-2.87
VA271	4417	2.32	-2.95
VA272	4367	2.36	-2.97
VA273	4347	2.27	-2.89
VA274	4322	2.36	-3.04
VA275	4297	2.34	-3.07
VA276	4267	2.32	-3.14
VA277	4212	2.32	-2.94
VA278	4142	2.30	-3.13
VA279	4077	2.32	-3.03
VA280	4022	2.23	-3.16
VA281	3932	2.27	-3.19
VA282	3882	2.29	-3.46
VA283	3867	2.26	-3.24
VA284	3772	2.26	-3.10
VA285	3672	2.40	-3.24
VA286	3502	2.50	-3.08
VA287	3447	2.47	-3.00
VA288	3392	2.53	-3.14
VA289	3352	2.52	-3.07
VA290	3262	2.64	-3.14
VA291	3142	2.52	-3.08
VA292	3077	2.56	-3.13
VA293	2992	2.69	-3.03
VA294	2902	2.56	-3.18
VA295	2832	2.56	-3.52
VA296	2762	2.71	-3.27
VA297	2687	2.55	-3.56
VA298	2642	2.64	-3.44
VA299	2617	2.70	-3.10
VA300	2567	2.75	-3.17
VA301	2502	2.83	-3.24
VA302	2412	2.80	-3.18
VA303	2392	2.68	-3.13
VA304	2322	2.72	-3.09
VA305	2202	2.66	-3.19
VA306	2135	2.61	-3.44
VA307	2080	2.54	-3.47
VA308	2020	2.53	-3.42
VA309	1900	2.65	-3.31
VA310	1855	2.58	-3.22
VA311	1823	2.56	-3.29

Valsloch

Sample	Depth (cm)	$\delta^{13}\text{C}$	$\delta^{18}\text{O}$
VA312	1795	2.55	-3.20
VA313	1675	2.02	-3.31
VA314	1575	1.88	-3.83
VA315	1545	2.02	-3.53
VA316	1500	1.96	-3.34
VA317	1450	1.85	-3.41
VA318	1415	1.76	-3.44
VA319	1360	1.76	-3.50
VA320	1315	1.83	-3.64
VA321	1295	1.79	-3.59
VA322	1235	1.77	-3.49
VA323	1225	1.86	-3.33
VA324	1140	1.78	-3.49
VA325	1055	1.76	-3.53
VA326	1010	1.46	-3.74
VA327	955	1.57	-3.72
VA328	920	1.49	-3.71
VA329	875	1.49	-3.75
VA330	740	1.53	-3.63
VA331	670	1.48	-3.79
VA332	610	1.29	-3.90
VA333	560	1.25	-3.97
VA334	495	1.01	-3.93
VA335	440	1.21	-3.90
VA336	320	1.00	-4.53
VA336b	235	0.91	-3.85
VA337	225	0.74	-4.25
VA338	150	0.50	-4.69
VA339	75	0.24	-4.93
VA340	25	0.37	-4.98

Harder

Sample	Depth (cm)	$\delta^{13}\text{C}$	$\delta^{18}\text{O}$
HA 1	0	1.01	-1.70
HA 6	123	1.04	-1.73
HA10	254	1.02	-3.06
HA 11	285	1.16	-2.57
HA12	300	1.28	-2.60
HA13	315	1.15	-2.71
HA15	390	1.16	-2.67
HA 16	454	1.37	-2.91
HA17	473	1.37	-2.78
HA18	506	1.47	-2.89
HA19	551	1.20	-3.52
HA20	601	1.42	-2.69
HA 21	608	1.42	-2.83
HA22	713	1.55	-2.70
HA25	878	1.89	-3.09
HA 26	971	2.15	-2.39
HA27	991	2.01	-2.52
HA29	1058	1.93	-2.74
HA30	1130	2.02	-3.01
HA 31	1161	1.85	-2.83
HA32	1218	2.16	-3.17
HA34	1293	2.08	-2.93
HA 36	1338	2.16	-2.42
HA39	1443	1.95	-2.30
HA 41	1553	2.54	-2.69
HA42	1580	2.34	-2.82
HA45	1818	2.30	-5.12
HA 46	1888	2.47	-4.70
HA48	2024	2.63	-3.14
HA49	2043	2.25	-2.87
HA50	2110	2.46	-3.01
HA 51	2178	2.66	-3.29
HA52	2258	2.66	-3.13
HA53	2300	2.32	-4.17
HA54	2370	2.38	-3.15
HA 55	2410	2.38	-3.03
HA58	2532	2.57	-2.91
HA59	2567	2.61	-2.89
HA 61	2614	2.68	-3.00
HA65	2796	2.68	-3.03
HA 66	2839	2.74	-3.15
HA68	3008	2.80	-3.33
HA69	3052	2.79	-3.35
HA 71	3142	2.93	-3.00
HA73	3194	2.89	-3.33
HA75	3259	2.91	-3.35
HA 76	3347	2.89	-3.49
HA77	3435	2.91	-3.20
HA78	3443	2.92	-3.25
HA80	3548	3.01	-2.82
HA 81	3600	3.03	-3.11
HA82	3648	3.08	-3.10
HA84	3722	3.07	-3.30
HA 86	3864	3.11	-3.39
HA91	4008	3.25	-3.18
HA 96	4287	3.12	-3.08
HA101	4520	3.25	-3.11
HA106	5010	2.96	-3.10
HA111	5334	2.37	-3.24
HA116	5620	2.40	-2.98
HA121	5874	2.56	-3.19
HA126	6138	2.63	-2.95

Harder

Sample	Depth (cm)	$\delta^{13}\text{C}$	$\delta^{18}\text{O}$
HA 131	6284	2.66	-2.76
HA 136	6587	2.91	-2.86
HA 141	6787	2.97	-2.80
HA 146	6976	2.92	-3.22
HA 151	7339	2.78	-3.07
HA 156	7596	2.75	-3.20
HA 161	7813	2.77	-3.01
HA 166	7959	2.64	-3.25
HA 171	8389	2.30	-2.63
HA 176	8601	2.46	-2.56
HA 181	9015	2.42	-2.96
HA 186	9336	1.92	-2.52
HA 191	9659	2.71	-3.43
HA 196	9988	2.54	-3.59
HA 201	10268	2.68	-3.35
HA 206	10618	2.76	-2.98
HA 211	10931	2.74	-2.64
HA 216	11244	2.93	-2.63
HA 221	11517	2.65	-2.94
HA 226	11944	2.73	-3.18
HA 231	12280	2.69	-2.84
HA 236	12702	2.82	-2.71
HA 241	13637	2.46	-3.20
HA 246	14237	2.55	-2.88
HA 251	14852	3.17	-2.65
HA 261	15727	2.71	-3.34
HA 266	16149	2.79	-3.02
HA 271	16542	2.88	-2.61
HA 276	17417	2.18	-3.16
HA 281	18091	2.38	-2.55
HA 286	18626	2.46	-3.09
HA 291	19592	2.78	-2.77
HA 296	20110	2.48	-3.20
HA 301	20648	2.68	-3.07
HA 306	21343	2.85	-2.80
HA 311	21848	2.45	-3.04
HA 316	22469.5	2.48	-2.56
HA 321	23114.5	2.34	-2.72
HA322	23209.5	2.42	-3.02
HA323	23284.5	2.15	-2.80
HA324	23354.5	2.24	-2.70
HA325	23419.5	2.07	-3.42
HA 326	23649.5	2.23	-3.01
HA327	23676.5	2.11	-2.41
HA328	23751.5	1.95	-3.22
HA329	23811.5	1.90	-3.18
HA330	23819.5	2.47	-2.60
HA 331	23904.5	2.11	-2.48
HA332	23993.5	2.50	-2.51
HA333	24078.5	2.11	-2.52
HA334	24173.5	1.86	-3.05
HA335	24223.5	2.02	-2.66
HA 336	24331.5	2.15	-2.63
HA337	24413.5	1.95	-3.22
HA340	24685.5	2.17	-3.37
HA 341	24745.5	2.21	-2.83
HA342	24850.5	2.20	-3.69
HA 346	25155.5	2.01	-2.75
HA 351	25546.5	2.10	-2.98
HA 356	26061.5	2.25	-3.33
HA 362	26603.5	2.86	-2.54
HA 366	26783.5	2.99	-2.45

Sample	Depth (cm)	$\delta^{13}\text{C}$	$\delta^{18}\text{O}$
HA 371	27208.5	2.90	-2.26
HA 376	27667.5	2.98	-2.54
HA 381	28037.5	2.81	-2.60
HA 386	28507.5	2.24	-2.44
HA 391	28952.5	2.30	-2.87
HA 397	29597.5	2.09	-3.04
HA 402	30097.5	2.16	-3.05
HA 405	30392.5	2.18	-2.41
HA 411	30907.5	2.05	-1.88
HA 415	31197.5	2.23	-1.75

Justistal

Sample	Depth (cm)	$\delta^{13}\text{C}$	$\delta^{18}\text{O}$
LB 233	5	0.68	-3.00
LB 232	95	0.64	-3.04
LB 231bis	600	0.96	-2.88
LB 231	1110	0.86	-3.06
LB 230	1225	1.20	-2.60
LB 229	1365	1.33	-3.57
LB 228	1445	1.33	-2.86
LB 227	1545	1.43	-2.90
LB 226	1665	1.61	-2.91
LB 225	1780	1.60	-2.85
LB 224	2580	1.43	-3.69
LB 223	2600	1.62	-3.23
LB 222	2680	1.85	-2.95
LB 221	2780	1.62	-3.43
LB 220	2880	1.68	-3.58
LB 219	2980	1.59	-3.27
LB 218	3080	1.76	-3.50
LB 217	3180	1.63	-3.13
LB 216	3280	1.56	-3.82
LB 215	3340	1.66	-3.45
LB 214	3400	1.91	-3.16
LB 213	3500	1.46	-3.85
LB 212	3600	1.74	-3.53
LB 211	3700	1.74	-4.02
LB 210	3800	1.57	-3.95
LB 209	3900	1.70	-3.72
LB 208	4080	1.61	-3.65
LB 207	4500	1.87	-4.03
LB 206	4600	1.81	-3.76
LB 205	4700	1.87	-3.76
LB 204	4800	1.79	-3.84
LB 203	4900	1.67	-4.04
LB 202	5000	1.59	-4.03
LB 201	5100	1.55	-4.09
LB 200	5200	1.63	-3.86
LB 199	5300	1.77	-3.84
LB 198	5400	1.69	-3.77
LB 197	5500	1.51	-4.24
LB 196	5600	1.59	-3.86
LB 195	5700	1.73	-3.67
LB 194	5800	1.70	-3.76
LB 193	5900	1.81	-3.50
LB 192	6000	1.70	-3.81
LB 191	6100	0.34	-7.33
LB 190	6200	1.97	-3.47
LB 189	6300	2.17	-4.04
LB 188	6400	1.70	-3.77
LB 187	6500	1.62	-4.17
LB 186	6600	1.64	-4.06
LB 185	6700	1.64	-3.72
LB 184	6820	1.69	-3.76
LB 183	6920	1.69	-3.69
LB 182	7020	1.74	-3.88
LB 181	7120	1.91	-2.95
LB 180	7220	1.57	-4.28
LB 179	7320	1.57	-3.81
LB 178	7420	1.61	-3.89
LB 177	7520	1.70	-3.77
LB 176	7620	2.13	-2.80
LB 175	7720	2.33	-2.44
LB 174	7820	2.04	-2.96
LB 173	7920	1.87	-3.45

Sample	Depth (cm)	$\delta^{13}\text{C}$	$\delta^{18}\text{O}$
LB 172	8020	1.87	-3.75
LB 171	8120	1.86	-3.58
LB 170	8220	1.94	-3.65
LB 169	8320	1.77	-4.01
LB 168	8420	1.80	-3.80
LB 167	8520	1.82	-3.85
LB 166	8620	1.84	-3.79
LB 165	8720	1.88	-3.78
LB 164	8820	1.85	-3.94
LB 163	8920	1.81	-3.66
LB 162	9020	1.95	-3.41
LB 161	9120	2.03	-3.19
LB 160	9220	1.57	-4.34
LB 159	9320	1.88	-3.89
LB 158	9420	1.80	-3.91
LB 157	9520	1.79	-3.76
LB 156	9620	1.88	-3.42
LB 155	9720	2.02	-3.02
LB 154	9820	1.93	-2.97
LB 153	9920	1.73	-3.74
LB 152	10020	1.79	-3.56
LB 151	10120	2.04	-3.54
LB 150	10220	2.02	-4.29
LB 149	10320	1.72	-3.60
LB 148	10420	1.85	-3.30
LB 147	10520	1.79	-3.76
LB 146	10580	1.97	-2.90
LB 145	10680	1.85	-3.42
LB 144	10780	2.19	-2.04
LB 143	10880	2.09	-2.16
LB 142	10980	1.95	-2.83
LB 141	11050	2.15	-1.92
LB 140	11150	2.71	-6.01
LB 139	11250	2.23	-2.47
LB 138	11350	2.45	-5.74
LB 137	11450	2.14	-2.40
LB 136	11640	1.79	-3.22
LB 135	11750	2.10	-2.70
LB 134	11860	1.66	-3.44
LB 133	11950	1.63	-4.27
LB 132	12050	1.71	-3.55
LB 131	12150	1.70	-3.73
LB 130	12260	1.60	-3.55
LB 129	12370	1.68	-3.81
LB 128	12470	1.78	-3.75
LB 127	12570	1.60	-3.68
LB 126	12680	1.67	-3.44
LB 125	12770	1.62	-3.48
LB 124	13180	1.76	-3.05
LB 123	13290	1.77	-3.42
LB 122	13400	1.92	-3.32
LB 121	13510	1.92	-3.54
LB 120	13620	1.95	-3.42
LB 119	13730	1.95	-3.55
LB 117	13840	2.00	-3.53
LB 116	13960	2.04	-3.47
LB 115	14070	2.08	-3.31
LB 114	14170	2.11	-3.29
LB 113	14290	2.22	-3.48
LB 112	14400	2.19	-3.21
LB 111	14500	2.10	-3.42
LB 110	14610	2.22	-3.58

Justistal

Sample	Depth (cm)	$\delta^{13}\text{C}$	$\delta^{18}\text{O}$
LB109	14720	2.26	-3.04
LB108	14830	2.28	-3.26
LB107	14940	2.30	-3.47
LB106	15050	2.29	-3.33
LB105	15160	2.38	-3.31
LB104	15260	2.29	-3.96
LB103	15360	2.42	-3.24
LB102	15480	2.10	-3.80
LB101	15580	2.60	-2.74
LB100	15710	2.28	-3.42
LB99	15810	2.68	-2.48
LB98	15910	2.48	-2.71
LB97	16010	2.15	-3.35
LB96	16110	2.09	-3.78
LB95	16210	2.22	-3.19
LB94	16310	2.17	-3.37
LB93	16410	2.23	-3.68
LB92	16510	2.37	-3.65
LB91	16620	2.31	-3.61
LB90	16670	2.40	-3.26
LB89	16770	2.35	-3.62
LB88	16880	2.35	-3.44
LB87	16910	2.54	-3.21
LB86	17020	2.41	-3.28
LB85	17120	2.47	-3.54
LB 84	17220	2.59	-3.23
LB83	17340	2.55	-3.11
LB82	17430	2.54	-3.10
LB81	17590	2.67	-2.94
LB80	17720	2.49	-3.00
LB79	17800	2.44	-3.03
LB78	17850	2.28	-3.50
LB77	17950	2.38	-3.02
LB76	18050	2.33	-3.21
LB75	18140	2.09	-3.80
LB74	18650	2.09	-3.36
LB73	18800	2.17	-2.96
LB72	18900	1.84	-4.04
LB71	18995	2.32	-2.70
LB70	19095	2.08	-3.29
LB69	19195	2.22	-3.06
LB68	19295	2.20	-3.05
LB67	19395	2.30	-3.18
LB66	19495	2.13	-3.00
LB65	19595	2.01	-3.43
LB64	19685	1.92	-3.44
LB63	19780	2.01	-2.93
LB62	19875	2.34	-3.51
LB61	19875	2.26	-3.17
LB60	20040	2.18	-3.29
LB59	20105	1.96	-3.36
LB58	20155	2.13	-3.15
LB57	20165	2.12	-3.12
LB56	20255	2.18	-3.06
LB55	20285	2.08	-3.25
LB54	20355	2.17	-3.28
LB53	20430	2.18	-3.00
LB52	20515	2.07	-3.16
LB51	20540	2.08	-3.12
LB50	20620	1.98	-2.96
LB49	20685	1.94	-3.09
LB48	20735	2.10	-2.77

Sample	Depth (cm)	$\delta^{13}\text{C}$	$\delta^{18}\text{O}$
LB47	20780	2.09	-2.93
LB46	20845	2.00	-2.81
LB45	20910	1.97	-2.67
LB44	20970	1.93	-2.22
LB43	21050	2.56	-3.50
LB42	21130	2.48	-3.32
LB41	21245	2.46	-3.38
LB40	21345	2.59	-3.27
LB39	21395	2.53	-3.19
LB 38	21450	2.35	-3.54
LB 37	21545	2.42	-3.18
LB 36	21620	2.25	-3.30
LB 35	21700	2.19	-3.24
LB 34	21780	2.06	-3.25
LB 33	21845	2.20	-2.96
LB 32	21910	2.19	-3.33
LB 31	21990	2.08	-3.16
LB 30	22070	1.98	-3.35
LB 29	22110	1.94	-3.42
LB 28	22145	1.95	-3.51
LB 27	22260	1.66	-3.39
LB 26	22320	1.88	-3.41
LB 25	22440	1.91	-3.65
LB 24	22560	2.20	-3.07
LB 23	22605	2.15	-3.89
LB 22	22710	2.02	-3.03
LB 21	22805	1.95	-3.43
LB 20	22875	1.59	-3.24
LB 19	22900	2.07	-3.54
LB 18	23005	1.75	-3.49
LB 17	23150	1.72	-3.10
LB 16	23210	1.93	-2.47
LB 15	23275	2.99	-2.55
LB 14	23295	3.07	-2.63
LB 13	23373	3.11	-2.23
LB 12	23405	2.58	-3.66
LB 11	23430	3.01	-2.37
LB 10	23450	3.18	-2.42
LB 9	23475	3.12	-2.18
LB 8	23495	3.29	-2.56
LB 7	23590	3.38	-2.84
LB 6	23630	3.30	-2.55
LB 5	23655	3.15	-2.73
LB 4	23700	3.19	-2.86
LB 3	23710	3.37	-2.60
LB 2	23780	3.16	-2.85
LB 1	23860	3.07	-2.76

Morschach

Sample	Depth (cm)	$\delta^{13}\text{C}$	$\delta^{18}\text{O}$
MC1	0	2.96	-1.81
MC2	-15	4.72	-1.94
MC2BIS	-32	4.22	-2.88
MC3	-45	4.02	-2.68
MC3a	-73	4.00	-3.20
MC3b	-89	4.10	-3.20
MC4	-100	3.96	-3.28
MC4	-100	4.00	-3.20
MC4a	-119	3.90	-2.30
MC4b	-128	3.70	-2.30
MC5	-230	3.36	-3.51
MC6	-351	3.55	-3.39
MC7	-447	3.66	-3.48
MC8	-535	3.53	-4.19
MC9	-635	3.75	-4.57
MC10	-695	3.48	-3.98
MC11	-760	3.59	-3.61
MC12	-845	3.66	-3.90
MC13	-945	3.52	-4.02
MC14	-1050	3.50	-3.53
MC15	-1150	3.43	-3.75
MC16	-1260	3.38	-3.36
MC17	-1365	3.30	-3.75
MC18	-1445	3.39	-3.46
MC19	-1550	3.24	-3.36
MC20	-1638	3.19	-3.61
MC21	-1750	3.19	-3.82
MC22	-1805	3.28	-3.82
MC23	-1945	3.33	-3.97
MC24	-2035	3.50	-3.94
MC25	-2130	3.44	-3.54
MC26	-2235	3.32	-3.74
MC27	-2360	3.65	-3.70
MC28	-2450	3.74	-3.57
MC29	-2550	3.69	-3.37
MC30	-2630	3.66	-3.51
MC31	-2740	3.62	-3.45
MC32	-2835	3.62	-3.23
MC33	-2952	3.58	-3.55
MC34	-3050	3.56	-2.68
MC35	-3135	3.40	-2.82
MC36	-3215	2.97	-3.22
MC37	-3245	1.68	-3.25
MC38	-3350	2.44	-3.41
MC39	-3435	2.69	-3.56
MC40	-3515	2.45	-3.67
MC41	-3575	1.98	-3.49
MC42	-3695	-1.85	-4.28
MC43	-3835	-0.19	-4.38
MC44	-3900	-0.86	-4.43
MC45	-4022	-0.83	-4.38
MC46	-4135	3.09	-3.39
MC47	-4220	2.68	-2.87
MC47bis	-4240	1.99	-4.26
MC49	-4305	2.82	-3.38
MC50	-4320	1.39	-3.53
MC51	-4430	1.56	-3.87
MC52	-4535	2.02	-4.06
MC53	-4625	-2.62	-4.64
MC54	-4705	-1.58	-4.77
MC55	-4785	-0.26	-4.71
MC56	-4835	-1.54	-4.59

Sample	Depth (cm)	$\delta^{13}\text{C}$	$\delta^{18}\text{O}$
MC57	-4875	-0.56	-4.47
MC58	-4940	-0.11	-4.38
MC59	-5035	0.62	-4.36
MC60	-5110	0.63	-4.42
MC61	-5215	1.36	-4.13
MC62	-5325	0.95	-4.19
MC63	-5435	2.12	-4.15
MC64	-5505	2.47	-3.07
MC65	-5650	2.34	-2.89
MC66	-5725	2.46	-3.31
MC67	-5850	2.75	-3.27
MC68	-5952	2.79	-3.13
MC69	-6035	2.86	-3.62
MC70	-6150	3.03	-3.43
MC71	-6195	2.46	-2.88
MC72	-6350	2.93	-3.90
MC73	-6450	2.97	-3.73
MC74	-6530	3.05	-3.13
MC75	-6640	2.71	-4.32
MC76	-6745	3.04	-4.10
MC77	-6825	2.98	-3.79
MC78	-6925	3.04	-4.10
MC79	-7053	3.21	-3.68
MC80	-7135	3.21	-3.97
MC81	-7251	3.42	-3.38
MC82	-7335	3.28	-3.82
MC83	-7449	3.34	-3.74
MC84	-7518	3.18	-4.11
MC85	-7650	3.22	-3.39
MC86	-7695	3.16	-2.42
MC87	-7790	3.38	-3.66
MC88	-7900	3.58	-3.45
MC89	-8045	3.61	-3.46
MC90	-8150	3.46	-3.49
MC91	-8220	3.28	-3.53
MC92	-8340	3.13	-4.30
MC93	-8435	3.05	-4.18
MC94	-8550	3.12	-3.52
MC95	-8605	3.23	-3.75
MC96	-8705	3.33	-3.71
MC97	-8823	3.32	-3.92
MC98	-8928	3.28	-3.52
MC99	-9020	3.15	-2.97
MC100	-9125	3.12	-3.60
MC101	-9252	3.16	-3.36
MC102	-9350	3.26	-3.54
MC103	-9440	3.41	-3.44
MC104	-9535	3.40	-3.14
MC105	-9630	3.44	-2.72
MC106	-9745	3.03	-3.37
MC107	-9850	3.08	-2.98
MC108	-9945	3.14	-3.06
MC109	-9970	2.93	-3.03
MC110	-10045	3.13	-3.14
MC111	-10100	3.17	-3.18
MC112	-10232	3.47	-3.10
MC113	-10350	3.48	-3.65
MC114	-10450	3.57	-3.29
MC115	-10475	3.53	-3.20
MC116	-10585	3.33	-3.00
MC117	-10727	3.85	-2.83
MC118	-10745	3.55	-3.28

Morschach

Sample	Depth (cm)	$\delta^{13}\text{C}$	$\delta^{18}\text{O}$
MC119	-10820	3.65	-4.35
MC120	-10875	3.55	-2.80
MC121	-10975	3.29	-3.27
MC122	-11020	3.27	-3.04
MC123	-11040	3.21	-3.17
MC124	-11145	3.40	-3.36
MC125	-11185	3.39	-3.44
MC126	-11230	3.39	-3.14
MC127	-11350	3.05	-2.13
MC128	-11450	3.36	-2.95
MC129	-11490	3.24	-2.91
MC130	-11515	3.47	-3.04
MC131	-11550	3.30	-3.31
MC132	-11630	3.46	-3.05
MC133	-11735	3.13	-3.85
MC134	-11787	3.48	-4.31
MC135	-11850	2.98	-3.68
MC136	-11890	3.55	-3.17
MC137	-11935	3.02	-2.54
MC138	-12035	3.50	-3.21
MC139	-12065	3.52	-3.01
MC140	-12120	3.54	-3.76
MC141	-12240	3.87	-3.13
MC142	-12335	3.67	-2.92
MC143	-12415	3.61	-3.45
MC144	-12545	3.66	-3.21
MC145	-12635	3.70	-3.55
MC146	-12745	3.59	-2.90
MC147	-12850	4.01	-2.17
MC148	-12950	3.60	-2.55
MC149	-13052	3.56	-3.15
MC150	-13130	3.76	-2.99
MC151	-13235	3.22	-3.16
MC152	-13295	3.12	-2.90
MC153	-13410	3.55	-3.27
MC154	-13525	3.59	-3.38
MC155	-13640	3.73	-3.04
MC156	-13740	3.44	-3.19
MC157	-13780	3.83	-2.51
MC158	-13935	3.15	-3.36
MC159	-14025	3.02	-3.36
MC160	-14147	3.13	-4.67
MC161	-14228	3.11	-4.73
MC162a	-14232	1.03	-3.82
MC162b	-14233	3.20	-3.68
MC163	-14327	3.01	-3.77
MC164	-14440	3.14	-3.67
MC165	-14535	3.09	-4.63
MC166	-14585	2.96	-4.45
MC167	-14750	2.99	-3.71
MC168	-14800	3.11	-4.61
MC169	-14880	2.70	-3.69
MC170	-14945	1.61	-4.36
MC171	-15025	2.28	-3.93
MC172	-15125	1.93	-4.06
MC173	-15240	1.82	-4.69
MC174	-15340	1.74	-4.80
MC175	-15422	1.64	-4.20
MC176	-15505	1.97	-4.50
MC177	-15590	2.28	-4.62

Sample	Depth (cm)	$\delta^{13}\text{C}$	$\delta^{18}\text{O}$
MC178	-15735	2.39	-4.15
MC179b	-15790	1.87	-4.25
MC179a	-15790	2.24	-4.38
MC180	-15915	2.20	-4.00
MC181	-16040	2.23	-3.97
MC182	-16142	2.28	-3.94
MC183	-16210	2.51	-4.30
MC184	-16290	2.53	-4.39
MC185	-16385	2.56	-4.27
MC186	-16530	2.67	-4.26
MC187	-16645	2.59	-4.32
MC188	-16745	2.56	-4.17
MC189	-16853	2.53	-4.21
MC190	-16935	2.50	-4.31
MC191	-17045	2.55	-4.15
MC192	-17130	2.41	-4.05
MC193	-17250	2.34	-4.54
MC194	-17312	2.36	-4.56
MC195	-17452	1.96	-4.51
MC196	-17545	1.92	-3.82
MC197	-17620	1.95	-4.46
MC198	-17740	1.84	-4.36
MC200	-17805	1.79	-4.16
MC201	-17807	1.89	-4.10
MC199	-17835	1.71	-3.19
MC202	-18060	1.93	-3.42
MC203	-18253	2.00	-2.85
MC204	-18348	2.91	-0.60
MC205	-18450	2.15	-2.38
MC206	-18575	1.66	-3.47
MC207	-18700	1.97	-3.37
MC208	-18885	2.07	-3.14
MC209	-18950	2.13	-3.17
MC210	-19130	2.28	-3.18
MC211	-19332	2.36	-3.34
MC212	-19425	2.22	-3.09
MC213	-19515	2.27	-3.04
MC214	-19735	2.42	-3.09
MC215	-20030	2.44	-3.48
MC217	-20315	2.47	-3.38
MC218	-20425	2.29	-3.62
MC219	-20560	2.40	-3.94
MC220	-20675	2.27	-3.83
MC221	-20825	2.29	-3.32
MC222	-20920	2.73	-2.82
MC223	-20965	2.42	-3.06
MC224	-21095	2.45	-3.12
MC216	-21120	2.23	-3.41
MC225	-21160	2.22	-3.14
MC226	-21385	2.05	-3.25
MC227	-21485	2.10	-3.58
MC228	-21710	2.52	-2.75
MC229	-21775	2.31	-2.99
MC230	-21875	2.08	-3.24
MC231	-21980	2.34	-2.75
MC232	-22052	2.38	-3.00
MC233	-22150	2.28	-3.09
MC234	-22260	2.14	-3.59
MC235	-22325	2.14	-3.77
MC236	-22480	2.15	-3.65
MC237	-22545	2.11	-3.66
MC238	-22700	2.18	-3.28

Morschach

Sample	Depth (cm)	$\delta^{13}\text{C}$	$\delta^{18}\text{O}$
MC239	-22760	2.22	-3.39
MC240	-22870	2.17	-3.65
MC241	-23035	2.15	-3.45
MC243	-23240	1.99	-3.31
MC242	-23265	2.11	-3.13
MC244	-23360	2.02	-3.14
MC245	-23455	1.99	-3.28
MC246	-23565	1.97	-3.30
MC247	-23665	2.18	-3.21
MC248	-23725	2.29	-2.76
MC249	-23830	2.28	-3.18
MC250	-23955	2.20	-3.00
MC251	-24025	2.07	-4.23
MC252	-24235	2.38	-2.93
MC253	-24345	2.43	-3.05
MC254	-24442	2.46	-2.75
MC255	-24552	2.49	-3.10
MC256	-24652	2.49	-3.89
MC257	-24750	2.72	-2.98
MC258	-24860	2.53	-3.36
MC259	-24930	2.50	-3.30
MC260	-25035	2.71	-2.39
MC261	-25145	2.63	-2.96
MC262	-25250	2.36	-3.64
MC263	-25350	2.30	-2.92
MC264	-25450	2.50	-2.76
MC265	-25530	2.46	-3.35
MC266	-25640	2.62	-3.10
MC267	-25715	2.64	-2.19
MC268	-25835	2.70	-2.91
MC269	-25920	2.37	-3.40
MC270	-26045	2.74	-3.16
MC271	-26138	2.68	-3.14
MC272	-26230	2.77	-2.87
MC273	-26320	2.60	-3.03
MC274	-26435	2.61	-3.07
MC275	-26495	2.58	-2.94
MC276	-26630	2.41	-2.89
MC277	-26705	2.43	-3.08
MC278	-26795	2.41	-3.08
MC279	-26915	2.59	-3.16
MC280	-27015	2.58	-3.35
MC281	-27115	2.76	-3.22
MC282	-27220	2.71	-3.10
MC283	-27312	2.63	-3.59
MC284	-27405	2.79	-2.98
MC285	-27505	2.63	-3.06
MC286	-27595	2.53	-3.28
MC287	-27705	2.50	-2.98
MC288	-27802	2.60	-2.89
MC290	-27975	2.60	-2.89
MC289	-28005	2.41	-3.03
MC291	-28075	2.29	-3.19
MC292	-28185	2.29	-3.75
MC293	-28285	2.34	-2.89
MC294	-28385	2.27	-3.10
MC295	-28485	2.29	-2.97
MC296	-28585	2.16	-3.43
MC297	-28685	2.20	-3.15
MC298	-28705	2.18	-3.12

Rawil

Sample	Depth (cm)	$\delta^{13}\text{C}$	$\delta^{18}\text{O}$
RW1	11075	3.29	-4.70
RW2	11050	2.56	-3.52
RW3	11040	2.48	-3.77
RW4	10980	2.55	-3.59
RW5	10900	2.46	-3.75
RW6	10860	2.66	-3.91
RW7	10710	2.58	-3.72
RW8	10560	2.76	-3.71
RW9	10410	2.82	-3.75
RW10	10290	2.80	-3.87
RW11	10170	3.11	-3.73
RW12	10070	2.95	-3.95
RW13	9910	2.91	-3.85
RW14	9810	2.92	-3.76
RW15	9730	2.89	-3.73
RW16	9660	1.65	-3.84
RW17	9580	2.39	-4.06
RW18	9550	2.07	-3.49
RW19	9480	2.49	-3.64
RW20	9390	2.28	-4.28
RW21	9350	2.34	-3.47
RW22	9230	2.15	-3.65
RW23	9150	2.24	-3.53
RW24	8990	2.01	-3.55
RW25	8890	2.16	-3.12
RW26	8860	2.04	-3.51
RW27	8780	2.07	-3.35
RW28	8680	2.20	-3.69
RW29	8570	2.18	-3.41
RW30	8450	2.12	-3.67
RW31	8320	2.17	-3.87
RW32	8040	2.21	-3.49
RW33	7880	2.09	-3.47
RW34	7560	1.81	-3.46
RW35	7070	2.60	-3.21
RW36	6820	2.75	-3.14
RW37	6660	2.84	-3.20
RW38	6520	2.75	-3.40
RW39	6390	1.67	-3.32
RW40	6320	-2.41	-18.06
RW41	6230	2.63	-3.26
RW42	6150	2.53	-3.08
RW43	6080	2.31	-3.23
RW44	6040	2.94	-3.18
RW45	5975	2.93	-3.56
RW46	5925	2.45	-2.74
RW47	5845	2.45	-3.77
RW48	5725	2.53	-3.70
RW49	5645	2.58	-3.24
RW50	5575	2.60	-3.56
RW51	5475	2.85	-3.30
RW52	5420	2.61	-3.51
RW53	5280	2.52	-3.46
RW54	5190	2.66	-3.09
RW55	5040	2.58	-3.47
RW56	4930	2.91	-5.57
RW57	4880	3.20	-3.51
RW58	4760	2.87	-3.15
RW59	4715	0.56	-4.11
RW60	4660	2.63	-3.07
RW61	4610	2.62	-3.18
RW62	4560	2.71	-2.96

Rawil

Sample	Depth (cm)	$\delta^{13}\text{C}$	$\delta^{18}\text{O}$
RW63	4440	2.55	-3.45
RW64	4380	2.20	-3.23
RW65	4290	2.64	-3.36
RW66	4220	2.32	-3.22
RW67	4160	2.66	-3.32
RW68	4090	2.33	-3.77
RW69	3970	-2.94	-4.70
RW70	3920	0.15	-4.50
RW71	3830	1.38	-4.11
RW72	3740	2.22	-3.17
RW73sed	3700	0.93	-3.68
RW73biot	3700	1.34	-4.05
RW74	3620	2.44	-3.18
RW75	3530	1.97	-3.09
RW76	3510	2.52	-2.94
RW77	3450	2.25	-3.20
RW78	3370	2.21	-3.55
RW79	3290	1.95	-3.16
RW80	3230	1.55	-3.21
RW81	3155	1.78	-3.31
RW82	3040	2.57	-3.83
RW83	2990	2.05	-4.12
RW84	2880	2.19	-3.48
RW85	2830	2.25	-4.79
RW86	2770	1.98	-3.88
RW87	2600	2.38	-3.49
RW88	2480	2.10	-3.75
RW89	2380	2.08	-3.84
RW90	2260	1.68	-3.86
RW91	2135	1.74	-4.08
RW92	2010	1.70	-3.78
RW93	1920	1.65	-3.80
RW94	1790	1.74	-3.61
RW95	1580	1.64	-3.70
RW96	1450	1.64	-3.97
RW97	1380	1.68	-3.87
RW98	1300	2.03	-3.90
RW99	1180	1.62	-4.19
RW100	1080	1.55	-4.11
RW101	940	1.43	-3.91
RW102	780	1.47	-4.24
RW103	650	1.61	-3.82
RW104	540	1.61	-3.84
RW105	430	1.55	-3.99
RW106	370	1.57	-3.77
RW107	270	1.60	-4.05
RW108	150	1.53	-3.98

Kistenpass

Sample	Depth (cm)	$\delta^{13}\text{C}$	$\delta^{18}\text{O}$
KP1	7554	1.30	-7.34
KP2	7509	1.10	-6.43
KP5	7204	0.45	-4.55
KP7	7004	1.36	-4.66
KP9	6814	1.26	-4.37
KP12	6544	1.62	-4.26
KP14	6344	1.92	-4.30
KP17	6044	1.45	-4.47
KP21	5634	0.32	-4.54
KP24	5344	0.89	-4.35
KP26	5184	1.53	-4.21
KP27	5114	1.42	-4.25
KP29	4989	1.49	-4.33
KP31	4815	1.36	-4.43
KP33	4615	1.45	-4.56
KP38	4270	1.49	-4.33
KP40	4085	1.46	-4.17
KP43	3875	1.47	-4.15
KP46	3680	1.74	-4.71
KP49	3575	1.63	-5.01
KP52	3155	1.54	-5.04
KP53	3055	1.47	-5.13
KP57	2795	1.35	-4.90
KP61	2625	1.46	-4.91
KP63	2560	1.27	-5.00
KP65	2090	1.17	-5.03
KP69	1940	1.07	-4.95
KP71	1760	1.19	-5.13
KP72	1650	1.32	-4.92
KP73	1600	1.25	-5.08
KP74	1550	1.20	-5.02
KP75	1440	1.29	-5.15
KP76	1380	1.10	-5.26
KP77	1290	1.13	-4.99
KP78	1170	0.41	-4.81
KP80	900	0.55	-4.68
KP81	720	0.43	-4.84
KP82	540	0.38	-5.44
KP83	460	0.43	-4.82
KP84	370	0.52	-4.76
KP85	100	0.42	-4.90

Interlaken

Sample	Depth (cm)	$\delta^{13}\text{C}$	$\delta^{18}\text{O}$
IN 1	61.2	2.21	-3.17
IN 7	58.2	2.44	-2.83
IN 11	52.2	2.36	-3.04
IN 16	48.2	2.22	-2.15
IN 21	43.2	2.06	-2.42
IN 26	39.2	1.99	-2.90
IN 30	32.2	1.49	-2.76
IN 35	27.2	2.15	-2.71
IN 42	23.6	2.36	-2.68
IN 46	18.5	2.84	-2.12
IN 51	14.5	2.66	-2.28
IN 55	9.5	3.23	-2.21
IN 61	5.5	2.06	-2.77
IN 66	0.5	2.59	-2.25

Lämmerenplaten

Sample	Depth (cm)	$\delta^{13}\text{C}$	$\delta^{18}\text{O}$
LP54	3900	-2.40	-5.77
LP53	3840	-0.87	-6.23
LP52	3825	-1.48	-5.64
LP51	3745	-4.57	-4.94
LP50	3605	-2.99	-4.67
LP49	3505	-2.56	-4.68
LP48	3415	-2.13	-4.65
LP47	3335	-2.65	-4.85
LP46	3320	-2.69	-4.84
LP45	3230	-2.83	-4.71
LP44	3190	-3.00	-4.72
LP43	3110	-3.75	-4.87
LP42	3035	-3.99	-4.56
LP 41	2965	-2.25	-5.16
LP 40	2875	-3.24	-5.01
LP 39	2770	-3.53	-4.57
LP 38	2685	-2.83	-4.91
LP 37	2575	-4.76	-4.61
LP 36	2505	-1.17	-4.79
LP 35	2400	0.16	-4.82
LP 33	2330	-2.26	-4.74
LP 34	2230	-2.13	-5.06
LP32	2175	-0.20	-4.70
LP31	2075	-2.04	-4.52
LP30	1975	-3.52	-4.43
LP29	1875	-2.10	-4.68
LP28	1825	-1.58	-4.38
LP27	1795	-2.04	-4.34
LP27BIS	1740	-1.60	-4.90
LP26	1665	-1.10	-4.80
LP25	1630	-0.24	-4.53
LP24	1535	0.37	-4.34
PL23	1490	0.87	-4.89
LP22	1415	1.41	-4.78
LP21	1340	1.20	-4.72
LP20	1290	0.93	-4.24
LP19	1255	0.96	-5.00
LP18	1220	1.39	-4.85
LP17	1200	0.67	-5.26
LP16	1150	0.80	-4.60
LP15	1050	0.50	-5.30
LP14	945	0.80	-4.60
LP13	845	1.00	-4.50
LP12	795	1.10	-4.50
LP11	700	0.80	-4.30
LP10	605	-0.30	-4.40
LP9	545	0.20	-4.30
LP8	455	-0.70	-4.50
LP7	405	1.60	-4.80
LP6	370	0.70	-4.10
LP5	325	1.50	-4.70
LP4	230	1.10	-4.30
LP3	145	1.30	-4.10
LP 2	25	0.95	-4.45
LP 1	5	0.53	-4.62

Cluses

Sample	Depth (cm)	$\delta^{13}\text{C}$	$\delta^{18}\text{O}$
CL1	0	0.78	-3.69
CL2	75	0.51	-2.95
CL3	103	0.48	-3.88
CL4	115	0.23	-4.00
CL5	195	0.48	-3.33
CL6	290	0.42	-3.77
CL7	405	0.74	-4.30
CL8	500	0.85	-4.02
CL9	560	0.66	-3.43
CL11	685	0.68	-3.44
CL12	785	0.54	-3.55
CL13	880	0.58	-3.99
CL14	959	0.54	-3.90
CL15	1039	0.50	-3.17
CL16	1134	0.59	-3.73
CL17	1144	0.60	-3.61
CL18	1224	0.61	-2.74
CL19	1384	0.60	-3.26
CL20	1464	0.52	-3.05
CL21	1524	0.61	-2.87
CL22	1528	0.61	-2.64
CL23	1531	0.64	-3.41
CL24	1649	0.62	-3.22
CL25	1749	0.63	-3.94
CL26	1869	0.52	-3.55
CL27	1969	0.70	-3.62
CL27BIS	2009	0.52	-3.71
CL28	2089	0.68	-2.63
CL28BIS	2149	0.67	-3.70
CL29	2209	0.62	-2.85
CL29BIS	2269	0.72	-3.38
CL30	2324	0.60	-3.17
CL30a	2404	0.72	-2.76
CL30b	2454	0.67	-3.46
CL31	2504	0.60	-2.92
CL31BIS	2604	0.38	-3.73
CL32	2664	0.43	-2.71
CL33	2734	0.59	-3.08
CL34	2809	0.64	-2.99
CL35	2929	0.61	-2.83
CL36	2994	0.57	-2.64
CL37	3059	0.75	-2.28
CL38	3074	0.57	-2.33
CL39	3096	0.79	-3.09
CL40	3169	0.46	-2.71
CL41	3224	0.56	-3.41
CL42	3364	0.60	-3.16
CL43	3414	0.56	-3.20
CL43BIS	3479	0.51	-3.31
CL44	3539	0.51	-2.95
CL44BIS	3579	0.64	-2.58
CL45	3629	0.53	-2.98
CL46	3669	0.60	-3.09
CL47	3769	0.62	-3.11
CXL48	3879	0.72	-2.40
CL49	3909	0.79	-2.96
CL50	3939	0.75	-2.52
CL51	3999	0.68	-2.77
CL51BIS	4034	0.60	-2.96
CL52	4059	0.83	-2.91
CL53	4129	0.34	-2.18
CL54	4179	0.60	-3.68

Sample	Depth (cm)	$\delta^{13}\text{C}$	$\delta^{18}\text{O}$
CL55	4259	0.92	-2.89
CL56	4339	0.83	-3.12
CL57	4399	0.81	-2.88
CL58	4609	0.96	-3.37
CL59	4684	0.96	-3.40
CL60	4744	1.06	-3.75
CL61	4844	1.12	-3.90
CL62	4904	1.19	-4.07
CL63	5004	1.05	-5.00
CL64	5084	1.37	-5.11
CL65	5129	1.35	-5.14
CL66	5179	1.39	-4.84
CL67	5189	1.31	-5.95
CL68	5254	1.32	-5.08
CL69	5344	1.45	-4.85
CL70	5414	1.46	-4.80
CL71	5494	1.69	-4.74
CL72	5134	1.82	-4.39
CL74	5219	1.74	-4.74
CL76	5274	1.75	-4.30
CL78	5319	1.93	-3.63
CL78a	5379	1.92	-4.27
CL78b	5429	1.95	-3.52
CL79	5474	1.90	-3.70
CL80	5589	1.69	-4.35
CL81	5729	1.69	-4.23

6.3 Total Phosphorus data

Valsloch

Sample	Depth (cm)	[P] mg/g	[P] ppm
VA 1	30983	0.23	229
VA2	30863	0.00	46
VA3	30693	0.00	35
VA 4	30683	0.03	34
VA5	30618	0.00	34
VA6	30588	0.00	32
VA7	30518	0.00	33
VA8	30393	0.01	14
VA9	30308	0.00	19
VA10	30178	0.00	14
VA11	30048	0.00	14
VA12	29888	0.02	18
VA13	29868	0.00	14
VA15	29623	0.02	16
VA16	29543	0.00	14
VA17	29463	0.02	22
VA18	29388	0.00	17
VA19	29298	0.00	14
VA20	29258	0.02	16
VA21	29158	0.00	19
VA22	29048	0.00	16
VA23	28998	0.01	14
VA24	28778	0.00	18
VA25	28758	0.03	29
VA26	28708	0.00	25
VA27	28618	0.03	32
VA28	28453	0.00	34
VA29	28363	0.00	33
VA30	28333	0.06	57
VA31	28278	0.00	37
VA32	28253	0.00	38
VA33	28138	0.04	43
VA34	28013	0.00	46
VA35	27978	0.00	40
VA36	27928	0.05	49
VA37	27888	0.00	42
VA38	27733	0.00	50
VA39	27658	0.05	45
VA40	27588	0.00	38
VA41	27493	0.05	47
VA42	27433	0.00	33
VA43	27383	0.00	44
VA44	27268	0.00	40
VA45	27248	0.00	54
VA46	27148	0.07	71
VA47	27138	0.00	72
VA48	27108	0.00	246
VA49	26938	0.03	31
VA50	26808	0.00	21
VA51	26708	0.00	20
VA52	26613	0.02	24
VA54	26558	0.00	25
VA55	26488	0.04	43
VA56	26403	0.00	29
VA57	26388	0.00	26
VA58	26268	0.04	36
VA59	26233	0.00	22
VA60	26133	0.00	16
VA61	26033	0.00	22
VA62	25933	0.03	33
VA63	25833	0.00	12
VA64	25733	0.01	14

Sample	Depth (cm)	[P] mg/g	[P] ppm
VA65	25583	0.00	10
VA66	25563	0.00	14
VA67	25483	0.00	10
VA68	25353	0.03	26
VA69	25233	0.00	14
VA70	25133	0.03	25
VA71	25073	0.00	17
VA72	24993	0.00	14
VA73	24893	0.00	16
VA74	24823	0.00	13
VA75	24663	0.02	22
VA76	24533	0.00	15
VA77	24493	0.00	22
VA78	24403	0.00	14
VA79	24283	0.00	14
VL7	24083	0.02	18
VL6	24033	0.01	14
VL5	23998	0.02	18
VL4	23943	0.02	18
VL3	23833	0.02	15
VL2	23773	0.01	14
VL1	23653	0.02	22
VA80	23553	0.03	29
VA81	23413	0.00	13
VA82	23393	0.00	23
VA83	23263	0.04	39
VA84	23173	0.00	20
VA85	23100	0.00	27
VA86	23040	0.03	26
VA87	23005	0.00	16
VA88	22985	0.00	23
VA89	22915	0.03	32
VA90	22835	0.00	21
VA91	22775	0.02	22
VA92	22670	0.00	21
VA93	22615	0.03	26
VA94	22525	0.00	22
VA95	22425	0.00	16
VA96	22310	0.00	28
VA97	22190	0.05	46
VA98	22165	0.00	18
VA99	21925	0.02	25
VA101	21860	0.03	26
VA102	21795	0.00	13
VA103	21735	0.00	19
VA104	21720	0.00	19
VA105	21620	0.04	37
VA107	21480	0.00	18
VA108	21455	0.03	29
VA109	21325	0.00	16
VA110	21280	0.00	14
VA111	21240	0.03	29
VA113	21170	0.03	26
VA114	21155	0.00	16
VA115	21085	0.04	35
VA116	21070	0.00	21
VA117	21010	0.00	21
VA118	21000	0.02	24
VA119	20945	0.00	18
VA120	20920	0.03	35
VA121	20840	0.00	21
VA122	20785	0.02	20

Valsloch

Sample	Depth (cm)	[P] mg/g	[P] ppm
VA123	20725	0.00	10
VA124	20545	0.00	16
VA 125	20445	0.03	31
VA126	20425	0.00	26
VA127	20325	0.00	22
VA 128	20225	0.02	22
VA 129	20125	0.03	30
VA 130	20035	0.03	33
VA131	20005	0.00	26
VA 132	19885	0.04	41
VA 133	19845	0.09	87
VA134	19830	0.00	28
VA 135	19745	0.03	30
VA136	19725	0.00	34
VA 137	19505	0.04	36
VA138	19405	0.00	34
VA 139	19325	0.03	29
VA140	19215	0.00	21
VA 141	19015	0.07	66
VA 142	18815	0.09	87
VA143	18715	0.00	49
VA144	18615	0.00	55
VA145	18515	0.00	39
VA 146	18355	0.05	52
VA147	18195	0.00	65
VA 148	18165	0.08	82
VA149	18105	0.00	55
VA 150	18065	0.07	73
VA151	17965	0.00	84
VA153	17825	0.00	74
VA 154	17695	0.10	97
VA155	17675	0.00	60
VA 156	17605	0.12	115
VA157	17515	0.00	107
VA 158	17495	0.18	177
VA159	17375	0.00	132
VA 160	17345	0.16	163
VA161	17245	0.00	105
VA 163	17155	0.15	148
VA164	17045	0.00	190
VA 165	17015	0.27	273
VA166	16925	0.00	61
VA 167	16825	0.09	87
VA168	16795	0.00	60
VA 169	16695	0.05	50
VA 170	16645	0.06	61
VA171	16625	0.00	42
VA172	16445	0.00	45
VA 173	16285	0.09	89
VA 174	16195	0.06	62
VA175	16015	0.00	49
VA 176	15895	0.07	67
VA177	15735	0.00	40
VA 178	15615	0.08	76
VA179	15465	0.00	40
VA180	15285	0.00	37
VA 181	15110	0.08	75
VA 182	14860	0.08	76
VA183	14660	0.00	52
VA184	14540	0.00	61
VA 185	14350	0.10	103
VA186	14150	0.00	62

Sample	Depth (cm)	[P] mg/g	[P] ppm
VA 187	13970	0.10	102
VA188	13670	0.00	49
VA189	13550	0.00	54
VA 190	13275	0.08	80
VA191	13105	0.00	60
VA 192	13095	0.10	101
VA193	12935	0.00	75
VA 194	12835	0.10	95
VA195	12685	0.00	67
VA196	12495	0.00	91
VA 197	12295	0.10	101
VA198	12010	0.00	68
VA199	11820	0.00	66
VA200	11725	0.00	86
VA 201	11615	0.11	107
VA 203	11375	0.16	163
VA 204	11155	0.14	142
VA205	10980	0.00	177
VA 207	10820	0.10	97
VA 210	10505	0.09	95
VA 212	10200	0.12	122
VA 213	10170	0.18	175
VA 215	10100	0.09	90
VA 216	10065	0.14	139
VA 218	9940	0.13	128
VA 220	9785	0.14	143
VA221	9640	0.00	69
VA222	9580	0.00	67
VA223	9520	0.00	71
VA 224	9460	0.11	114
VA225	9265	0.00	102
VA226	9200	0.00	89
VA 227	9125	0.12	116
VA 228	9080	0.12	122
VA 230	8935	0.13	125
VA232	8820	0.00	74
VA 233	8755	0.11	112
VA 235	8570	0.16	163
VA 236	8480	0.12	116
VA 238	8315	0.13	129
VA 239	8297	0.12	117
VA 241	8202	0.08	75
VA 243	8012	0.11	108
VA244	7927	0.00	80
VA 246	7707	0.10	104
VA 248	7467	0.09	94
VA 249	7367	0.11	109
VA 250	7217	0.12	115
VA 252	6962	0.08	84
VA253	6862	0.00	74
VA 255	6647	0.12	116
VA256	6542	0.00	102
VA 257	6347	0.13	127
VA 258	6192	0.15	146
VA 260	6002	0.11	112
VA 262	5732	0.17	174
VA 264	5347	0.16	157
VA 265	5317	0.13	127
VA266	5027	0.00	98
VA 267	4907	0.14	139
VA268	4847	0.00	105
VA 269	4517	0.14	140

Valsloch

Sample	Depth (cm)	[P] mg/g	[P] ppm
VA 270	4462	0.16	156
VA271	4417	0.11	108
VA272	4367	0.13	128
VA273	4347	0.12	115
VA274	4322	0.17	171
VA275	4297	0.14	139
VA276	4267	0.09	90
VA277	4212	0.10	101
VA278	4142	0.08	80
VA279	4077	0.09	92
VA280	4022	0.11	111
VA281	3932	0.13	126
VA282	3882	0.14	136
VA283	3867	0.09	85
VA284	3772	0.08	76
VA285	3672	0.09	87
VA286	3502	0.11	112
VA287	3447	0.11	106
VA288	3392	0.11	105
VA289	3352	0.11	111
VA290	3262	0.13	126
VA291	3142	0.08	82
VA293	2992	0.08	83
VA294	2902	0.07	66
VA295	2832	0.08	77
VA296	2762	0.08	75
VA297	2687	0.10	98
VA298	2642	0.09	92
VA299	2617	0.09	86
VA300	2567	0.26	259
VA301	2502	0.11	115
VA302	2412	0.08	84
VA303	2392	0.13	125
VA304	2322	0.10	98
VA305	2202	0.09	92
VA306	2135	0.11	107
VA307	2080	0.10	102
VA308	2020	0.11	107
VA309	1900	0.13	125
VA310	1855	0.12	119
VA311	1823	0.15	145
VA312	1795	0.12	124
VA313	1675	0.15	154
VA314	1575	0.20	199
VA315	1545	0.23	228
VA316	1500	0.19	191
VA317	1450	0.23	228
VA318	1415	0.17	168
VA319	1360	0.15	149
VA320	1315	0.17	165
VA321	1295	0.14	138
VA322	1235	0.22	224
VA323	1225	0.15	149
VA324	1140	0.24	242
VA325	1055	0.21	212
VA326	1010	0.23	230
VA327	955	0.16	160
VA328	920	0.17	168
VA329	875	0.23	227
VA330	740	0.16	162
VA331	670	0.27	267
VA332	610	0.32	320

Sample	Depth (cm)	[P] mg/g	[P] ppm
VA333	560	0.26	256
VA334	495	0.22	221
VA335	440	0.25	253
VA336	320	0.21	205
VA336b	235	0.21	206
VA337	225	0.24	237
VA338	150	0.85	847
VA339	75	0.61	609
VA340	25	0.58	583

Tierwis

Sample	Depth (cm)	[P] mg/g	[P] ppm
TW 160	19165	7.40	7397
TW 159	19155	5.79	5786
TW158	19070	0.01	12
TW 157	18990	0.05	54
TW156	18970	0.01	9
TW 155	18890	0.07	66
TW154	18875	0.01	11
TW153	18780	0.01	12
TW152	18765	0.01	8
TW 151	18685	0.05	48
TW150	18665	0.01	9
TW149	18565	0.01	8
TW 148	18525	0.04	40
TW147	18425	0.01	9
TW146	18275	0.02	16
TW 145	18135	0.04	40
TW144	18115	0.02	16
TW143	17965	0.02	16
TW 142	17895	0.03	34
TW141	17835	0.02	19
TW 140	17720	0.05	51
TW139	17615	0.02	24
TW138	17590	0.03	25
TW 137	17475	0.05	49
TW 136	17442	0.05	48
TW 135	17417	0.00	14
TW 134	17387	0.04	43
TW 132	17297	0.00	21
TW 131	17207	0.00	23
TW 130	17132	0.05	50
TW 129	17122	0.00	24
TW 128	17082	0.04	44
TW 127	17012	0.00	21
TW 125	16942	0.03	26
TW 124	16852	0.00	19
TW 123	16772	0.03	34
TW 122	16747	0.05	53
TW 120	16647	0.00	33
TW 119	16517	0.06	56
TW 118	16477	0.00	29
TW 117	16437	0.05	52
TW 116	16402	0.06	59
TW 115	16322	0.06	64
TW 114	13038	0.00	30
TW 113	12938	0.05	46
TW 112	12923	0.00	2
TW 111	12898	0.00	8
TW 110	12808	0.00	18
TW 108	12788	0.04	41
TW 107	12668	0.00	6
TW 106	12563	0.00	4
TW 105	12428	0.03	29
TW 104	12328	0.00	12
TW 103	12238	0.00	10
TW 102	12218	0.04	37
TW 101	12118	0.00	13
TW 100	12098	0.00	6
TW 99	11958	0.03	32
TW 98	11938	0.00	2
TW 97	11848	0.04	42
TW 96	11768	0.00	17
TW 95	11738	0.03	26

Sample	Depth (cm)	[P] mg/g	[P] ppm
TW 94	11628	0.00	12
TW 93	11598	0.00	17
TW 92	11478	0.00	15
TW 91	11458	0.00	17
TW 90	11378	0.03	33
TW 89	11308	0.00	16
TW 88	11258	0.04	44
TW 87	11128	0.00	25
TW 86	11108	0.00	35
TW 85	10978	0.00	27
TW 84	10938	0.05	50
TW 83	10858	0.00	39
TW 82	10838	0.00	57
TW 81	10718	0.00	45
TW 80	10688	0.08	80
TW 79	10588	0.00	51
TW 78	10508	0.05	48
TW 77	10448	0.00	35
TW 76	10433	0.00	38
TW 75	10343	0.00	41
TW 74	10318	0.04	39
TW 73	10248	0.00	33
TW 72	10218	0.00	39
TW 71	10193	0.00	54
TW 70	10123	0.05	47
TW 69	10098	0.00	40
TW 68	10068	0.00	36
TW 67	9928	0.04	40
TW 66	9868	0.00	41
TW 65	9578	0.00	44
TW 64	9558	0.00	51
TW 63	9558	0.05	49
TW 62	9448	0.00	49
TW 61	9358	0.00	34
TW 60	9343	0.08	82
TW 59	9283	0.00	43
TW 57	9163	0.00	47
TW 56	9023	0.07	70
TW 54	8903	0.05	50
TW 53	8768	0.00	57
TW 52	8688	0.00	65
TW 51	8613	0.06	57
TW 50	8553	0.00	60
TW 49	8518	0.06	63
TW 48	8453	0.00	59
TW 47	8393	0.00	57
TW 46	8323	0.00	50
TW 45	8298	0.00	46
TW 44	8248	0.00	45
TW 43	8178	0.06	59
TW 42	8108	0.00	55
TW 40	8038	0.05	45
TW 39	7948	0.00	47
TW 37	7858	0.00	63
TW 36	7805	0.05	51
TW 35	7765	0.07	74
TW 34	7720	0.00	1277
TW 33	7620	0.00	20
TW 32	7550	0.04	41
TW 31	7445	0.00	35
TW 30	7395	0.00	128
TW 29	7355	0.00	87

Tierwis

Sample	Depth (cm)	[P] mg/g	[P] ppm
TW 28	7245	0.05	53
TW 27	7185	0.00	46
TW 26	7125	0.00	64
TW 25	7090	0.08	76
TW 24	7025	0.00	55
TW 23	6965	0.00	51
TW 22	6850	0.06	57
TW 21	6780	0.00	89
TW 20	6683	0.00	60
TW 19	6641	0.06	62
TW 18	6596	0.00	62
TW 17	6556	0.00	48
TW 16	6476	0.00	58
TW 15	6386	0.09	91
TW 14	6316	0.00	74
TW 13	6274	0.00	102
TW 12	6185	0.11	112
TW 11	6140	0.00	95
TW 10	6095	0.00	107
TW 9	6017	0.00	123
TW 8	5985	0.10	97
TW 7	5933	0.00	77
TW 6	5858	0.00	79
TW 5	5778	0.00	94
TW 4	5708	0.14	138
TW 3	5643	0.11	110
TW 1	5600	0.09	92
SA LB 1	5063	0.12	122
SA LB 2	4998	0.10	99
SA LB 3	4923	0.18	176
SA LB 4	4823	0.13	134
SA LB 6	4718	0.18	184
SA LB 7	4673	0.26	256
SA LB 8	4568	0.11	113
SA LB 9	4468	0.25	245
SA LB 10	4448	0.14	141
SA LB 11	4173	0.14	137
SA LB 12	4043	0.17	174
SA LB 13	3993	0.16	160
SA LB 14	3893	0.13	135
SA LB 15	3878	0.15	152
SA LB 16	3823	0.37	370
SA LB 17	3778	0.17	173
SA LB 18	3743	0.17	171
SA LB 19	3703	0.19	191
SA LB 20	3633	0.27	267
SA LB 22	3528	0.24	243
SA LB 26	3153	0.16	156
SA LB 30	2663	0.19	191
Sa SB 49	5083	0.09	94
Sa SB 48b	4960	0.16	162
Sa SB 47	4783	0.11	106
Sa SB 45	4239	0.15	148
Sa SB 44	4161	0.14	144
Sa SB 43	3892	0.15	154
Sa SB 41	3765	0.18	177
Sa SB 40	3745	0.24	243
Sa SB 39	3630	0.25	247
Sa SB 38	3565	0.65	657
Sa SB 37	3540	0.37	365
Sa SB 36	3515	0.34	342
Sa SB 35	3470	0.36	358

Sample	Depth (cm)	[P] mg/g	[P] ppm
Sa SB 34	3420	0.13	127
Sa SB 33	3360	4.52	11757
Sa SB 32	3310	0.27	271
Sa SB 31	3240	0.14	144
Sa SB 30b	3195	0.11	108
Sa SB 30a	3160	0.16	158
Sa SB 29	3065	0.14	136
Sa SB 28b	3025	0.12	122
Sa SB 28a	2980	1.75	1815
Sa SB 27b	2940	0.14	139
Sa SB 27a	2865	0.22	217
Sa SB 26	2820	0.42	422
Sa SB 25	2760	0.27	268
Sa SB 24c	2630	0.19	188
Sa SB 24b	2170	0.13	126
Sa SB 24a	1720	0.10	97
Sa SB 23	1500	0.13	135
Sa SB 22	1370	0.16	157
Sa SB 20	1250	0.76	761
Sa SB 19	1250	1.68	1682
Sa SB 18c	1210	0.19	195
Sa SB 18b	1180	0.18	180
Sa SB 18a	1120	0.29	293
Sa SB 17	1055	0.75	749
Sa SB 16b	1020	0.68	677
Sa SB 16a	985	0.59	592
Sa SB 15c	900	0.88	881
Sa SB 15b	875	0.58	580
Sa SB 15a	860	0.73	731
Sa SB 14b	825	0.79	787
Sa SB 14a	795	0.40	400
Sa SB 13	760	0.88	884
Sa SB 12	735	1.16	1162
Sa SB 11	705	0.86	858
Sa SB 10	530	0.84	843
Sa SB 9	420	0.75	747
Sa SB 8	335	0.49	491
Sa SB 7	240	0.16	155
Sa SB 2	15	0.07	74

Kistenpass

Sample	Depth (cm)	[P] mg/g	[P] ppm
KP 1	7554	1.61	1606
KP 2	7509	0.07	71
KP 5	7204	0.02	19
KP 7	7004	0.02	16
KP 9	6814	0.02	21
KP 12	6544	0.02	23
KP 14	6344	0.02	22
KP 17	6044	0.02	16
KP 21	5634	0.03	33
KP 24	5344	0.04	40
KP 26	5184	0.07	68
KP 27	5114	0.08	83
KP 29	4989	0.10	97
KP 31	4815	0.06	62
KP 33	4615	0.11	107
KP 38	4270	0.10	98
KP 40	4085	0.05	51
KP 43	3875	0.08	85
KP 46	3680	0.19	189
KP 49	3575	0.20	198
KP 52	3155	0.16	160
KP 53	3055	0.16	164
KP 57	2795	0.17	165
KP 61	2625	0.19	191
KP 63	2560	0.34	337
KP 65	2090	0.36	365
KP 69	1940	0.25	250
KP 72	1650	1.17	1170
KP 75	1440	0.12	122
KP 78	1170	1.78	1784
KP 80	900	0.84	839
KP 84	370	0.78	783
KP 52	3155	0.16	160
KP 53	3055	0.16	164
KP 57	2795	0.17	165
KP 61	2625	0.19	191
KP 63	2560	0.34	337
KP 65	2090	0.36	365
KP 69	1940	0.25	250
KP 72	1650	1.17	1170
KP 75	1440	0.12	122
KP 78	1170	1.78	1784
KP 80	900	0.84	839
KP 84	370	0.78	783

Harder

Sample	Depth (cm)	[P] mg/g	[P] ppm
HA 415	31197.5	0.06	55
HA 411	30907.5	0.08	83
HA 405	30392.5	0.04	40
HA 402	30097.5	0.03	28
HA 397	29597.5	0.06	59
HA 391	28952.5	0.07	68
HA 386	28507.5	0.07	68
HA 381	28037.5	0.06	57
HA 376	27667.5	0.06	62
HA 371	27208.5	0.07	72
HA 366	26783.5	0.08	84
HA 362	26603.5	0.09	85
HA 356	26061.5	0.07	71
HA 351	25546.5	0.05	47
HA 346	25155.5	0.11	111
HA 341	24745.5	0.06	64
HA 336	24331.5	0.07	66
HA 331	23904.5	0.09	86
HA 326	23649.5	0.03	33
HA 321	23114.5	0.05	46
HA 316	22469.5	0.11	106
HA 311	21847.5	0.08	80
HA 306	21342.5	0.16	163
HA 301	20647.5	0.08	76
HA 296	20109.5	0.09	89
HA 291	19591.5	0.08	75
HA 286	18625.5	0.08	83
HA 281	18090.5	0.13	128
HA 276	17416.5	0.11	106
HA 271	16542	0.13	127
HA 266	16149	0.09	88
HA 261	15727	0.10	103
HA 251	14852	0.10	98
HA 246	14237	0.10	95
HA 241	13637	0.08	76
HA 236	12702	0.12	122
HA 231	12280	0.09	94
HA 226	11944	0.11	115
HA 221	11517	0.10	99
HA 216	11244	0.09	94
HA 211	10931	0.10	97
HA 206	10618	0.07	74
HA 201	10268	0.09	87
HA 196	9988	0.07	67
HA 191	9659	0.09	89
HA 186	9336	0.05	52
HA 181	9015	0.05	54
HA 176	8601	0.17	165
HA 171	8389	0.10	96
HA 166	7959	0.10	101
HA 161	7813	0.14	140
HA 156	7596	0.13	134
HA 151	7339	0.11	107
HA 146	6976	0.12	124
HA 141	6787	0.11	109
HA 136	6587	0.12	120
HA 131	6284	0.10	99
HA 126	6138	0.23	233
HA 121	5874	0.12	118
HA 116	5620	0.12	124
HA 111	5334	0.12	125
HA 106	5010	0.19	188

Harder

Sample	Depth (cm)	[P] mg/g	[P] ppm
HA 101	4520	0.16	164
HA 96	4287	0.14	140
HA 91	4008	0.19	185
HA 86	3864	0.13	127
HA84	3722	0.11	106
HA82	3648	0.14	144
HA 81	3600	0.14	136
HA80	3548	0.11	110
HA78	3443	0.11	115
HA77	3435	0.11	113
HA 76	3347	0.14	140
HA75	3259	0.08	85
HA73	3194	0.10	104
HA 71	3142	0.12	124
HA69	3052	0.12	116
HA68	3008	0.11	107
HA 66	2839	0.17	174
HA65	2796	0.15	145
HA 61	2614	0.13	127
HA59	2567	0.09	93
HA58	2532	0.09	91
HA 56	2465	0.10	98
HA54	2370	0.07	72
HA53	2300	0.06	56
HA52	2258	0.06	61
HA 51	2178	0.11	107
HA50	2110	0.05	51
HA49	2043	0.05	49
HA48	2024	0.08	79
HA 46	1888	0.06	62
HA45	1818	0.04	39
HA44	1769	0.06	57
HA42	1580	0.08	80
HA 41	1553	0.11	106
HA40	1526	0.08	81
HA39	1443	0.34	339
HA 36	1338	0.13	134
HA34	1293	0.17	170
HA32	1218	0.22	225
HA 31	1161	0.41	407
HA30	1130	0.66	662
HA29	1058	0.19	192
HA27	991	0.20	197
HA 26	971	0.22	216
HA25	878	0.25	246
HA24	803	0.38	380
HA23	753	0.25	245
HA22	713	0.58	576
HA 21	608	0.32	323
HA20	601	0.18	179
HA19	551	0.24	236
HA18	506	0.81	807
HA17	473	0.36	357
HA 16	454	1.43	1434
HA15	390	0.30	297
HA13	315	0.33	331
HA12	300	0.91	906
HA 11	285	0.88	875
HA10	254	0.33	333
HA8	168	0.30	301
HA 6	123	0.11	114
HA4	58	0.53	525

Sample	Depth (cm)	[P] mg/g	[P] ppm
HA3	28	0.28	284
HA2	11	0.81	813
HA1	0	0.72	723

L'Ecuelle

Sample	Depth (cm)	[P] mg/g	[P] ppm
EC 257	23665	0.13	131
EC 256	23515	0.74	744
EC 255	23445	0.01	13
EC 254	23375	0.01	12
EC 253	23305	0.14	140
EC 252	23265	0.01	9
EC 251	23215	0.02	17
EC 250	23160	0.04	40
EC 249	23100	0.02	25
EC 248	23030	0.01	12
EC 247	22965	0.01	14
EC 246	22950	0.01	10
EC 245	22935	0.01	10
EC 244	22895	0.01	12
EC 243	22845	0.01	13
EC 242	22765	0.02	15
EC 241a	22745	0.01	13
EC 240	22695	0.01	10
EC 238	22595	0.04	45
EC 237	22570	0.07	73
EC 236	22525	0.02	19
EC 235	22465	0.01	12
EC 234	22405	0.01	10
EC 233	22370	0.01	11
EC 232	22355	0.01	13
EC 231	22285	0.01	8
EC 230	22235	0.01	12
EC 229	22175	0.01	12
EC 228	22160	0.01	12
EC 227	22085	0.01	12
EC 226	22015	0.02	20
EC 225	22000	0.02	16
EC 224	21915	0.02	25
EC 223	21905	0.02	21
EC 222	21895	0.01	10
EC 221	21820	0.01	10
EC 220	21755	0.01	11
EC 219	21665	0.01	10
EC 218	21650	0.04	37
EC 217	21605	0.02	16
EC 216	21545	0.02	16
EC 215	21480	0.02	19
EC 214	21465	0.01	14
EC 213	21405	0.01	14
EC 212	21315	0.03	26
EC 211	21240	0.02	19
EC 210	21190	0.02	19
EC 209	21135	0.05	50
EC 208	21085	0.03	30
EC 207	21065	0.03	28
EC 206	21005	0.02	18
EC 205	20925	0.02	24
EC 204	20905	0.02	22
EC 203	20835	0.03	28
EC 202	20815	0.02	24
EC 201	20755	0.05	48
EC 200	20695	0.03	34
EC 199	20675	0.07	68
EC 198	20635	0.03	26
EC 197	20574	0.04	40
EC 196	20565	0.02	20
EC 195	20515	0.01	12

Sample	Depth (cm)	[P] mg/g	[P] ppm
EC 194	20475	0.02	20
EC 193	20405	0.02	22
EC 192	20315	0.03	28
EC 191	20275	0.06	58
EC 190	20260	0.02	24
EC 189	20205	0.02	18
EC 188	20125	0.03	27
EC 187	20060	0.04	38
EC 185	19985	0.04	37
EC 184	19940	0.03	32
EC 183	19913	0.03	31
EC 182	19850	0.03	31
EC 181	19805	0.03	30
EC 180	19770	0.06	57
EC 179	19725	0.06	59
EC 178	19645	0.05	48
EC 177	19623	0.13	131
EC 176	19620	0.06	59
EC 175	19565	0.08	76
EC 174	19513	0.04	42
EC 173	19460	0.11	105
EC 172 carb	19390	0.10	101
EC 171	19370	0.05	48
EC 169	19235	0.03	29
EC 168	19222	0.07	67
EC 166	19175	0.02	16
EC 165	19120	0.03	30
EC 164	19050	0.03	33
EC 163	19025	0.02	20
EC 162	18925	0.02	18
EC 161	18825	0.04	39
EC 160	18725	0.03	26
EC 159	18635	0.02	25
EC 158	18495	0.03	35
EC 157	18385	0.03	26
EC 156	18295	0.03	27
EC 155	18165	0.05	49
EC 154	18095	0.02	16
EC 153	17995	0.01	12
EC 152	17945	0.02	17
EC 151	17845	0.01	14
EC 150	17745	0.02	25
EC 149	17645	0.02	21
EC 148	17545	0.03	30
EC 147	17445	0.01	12
EC 146	17345	0.01	15
EC 145	17145	0.05	54
EC 144	16845	0.02	21
EC 143	16695	0.02	20
EC 142	16545	0.02	17
EC 141	16415	0.01	14
EC 140	16310	0.01	13
EC 139	16200	0.02	20
EC 138	16045	0.02	18
EC 137	15935	0.01	12
EC 136	15795	0.02	25
EC 135	15715	0.02	21
EC 134	15620	0.02	18
EC 133	15595	0.02	17
EC 132	15525	0.03	26
EC 131	15410	0.02	25

L'Ecuelle

Sample	Depth (cm)	[P] mg/g	[P] ppm
EC130	15375	0.04	43
EC129	15335	0.07	66
EC128	15240	0.10	104
EC127	15190	0.02	20
EC126	15070	0.02	19
EC125	15060	0.02	17
EC124	14940	0.04	36
EC123	14930	0.04	38
EC122	14835	0.02	19
EC121	14735	0.02	22
EC120	14635	0.02	22
EC119	14535	0.02	15
EC118	14395	0.03	26
EC117	14265	0.02	15
EC115	14135	0.02	20
EC114	14113	0.02	18
EC113	13995	0.02	18
EC112	13925	0.02	20
EC111	13785	0.02	17
EC110	13715	0.02	24
EC109	13615	0.02	17
EC108	13535	0.02	22
EC107	13420	0.02	24
EC106	13340	0.02	20
EC105	13290	0.03	29
EC104	13220	0.02	22
EC103	13015	0.02	21
EC102	12915	0.01	13
EC101	12810	0.02	16
EC100	12690	0.02	17
EC99	12485	0.02	15
EC98	12375	0.02	20
EC97	12275	0.02	17
EC96	12170	0.02	23
EC95	12070	0.05	54
EC94	11980	0.03	29
EC93	11775	0.03	32
EC92	11670	0.02	25
EC91	11625	0.02	22
EC90	11530	0.02	22
EC89	11430	0.02	22
EC88	11315	0.02	23
EC 87	11140	0.03	33
EC86	11060	0.02	23
EC 85	11050	0.02	24
EC 84	11000	0.03	30
EC 83	10925	0.05	54
EC 82	10845	0.03	26
EC 81	10770	0.04	41
EC 80	10705	0.07	68
EC 79	10675	0.03	29
EC 78	10620	0.06	60
EC 77	10560	0.04	42
EC 76	10495	0.04	43
EC 75	10425	0.03	25
EC 74	10390	0.03	27
EC 73	10290	0.02	23
EC 72	10190	0.03	33
EC 71	10090	0.03	25
EC 70	9960	0.03	27
EC 69	9860	0.03	31
EC 68	9755	0.04	36

Sample	Depth (cm)	[P] mg/g	[P] ppm
EC 67	9650	0.10	103
EC 66	9510	0.05	46
EC 65	9230	0.05	53
EC 64	9075	0.13	135
EC 63	8985	0.06	59
EC 62	8946	0.07	70
EC 61	8867	0.07	67
EC 60	8860	0.06	65
EC 59	8760	0.09	91
EC 58	8694	0.09	87
EC 57	8629	0.07	71
EC 56	8524	0.09	94
EC 55	8439	0.08	82
EC 54	8369	0.09	87
EC 53	8194	0.04	45
EC 52	8134	0.05	48
EC 51	8047	0.05	48
EC 50	7959	0.06	57
EC 49	7870	0.05	53
EC 48	7780	0.04	43
EC 47	7720	0.05	52
EC 46	7655	0.06	58
EC 45	7575	0.06	64
EC 44	7475	0.09	90
EC 43	7375	0.08	82
EC 42	7275	0.06	64
EC 41	7175	0.06	56
EC 40	7075	0.04	44
EC 39	6975	0.07	70
EC 38	6875	0.06	63
EC 37	6775	0.08	82
EC 36	6675	0.09	88
EC 35	6575	0.11	113
EC 34	6475	0.09	87
EC 33	6380	0.05	53
EC 32	6290	0.07	68
EC 31	6240	0.06	64
EC 30	6205	0.07	68
EC 29	6180	0.11	111
EC 28	6085	0.15	150
EC 27	5985	0.10	104
EC 26	5890	0.09	88
EC 25	5885	0.08	78
EC 24	5815	0.13	131
EC 23	5725	0.15	146
EC 22	5625	0.12	122
EC 21	5575	0.10	101
EC 20	5465	0.16	164
EC 19	5365	0.14	143
EC 18	5165	0.21	211
EC 17	5065	0.13	130
EC 16	5035	0.16	163
EC 15	4885	0.15	150
EC 14	4815	0.13	125
EC 13	4705	0.20	204
EC 12	4655	0.11	114
EC 11	4605	0.16	156
EC 10	4485	0.17	167
EC 9	4385	0.13	128
EC 8	4275	0.16	163
EC 7	4195	0.18	179
EC 6	4095	0.11	105

L'Ecuelle

Sample	Depth (cm)	[P] mg/g	[P] ppm
EC 5	3360	0.11	113
EC 4	3240	0.09	91
EC 3	3230	0.12	118
EC 2	3200	0.13	129
EC 1	3050	0.16	160
ECU24	2745	0.18	178
ECU23	2655	0.10	101
ECU22	2600	0.11	108
ECU21	2505	0.14	144
ECU20	2455	0.13	131
ECU19	2375	0.11	114
ECU18	2270	0.11	107
ECU17	2175	0.12	115
ECU16	1170	0.15	155
ECU15	1070	0.34	341
ECU14	950	0.15	148
ECU12	830	0.14	140
ECU11	740	0.15	147
ECU10	660	0.13	127
ECU9	580	0.15	145
ECU8	510	0.15	148
ECU7	407	0.38	377
ECU6	385	0.40	405
ECU5	355	0.42	423
ECU4	320	0.46	460
ECU3	200	0.50	500
ECU2	120	0.39	385
ECU1	5	0.66	658

Interlaken

Sample	Depth (cm)	[P] mg/g	[P] ppm
IN 1	0	0.04	39
IN 7	550	0.02	19
IN 11	950	0.02	21
IN 16	1450	0.03	30
IN 21	1850	0.03	34
IN 26	2360	0.15	153
IN 30	2720	0.02	21
IN 35	3220	0.01	13
IN 42	3920	0.02	17
IN 46	4320	0.04	36
IN 51	4820	0.03	32
IN 55	5220	0.05	51
IN 61	5820	0.04	36
IN 66	6120	0.03	30

6.4 XRD (bulk rock) data

Valsloch

Samples	Depth (cm)	Phyllosilicates	Quartz	Feldspat-K	Plagioclase-Na	Calcite	Dolomite	Goethite	Ankérite	Indices
VA1	30983	6.73	2.35	0.00	0.00	87.34	0.00	0.00	0.00	3.58
VA3	30693	0.00	1.89	0.00	0.00	95.33	0.00	0.00	0.00	2.78
VA6	30588	0.00	0.44	0.00	0.00	97.12	0.00	0.00	0.00	2.44
VA8	30393	4.77	0.48	0.35	0.34	90.45	0.00	0.00	0.00	3.61
VA10	30178	0.00	0.30	0.00	0.00	97.45	0.00	0.00	0.00	2.25
VA12	29888	0.00	1.87	0.00	0.00	95.23	0.00	0.00	0.00	2.90
VA15	29623	0.00	1.00	0.00	0.37	93.11	0.00	0.00	0.00	5.52
VA18	29388	0.00	1.09	0.00	0.00	92.34	0.00	0.00	0.00	6.57
VA20	29258	8.67	1.45	0.00	0.00	83.22	0.00	0.00	0.00	6.66
VA23	28998	0.00	0.85	0.00	0.00	98.04	0.00	0.00	0.00	1.11
VA25	28758	0.00	0.32	0.00	0.00	97.33	0.00	0.00	0.00	2.35
VA28	28453	11.71	5.67	0.00	0.00	80.34	0.00	0.00	0.00	2.28
VA30	28333	3.38	0.35	0.00	0.43	94.67	0.00	0.00	0.00	1.16
VA33	28138	0.00	2.43	0.00	0.00	95.12	0.00	0.00	0.00	2.45
VA36	27928	6.90	3.03	0.00	0.00	86.23	0.00	0.00	0.00	3.84
VA39	27658	10.83	6.23	0.00	0.83	78.33	0.00	1.18	0.00	2.60
VA41	27493	0.00	1.78	0.00	0.00	96.00	0.00	0.00	0.00	2.22
VA44	27268	0.00	1.23	0.00	3.09	92.67	0.00	0.00	0.00	3.01
VA45	27138	4.40	1.58	0.00	0.21	91.45	0.00	0.00	0.00	2.36
VA47	26938	0.00	2.33	0.61	0.00	95.03	0.00	0.00	0.00	2.02
VA52	26613	0.00	0.35	0.00	0.00	97.32	0.00	0.00	0.00	2.33
VA55	26488	5.05	0.88	0.42	0.00	91.34	0.00	0.00	0.00	2.30
VA57	26388	0.00	1.53	0.00	0.00	96.14	0.00	0.00	0.00	2.33
VA60	26133	0.00	0.94	0.00	0.00	98.05	0.00	0.00	0.00	1.01
VA62	25933	5.45	9.18	0.52	0.00	83.11	0.00	0.00	0.00	1.73
VA65	25583	0.00	0.53	0.00	0.00	97.21	0.00	0.00	0.00	2.26
VA68	25353	0.00	0.48	0.00	0.00	93.90	0.00	0.00	0.00	5.62
VA70	25133	0.00	0.43	0.00	0.00	97.34	0.00	0.00	0.00	1.74
VA73	24893	0.00	0.43	0.00	0.00	96.97	0.00	0.00	0.00	2.60
VA75	24663	0.00	0.48	0.46	0.42	95.12	0.00	0.00	0.00	3.53
VA78	24403	15.49	0.61	0.00	0.00	81.34	0.00	0.00	0.00	2.55
VA79	24283	0.00	2.31	0.34	0.57	94.33	0.00	0.00	0.00	2.45
VA80	23553	0.00	0.96	0.00	0.00	96.22	0.51	0.00	0.00	2.31
VA83	23263	4.41	0.47	0.00	0.00	90.89	0.00	0.00	0.00	4.22
VA86	23040	0.00	0.43	0.00	0.00	97.02	0.38	0.00	0.00	2.17
VA89	22915	0.00	0.92	0.00	0.00	96.02	0.00	0.00	0.00	3.06
VA93	22615	0.00	1.13	0.28	0.28	94.28	0.00	0.00	0.00	4.03
VA96	22310	0.00	0.66	0.76	0.00	96.12	0.00	0.00	0.00	2.46
VA99	21925	6.24	0.23	0.00	0.30	91.33	0.00	0.00	0.00	1.89
VA102	21795	0.00	0.41	0.00	0.00	97.45	0.60	0.00	0.00	1.54
VA105	21620	6.84	0.51	0.00	0.26	87.22	0.00	0.00	0.00	5.17
VA108	21455	0.00	0.56	0.00	0.00	98.12	0.00	0.00	0.00	1.32
VA111	21240	0.00	0.49	0.00	0.48	95.09	0.00	0.00	0.00	3.94
VA115	21085	5.57	0.28	0.00	0.00	88.33	0.00	0.00	0.00	5.81
VA117	21010	12.49	0.54	0.00	0.53	84.10	0.00	0.00	0.00	2.34
VA120	20920	5.41	0.22	0.00	0.00	89.98	0.00	0.00	0.00	4.39
VA123	20725	0.00	0.38	0.00	0.00	98.23	0.98	0.00	0.00	0.41
VA125	20445	6.89	0.18	0.00	0.51	86.74	0.00	0.00	0.00	5.68
VA129	20125	4.57	0.18	0.00	0.00	92.45	0.00	0.00	0.00	2.80
VA132	19885	0.00	0.91	0.00	0.40	97.33	0.00	0.00	0.00	1.36
VA135	19745	5.81	1.09	0.33	0.29	90.90	0.00	0.00	0.00	1.58
VA139	19325	5.64	0.33	0.00	0.00	92.45	0.00	0.00	0.00	1.57
VA142	18815	0.00	0.29	0.60	0.33	96.12	0.00	0.00	0.00	2.66

Valsloch

Samples	Depth (cm)	Phyllosilicates	Quartz	Feldspath-K	Plagioclase-Na	Calcite	Dolomite	Goethite	Ankérite	Indices
VA145	18515	0.00	0.61	0.00	0.00	97.56	0.00	0.00	0.00	1.83
VA148	18165	3.10	0.59	0.00	0.00	90.34	0.00	0.00	0.00	5.98
VA152	17845	7.00	0.59	0.31	0.33	85.86	0.00	0.00	0.00	5.92
VA156	17605	5.54	0.94	0.25	0.00	90.34	0.00	0.00	0.00	2.93
VA160	17345	5.30	1.67	0.38	0.33	87.78	0.00	0.00	0.00	4.54
VA165	17015	3.08	1.80	0.37	0.41	88.93	0.00	0.00	0.00	5.40
VA169	16695	3.24	0.27	0.38	0.00	92.58	0.00	0.00	0.00	3.52
VA173	16285	6.41	0.85	0.00	0.44	88.34	0.00	0.00	0.00	3.96
VA176	15895	5.09	1.24	0.58	0.21	87.23	0.00	0.00	0.00	5.65
VA181	15110	2.96	0.81	0.35	0.00	90.46	0.00	0.00	0.00	5.42
VA185	14350	4.87	3.48	0.36	2.19	87.33	0.00	0.00	0.00	1.76
VA190	13275	3.54	0.51	0.00	0.00	90.10	0.00	0.00	0.00	5.86
VA194	12835	5.36	0.22	0.00	0.00	92.17	0.00	0.00	0.00	2.25
VA197	12295	0.00	1.68	0.00	0.00	95.89	0.00	0.00	0.00	2.43
VA201	11615	7.06	2.15	0.25	0.39	86.23	0.00	0.00	0.00	3.92
VA204	11155	8.77	5.48	0.45	0.25	80.12	0.00	0.00	0.00	4.93
VA207	10820	7.09	3.08	0.00	0.75	87.45	0.00	0.00	0.00	1.62
VA210	10505	9.26	1.17	0.46	0.46	85.22	0.00	0.00	0.00	3.44
VA213	10170	0.00	3.13	0.00	0.89	93.21	0.00	0.00	0.00	2.77
VA216	10065	5.59	1.61	0.56	0.00	86.45	0.00	0.00	0.00	5.79
VA220	9785	6.70	2.15	0.00	0.66	85.11	0.00	0.00	0.00	5.38
VA224	9460	0.00	2.15	0.41	1.34	91.56	0.00	0.00	0.00	4.54
VA227	9125	5.74	3.44	0.36	0.00	84.23	0.00	0.00	0.00	6.23
VA230	8935	7.97	0.92	0.27	0.45	85.40	0.00	0.00	0.00	5.00
VA235	8570	0.00	5.19	0.00	0.79	90.10	0.00	0.00	0.00	3.91
VA238	8315	4.60	3.83	0.00	1.06	85.45	0.00	0.00	0.00	5.06
VA241	8202	0.00	1.36	0.58	0.39	94.23	0.00	0.00	0.00	3.44
VA246	7707	8.15	5.71	0.00	0.62	80.44	0.00	0.00	0.00	5.09
VA249	7367	14.13	6.74	0.59	0.54	74.16	0.00	0.00	0.00	3.84
VA252	6962	4.95	3.50	0.36	1.20	84.33	0.00	0.00	0.00	5.66
VA255	6647	6.25	2.48	0.00	0.54	85.09	0.00	0.00	0.00	5.64
VA257	6347	9.60	4.93	0.49	0.62	81.42	0.00	0.00	0.00	2.93
VA260	6002	6.48	5.95	0.31	1.34	84.91	0.00	0.00	0.00	1.02
VA262	5732	8.32	4.08	0.43	1.09	82.56	0.00	0.00	0.00	3.52
VA264	5347	12.01	4.48	0.43	0.63	78.22	0.00	0.00	0.00	4.23
VA267	4907	6.95	2.95	0.00	0.61	85.22	0.00	0.00	0.00	4.27
VA270	4462	5.23	4.76	0.00	0.00	86.04	0.00	0.00	0.00	3.97
VA274	4322	9.98	11.36	0.00	0.00	74.78	1.49	0.00	0.00	2.39
VA278	4142	0.00	10.91	0.00	3.86	82.18	0.00	0.00	0.00	3.05
VA282	3882	9.46	10.11	0.00	2.34	75.09	0.00	0.00	0.00	3.01
VA286	3502	7.56	11.07	0.00	0.93	78.43	0.00	0.00	0.00	2.01
VA290	3262	9.58	13.01	0.00	0.00	72.18	0.00	0.00	0.00	5.23
VA294	2902	0.00	14.25	0.00	3.10	77.46	0.00	0.00	0.00	5.19
VA298	2642	10.86	12.19	0.00	4.66	70.33	0.00	0.67	0.00	1.29
VA301	2502	3.80	10.58	0.00	4.64	75.33	0.00	1.15	0.00	4.50
VA305	2202	6.06	7.10	0.00	0.96	84.00	0.00	0.00	0.00	1.87
VA309	1900	0.00	12.74	0.00	3.16	83.27	0.00	0.00	0.00	0.83
VA313	1675	0.00	7.17	0.00	0.00	89.05	0.00	0.00	0.00	3.78
VA317	1450	5.30	7.71	0.00	2.94	80.56	0.00	0.00	0.00	3.49
VA321	1295	3.93	12.40	0.00	0.00	82.34	0.00	0.00	0.00	1.33
VA325	1055	5.33	11.89	0.00	0.00	79.49	0.00	0.00	0.00	3.30
VA330	875	6.97	4.50	0.00	0.51	84.33	0.00	0.00	0.00	3.68
VA336	320	32.57	20.77	2.56	2.67	34.77	0.00	0.00	0.00	6.66
VA340	25	7.53	26.46	0.00	0.49	62.14	0.00	0.00	0.00	3.38

Cluses

Samples	Depth (cm)	Phyllosilicates	Quartz	Feldspath-K	Plagioclase-Na	Calcite	Dolomite	Goethite	Ankérite	Indicies
CL3	103	9.32	38.00	0.00	0.00	49.33	0.00	0.00	0.00	3.35
CL5	195	13.67	31.33	0.00	1.73	45.88	0.00	0.00	1.43	5.96
CL7	405	20.45	34.78	0.00	1.57	36.87	0.00	0.00	0.00	6.33
CL9	405	13.76	34.64	0.00	1.00	44.78	0.00	0.00	0.30	5.52
CL11	685	10.22	22.12	0.00	0.67	62.82	0.00	0.00	0.00	4.17
CL13	880	21.12	28.90	0.00	0.46	48.72	0.00	0.00	0.00	0.80
CL15	1039	8.45	20.45	0.00	0.00	65.33	0.00	0.00	0.00	5.77
CL18	1224	4.55	15.44	0.00	0.00	76.31	0.00	0.00	0.00	3.70
CL22	1528	4.68	11.34	0.00	0.00	80.34	0.00	0.00	0.00	3.64
CL25	1749	7.67	36.44	0.00	0.80	50.23	0.00	0.00	0.00	4.86
CL27	1969	12.56	38.56	0.00	0.73	42.11	0.00	0.00	0.00	6.04
CL27BIS	2009	8.55	21.66	0.00	0.00	67.33	0.31	0.00	0.19	1.96
CL29	2269	6.66	16.78	0.00	1.05	67.12	0.00	0.00	0.00	8.39
CL29BIS	2269	12.45	25.34	0.86	0.88	52.55	0.13	0.00	0.09	7.70
CL30A	2404	6.02	18.61	0.00	0.60	72.53	0.00	0.00	0.23	2.02
CL31	2504	8.24	17.33	0.00	0.53	71.45	0.00	0.31	0.00	2.14
CL32	2664	4.41	14.22	0.00	0.60	79.10	0.00	0.00	0.00	1.67
CL34	2809	5.34	20.45	0.00	0.59	71.22	0.00	0.00	0.00	2.40
CL36	2994	9.56	15.33	0.50	0.31	68.19	0.00	0.00	0.00	6.11
CL38	3074	6.89	12.00	0.00	0.00	73.29	0.00	0.00	0.00	7.82
CL40	3169	12.28	9.79	0.00	0.00	75.94	0.00	0.00	0.00	1.99
CL41	3224	4.01	17.70	0.00	0.00	75.29	0.00	0.18	0.37	2.45
CL42	3364	6.03	25.61	0.00	4.28	60.34	0.46	0.00	0.38	2.90
CL43	3414	9.62	26.93	0.00	0.56	59.73	0.00	0.00	0.00	3.16
CL44	3539	7.76	18.98	0.00	0.95	70.33	0.00	0.00	0.00	1.98
CL44BIS??	3579	7.05	17.67	0.00	0.63	71.22	0.00	0.00	0.00	3.43
CL45	3629	8.90	21.49	0.00	0.00	62.78	0.00	0.00	0.00	6.83
CL46BIS (?)	3669	9.02	18.17	0.00	0.00	72.10	0.00	0.00	0.00	0.71
CL47	3769	7.04	15.78	1.02	1.43	70.66	0.00	0.00	0.00	4.07
CL48	3879	6.78	10.33	1.34	0.00	74.98	0.00	0.00	0.00	6.57
CL49	3909	10.77	15.37	0.00	0.95	69.30	0.00	0.00	0.10	3.51
CL50	3939	13.78	10.46	0.44	0.70	70.33	0.00	0.00	0.07	4.23
CL51	3999	4.24	9.45	0.00	0.00	86.20	0.00	0.00	0.00	0.11
CL51BIS	4034	11.45	17.90	0.00	0.00	67.16	0.00	0.22	0.00	3.27
CL52	4059	13.56	19.66	0.00	0.00	61.73	0.00	0.00	0.00	5.05
CL53	4129	7.22	7.13	0.00	0.00	80.77	0.00	0.00	0.00	4.89
CL54	4179	21.31	17.07	0.00	0.66	59.05	0.00	1.04	0.00	0.87
CL55	4259	11.37	16.34	0.00	0.58	67.22	0.00	0.00	0.00	4.49
CL57	4399	7.66	8.06	0.27	0.42	82.08	0.00	0.00	0.17	1.33
CL58	4609	6.44	12.09	0.00	0.35	76.92	0.00	0.00	0.00	4.20
CL60	4744	11.90	17.00	0.00	0.00	65.23	0.16	0.00	0.17	5.54
CL61	4844	6.87	11.72	0.00	0.00	80.45	0.13	0.00	0.09	0.73
CL63	5004	8.94	5.97	0.00	0.00	83.12	0.00	0.00	0.15	1.82
CL65	5129	3.95	4.66	0.00	0.00	87.06	0.60	0.00	0.11	3.63
CL68	5254	0.00	6.04	0.00	0.00	90.34	1.84	0.00	0.00	1.78
CL70	5414	3.17	5.59	0.00	0.00	89.13	1.74	0.00	0.00	0.37
CL71	5494	2.94	3.02	0.00	0.00	90.23	1.14	0.00	2.47	0.20
CL74	5619	4.72	1.40	0.00	0.00	91.34	1.33	0.00	1.16	0.05
CL76	5674	2.25	8.36	0.21	0.00	81.22	2.40	0.00	4.66	0.90
CL78	5719	2.61	2.46	0.00	0.00	60.80	5.37	0.00	24.09	4.66
CL78B	5829	3.92	2.68	0.00	0.21	69.35	11.99	0.00	10.73	1.13
CL80	5989	3.54	0.60	0.41	0.00	91.03	1.18	0.24	2.33	0.67
CL81	6129	4.77	0.39	0.00	0.00	93.20	0.00	0.00	0.15	1.50

6.5 Valsloch component counting data

Sample	Prætericulina curvilliferi	Rudistites a canaux	Sabaudia capitata	Troccholina modesta	Textrulariidae ind.	Trocholina	Bacinella	Dncoctites à Bacinella	Dncoctites à Lithocodium	Arrenobilimina petite taille interne	Girardella petite taille	Glomospira petite taille	Istiloculina petite taille interne	Nubecularia millieux confinées	Assemblyage 1 (%)	Assemblyage 2 (%)	Assemblyage 3 (%)	Assemblyage 4 (%)	Assemblyage 5 (%)	Assemblyage 6 (%)	Assemblyage 7 (%)	Assemblyage 8 (%)	Assemblyage 9 (%)
V/A 20	3	12	2	6				4	1	4	3				0	1	4	0	2	55	37	2	0
V/A 21															1	0	4	0	0	1	14	0	4
V/A 22	7	5	8	1	35										0	2	11	0	2	20	34	13	0
V/A 23	3	5	2	1	26	9									0	0	1	0	0	12	17	12	0
V/A 24	7	7	1	1	18	6									0	0	5	1	1	8	43	8	0
V/A 25						3									1	1	52	74	2	7	4	1	0
V/A 26						2									1	4	55	127	0	9	4	1	0
V/A 27															0	0	8	604	0	0	0	0	0
V/A 28							1								1	2	16	184	0	4	2	0	0
V/A 29															0	1	15	577	0	1	0	0	0
V/A 30						1									6	1	310	8	0	4	10	0	0
V/A 31															13	2	218	5	0	2	0	0	0
V/A 32															1	3	259	13	0	4	10	0	0
V/A 33															1	4	129	9	3	8	5	0	0
V/A 34															1	0	187	8	1	7	6	0	0
V/A 35															8	2	175	49	0	4	0	0	0
V/A 36															0	4	48	13	1	8	2	0	0
V/A 37															0	2	104	26	1	2	6	0	0
V/A 38															0	2	20	27	0	14	3	0	0
V/A 39	1														2	2	21	87	1	9	0	1	0
V/A 40															13	2	202	1	0	1	1	0	0
V/A 41															5	8	57	3	0	3	0	0	1
V/A 42															4	4	60	7	1	2	0	0	0
V/A 43															1	3	30	1	2	17	0	2	0
V/A 44															15	4	65	0	0	0	0	1	0
V/A 45															5	10	5	0	1	14	0	0	0
V/A 46															30	2	26	0	0	2	0	0	2
V/A 47															22	3	20	0	1	0	0	0	1
V/A 48	2														0	2	4	0	1	3	1	1	0
V/A 49	3														0	2	2	0	2	1	1	4	0
V/A 50	2		1												0	0	32	0	4	6	7	0	0
V/A 51	1		2												1	1	53	1	2	8	17	0	0
V/A 52	1		5			3									2	0	31	0	2	12	20	1	0
V/A 55	7		1												0	0	4	0	2	2	4	7	0
V/A 56															2	0	91	0	1	6	9	2	0
V/A 57	2														0	1	8	0	1	14	1	1	0
V/A 58	6		3												1	1	14	0	2	5	11	2	0
V/A 59	5														0	0	2	0	2	14	6	5	0
V/A 61	11														0	0	2	0	4	4	6	3	0
V/A 62	7														0	1	3	0	1	5	8	10	0
V/A 63	1		1												0	1	2	9	1	10	17	4	0

ASSOCIATION 1		ASSOCIATION 2		ASSOCIATION 3 (ECHINO)		ASSOCIATION 4 (TOT OUTLES)		ASSOCIATION 5		ASSOCIATION 6		ASSOCIATION 7		ASSOCIATION 8		ASSOCIATION 9		ASSOCIATION 10	
Sample																			
VA 64																			
VA 65																			
VA 66																			
VA 67																			
VA 68																			
VA 69																			
VA 70																			
VA 71																			
VA 72																			
VA 73																			
VA 74																			
VA 75																			
VA 76																			
VA 77																			
VA 78																			
VA 79																			
VA 80																			
VA 81																			
VA 82																			
VA 83	8		1																
VA 84																			
VA 85																			
VA 86																			
VA 87																			
VA 88																			
VA 89																			
VA 90																			
VA 91																			
VA 92																			
VA 93																			
VA 94																			

Sample	Præreticulina cultilliferi	Rudistites	Rudistites a canaux	Sabaudia capitata	Trocholina molesta	Valvulinifera sp.2	Vercoresella	Bacinella	Galet	Oncocilles à Bacinella et Lithcodium	ASSOCIATION 9	Arrenobulima petite taille interne	Giriarella petite taille	Glomospira petite taille	Istriloculima petite taille interne	Nubecularia milieux confinés	
V/A 64	2	3								28							
V/A 65	4	2								22							
V/A 66	4	1	9							3							
V/A 67	3									21	1						
V/A 68										26	3	2					
V/A 69	1									32	4						
V/A 70	1									51							
V/A 71	3		1							2	38						
V/A 72	5		3							3	23						
V/A 73	8		2							2	47						
V/A 74	1		4							6	49						
V/A 75	3									8	2	1					
V/A 76			1							2	24						
V/A 77	6		4								12						
V/A 78	8		8								24						
V/A 79	1	2		1						1	56	1					
V/L7	5		6								17	10		1			
V/L5	1									2				32			
V/L4	1																
V/L3																	
V/L2														1			
V/A 80										4		2		23			
V/A 81	9		3	1						1				14			
V/A 82	18									2							
V/A 83										2				1			
V/A 87	5		7											57			
V/A 88			12							4		2		1	52		
V/A 89			18							1				25			
V/A 90	17									8				46			
V/A 91	14		7							1				41			
V/A 93	15													21			
V/A 94	16													1			5

6.6 Microfacies and Dunham data

Justistal

Sample	Deph (cm)	Dunham	Microfacie s
LB1	23860	P	FT
LB2	23780	W/P	FT
LB3	23710	P	F8/FT
LB4	23700	P	F9/10
LB5	23655	P/G	FT
LB6	23630	P	F8
LB7	23590	P/G	F8
LB8	23495	W	FT
LB9	23475	P	FT
LB10	23450	P	FT
LB11	23430	P	FT
LB12	23405	P	FT
LB13	23373	P	FT
LB14	23295	P	FT
LB15	23275	P	FT
LB16	23210	W	F9/FT
LB17	23150	W	F9/FT
LB18	23005	G/P	F8
LB19	22900	P	F9
LB20	22875	G/P	F8
LB21	22805	G/P	F11 sandy
LB22	22710	P	F8/9?
LB23	22605	P	F10
LB24	22560	P	F8/9
LB25	22440	G/P	F10
LB26	22320	P	F9/10
LB27	22260	P	F9
LB28	22145	P	F8/9/11?
LB29	22110	P	F8/9
LB30	22070	P	F10
LB31	21990	P	F10/11
LB32	21910	G	F5/11
LB33	21845	G	F8
LB34	21780	P	F10
LB35	21700	G	F8
LB36	21620	P/G	F8
LB37	21545	P	F8
LB38	21450	P	F8/9
LB39	21395	P	F9
LB40	21345	P	F10
LB41	21245	P	F10
LB42	21130	P	F10
LB43	21050	P	F9
LB44	20970	M/W	F11 muddy
LB45	20910	W	F8
LB46	20845	G/P	F6
LB47	20780	G/P	F6
LB48	20735	G/P	F6
LB49	20685	G	F6
LB50	20620	G	F6
LB51	20540	G	F6
LB52	20515	P	F5/6
LB53	20430	G	F6
LB54	20355	G	F5/6
LB55	20285	P	F5/6
LB56	20255	G/P	F5/6
LB57	20165	G	F5/6/11
LB58	20155	G	F4
LB59	20105	G	F4/5
LB60	20040	G	F11
LB61	19875	G	F4/5
LB62	19875	G/P	F5

Sample	Deph (cm)	Dunham	Microfacie s
LB63	19780	G	F6
LB64	19685	G	F5/8
LB65	19595	G	F5
LB66	19495	G	F4
LB67	19395	G	F5
LB68	19295	G	F5
LB69	19195	G	F5
LB70	19095	G	F5
LB71	18995	P	F5/6
LB72	18900	G	F4
LB73	18800	G	F4
LB74	18650	G	F5/6
LB75	18140	G	F5/6
LB76	18050	G	F5/6
LB77	17950	G/P	F4/FT
LB78	17850	G/P	F3
LB79	17800	G	F6
LB80	17590	G	F5/6
LB81	17430	G	F5/6
LB82	17340	G	F5/6
LB83	17220	G	F5/6
LB84	17120	P/W	F2/4
LB85	17020	G	F5/6
LB86	16910	G	F5/6
LB87	16880	G	F5/6
LB88	16770	G	F5/6
LB89	16670	G	F5
LB90	16620	G	F5
LB91	16510	G	F5
LB92	16410	W	F2/4
LB93	16310	G	F5
LB94	16210	G	F6
LB95	16110	G	F5/6
LB96	16010	G	F5/F11
LB97	15910	P	F4
LB98	15810	P	F4
LB99	15710	dolomitized	dolomitized
LB100	15580	G	F3/5
LB101	15480	dolomitized	dolomitized
LB102	15360	G	F5
LB103	15260	G	F5
LB104	15160	G	F5
LB105	15050	G	F5
LB106	14940	G	F5
LB107	14830	P	F4
LB108	14720	G	F5
LB109	14610	G	F5
LB110	14500	P	F4
LB111	14400	P	F4
LB112	14290	P	F4
LB113	14170	G	F5
LB114	14070	G	F4
LB115	13960	G	F5
LB116	13840	G/P	F4
LB117	13730	G/P	F4
LB118	13620	G/P	F4
LB119	13510	G	F3
LB120	13400	G	F4
LB121	13290	G	F5
LB122	13180	G	F5
LB123	12770	G	F5
LB124	12680	G	F5
LB125			

Justistal

Sample	Deph (cm)	Dunham	Microfacie s
LB126	12570	G	F5
LB127	12470	G	F5
LB128	12370	G	F5
LB129	12260	G	F5
LB130	12150	G	F5
LB131	12050	G	F5
LB132	11950	G	F5
LB133	11860	G	F4
LB134	11750	G	F3
LB135	11640	dolomitized	dolomitized
LB136	11450	G	F3
LB137	11350	dolomitized	dolomitized
LB138	11250	dolomitized	dolomitized
LB139	11150	dolomitized	dolomitized
LB140	11050	dolomitized	dolomitized
LB141	10980	dolomitized	dolomitized
LB142	10880	P/W	F3
LB143	10780	P/W	F2/4
LB144	10680	P/W	F2/4
LB145	10580	G	F3/5
LB146	10520	P/W	F2/4
LB147	10420	G	F3/5
LB148	10320	G/P	F3
LB149	10220	G	F3/5
LB150	10120	P/W	F2/4
LB151	10020	G	F3
LB152	9920	G	F3/4
LB153	9820	G/P	F3
LB154	9720	P/W	F2/3
LB156	9620	G	F3
LB157	9520	G	F3
LB158	9420	P	F4/6?
LB159	9320	G	F3
LB160	9220	G	F3
LB161	9120	P/W	F2/3
LB162	9020	P?	F4?
LB163	8920	G	F5
LB164	8820	G	F5
LB165	8720	G	F5
LB166	8620	G	F5
LB167	8520	G	F5
LB168	8420	G	F5
LB169	8320	G	F5
LB170	8220	G	F5?
LB171	8120	P/W	F2/4
LB172	8020	P/G	F3
LB173	7920	P/W	F2/3
LB174	7820	P/W	F2/3
LB175	7720	dolomitized	dolomitized
LB176	7620	dolomitized	dolomitized
LB177	7520	G	F5
LB178	7420	G	F5
LB179	7320	G	F5
LB180	7220	P	F4
LB181	7120	P/W	F2/4
LB182	7020	P/W	F2/4
LB183	6920	P/W	F2/4
LB184	6820	P/W	F2/4
LB185	6700	G	F5
LB186	6600	G	F5
LB187	6500	G	F5
LB188	6400	G	F5

Sample	Deph (cm)	Dunham	Microfacie s
LB189	6300	P	F1/2
LB190	6200	P	F1/2
LB191	6100	P	F1/2
LB192	6000	P	F1/2
LB193	5900	P	F1/2
LB194	5800	P	F1/2
LB195	5700	P	F1/2
LB196	5600	P	F1/2
LB197	5500	G	F3
LB198	5400	P	F2/3
LB199	5300	P	F2/3
LB200	5200	P	F1/2
LB201	5100	P	F4
LB202	5000	G	F3
LB203	4900	P	F1/2
LB204	4800	P	F1/2
LB205	4700	P	F1/2
LB206	4600	P	F1/2
LB207	4500	G/P	F4/5
LB208	4080	G	F5/6
LB209	3900	W	F3
LB210	3800	G	F5
LB211	3700	G/P	F4/5
LB212	3600	G	F5
LB213	3500	P	F2/4
LB214	3400	P	F4
LB215	3340	P	F4
LB216	3280	P	F4
LB217	3180	P/G	F4/6
LB218	3080	G	F3/5
LB219	2980	G/P	F2/5
LB220	2880	G	F5
LB221	2780	P	F4
LB222	2680	WP	F4
LB223	2600	P	F4
LB224	2580	P	F4/6
LB225	1780	P/G	F4/5
LB226	1665	P/G	F4/5
LB227	1545	P/G	F4/5
LB228	1445	G/W	F5
LB229	1365	W	F1
LB230	1225	W	F4/6
LB231	1110	G	F4
LB231bis	600	G	F5/6
LB232	95	P	FT
LB233	5	P	FT

Alvier

Sample	Deph (cm)	Dunham	Microfacie s
68/259	445.6	G	F3
68/260	444.6	P/G	F3
68/261	443.6	P	F2-3
68/262	442.6	G	F3
68/263	440.6	W/P	F2-3
68/264	440.1	W/P	F2-3
68/265	439.6	G	F3
68/266	439.1	G	F3
68/267	437.6	W/P	F4
68/268	435.6	P	F3
68/269	435.1	P/G	F3
68/270	433.6	W/P	F3/4
68/271	430.6	P	F3
68/272	429.6	P	F2/3
68/273	428.6	W/P	F2/3
68/273.5	428.1	dolomitized	dolomitized
68/274	427.6	W	(F8??) F4
68/275	425.6	G	F5
68/276	423.6	G	F5/6
68/277	421.6	P/G	F3
68/235	413	P	F3
68/234	411.5	P	F3
68/233	410	P/G	F3
68/232	409	P/G	F2
68/231	406.5	P/G	F3
68/236	405.5	P	F3
68/237	402.5	P	F4
68/238	397.5	P	F3
68/239	396.5	P	F2
68/240	394.5	W	F1
68/241	392.5	W	F2
68/242	389.5	W	F2
68/243	385.5	P	F2/3
68/245	381.5	W	F2/3
68/246	379.5	W/P	F2
68/247	378.5	P/G	F2
68/248	377.5	P	F1
68/249	376.5	P	F4
68/250	375.5	P	F4
68/251	373.5	W	F2
68/252	372	W	F2
68/253	369.5	W	FT
68/254	368.5	P	F5
68/254.5	366.5	P	F5
68/256	365.5	P/G	F3
68/257	363.5	G	F3
68/258	360	P	F3
68/230	359	P/G	F3
68/229	357.5	P/G	F4
68/228.5	354.5	P/G	F4/8
68/228	353.5	W	F4/8
68/227	349.5	W	F4
68/226	349	W	F3
68/225	348.5	G	F5
68/224	347.5	P	F3
68/223	345.5	W	F2/3
68/222	342.5	W	F3
68/221	340.5	G	F3
68/220	339	W	F2/3
68/219	337.5	W	F5/FT?
68/218	335.5	P	FT
68/217	333	P	F3/8

Sample	Deph (cm)	Dunham	Microfacie s
68/216	330.5	P/G	F3
68/215	329.5	P	F3
68/214	326.5	W	F2/3
68/213	325.5	W	F3/2
68/212	322.5	W	F3
68/211	319.5	P/G	F5/8
68/210	318.5	W/P	F5/8
68/209	317.5	P/G	F8
68/208	313.5	P/W	F3
68/207	312.5	W	F8
68/206	310.5	W	F3/8
68/205	308.5	P	F3/8
68/204	306.5	W	F3/8
68/203	305.5	W	F3/2
68/202	302.5	W	F3/2
68/201	300.5	P	F2
68/200	298.5	P	F2/FT
68/199	295.5	W	F2/3
68/198	294.5	W	F3
68/195	293.5	P	F5
68/193	290.5	W	F2/3
68/192	289.5	W	F2
68/191	288.5	P	F2
68/190	287.5	P	F2
68/189	286.5	P/G	F2/3
68/188	285.5	P	F2/3
68/187	285	W	F2/3
68/186.3	284.5	P	F3
68/186	284	W/P	F3
68/184	283.5	W	F1
68/182	281.5	W	F1
68/180	278.5	W	F2/3
68/179	276	W	F1
68/178	275	W	F1
68/177	274.5	W	F1
68/176	273.5	W	F1
68/175	272	P	F2
68/174	270	W	F1/2
68/172	268.5	W	F1
68/171	257.5	W	F0/1
68/170	251.5	P/W	F1/2
68/169	243.5	P	F2
68/168	242.5	P	F2
68/167	241.5	W	F0
68/166	240.5	W	F2
68/165	239.5	W	F1/2
68/164	238.5	P/G	F1/2
68/163	237	P/W	F1/2
68/162	237.5	W/P	F3/4
68/161	236	P/W	F1/2
68/160	234.5	W	F2
68/158	233.5	P/W	F3
68/157	232.5	P/W	F3
68/156	231.5	W	F2
68/155	230.5	P	F2
68/154	229.5	P/W	F3
68/153	227	P	F2
68/152	225.5	P/W	F1
68/151	224	P	F2
68/150	222.5	W	F1
68/149	221.5	W	F1
68/148	220.5	W	F2

Alvier

Sample	Depth (cm)	Dunham	Microfacies
68/147	219.5	W	F2
68/146	218.5	W	F2
68/145	217.5	W	F2
68/144	216.5	P	FT
68/143	215.5	P/G	F4/5?

Sample	Depth (cm)	Dunham	Microfacies
Ri 46	196	M/W	F3?
Ri 45	191	M/W	F3?
Ri 44	186	M	F0
Ri 43	181	M/W	F1
Ri 42	178	M/W	F2
Ri 40	165	W/P	F2/3?
Ri 38	160	W	F3
Ri 37	157	M/W	F0
Ri 36	153	M/W	F1
Ri 35	149	M/W	F1
Ri 34	147	M/W	F0/1
Ri 33	143	M/W	F0/1
Ri 32	139	M/W	F1
Ri 31	134	M/W	F1
Ri 30	130	M/W	F1
Ri 29	126	M/W	F0/1
Ri 28	121	M/W	F1
Ri 27	118	M/W	F0
Ri 26	114	M/W	F1
Ri 25	110	M/W	F1
Ri 24	106	M/W	F0
Ri 23	103	M/W	F1
Ri 22	98	M/W	F1
Ri 21	93	M/W	F1
Ri 20	89	M/W	F2
Ri 19	85	M/W	F1
Ri 18	83	M/W	F2
Ri 17	79	M/W	F1
Ri 16	73	M/W	F1
Ri 15	70	M/W	F1
Ri 14	67	M/W	F1
Ri 13	60	M/W	F1
Ri 11	51	W	F2
Ri 10	45	M/W	F1
Ri 9	40	M/W	F2
Ri 8	34	M/W	F1
Ri 7	30	M	F0
Ri 6	25	M/W	F0
Ri 5	18	M/W	F0/1
Ri 4	13	M/W	F1
Ri 3	9	M/W	F0
Ri 2	4	M/W	F0
Ri 1	0	W	F0

L'Ecuelle

Sample	Deph (cm)	Dunham	Microfacie s
EC257	20620	G	FT
EC256	20470	G	FT
EC253	20260	G	F11
EC252	20220	G	F10
EC250	20115	G	F10
EC247	19920	G	F11
EC246	19905	G	FT
EC244	19850	?	F8/FT?
EC242	19720	P	FT
EC241c	19700	P	FT
EC241a	19700	G	F11
EC240	19650	G	F11
EC237	19525	G	F11
EC236	19480	G	F11
EC235	19420	G	F11
EC233	19325	W	F10
EC232	19310	W	F8/9
EC231	19240	P/G	F8/9
EC229	19130	G	F11
EC226	18970	G	F8
EC224	18870	P	F8/9
EC223	18860	P	F8/9
EC221	18775	P	F9
EC220	18710	P	F9
EC217	18560	W	FT
EC213	18360	W	F3
EC211	18195	W	F3
EC210	18145	W	F3
EC206	17960	W	F3
EC203	17790	W	F3
EC201	17710	W/P	FT
EC199	17630	W/P	FT
EC197	17529	W/P	FT
EC196	17520	B	F7
EC195	17470	P	FT
EC194	17430	P	FT
EC193	17360	P	FT
EC192	17270	P	FT
EC191	17230	P	FT
EC190	17215	P	FT
EC188	17080	P/G	FT
EC187	17015	P	FT
EC186	17010	siltstone	F1
EC185	16940	P	FT
EC184	16895	P	FT
EC183	16868	P	FT
EC182	16805	P/G	FT
EC181	16760	G	F11
EC180	16725	P	F3/4
EC179	16680	W	F1
EC178	16600	P	FT
EC177	16578	M/P	F1/F3?
EC176	16575	M/G	F1/F3
EC175	16520	P	FT
EC174	16468	P	FT
EC173	16415	M	F1
EC172	16359	sandstone	sandstone
EC171	16345	G	F11?
EC170	16325	P	F9/FT
EC169	16310	P/G	F11
EC168	16190	W/P	FT
EC167	16177	G	FT?

Sample	Deph (cm)	Dunham	Microfacie s
EC166	16170	G	FT
EC165	16130	G	F11
EC164	16075	G	F11
EC163	16005	G	FT
EC162	15980	G/W	F11
EC161	15880	G	F11
EC160	15780	P	F11
EC159	15680	G	F11
EC158	15590	P	F9
EC157	15450	P	F9
EC156	15340	P/G	F9
EC155	15250	P/G	F10
EC154	15120	P	F9
EC153	15050	P	F10
EC152	14950	P	F9
EC151	14900	P	F8
EC150	14800	P	F11
EC149	14700	P	F10
EC148	14600	P	F10
EC147	14500	P/G	F9
EC146	14400	P/G	F9
EC145	14300	P/G	F9
EC144	14100	W	F10
EC143	13800	W	F10
EC142	13650	W	F10
EC141	13500	P/G	F10
EC140	13370	P	F9
EC139	13265	P/G	F10
EC138	13155	G	F11
EC136	12890	P	F8
EC135	12750	W/P	F8
EC134	12670	W/P	F8
EC133	12575	W/P	F8
EC132	12550	W/P	F8
EC131	12480	W/P	F8
EC129	12330	W/P	F4
EC128	12290	W/P	F4
EC127	12195	G	F9
EC126	12145	G	F9
EC125	12025	G	F9
EC123	11895	W	F10
EC122	11885	G	F10
EC121	11790	G	F9
EC120	11690	P/G	F11
EC119	11590	G	F10
EC118	11490	P/G	F11
EC117	11350	G	F10
EC115	11220	G	F10
EC114	11090	G	F9
EC113	11068	G	F9
EC111	10880	G	F9
EC110	10740	G	F9
EC109	10670	G	F9
EC108	10570	P	F10
EC107	10490	P	F10
EC106	10375	G	F9
EC105	10295	P/G	F11
EC104	10245	P/G	F11
EC103	10175	P/G	F11
EC102	9970	G	F10
EC99	9645	G	F10
EC98	9440	P	FT

L'Ecuelle

Sample	Deph (cm)	Dunham	Microfacie s
EC97	9330	W	F3
EC95	9125	W	F4
EC94	9025	G	F4
EC93	8935	P/G	F4
EC89	8485	G	F3/4
EC88	8385	G	F3/4
EC86	8095	G	F3/4
EC85	8015	G	F3/4
EC84	7955	G	F3/4
EC83	7880	G	F4
EC82	7800	G	F3/4
EC81	7725	P/G	F4
EC80	7660	P/G	F4/5
EC77	7515	P/G	F4/5
EC74	7345	P/G	F4/5
EC72	7145	P/G	F4/5
EC70	6915	P/G	F4/5
EC69	6815	P/G	F4/5
EC68	6710	P/G	F5
EC67	6605	P	F3
EC66	6465	P	F3
EC64	6030	P	F3
EC63	5940	P	F3
EC62	5901	W	F3
EC61	5822	P/G	F4/5
EC60	5815	P/G	F3
EC59	5715	P/G	F3
EC58	5649	P/G	F3
EC57	5584	P/G	F3
EC56	5479	P/G	F3
EC55	5394	P	F3
EC54	5324	P/G	F3
EC53	5149	P/G	F5?
EC52	5089	G	F5
EC51	5002	G	F5
EC50	4914	G	F5/3
EC49	4825	G	F5/3
EC48	4735	G	F5/3
EC47	4675	G	F5
EC46	4610	W	F3
EC45	4530	W	F3
EC44	4430	P	F3/4
EC43	4330	P	F3/4
EC41	4130	G	F5/3
EC40	4030	G	F5/3
EC39	3930	P/G	F4
EC38	3830	P/G	F3/4
EC36	3630	W	F3
EC35	3530	W	F3
EC34	3430	W	F3
EC33	3335	W	F3
EC32	3245	W	F3/4
EC30	3160	P	F4/5?
EC29	3135	P/G	F5
EC28	3040	P	F4
EC27	2940	P	F4
EC26	2845	P	F4
EC25	2840	P	F4
EC24	2770	W	F1?
EC23	2680	W	F0?
EC22	2580	W-P	F3?
EC21	2530	W-P	F3?

Sample	Deph (cm)	Dunham	Microfacie s
EC19	2320	W	F2?
EC18	2120	W	F1?
EC17	2020	W	F1?
EC14	1770	W	F0?
EC12	1610	W-P	F3?
EC11	1560	W-P	F3?
EC10	1440	W-P	F3?
EC9	1340	W-P	F4?
EC8	1230	W-P	F4?
EC6	1050	W	F2?
EC5	315	P-G?	F3?
EC4	195	P	F3?
EC2	155	P-G?	F5/FT?
EC1	5	W-P	F3

Morschach

Sample	Deph (cm)	Dunham	Microfacie s
MC2	15	P/G	F4
MC2bis	32	P/G	F4
MC3	45	P/G	F4
MC3a	73	P/G	F4
MC3b	89	P/G	F4
MC4	100	P/G	F4
MC4a	119	P/G	F4
MC4b	128	W/P	F10
MC5	230	W/P	F10
MC8	535	W/P	F10?F11?
MC10	695	W	F10
MC11	760	W	F10
MC12	845	W	F10
MC13	945	W	F10
MC14	1050	W	F8/9
MC15	1150	W	F8/9
MC16	1260	W	F8/9
MC17	1365	W	F8/9
MC18	1445	W	F8/9
MC19	1550	P	F8
MC20	1638	P	F9
MC21	1750	P	F10
MC22	1805	P	F10
MC23	1945	P	F8
MC24	2035	P/G	F8?
MC25	2130	P/G	F10
MC26	2235	P	F8/9
MC27	2360	P	F8
MC28	2450	P	F8
MC29	2550	G/P	F10
MC30	2630	G/P	F10
MC31	2740	G	F9/F10
MC32	2835	W	F9/F10
MC33	2952	G	F8
MC34	3050	G	F8/3
MC35	3135	W	F8
MC36	3215	G	F3
MC37	3245	W	F11
MC38	3350	G	F9/11
MC39	3435	P	F9
MC40	3515	W	F9/11
MC41	3575	M	F1
MC42	3695	G	F2/3
MC43	3835	G	F5
MC44	3900	G/P	F2/3
MC45	4022	G	F5
MC46	4135	M	F11
MC47	4220	M	F11
MC47bis	4240	G	F11
MC48	4280	sandstone	FT
MC49	4305	G	F3
MC50	4320	G	F11
MC51	4430	G	F11
MC52	4535	W/P	F9/11
MC53	4625	G	F3
MC54	4705	G	F3
MC55	4785	G	F5
MC56	4835	G	F5
MC57	4875	G	F3/5
MC58	4940	G	F3/5
MC59	5035	G	F3?
MC60	5110	G	F3/11

Sample	Deph (cm)	Dunham	Microfacie s
MC61	5215	G	F11
MC62	5325	G	F11
MC63	5435	G/P	F9/10
MC64	5505	G/P	F9/11
MC65	5650	W	F11
MC66	5725	W	F9/10
MC67	5850	W	FT/FT
MC68	5952	P	F8/F11
MC69	6035	G	F11 temp
MC70	6150	W	F8?
MC71	6195	W/G	F11
MC72	6350	W	FT?
MC73	6450	P/G	F10/11
MC74	6530	P/G	F10
MC75	6640	W/P	F9/10
MC77	6825	P/G	F10
MC78	6925	G/P	F8
MC79	7053	G/W	FT
MC80	7135	G	F11 temp
MC82	7335	W/P	F9/10
MC83	7449	P/G	F8/9
MC84	7518	W/P	F8/9
MC85	7650	G/P	F9
MC86	7695	G	F8
MC87	7790	G	F11 temp
MC88	7900	P/G	F10?
MC89	8045	G	F11 temp
MC91	8220	G	F5/F11?
MC92	8340	P/G	FT
MC93	8435	W/P/G	F4?/F8/FT
MC94	8550	P	F10
MC95	8605	P/G	F8/9
MC96	8705	G	F11
MC97	8823	G	F11
MC98	8928	W	F8
MC99	9020	P/G	F8/9
MC100	9125	G	F8/9
MC101	9252	P	F9?
MC102	9350	G	F8
MC103	9440	G	F3/F5?
MC104	9535	P	F9?
MC105	9630	W/P	F11
MC106	9745	P/G	F9/10
MC107	9850	P	F9
MC108	9945	P	FT?
MC109	9970	P/G	FT
MC110	10045	P/G	FT
MC111	10100	W	F10/11
MC112	10232	P	F8/9
MC113	10350	P/G	FT?
MC114	10450	W	F8
MC115	10475	G/P	F8/FT
MC116	10585	P	F8
MC117	10727	W	FT?
MC118	10745	sandstone	sandstone
MC119	10820	W	FT
MC120	10875	W	F11
MC121	10975	W	FT/F3
MC122	11020	P	FT?FPN?
MC123	11040	W/P	F8/FT
MC124	11145	G	F3
MC125	11185	W/P	FT

Morschach

Sample	Deph (cm)	Dunham	Microfacie s
MC126	11230	P/G	F9
MC127	11350	P	10/11?
MC128	11450	P	FT
MC129	11490	P	FT
MC130	11515	W	FT
MC131	11550	G	F9/10
MC132	11630	P	F8
MC133	11735	G	F11
MC134	11787	P	F8/9
MC135	11850	G	F11
MC136	11890	P	F8
MC137	11935	G	F11
MC138	12035	P	F9
MC139	12065	P/G	F8/9
MC140	12120	P	F9
MC141	12240	G/P	F9/11?
MC142	12335	G	F10?
MC143	12415	W	F9/10/FT
MC144	12545	W	F9/10/FT
MC145	12635	P/G	F9
MC146	12745	P/G	F9
MC147	12850	P/G	F9
MC148	12950	P	F9/10/FT
MC149	13052	W	F9/10/FT
MC150	13130	W/P	F9
MC151	13235	W/P	F8/9
MC152	13295	W	F8/11
MC153	13410	P	FT
MC154	13525	W/P	F8/9
MC155	13640	W/P	F8
MC156	13740	W/P	F8/9
MC157	13780	W/P	F8
MC158	13935	W	FT/F8
MC159	14025	W	FT
MC160	14147	P	F8
MC161	14228	P	F8
MC162	14233	G/P	F8
MC163	14327	G	F9
MC164	14440	P/G	F9
MC165	14535	P	F10
MC166	14585	W/P	F8
MC167	14750	G/P	F8
MC169	14880	P	F8
MC170	14945	G	F5
MC171	15025	G	F4/5
MC172	15125	G	F4/5
MC173	15240	G	F7/8
MC174	15340	P	F4
MC175	15422	G/P	F5/6
MC176	15505	G	F5?
MC177	15590	P	F4
MC178	15735	W/G	F3
MC179	15790	G	F6
MC180	15915	G	F3/5
MC181	16040	G	F5/6
MC182	16142	G	F5
MC183	16210	G	F4/5
MC184	16290	G	F4/5
MC185	16385	G	F4/5
MC186	16530	G	F4/5
MC188	16745	G	F4/5
MC190	16935	G	F4/5

Sample	Deph (cm)	Dunham	Microfacie s
MC191	17045	G	F4/5
MC193	17250	P	F4
MC194	17312	W/G	F3
MC195	17452	W/G	F3
MC197	17620	W/G	F3
MC200	17805	P	F4
MC201	17807	W/P	F2/3
MC202	18060	W	F2
MC203	18253	W	F2
MC204	18348	P	F2?
MC205	18450	W	F2
MC206	18575	P	FT
MC207	18700	W	F2
MC208	18885	W?	F2
MC209	18950	W	F1
MC210	19130	W	F2
MC211	19332	W	F2
MC213	19515	W	F2
MC214	19735	G	F4/5/6
MC216	20030	W	F2
MC217	20315	G	F5
MC218	20425	G	F5
MC219	20560	G	F5
MC221	20825	W?	F2
MC222	20920	W	F2
MC223	20965	G	F3
MC224	21095	G	F3?
MC225	21160	G	F5/6
MC226	21385	G/P	F4
MC227	21485	G	F5
MC228	21710	W?	F2
MC230	21875	W	F2
MC232	22052	W	F2
MC234	22260	W	F2
MC238	22700	W	F2/3
MC241	23035	W/G	F3
MC242	23265	W/G	F3
MC245	23455	W	F2
MC248	23725	W	F1
MC251	24025	W	F2
MC259	24930	W	F2
MC262	25250	W	F2
MC265	25530	W	F2
MC267	25715	W	F2
MC272	26230	W	F0?
MC275	26495	W	F2
MC277	26705	W	F2
MC280	27015	W	F1
MC283	27312	W	F1
MC285	27505	W	F1
MC286	27595	W	F1
MC289	27802	W	F1
MC290	27975	W	F1
MC298	28705	W	F1

Tierwis

Sample	Deph (cm)	Dunham	Microfacies
TW159	19250	W	F9
TW 158	19165	W	F9
TW157	19085	W	F9
TW156	19065	W	F8
TW155	18985	W	F9
TW154	18970	W/P	F10
TW153	18875	W	F11
TW152	18860	G/P	F8
TW151	18780	W	F8
TW150	18760	W	F8
TW149	18660	W	F10
TW148	18620	W	F9
TW147	18520	W	F10
TW146	18370	G	F11
TW145	18230	W	F8
TW144	18210	W	F8
TW143	18060	W	F8
TW142	17990	P	F8
TW140	17815	P/W	F8
TW139	17710	P/W	F8
TW137	17570	G	F9.5
TW136	17537	G	F11
TW135	17512	G	F11
TW134	17482	G	F8
TW132	17372	G	F8
TW131	17302	W	F8
TW130	17227	G	F8
TW129	17217	G	F8
TW128	17177	G	F8
TW127	17107	G	F7
TW126	17037	G	F8
TW125	16947	G	F8/9
TW124	16867	G	F9
TW123	16842	W	F8
TW122	16742	G	F6
TW120	16612	G	F5/6
TW119	16572	P	FT/F6
TW118	16532	G	F5
TW117	16497	G	F5
TW116	16417	P	F11
SA MS 86	16332	G	F6
SA MS 85	16202	G	F5
SA MS 84	16190	W	FT
SA MS 83	16177	P/G	FT
SA MS 82	16105	P/G	F6/8
SA MS 81	16028	G	F3
SA MS 80	16017	G	F3
SA MS 79	15924	G	FT
SA MS 78	15830	W	F2-F3
SA MS 77	15818	W	F2
SA MS 76	15803	G	F3
SA MS 75	15786	G	F3
SA MS 74	15736	W	FT/F2
SA MS 73	15685	W	FT
SA MS 72	15681	W/P	FT
SA MS 71	15673	G	FT F3
SA MS 70	15662	P/W	FT
SA MS 69	15607	P/G	F8
SA MS 68	15599	G	F5/6
SA MS 67	15510	G	F5/6
SA MS 66	15499	G	F5
SA MS 65	15497	P/G	F4/5

Sample	Deph (cm)	Dunham	Microfacies
SA MS 64	15444	W	F2
SA MS 63	15425	P/W	FT
SA MS 62	15257	G	F3
SA MS 61	15246	G	F2-F3
SA MS 60	15097	W/P	FT
SA MS 59	15068	W/P	F2-F3?
SA MS 58	15030	W	F1-2
SA MS 57	14993	W	F3
SA MS 56	14952	W	F2-F3
SA MS 55	14928	W	F4
SA MS 54	14893	W	F4
SA MS 53	14882	G	F3
SA MS 52	14818	G	F3
SA MS 51	14807	P	F8?
SA MS 50	14782	G/P	F8
SA MS 49	14709	P/W	F8
SA MS 48	14605	P/W	F8
SA MS 47	14592	P/W	F8
SA MS 46	14448	P/G	F5
SA MS 45	14435	G	F3
SA MS 44	14341	P/W	F4
SA MS 43	14247	W	F8
SA MS 42	14237	G	F5
SA MS 41	14130	W/P	FT
SA MS 40	14105	W/P	FT
SA MS 39	14082	W/P	FT
SA MS 38	14031	P/G	FT
SA MS 37	14006	W	F8
SA MS 36	13981	W/P	FT
SA MS 35	13941	W	FT
SA MS 34	13891	W	F8
SA MS 33	13883	W	FT
SA MS 32	13777	W/P	FT
SA MS 31	13692	W/P	F11
SA MS 30	13673	W/P	F11
SA MS 29	13632	W/P	FT
SA MS 28	13609	-	-
SA MS 27	13601	-	-
SA MS 26	13571	G	F6
SA MS 25	13554	G	F11
SA MS 24	13475	W/P	F8?
SA MS 23	13465	W/P	F8?
SA MS 22	13379	W	FT
SA MS 21	13360	W	FT
SA MS 20	13331	W	FT
SA MS 19	13307	W	FT
SA MS 18	13296	W	FT
SA MS 17	13282	W	FT
SA MS 16	13241	M/W	F11
SA MS 15	13228	sandstone	FT
SA MS 14	13208	sandstone	FT
SA MS 13	13159	sandstone	FT
SA MS 12	13153	sandstone	FT
TW115	13128	P	F9
TW114	13028	P	F8
TW113	13013	G	F6
TW112	12988	G	F11
TW110	12878	P	F8
TW108	12758	G	F6
TW107	12653	G	F8
TW105	12418	G/P	F5
TW104	12328	W	F11

Tierwis

Sample	Deph (cm)	Dunham	Microfacie s
TW103	12308	G/P	F8
TW102	12208	G	F5
TW101	12188	W	F11
TW100	12048	P	F8
TW99	12028	P	F4
TW98	11938	G	F9/10
TW97	11858	G	F5
TW96	11828	W	F11
TW95	11718	G	F6
TW94	11688	P	F9
TW93	11568	P/G	F8 ?
TW91	11468	W	F9
TW90	11398	P	F7
TW89	11348	W	F9
TW88	11218	G	F5
TW87	11198	G	F6
TW86	11068	P/G	FT
TW85	11028	G	F6/11
TW84	10948	G	F5
TW83	10928	G	F6
TW82	10808	P/G	F4
TW81	10778	G	F5
TW80	10678	G	F5
TW79	10598	G	F3
TW78	10538	G	F5
TW77	10523	G	F5/F6
TW76	10433	G	F6
TW74	10338	G	F4
TW73	10308	G	F5
TW72	10283	G	F5
TW71	10213	G	F5
TW70	10188	P/G	F3
TW69	10158	G	F6
TW67	9958	G	F4
TW66	9668	G/P	F6
TW65	9648	G/P	F6
TW64	9648	P/G	F5
TW63	9538	W	F1/F4
TW62	9448	G	F5
TW61	9433	G	F5
TW60	9373	W/P	F1
TW59	9253	G	F6
TW58	9133	P/G?	F6?
TW57	9113	G	F5
TW56	8993	G/P	F4?
TW54	8858	G/P	F8
TW53	8778	G	F6
TW52	8703	P	F6
TW51	8643	G	F7/8
TW50	8608	G	F7
TW49	8543	P/G	F10
TW48	8483	G	F5
TW47	8413	G	F5
TW46	8388	G	F5
TW45	8338	G	F5/8?
TW44	8268	G	F5
TW43	8198	G	F9-10
TW42	8128	G	F8
TW40	8038	W/P	F10
TW39	7948	G	F6
TW38	7925	G	F6
TW37	7895	P	F11?

Sample	Deph (cm)	Dunham	Microfacie s
TW36	7855	G	F11
TW35	7810	M/W	F11
TW34	7710	P	F11
TW33	7640	G	F4/5
TW32	7535	M/W	F11
TW31	7485	P/G	F5/8
TW30	7445	G	F6
TW29	7335	G	F5
TW28	7275	P	F8
TW27	7215	G	F5
TW26	7180	G	F5
TW25	7115	G	F6
TW24	7055	G	F5
TW23	6940	G	F5
TW22	6870	G	F3?
TW21	6773	G	F4/5
TW20	6731	G	F4/6
TW19	6686	G	F6
TW18	6646	G	F5
TW17	6566	G	F4
TW16	6476	G	F5
TW15	6406	G	F4/5
TW14	6364	G	F5/6
TW13	6275	P/G	F3/4
TW12	6230	G	F5/F6
TW11	6185	G	F3
TW10	6139	P	F3/4
TW9	6107	P	F4
TW8	6075	G	F5
TW7	6023	P	F2/3
TW6	5948	P/G	F3/4
TW5	5868	W	F3
TW4	5798	G	F4/5
TW3	5733	G	F5
TW1	5690	G	F4/5
SA SB 49	5091	M/W	F0/1
SA LB 1	5019	M/W	F0/1
SA SB 48b	4968	M/W	F0/1
SA LB 2	4954	M/W	F0/1
SA LB 3	4879	M/W	F0/1
SA SB 47	4790	M/W	F1
SA LB 4	4779	M/W	F0/1
SA LB 6	4729	M/W	F0/1
SA SB 46	4674	M/W	F1
SA LB 7	4629	M/W	F0/1
SA LB 8	4524	M/W	F0/3
SA LB 9	4424	M/W	F0/1
SA LB 10	4274	M/W	F0/1
SA SB 45	4246	M/W	F1
SA SB 44	4168	M/W	F1
SA LB 11	4129	M/W	F0/1
SA LB 12	3999	M/W	F0/1
SA LB 13	3949	M/W	F0/1
SA SB 43	3898	M/W	F1
SA LB 14	3849	M/W	F0/1
SA LB 15	3834	M/W	F0/1
SA LB 16	3779	W	F1/2
SA SB 41	3763	M/W	F1/2
SA SB 40	3735	M/W	F1
SA LB 17	3734	W	F1/2
SA LB 18	3699	M/W	F0/1
SA LB 19	3659	W	F1/2

Tierwis

Sample	Deph (cm)	Dunham	Microfacies
SA SB 39	3627	M/W	F1
SA LB 20	3589	W	F1/2
SA SB 38	3565	marl	F0?
SA SB 37	3533	M/W	F1
SA SB 36	3505	P/G?	F3
SA LB 22	3484	W	F1/2
SA SB 35	3468	M/W	F2/3
SA SB 34	3408	M/W	F2/3
SA SB 33	3354	W	F4
SA SB 32	3300	M/W	F2/3
SA SB 31	3234	M/W	F2/3
SA SB 30b	3193	M/W	F2/3
SA SB 30a	3166	M/W	F1/2
SA LB 26	3109	W	F3/4
SA SB 29	3068	M/W	F2/3
SA SB 28b	3017	M/W	F1/2
SA SB 28a	2973	marl	F0?
SA SB 27b	2931	M/W	F1/2
SA SB 27a	2881	M/W	F2/3
SA SB 26	2809	P/G	F3/4
SA SB 25	2752	P/G	F3/4
SA LB 30	2619	W	F3/4
SA SB 24c	2607	M/W	F2/3
SA SB 24b	2138	M/W	F2/3
SA SB 24a	1684	M/W	F1/2
SA SB 23	1504	M/W	F1/2
SA SB 22	1380	M/W	F1/2
SA SB 21	1300	P/G?	F3
SA SB 20	1235	M/W	F1/2
SA SB 19	1201	M/W	F1
SA SB 18c	1169	WP	F2
SA SB 18b	1110	M/W	F1
SA SB 18a	1059	M/W	F1
SA SB 17	1008	marl	F0?
SA SB 16b	980	marl	F0?
SA SB 16a	924	M/W	F1
SA SB 15c	873	WP	F2
SA SB 15b	848	M/W	F1
SA SB 15a	815	M/W	F1
SA SB 14b	783	WP	F2
SA SB 14a	758	M/W	F1
SA SB 13	723	WP	F2
SA SB 12	691	P/G	F4/5
SA SB 10	514	P/G	F4?
SA SB 9	411	P/G	F3/4
SA SB 8	325	W/P	F2
SA SB 7	239	W/P	F2
SA SB 2	64	W/P	F2

Valsloch

Sample	Deph (cm)	Dunham	Microfacies
VA1	30983	W/P	F9
VA2	30863	W/P	F9
VA3	30693	W/P	F9
VA4	30683	W	F10?
VA5	30618	W/P	F9/10
VA6	30588	P	F9
VA7	30518	W	F9
VA8	30393	P	F9
VA10	30178	W/P	F8
VA12	29888	W/P	F9
VA13	29868	P	F10
VA15	29623	W	F10
VA16	29543	W	F10
VA17	29463	P/G	F8
VA18	29388	W/P	F10
VA19	29298	P/G	F9
VA20	29258	P	F9
VA21	29158	M/W	F11
VA22	29048	W/P	F9
VA23	28998	W/P	F10
VA24	28778	P/G/B	F8
VA25	28758	G	F5/6
VA26	28708	P/G	F11
VA27	28618	G	F6
VA28	28453	P/G	F5
VA29	28363	P	F6
VA30	28333	P/G	F5
VA31	28278	P/G	F5
VA32	28253	P/G	F5
VA33	28138	G	F4/5
VA34	28013	P/G	F3/4
VA35	27978	P	F3
VA36	27928	G	F5
VA37	27888	P	F3
VA38	27733	G	TF?
VA39	27658	G	F5/6
VA40	27588	P	F3
VA41	27493	G	F3/4
VA42	27433	G	F3/4
VA43	27383	G	F3/4
VA44	27268	G	F2/4
VA45	27248	G/P	FT?
VA46	27148	W	F3
VA47	27138	W	F3
VA48	27108	G	F5
VA49	26938	G	F5
VA50	26808	G/P	F4
VA51	26708	P	F4
VA52	26613	P	F4
VA55	26488	G/P	F8
VA56	26403	P	F4
VA57	26388	P	F8/9
VA58	26268	P/G	F4?
VA59	26233	G	F4?
VA61	26033	G	F7
VA62	25933	W/P	F9
VA63	25833	W/P	F8??
VA64	25733	G	F8
VA65	25583	G	F5/11
VA66	25563	G	F11
VA67	25483	W	F10?
VA68	25353	P/G	F10?

Valsloch

Sample	Deph (cm)	Dunham	Microfacie s
VA69	25233	G	F10
VA70	25133	P/W	F8/9
VA71	25073	P/W	FPN
VA72	24993	P/G	F8
VA73	24893	G	F9
VA74	24823	G	F8
VA75	24663	G	F9/10
VA76	24533	G	F9
VA77	24493	G/W	F9/10
VA78	24403	P/W	F8
VA79	24283	P/G	FT
VA80	23553	P/W	F8
VA81	23413	W	FT
VA82	23393	W/P	F8
VA83	23263	W	FT
VA84	23173	W	F8
VA85	23100	P	FT
VA86	23040	P	F8/T
VA87	23005	G/P	F8/T
VA88	22985	P	F8/T
VA89	22915	G/P	F8/T
VA90	22835	P	F9
VA91	22775	P/G	FT
VA93	22615	P/G	F8
VA94	22525	P/B	F7/8
VA95	22425	G/P	F8
VA96	22310	G/P	F8
VA97	22190	W/P	F8
VA98	22165	P	F8
VA99	21925	W	F8
VA101	21860	W	F9
VA102	21795	W/P	F8
VA103	21735	P/G	F8
VA104	21720	P	F9/10
VA105	21620	P/W	F10
VA106	21600	P	F8
VA107	21480	P/W	F9
VA108	21455	P	F9
VA109	21325	P/G	F8
VA110	21280	P	F9
VA111	21240	P	F9
VA113	21170	P	F9
VA114	21155	G/P	F8
VA115	21085	W/P	F9
VA116	21070	P	F8
VA117	21010	P	F8
VA118	21000	P	F8
VA119	20945	W/P	F8
VA120	20920	W/P	F9/8
VA121	20840	P	F9/11
VA122	20785	G/P	F8/11
VA123	20725	W/P	F8
VA124	20545	W	F8
VA125	20445	W	F8?
VA126	20425	G	F8/11
VA127	20325	G	F8/11
VA128	20225	G	F8/11
VA129	20125	P	F8
VA130	20035	G	F5
VA131	20005	P	F5
VA132	19885	G	F5
VA133	19845	G	F5

Sample	Deph (cm)	Dunham	Microfacie s
VA134	19830	G	F5
VA135	19745	G	F5
VA136	19725	G	F5
VA137	19505	P	F8/7
VA138	19405	G/P	F5
VA139	19325	G/P	F3/5
VA140	19215	P	F3/5
VA141	19015	P	F7/8
VA142	18815	P	F8
VA143	18715	P	F7
VA144	18615	G	F7
VA145	18515	G	F3/5
VA146	18355	G	F3/5
VA147	18195	P	F3
VA148	18165	G	F3
VA149	18105	P	F3
VA150	18065	G	F3
VA151	17965	P	F3
VA152	17845	P	F3
VA154	17695	P	F3
VA156	17605	W	F3
VA157	17515	W	F3
VA158	17495	W	F2/3
VA159	17375	W	F2/3
VA160	17345	W	F3
VA161	17245	P	F3
VA163	17155	P	F2/3
VA164	17045	P	F3
VA165	17015	W	F3
VA166	16925	G	F2
VA167	16825	G	FT
VA168	16795	G/P	F7
VA169	16695	G	F6
VA170	16645	G	F6
VA171	16625	G	F6
VA172	16445	G	F6
VA173	16285	G	F6
VA174	16195	G	F6
VA175	16015	G	F5
VA176	15895	G	F5/6
VA177	15735	G	F5/6/4/7
VA178	15615	G	F6
VA179	15465	P	F5/6
VA180	15285	P	F5
VA181	15110	G	F2/5
VA182	14860	G	F5
VA183	14660	G	F5/6
VA184	14540	G	F5/6
VA185	14350	G	F3/5/6
VA186	14150	P/G	F3
VA187	13970	G	F3
VA188	13670	G	F2/6
VA189	13550	W/G	F2/3/6
VA190	13275	G	F5/6
VA191	13105	W/G	F2/5
VA192	13095	G	F2/5
VA193	12935	G	F5
VA194	12835	G	F5/6
VA195	12685	G	F5/6
VA196	12495	G	F5/6
VA197	12295	G	F3
VA198	12010	G	F4

Valsloch

Sample	Depth (cm)	Dunham	Microfacies
VA199	11820	G	F2/3
VA200	11725	P	F3
VA201	11615	P	F2/3
VA203	11375	W/P	FT
VA204	11155	W/P	dolom.
VA206	10910	W/P	FT
VA207	10820	W/P	F4?
VA210	10505	P/G	F3/6
VA212	10200	G/P	F3
VA213	10170	W/P	F3
VA215	10100	P/G	F6
VA216	10065	G	F3/6
VA218	9940	G	F3/6
VA220	9785	W	F3/T
VA221	9640	W	FT
VA222	9580	W	FT/2/6
VA223	9520	W	FT?
VA224	9460	W	FT
VA225	9265	W	FT
VA226	9200	W	FT
VA227	9125	W	FT
VA228	9080	W	F2
VA230	8935	W	F2
VA232	8820	W	F1
VA233	8755	W	F1
VA235	8570	W	F3
VA236	8480	W	F1?
VA238	8315	W	F2
VA239	8297	W	F2
VA241	8202	P	F1
VA243	8012	W/P	F3
VA244	7927	W/P	F3
VA246	7707	W/P	F2/3
VA248	7467	W/P	F3
VA249	7367	W/G	F0/3
VA250	7217	W	F2
VA252	6962	W/P	F1/2
VA253	6862	W/P	F2/3
VA255	6647	W/P	F2/4
VA256	6542	W/P	F3
VA257	6347	W	F2
VA258	6192	W	F2
VA260	6002	W	F1/FT
VA262	5732	W	F2
VA264	5347	W	F1
VA265	5317	W	F2/1
VA266	5027	M/W	F3
VA267	4907	M	F3
VA268	4847	M	F3
VA269	4517	M	F0/2
VA270	4462	M	F0
VA271	4417	M	F0
VA274	4322	M	F1
VA276	4267	M	F1
VA277	4212	M	F2
VA279	4077	M	F2
VA280	4022	M	F1
VA281	3932	M	F2
VA282	3882	M	F2
VA285	3672	M	F1
VA286	3502	M	F1
VA287	3447	M	F1

Sample	Depth (cm)	Dunham	Microfacies
VA289	3352	M	F1
VA294	2902	M	F1
VA295	2832	M	F1
VA296	2762	M	F1
VA297	2687	M	F2
VA298	2642	M	F1
VA301	2502	M	F1
VA302	2412	M	F1
VA304	2322	M	F1
VA305	2202	M	F1
VA309	1900	M	F1
VA314	1575	M	F1
VA316	1500	M	F2
VA317	1450	M	F0
VA318	1415	M	F0
VA319	1360	M	F0
VA320	1315	M	F2
VA324	1140	M	F0
VA327	955	M	F1
VA330	740	M	F1
VA335	440	M	F1
VA336b	235	M	F0
VA338	150	sandstone	FT
VA340	25	sandstone	FT

Rawil

Sample	Deph (cm)	Dunham	Microfacie s
RW1	11075	P	F4??
RW2	11050	G	F7/8
RW3	11040	G	F11
RW4	10980	G	F11?
RW5	10900	G	F11?
RW6	10860	G	F11?
RW7	10710	G	F9/10
RW8	10560	G	F9/10
RW9	10410	P/G	F9/10
RW10	10290	P/W	F10
RW11	10170	P/W	F9/10
RW12	10070	P/W	F9/10
RW13	9910	P/W	F9/10
RW14	9810	P/W	F9/10
RW15	9730	P/W	F9/10
RW16	9660	P	F8/FT?
RW17	9580	sandstone	F3
RW18	9550	W	F10
RW19	9480	P/W	F9
RW20	9390	P/W	F9
RW21	9350	P/W	F9
RW22	9230	P	F5/F8?
RW23	9150	P	F5/F8?
RW24	8990	G	F7-F5
RW25	8890	G	F7-F5
RW26	8860	G	F5
RW27	8780	G	F4-5?
RW28	8680	G	F4-5?
RW29	8570	G	F4-5?
RW30	8450	G	F5
RW31	8320	G/W	F5
RW32	8040	P	F4
RW33	7880	G thin	F3
RW34	7560	G thin	F3/4?
RW35	7070	W/P	F9?
RW36	6820	P/G	F8?/FT
RW37	6660	W/P	FT?
RW38	6520	P/G	FT
RW39	6390	P sandy	FT
RW40	6320	P	FT/F7?
RW41	6230	P	FT
RW42	6150	G	F11?
RW43	6080	W/P	FT
RW44	6040	W	FT
RW45	5975	P sandy	FT
RW46	5925	P/G	F9
RW47	5845	P/G	FT?
RW48	5725	G/P	FT?
RW49	5645	P sandy	FT/FT
RW50	5575	P/G	FT
RW51	5475	P	F8/FT
RW52	5420	G	F11
RW53	5280	G/P	FT
RW54	5190	P	FT
RW55	5040	P	FT
RW56	4930	W	FT/FT
RW57	4880	P	FT/FT
RW58	4760	W sandy	FT
RW59	4715	G	F11
RW60	4660	W sandy	FT
RW61	4610	W sandy	FT
RW62	4560	p	FT/FT

Sample	Deph (cm)	Dunham	Microfacie s
RW63	4440	W	FT
RW64	4380	G	F8
RW65	4290	G/P	F8?
RW66	4220	G	F10?
RW67	4160	M/W sandy	F10?
RW68	4090	M/W sandy	F10?
RW69	3970	G	F11/FT
RW70	3920	G/P	FT?
RW71	3830	G	F11/FT
RW72	3740	G	F11
RW73	3700	M sandy	FT?
RW74	3620	W	FT/FT
RW75	3530	W	F3/8
RW76	3510		F8
RW77	3450	P/G	FT
RW78	3370	G/P	FT
RW79	3290	W sandy	F11
RW80	3230	W	FT
RW81	3155	P/W	F9/10
RW82	3040	W	F9?
RW83	2990	P	F10
RW84	2880	P/G	F9/10
RW85	2830	W	F8
RW86	2770	P	F7/FT
RW87	2600	G	F9
RW88	2480	P	F9
RW89	2380	P	F9
RW90	2260	P	F4
RW91	2135	P	F4
RW92	2010	P	F4
RW93	1920	P	F4
RW94	1790	M/W	F1
RW95	1580	P?	F4
RW96	1450	P?	F4
RW97	1380	P	F4
RW98	1300	G	F5
RW99	1180	P/G	F3/7?
RW100	1080	P/G	F3/5??
RW101	940	B	F7
RW102	780	B	F7
RW103	650	G	F5
RW104	540	P	F4
RW105	430	G	F5/6
RW106	370	P	F7
RW107	270	G	F7
RW108	150	P	F3/4
RW109	130	G	F3/4

Interlaken

Sample	Depth (cm)	Dunham	Microfacies
IN 1	80	G	F10/Temp.
IN 3	250	P	F8?
IN 7	550	P	F8?
IN 9	670	G/W	F5?Temp.
IN 13	1090	G	F3/5
IN 16	1450	G	F3/6
IN 20	1850	G	F3/4/5
IN 24	2240	P/G	FPN
IN 29	2620	P/G	F3
IN 33	3020	G/P	F9
IN 36	3320	G/P	F9
IN 40	3720	G	F8?11?6?
IN 51	4820	G	F10
IN 56	5320	sandstone	FT?
IN 60	5620	W	F11? F9?
IN 62	5920	P	F10/FT
IN 63	6020	P/G	F10
IN 66	6250	W	F10

Harder

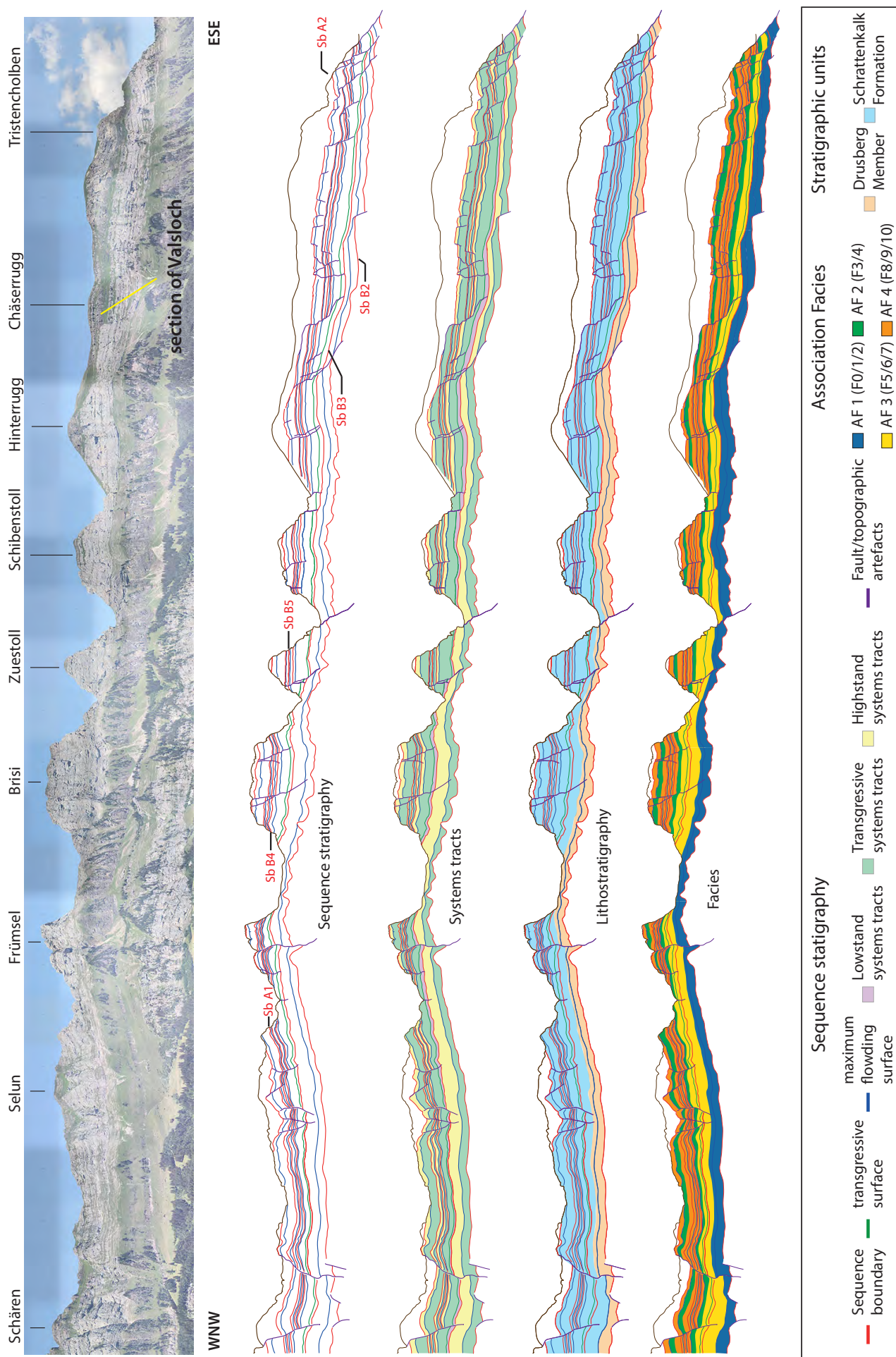
Sample	Depth (cm)	Dunham	Microfacies
HA414	31132.5	P	F10
HA407	30512.5	B/P	F7
HA401	29997.5	G	F7/5
HA397	29597.5	P	F8
HA392	29022.5	G	F7/5?
HA387	28592.5	G	F5
HA381	28037.5	G	F5/11?
HA378	27742.5	G	F3
HA372	27253.5	G	F6/T?
HA366	26783.5	P	F3?
HA362	26603.5	P	F3?
HA356	26061.5	P/G	F5
HA353	25756.5	G	F5/11?
HA349	25396.5	P?	FT??
HA346	25155.5	P	F4
HA343	24945.5	P	F4?
HA341	24745.5	P	F3
HA337	24413.5	G	FT
HA336	24331.5	P	FT?
HA335	24223.5	P	F3?
HA331	23904.5	W/P	F5
HA330	23819.5	W/P	F5
HA329	23811.5	W/P	F5
HA328	23751.5	P	F4
HA323	23284.5	G	F5
HA322	23209.5	G	F5
HA320	23004.5	G	F4
HA318	22769.5	G	F5
HA317	22609.5	G	F5/6
HA314	22259.5	G	F5
HA313	22097.5	G	F3
HA312	21957.5	G	F5
HA310	21722.5	G	F6
HA309	21567.5	G	F5
HA307	21422.5	G	F5
HA306	21342.5	G	F5
HA304	21172.5	G	F5/6
HA302	20962.5	G	F6
HA301	20762.5	G	F6
HA298	20467.5	P	F4?
HA294	20039.5	G	F5
HA292	19924.5	G?	F4/5
HA290	19591.5	G	F5/4
HA289	19481.5	G	F4/5
HA288	19146.5	G	F5/6
HA287	18873.5	G	F5
HA286	18765.5	P/G	F5/4
HA285	18625.5	P/G	F5/4
HA284	18550.5	G?	F4
HA283	18480.5	G	F4/5/6
HA281	18210.5	G/P	F5
HA280	18090.5	G/P	F5/6
HA278	17783.5	P	F5/6
HA276	17491.5	P	F4?
HA275	17416.5	P	F3
HA271	16604	W/P	F3
HA267	16323	W/P	F3
HA263	15953	P/G	F3/5?
HA260	15727	P/G	F5?
HA253	15181	?	F3???
HA252	15053	G	F4
HA251	14952	?	

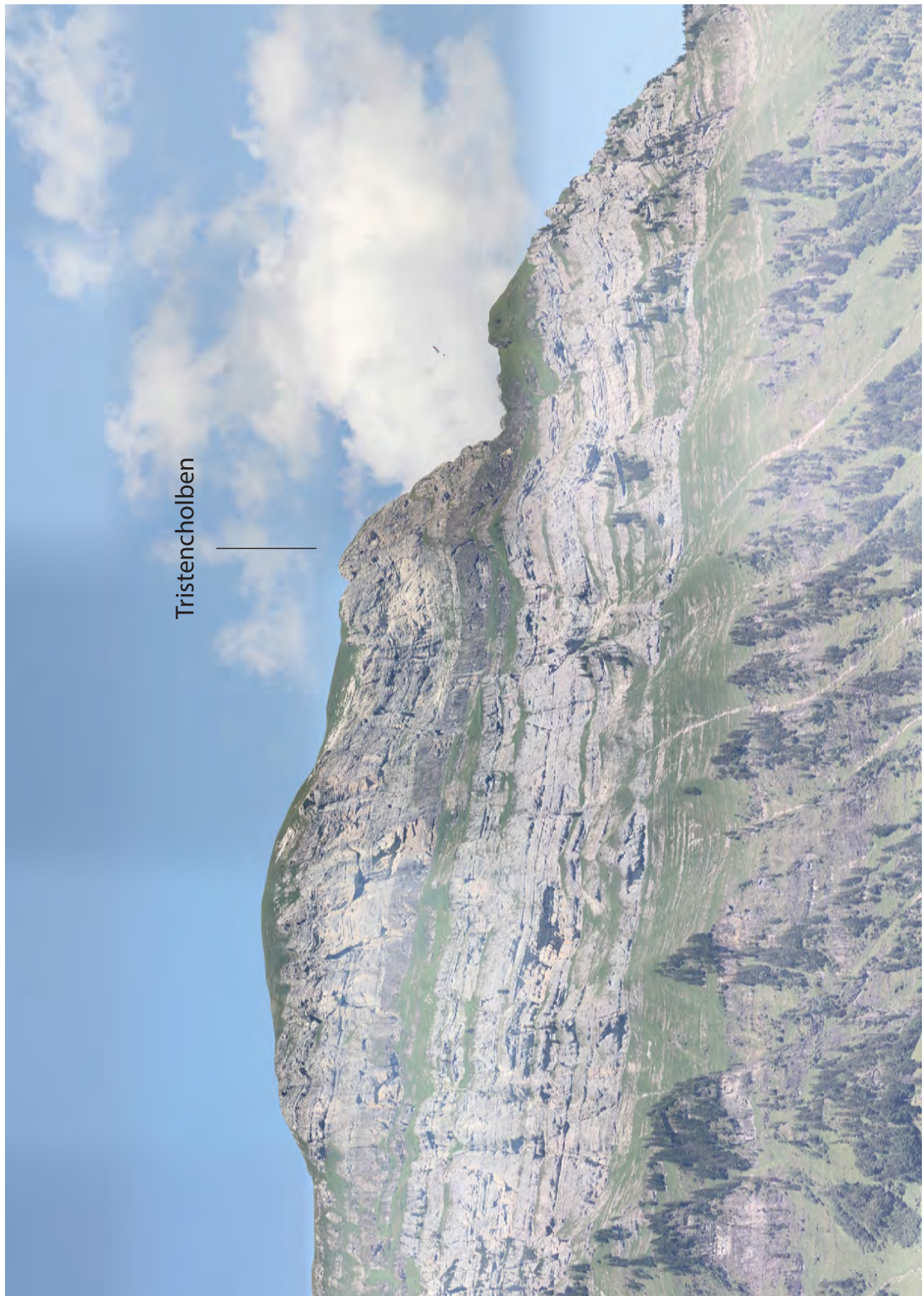
Harder

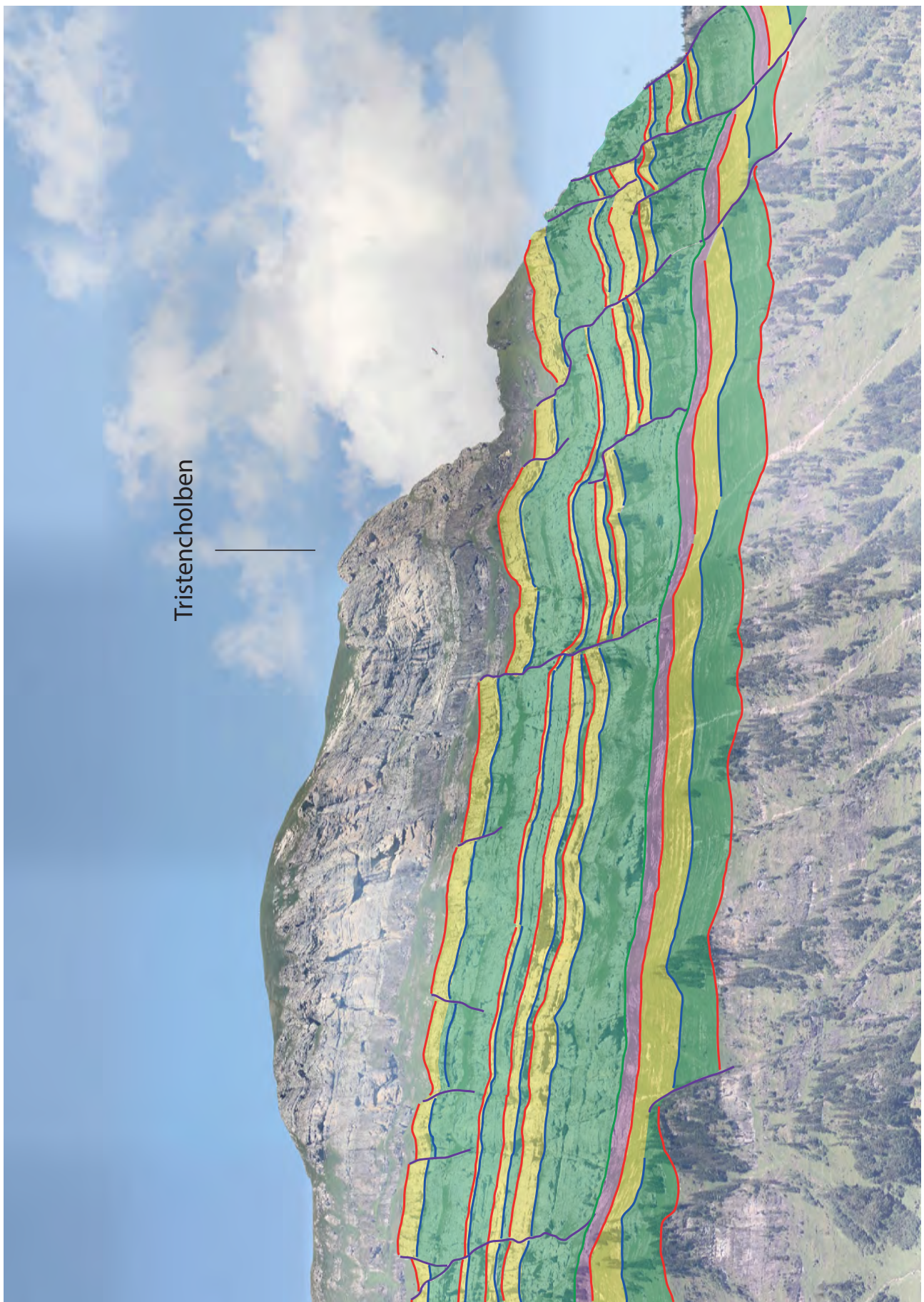
Sample	Depth (cm)	Dunham	Microfacies
HA250	14852	G/P	F4
HA249	14802	G	F4/5
HA245	14137	G	F3/4
HA243	13876	G	F6
HA240	13496	G	F6?
HA239	13296	G	F5/6
HA237	12811	G	F5/6
HA231	12280	P/G	F4?
HA225	11834	P/G	F3/4
HA223	11696	P/G	F3/4
HA219	11472	P/G	F3/4
HA216	11244	P/G	F3/4
HA214	11173	G	F3/4
HA212	10944	G	F3/4
HA211	10931	G	F3/4
HA210	10895	G	F3/4
HA209	10767	G	F3/4
HA208	10724	G	F3/4
HA206	10618	G	F3/4
HA205	10528	G	F3/4
HA204	10438	G	F3/4
HA203	10388	G	F3/4
HA202	10378	W/P	F3/4
HA201	10268	W/P	F4/5
HA200	10258	W/P	F3/4
HA196	9988	W/P	F3/4
HA195	9933	W/P	F3/4
HA194	9833	W/P	F3
HA193	9783	W/P	F7??
HA191	9659	W/P	F4
HA190	9643	W/P	F4
HA189	9563	W/P	F4
HA188	9498	W/P	F4?
HA187	9458	W/P	F4?
HA182	9045	G	F5
HA181	9015	G	F5
HA180	8885	G	F5
HA179	8750	G	F5
HA174	8505	W	F2
HA169	8254	W	F3
HA168	8194	W	F2
HA167	8034	W/P	F1
HA166	7959	W	F1
HA159	7714	M?	F0?
HA148	7195	W	F1
HA147	7035	W	F1
HA133	6459	W	F3
HA132	6339	W	F1/F3?
HA121	5874	W	F3
HA115	5602	P	FT?
HA114	5502	P	FT
HA113	5397	P	FT
HA104	4867	W	F2
HA94	4138	W	F2
HA82	3648	W	F3
HA75	3259	W	FT/2/?
HA65	2796	W	F0 ??
HA63	2748	M	F0?
HA59	2567	W	F2
HA55	2410	G	F4/5
HA54	2370	P/G	F3/F4?
HA53	2300	P	F4?

Sample	Depth (cm)	Dunham	Microfacies
HA52	2258	G	F5?3
HA51	2178	G	F5?3
HA50	2110	G	F5?3
HA49	2043	G	F5
HA48	2024	P	F2/3
HA47	1948	W	?
HA46	1888	G	F3
HA45	1818	G	F3/4
HA44	1769	P/G	F3
HA42	1580	P	FT?
HA39	1443	P	F4
HA36	1338	W	F1/2
HA34	1293	W	F1
HA30	1130	P	F2/3
HA26	971	M	F1
HA22	713	W/P	F2/3
HA20	601	W	F2
HA19	551	W	F1
HA18	506	W/P	F3
HA17	473	W	F2
HA15	390	W	F1
HA13	315	W	F1
HA10	254	W	F1
HA8	168	W	F1
HA6	123	M	F0
HA5	98	M	F0
HA4	58	W	F0
HA1	0	P	F0

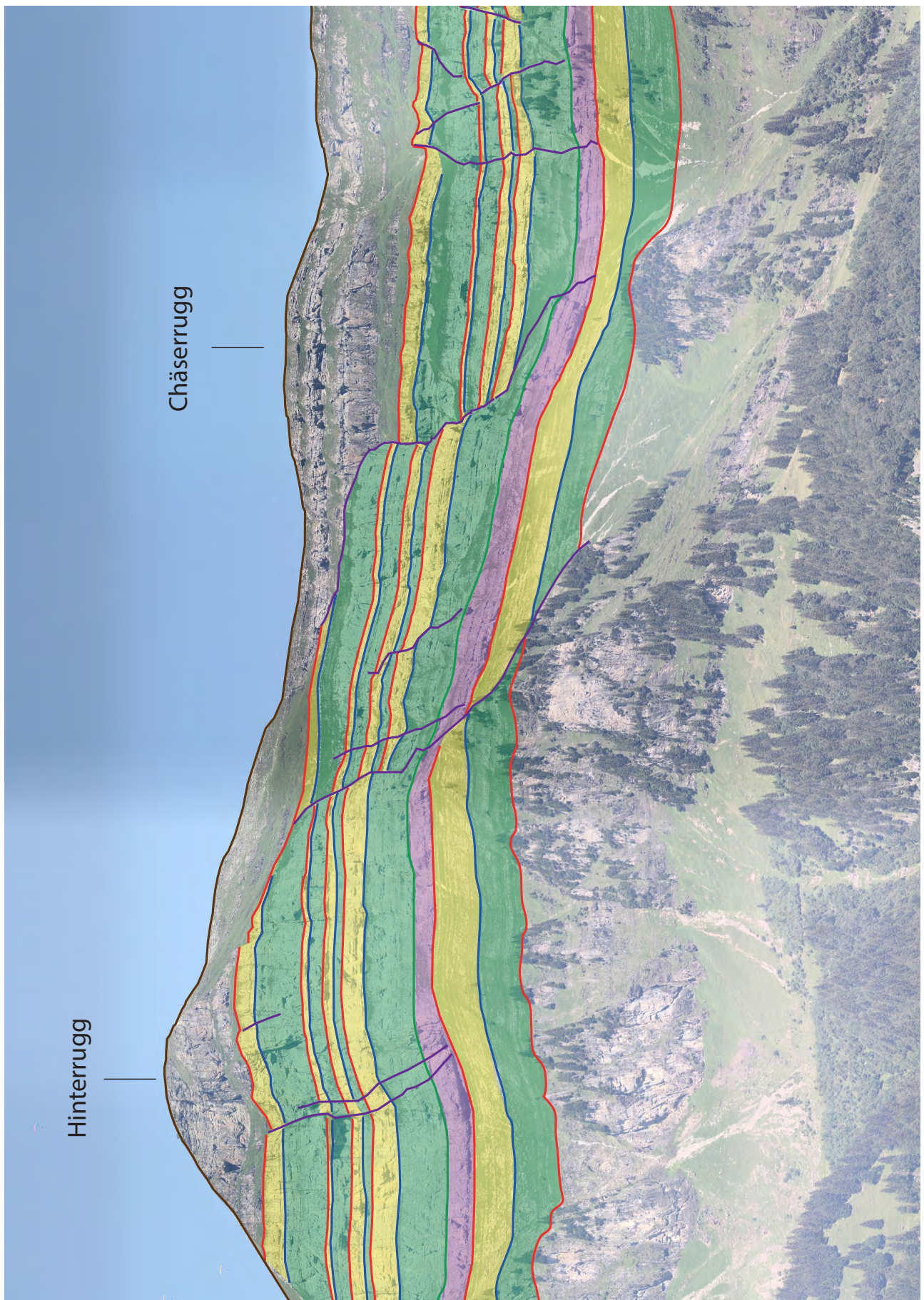
6.7 Panorama



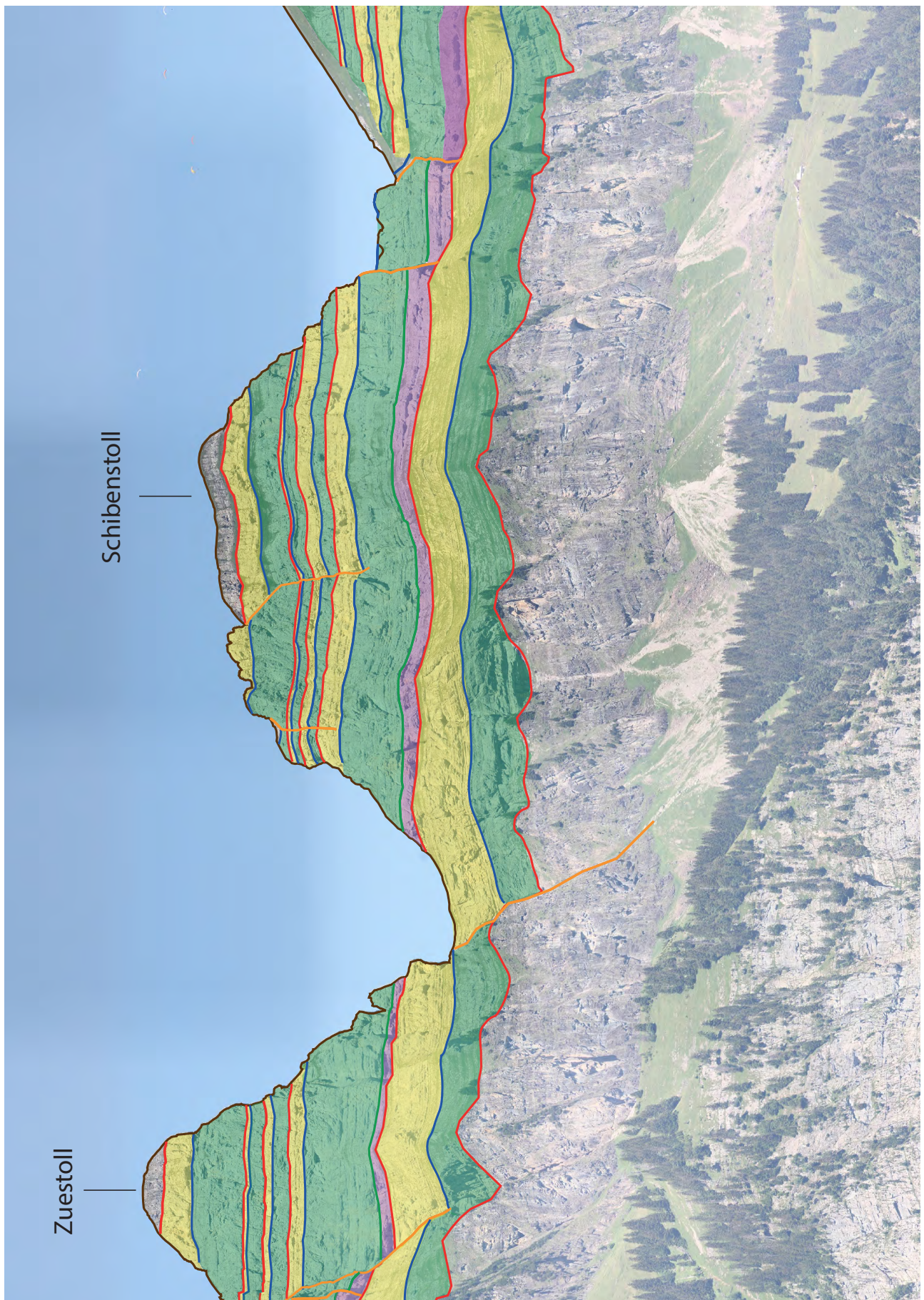


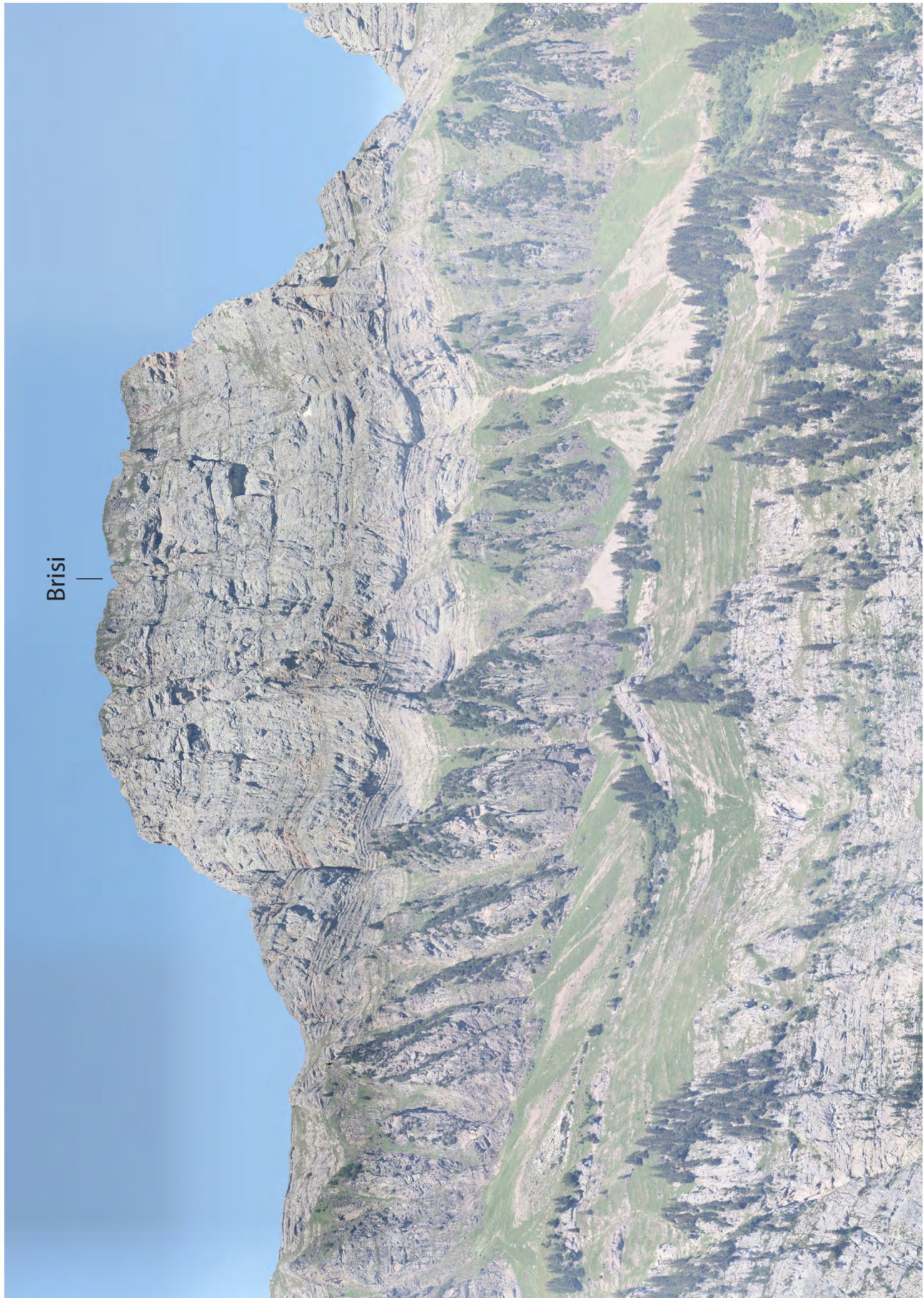


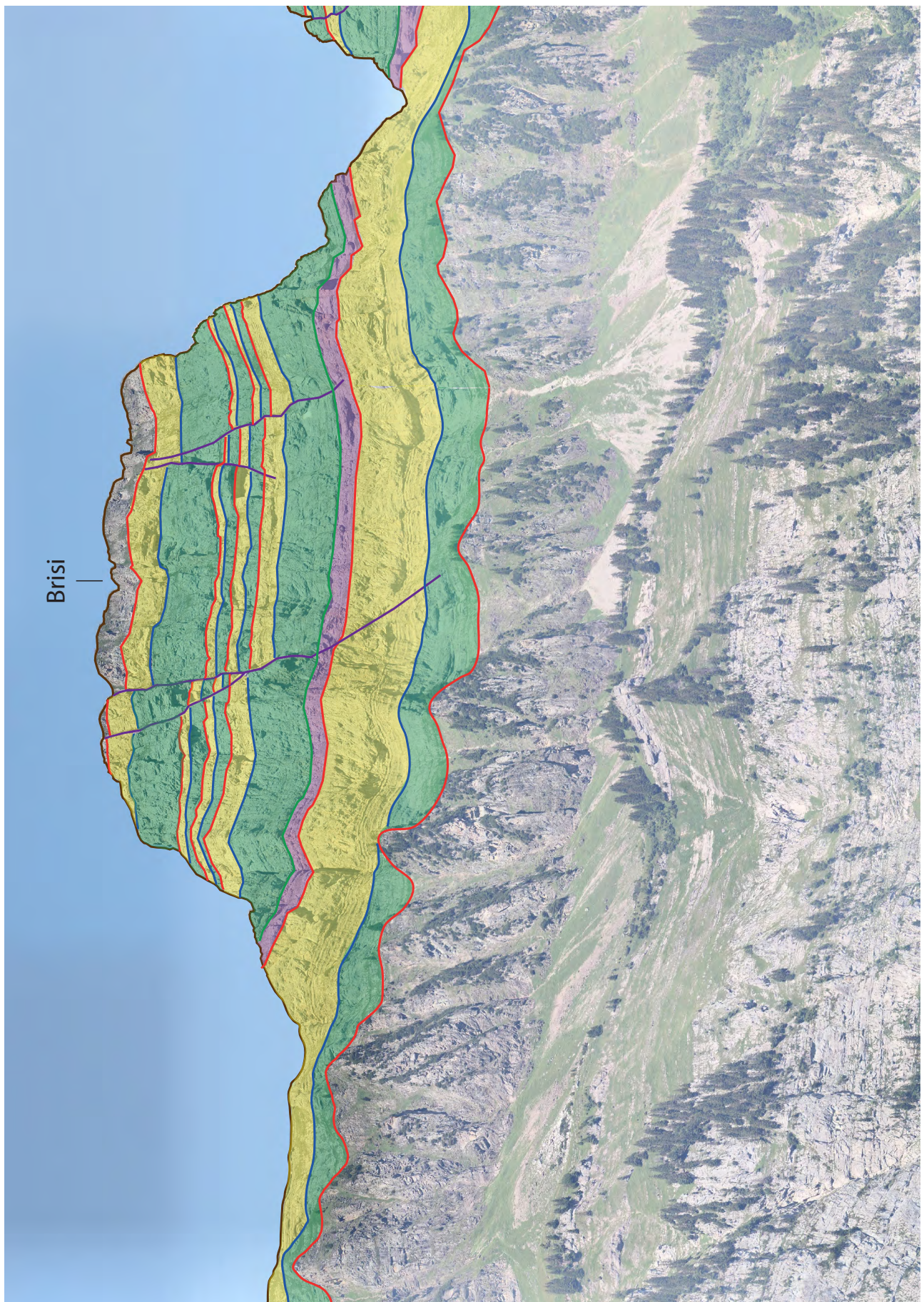


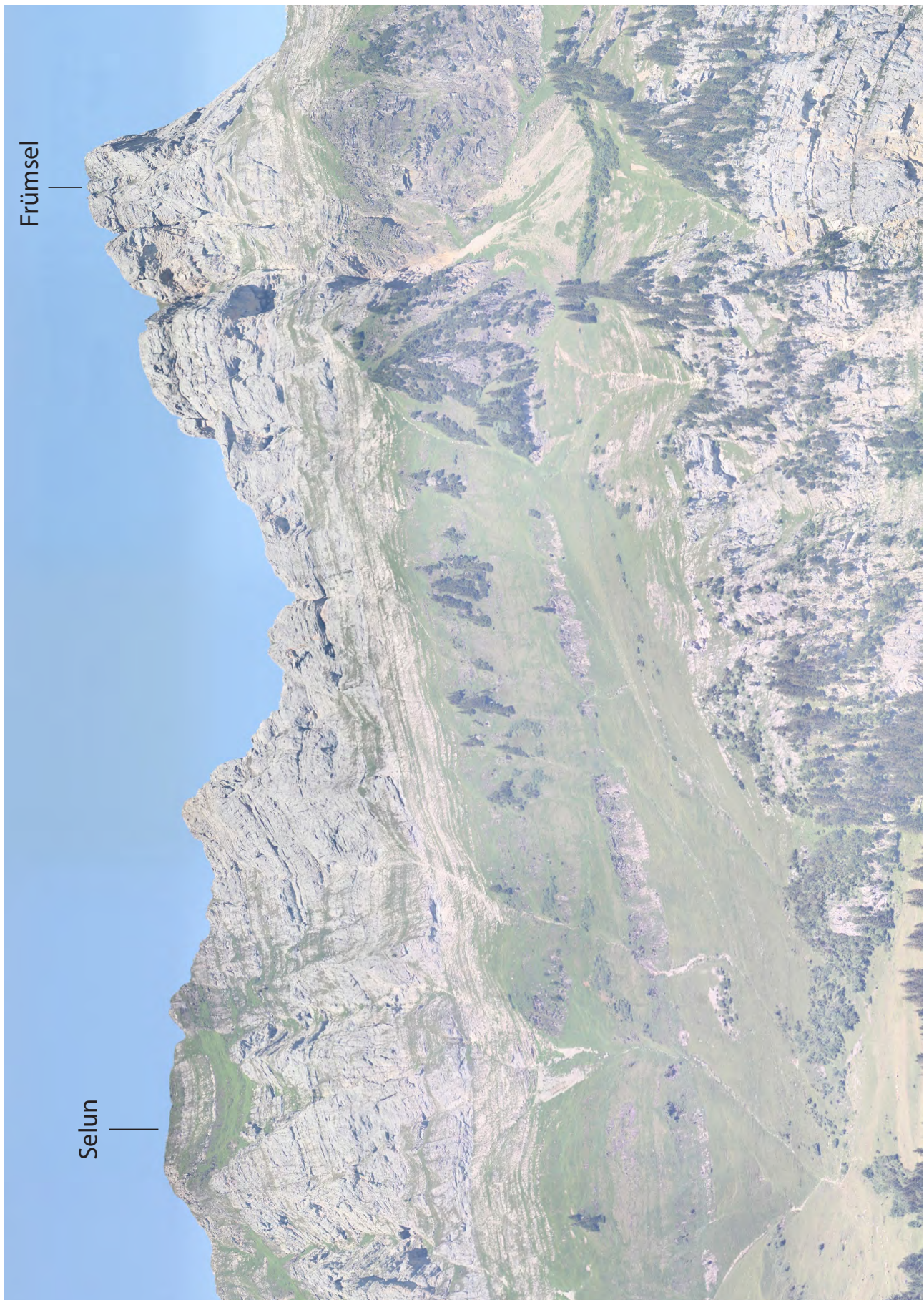


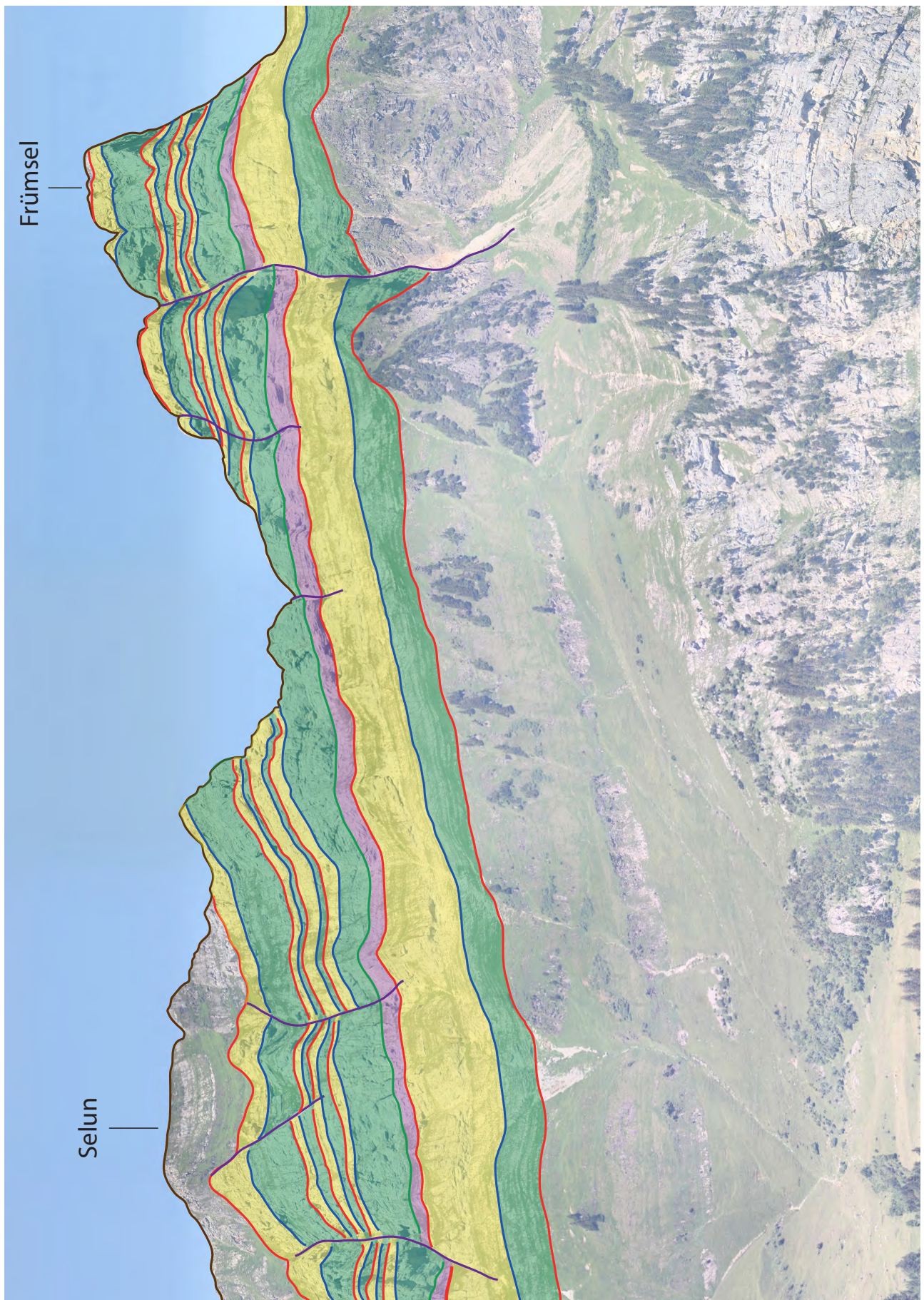




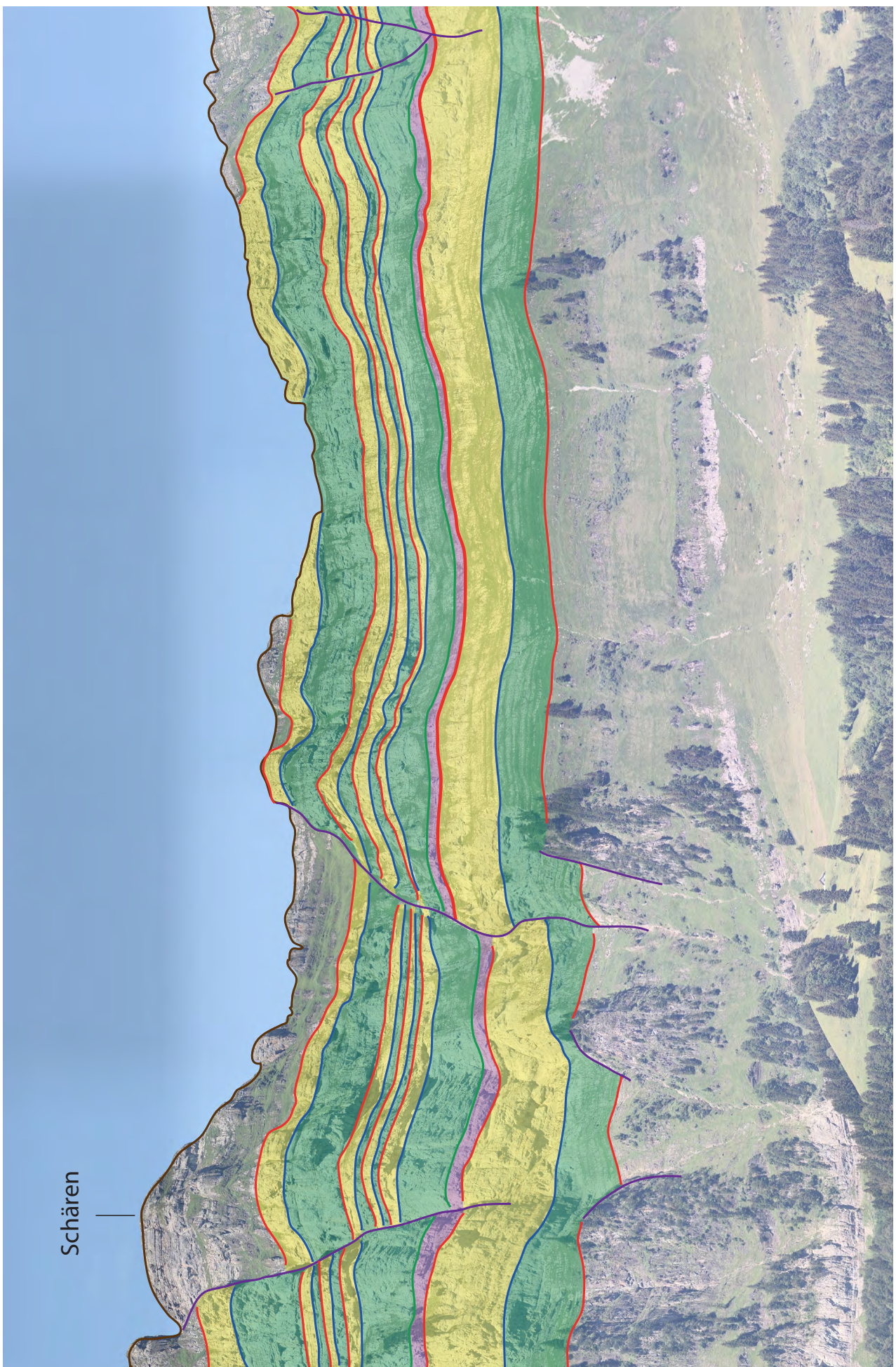


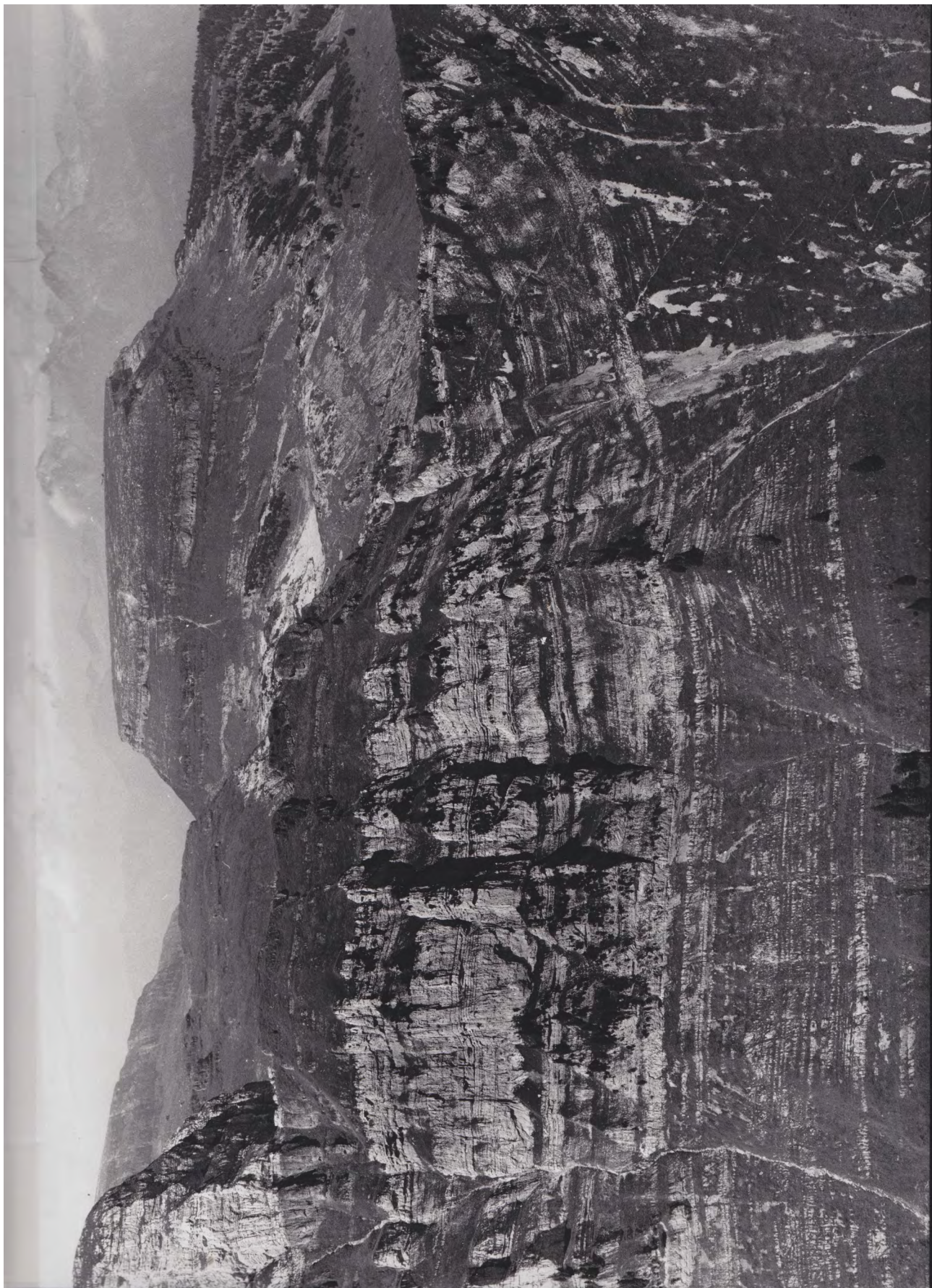




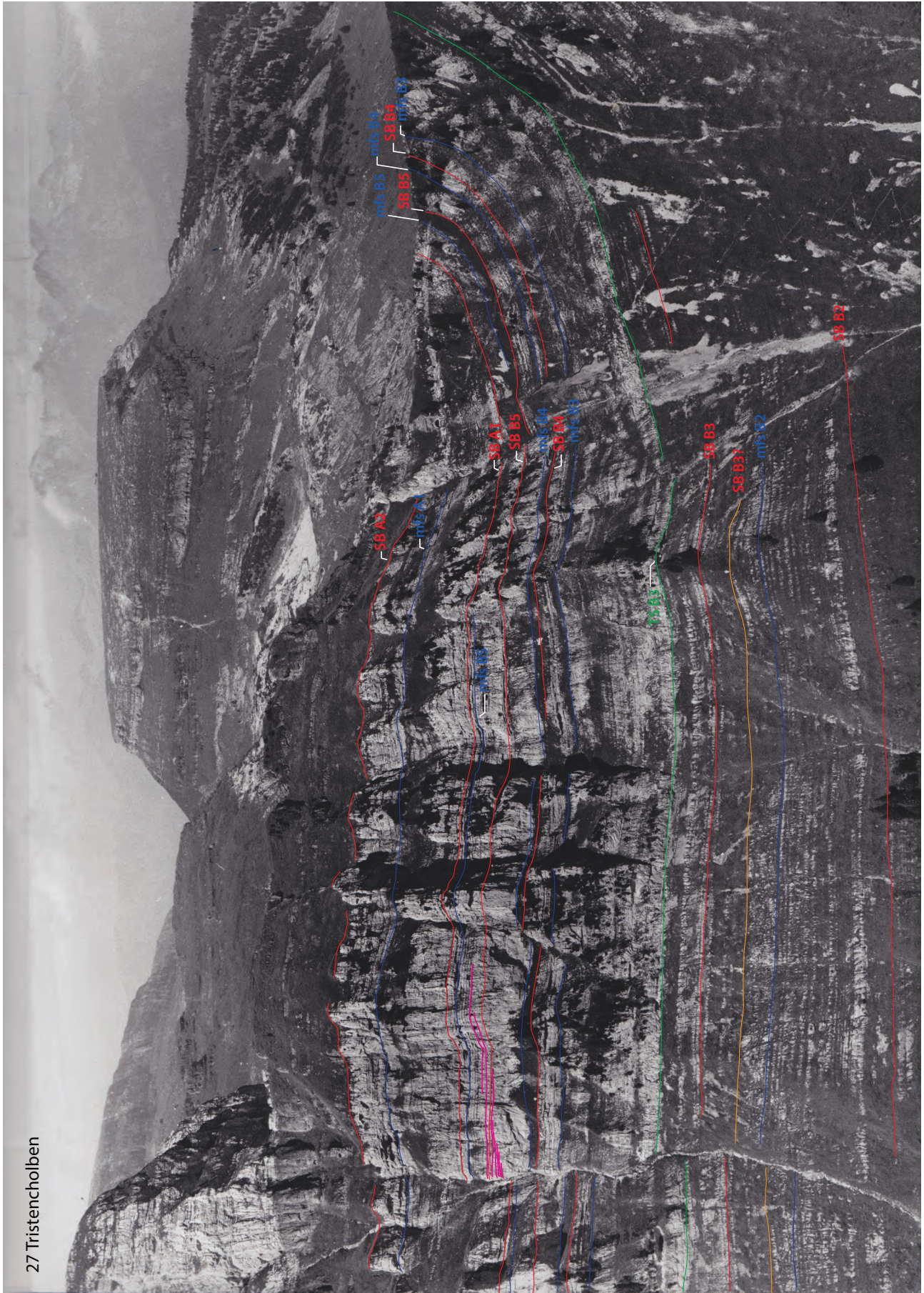


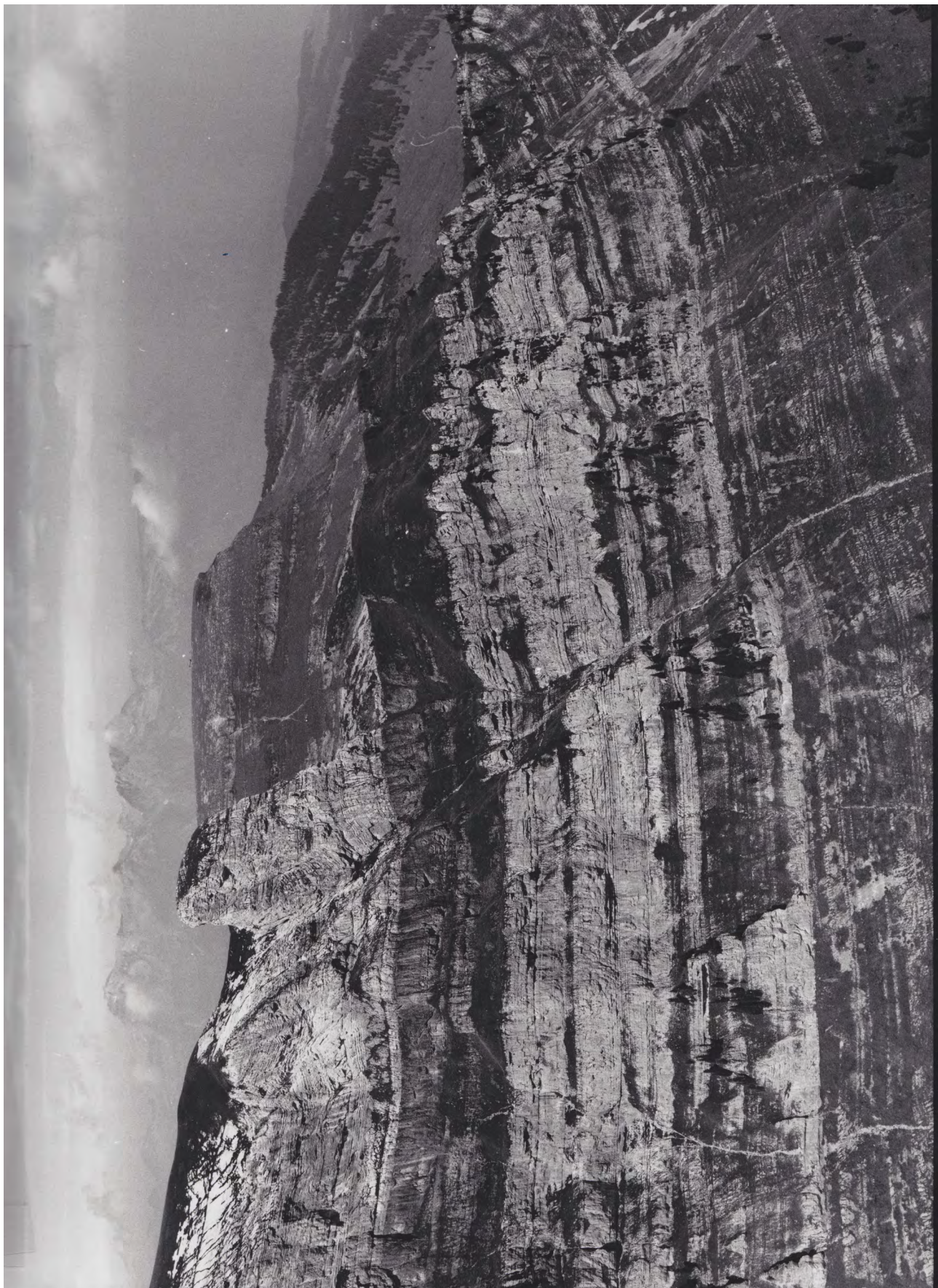




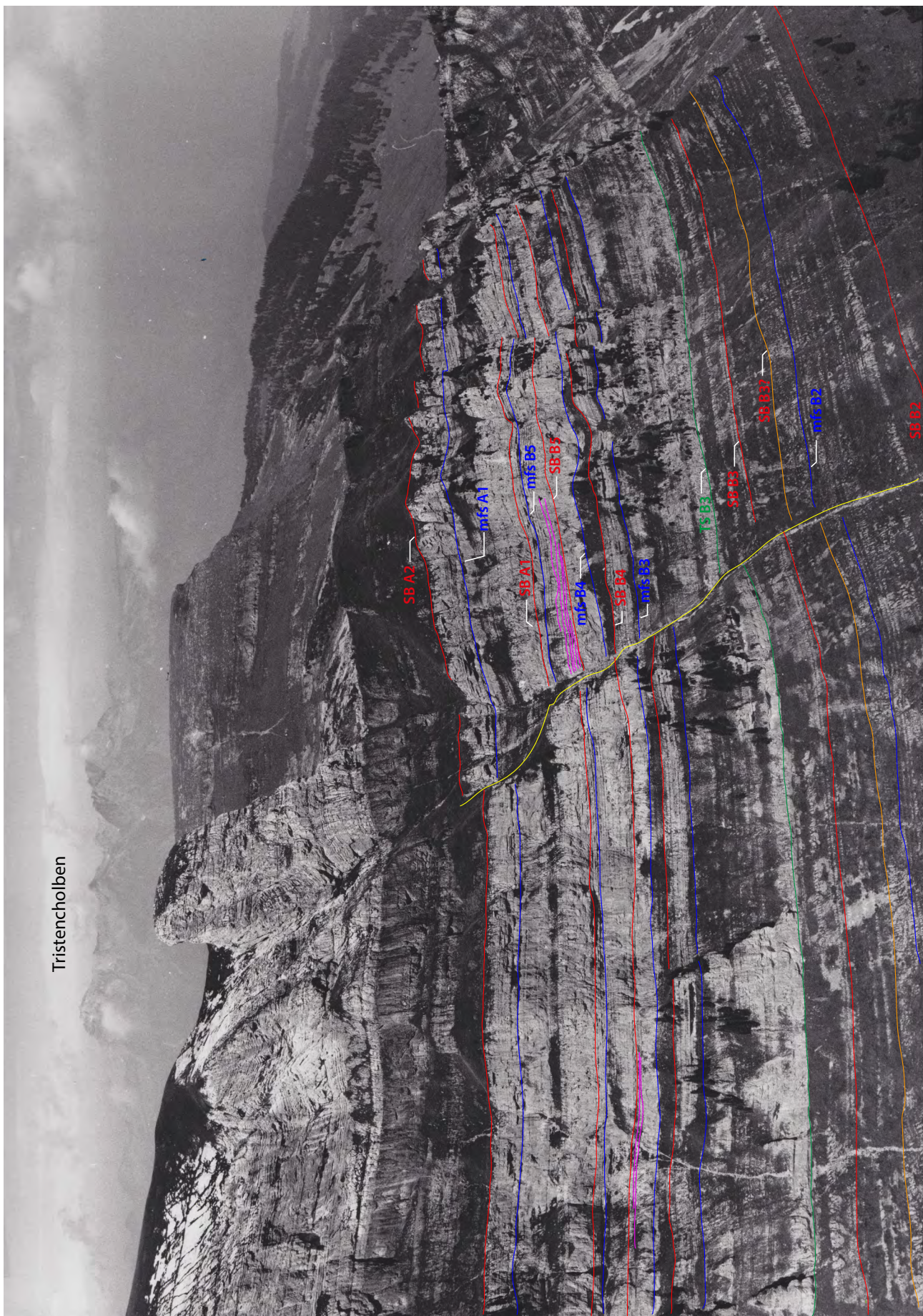


27 Tristencholben





Tristencholben

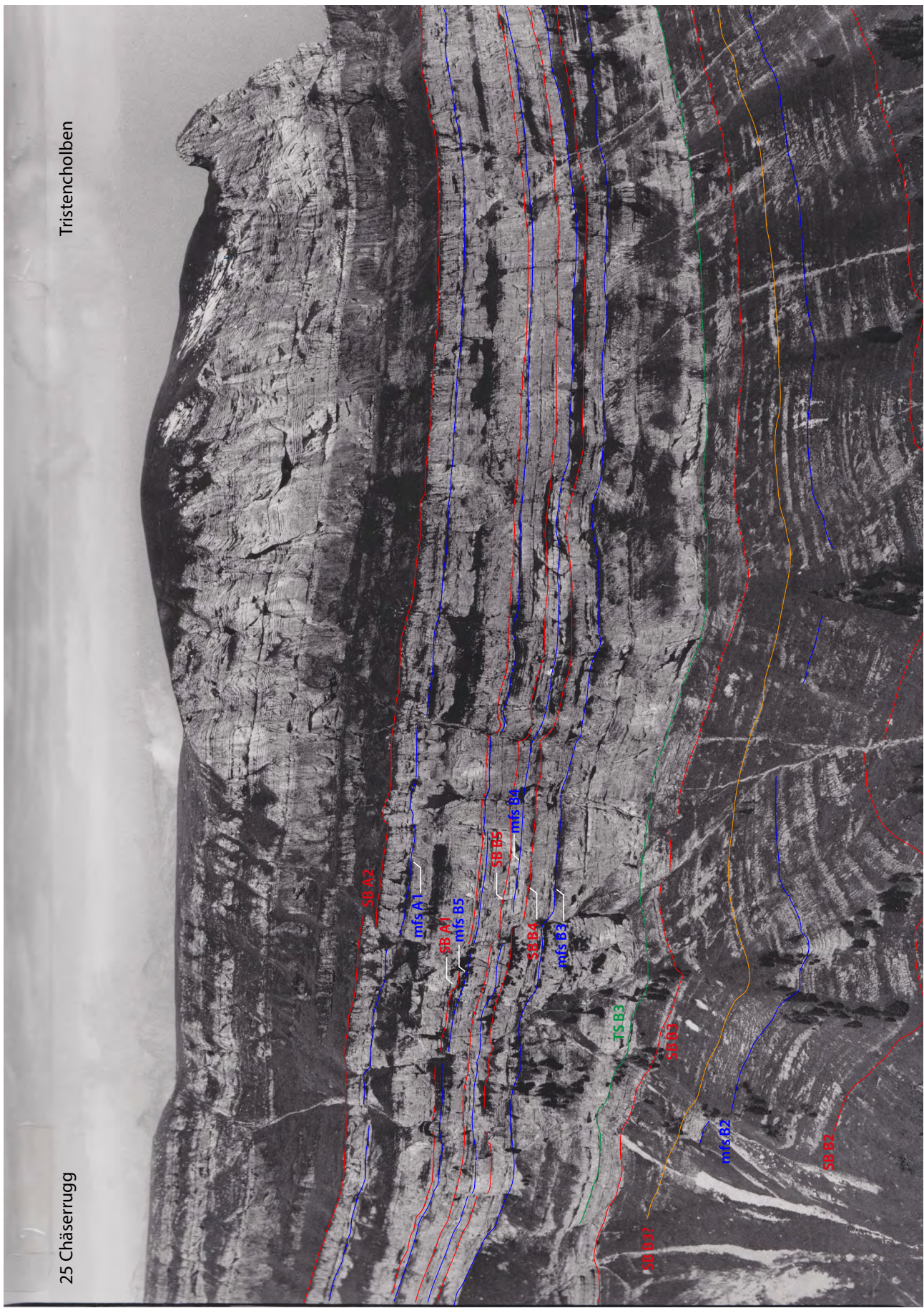




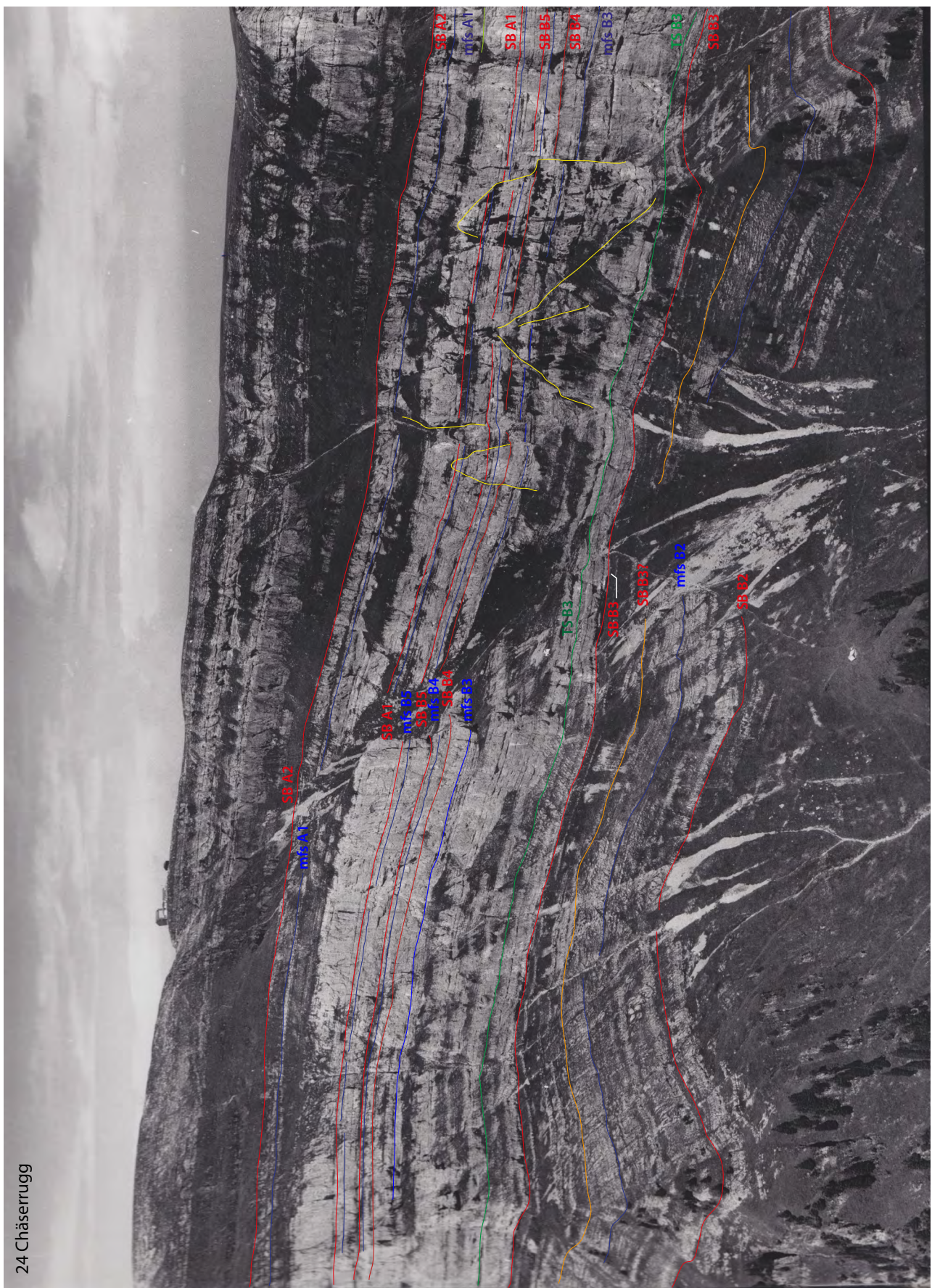
25

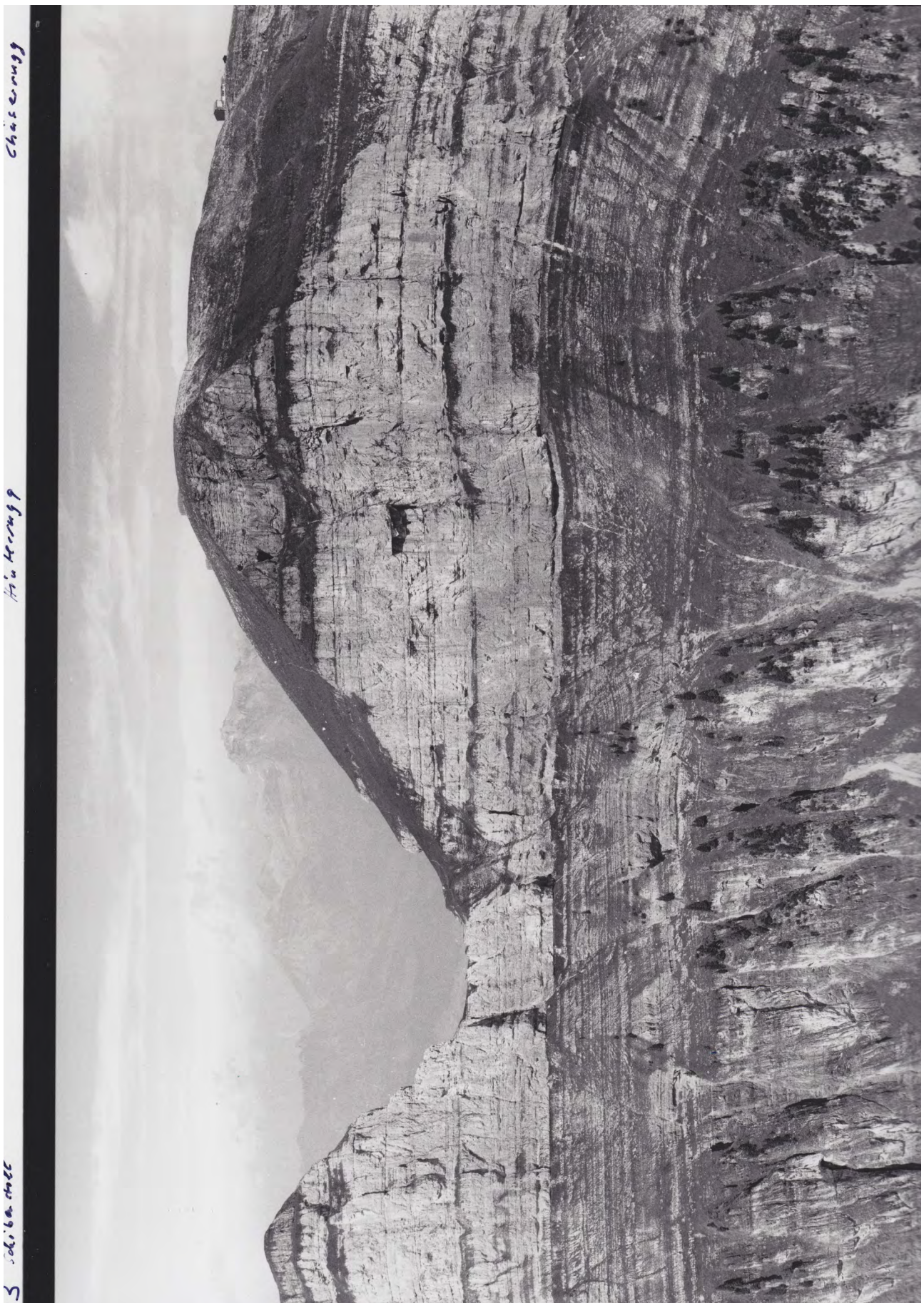
25 Chässerrugg

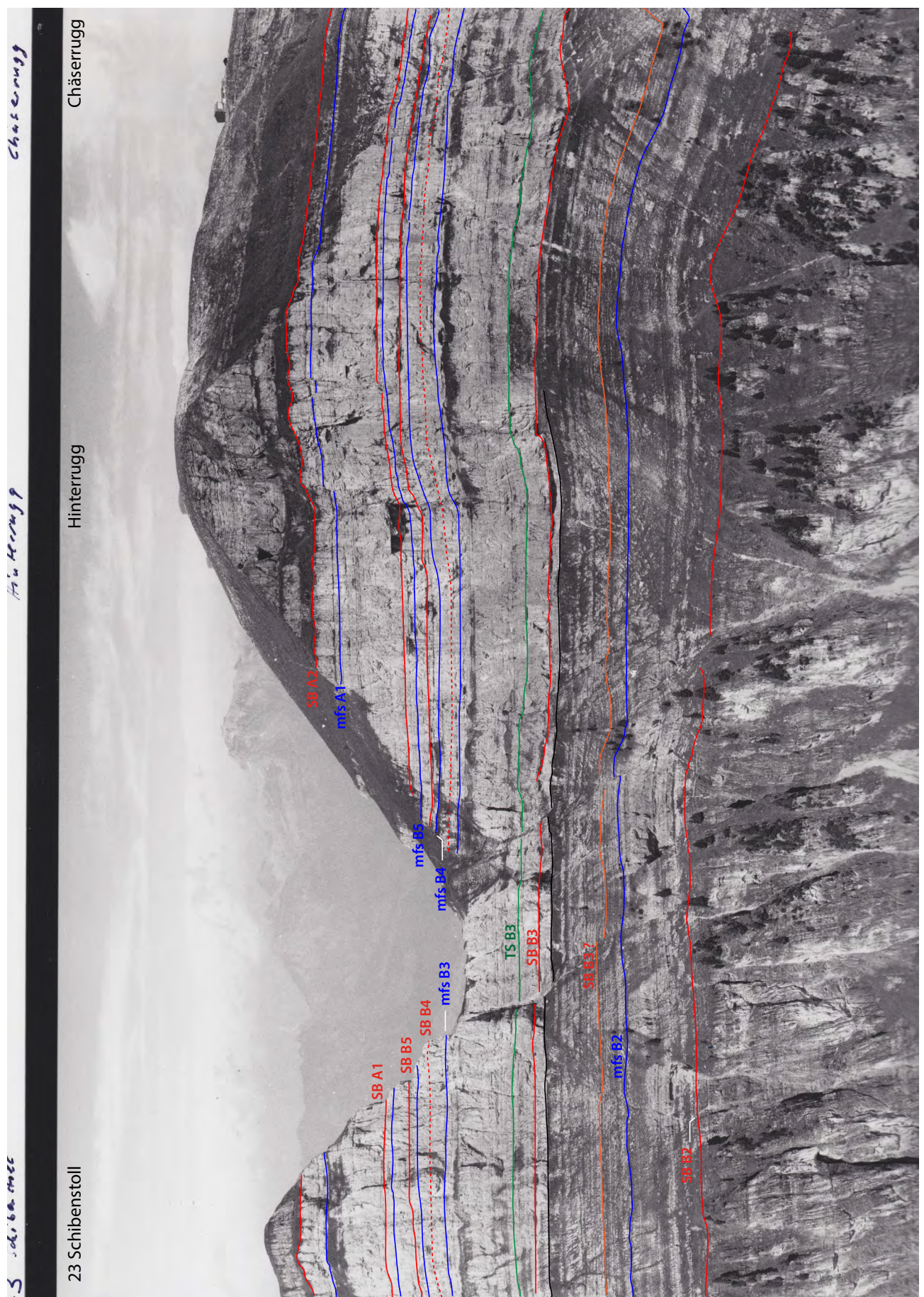
Tristencholben







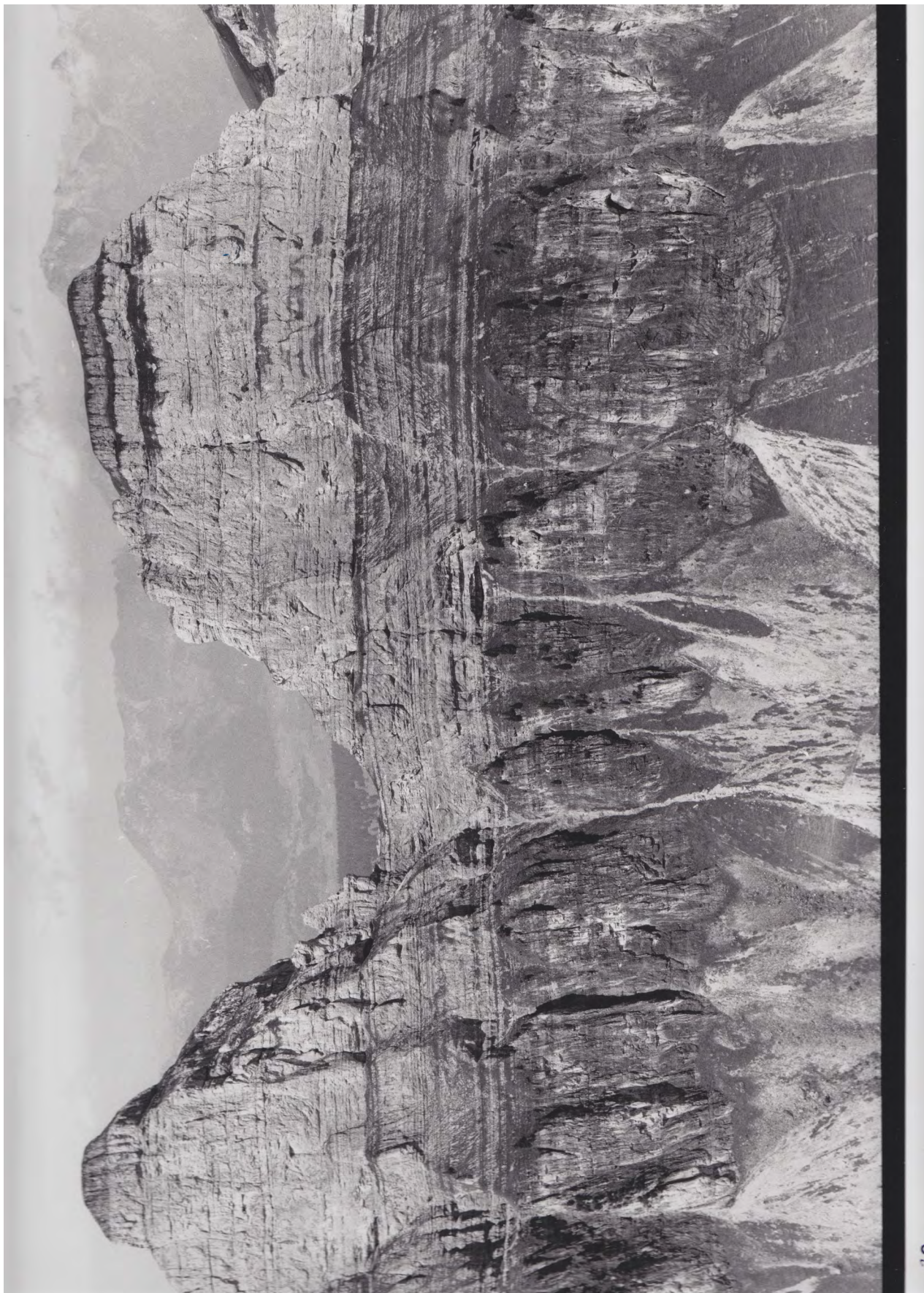


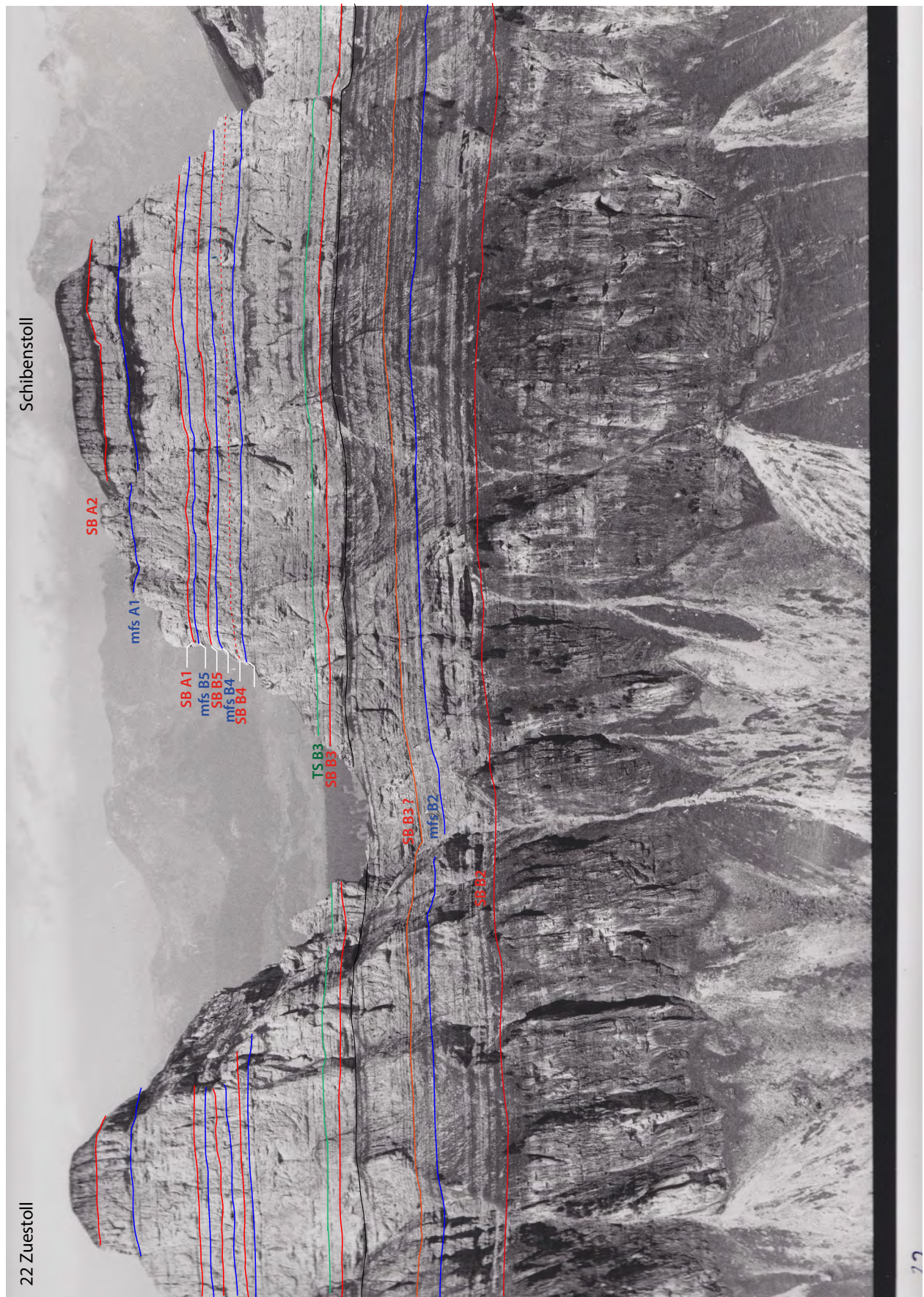


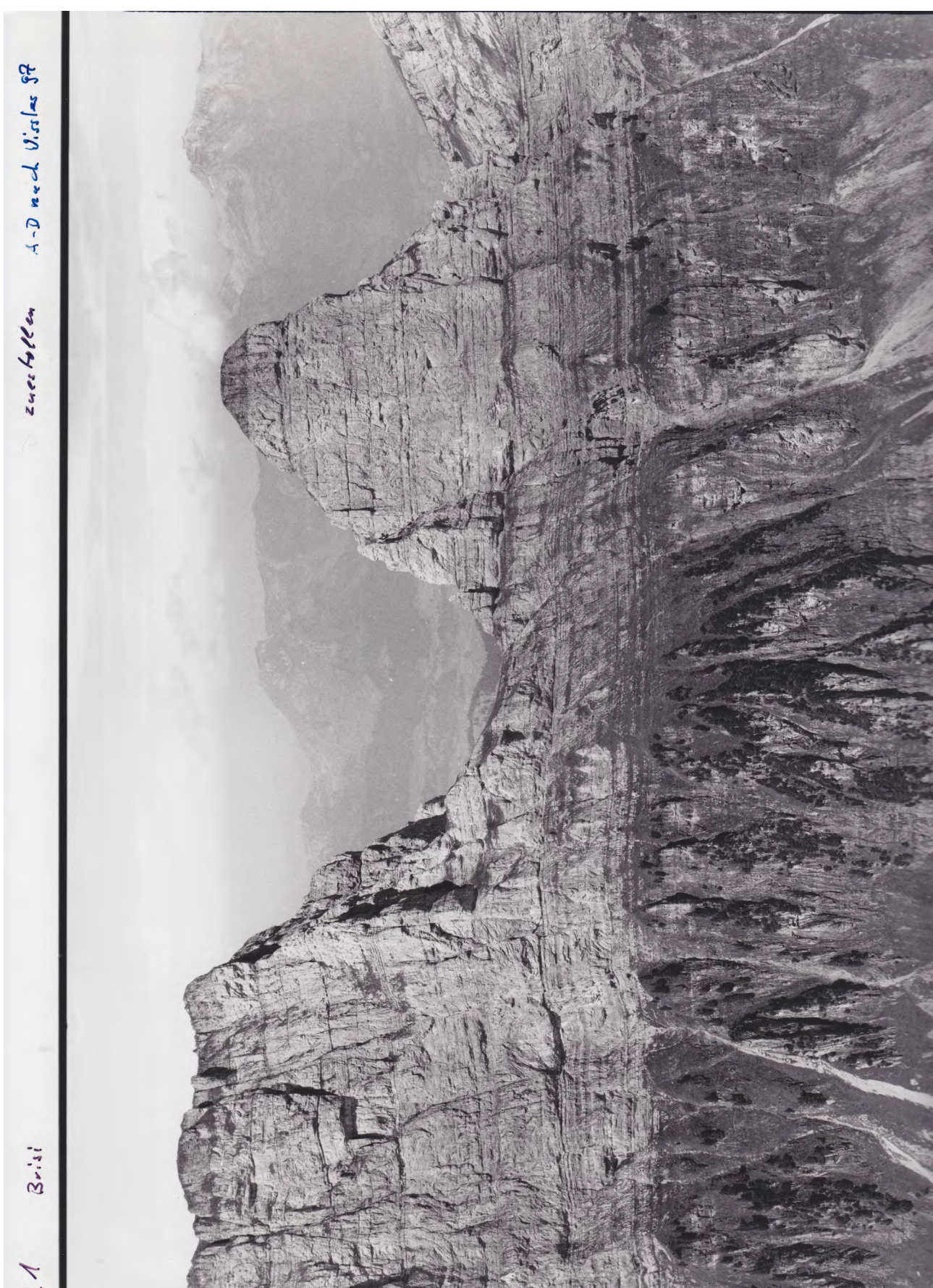
23 Schibenstoll

Hinterrugg

Chäserrugg





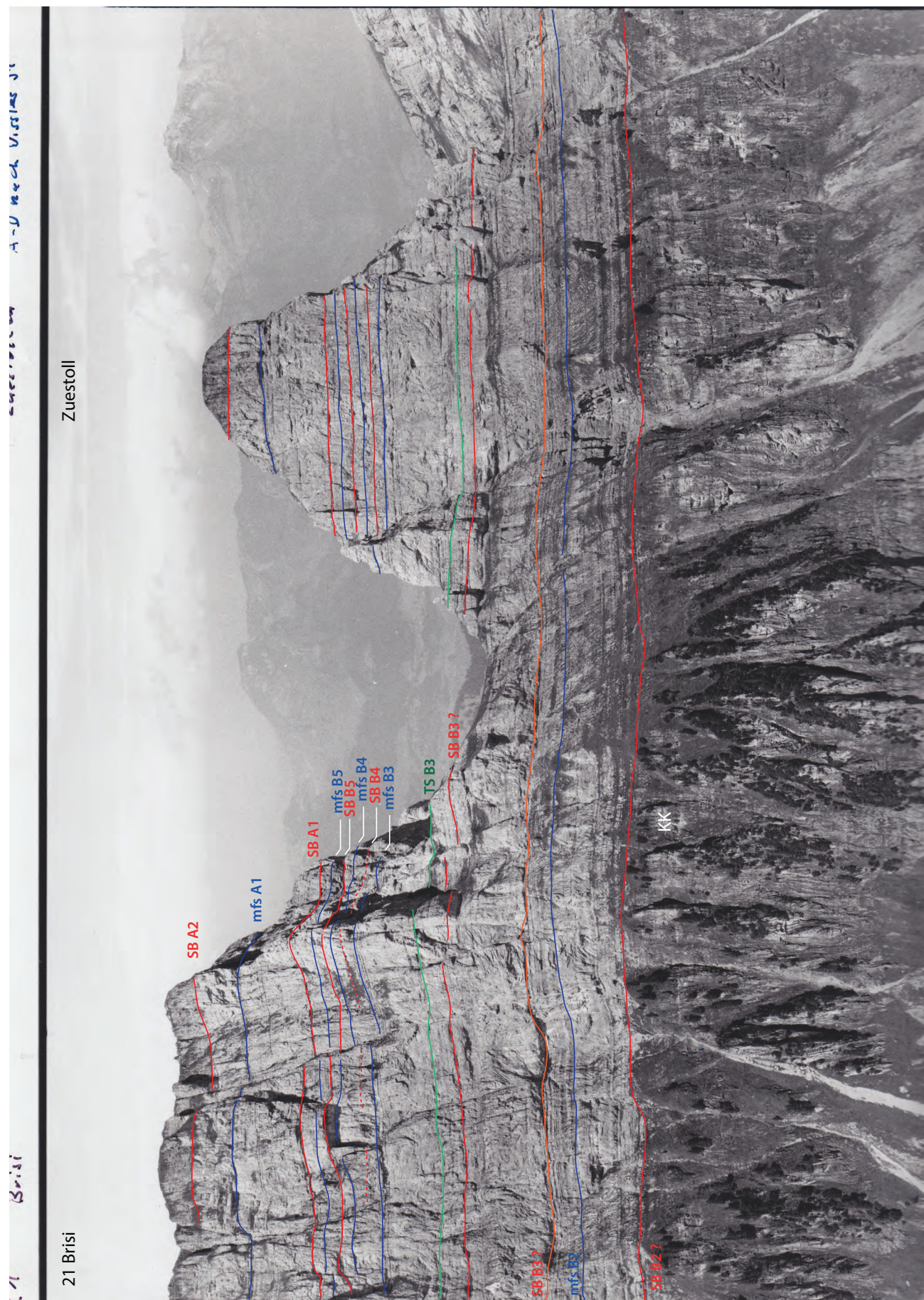


zurhellen A-D nach Uissas §7

D

Briit

1



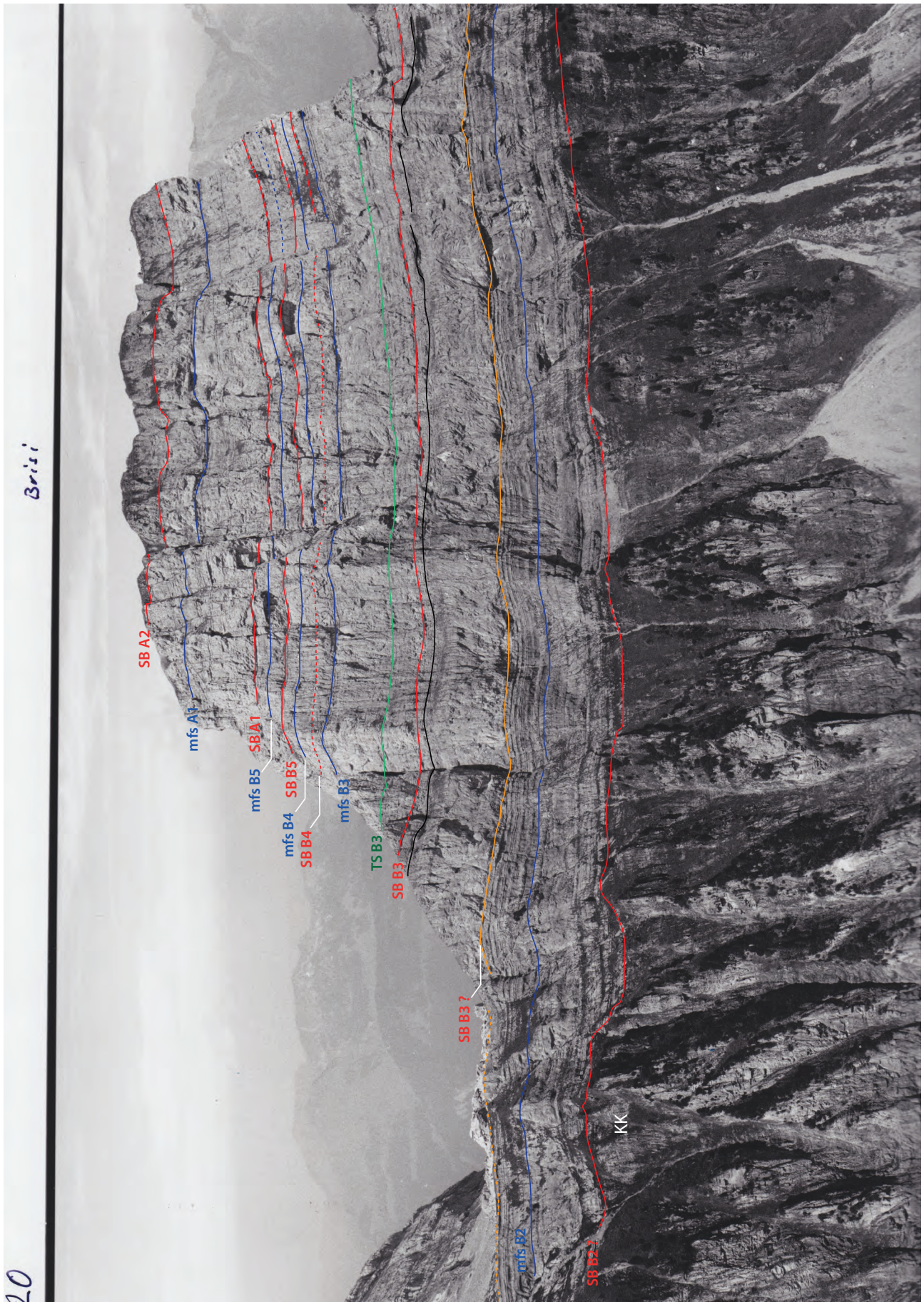
Brisi

20

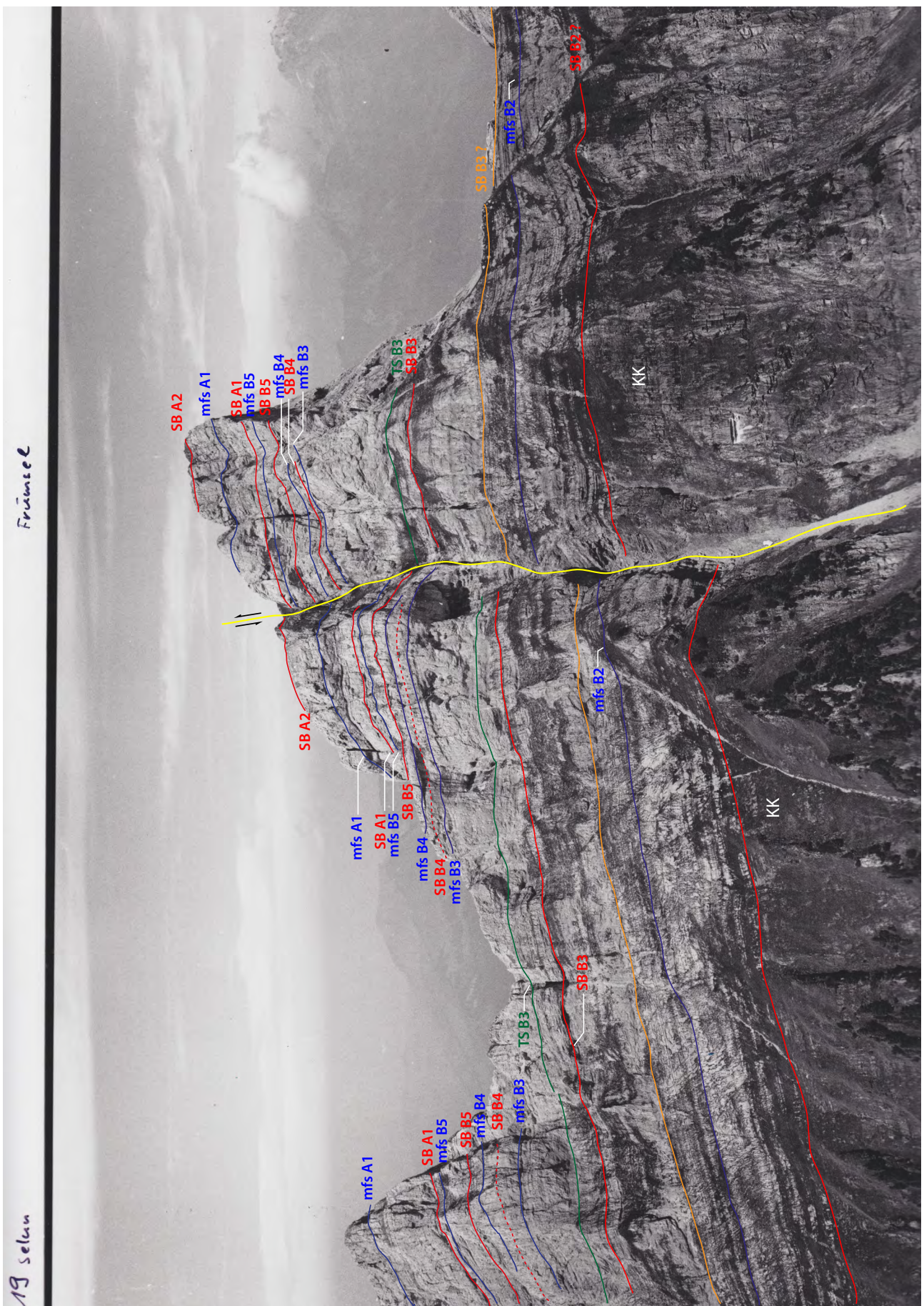


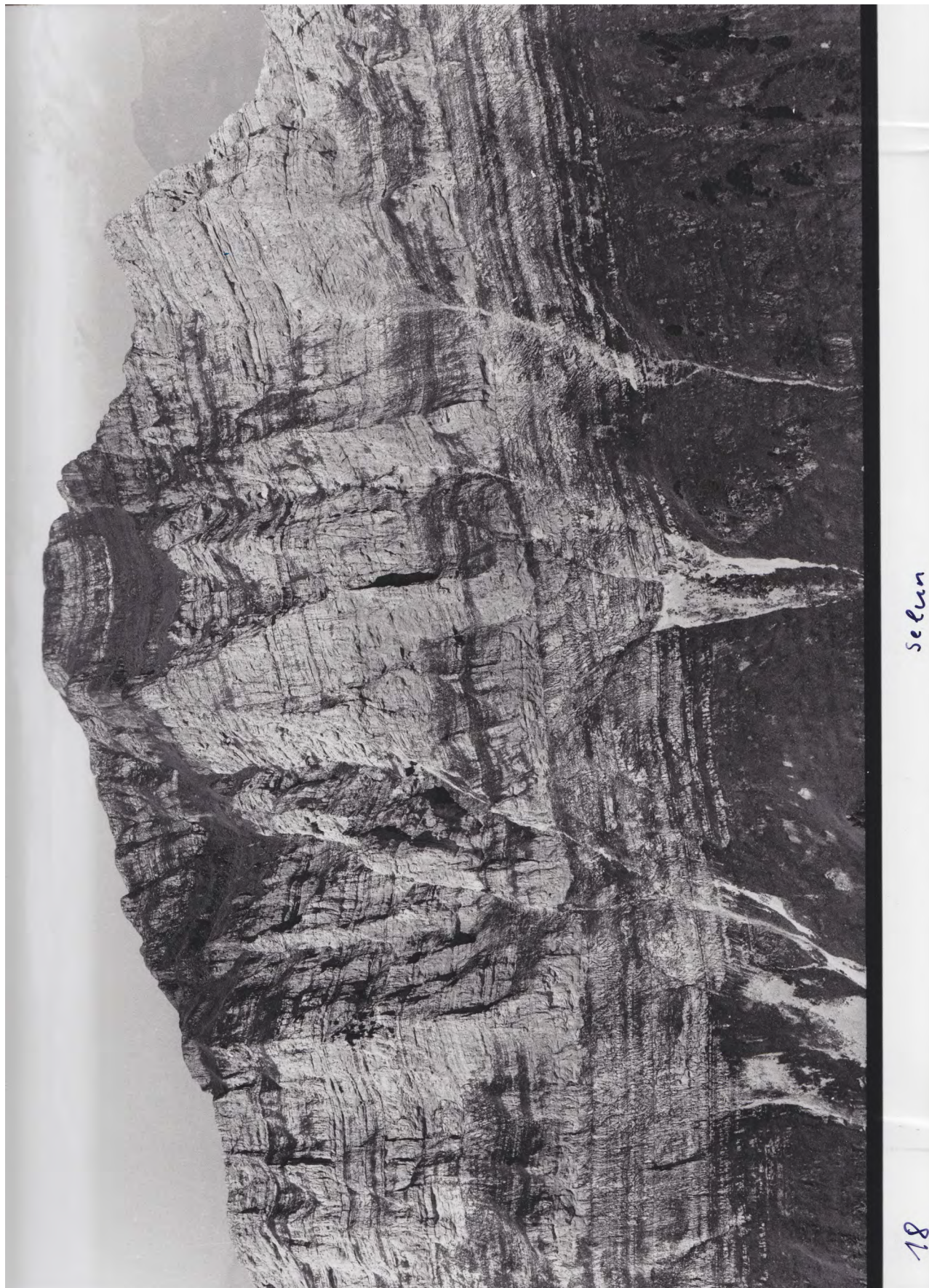
Brixi

20



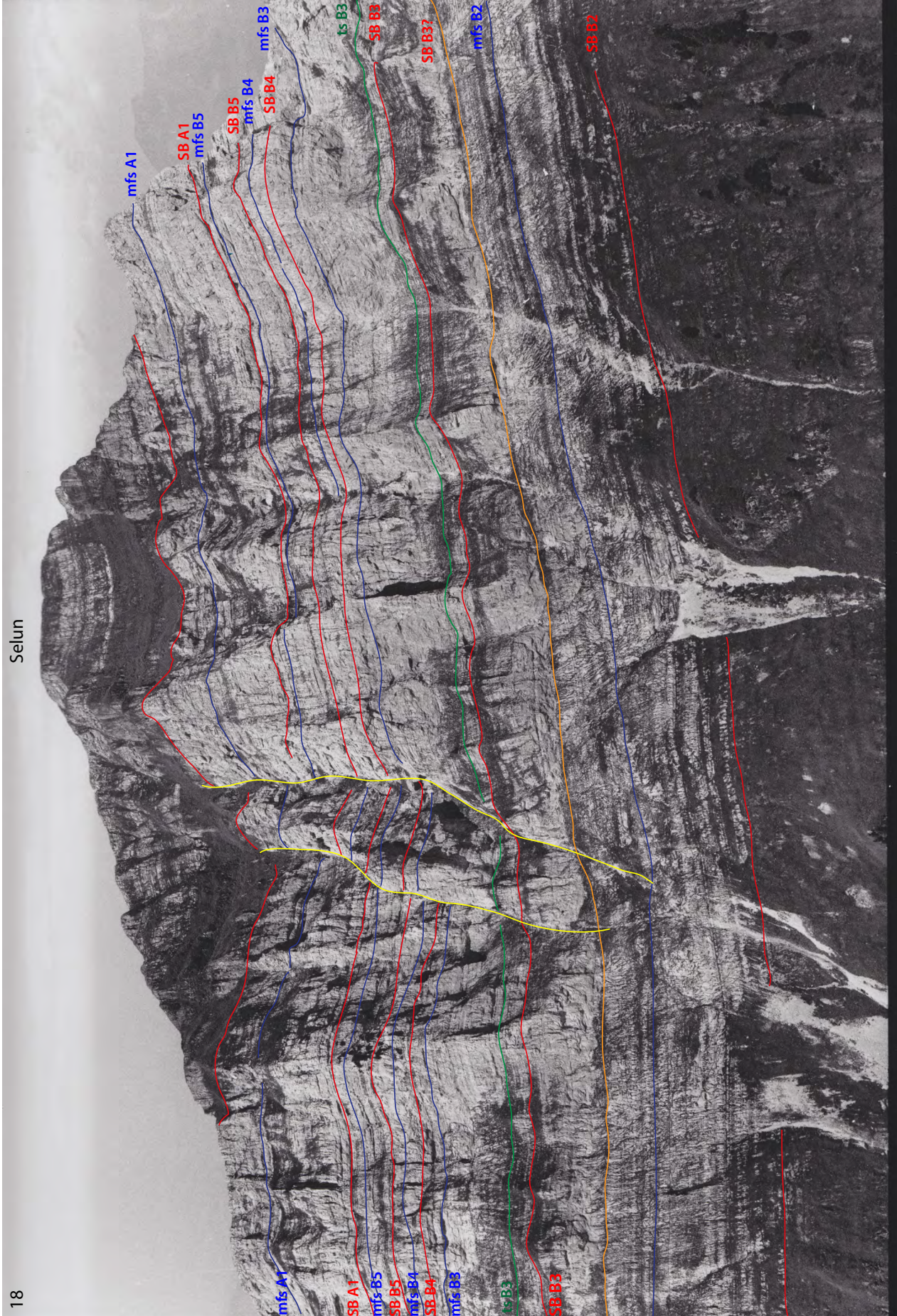


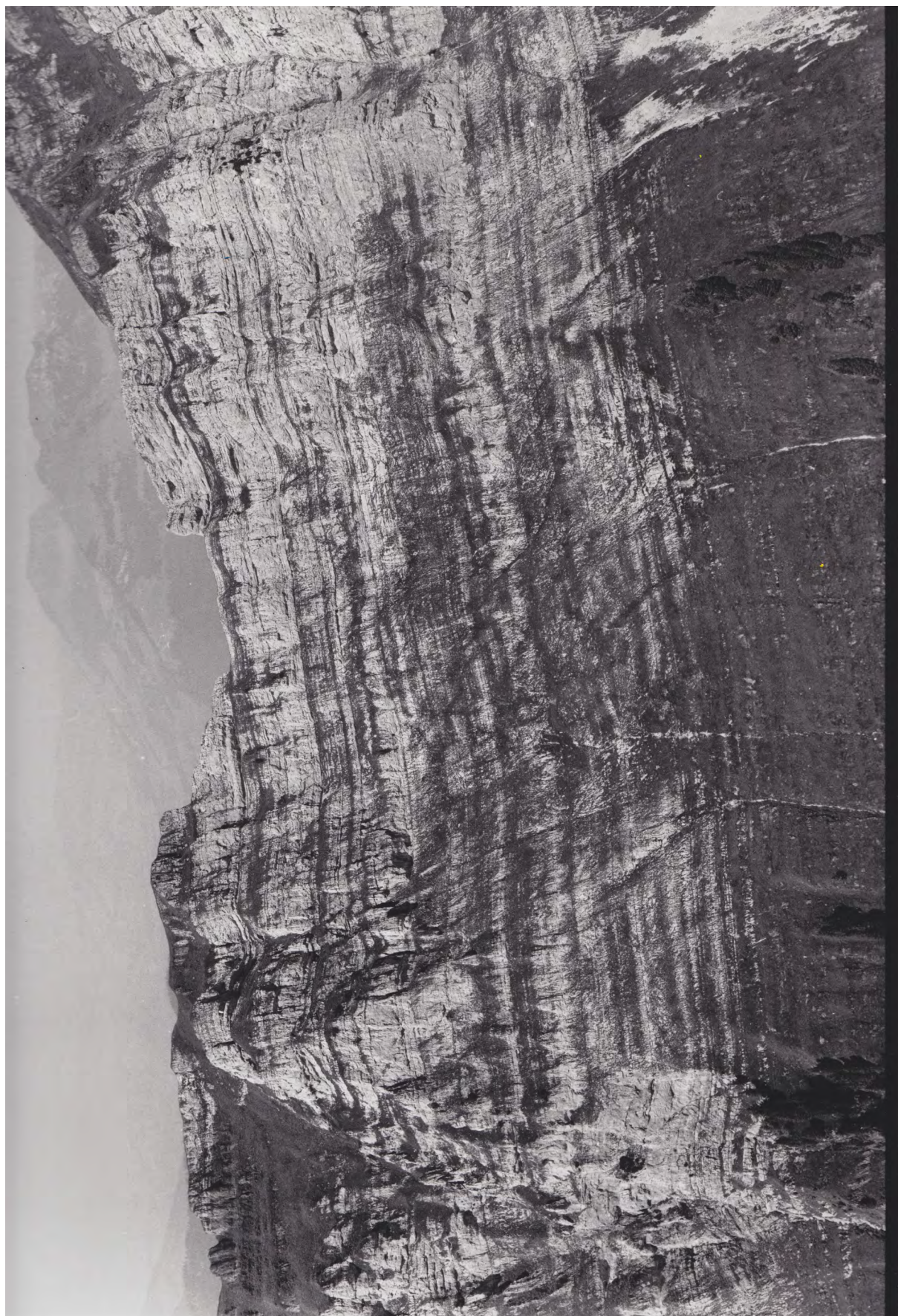




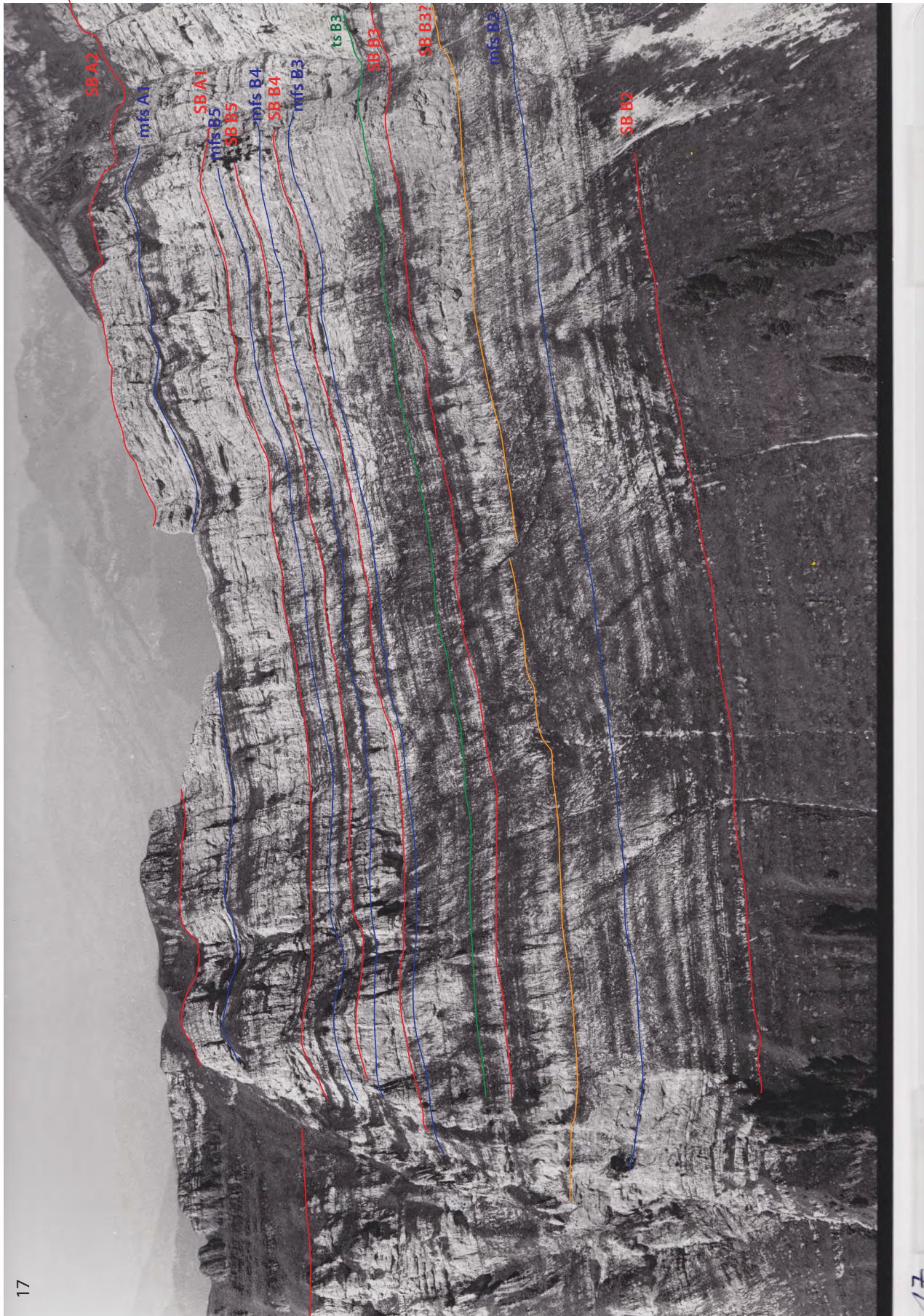
Sección

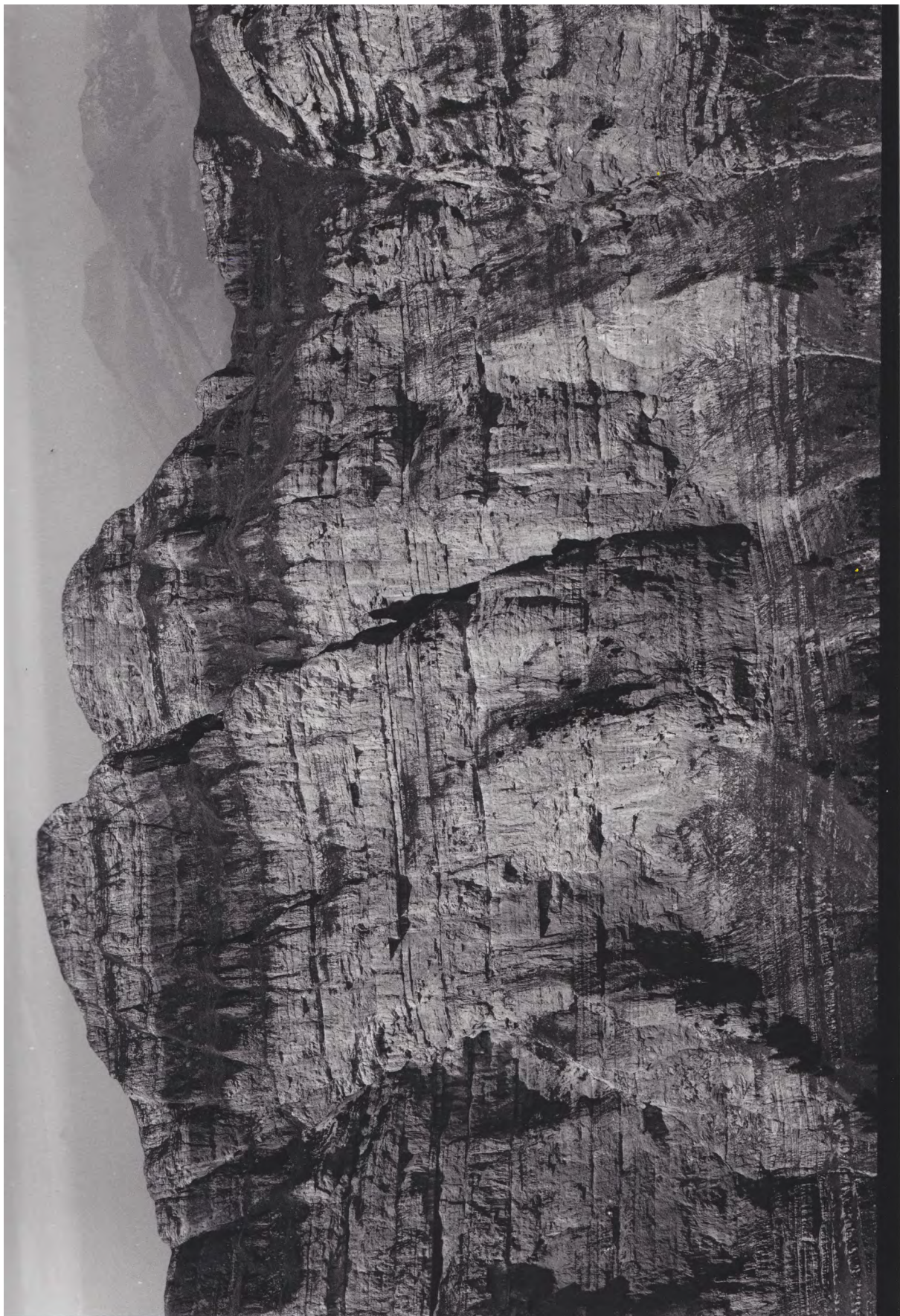
18





17





2181

Schären

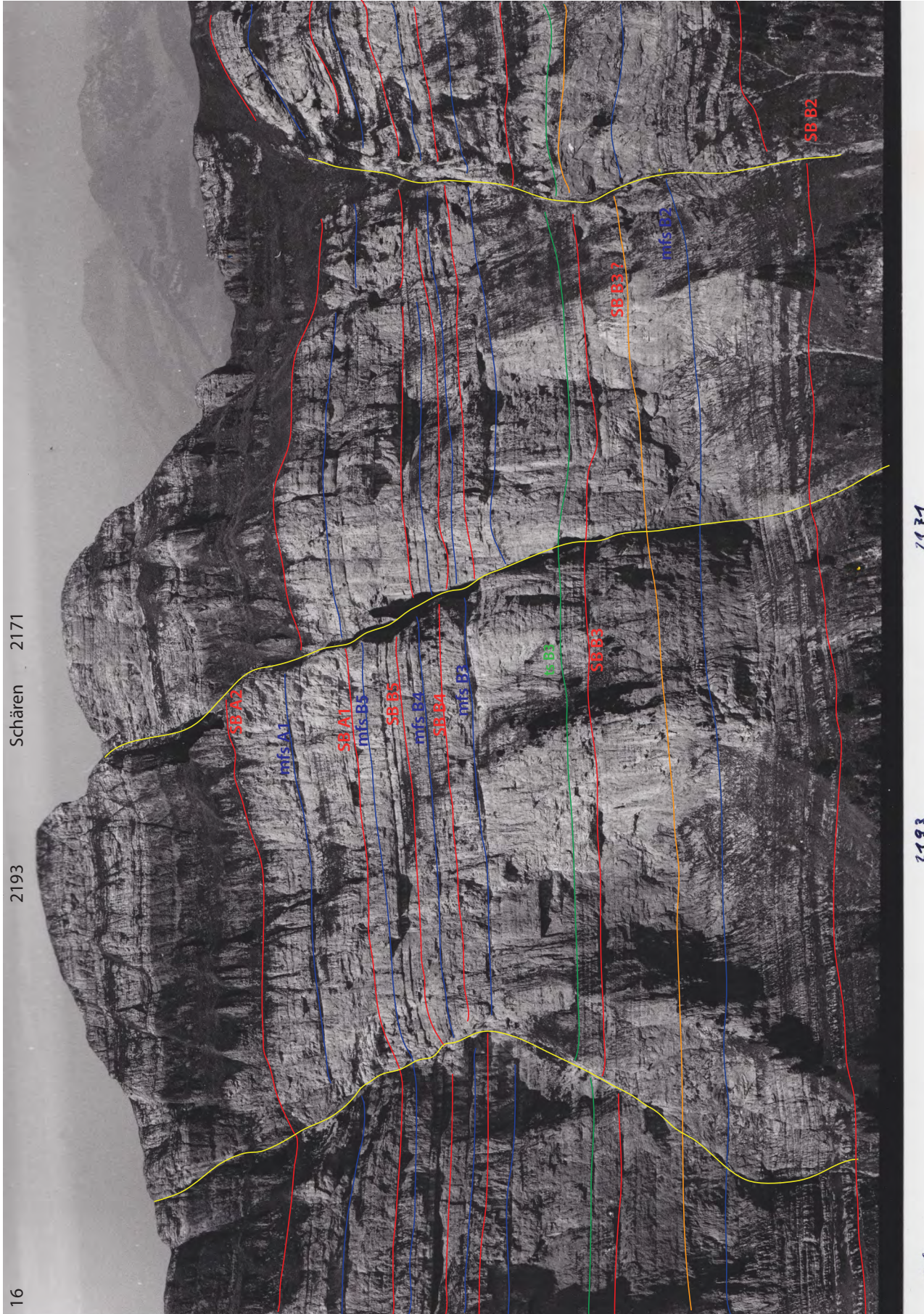
2182

16

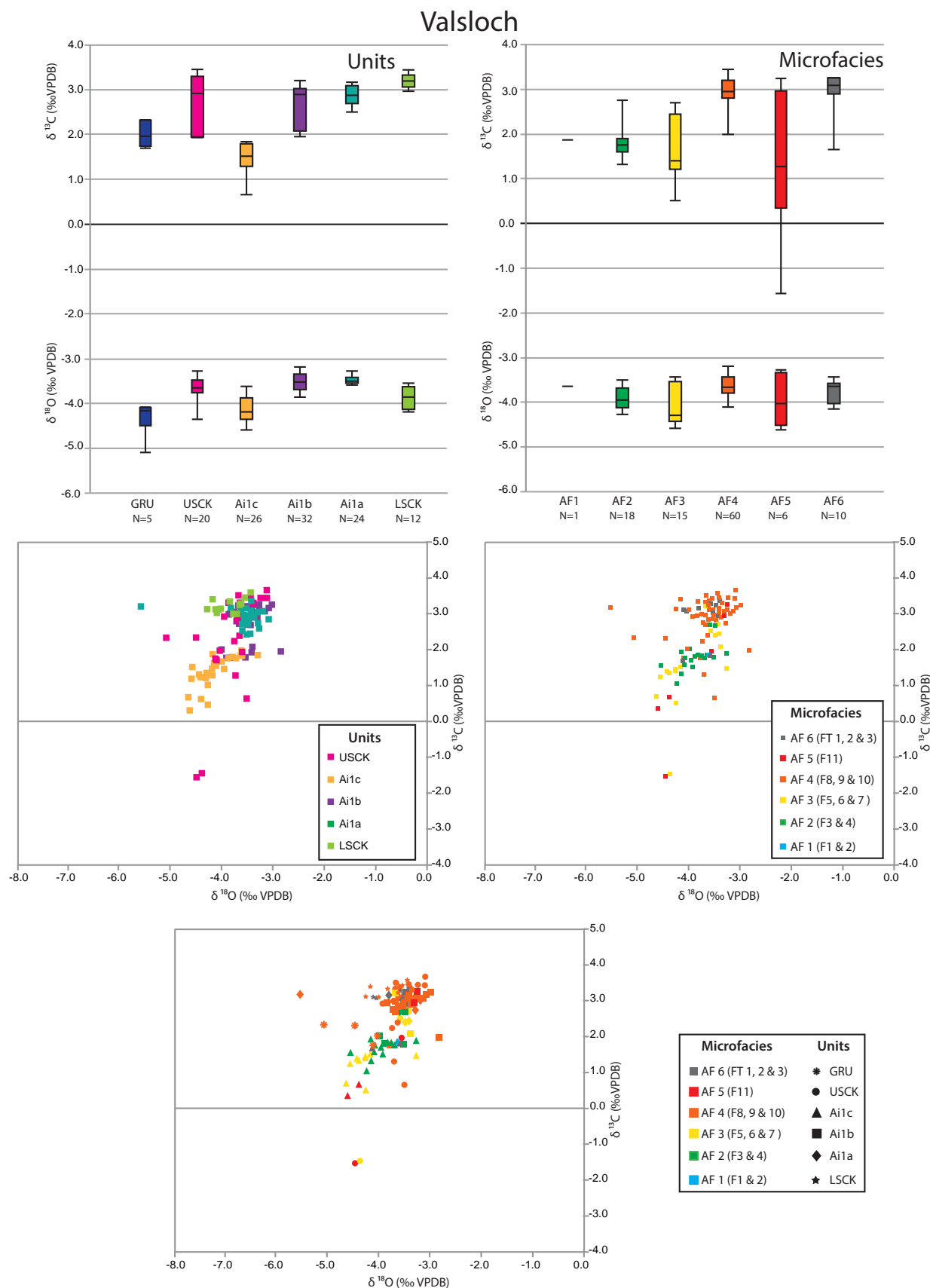
Schären 2171

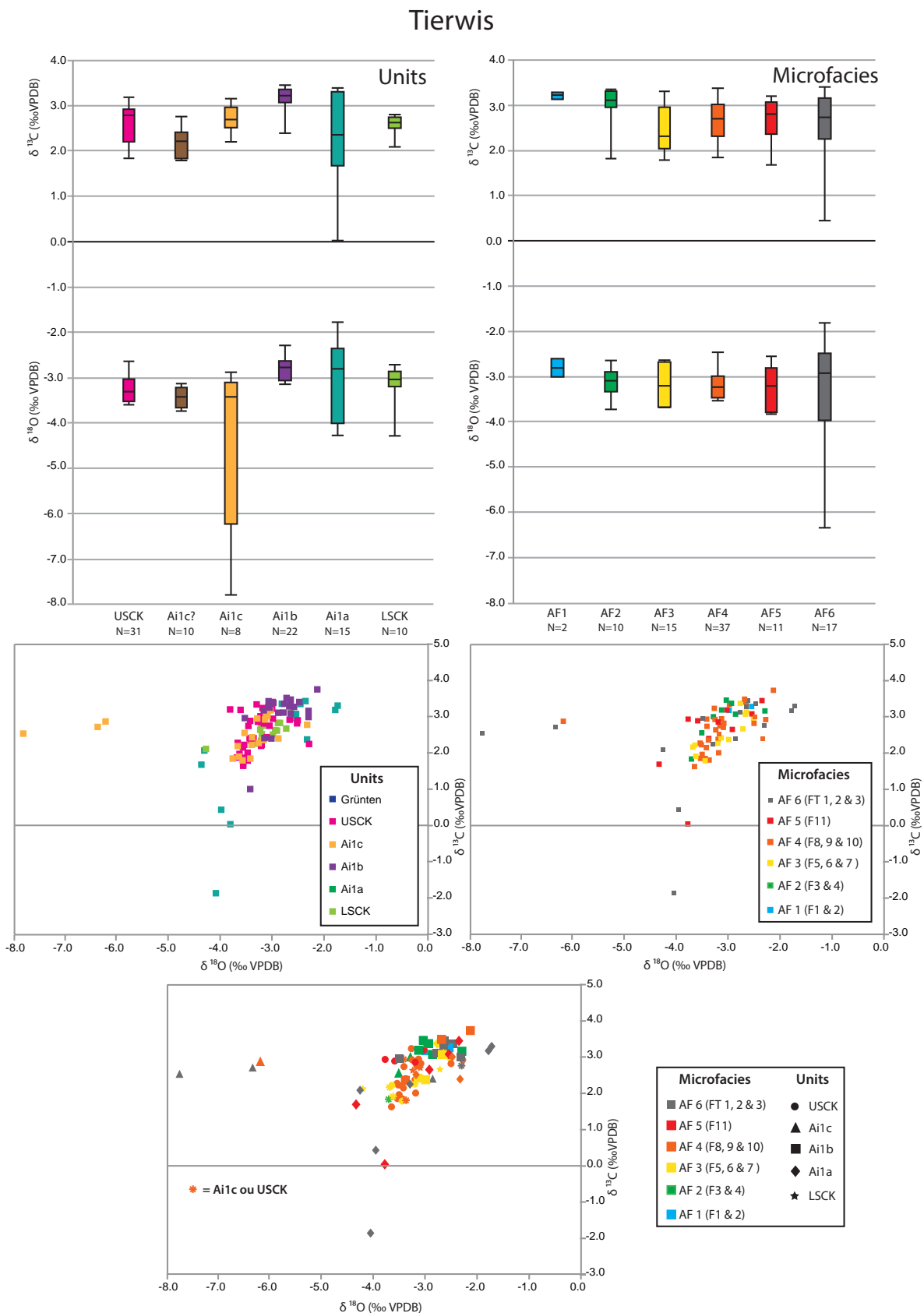
2193

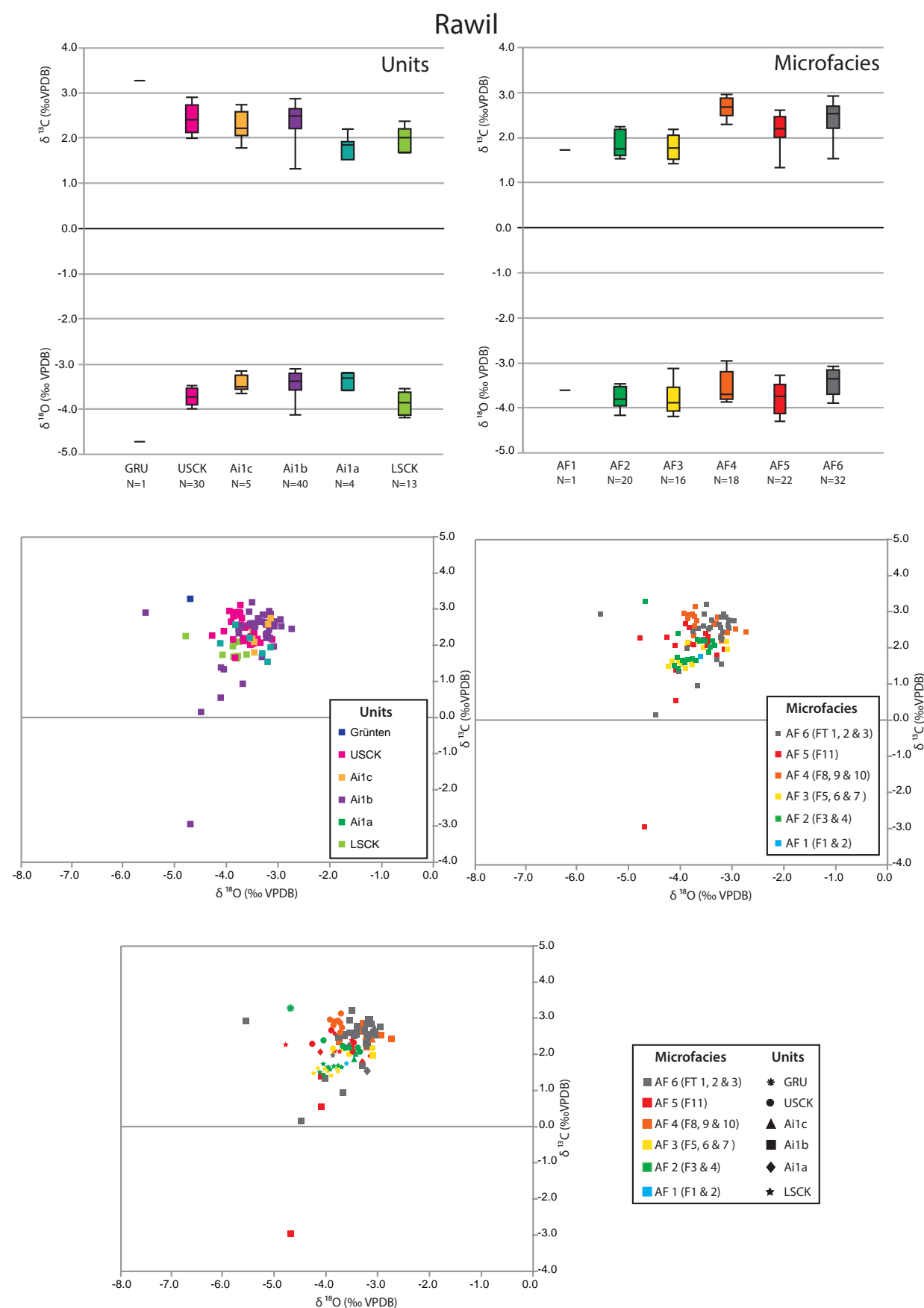
16

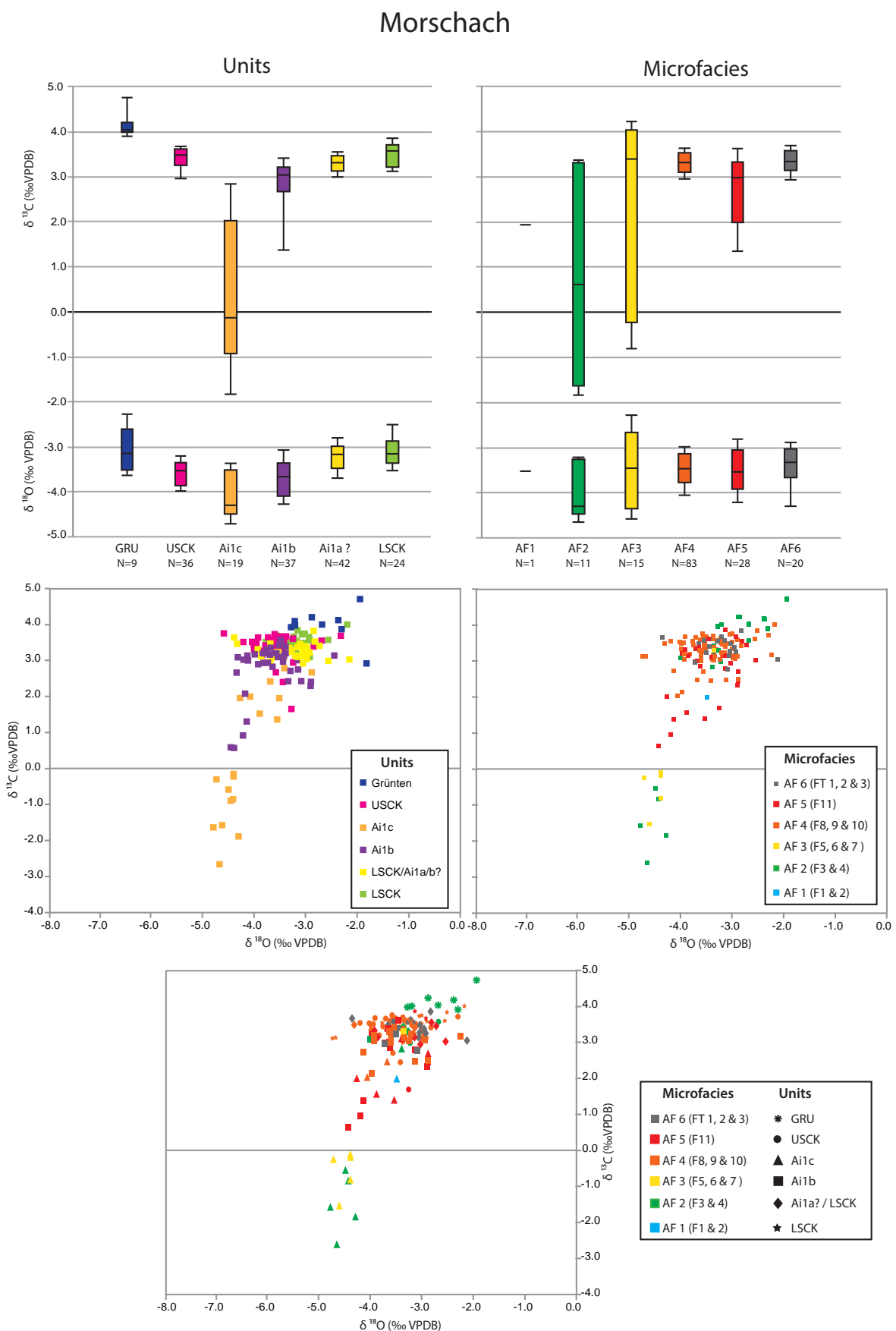


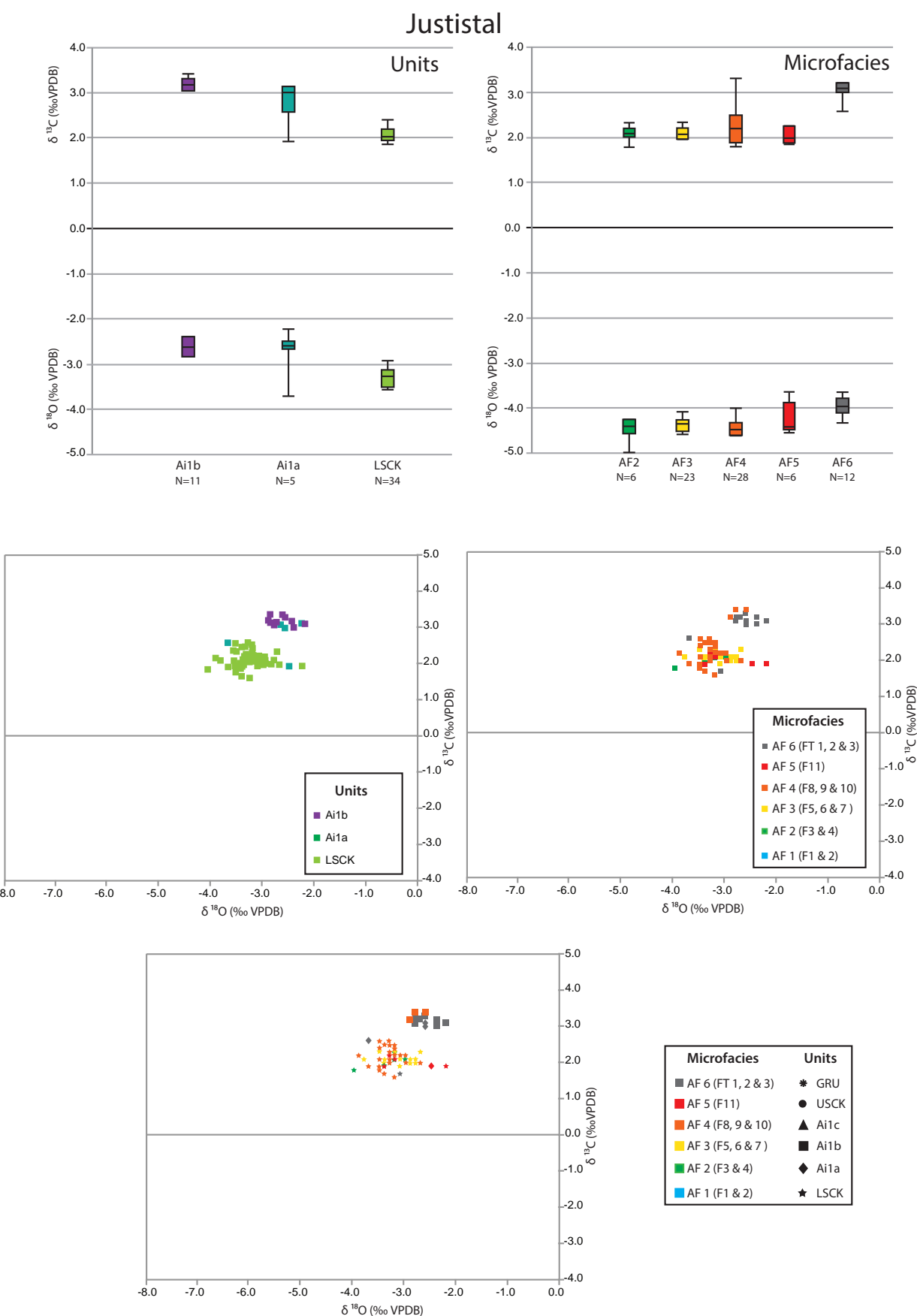
6.8 Additional boxplots for the chapter 3

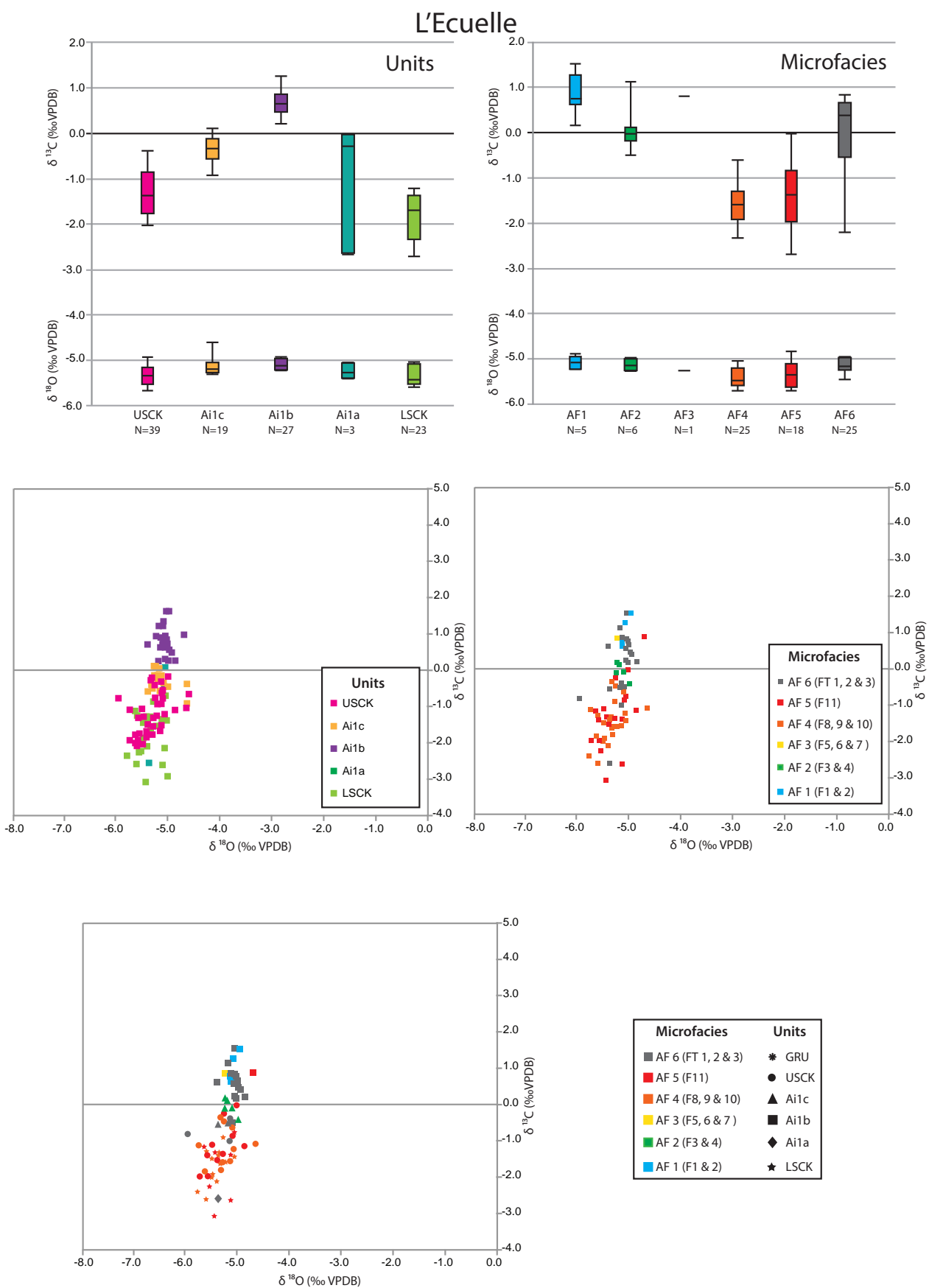












6.9 Cluses section (Subalpine Chains)

